FORCED-CONVECTION, LIQUID-COOLED, MICROCHANNEL HEAT SINKS

by

Richard J. Phillips

SUBMITTED TO THE
DEPARTMENT OF MECHANICAL ENGINEERING
IN PARTIAL FULFILLMENT OF THE REQUIREMENTS
FOR THE DEGREE OF

MASTER OF SCIENCE IN MECHANICAL ENGINEERING

at the

MASSACHUSETTS INSTITUTE OF TECHNOLOGY
16 January 1987

c Massachusetts Institute of Technology 1987

Signature of Author ______________________
Department of Mechanical Engineering
16 January 1987

Certified by ______________________
Leon R. Glicksman
Thesis Supervisor

Accepted by ______________________
Ain A. Sonin
Chairman, Department Graduate Committee

"The views expressed are those of the author and do not reflect the offical policy or postition of the U.S. government."

This work was sponsored by the Department of the Air Force.

VOL 1

MASSACHUSETTS INSTITUTE OF TECHNOLOGY
MAR 09 1987
LIBRARIES
ARCHIVES

ABSTRACT

It was recently shown by Tuckerman and Pease that heat loads on the order of 1000 W/cm^2 can be dissipated from silicon integrated circuit chips. The high power dissipation was obtained while maintaining chip temperatures below 110°C, by forcing water through microchannels fabricated directly into the back of the chip. The coolant (water) pressure drop was typically 345 kPa (50 psi) or smaller, and thermal resistance as low as 0.083 °C/(W/cm^2) has been obtained for a 1.0 cm square heat source. The theoretical analysis of Tuckerman and Pease was simplified in that the coolant flow was assumed to be laminar and fully developed, which implies an "optimum" design channel width (typically $w_c \approx \sim 50$ μm).

The current study extends the theoretical analysis of Tuckerman and Pease to include small, moderate, and large aspect ratio channels, for fully-developed and developing flow in the laminar and turbulent regimes. The channel surfaces may be smooth or roughened with repeated-ribs. Variable property effects are included for the chip material and the liquid coolant (compressibility effects have not been included). Thermal spreading at the periphery of the simulated integrated circuit heat source is also accounted for using simplified one-dimensional models. A novel method to enhance the temperature uniformity of integrated circuits, which uses "compensation heaters," is introduced.

To facilitate numerical computation, a new computer program has been created which computes the thermal and fluid performance for a large variety of coolant flow rate constraints and heat sink designs. The numerical results clearly show that essentially the same thermal performance can be obtained by increasing the channel width from that suggested by the analytical results of Tuckerman and Pease. Increasing the channel width causes the flow to become less fully developed at the channel exit (for the same coolant pressure drop), and also causes the flow to become turbulent if the Reynolds number is large enough. The pumping power requirements for the larger channel designs can be kept below 10 W/cm^2. The larger channel width designs, which are commonly on the order of w_c = 200 to 400 μm, are also much easier to fabricate.

The computer program, called MICROHEX, can be used as a design tool because it quite accurately predicts the thermal and fluid performance data for silicon microchannel heat sinks that were obtained by Tuckerman and Pease. The computer program also predicts quite well the thermal and fluid performance data for indium phosphide microchannel heat sinks that were obtained by this author. The indium phosphide microchannel heat sinks have been tested to a pressure drop as high as about 414 kPa (60 psi), and a thermal resistance as low as 0.072 °C/(W/cm^2) for a 0.25 cm square resistor heat source.

ACKNOWLEDGEMENTS

I would like to express my gratitude to M.I.T. Lincoln Laboratory for providing financial support and facilities for this project. I would also like to acknowledge the financial support provided by the Digital Equipment Corporation.

I wish to thank my thesis supervisor, Dr. Leon Glicksman, for his enthusiastic technical support and guidance. I wish to also thank Ralph Larson (Digital Equipment Corporation, Maynard, MA, U.S.A.) and Dr. Tom Bligh (Cambridge University, Cambridge, England) for their technical contributions.

There are many other people from M.I.T. Lincoln Laboratory who worked on this project that I want to thank for their guidance and assistance. Dr. Jim Walpole provided several invaluable contributions in working out the fabrication process. The consultations with Dr. Steve Groves, Dr. Jerry Iseler, and Dr. Zong-Long Liau were very helpful. Pete Daniels made several helpful recommendations on the packaging design.

There are several people who helped in various ways to fabricate the indium phosphide test chips. Steve Connor fabricated the test chip resistors and did the photolithography for orientation dependent acid etching of the microchannels. Dana Dedek, Yvette Grinbush, and Deborah Landers did the wire bonding of the test chips. Ben DiGiorgio polished test chips, and Mark McAleese implanted the test chip wafers. Dr. Jerry Iseler provided the indium phosphide wafers.

I wish to thank Skip Hoyt and Dan Calawa for their guidance and assistance in sawing the microchannels in indium phosphide chips. Pat Doherty, Danny Dufour, and Don Paquet developed the machining process for making microchannels in aluminum.

Thanks go out to Buddy Bradley, Bob Perle, Bob Pitts, and Bob Steeves for their assistance in setting up the test apparatus. Sarah Coley and Tim Sullivan programmed the data acquisition system.

I am very grateful to Joan Daugherty and Diane Valcourt for typing this thesis. Their patience and attention to detail go beyond description. Kris Gastongway typed some of the draft portions of the thesis.

TABLE OF CONTENTS

TITLE PAGE 1

ABSTRACT 2

ACKNOWLEDGMENTS 3

TABLE OF CONTENTS 4

LIST OF FIGURES 8

LIST OF TABLES 14

NOMENCLATURE 16

1.0 THERMAL MANAGEMENT OF MICROELECTRONICS 27

1.1 Trends In Computer Microelectronics 27

1.2 State-Of-The-Art Single-Chip and Multi-Chip-Module

Heat Sink Technology 30

1.3 Overview of Microchannel Heat Sink Design 35

1.3.1 Previous Works 36

1.3.2 This Investigation 41

1.4 Thesis Organization 45

2.0 FORCED CONVECTION FLOW IN DUCTS 48

2.1 Smooth Ducts 48

2.1.1 Distinction Between Laminar,

Transitional, and Turbulent Flow 48

2.1.2 Friction Coefficients In Channel Flow 50

2.1.3 Pressure Drop 66

2.1.4 Heat Transfer Coefficients 73

2.2 Roughened Ducts 89

2.2.1 Overview of Heat Transfer Augmentation By

Surface Roughening 90

2.2.2 Friction Coefficients and Pressure Drop 91

2.2.3 Heat Transfer Coefficients 96

2.3 Effect of Axial Heat Conduction 97

2.4 Effect of Viscous Dissipation 98

2.5 Effect of Natural Convection 99

2.6 Effect of Temperature Varying Properties 102

2.7 Effect of Non-uniform Passages 103

2.8 Interrupted Fins 104

2.9 Chapter Summary 117

3.0 CONDUCTION HEAT TRANSFER 120

3.1 Physics of The Heat Conduction Process 120

3.2 Continuous and Discrete Heat Sources and Sinks 123

3.3 Fin Heat Transfer 128

3.4 Thermal Spreading At The Heat Source Perimeter 143

3.5 Chapter Summary 147

4.0 MICROCHANNEL HEAT SINK DESIGN 150

4.1 Components of Thermal Resistance 150

4.2 Thermal Resistance Models 160

4.3 Simplified Solution of The Large Aspect Ratio Channel Models 163

4.4 Iterative Solution Procedure 166

4.5 Computer Solution of The Thermal Resistance Models 172

4.5.1 The MICROHEX Computer Program 172

4.5.2 Sample Numerical Results 181

4.6 Use of Compensation Heaters 213

4.7 Use of Interrupted Fins 219

4.8 Chapter Summary 221

5.0 EXPERIMENTAL VERIFICATION OF MICROCHANNEL HEAT SINK PERFORMANCE 224

5.1 Purpose of The Experimental Investigation 224

5.2 Heat Sink Fabrication 225

5.2.1 Manufacturing The Microchannels In InP 225

5.2.1.1 Precision Sawing 225

5.2.1.2 Orientation Dependent Etching 227

5.2.2 Packaging and Headering 230

5.2.3 Resistor Heat Source Fabrication 232

5.2.4 Summary of Manufacturing Process Steps For Indium Phosphide Chips 236

5.2.5 Manufacturing The Microchannels In Aluminum 242

5.3 Experiments 243

5.3.1 Test Apparatus 243

5.3.2 Data Acquisition and Reduction 246

5.3.3 Experimental Errors 251

5.4 Chapter Summary 254

6.0 COMPARISON OF ANALYTICAL AND EXPERIMENTAL RESULTS 255

6.1 Heat Sink Geometry 255

6.2 Fluid Performance 258

6.3 Thermal Performance 262

6.4 Modes of Failure 278

6.5 Chapter Summary 281

7.0 SUMMARY AND CONCLUSIONS 282

7.1 Conclusions 282

7.2 Future Work 284

BIBLIOGRAPHY 286

APPENDIX A: Fins With Non-uniform Thermal Conductivity, Heat Transfer Coefficient, and Coolant Temperature 292

APPENDIX B: Fin With Internal Heat Generation 295

APPENDIX C: Optimum Fin Aspect Ratio 297

APPENDIX D: Microcapillary Thermal Interface 300

APPENDIX E: MICROHEX Computer Program Listing 304

APPENDIX F: MICROHEX Numerical Results for the Reference Case 373

LIST OF FIGURES

FIGURE NUMBER	TITLE	PAGE
1.1	Power-delay continuums of important transistor technologies	29
1.2	General trends for MIPS versus power	29
1.3	Perspective of microelectronic heat flux	31
1.4	Schematic of a forced-convection, liquid-cooled microchannel heat sink	37
1.5	Silicon "pin-fins" manufactured by precision sawing	40
1.6	Microcapillary thermal interface	40
1.7	Thermal spreading at the heater periphery	43
2.1	Laminar flow friction coefficients used for computer simulation	55
2.2	Friction pressure drop data plotted as a function of Re* and Re	58
2.3	Local friction factor based on static pressure gradient for the entrance region of circular tubes	59
2.4	Average friction factor based on static pressure drop for the entrance region of circular tubes	59
2.5	Numerically integrated average friction factor for turbulent flow in circular tubes	61
2.6	Numerically integrated average friction factor for turbulent flow in circular tubes	62
2.7	Ratio of numerically integrated average friction factor to the fully developed friction factor based on static pressure drop	62
2.8	Comparison of fully-developed-flow friction factors with respect to the Karman-Nikuradse correlation	67
2.9	Microchannel heat sink pressure drop components	68

FIGURE NUMBER	TITLE	PAGE

2.10	Entrance and exit loss coefficients for flow in circular tubes	71
2.11	Entrance and exit loss coefficients for flow between parallel plates	72
2.12	Nusselt number for fully developed flow in rectangular ducts with one or more walls transferring heat. Uniform axial heat flux and uniform peripheral wall temperature	77
2.13	Laminar flow Nusselt numbers used for computer simulation	83
2.14	Thermal entrance results for oil flow in circular tubes	86
2.15	Flow patterns as a function of p/e for flow past repeated-ribs	92
2.16	Repeated-rib geometric parameters	93
2.17	Regimes for free, forced, and mixed convection for flow through tubes	101
2.18	Schematic of interrupted fins	106
2.19	Recirculation zones on a plat plate aligned parallel to the flow	108
2.20	Schematic of co-linear plates	110
2.21	Nusselt number variation with inter-plate spacing	110
2.22	Dimensionless pressure drop variation with inter-plate spacing	111
2.23	Conditions for the onset of periodic flow between co-linear plates	111
2.24	Comparison of interrupted-fin and continuous-fin mean Nusselt numbers	115

FIGURE NUMBER	TITLE	PAGE

3.1 Thermal conductivity versus temperature of various materials........ 122

3.2 Thermal conductivity of In-As-P........ 124

3.3 Heat transfer by conduction through a plane slab....... 124

3.4 Heat flow "constriction effect."........ 125

3.5 Schematics of discrete heat sources........ 127

3.6 Channel configurations obtained by precision sawing and orientation dependent etching........ 129

3.7 Heat flow paths in the region of the fin tip........ 133

3.8 Flow channel configuration used by Han (1959)........ 138

3.9 Correction factor for finite fin conductivity........ 138

3.10 Flow channel configuration used by Sparrow, Baliga, and Patankar (1978), and Kadle and Sparrow (1986)...... 140

3.11 One-dimensional fin model........ 142

3.12 Fin model for thermal spreading at the heater perimeter........ 145

3.13 Example of chip thermal spreading........ 148

4.1 Temperature trends in the streamwise direction........ 159

4.2 Flow chart of the iterative solution procedure........ 173

4.3 Flow chart of subroutine calls for program MICROHEX.... 177

4.4 Thermal resistance and pumping power versus channel width for the reference case........ 184

4.5 Thermal resistance as a function of distance from the upstream heater edge for several reference case channel widths........ 191

FIGURE NUMBER	TITLE	PAGE

4.6 Thermal resistance and pumping power versus channel width for the reference case and fully-developed laminar flow at two channel aspect ratios.............. 194

4.7 Thermal resistance and pumping power versus channel width for the reference case with several coolant velocity constraints.................................... 196

4.8 Thermal resistance and pumping power versus channel width for the reference case with several heat sink materials... 198

4.9 Thermal resistance and pumping power versus channel width for the reference case with several liquid coolants.. 200

4.10 Thermal resistance and pumping power versus channel width for the reference case with several inlet coolant temperatures............................... 201

4.11 Thermal resistance and pumping power versus channel width for the reference case with several surface heating rates.................................... 203

4.12 Thermal resistance and pumping power versus channel width for the reference case with several channel lengths.. 205

4.13 Thermal resistance and pumping power versus channel width for the reference case with several values of the fin thickness to channel width ratio..... 207

4.14 Thermal resistance and pumping power versus channel width for the reference case with several constant fin heights.................................... 208

4.15 Thermal resistance and pumping power versus channel width for the reference case with several solid substrate thicknesses............................ 210

4.16 Thermal resistance and pumping power versus channel width for the reference case with several channel aspect ratios.................................... 211

FIGURE NUMBER	TITLE	PAGE

4.17 Thermal resistance and pumping power versus channel width for the reference case with and without entrance and exit losses....................... 212

4.18 Thermal resistance and pumping power versus channel width for the reference case with smooth and repeated-rib-roughened surfaces.................... 214

4.19 Compensation heater concept............................ 216

4.20 Thermal resistance as a function of distance from the upstream heater edge with and without a compensation heater energized for the reference case channel width of 300 μm.......................... 218

5.1 Views of microchannels fabricated in Indium Phosphide using orientation dependent etching with H_3PO_4:HCl (3:1).. 229

5.2 Test block assembly and coolant flow path.............. 231

5.3 Test chip resistor electrical connection............... 234

5.4 Test loop schematic.................................... 244

5.5 Microchannel heat sink test apparatus.................. 247

5.6 Manifold electronics substage.......................... 249

6.1 Comparison of experimental data and MICROHEX program predictions for pressure drop versus Reynolds number... 261

6.2 Comparison of experimental data and MICROHEX program predictions for pressure drop versus hydrodynamic entrance length....................................... 263

6.3 Comparison of experimental data and MICROHEX program predictions for thermal resistance versus thermodynamic entrance length....................................... 265

6.4 Comparison of experimental data and MICROHEX program predictions for thermal resistance versus distance from the upstream heater edge............................. 265

FIGURE NUMBER	TITLE	PAGE

6.5	Surface temperature for HEX3 as a function of the microscope substage micrometer position................	268
6.6	Surface temperature for HEX4 as a function of the microscope substage micrometer position................	271
6.7	Comparison of experimental data and MICROHEX program predictions for thermal resistance versus distance from the upstream heater edge of HEX4 resistor R2...........	272
6.8	Peak surface temperature versus dissipated power for HEX4 at two coolant flow rates.....................	274
6.9	Thermal resistance versus dissipated power for HEX4 at two coolant flow rates..............................	275
6.10	Roughness height criterion versus flow Reynolds number...	277
6.11	Comparison of experimental data and MICROHEX program predictions for thermal resistance versus dissipated power..	279
A.1	Sub-divided fin model.................................	294
B.1	Fin with internal heat generation......................	296
D.1	Microcapillary thermal interface concept...............	303

LIST OF TABLES

TABLE NUMBER	TITLE	PAGE
1.1	PRIMARY COOLING METHODS FOR CHIPS	33
1.2	STATE-OF-THE-ART SINGLE-CHIP AND MULTI-CHIP MODULE THERMAL PERFORMANCE	34
2.1	CRITICAL REYNOLDS NUMBERS FOR ABRUPT-ENTRANCE DUCTS	50
2.2	FULLY-DEVELOPED, LAMINAR-FLOW FRICTION COEFFICIENTS IN RECTANGULAR DUCTS	51
2.3	DEVELOPING, LAMINAR-FLOW FRICTION COEFFICIENTS IN RECTANGULAR DUCTS	52
2.4	DEVELOPING, LAMINAR-FLOW FRICTION COEFFICIENTS BETWEEN PARALLEL PLATES	53
2.5	LAMINAR-FLOW FRICTION COEFFICIENTS USED FOR COMPUTER SIMULATION	54
2.6	NUMERICALLY INTEGRATED AVERAGE FRICTION FACTORS	63
2.7	CORRELATION EQUATIONS FOR AVERAGE FRICTION FACTORS	65
2.8	NUSSELT NUMBER FOR FULLY DEVELOPED FLOW IN RECTANGULAR DUCTS WITH ONE OR MORE WALLS TRANSFERRING HEAT, WITH UNIFORM AXIAL HEAT FLUX AND UNIFORM PERIPHERAL WALL TEMPERATURE	76
2.9	NUSSELT NUMBER FOR THERMALLY DEVELOPING FLOW IN RECTANGULAR DUCTS, WITH ALL FOUR WALLS TRANSFERRING HEAT AND UNIFORM PERIPHERAL WALL TEMPERATURE	79
2.10	NUSSELT NUMBER FOR THERMALLY DEVELOPING FLOW BETWEEN PARALLEL PLATES WITH ONE OR BOTH WALLS HEATED	80
2.11	LAMINAR FLOW NUSSELT NUMBERS USED FOR COMPUTER SIMULATION	82
2.12	THERMAL ENTRANCE LENGTH RESULTS FOR OIL FLOW IN CIRCULAR TUBES	85
2.13	PROPERTY RATIO METHOD EXPONENTS	103

TABLE NUMBER	TITLE	PAGE
4.1	OVERVIEW OF MICROHEX ROUTINES	175
4.2	MICROHEX DATA STATEMENT VARIABLES	178
4.3	INPUT DATA FOR MICROHEX COMPUTATIONS	183
5.1	RESISTANCE VALUES FOR TEST CHIPS	235
5.2	SUMMARY OF MANUFACTURING PROCESS FOR INDIUM PHOSPHIDE TEST CHIPS	236
6.1	HEAT SINK GEOMETRY	257
6.2	COMPARISON OF PRESSURE DROP PREDICTED BY THE MICROHEX COMPUTER PROGRAM AND EXPERIMENTAL DATA OBTAINED BY THE STANFORD RESEARCHERS	260
6.3	EXPERIMENTAL THERMAL PERFORMANCE OF InP TEST CHIPS	267
F.1	MICROHEX OUTPUT1 FOR THE REFERENCE CASE	374
F.2	MICROHEX OUTPUT2 FOR THE REFERENCE CASE	377
F.3	MICROHEX OUTPUT3 FOR THE REFERENCE CASE	380
F.4	MICROHEX OUTPUT4 FOR THE REFERENCE CASE	380

NOMENCLATURE

a	...	constriction effect dimension (m)
A	...	channel cross-sectional flow area (m^2)
	also,	parameter for Equation 2.6 (-)
	also,	surface area for heat transfer (m^2)
A_{bc}	...	area of channel base (m^2)
A_{bf}	...	area of fin base (m^2)
Ac	...	minimum free-flow area (m^2)
A_{cross}	...	surface area for heat input (m^2)
Ac/Ap	...	ratio of inlet and exit plenum cross-sectional areas (-)
A_p	...	fin profile area (m^2)
A_{surf}	...	fin surface area (m^2)
Aw	...	repeated-rib-roughened, total heat transfer surface area (m^2)
b	...	constriction effect dimension (m)
	also,	fin and channel height (m)
	also,	interrupted-fin boundary layer thickness (m)
B	...	parameter for Equation 2.16 (-)
c	...	constriction effect dimension (m)
C_1, C_2	...	parameters for Table 2.7 (-)
c_j	...	carrier specific heat per unit volume (J/m^3°C)
Cp_f	...	coolant specific heat (J/(kg°C))
d	...	constriction effect dimension (m)
	also,	rod diameter (m)

NOMENCLATURE (continued)

D_e	...	channel hydraulic diameter (m)
D_{le}	...	laminar equivalent diameter (m)
e	...	repeated-rib height (m)
e^+	...	roughness Reynolds number (-)
E_A	...	activation energy (J/molecule)
f, f_0	...	smooth-channel, fully-developed-flow friction factor (-)
f_1	...	one-side-roughened, fully-developed-flow friction factor (-)
f_2	...	two-sides-roughened, fully-developed-flow friction factor (-)
f_{app}	...	apparent friction factor (-)
Fc	...	correction factor in Equation 3.10 (-)
f_{cold}	...	unheated-chip, total coolant flow rate (cm^3/s)
f_{cp}	...	constant-property friction factor (-)
f_{curve}	...	curve friction factor in Figure 2.8 (-)
f_{heated}	...	coolant flow rate under the heaters (cm^3/s)
f_{hot}	...	heated-chip, total coolant flow rate (cm^3/s)
f_{K-N}	...	Karman-Nikuradse fully-developed friction factor (-)
f_p	...	local friction factor based on static pressure gradient (-)
g	...	acceleration of gravity (m/s^2)
g_c	...	constant (1 kg m/N s^2)
Gr	...	Grashof number (-)
h	...	heat transfer coefficient ($W/m^2 °C$)

NOMENCLATURE (continued)

$h(z)$	...	heat transfer coefficient along fin height (W/m^2°C)
h_j	...	sectioned-fin heat transfer coefficient (W/m^2°C)
H	...	interrupted-fin transverse spacing (m)
H_e^+	...	heat transfer function (-)
H_{eff}	...	thermal spreading effective fin height (m)
h_x	...	local heat transfer coefficient (W/m^2°C)
i	...	parameter for Equation 2.19 (-)
I	...	electrical current (Amps)
j	...	Colburn modulus (-)
	also,	parameter for Equation 2.19 (-)
J	...	mechanical equivalent of heat (1 N m/J)
k	...	Boltzmann's constant (J/molecule°K)
K	...	fin parameter (-)
	also,	overall pressure loss coefficient (-)
Kc	...	entrance pressure loss coefficient (-)
Ke	...	exit pressure loss coefficient (-)
K_{90}	...	90° bend pressure loss coefficient (-)
k_f	...	coolant thermal conductivity (W/(m°C))
k_w	...	heat sink material thermal conductivity (W/(m°C))
k_{wj}	...	sectioned-fin thermal conductivity (W/m°C)
l	...	streamwise length of flow recirculation (m)
L	...	streamwise fin length (m)
L_1, L_2	...	thermal spreading fin lengths (m)
L_{ex}	...	heat exchanger length (m)

NOMENCLATURE (continued)

L_d	...	thermal spreading diffusion length (m)
L_s	...	streamwise thermal spreading diffusion length (m)
L_t	...	transverse thermal spreading diffusion length (m)
L^*	...	interrupted-fin thermal entrance length (-)
L^+	...	hydrodynamic entrance length (-)
m	...	fin parameter (m^{-1})
	also,	parameter for Equation 2.16 (-)
m_j	...	sectioned-fin parameter (m^{-1})
M	...	property ratio method exponent (-)
$\dot{m}$	...	coolant mass flow rate (kg/s)
n	...	parameter for Equation 2.16 (-)
	also,	total number of channels (-)
N	...	property ratio method exponent (-)
Nu	...	Nusselt number (-)
$Nu_{case\ 1}$	...	four-sides-heated, fully-developed Nusselt number (-)
$Nu_{case\ 2}$	...	three-sides-heated, fully-developed Nusselt number (-)
Nu_{cp}	...	constant-property Nusselt number (-)
Nu_m	...	mean Nusselt number (-)
$Nu_{m,T}$	...	constant-surface-temperature mean Nusselt number (-)
Nu_x	...	local Nusselt number (-)
$Nu_{x,3}$	...	three-sides-heated, developing Nusselt number (-)
$Nu_{x,4}$	...	four-sides-heated, developing Nusselt number (-)
p	...	distance between repeated-ribs (m)

NOMENCLATURE

Symbol		Definition
P	...	channel perimeter (m)
	also,	convective heat transfer perimeter (m)
Pe	...	Peclet number (-)
Pr	...	coolant Prandtl number (-)
P''	...	coolant pumping power (W/cm^2)
q'	...	fin base heating rate per unit length (W/m)
q''	...	uniform surface heat flux (W/cm^2)
q''_b	...	heat flux at fin base (W/m^2)
q''_j	...	sectioned-fin heat flux at fin base (W/m^2)
$q''_{w,x}$	...	local, wall heat flux (W/m^2)
Q	...	total heating rate (W)
Q_{fj}	...	sectioned-fin coolant heating rate (W)
Q_j	...	sectioned-fin base heating rate (W)
Q_{j+1}	...	sectioned-fin tip heating rate (W)
R	...	electrical resistance (Ω)
R^2	...	coefficient of determination (-)
R''	...	modified thermal resistance (°C/(W/cm^2))
R''_{bulk}	...	coolant bulk temperature rise modified thermal resistance (°C/(W/cm^2))
R''_{conv}	...	contraction modified thermal resistance (°C/(W/cm^2))
R''_{conv}	...	convective modified thermal resistance (°C/(W/cm^2))
$R''_{conv,continuous}$	...	continuous-fin convective modified thermal resistance (°C/(W/cm^2))

NOMENCLATURE (continued)

$R''_{conv,interrupted}$	...	interrupted-fin convective modified thermal resistance (°C/(W/cm^2))
R''_{int}	...	interface modified thermal resistance (°C/(W/cm^2))
R''_{solid}	...	solid substratge modified thermal resistance (°C/(W/cm^2))
R_{spread}	...	gate thermal spreading thermal resistance (°C/W)
R''_{spread}	...	gate thermal spreading modified thermal resistance (°C/(W/cm^2))
R_{tot}	...	total thermal resistance (°C/W)
R''_{tot}	...	total modified thermal resistance (°C/(W/cm^2))
$R''_{tot,large}$	...	large aspect ratio channel modified thermal resistance (°C/(W/cm^2))
$R''_{tot,moderate}$	...	moderate aspect ratio channel modified thermal resistance (°C/(W/cm^2))
$R''_{tot,small}$	...	small aspect ratio channel modified thermal resistance (°C/(W/cm^2))
$R''_{tot,spread}$	...	total modified thermal resistance including thermal spreading at the heater perimeter (°C/(W/cm^2))
R^+_e	...	roughness function (-)
Re, Re_d	...	Reynolds number based on D_e (-)
Re_b	...	Reynolds number based on momentum thickness (-)
Re*	...	laminar equivalent Reynolds number (-)
Re_{crit}	...	flow transition Reynolds number (-)

NOMENCLATURE (continued)

Re_t	...	Reynolds number based on interrupted-fin thickness (-)
S	...	interrupted-fin streamwise spacing (m)
St	...	Stanton number (-)
t	...	epoxy spin-down time (s)
	also,	interrupted-fin thickness (m)
	also,	substrate thickness (m)
T	...	failure rate chip temperature (°K)
T_1, T_2	...	wall conduction temperatures (°K)
T_b	...	coolant bulk temperature (°C)
T_{bj}	...	sectioned-fin coolant bulk temperature (°C)
t_{epox}	...	epoxy thickness (m)
$T_f(z)$	...	coolant temperature along fin height (°C)
$T_{f,in}$	...	inlet coolant temperature (°C)
$T_{m,x}$	...	local, streamwise mixed-mean coolant temperature (°C)
T_r	...	failure rate reference temperature (°K)
$T_w(z)$	...	fin temperature along fin height (°C)
$T_{wj}(z)$	...	sectioned-fin temperature along fin height (°C)
$T_{w,x}$	...	local, streamwise wall temperature (°C)
U	...	overall heat transfer coefficient ($W/m^2 {}^\circ C$)
V	...	coolant volumetric flow rate per channel (cm^3/s)
	also,	fin volume (m^3)
V"	...	coolant volumetric flow rate per unit heater surface area ($(cm^3/s)/cm^2$)

NOMENCLATURE (continued)

V_c	...	channel coolant velocity (m/s)
v_j	...	carrier velocity (m/s)
V_p	...	plenum coolant velocity (m/s)
V_{p1}	...	inlet plenum coolant velocity (m/s)
V_{p4}	...	output plenum coolant velocity (m/s)
w	...	repeated-rib width (m)
W	...	fin width used for convective perimeter (m)
	also,	transverse heater width (m)
w_c	...	channel width (m)
w_j	...	fin internal heating rate (J/m^3)
W_{max}	...	microcapillary channel base width (m)
W_{min}	...	microcapillary channel throat width (m)
w_s	...	plenum slot length (m)
w_w	...	fin width (m)
x	...	coordinate direction (-)
	also,	distance from channel entrance (m)
x_s	...	plenum slot width (m)
x_1, x_2	...	distance from heater perimeter (m)
x*	...	thermodynamic entrance length (-)
y	...	coordinate direction (-)
	also,	plate spacing (m)
z, z_j	...	coordinate direction (-)

NOMENCLATURE (continued)

GREEK

α	...	channel aspect ratio (-)
α^*	...	inverse of the channel aspect ratio (-)
β	...	fin optimizing parameter (-)
	also,	volumetric coefficient of expansion (°C^{-1})
δ	...	fin aspect ratio (-)
	also,	surface area multiplication factor (-)
ΔP	...	coolant pressure drop (Pa)
$\Delta R''_{tot}$	...	differential total modified thermal resistance (°C/(W/cm^2))
ΔT	...	chip temperature rise above ambient (°C)
ΔT_0	...	temperature difference for uniform sources (°C)
ΔT_{bulk}	...	bulk coolant temperature rise (°C)
ΔT_c	...	constriction effect temperature rise (°C)
ΔT_{c1}, ΔT_{c2}, ΔT_{c3}		
	...	parameters for Equation 3.6 (°C)
ΔT_{conv}	...	coolant convective temperature rise (°C)
ΔT_{cont}	...	contraction temperature rise (°C)
$\Delta T_{f,in}$	...	inlet coolant temperature (°C)
ΔT_{pump}	...	viscous heating temperature rise (°C)
ΔT_{solid}	...	solid substrate temperature rise (°C)
ΔT_{tot}	...	peak surface temperature rise (°C)
ϵ	...	emissivity (-)
	also,	surface roughness height (m)
λ	...	failure rate (-)

NOMENCLATURE (continued)

λ_j	...	carrier mean free path (m)
μ_b	...	bulk dynamic viscosity (kg/(m s))
μ_f	...	dynamic viscosity (kg/(m s))
μ_w	...	bulk dynamic viscosity (kg/(m s))
ν	...	epoxy kinematic viscosity (m^2/s
ν_f	...	coolant kinematic viscosity (m^2/s)
ϕ	...	repeated-rib shape angle (degrees)
π	...	3.14159...
π	...	electrical resistivity (Ω-m)
ρ_f	...	coolant density (kg/m^3)
ρ_m	...	channel mean coolant density (kg/m^3)
ρ_1	...	channel inlet coolant density (kg/m^3)
ρ_4	...	channel exit coolant density (kg/m^3)
η_f	...	fin efficiency (-)
∞	...	infinity (-)
σ	...	ratio of free-flow and frontal cross-sectional areas (-)
θ	...	fin temperature (°C)
	also,	momentum thickness (m)
θ_1, θ_2	...	fin temperature (°C)
θ_b, θ_{base}	...	fin base temperature (°C)
$\theta_{base,j}$	...	sectioned-fin base temperature (°C)
ω	...	epoxy spin rate (rpm)

NOMENCLATURE (continued)

ψ	...	repeated-rib flow attack angle (degrees)
$\Box$	...	resistance characteristic shape (square)

1.0 THERMAL MANAGEMENT OF MICROELECTRONICS

The discussion in this chapter will first review the trends in computer microelectronics which continue to cause increasingly denser circuit integrations, larger power densities, and more stringent temperature constraints. The discussion then turns to a brief overview of the heat dissipation capabilities of state-of-the-art heat sink technology used to cool "today's" computers. A relatively new technology, microchannel heat sinks, will be introduced that can offer two, three, and perhaps larger orders-of-magnitude increases in the heat allowable dissipation of microelectronics. Microchannel heat sinks are the primary topic of this thesis, and the discussion at the end of this chapter outlines the presentation in the remainder of this treatise.

1.1 Trends in Computer Microelectronics

Discounting the abacus and the slide rule, computing machines have existed since the time of Pascal. The computer revolution, though, really didn't get started until 1958 when the silicon integrated circuit was invented. Since then, the development of microelectronics has been characterized by successive revolutions in device technology. The path of development has been primarily from TTL to ECL to NMOS and most recently to CMOS. Other device technologies exist, but many are still in the development stage.

Since the invention of the silicon integrated circuit, there has been in excess of a five-orders-of-magnitude increase in circuit integration (the total number of components on a chip). Part of this increase can be traced to growth in chip size, where the characteristic dimensions

have gone from about 1 mm in 1965 to about 4-8 mm in 1985. The remainder of the increase in circuit integration can be primarily traced to the reduction in the integrated circuit feature size, which is today generally less than 1.0 μm and rapidly approaching the size of 0.1 μm. In fact, silicon MOSFET's have been made with features as small as 0.025 μm, which is on the order of one hundred atoms across [Howard (1986)].

The increase in circuit integration continues to be driven by the need for increased processing speed. Processing speed is dependent upon the signal delay times which are directly proportional to the physical length of interconnections between circuit components. The characteristic signal delay times of several important device technologies are shown in Figure 1.1. A measure of the processing speed is how many millions of instructions per second (MIPS) can be executed. The number of MIPS and the total power dissipation of a chip are both directly proportional to the packaging density. As shown in Figure 1.2, the power dissipation per MIPS has been decreasing on the system level. At the component level, the chip power dissipation has been rapidly increasing due to the tremendous increase in the MIPS per chip (which may be crudely estimated by multiplying the upper and lower portions of Figure 1.2).

The increase in the chip power dissipation has greatly complicated thermal management of microelectronics. To appreciate the magnitude of the problem, consider a state-of-the-art single chip module which has a maximum chip heat flux of 40 W/cm^2 (Sperry Compact HX discussed in Section 1.2.). The heat flux of this chip is only about 150 times less than the heat flux at the surface of the sun which is about 6000 W/cm^2!

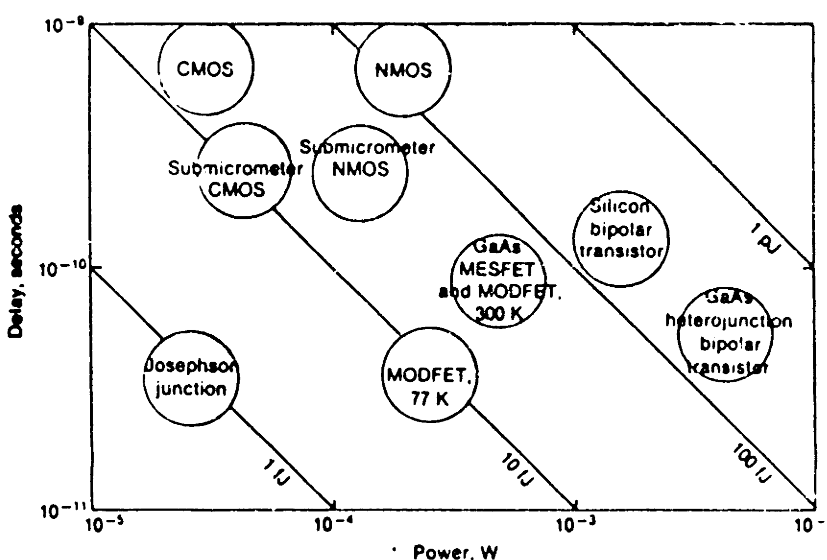

Figure 1.1. Power-delay continuums of important transistor technologies. [Taken from Morkoc and Solomon (1984).]

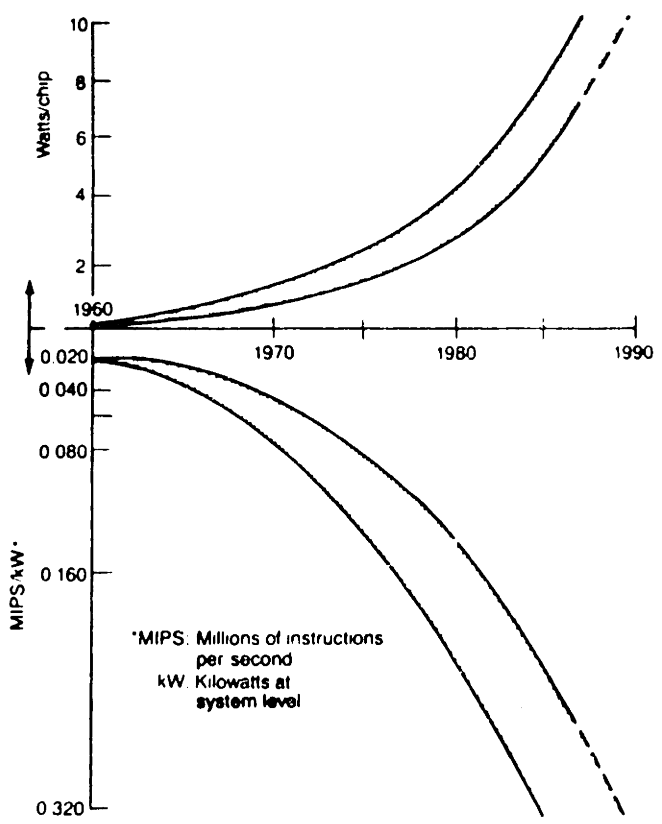

Figure 1.2. General trends for MIPS versus power. [Taken from Oktay, Hannemann, and Bar-Cohen (1986).]

As shown in Figure 1.3, the chip heat flux is similar to that of re-entry from earth orbit!

Clearly the chip heat flux is large, but the chip must also operate at much lower temperatures - typically lower than 120°C. Such a low temperature is dictated by stringent reliability constraints. A simplified expression for the failure rate of microelectronics is the Arrehenius relation,* which is given by

$$\lambda(T) = \lambda(Tr) \exp\left[(E_A/k)\,(Tr^{-1} - T^{-1})\right] \qquad (1.1)$$

where $\lambda(T)$ is the failure rate at temperature T (°K), $\lambda(Tr)$ is the normalized failure rate at temperature Tr (°K), E_A is the activation energy, and k is Boltzmann's constant. Clearly, the failure rate decreases exponentially with decreasing component temperature. In fact, a commonly used rule of thumb for microelectronic reliability is that a 20°C decrease in component temperature will typically result in a 50 percent reduction in the failure rate. Continued pressure to enhance reliability will therefore demand reduction in the component temperatures, as well as more uniform component temperatures.

1.2 State-of-the-Art Single-Chip and Multi-Chip-Module Heat-Sink Technology

Computers can be more-or-less lumped into two groups or classes. One group is the cost-performance class which includes desk-top, mini,

---

* The discussion of reliability in this thesis is limited to a general discussion of component temperature. Note that component temperature is not the only factor affecting reliability, but it is perhaps the most important. Good references to obtain more information on this topic are Baker (1971) and MIL HANDBOOK 217D (1983).

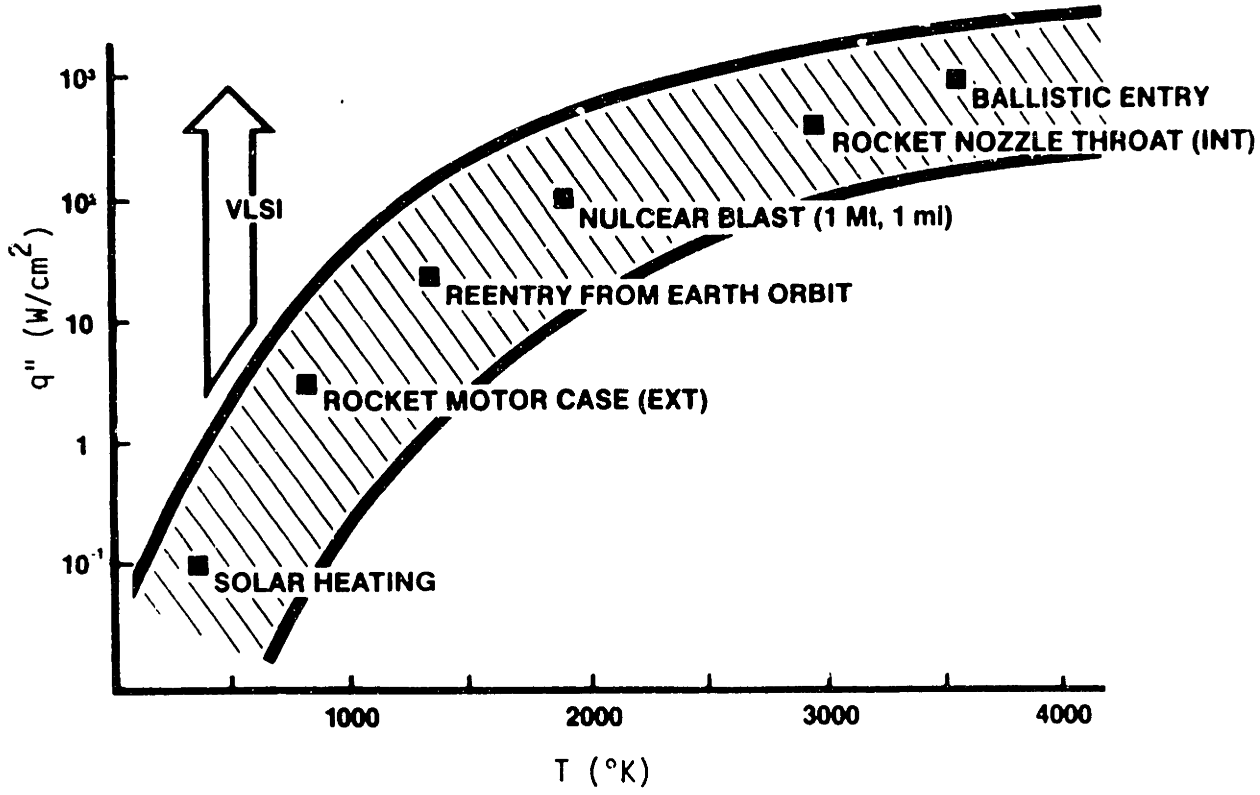

Figure 1.3. Perspective of microelectronic heat flux. [Taken from Bar-Cohen (1985).]

and even super-minicomputers. The other group is the high-performance class which includes mainframes and supercomputers. With time, heat transfer technology used for the high-performance class will make its way into the cost-performance class. Consequently, the discussion here is limited to heat-transfer techniques used for the high-performance class, which currently has chip internal thermal resistance of order 10°C/W and smaller.

The primary cooling methods used for chips have been compared in a trade-off study by Hannemann (1980). His results are shown in Table 1.1. From this table, it can be seen that a cooling mechanism which performs relatively better in one area also performs relatively poorer in others. In part because of this, most state-of-the-art computers will use more than one cooling mechanism. The detailed designs of the cooling systems currently used in several state-of-the-art computers have been reviewed and will not be reconsidered here [see for example Bar-Cohen (1985) and Oktay, Hannemann, and Bar-Cohen (1986)].

What is important for this study is the ultimate heat transfer capabilities of the high-performance class of single-chip and multi-chip modules listed in Table 1.2. A glance at this table shows that the chip heat flux is typically less than only 40 W/cm^2. For the multi-chip modules, the average heat transfer over the circuit board is limited to no more than 2.2 W/cm^2, and the heat density to less than 1 W/cm^3!

What are the heat dissipation requirements of the future? Consider for example the requisites for artificial intelligence [see Bar-Cohen (1985)]. It has been claimed that superchips with 10^9 transistors will

TABLE 1.1

PRIMARY COOLING METHODS FOR CHIPS*

Cooling Mechanism	Relative Effectiveness	Achievable Density	Complexity	Relative Cost	Acoustic Noise	Relative Reliability	Relative Maintainability
Natural Convection (AIR)	0.2	LOW	VERY LOW	LOW	VERY LOW	HIGH	HIGH
Forced Convection (AIR)	1	MEDIUM	LOW	LOW	HIGH	MEDIUM-HIGH	HIGH
Natural Convection (Liquid)	1	MEDIUM	MEDIUM	MEDIUM	LOW	MEDIUM-HIGH	LOW
Forced Convection (Liquid)	20	HIGH	HIGH	HIGH	MEDIUM	LOW	LOW
Immersion/Pool Boiling	100	HIGH	HIGH	HIGH	MEDIUM	MEDIUM	LOW
Heat Pipe Assisted Convection	10	MEDIUM-HIGH	MEDIUM	LOW-MEDIUM	MEDIUM	HIGH	MEDIUM-HIGH

* [Taken from Hannemann (1980).]

TABLE 1.2

STATE-OF-THE-ART SINGLE-CHIP AND MULTI-CHIP MODULE THERMAL PERFORMANCE*

Single-Chip Modules

Technology	Max. Chip Flux (W/cm^2)
Mitsubishi Alumina HTCP	6.25
Mitsubishi SiC	6.25
Hewlett-Packard Finstrate	10.1
Hitachi S-810	13.1
Fujitsu MCC	19.7
Burroughs PGA	24.3
Motorola MCA-2	24.5
Sperry Compact HX	40.0

Multi-Chip Modules

Technology	Max. Chip Flux (W/cm^2)	Avg. Heat Flux (W/cm^2)	Heat Density (W/cm^3)
Mitsubishi HTCM	6.25	0.83	0.4
Hitachi RAM	13.1	0.8	0.5
Honeywell SLIC	--	0.93	0.2
NEC SX LCM	> 8.4	1.6	0.3
IBM 4381 IMPNG	17.0	2.2	0.5
IBM 3090 TCM	29.8	2.2	0.4

* [Abstracted from Bar-Cohen (1985).]

be barely adequate to meet the demands of artificial intelligence, and that such applications will require 10^{14} operations per second! Several tactics will be required just to build the circuitry (for example, wafer scale integration, parallel processing, 3-D packaging, laser interconnects, etc.). The required heat dissipation capabilities for artificial intelligence are indeed enormous. A quick scan of Figure 1.1 shows that power dissipations of order 10^{-5} watts per transistor are available. Multiplying by 10^9 transistors per chip results in 10^4 watts per chip! No wonder that several researchers have suggested that power dissipations of 20 kW/liter is needed for future systems [see for example Trimberger (1983)]. Projected needs for 100 to 1000 kW/liter are also being suggested for systems related to SDI.

Given the current status of the heat density of todays state-of-the-art computers (see Table 1.2), the situation requires innovative cooling techniques. There is a method of heat sinking which can provide the required heat dissipations! It is the topic of this thesis and is introduced in the next section.

1.3 Overview of Microchannel Heat Sink Design

The use of forced-convection, liquid-cooled, microchannel heat sinks is introduced in this section. Heat dissipation rates of greater than 1000 W/cm^2 can be handled by this method of heat sinking. The use of microchannel heat sinks is not limited to microelectronics. They can be used most anywhere there is a need to cool bodies with large heating rates. Other potential applications include laser resonators, optical surfaces of high-power laser systems, central-station solar receivers, rocket casings, leading surfaces of hypersonic aircraft, etc.

1.3.1 Previous Works

Forced-convection, liquid-cooled, microchannel heat sinks were originally studied at Stanford University, U.S.A. The first technical publications appeared in the early 1980's*, which since then have caused considerable interest in the heat transfer community. This author is currently not aware of any other researchers who have attempted to replicate the original Stanford work, and who have published unclassified analytical and/or experimental results.

The configuration of a typical microchannel heat sink is shown in Figure 1.4. The heat sink is a finned structure which is cooled by forced convection. The coolant flows from the inlet plenum, through the channels, and out into the discharge plenum. Power is dissipated on the "circuit" side of the heat sink, and the heat is conducted through the substrate to the fins where it is conducted to the coolant. The coolant can be either a liquid or a gas, but the pumping power requirements for gases are much larger for the same thermal performance [see Tuckerman (1984)]. The microchannels used by the Stanford researchers were nearly rectangular and generally of large aspect ratios. The channels were fabricated in silicon substrates by precision sawing or orientation dependent etching. The fourth side of the channels was formed by attaching a "cover plate" to the heat sink by "anodic bonding" or by a suitable epoxy.

---

* See Tuckerman and Pease (1981a, b), (1982), (1983), and Tuckerman (1984).

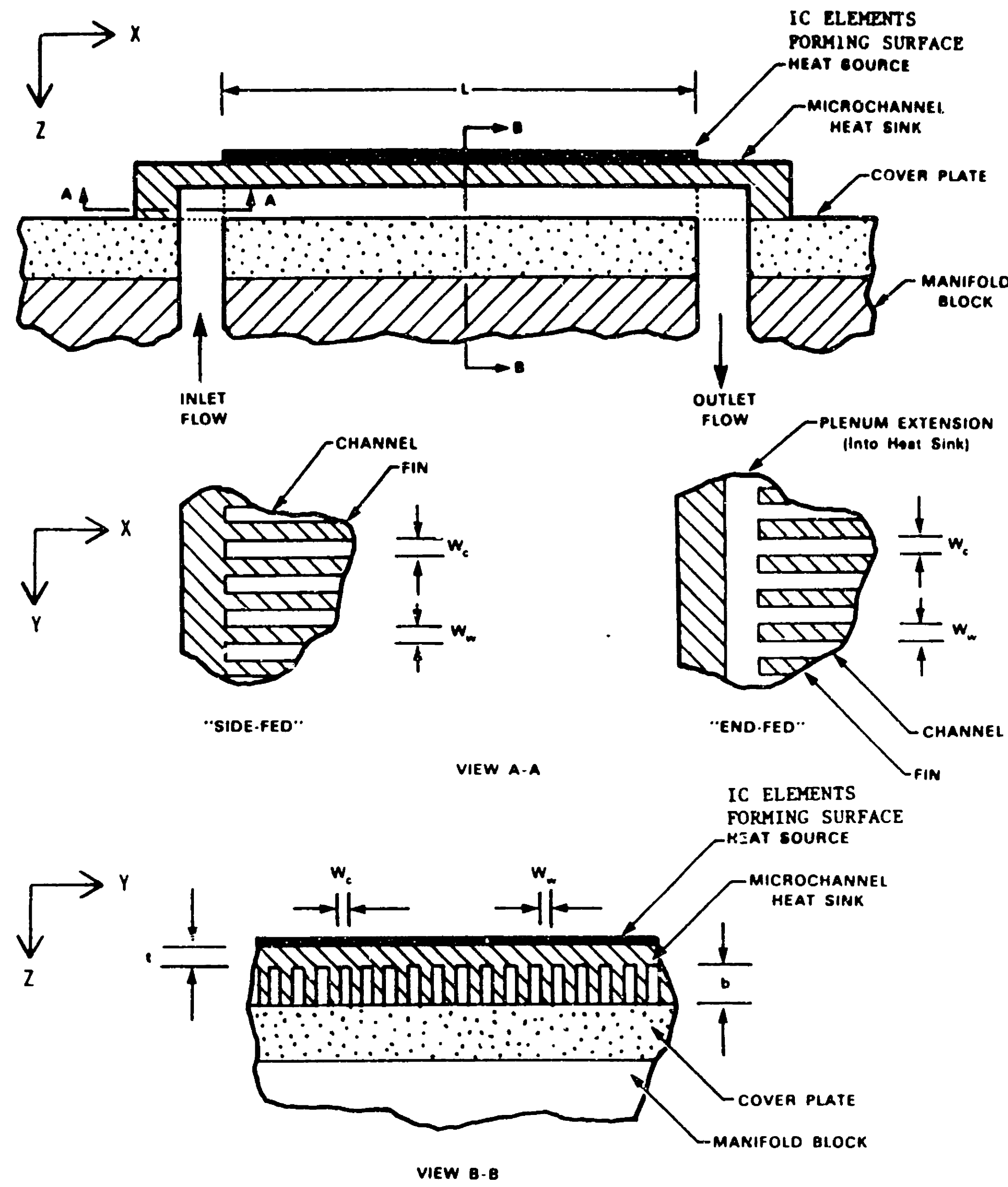

Figure 1.4. Schematic of a forced-convection, liquid-cooled, microchannel heat sink.

The physical dimensions of the silicon microstructures were of the following orders of magnitude. The channel width w_c was typically about 55 μm, and the fin thickness w_w was typically about 40-45 μm. The substrate height t was typically about 100-200 μm, and the fin height b was typically about 300-400 μm. The channel length was typically 1.4-2.0 cm.

Why are the channel dimensions so small? Consider the overall-heat-transfer equation $Q = (UA)\Delta T$, where Q is the chip heat-dissipation rate, U is the overall-heat-transfer coefficient, A is the surface area for heat transfer, and ΔT is the chip peak temperature rise over the ambient temperature. If Q is to be increased while keeping ΔT the same (or smaller due to reliability considerations), then the UA product must increase. Large increases in UA are not easily obtained by increasing the surface area. Large increases in U can be obtained by increasing the convective-heat-transfer coefficient h. Large increases in h can be obtained by applying heat transfer fundamentals. If the flow in a channel is fully developed, then the Nusselt number $Nu = hD_e/k_f$ is a constant where D_e is the channel hydraulic diameter, and k_f is the coolant thermal conductivity. Since k_f is constant for a given coolant, then h can be increased proportional to the decrease in channel hydraulic diameter $D_e = 4w_c b/(2w_c + 2b)$. Therefore, for fully-developed flow (Nu of order 5.0) of water (k_f of order 0.6 W/m°C) through a typical microchannel (D_e of order 100 μm), the heat transfer coefficient is of order 30,000 $W/m^2 {}^\circ C$! Perhaps now it is clear to the reader why the channel dimensions are so small.

The channels of the type shown in Figure 1.4 do not allow for transverse mixing of the coolant, which would be desirable if a channel happened to get plugged. Other channel geometries, in particular "pin-fins" as shown in Figure 1.5, were also studied by the Stanford researchers. It was found that the use of such structures did provide better transverse mixing. The enhancement of the heat transfer owing to increases in the Nusselt number due to vortex generation did not occur as had been hoped.

In addition to their original work in microchannel heat sinks, the Stanford researchers also developed a "microcapillary thermal interface" as shown in Figure 1.6. This interface used the inherent attractive force (suction due to the liquids surface tension) to hold the two surfaces together. This interface also helped to reduce wafer warpage. This interface technique allows the heat sink to be manufactured separately from the heat source. Therefore, the heat sink can be made of materials of high thermal conductivity which the heat source substrate may not have. The microcapillary channels were typically about 30 μm deep with a throat width of about 1 μm.

The typical thermal performance of these heat sinks is as follows. The typical thermal resistance of the microcapillary thermal interface was of order 0.02 °C/(W/cm^2). The thermal resistance of the microchannel heat sinks including the coolant bulk temperature rise was typically of order 0.08 - 0.09 °C/(W/cm^2) exclusive of the microcapillary interface! The heat sinks were shown experimentally to dissipate as much as about 1300 W/cm^2 from a 1.0 cm square metal film heater. The coolant flow rate

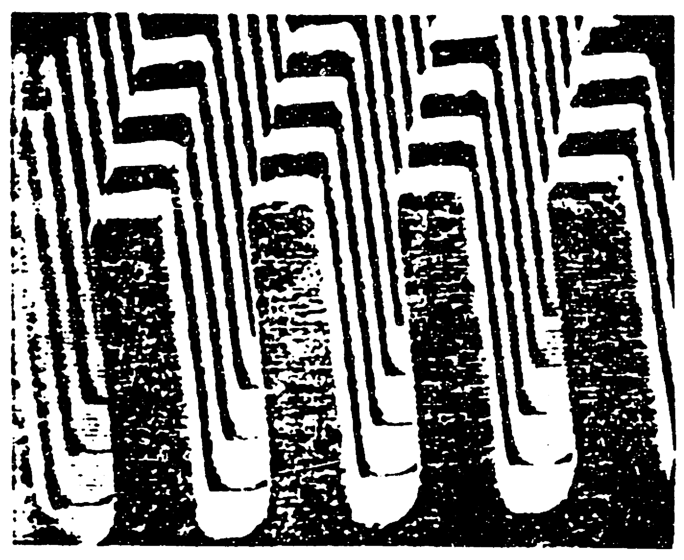

Figure 1.5. Silicon "pin-fins" manufactured by precision sawing. [Taken From Tuckerman and Pease (1981b).]

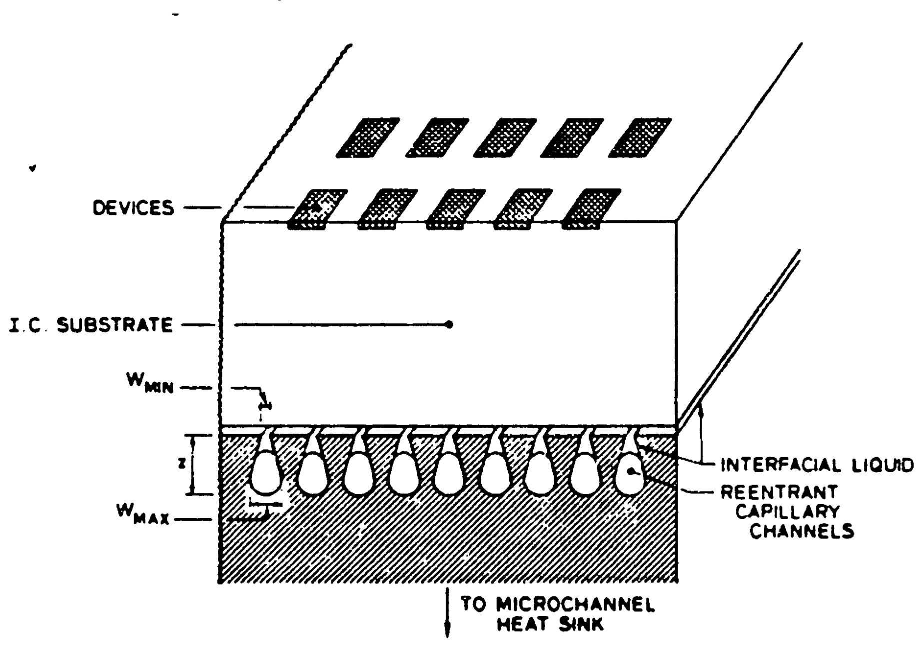

Figure 1.6. Microcapillary thermal interface. [Taken from Tuckerman (1984).]

in this particular example was 14.2 cm^3/sec of water with a pressure drop of 53 psi across the chip. The length of the coolant channel was 2.0 cm, and the flow was provided to a 1.5 cm wide section of the chip.

The ultimate limit of this heat sinking method in silicon has been predicted by the Stanford researchers. They estimate that up to 50 kW/cm^2 may be dissipated using 100 μm long channels, a water pressure drop of 1000 atmospheres, and allowing a maximum surface temperature of no more than 120°C!

1.3.2 This Investigation

This study was initiated to survey the methods of removing dissipated power from an array of electronic devices constructed in indium phosphide. These devices are anticipated to dissipate on the order of 100-300 W/cm^2 continuously over a large two-dimensional array that may exceed tens of centimeters on each side. After an extensive review of the heat transfer literature, it was decided that forced-convection, liquid-cooled, microchannel heat sinking would be the most viable thermal control method. This thesis is a direct result of the theoretical, numerical, and experimental efforts that were concentrated at generalizing and extending the work originally done by the Stanford researchers.

The current study extends the theoretical analysis of Tuckerman and Pease to include small, moderate, and large aspect ratio channels, for fully-developed and developing flow in the laminar and turbulent regimes. The channel surfaces can be smooth or roughened with repeated-ribs. Variable property effects are included for the chip material and

the liquid coolant (compressibility effects have not been included). The effect of viscous dissipation in the liquid coolant is included. Thermal spreading at the periphery of the simulated integrated circuit heat source is also accounted for using simplified one-dimensional models.

To facilitate numerical computation, a new computer program has been created which computes the thermal and fluid performance for a large variety of coolant flow rate constraints and heat sink designs. A complete listing of this computer program has been included in Appendix E.

The numerical results clearly show that developing laminar flow has essentially the same thermal and fluid performance over a large range of channel widths (assuming constant, coolant pressure drop). At larger channel widths, turbulent flow is encountered, which results in better thermal performance with only small increases in the pumping power requirement. It will be shown that the computer program quite accurately predicts the experimental data for the thermal and fluid performance of microchannel heat sinks obtained by both the Stanford study and this study.

A new method of surface temperature uniformity enhancement at the chip level which uses a "compensation heater" about the periphery of the heat source (for example an integrated circuit) will be introduced. As shown in Figure 1.7, the thermal spreading at the periphery of the heater can cause significant thermal gradients across the integrated circuit. If there is a heater providing an equivalent heat flux over a sufficiently wide region around the integrated circuit, the temperature profiles in the integrated circuit are much more uniform. The author is

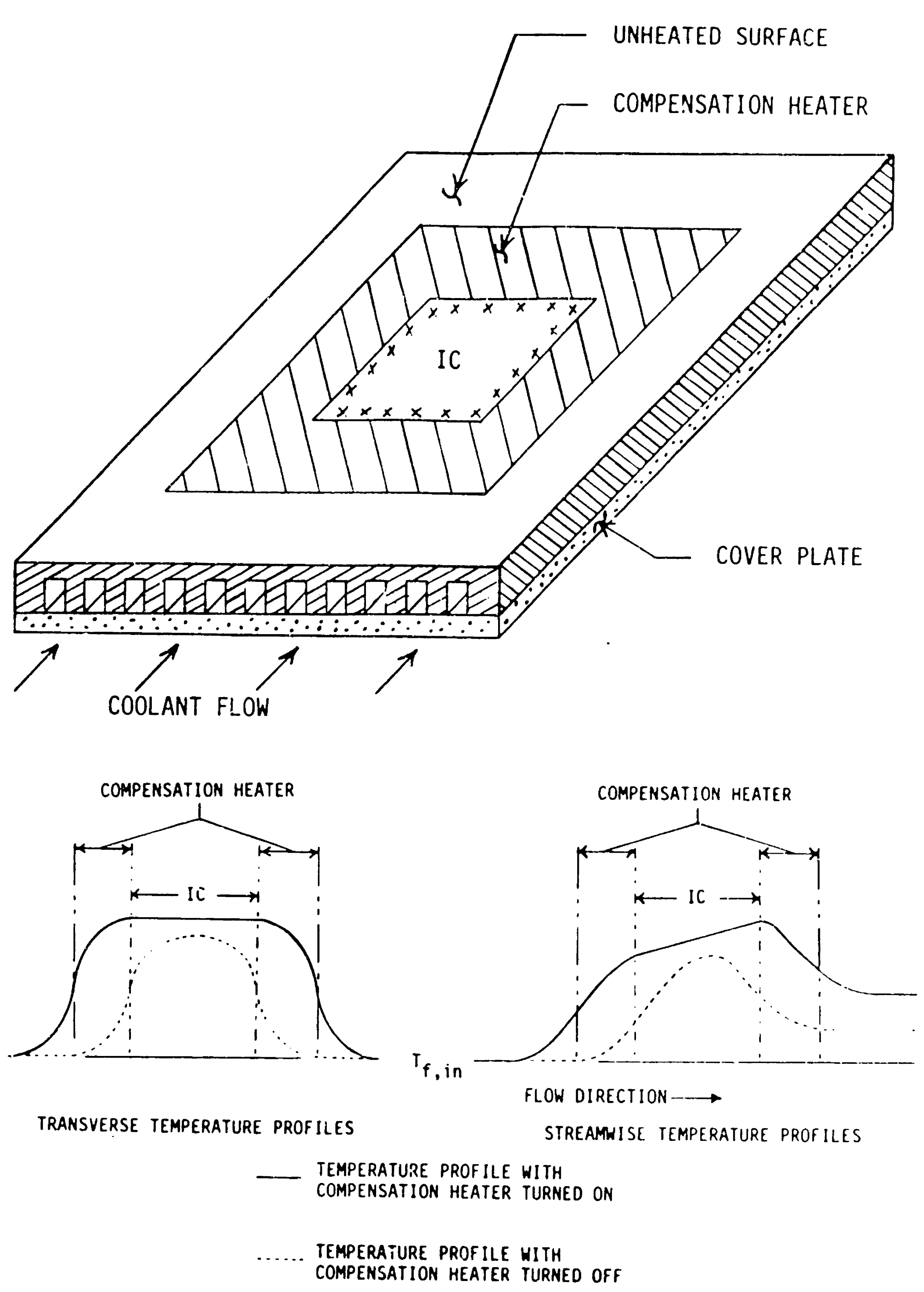

Figure 1.7. Thermal spreading at the heater periphery.

not aware of other applications in microelectronics where this method has been used at the chip level. Therefore, the concept of a "compensation heater" is considered to be original.

It is necessary to clarify several terms and geometrical analysis parameters used in this study - many of which are identical to the notation used in the Stanford studies. The coordinate system shown in Figure 1.4 should be carefully noted by the reader. The location of the origin is somewhat arbitrary. The positive y- and z-directions will be defined as required in the other chapters. In general, the x-direction is parallel to the fin base and channel base plane, and parallel to the flow direction. The y-direction is parallel to the fin base and channel base plane, and perpendicular to the flow direction. The z-direction is perpendicular to the fin base and channel base plane, and is also perpendicular to the flow direction. The x-direction is often referred to as the "length," the y-direction is often referred to as the "thickness" or "width," and the z-direction is often referred to as the "height." For example, in Figure 1.4, the fin length and channel length are defined as L, the fin thickness or width is defined as w_w, and the substrate height is defined as t.

The channel aspect ratio is defined as $\alpha = b/w_c$. The three categories of channel aspect ratios used in this study are: small ($\alpha < 0.1$), moderate ($0.1 < \alpha < 10.0$), and large ($\alpha > 10.$). In this study, the heat transfer from the channel bottom (from the cover plate) is ignored in all cases (primarily due to the poor thermal conductivity of the cover plate material used in this study). Small aspect ratio channels provide

cooling from one surface - the channel base. The fins in the small aspect ratio designs are used primarily for structural purposes and do not contribute significantly to the overall heat transfer (especially when w_w is small and $\alpha \ll 0.1$). Moderate aspect ratio channels provide cooling from three surfaces - the fin sides and the channel base. Large aspect ratio channels provide cooling from two surfaces - the fin sides. The heat transferred from the channel base of large aspect ratio channels is small and is ignored (especially when w_c is small and $\alpha \gg 10.0$).

1.4 Thesis Organization

Chapter 1 has been dedicated to introducing the trends in computer microelectronics which have led to ever-increasing power dissipation rates. The state-of-the-art methods used for thermal control of today's computers were quickly reviewed. A "new" heat sinking method, microchannel heat sinks, was introduced that will play a significant role in the continuing development of microelectronics. The reminder of this section outlines the analysis and discussion presented in the rest of this thesis.

Chapter 2 deals with forced convection flow in smooth and repeated-rib roughened ducts. The transition between the laminar and turbulent flow regimes is specified. The friction factors and Nusselt numbers for channel flow are presented in the form of analytical equations or tabular data. The pressure drop through the microchannel heat sink is also discussed. Finally, the effect of axial heat conduction, viscous dissipation, superimposed natural convection, temperature varying properties, non-uniform passages, and interrupted-fins are investigated.

Chapter 3 deals with conduction heat transfer. The physics of the heat conduction process is introduced, and trends of various factors affecting the thermal conductivity are briefly discussed. The contraction thermal resistance owing to discrete heat sources is presented. The validity of the assumptions used to formulate the fin heat transfer analysis will be discussed in detail. The fin thermal response equations will be presented followed by a simple model of thermal spreading at the periphery of a surface heater.

Chapter 4 presents the details of the heat sink design process. Thermal resistance models will be formulated for large, moderate, and small aspect ratio ducts. Models are provided for constant pressure drop, constant pumping power, and constant volumetric flow. The new computer program created especially for this study will be reviewed. Typical numerical predictions obtained using the computer program will be presented and discussed.

Chapter 5 presents details of the testing program used to determine the thermal performance of microchannel heat sinks. The methods of microchannel fabrication including precision sawing and orientation dependent etching are discussed. The methods of packaging and headering, and the resistor heat source fabrication process will be reviewed. The test apparatus, the experimental procedure, and the estimate of the experimental error will be presented.

Chapter 6 presents detailed discussion of the experimental results of this study and those of the Stanford study. The experimental results will be compared with the theoretical and numerical predictions.

Chapter 7 presents the summary and conclusions of this study. Design recommendations are summarized, and suggestions are listed for future work in the analysis and design of microchannel heat sinks.

2.0 FORCED CONVECTION FLOW IN DUCTS

The purpose of this chapter is to review the thermal and fluid characteristics of flow through rectangular ducts as it applies to this study. Smooth ducts will be considered first, beginning with the establishment of the transition Reynolds number. The smooth-duct, fully-developed and developing-flow friction factors are determined for the laminar regime, and then the turbulent regime. Following this, there will be an analysis of the pressure drop through microchannel heat sinks. The discussion then turns to determining the Nusselt numbers for fully-developed and developing-flow in the laminar regime, and then the turbulent regime. After this, there will be a discussion of heat transfer augmentation by surface roughening. The friction factors and Nusselt numbers will be determined for channels with repeated-rib roughness in fully developed turbulent flow. The discussion then turns to analysis of the effects of viscous dissipation, superimposed natural convection, temperature varying properties, and non-uniform passages. Following this, there will be an overview of how interrupted fins (as opposed to continuous fins) might be used to improve the thermal and fluid performance.

2.1 Smooth Ducts

The purpose of this section is to present the hydrodynamic and heat transfer characteristics of fully developed and developing flows in smooth ducts for the laminar and turbulent regimes.

2.1.1 Distinction Between Laminar, Transitional, and Turbulent Flow

The hydrodynamic and heat transfer properties of flow through rectangular ducts depends on the flow regime. The parameter used to

define the flow regime is the Reynolds number which is given by

$$Re = \frac{\rho_f V_c D_e}{\mu_f} \tag{2.1}$$

where Re is the Reynolds number, ρ_f the coolant density, μ_f the coolant dynamic viscosity, V_c the average coolant velocity in the duct, and D_e the hydraulic diameter.

The transition between laminar and turbulent flow occurs over a range of Reynolds numbers. This range is large if the tube entrance is "bell-mouthed" and much smaller if there is an "abrupt" reduction in the flow cross-sectional area at the entrance. In the latter, the flow tends to "trip" at a "critical" Reynolds number, for which the flow is laminar if $Re < Re_{crit}$, and the flow is turbulent if $Re > Re_{crit}$. In this study, the liquid coolant enters the duct via an abrupt contraction immediately after a 90° bend. Consequently, it is assumed that, for all practical purposes, the flow undergoes a "sudden" transition between laminar and turbulent flow regimes at the critical Reynolds number.

The transition Reynolds numbers used for this study were reported by Hartnett, Koh, and McComas (1962). They are listed in Table 2.1 as a function of the duct aspect ratio which is given by

$$\alpha = \frac{b}{w_c} \tag{2.2}$$

where α is the duct aspect ratio, b the duct height, and w_c the duct width.

TABLE 2.1

CRITICAL REYNOLDS NUMBERS FOR ABRUPT-ENTRANCE RECTANGULAR DUCTS
[DUE TO HARTNETT, KOH, AND McCOMAS (1962).]

α	Re_{crit}**
$\leq$ 0.2*	2500.
1.0	2200.
$\geq$ 5.0*	2500.

* Inferred from data for α = 5 and α = 10.

** Linear interpolation will be assumed for 0.2 < α < 1.0 and 1.0 < α < 5.0.

2.1.2 Friction Coefficients In Channel Flow

Shah and London (1978) have computed the fully developed laminar friction factors in rectangular ducts. Their results are listed in Table 2.2. Shah and London (1978) also present the results of Curr, Sharma, and Tatchell (1972) for hydrodynamically developing laminar flow in rectangular ducts as shown in Table 2.3. The friction factor for laminar developing flow between infinite parallel plates, as computed by Liu (1974), are also presented by Shah and London (1978) and are listed in Table 2.4.

The friction coefficients listed in Table 2.5 and plotted in Figure 2.1 were extracted from Tables 2.2 through 2.4, and will be used for computer solution purposes (see Chapter 4).

Shah and London (1978) present results by Bodoia (1959) for α^* = 0. which suggest that $f_{app}Re$ should be much larger near $(x/D_e)/Re \approx 0$. (the same result for $(x/D_e)/Re \approx 0$. is also expected for the other

TABLE 2.2

FULLY-DEVELOPED, LAMINAR-FLOW FRICTION COEFFICIENTS IN RECTANGULAR DUCTS+ [TAKEN FROM SHAH AND LONDON (1978).]

α^*	fRe
1.000	14.22708
0.900	14.26098
1/1.2	14.32808
0.800	14.37780
0.750	14.47570
1/1.4	14.56482
0.700	14.60538
2/3	14.71184
0.600	14.97996
0.500	15.54806
0.400	16.36810
1/3	17.08967
0.300	17.51209
0.250	18.23278
0.200	19.07050
1/6	19.70220
1/7	20.19310
0.125	20.58464
1/9	20.90385
1/10	21.16888
1/12	21.58327
1/15	22.01891
1/20	22.47701
1/50	23.36253
0	24.00000

+ $\alpha^* = \frac{\text{short side length}}{\text{long side length}}$

Re based on $D_e = 4A/P$

TABLE 2.3

DEVELOPING, LAMINAR-FLOW FRICTION COEFFICIENTS IN RECTANGULAR DUCTS+
(DUE TO CURR, SHARMA, AND TATCHELL.)
[TAKEN FROM SHAH AND LONDON (1978).]

$(x/D_e)/Re$	$f_{app}Re$		
	$\alpha^* = 1.0$	$\alpha^* = 0.5$	$\alpha^* = 0.2$
0.001	142.0	142.0	142.0
0.002	80.2	80.2	80.2
0.003	66.0	66.0	66.1
0.004	57.6	57.6	57.9
0.005	51.8	51.8	52.5
0.006	47.6	47.6	48.4
0.007	44.6	44.6	45.3
0.008	41.8	41.8	42.7
0.009	39.9	40.0	40.6
0.010	38.0	38.2	38.9
0.015	32.1	32.5	33.3
0.020	28.6	29.1	30.2
0.030	24.6	25.3	26.7
0.040	22.4	23.2	24.9
0.050	21.0	21.8	23.7
0.060	20.0	20.8	22.9
0.070	19.3	20.1	22.4
0.080	18.7	19.6	22.0
0.090	18.2	19.1	21.7
0.100	17.8	18.8	21.4

+ $\alpha^* = \frac{\text{short side length}}{\text{long side length}}$

Re based on $D_e = 4A/P$

TABLE 2.4

DEVELOPING, LAMINAR-FLOW FRICTION COEFFICIENTS BETWEEN PARALLEL PLATES+
(DUE TO LIU.) [TAKEN FROM SHAH AND LONDON (1978).]

$(x/D_e)/Re$	$f_{app}Re$
0.0001183	-
0.0001479	-
0.0002656	209.1
0.0003839	174.5
0.0005023	153.2
0.0007391	127.1
0.001209	100.4
0.001683	86.00
0.002156	76.76
0.002630	70.16
0.004985	53.04
0.006882	46.44
0.008772	42.44
0.01067	39.29
0.01256	37.13
0.02011	32.34
0.02768	30.07
0.03525	28.77
0.04283	27.93
0.05040	27.34
∞	24.00

+ Re based on $D_e = 2w_c$, where w_c is the plate spacing.

TABLE 2.5

LAMINAR-FLOW FRICTION COEFFICIENTS USED FOR COMPUTER SIMULATION+

$(x/D_e)/Re$	$f_{app}Re$			
	α = 1.0	α = 2.0	α = 5.0	$\alpha \leq 0.1$ $\alpha \geq 10.$
≈ 0.*	142.0	142.0	142.0	287.0
0.001	111.0	111.0	111.0	112.0
0.003	66.0	66.0	66.1	67.5
0.005	51.8	51.8	52.5	53.0
0.007	44.6	44.6	45.3	46.2
0.009	39.9	40.0	40.6	42.1
0.01	38.0	38.2	38.9	40.4
0.015	32.1	32.5	33.3	35.6
0.02	28.6	29.1	30.2	32.4
0.03	24.6	25.3	26.7	29.7
0.04	22.4	23.2	24.9	28.2
0.05	21.0	21.8	23.7	27.4
0.06	20.0	20.8	22.9	26.8***
0.07	19.3	20.1	22.4	26.4***
0.08	18.7	19.6	22.0	26.1***
0.09	18.2	19.1	21.7	25.8***
0.10	17.8	18.8	21.4	25.6***
0.20**	15.8	17.0	20.1	24.7***
> 1.00	14.2	15.5	19.1	24.0

+ $\alpha = \frac{\text{long side length}}{\text{short side length}}$

Re based on $D_e = 4A/P$

* Linear extrapolation based on $(x/D_e)/Re$ of 0.001 and 0.002.

** Linear interpolation based on inverses of $(x/D_e)/Re$ = 0.1 and 1.0 (≈ ∞).

*** Linear interpolation based on inverses of $(x/D_e)/Re$ = 0.05 and 1.0 (≈ ∞).

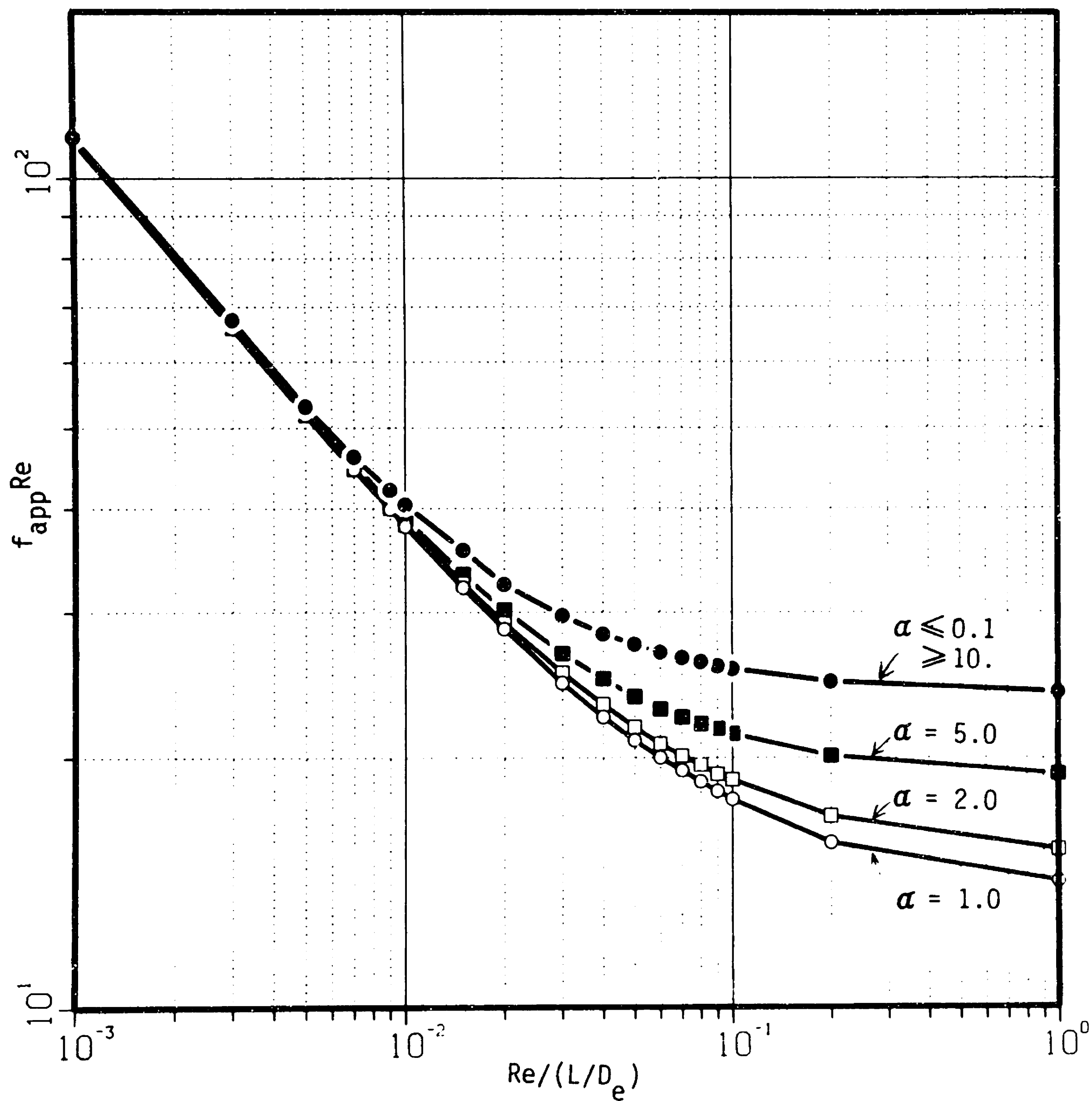

Figure 2.1. Laminar flow friction coefficients used for computer simulation.

α^*'s). The numerical solutions used to predict the $f_{app}Re$ values assume highly idealized inlet flow conditions. These conditions probably do not exist for this study due to the sudden contraction at the channel entrance which is preceded by a 90° bend. Therefore, the computer results for the thermal response should be viewed with caution when $(x/D_e)/Re < 0.001$.

Turbulent friction factors for fully developed flow in rectangular ducts appear to be affected by the aspect ratio of the duct. The friction factors are larger than those obtained using the usual definition of the equivalent diameter in the Karman-Nikuradse relation. Jones (1976) defines a "laminar equivalent diameter" given as

$$D_{le} = [(2/3) + (11/24)\alpha^*(2-\alpha^*)]D_e \tag{2.3}$$

where D_{le} is the laminar equivalent diameter, α^* is the inverse of the duct aspect ratio (short side length/long side length), and D_e is the equivalent diameter (D_e = 4A/P). The laminar equivalent diameter is used in the formulation of the "laminar equivalent Reynolds number" given by

$$Re^* = \frac{\rho_f \, V_c \, D_{le}}{\mu_f} \tag{2.4}$$

where Re^* is the laminar equivalent Reynolds number.

Jones (1976) showed that the friction factors for fully-developed flow in rectangular ducts can be accurately predicted using the

Karman-Nikuradse equation with Re replaced by Re^*. The revised form of the Karman-Nikuradse equation is

$$(f)^{-0.5} = 1.737 \ln \left[Re^*(f)^{0.5}\right] - 0.4 \quad . \tag{2.5}$$

where f is the fully-developed flow friction factor. Shah and Johnson (1981) have found that the values for the friction coefficient are 3 percent lower for a square duct and 11 percent higher for infinite parallel plates when compared with the values for flow through a circular tube at the same Re. Jones (1976) claims that a 5 percent uncertainty should be placed on the friction factors obtained using Equation 2.5. As shown in Figure 2.2, the scatter of the data is considerably reduced when Re^* is used in place of Re.

Turbulent boundary layers develop much faster than laminar boundary layers because of the rapid diffusion of momentum and heat due to turbulence. Deissler (1955) has computed the friction factor based on local shear stress for a circular tube with a uniform velocity profile at the entrance, constant properties, and a turbulent boundary layer originating at the entrance. Using those results, Kays and Perkins in Rohsenow, Hartnett, and Ganic' (1985b) present results for the local friction factor based on the static pressure gradient. They also present results for the average friction factor based on the total static pressure drop. The results are presented in Figures 2.3 and 2.4, respectively.

From Figure 2.3, it is clear that the local friction factor based on static pressure drop has essentially reached the fully developed values when x/D_e is about 10. Figure 2.4, which was obtained by simple

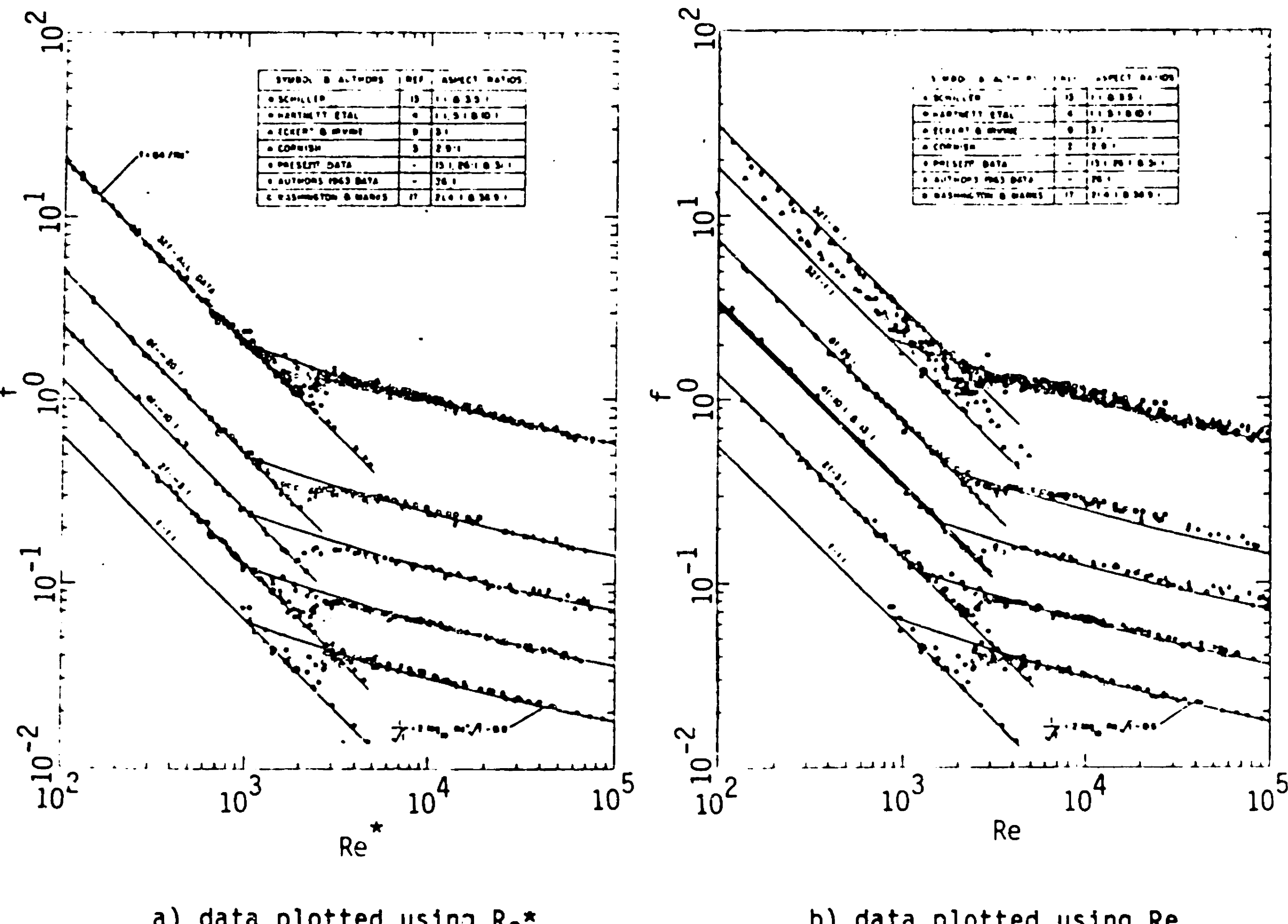

a) data plotted using R_e*

b) data plotted using Re

Figure 2.2. Friction pressure drop data plotted as a function of Re^* and Re. [Taken from Jones (1976).]

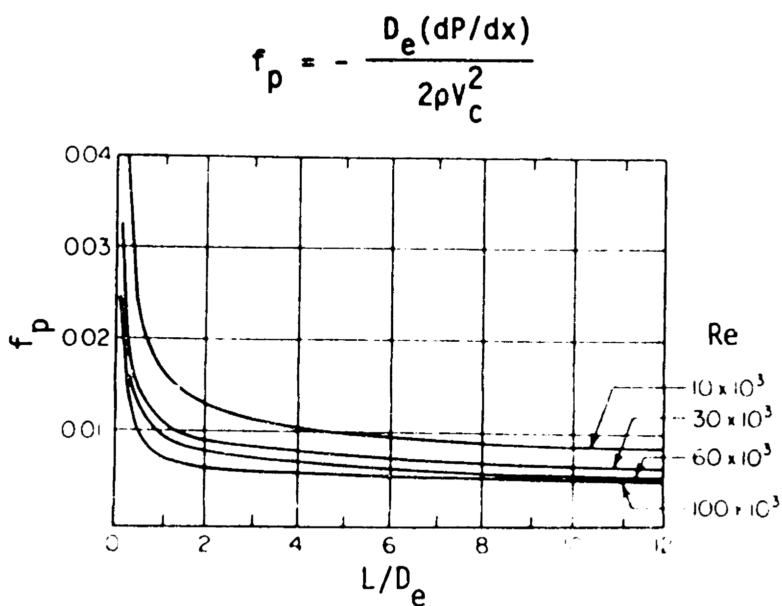

Figure 2.3. Local friction factor based on static pressure gradient for the entrance region of circular tubes. [Taken from Kays and Perkins in Rohsenow, Hartnett, and Ganic' (1985b).]

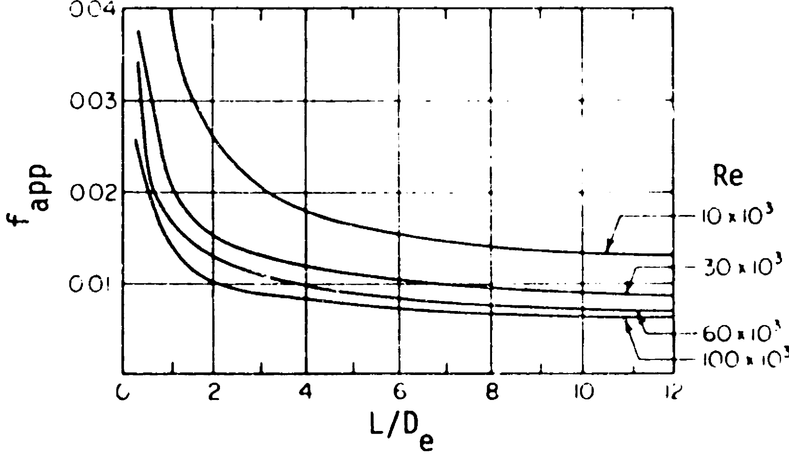

Figure 2.4. Average friction factor based on static pressure drop for the entrance region of circular tubes. [Taken from Kays and Perkins in Rohsenow, Hartnett, and Ganic' (1985b).]

integration of the curves shown in Figure 2.3, clearly shows that the effect of the local friction factor in the inlet region extends much further down the tube. At $x/D_e = 12$, the average friction factors are still approximately 50 percent higher than the fully developed values.

This author is not aware of published results of the developing-turbulent-flow average friction factor for $x/D_e > 20$ [Rohsenow and Choi (1961)] present limited results for $12 < x/D_e < 19.5$]. Consequently, it was decided to numerically re-integrate the curves of the local friction factor (Figure 2.3). Figure 2.5 shows that this integration provides results very similar to those shown in Figure 2.4.* Figure 2.6 plots the results over a longer range of x/D_e. The values for turbulent flow appear to be close to the asymptotic limit when $x/D_e \approx 100$. Figure 2.7 shows the ratio of the average and fully developed friction factors. For $x/D_e = 100$, the turbulent-flow average friction factors are within about five percent of their fully developed values. This result appears to be in agreement with results presented in Chapter 7 of Kays and London (1984).

For the purposes of this study, it is necessary to extrapolate the numerical integration results down to Re_{crit}. Table 2.6 lists the numerically integrated average friction factors upon which the

* The integration assumes that the values at $x/D_e = 12$ (Figure 2.4) are fully developed and persist throughout the remainder of the tube. The numerical integration is expected to be accurate to within five percent. Differences between Figures 2.4 and 2.5 for $x/D_e < 1.0$ are probably due to the assumed value of the local friction factor at $x/D_e \approx 0$. This "error" is small for $x/D_e > 1.0$.

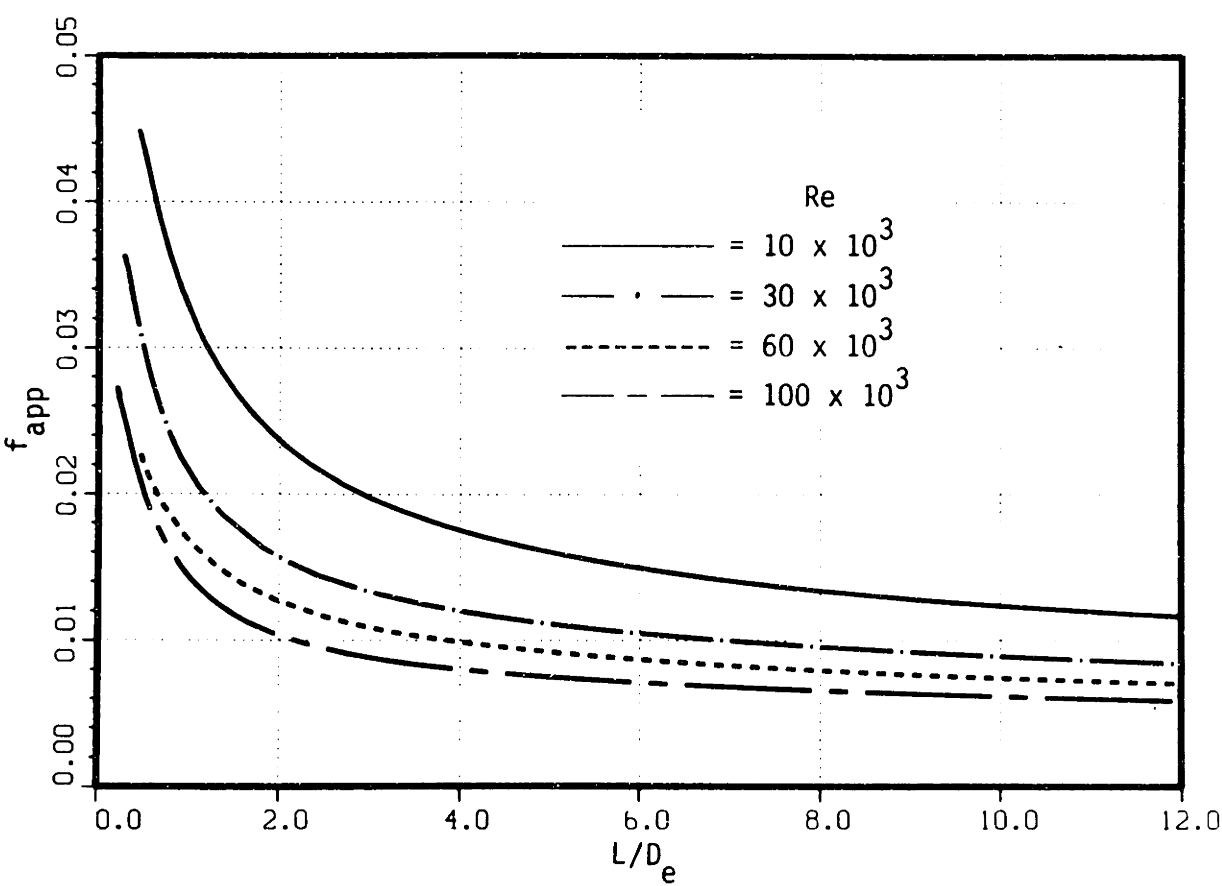

Figure 2.5. Numerically integrated average friction factor for turbulent flow in circular tubes.

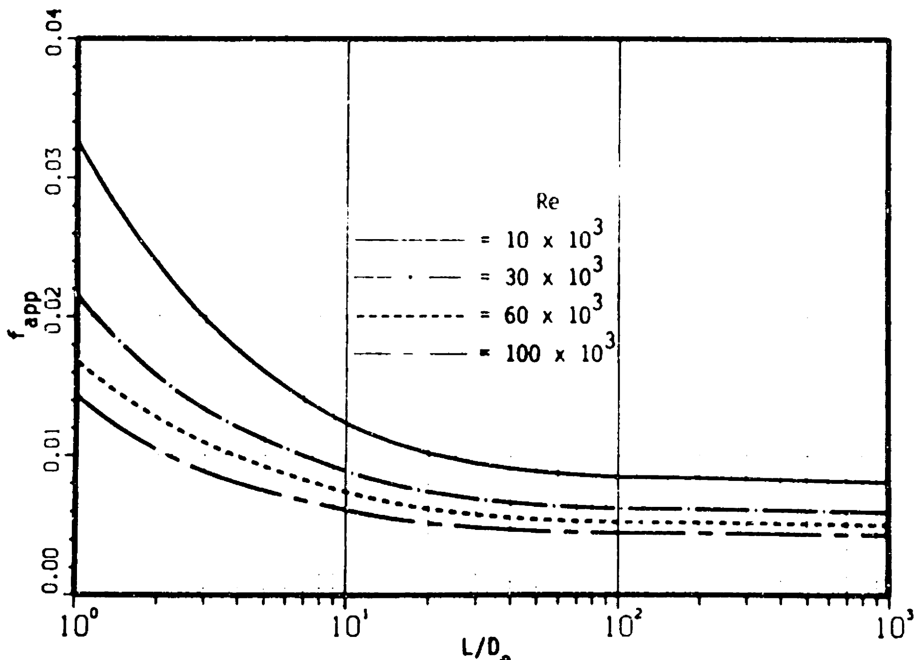

Figure 2.6. Numerically integrated average friction factor for turbulent flow in circular tubes.

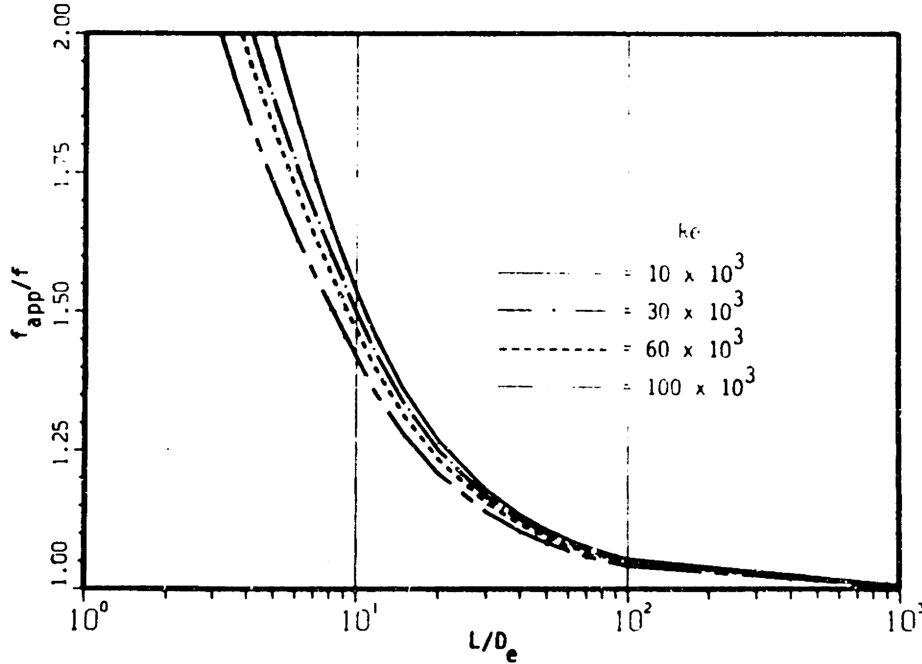

Figure 2.7. Ratio of numerically integrated average friction factor to the fully developed friction factor based on static pressure drop.

TABLE 2.6

NUMERICALLY INTEGRATED AVERAGE FRICTION FACTORS

Re	f_{app}					
	x/D_e					
	∞**	$1000 \approx \infty$	100	50	25	10
2,300*	0.01141	0.01195	0.01261	0.01335	0.01495	0.01925
10,000	0.07900	0.008093	0.008482	0.008915	0.009852	0.012370
30,000	0.00600	0.005974	0.006243	0.006541	0.007188	0.008910
60,000	0.00505	0.005077	0.005291	0.005527	0.006041	0.007412
100,000	0.00444	0.004348	0.004511	0.004691	0.005083	0.006145

* Values for Re = 2300 actually were obtained from the equations presented in Table 2.7.

** Values for this column were obtained using the Blasius equation, and are presented only for comparison with the $x/D_e = 1000 \approx \infty$ results.

extrapolation is based. "Best fit" equations* of the average friction factors were obtained as a function of the Reynolds number for several values of x/D_e. The correlations, with their respective coefficients of determination (R^2 - a measure of the goodness of fit), are listed in Table 2.7. Values for the average friction factor have been computed using those correlations for Re = 2300, and have been included in Table 2.6. "Best fit" equations* were also obtained for the "constants" listed in Table 2.7. The resulting equation for the average turbulent friction factor is

$$f_{app} = A(Re)^B \tag{2.6}$$

where

$$A = 0.09290 + \frac{1.01612}{(x/D_e)}$$

$$B = -0.26800 - \frac{0.31930}{(x/D_e)}$$

Equation 2.6 correlates the values listed in Table 2.7 to within $\mp$ 4.1 percent (R^2 for A and B is 0.99961 and 0.98513, respectively). Equation 2.6 applies for circular tubes. To obtain the friction factor for rectangular ducts, Re is replaced by Re^*.

Equation 2.6 will be used to obtain the friction factors for both fully-developed and developing turbulent flow. A comparison of the fully-developed-flow friction factors obtained using Equation 2.5 and

---

* The best fit equations were obtained on an HP-41C using the STAT PAC programs ∑LIN and ∑POW.

TABLE 2.7

CORRELATION EQUATIONS FOR AVERAGE FRICTION FACTORS*

x/D_e	$f_{app} = C_1(Re)^{C_2}$		
	C_1	C_2	R^2
1000 ≈ ∞	0.09404	-0.26649	0.9986
100	0.10249	-0.27066	0.9985
50	0.11226	-0.27506	0.9984
25	0.13384	-0.28315	0.9981
10	0.19464	-0.29889	0.9976

* Based on Table 2.6 data for $10,000 \leq Re \leq 100,000$.

Equation 2.6 (with $x/D_e = \infty$) is shown in Figure 2.8. Equation 2.6 predicts results which agree with the Karman-Nikuradse correlation to within about -1.5 percent and +2.0 percent. The agreement of the Blasius equation is in comparison slightly worse over the Reynolds number range of interest for this study. This fact, that Equation 2.6 quite accurately predicts the fully-developed-flow results, also suggests that Equation 2.6 is a reasonably accurate model for predicting the developing-flow friction factors. Note that Equation 2.6 predicts fully developed friction factors which are too small for $Re > 28,000$. Therefore, the thermal and fluid predictions for $Re > 28,000$ will be viewed with caution.

2.1.3 Pressure Drop

In the design of microchannel heat sinks, it is necessary to predict the overall pressure drop between the inlet and outlet plenums. The pressure drops associated with the distribution of the coolant to the inlet plenum and from the outlet plenum are not included here since they vary considerably based on the manifolding technique. For the purpose of this study, the pressure drop components diagram shown in Figure 2.9 will be used to formulate the pressure drop models ("end-fed" microchannel design - see Figure 1.4). The overall pressure drop has been divided into six components. The flow from the inlet plenum first goes through a 90° bend. It then experiences a sudden contraction which causes the flow to separate and undergo an irreversible free expansion. In the core, the coolant experiences skin friction and a density change due to heating. At the exit, there is another irreversible free

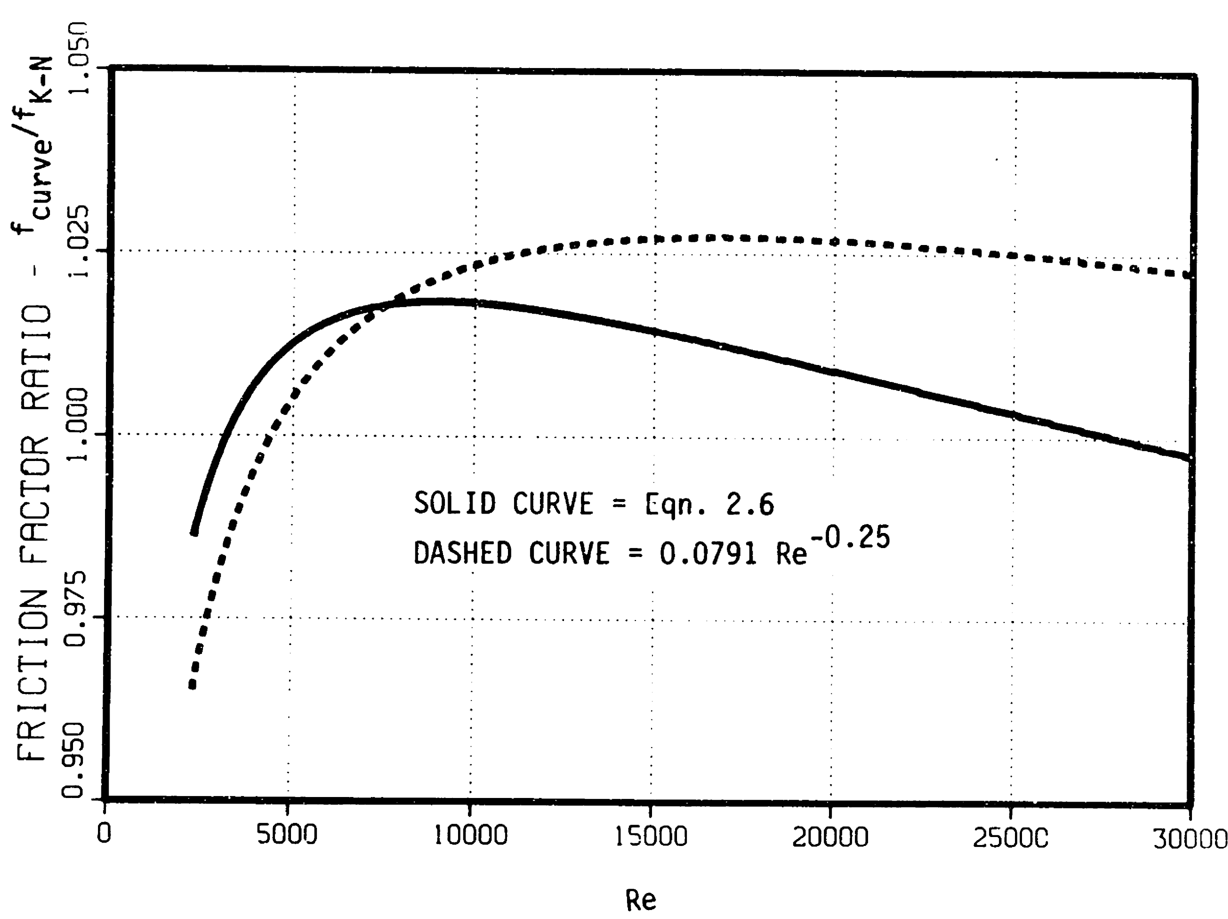

Figure 2.8. Comparison of fully-developed-flow friction factors with respect to the Karman-Nikuradse correlation.

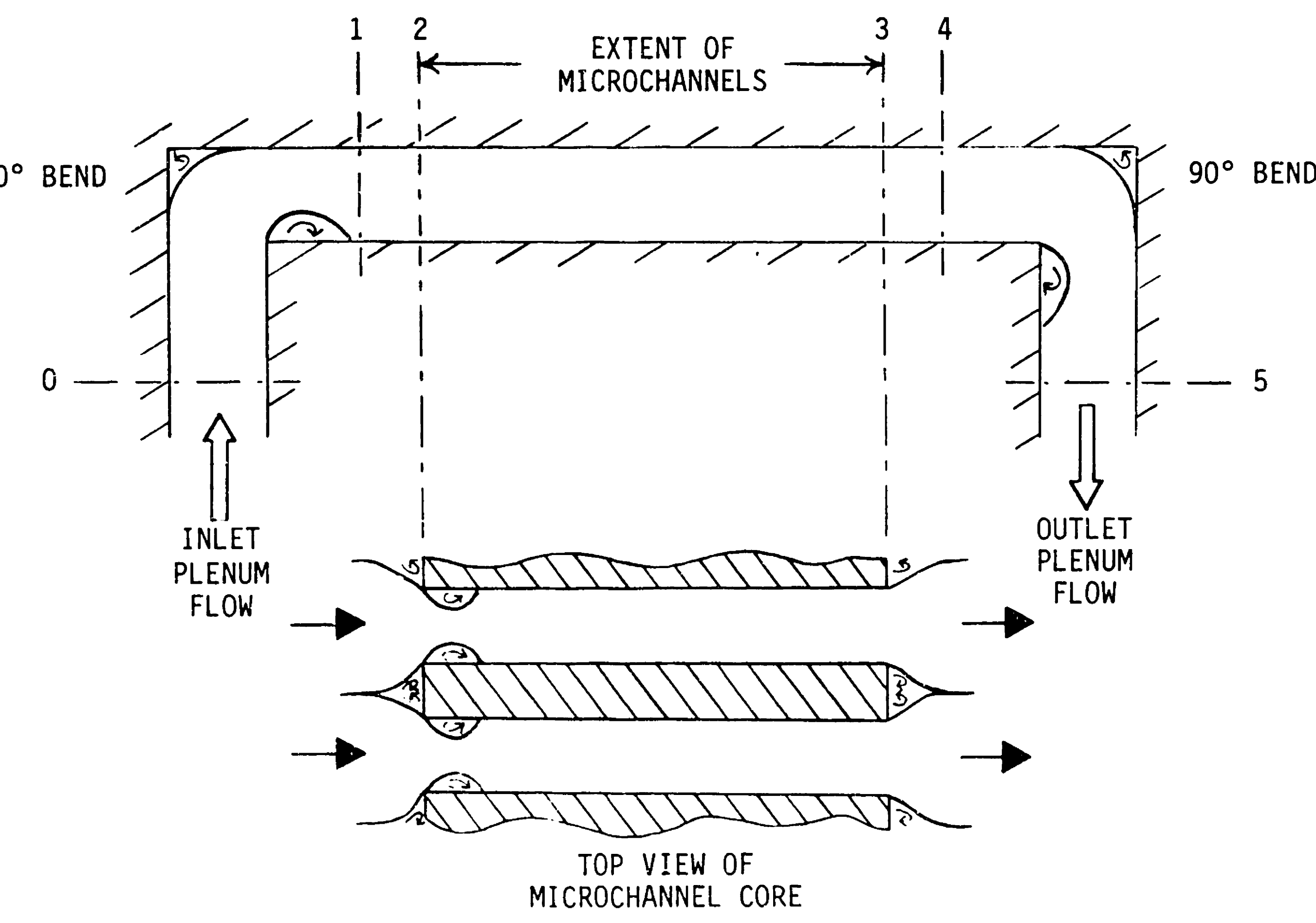

Figure 2.9. Microchannel heat sink pressure drop components.

expansion. The flow finally goes through another 90° bend as it enters the outlet plenum.

The pressure drop model based on Figure 2.9 is given by

$$\Delta P = \frac{\rho_1 V_{p1}^2}{2\, g_c} K_{90}$$
$$+ \frac{\rho_1 V_c^2}{2\, g_c} \left[(1 - \sigma^2 + Kc) + 2\left(\frac{\rho_1}{\rho_4} - 1\right) + 4f\, \frac{x}{D_e}\, \frac{\rho_1}{\rho_m} - (1 - \sigma^2 - Ke)\right]$$
$$+ \frac{\rho_4 V_{p4}^2}{2\, g_c} K_{90} \qquad (2.7)$$

where K_{90} is the 90° bend loss coefficient, Kc and Ke are the entrance and exit loss coefficients, σ is the ratio of the core free flow to frontal cross-sectional areas, and ρ_m is the average density which is given by

$$\frac{1}{\rho_m} = \frac{1}{L} \int_0^L \frac{1}{\rho}\, dx \approx \frac{2}{\rho_1 + \rho_4} \; . \qquad (2.8)$$

Assuming that the plenum cross-sectional areas are the same, and that the coolant density undergoes negligible variations, then Equation 2.7 simplifies to

$$\Delta P = \frac{\rho_f V_p^2}{2\, g_c} (2\, K_{90}) + \frac{\rho_f V_c^2}{2\, g_c} \left[(Kc + Ke) + 4f \frac{x}{D_e}\right] \; . \qquad (2.9)$$

The problem now is to determine the loss coefficients and the friction factor.

The model given by Figure 2.9 is highly idealized in that the velocity profiles at Sections 0 through 5 are assumed to be fully developed (the case of developing flow at Section 3 will be discussed soon). The entrance and exit loss coefficients can be determined from Figures 2.10 and 2.11. Figure 2.11 may be directly used for small and large aspect ratio ducts. Some judgement is required to determine the loss coefficients for moderate aspect ratio ducts. For this study, it is assumed that Figure 2.10 applies when $0.1 < \alpha < 10.0$. The usual Reynolds number with $D_e = 4A/P$ is used. The 90° bend loss coefficient is estimated to be $K_{90} \approx 1.2$.*

The loss coefficients Kc and Ke in Figures 2.10 and 2.11 were obtained assuming essentially uniform velocity in the inlet and exit plenums, and fully developed flow at the exit of the channel core [Kays and London (1984)]. They already include the pressure change associated with the change of the velocity profile in the core. Therefore, the channel friction factor used to evaluate the overall pressure drop in Equations 2.7 and 2.9 should be based on the mean wall shear. A less than fully developed velocity profile at the core exit will result in a smaller Kc and a larger Ke than those obtained for the fully-developed flow situation. This effect has been included for laminar flow in Figure 2.10, but the rest of the results apply for fully developed flow at the channel exit. Because of this discrepancy, the apparent friction factor

* This is an estimated average value for the loss coefficients listed in several commonly available fluids and heat transfer handbooks.

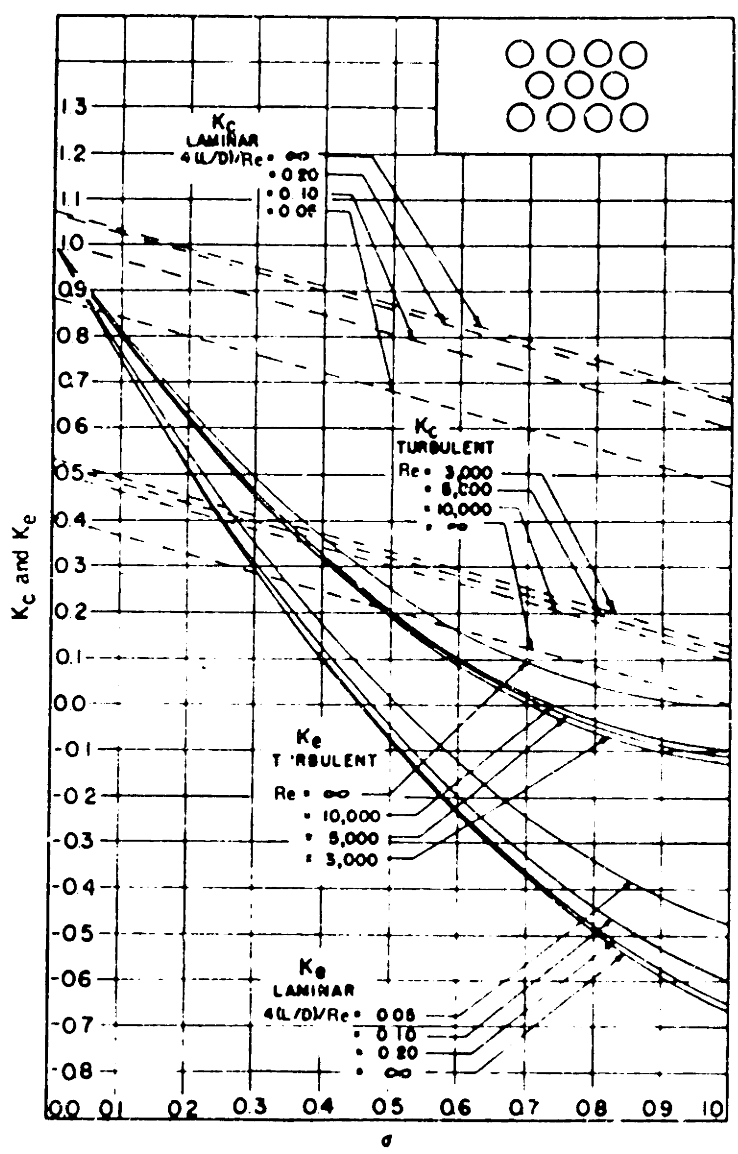

Figure 2.10. Entrance and exit loss coefficients for flow in circular tubes. [Taken from Kays and London (1984).]

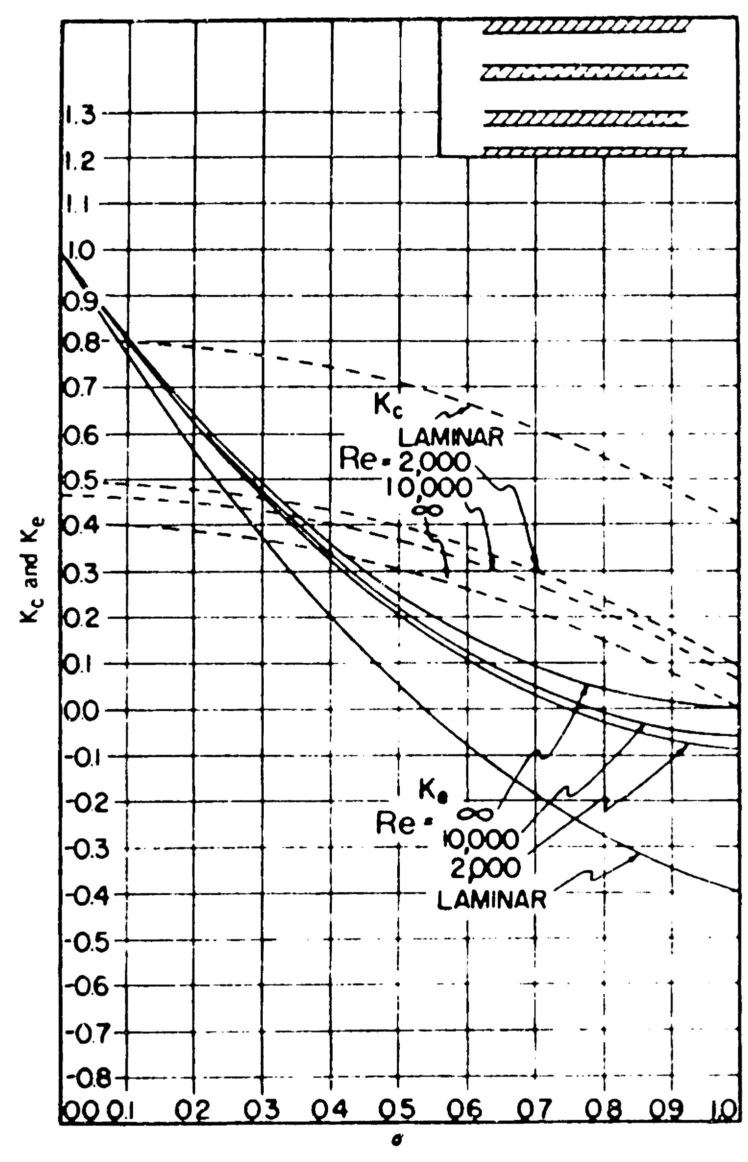

Figure 2.11. Entrance and exit loss coefficients for flow between parallel plates. [Taken from Kays and London (1984).]

(instead of the friction factor based on mean-wall shear) will be used in this study to provide a conservative estimate of the overall pressure drop. This action is conservative because the change in the core velocity profile is taken into account twice.

2.1.4 Heat Transfer Coefficients

To determine the thermal performance of microchannel heat sinks, it is necessary to know the value of the heat transfer coefficient, which is given by

$$h_x = \frac{q''_{w,x}}{T_{w,x} - T_{m,x}} \tag{2.10}$$

where h_w is the local heat transfer coefficient, $q''_{w,x}$ is the heat flux at the wall, $T_{w,x}$ is the local wall temperature, and $T_{m,x}$ is the mixed-mean temperature of the coolant. For convenience, the local heat transfer coefficient is expressed in the nondimensional form of a Nusselt number, which is given by

$$Nu_x = \frac{h_x D_e}{k_f} \tag{2.11}$$

where Nu_x is the local Nusselt number, D_e is the hydraulic diameter, and k_f is the thermal conductivity of the coolant evaluated at $T_{m,x}$. In the following, the subscript x is dropped for convenience.

The Nusselt number has been shown to be a function of several parameters. Some of them are: the coolant type (phase and properties), the coolant flow rate, the flow regime (laminar, transitional, or turbulent),

the channel geometry, the axial position in the channel (from the entrance), the heat input boundary conditions, the type of channel entrance (e.g. bell-mouthed or abrupt), the entrance velocity profile, and the entrance coolant temperature profile. In this study, it is assumed that the channel entrance is "abrupt," and that the heating rate is constant in the flow direction with uniform peripheral surface temperature.

In channel flow, the Nusselt number at the channel entrance is indefinitely high, and becomes smaller with downstream distance. If the channel is long enough, the Nusselt number monotonically approaches a fully developed limit (assumes small property variations). Due to this monotonic trend, the smallest Nusselt number will be obtained at the channel exit.

The Nusselt number for channel flow will be significantly affected by the entrance velocity and temperature profiles. Analytical solutions for the Nusselt number are usually done for the following entrance conditions:

1) fully-developed velocity and temperature profiles (the fully-developed-flow problem),

2) fully-developed velocity profile and uniform temperature profile (the thermal-entry-length problem), and

3) uniform velocity and temperature profiles (the combined thermal and hydrodynamic entry-length problem).

The Nusselt numbers for simultaneously developing flows (Item 3) are always higher than those for thermally developing flows (Item 2), which is in turn higher than those for fully developed flow (Item 1).

For this study, the flow should be well mixed at the channel entrance, and therefore will be very similar to the combined thermal and hydrodynamic entry-length problem (simultaneously developing flow). The correlations used to determine the Nusselt number should be obtained for this simultaneously developing flow condition if they are to be "accurate." The limited correlations available for simultaneously developing flow has forced the author to use correlations for thermally developing flow and/or fully developed flow to determine the Nusselt numbers.* It is recognized that Nusselt numbers obtained in this manner will be too low, and therefore will be slightly <u>conservative</u>.

Fully-developed laminar-flow heat transfer in rectangular ducts has been studied by Schmidt (1971). Table 2.8 presents his results of the Nusselt number for fully developed velocity and temperature profiles with one or more walls transferring heat (the local wall temperature of the heating walls is constant). Figure 2.12 is a plot of the values in Table 2.8. Note that Case 3 applies for large aspect ratio channels, Case 2 applies for moderate aspect ratio channels, and Case 4 applies for small aspect ratio channels. From Figure 2.12, it is apparent that Case 1 (all four sides heating) provides values of the Nusselt number for fully-developed flow that are the closest to those for Case 2 when $\alpha > 1.0$ (i.e., for large and moderate aspect ratio ducts). The Case 1 values, though, are as much as 10 percent lower than those for Case 2.

* Some literature is available on simultaneously developing flows (they are briefly discussed in this document). The correlations are usually limited in the range of Reynolds number or Prandtl number. Time pressures for this study did not allow the author to extend their results.

TABLE 2.8

NUSSELT NUMBER FOR FULLY DEVELOPED FLOW IN RECTANGULAR DUCTS WITH ONE OR MORE WALLS TRANSFERRING HEAT, WITH UNIFORM AXIAL HEAT FLUX AND UNIFORM PERIPHERAL WALL TEMPERATURE (DUE TO SCHMIDT.) [TAKEN FROM SHAH AND LONDON (1978).]

α^*	Nu				
	Case 1 (b, w_c)	Case 2	Case 3	Case 4	Case 5
0.0	8.235	8.235	8.235	0	5.385
0.1	6.700	6.939	7.248	0.538	4.410
0.2	5.704	6.072	6.561	0.964	3.914
0.3	4.969	5.393	5.997	1.312	3.538
0.4	4.457	4.885	5.555	1.604	3.279
0.5	4.111	4.505	5.203	1.854	3.104
0.6	3.884	--	--	--	2.987
0.7	3.740	3.991	4.662	2.263	2.911
0.8	3.655	--	--	--	2.866
0.9	3.612	--	--	--	2.843
1.0	3.599	3.556	4.094	2.712	2.836
1.43	3.740	3.195	3.508	3.149	2.911
2.0	4.111	3.146	2.947	3.539	3.104
2.5	4.457	3.169	2.598	3.777	3.279
3.33	4.969	3.306	2.182	4.060	3.538
5.0	5.704	3.636	1.664	4.411	3.914
10.0	6.700	4.252	0.975	4.851	4.410
∞	8.235	5.385	0	5.385	5.385

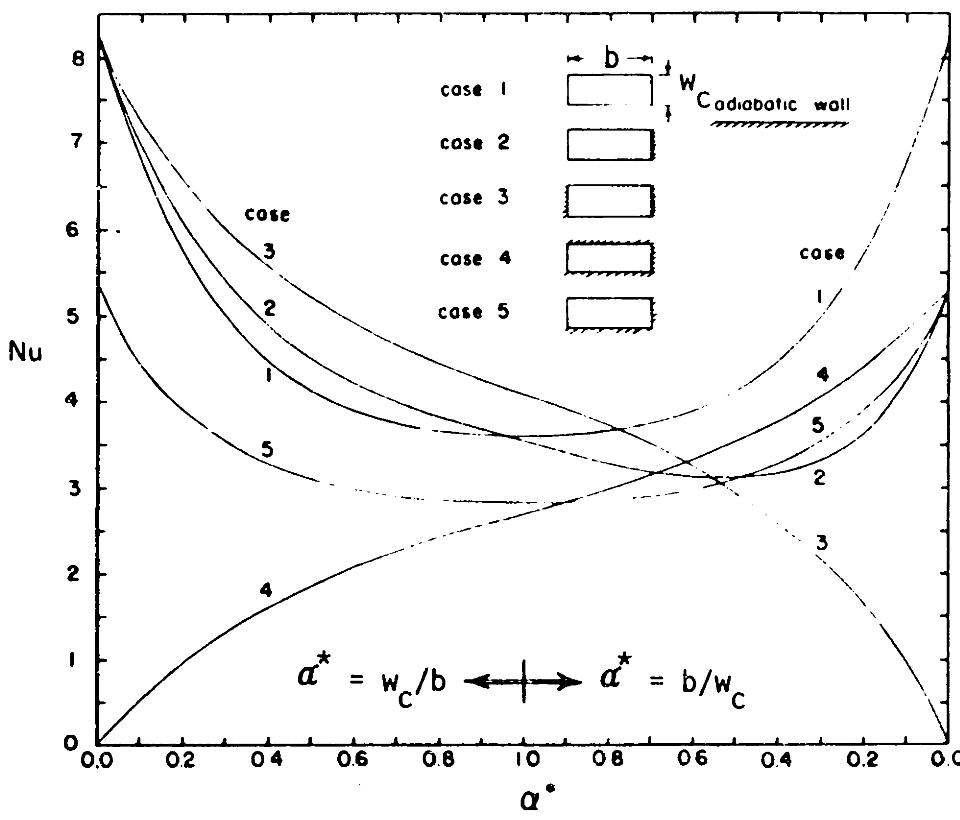

Figure 2.12. Nusselt number for fully developed flow in rectangular ducts with one or more walls transferring heat. Uniform axial heat flux and uniform peripheral wall temperature. (Due to Schmidt.) [Taken from Shah and London (1978).]

The author is not aware of any available solutions of the thermal entrance length problem for moderate aspect ratio rectangular ducts with one wall insulated (and the other three transferring heat - Case 2). Wibulswas (1966) has computed the Nusselt number for the thermal entrance length problem for rectangular ducts with all four sides transferring heat and constant local-peripheral-wall temperature (Case 1). His results are shown in Table 2.9.

An estimate of the Nusselt numbers for moderate aspect ratio channels with three sides heated may be obtained. The method used for this study is to multiply the developing flow Nusselt number obtained from Table 2.9 (4 sides heated) by the ratio of the fully-developed flow Nusselt numbers for Case 2 (3 sides heated), and Case 1 (4 sides heated) at the same aspect ratio. The developing flow, three-side-heated Nusselt number for moderate aspect ratio channels is therefore approximated by

$$Nu_{x,3}\ (x^*,\ \alpha) \approx Nu_{x,4}\ (x^*,\ \alpha)\ \frac{Nu_{Case\ 2}(\alpha)}{Nu_{Case\ 1}(\alpha)} \qquad (2.12)$$

where the axial length parameter, x^*, is given by

$$x^* = \frac{(x/D_e)}{RePr} \qquad (2.13)$$

and x is the axial distance downstream from the channel entrance.

The thermal entry length problem has been solved for flow between parallel plates by Lundberg, et al. (1963). The results are shown in Table 2.10 for large aspect ratio channels (both sides heated), and small aspect ratio channels (one side heated and the other insulated). The

TABLE 2.9

NUSSELT NUMBER FOR THERMALLY DEVELOPING FLOW IN RECTANGULAR DUCTS, WITH ALL FOUR WALLS TRANSFERRING HEAT AND UNIFORM PERIPHERAL WALL TEMPERATURE (DUE TO WIBULSWAS.) [TAKEN FROM SHAH AND LONDON (1978).]

$1/x^*$	Nu_x			
	α			
	1.0	2.0	3.0	4.0
0	3.60	4.11	4.77	5.35
10	3.71	4.22	4.85	5.45
20	3.91	4.38	5.00	5.62
30	4.18	4.61	5.17	5.77
40	4.45	4.84	5.39	5.87
60	4.91	5.28	5.82	6.26
80	5.33	5.70	6.21	6.63
100	5.69	6.05	6.57	7.00
120	6.02	6.37	6.92	7.32
140	6.32	6.68	7.22	7.63
160	6.60	6.96	7.50	7.92
180	6.86	7.23	7.76	8.18
200	7.10	7.46	8.02	8.44

TABLE 2.10

NUSSELT NUMBER FOR THERMALLY DEVELOPING FLOW BETWEEN PARALLEL PLATES WITH ONE OR BOTH WALLS HEATED (DUE TO LUNDBERG, ET AL.) [COMPUTED FROM KAYS AND CRAWFORD (1980).]

x^*	Nu_x	
	Both Sides Heated $\alpha = \infty$	One Side Heated $\alpha = 0$
0.00025	23.8	23.5
0.0025	11.9	11.2
0.01	8.80	7.49
0.05	8.25	5.55
0.125	8.24	5.39
$= \infty$	8.23	5.38

results shown in Table 2.10 are "exact" solutions in that they apply for $\alpha = 0$ and $\alpha = \infty$. Interpolation between these results and those for moderate aspect ratios at a given x^* will be required. For simplicity, it is assumed that the values in Table 2.10 apply for $\alpha < 0.1$ and $\alpha > 10.0$ (small and large aspect ratios, respectively).

For the combined thermal and hydraulic entry length problem, the Nusselt numbers are theoretically higher than those for the thermal entrance length problem. The theoretical models do not account for wake effects or secondary flow at the entrance, which are usually present in "abrupt" channel entrances. Based on experimental evidence, the heat transfer coefficients do not achieve the higher Nusselt numbers predicted by the simultaneously-developing-flow theoretical analyses. Shah and Mueller in Rohsenow, Hartnett, and Ganic' (1985a) recommend using the analytical results obtained for the thermal entry length problem (fully developed velocity profile at the entrance) because they agree better with the experimental data! Even if the flow had uniform velocity and temperature profiles at the entrance, it has been shown by Kays and Crawford (1980) that it is only significant if $Pr < \sim 5$ which is a small number for liquid coolants. It is for these reasons that the effect of the developing velocity profile on the laminar Nusselt number will be ignored.

The laminar flow Nusselt numbers listed in Table 2.11 and plotted in Figure 2.13 were extracted from Tables 2.8 through 2.10. They will be used for computer solution purposes (see Chapter 4).

Turbulent flow, which has a developing temperature profile but a fully developed velocity profile, will result in Nusselt numbers which

TABLE 2.11

LAMINAR FLOW NUSSELT NUMBERS USED FOR COMPUTER SIMULATION+

x/D_eRePr	Nu_x					
	$\alpha \leq .1$**	$\alpha = 1.0$	$\alpha = 2.0$	$\alpha = 3.0$	$\alpha = 4.0$	$\alpha \geq 10.0$**
0.0001≈0.*	31.6	25.2	23.7	27.0	26.7	31.4
0.0025*	11.2	8.9	9.2	9.9	10.4	11.9
0.005	9.0	7.10	7.46	8.02	8.44	10.0
0.00556	8.8	6.86	7.23	7.76	8.18	9.8
0.00625	8.5	6.60	6.96	7.50	7.92	9.5
0.00714	8.2	6.32	6.68	7.22	7.63	9.3
0.00833	7.9	6.02	6.37	6.92	7.32	9.1
0.01	7.49	5.69	6.05	6.57	7.00	8.80
0.0125	7.2	5.33	5.70	6.21	6.63	8.6
0.0167	6.7	4.91	5.28	5.82	6.26	8.5
0.025	6.2	4.45	4.84	5.39	5.87	8.4
0.033	5.9	4.18	4.61	5.17	5.77	8.3
0.05	5.55	3.91	4.38	5.00	5.62	8.25
0.1	5.4	3.71	4.22	4.85	5.45	8.24
≥ 1.0	5.38	3.60	4.11	4.77	5.35	8.23

+ $\alpha = \frac{\text{channel height}}{\text{channel width}} = \frac{b}{w_c}$

Re based on $D_e = 4A/P$.

* Values exponentially extrapolated.

** Values from Table 2.10 were graphically interpolated.

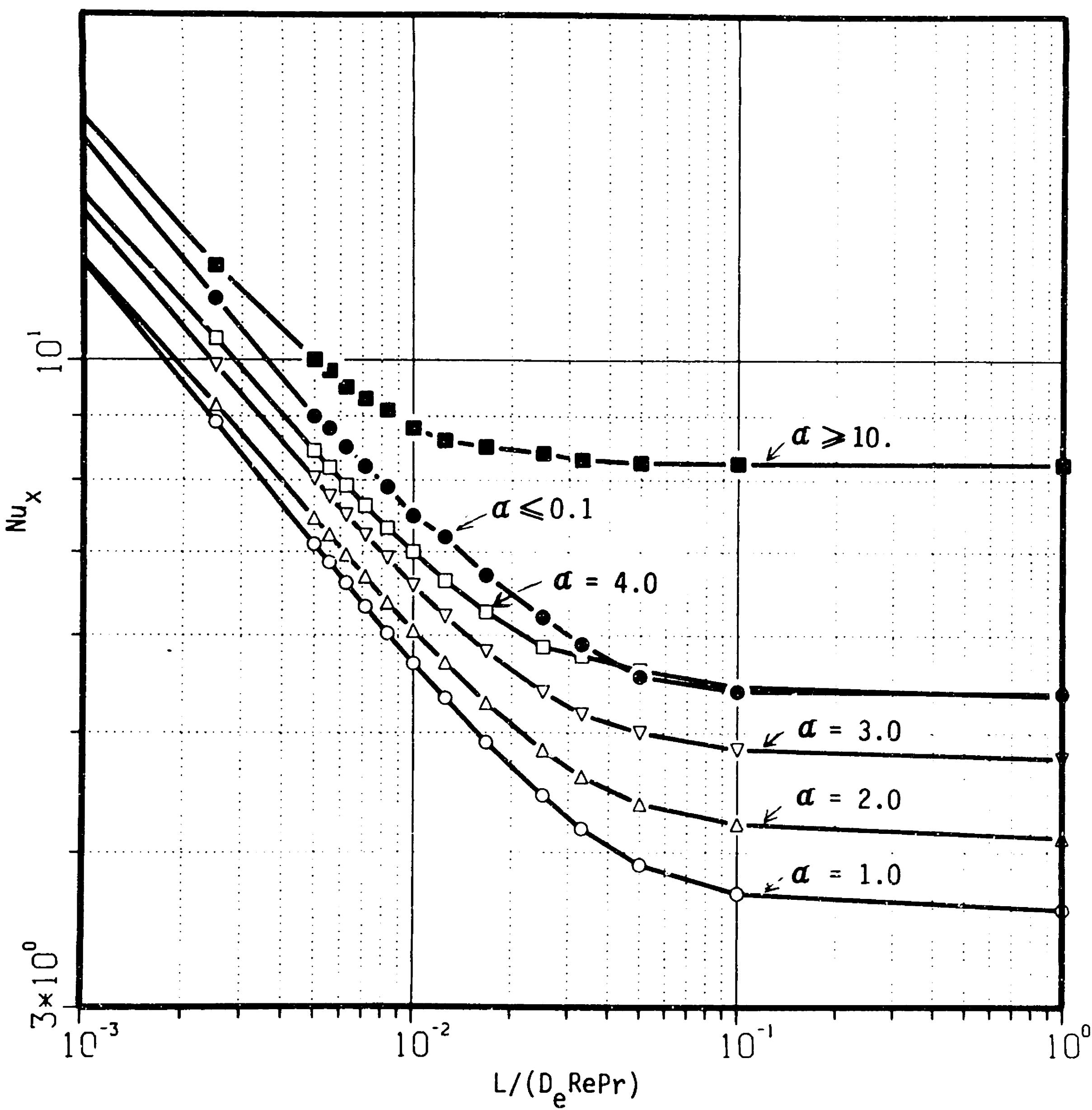

Figure 2.13. Laminar flow Nusselt numbers used for computer simulation.

are large at the entrance. They become smaller with axial distance downstream, and eventually will approach a fully developed value. Deissler (1955) has analyzed the thermal entry length problem. His results indicate that the local Nusselt number is within 10 percent of the fully developed value when $x/D_e \approx 10$. His results also show that for $Pr \approx 0.73$, the entrance length increases slightly with decreasing Reynolds number. Sparrow, Hallman, and Siegel (1957) have shown that the thermal entrance length becomes very small for Prandtl numbers above one. For example, when $x/D_e = 10$, the local Nusselt number is only two percent higher than the fully developed value for $Pr = 10$ and $Re = 50,000$. Malina and Sparrow (1964) present results for $12,000 < Re < 101,000$ which suggest that the thermal entry length is somewhat smaller. This author has crudely extrapolated their results down the Re_{crit}, and found that the thermal entrance length was still $(x/D_e) < 10$. The experimental results of Hartnett (1955) for $Re > 10,000$, indicate that the flow is essentially fully developed when $x/D_e \approx 10$. Hartnett (1955) also presents the results for thermal entry length tests of oil for lower Reynolds numbers. His results for the oil thermal entrance lengths are listed in Table 2.12, and Figure 2.14 is a plot of the ratio of the local and fully developed heat transfer coefficients. Clearly, the thermal entrance lengths can be quite large for Reynolds numbers at the lower end of the turbulent regime (down to Re_{crit} for this study for high Pr). This author has not found any additional experimental evidence showing a significant increase of the circular-tube local Nusselt numbers for $x/D_e > 10$. Therefore, the increase in the turbulent Nusselt number in

TABLE 2.12

THERMAL ENTRANCE LENGTH RESULTS FOR OIL FLOW IN CIRCULAR TUBES
[TAKEN FROM HARTNETT (1955).]

Re X 1000	Pr	x^*/D_e	$(x^*/D_e)5\%$
2.57	379	74^{α}	69
3.44	350	41	31
4.29	336	41	28
5.50	223	29	14
7.83	260	15.3	7.2
10.1	206	13.8	5.7
13.3	170	16.9	4.6
14.8	157	13.8	4.4
16.2	90	10.7	3.7
16.3	135	7.4	4.1
17.2	138	13.8	3.7
17.3	87	13.8	3.7
22.9	98	7.7	2.2
24.6	107	10.7	2.8
24.6	107	15.3	2.6
29.8	88	7.8	2.0
34.6	63	13.8	2.8
46.4	63	6.9	1.5
46.6	61	8.4	1.7

α = Thermal-entry length actually greater than tube length.

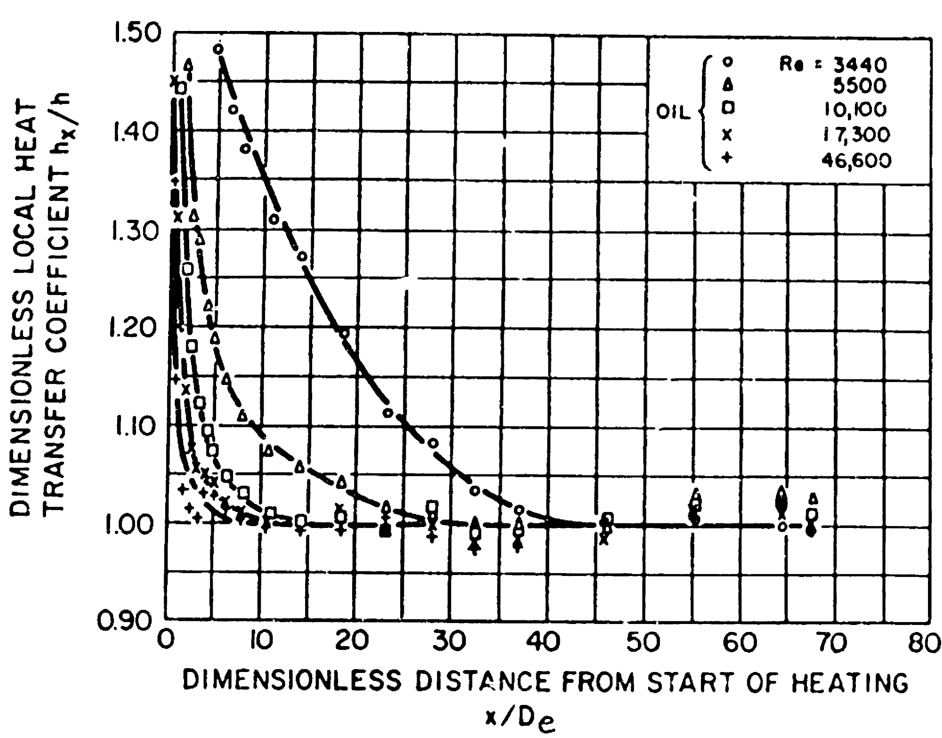

Figure 2.14. Thermal entrance results for oil flow in circular tubes. [Taken from Hartnett (1955).]

the thermal entrance region of moderate aspect ratio ducts will be ignored. This is a conservative assumption.

The thermal entrance length problem has been solved for flow between parallel plates. Solutions are available for the cases of one side heated uniformly (the other side is insulated), and with both sides uniformly heated. The solutions apply respectively for large and small aspect ratio ducts. The restriction this time is that the author is only aware of solutions which are presented for a limited range of Prandtl numbers [see Kays and Crawford (1980)]. Therefore, the increase in the turbulent Nusselt number in the thermal entrance region of large and small aspect ratio ducts will be ignored. This assumption is also conservative.

The combined thermal and hydrodynamic entry length problem for turbulent flow can be analytically solved if several assumptions are made. The solutions obtained are usually for "ideal" flow, and do not account for the separated flow at the entrance which tends to provide much larger heating rates (opposite to the impact in laminar flow). Kays and Crawford (1980) present experimental results obtained by Boelter, Young, and Iversen (1948) for air (Pr = 0.73) flowing in tubes with various inlet geometries. Their results show that the inlet Nu can be about twice as large as the fully developed flow value. They are only about 10 percent different though, when $x/D_e \approx 10$. For liquid coolants, which typically have large Prandtl numbers, the effect of simultaneously developing flows will be smaller. Consequently, the increase in the turbulent Nusselt number in the combined thermal and hydrodynamic entry length problem will be ignored. This assumption is conservative.

The Nusselt numbers for turbulent flow in rectangular ducts can be obtained by using circular tube correlations where the friction factor is computed using the Jones (1976) method. Gnielinski (1976) derived an equation for circular tube Nusselt numbers based on experimental data in the low Reynolds number range. It is given by

$$Nu = \frac{(f/2)\ (Re - 1000)Pr}{1 + 12.7(f/2)^{1/2}\ (Pr^{2/3} - 1)} \tag{2.14}$$

where Pr is the fluid Prandtl number, Re is based on D_e, and Nu is based on D_e. Equation 2.14 applies for $2300 < Re < 10{,}000$. Gnielinski (1976) used the Filonenko equation $f = (1.58\ \ln(Re) - 3.28)^{-2}$ to compute the friction factor for Equation 2.14.

When the flow is not fully developed, Gnielinski (1976) recommends multiplying the right-hand-side of Equation 2.14 by $[1 + (D_e/x)^{2/3}]$. Note that this conversion factor does not include the effects of Re and Pr. With this conversion, it was found that 80 percent of the experimental data fall within ±20 percent of the calculated values. Those experimental data points which fall outside of the ±20 percent accuracy limit were found to have calculated Nusselt numbers that were usually larger than the experimental values. That is, that the calculated values were more than 20 percent too large for nearly 20 percent of the data points. Such errors are deemed too large and indeed are not conservative. Therefore, the developing-flow conversion is not used.

A simplified form of Equation 2.14 was provided by Gnielinski (1976). It is given by

$$Nu = 0.012\ (Re^{0.87} - 280)Pr^{0.4} \tag{2.15}$$

and applies for fully-developed flow of liquids ($1.5 < Pr < 500$). Shah and Johnson (1981) have asserted that Equation 2.15 agrees with Equation 2.14 within -10 percent and +0 percent for fully-developed flow in circular tubes. This means that Equation 2.15 predicts a lower Nusselt number than Equation 2.14. If the enhancement in the Nusselt number caused by developing flow is ignored, then it appears that Equation 2.15 will predict Nusselt numbers that are no more than about 10 percent too large, and indeed the Nusselt numbers should be conservative most of the time. Note, though, that Equation 2.15 does not contain the friction coefficient, and therefore will not permit correction in the Nusselt number for duct shape. Fortunately, the duct geometry appears to have a second-order effect on the turbulent Nusselt number when compared to using the hydraulic diameter in place of the circular tube diameter. Therefore, Equation 2.15 will be used to predict the fully-developed and developing-turbulent-flow Nusselt numbers for this study.*

2.2 Roughened Ducts

The performance of conventional heat exchangers can be significantly enhanced by using several augmentation techniques. In this study, two

* It should be noted that there are many other turbulent-flow Nusselt-number correlations that are available. Shah and Johnson (1981) have compared many of them with the Gnielinski (1976) correlation. The results indicate that most of the other equations predict much higher Nusselt numbers and therefore are not conservative over the Prandtl number range of interest for this study. For example, the classical Dittus-Boelter equation $Nu = 0.023\ Re^{0.8}Pr^{0.4}$ overpredicts by as much as 20 percent for $Pr = 5.0$.

"passive" methods are used in that no direct application of external power is required.* They are: 1) extended surfaces (fins), and 2) surface roughening. Extended surfaces are used to increase the surface area for heat transfer (see Chapter 3). Surface roughening can be used to promote turbulence which increases the heat transfer coefficient.

An analysis is presented here that predicts the thermal and fluid performance of repeated-rib surface roughening for fully-developed turbulent flow between parallel plates.+

2.2.1 Overview of Heat Transfer Augmentation by Surface Roughening.

Rough surfaces have better thermal-hydraulic performance than smooth surfaces for the same flow conditions. A smooth duct must be operated at a higher Reynolds number, higher pressure drop, and higher pumping power to yield the same heat transfer rate as a duct equipped with discrete roughness. For this study, the most promising method of surface roughening appears to be the use of repeated-ribs of a specific shape which protrude from the channel surface at regular intervals. The main purpose of the ribs is to break down the turbulent-flow laminar sub-layer such that turbulent mixing is increased next to the wall. This increased mixing results in larger heat transfer coefficients, but a penalty is paid in that the friction coefficient is also increased.

The flow patterns near the wall depend on the relative rib spacing which is the ratio of the distance between repeated-ribs (p) and the rib

---

* Examples of augmentation techniques that require external power are surface and fluid vibration.

+ The author is not aware of correlations for developing flow.

height (e). Typical flow patterns are shown in Figure 2.15. The boundary layer re-attaches at 6-8 rib heights downstream, and usually does not re-attach if $p/e < 8$. This is important since the maximum heat transfer coefficient occurs in the vicinity of the re-attachment point.

The correlations presented by Han, et al. (1978) will be used in this study. Figure 2.16 shows the definitions of the geometric parameters of interest. The rib width is w, which is assumed in this study to equal the rib height e.* The plate spacing is y, the rib shape angle is ϕ, and the flow attack angle is ψ. Han, et al. (1978) suggests that $\psi \approx 45°$ and $p/e \approx 10$ for optimum performance. Having $\phi < 90°$ appears to be advantageous because data indicate that the reduction in the friction factor (w.r.t. $\phi = 90°$) is larger than the reduction in the heat transfer coefficient.+ The correlations presented in the following subsections were presented by Han, et al. (1978), and apply for $0.032 \leq e/D_e \leq 0.102$, $55° \leq \phi \leq 90°$, $20° \leq \psi \leq 90°$, $3{,}000 \leq Re \leq 30{,}000$, and $5 \leq p/e \leq 20$.

2.2.2 Friction Coefficients and Pressure Drop

The friction factor may be readily obtained for flow between repeated-rib-roughened parallel plates if the values of e/D_e, p/e, ϕ,

---

* The experiments of Han, et al. (1978) were done for $w/e = 1.0$ and $w/e = 1.5$. Apparently such small variations in w/e have only a small effect on the thermal-fluid performance - see Han, et al. (1978) for more details.

+ This trend is expected to apply only for moderate and large values of ϕ. Han, et al. (1978) does not have heat transfer coefficient data for $\phi < 55°$, but does have friction factor data for values as low as $\phi = 40°$.

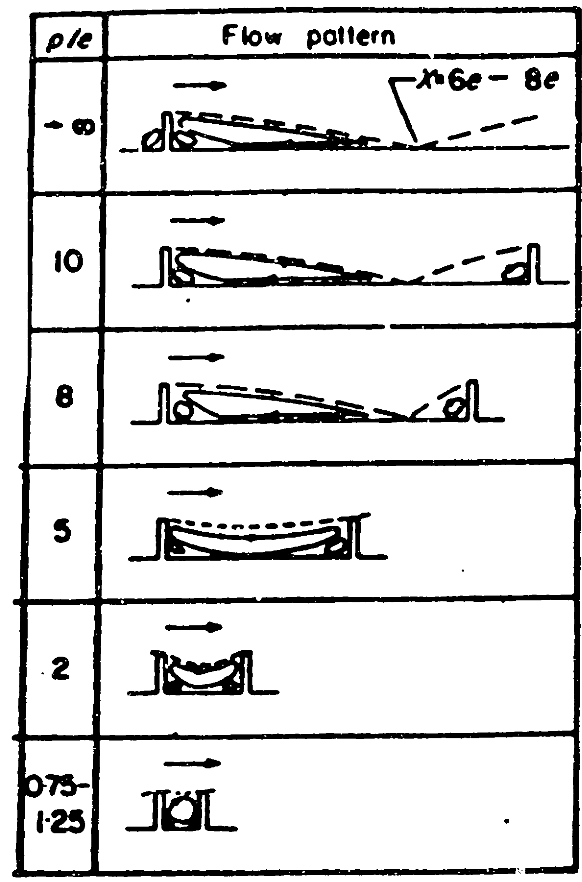

Figure 2.15. Flow patterns as a function of p/e for flow past repeated-ribs. [Taken from Webb, Eckert, and Goldstein (1971).]

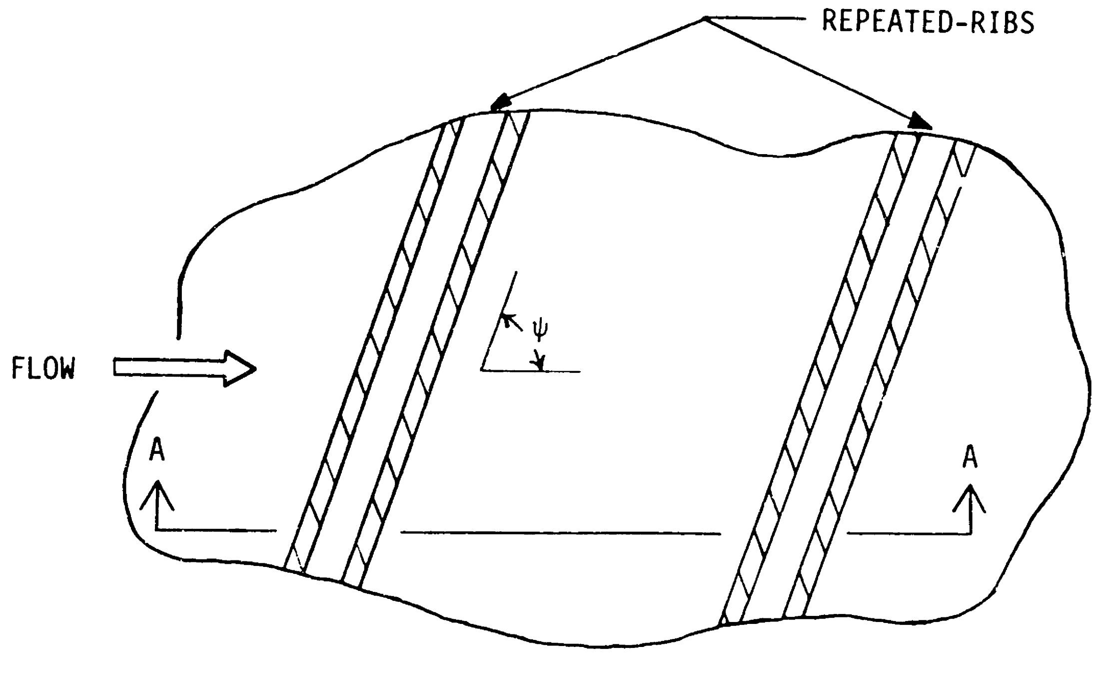

TOP VIEW OF ONE PLATE

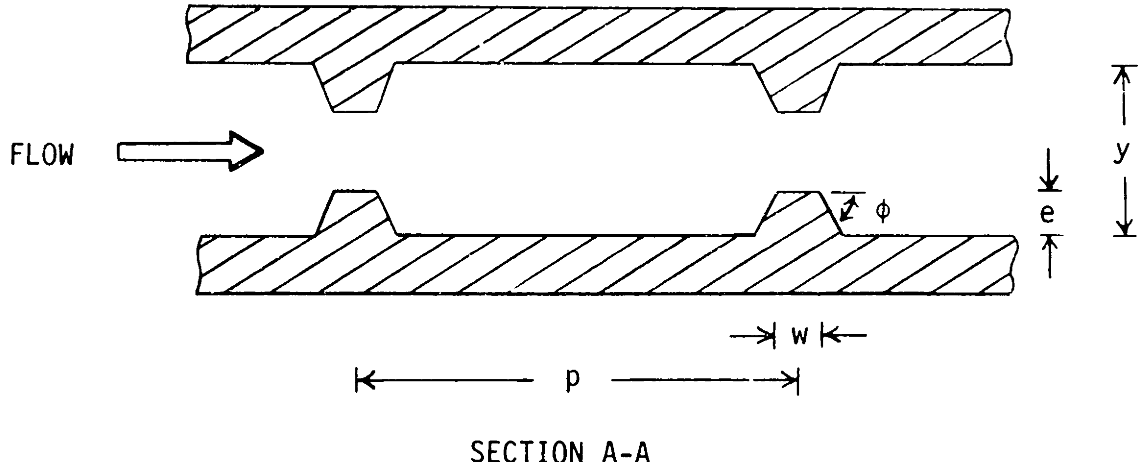

SECTION A-A

Figure 2.16. Repeated-rib geometric parameters.

and ψ are known.* The following equation is given by Han, et al. (1978)

$$R_e^+(e^+)(\phi/90°)^{0.35}\ (10/(p/e))^n\ (\psi/45°)^{0.57} = 4.9(e^+/35)^m \tag{2.16}$$

where

$$R_e^+(e^+) = (2/f_2)^{0.5} + 2.5\ \ln(2e/D_e) + 3.75$$

$$e^+ = (e/D_e)\text{Re}\ (f_2/2)^{0.5}$$

$$\begin{aligned} m &= -0.4 && \text{if } e^+ < 35 \\ m &= 0. && \text{if } e^+ \geq 35 \\ n &= -0.13 && \text{if } p/e < 10 \\ n &= 0.53(\psi/90°)^{0.71} && \text{if } p/e \geq 10 \ . \end{aligned}$$

The roughness Reynolds number is e^+, and Re is the usual Reynolds number based on D_e. The fully developed friction factor, f_2, is for both walls roughened, and applies directly for large aspect ratio

* Han, et al. (1978) does not define the method he used to obtain the value of the equivalent diameter. For this study, it is assumed that $D_e = 4Acx/Aw$ applies for roughened channels. This is the usual correlation used for heat exchanger design where Ac is the minimum free-flow area, and x is the axial flow length over which the total heat transfer surface area, Aw, is obtained.

channels. For small aspect ratio channels, heating occurs only at one surface (the other is insulated). To avoid the additional pressure drop penalty, only the heated wall needs to be roughened (the other wall is smooth). When only one wall is roughened, Webb, Eckert, and Goldstein (1971) recommend using the following to obtain the friction factor

$$f_1 = \frac{f_2 + f_0}{f_2} + f_0 \qquad (2.17)$$

where f_0 is the average friction factor for both channel sides smooth, f_1 is the average friction factor for one channel side smooth and the other roughened, and f_2 is the average friction factor for both channel sides roughened. The Blasius equation is used to compute f_0 and is given by

$$f_0 = 0.0791\ Re^{-0.25} \qquad (2.18)$$

where Re is the usual Reynolds number based on the hydraulic diameter. The pressure drop can be computed using Equations 2.7 through 2.9 with f_1 or f_2 used in the place of f.

2.2.3 Heat Transfer Coefficients

Han, et al. (1978) presents the following correlation to compute the Stanton number, St,

$$(H_e^+)\ (\psi/45°)^j = 10.0(e^+/35)^i \tag{2.19}$$

where

$$H_e^+ = (f_2/2St - 1)/\ (f_2/2)^{0.5} + R_e^+$$

$$R_e^+ = (2/f_2)^{0.5} + 2.5\ \ln(2e/D_e) + 3.75$$

$$e^+ = (e/D_e)Re\ (f_2/2)^{0.5}$$

$i = 0.$	if $e^+ < 35$
$i = 0.28$	if $e^+ \geq 35$
$j = 0.5$	if $\psi < 45°$
$j = -0.45$	if $\psi \geq 45°$

where f_2 is obtained from Equation 2.16. Sheriff and Gumley (1966) show that $e^+ \approx 35$ produces an optimum heat transfer condition.

The fully developed flow Nusselt number is obtained from the definition of the Stanton number using

$$Nu = StRePr \quad . \tag{2.20}$$

Han's equations were obtained from experimental data for air ($Pr = 0.72$). He recommends accounting for the Prandtl number effect by replacing H_e^+ in Equation 2.19 with $(H_e^+)(0.72/Pr)^{0.57}$, where $0.71 \leq Pr \leq 37.6$.*

2.3 Effect of Axial Heat Conduction

Axial heat conduction represents the process of transferring heat in the coolant due to the axial fluid-bulk-mean temperature gradient. This temperature gradient is constant for the case of uniform axial heat input. It will not be a constant for this study since there is an abrupt transition to zero heat flux at the perimeter of the heat source. When fluid axial conduction is considered, part of the energy transferred from the wall goes to fluid enthalpy rise, and the remainder is conducted by the fluid to the end headers of the duct.

The Peclet number represents the ratio of the thermal energy convected to the fluid (fluid enthalpy rise) to the thermal energy conducted within the fluid. It can be shown that the Peclet number, Pe,

---

* This conversion factor was proposed by Webb, Eckert,and Goldstein (1971).

is given by

$$Pe = RePr \quad . \tag{2.21}$$

The relative importance of axial heat conduction can be represented by the inverse of the Peclet number. As a general rule, axial heat conduction may be neglected if $(1/RePr) < 0.01$ [see Kays and Crawford (1980)]. In this study, this condition is satisfied since $Pr > 1.0$ and generally $Re \gg 100$. Therefore, the effect of axial heat conduction in the fluid will be ignored.

The effect of axial heat conduction in the chip substrate material can be significant. This topic is discussed in Section 3.4.

2.4 Effect of Viscous Dissipation

The work done by the fluid on adjacent layers due to the action of shear forces is usually referred to as "viscous dissipation." In "layman's terms," it represents the conversion of mechanical energy (fluid pressure*) into heat. As the fluid flows downstream, it experiences a pressure drop due to friction. This pressure drop is converted into thermal energy, which causes the fluid temperature to rise (assuming an adiabatic wall).

---

* For this study, it is assumed that the liquid coolants are essentially incompressible. Therefore, momentum changes due to variations of density with pressure do not exist.

An energy equation (with an adiabatic wall) that accounts for viscous dissipation is

$$\Delta P V = \dot{m} Cp_f \Delta T_{pump} J \tag{2.21}$$

where ΔP is the coolant pressure drop, V is the volumetric flow rate, $\dot{m}$ is the mass flow rate, Cp_f is the specific heat, ΔT_{pump} is the coolant temperature rise due to viscous heating, and J is the mechanical equivalent of heat (1 Nm/J in SI units, and 778.163 lbf ft/Btu in English units). Substituting $\dot{m} = \rho_f V$ and rearranging gives

$$\Delta T_{pump} = \frac{\Delta P}{\rho_f Cp_f J} \tag{2.22}$$

which is independent of the heat flux applied at the wall (assuming average coolant properties). Therefore, the effect of viscous heating can not be put into the form of a thermal resistance (see Chapter 4).

For this study, the effect of viscous dissipation on the thermal response is small, but can be significant if the pressure drop is large. For example, 21.11°C (70°F) water flowing under a pressure drop of 206.8 kPa (30 psi) will experience a temperature rise of about 0.05°C (0.09°F).

2.5 Effect of Natural Convection

A convective velocity will be generated by buoyancy forces resulting from fluid density changes near the heated microchannel surfaces. This type of convection is often referred to as "free" or "natural" convection. It may have a significant effect on the microchannel heat transfer

if the forced convection velocity through the microchannels is low enough.

Metais and Eckert (1964) have classified the flow regimes, and their results are shown in Figure 2.17.* The Grashof number Gr is the ratio of the buoyancy to viscous forces, and is given by

$$Gr = \frac{g \rho_f^2 D_e^3 \Delta T \beta}{\mu_f^2} \qquad (2.23)$$

where g is the acceleration of gravity, ρ_f is the coolant density, D_e is the equivalent diameter, β is the volumetric coefficient of expansion, μ_f is the coolant dynamic viscosity, and ΔT is the wall to bulk coolant temperature difference. Lines 1 and 2 in Figure 2.17 are used in this study to approximate the separation between the purely forced convection, and the mixed convection regions. They represent a <u>rough</u> estimate of the limit to the forced convection regime where natural convection affects are likely to be less than 10 percent.

If the Reynolds number is large enough, and the $GrPrD_e/L$ product is small enough, then superimposed natural convection will not be important. For flow of water at room temperature (ρ_f = 997.4 kg/m^3, μ_f = 9.8 x 10^{-4} kg/ms, β = 2.12 x 10^{-4} °C^{-1}) through a channel (D_e of order 200 µm) with ΔT of order 100°C (maximum) and g = 9.81 m/s^2, the Grashof number is about 0.2. Since Pr is of order 7.0 and D_e/L of order 1.0 or

* Figure 2.17 is for flow through vertical tubes. The results for horizontal tubes and non-circular cross-sections are reasonably similar.

$$(10^{-2} < PrDe/L < 1)$$

Line 1: $Re = 1.5\ (GrPrDe/L)^{0.8}$ for $(GrPrDe/L) < 35{,}000$

Line 2: $Re = 800\ (GrPrDe/L)^{0.2}$ for $(GrPrDe/L) > 35{,}000$

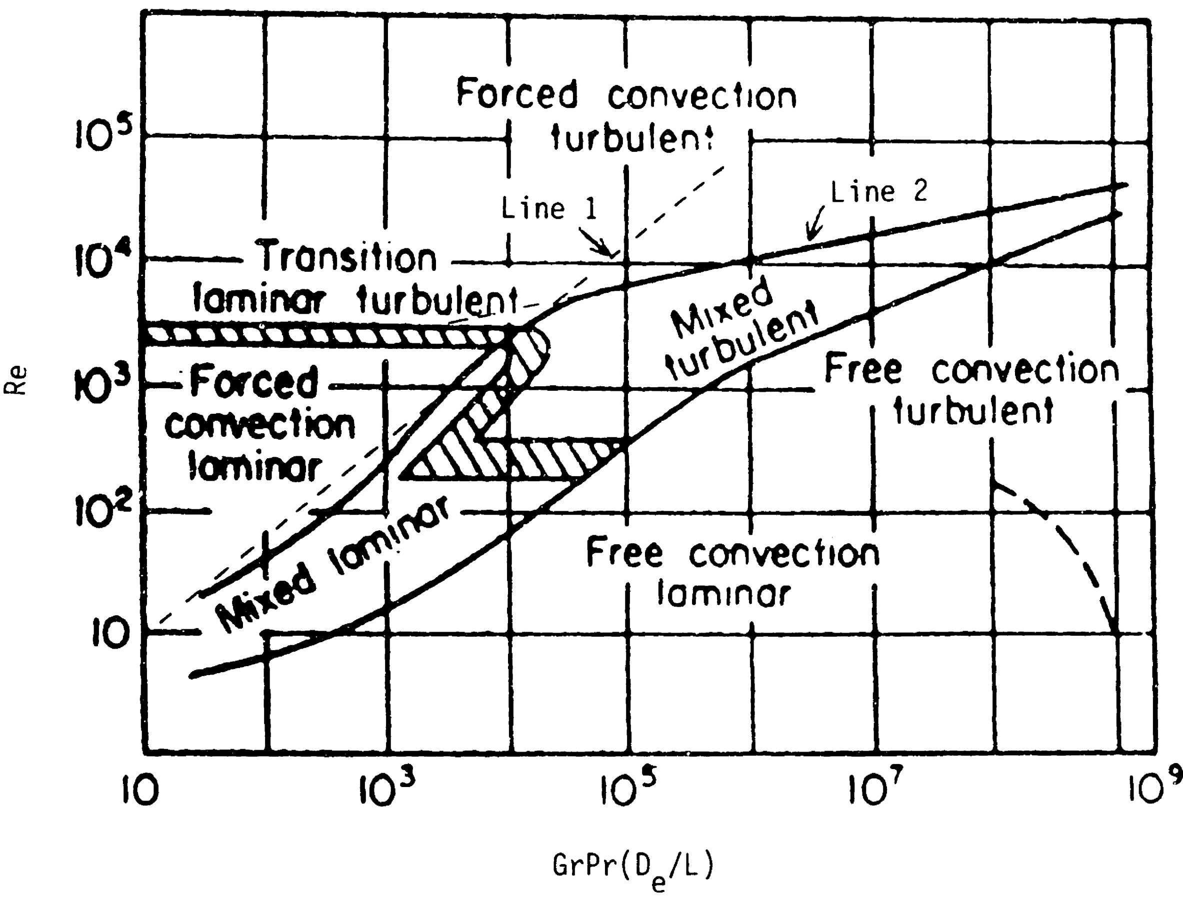

Figure 2.17. Regimes for free, forced, and mixed convection for flow through tubes. (Due to Metais and Eckert.) [Taken from Rohsenow, Hartnett, and Ganic' (1985b).]

smaller, the $GrPrD_e/L$ product is of order 1.4. This is indeed very small and suggests that superimposed natural convection is not important. Therefore, no attempt has been made to account for natural convection effects in the computer model.

2.6 Effect of Temperature Varying Properties

The flow friction and heat transfer solutions presented in the previous sections were based on the assumption of constant fluid properties throughout the entire flow field. Surface heat transfer necessitates that the temperature of the fluid near the wall is higher than the local "mixed-mean" temperature. Property variations due to temperature gradients within the fluid will cause "distortion" of the velocity and temperature profiles, which will affect the thermal-hydraulic performance.

For most liquids, the thermal conductivity, the density, and the specific heat are relatively independent of temperature. The dynamic viscosity, and consequently also the Prandtl number, are very temperature dependent.

The "property ratio" method is used in this study to account for fluid property variations. The values of the variable property friction factor and Nusselt number are obtained from

$$\frac{f}{f_{cp}} = \left[\frac{\mu_w}{\mu_b}\right]^M \qquad (2.24)$$

$$\frac{Nu}{Nu_{cp}} = \left[\frac{\mu_w}{\mu_b}\right]^N \qquad (2.25)$$

where the subscript cp represents the variable obtained using constant properties evaluated at the bulk temperature. Similarly, μ_w is evaluated at the average wall surface temperature, and μ_b is evaluated at the average bulk temperature. The values of the exponents N and M for fully developed laminar and turbulent flow used in this study are listed in Table 2.13. They were obtained from Kays and London (1984). It is assumed in this study that the values listed in Table 2.13 also apply for developing flow.

TABLE 2.13

PROPERTY RATIO METHOD EXPONENTS
[OBTAINED FROM KAYS AND LONDON (1984).]

Flow Regime	N	M
Laminar	-0.14	+0.58
Turbulent	-0.11	+0.25

2.7 Effect of Non-uniform Passages

In microchannel heat sinks, or any compact heat exchanger, the passage geometries are never uniform and identical. Cross-section non-uniformities can have a significant effect on the thermal and fluid performance. Differently sized and shaped passages will exhibit different flow resistance, and the fluid will be distributed unevenly. This effect is apparently most important for laminar flow in continuous passages which do not allow transverse flow mixing between passages.

Shah and London (1980) have analytically studied the changes in the friction factor and heat transfer coefficients due to passage-to-passage non-uniformity. Their results indicate that the effect on the Nusselt number is larger than that on the friction factor. For the case of uniform axial heat flux in a α = 8 channel, a 5 percent deviation in channel size results in about a 4 percent drop in the Nusselt number and about a 1 percent drop in the friction factor. If the channel deviation is doubled, the reductions are about 12 percent and 2.5 percent, respectively.

Shah and London (1980) consequently recommend that manufacturing tolerances should be kept to within 5 percent. The microchannel heat sinks used in the experimental portion of this study appear to meet this design recommendation (see Chapter 5). Consequently, no attempt was made to account for the effect of passage non-uniformities in the computer model.

2.8 Interrupted Fins

The numerical models that will be presented in Section 4.5 will show that the thermal performance is best when the flow at the channel exit is not fully developed. For the parallel-plate passages used there, the departure from fully developed flow is achieved in part by increasing the hydraulic diameter (by increasing the channel width). Given the same coolant velocity, the thermal-hydraulic boundary layers are less fully developed at the channel exit, and therefore both the heat transfer coefficient and the friction coefficient are larger.

Another method of attaining departure from fully-developed flow is to reduce the fin length while keeping the hydraulic diameter constant.

This so-called use of perforated surfaces or interrupted fins is shown schematically in Figure 2.18 for the two most common geometries: in-line and staggered. Interrupted-fins can augment the overall heat transfer coefficient by 50-100 percent due to flow separation, secondary flow, and periodic starting of the boundary layer on the fins. The boundary layers at the top and bottom of the channels, though, are more developed than those on the fins because of less effective flow mixing at the top and bottom. Interrupted-fin channels allow for transverse coolant mixing which spreads out the high coolant temperatures downstream from zones of high heat dissipation. They also draw more coolant to the hot-spots since the coolant viscosity is usually lower there [Tuckerman and Pease (1981b)]. Finally, interrupted-fin channels are less susceptible to catastrophic thermal failures due to channel clogging, and therefore are less susceptible to problems caused by manufacturing tolerance errors.

Clearly, interrupted fins offer several potential advantages if they are designed correctly. Unfortunately, even though design and analysis of compact heat exchangers has been in progress for several decades, there are very few generalized correlations that can predict their performance [Bergles in Rohsenow, Hartnett, and Ganic' (1985a)]. Those which are available are usually limited to flow of air through specific heat exchanger geometries. Ultimately, each interrupted-fin design must be evaluated experimentally to determine the performance.

Given the lack of general correlations, the remainder of this section presents results of several studies directed towards understanding the thermal-hydraulic characteristics of interrupted-fin heat

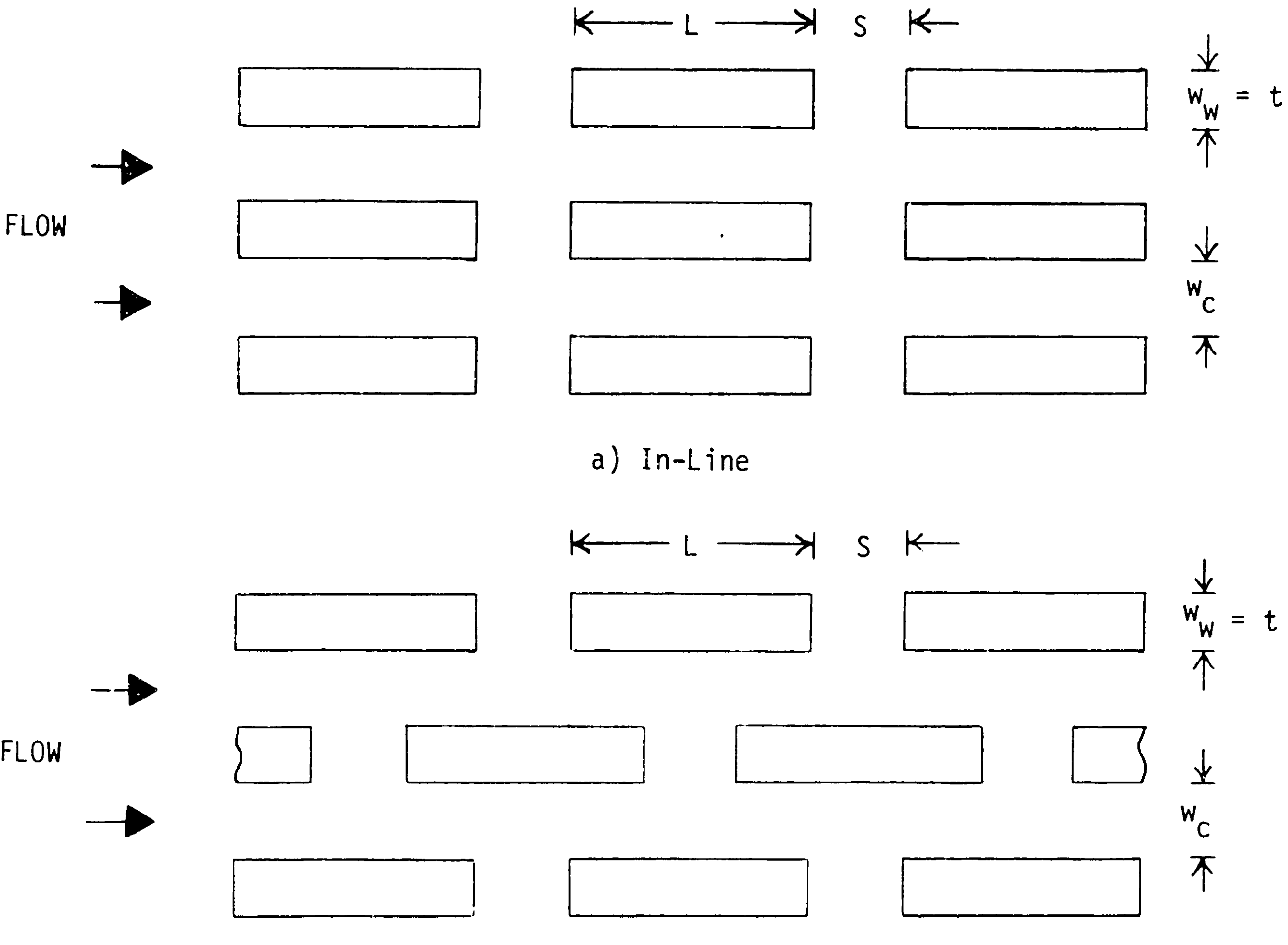

Figure 2.18. Schematic of interrupted fins.

exchangers. The flow past a single plate aligned parallel to the flow will first be reviewed to establish the potential size of the recirculation zones due to flow separation at the leading edge of the plate. The flow past a pair of co-linear plates aligned parallel to the flow will then be reviewed in order to establish the conditions for unsteady flow (transverse flow) between the two plates. There will also be a discussion of the possible excitation of resonance due to unsteady flow. The flow past arrays of interrupted fins will then be discussed to establish the conditions when in-line or staggered fin arrays are preferred. There will be a brief review of the work done by the Stanford researchers with "pin-fin" designs that did not provide the enhancement in heat transfer which they anticipated. At the end of this section, several design recommendations are presented which should provide interrupted-fin designs that are competitive with continuous-fin designs.

If the fin separation S and the channel width w_c are large, then each fin can be thought of as being a bluff body in a uniform-velocity, and uniform-temperature, flow field. If the Reynolds number is sufficiently large, a bluff-body plate aligned parallel to the flow will have recirculation zones form due to flow separation at the leading edge (see Figure 2.19). It is well known that these recirculation zones can have a significant insulating effect in laminar flow. In turbulent flow, these recirculation zones tend to be less insulative due to periodic shedding and mass transport across the recirculation boundary. For laminar flow of water past long plates ($8 < L/w_w < 16$), Lane and Loehrke (1980) found that a recirculation zone first forms when $Re_t = V_c t/\nu_f \approx 100$. As Re_t is increased, the recirculation zone grows to a maximum

size of $l = 6.5t$ at $Re_t = 325$. At higher Re_t the recirculation is unsteady which causes the zone to decrease in size due to increased momentum transfer. For $Re_t > 500$, the recirculation length is relatively constant at $l \approx 4t$ for both laminar and turbulent flow. For laminar flow of water past short plates ($2 < L/w_w < 4$), Lane and Loehrke (1980), found that the length of the recirculation zone tends to be smaller, but that the reattachment point tends to stick to the trailing edge ($l = L$) for $Re_t > 200$-400. From these results, it can be concluded that Re_t must be very small (say < 100) or that $L >> 4t$ for large Re_t (say > 500). Otherwise, the recirculation zones will extend over a significant portion of the fin length and therefore will retard heat transfer in that region (at least for laminar flow).

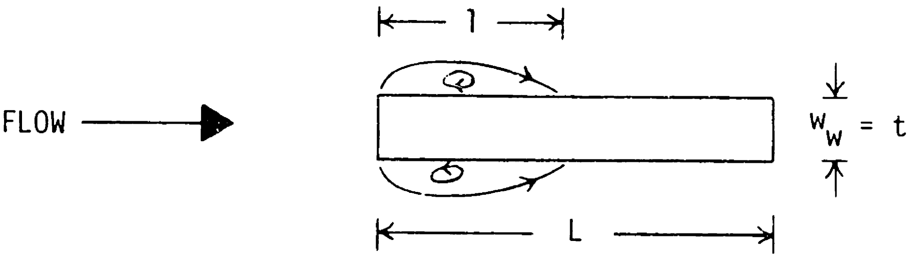

Figure 2.19. Recirculation zones on a flat plate aligned parallel to the flow.

The results for single plates apply for large plate separations. Lane (1980) has studied flow past multiple in-line plates, and found that there was no flow separation for small plate separation ($S < 4w_w$).

Therefore, flow separation and the associated recirculation zones may not be a problem if the plate separation is sufficiently small.

Pairs of co-linear plates aligned parallel to the flow (see Figure 2.20) have been studied by several researchers in order to gain insight into the flow phenomenon that apply to interrupted-fin heat exchangers. In such studies, it is presumed that the downstream plate is more or less representative of interrupted-fin arrays. Cur and Sparrow (1978) obtained the experimental results shown in Figure 2.21. From these results it can be inferred that increasing the Reynolds number and increasing the fin thickness promote flow homogenization with a corresponding reduction in the preheating effect of the upstream plate. The lowest Nusselt numbers are obtained for zero spacing, and there is a tendency of leveling off at higher spacings. It is also clear that the traditional spacing ratio of $S/L = 1.0$ is not necessarily the best spacing even though it is used in many conventional compact heat exchangers. For $w_w/L = 0.04$, if $Re_d = V_c D_e/\nu_f$ is very large, the best plate spacing appears to be $S/L \approx 0.25$. For $w_w/L = 0.04$ and 0.08, if a moderate Re_d is used, the best plate spacing appears to be $S/L \approx 0.5$. For $w_w/L = 0.12$, the best plate spacing appears to be $S/L \approx 0.5$ for low Re_d, and $S/L \approx 1.0$ for large Re_d. Cur and Sparrow (1978) also obtained experimental results for the dimensionless pressure drop shown in Figure 2.22. It is clear that the pressure drop goes up drastically as the plate thickness increases. The percentage increase in the pressure drop is larger than the increase in the mean Nusselt number. In addition, the pressure drop

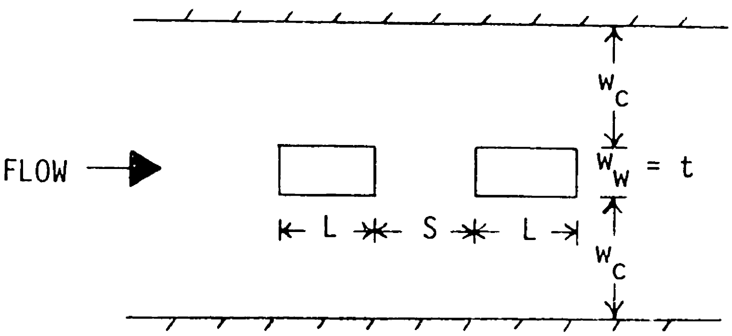

Figure 2.20. Schematic of co-linear plates.

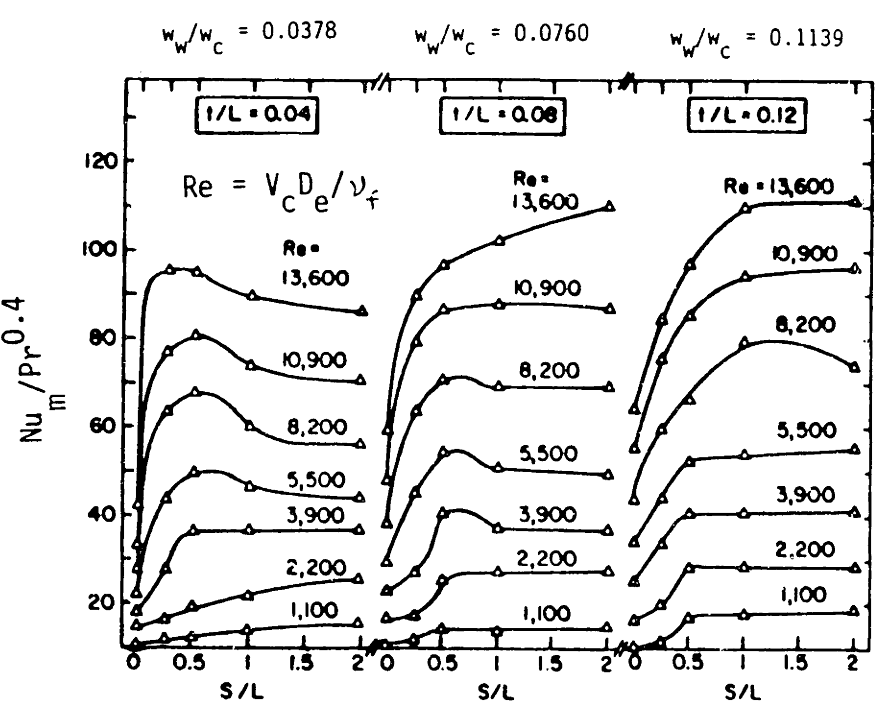

Figure 2.21. Nusselt number variation with inter-plate spacing. [Abstracted from Cur and Sparrow (1978).]

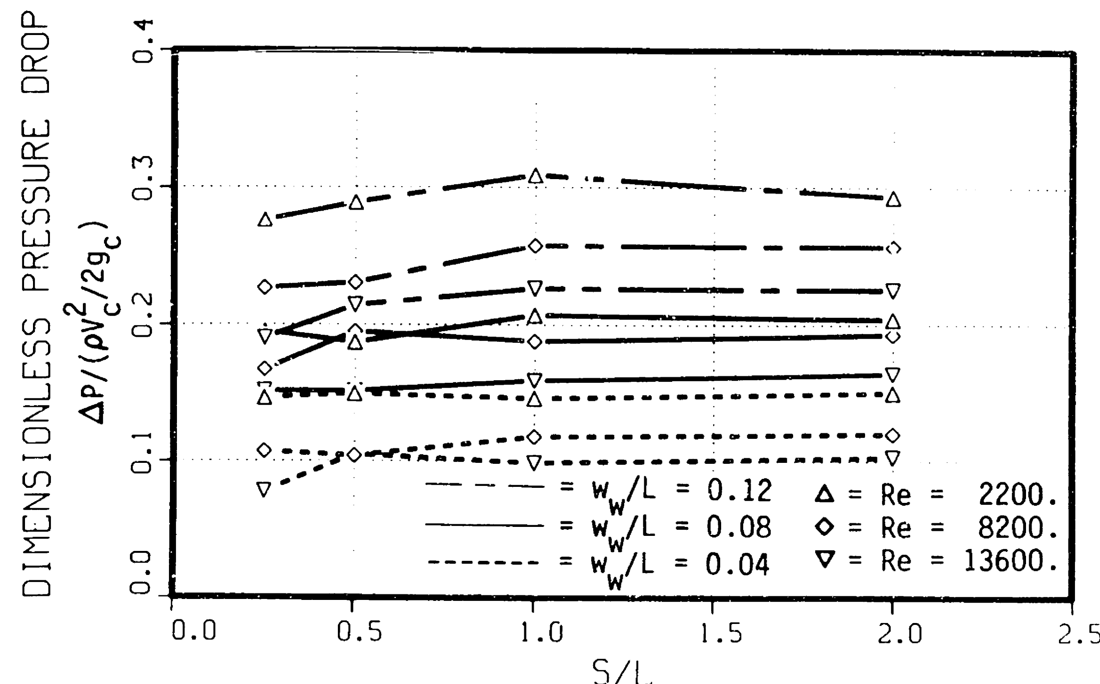

Figure 2.22. Dimensionless pressure drop variation with inter-plate spacing. [Abstracted from Cur and Sparrow (1978).]

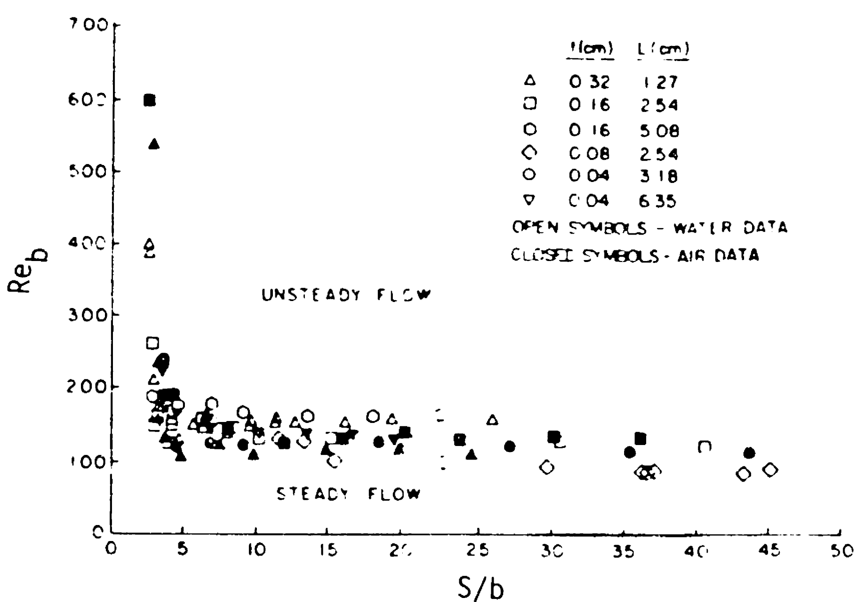

Figure 2.23. Conditions for the onset of periodic flow between co-linear plates. [Taken from Roadman and Loehrke (1983).]

is relatively insensitive to the plate separation, and therefore the plate separation should be selected based on heat transfer considerations.

Roadman and Loehrke (1983) have also investigated the co-linear plate problem. They found that unsteady flow begins for $S/b > 4$ when the Reynolds number based on wake width* $Re_b > \sim 150$ (see Figure 2.23). Higher Reynolds numbers must be achieved before the instability starts when $S/b < 4$. For a given plate separation, increasing the Reynolds number above the critical values increases the amplitude of the wake oscillations in channels.

Loehrke, Roadman, and Read (1976) found that interrupted fins may enhance laminar heat transfer as well as provide an early transition and augmentation in the turbulent regime. Shah and Osborne (1967) found that 1) there is little effect of the plate separation for $S/w_w < 1$ when $Re_t \approx 10{,}000$, 2) there is a transition to turbulence of the separated shear layers for $S/w_w > 1.25$, and 3) that oscillating cross-flow appears between the gap for $S/w_w > 2$. Liang (1975) found that for $Re_t \approx 500$, there is apparently no cross-flow for $S/w_w < 3$.

One potential problem that has not been mentioned is the possibility of exciting resonance conditions within the liquid coolant and/or the fins. Strong acoustic emission has been known to occur due to vortex shedding. It has been shown by Johnson and Loehrke (1984) that the purely hydrodynamic resonance condition (which is independent of the plate

---

* $Re_b = V_c b/\nu_f$ where $b = w_w + 2\theta$ is the boundary layer momentum thickness at the trailing edge of the upstream plate computed using the Blasius profile.

properties) for flow past a pair of co-linear plates can be obtained when $S \approx 4nw_W$ where n is an integer.* The measured sound is low when the plate spacing is out of phase, and highest when the plate spacing is in phase, with the first significant peak occurring when n = 2. This means that plate spacings of S ≈ 8t, 12t, ... should be avoided because they might excite vibration in the fins.

The empirical results obtained using co-linear plates are helpful in understanding the flow phenomenon of interrupted fin heat exchangers, but they do not address neither the effects of fins further downstream, nor the effects of the fins on the opposite side of the adjacent flow channels. Several researchers have numerically analyzed "fully developed" flow in the interrupted-fin arrays shown in Figure 2.18. The flow is "fully developed" in the sense that it obtains a "periodic" fully-developed behavior after a relatively short entrance region of five to ten ranks of plates. Unfortunately, this author is only aware of laminar flow analyses which fix S/L = 1, but a review of such numerical results will provide additional insight.

Sparrow and Liu (1979) analyzed both in-line and staggered arrays with the assumption that the fin thickness was negligible. For the fixed-mass-flow-rate constraint, the in-line arrays had a slightly higher effectiveness, but this was at the cost of a larger relative increment in the pressure drop than the effectiveness increment. For the fixed-pumping-power constraint, the results were mixed. In-line arrays were

* For comparison, S ≈ 4nd for cylindrical rods where d is the rod diameter.

found to have slightly better effectiveness if $Re_d > \sim 1000$ when $L_{ex}/L \approx 10$, and if $Re_d > \sim 1800$ when $L_{ex}/L \approx 20$, where L_{ex} is the heat exchanger length. For lower Re_d at the same and larger values of L_{ex}/L, it was found that staggered arrays had better performance with the cost of a higher mass flow rate (than in-line arrays) which results in system-wide pressure drops that may be larger.

Shah (1979) presents a discussion of a paper by Sparrow, Baliga, and Patankar (1977), in which it is shown that there "appears" to be no advantage in reducing the fin length below a certain value. For $L^* = L/(4HRe_dPr) < 0.0005$, $Nu_{m,T}$ is smaller than that for hydrodynamically developed flow, and for $L^* > 0.017$, $Nu_{m,T}$ is larger than that for simultaneously developing flow (see Figure 2.24). It is shown that $Nu_{m,T}$ approaches an asymptotic limit rather than infinity for small L^*. The conclusion that there is a minimum useful fin length seems plausible.

Patankar and Prakash (1981) have numerically analyzed "periodic" fully-developed laminar flow in staggered interrupted-fin arrays. They found that the heat transfer from the upstream end of the plate was rather small and that the downstream end of the plate was always rather inactive due to the separated flow there.

Wieting (1975) has provided correlations based on empirical data for the friction factor and the colburn modulus ($j = StPr^{2/3}$) for 22 configurations of staggered-fin arrays. The equations were limited to $S/L = 1$, which was shown previously to be not necessarily the best plate spacing. Even so, his results are important because he found that the flow was predominantly laminar for $Re_d < 1000$, and predominantly

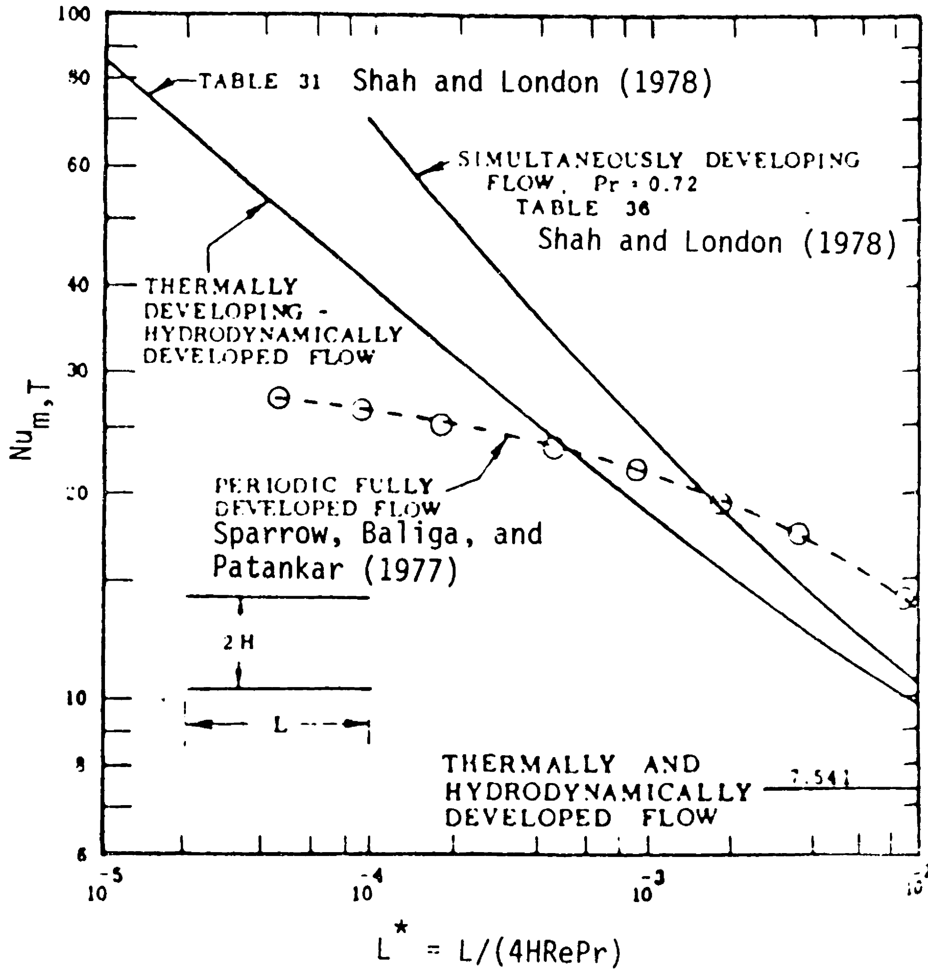

Figure 2.24. Comparison of interrupted-fin and continuous-fin mean Nusselt numbers. [Taken from Shah (1979).]

turbulent for $Re_d > 2000$. The transition region was between Re_d = 1000 and 2000.

Tuckerman and Pease (1981b, 1982) and Tuckerman (1984) have manufactured and tested microchannel heat sinks with interrupted fins. They used an in-line array of "pin-fins" with $w_c = S \approx 55$ µm and $w_w = L \approx 35$ µm. Their experimental results did not show the anticipated heat transfer augmentation, but instead showed a ten percent degradation in the thermal performance. There are several factors which may account for this result, but the most likely ones are that the Reynolds number may have been too low (generally $Re_d < 700$), the ratio of the fin width to the channel width may have been too large to allow vortex generation and unsteady flow to occur, the ratio of the fin length to the fin thickness may have been too low, and the ratio of the fin separation to the fin thickness may have been too small.

From the discussion presented earlier in this section, several design recommendations can be drawn which should provide enhancement in heat transfer. They are:

1) The ratio of the fin separation to the fin length of $S/L \approx 0.5$ appears to be best because of the peak in the curves for the mean Nusselt number at moderate Reynolds number (see Figure 2.21). Note that the pressure drop appears to be relatively insensitive to the fin separation S.

2) The ratio of the fin separation to the fin thickness should be in the range of about $2 < S/w_w < 4$ to insure enhanced mixing due to unsteady flow. Note that $S/w_w \approx 2$ applies for large

Re_t (~ 10^4), and $S/w_w \approx 4$ applies for small Re_t (~ 200). Note also that $S/w_w \approx 8$ was found to be the first significant acoustic peak, but that there is also a small acoustic peak at $S/w_w \approx 4$.

3) Given the two previous design recommendations, the ratio of the fin length to the fin thickness should be in the range of about $4 < L/W_w < 8$.

4) The ratio of the fin thickness to the channel width should be minimized to keep the pressure drop small (hopefully $w_w/w_c < 0.1$).

5) The flow Reynolds number should be about $Re_d > 1000 - 2000$ in order to ensure turbulent flow (if not at least highly mixed laminar flow).

6) Either in-line or staggered arrays can be used, but in-line arrays are generally easier to manufacture.

Interrupted-fin microchannel heat sink designs based on these recommendations should provide a thermal performance which is at least competitive with continuous-fin designs if the coolant flow rate is large enough. The actual thermal-hydraulic performance, though, will probably have to be determined experimentally.

2.9 Chapter Summary

To conclude this chapter, some of the major results will be summarized.

For analysis purposes, it is assumed that there is a "sudden" transition at the critical Reynolds number between laminar and turbulent flow.

The smooth-duct, fully-developed and developing flow, laminar friction factors will be obtained from Table 2.5.

The "laminar equivalent diameter" is used for turbulent flow because the turbulent friction factors predicted using the traditional hydraulic diameter in the Karman-Nikuradse relation are too low. Friction factors for fully-developed and developing turbulent flow in smooth ducts will be obtained using Equation 2.6. The use of this equation appears to be conservative.

The pressure drop in the microchannel heat sink will be obtained using Equation 2.9.

The smooth-duct Nusselt number for fully-developed and developing laminar flow will be obtained using Tables 2.8 and 2.11, and Equation 2.12.

The smooth-duct Nusselt number for turbulent flow will be obtained using the modified Gnielinski correlation (Equation 2.16). The use of this equation appears to be conservative.

The friction factor and Nusselt number for fully developed turbulent flow in repeated-rib roughened channels will be obtained using Equations 2.16 - 2.20. The pressure drop for repeated-rib roughened channels will be obtained using Equation 2.9 with f_1 or f_2 replacing f.

The effect of viscous dissipation will cause the coolant temperature to rise nearly independent of the heating rate (due to property variations). Equation 2.22 will be used to predict the temperature rise.

The effect of superimposed natural convection was studied and found to be small enough to ignore.

The effect of temperature varying properties was found to be important due to variations in the dynamic viscosity. Equations 2.24 and 2.25 will be used to account for the effect on the friction factor and the Nusselt number.

The effect of non-uniform passages was found to be important. Non-uniformity in channel sizes should be kept to within five percent to avoid significant changes in the friction factors and Nusselt numbers.

Finally, the use of interrupted-fin channels was reviewed, and several design recommendations were listed. It will be shown in Section 4.7 that interrupted-fins will be used primarily for thermal spreading enhancement downstream of "hot spots", and for prevention of catastrophic failure due to channel clogging.

3.0 CONDUCTION HEAT TRANSFER

The purpose of this chapter is to provide an overview of conduction heat transfer in solids as it applies to this study. The physics of the heat conduction process will be briefly discussed. Following this will be an overview of theoretical models used to predict the temperature drop through materials with continuous and discrete, heat sources and sinks. An analysis of heat transfer from extended surfaces (fins) will then be presented. An analysis will be presented that models the thermal spreading at the heater perimeter.

3.1 Physics of the Heat Conduction Process

The rate at which energy is diffused in a material is proportional to the temperature gradient and the thermal conductivity of the material. Several carriers of heat can contribute to the thermal conductivity. Some of them are: phonons (the quantized modes of vibration of the atoms in the solid), electron-hole pairs, and separate electrons and holes. The thermal conductivity k_w is composed of the contributions of each carrier. It can be shown that

$$k_w = \frac{1}{3} \sum_j C_j v_j \lambda_j \tag{3.1}$$

where j denotes each type of carrier, C_j is the contribution of the carrier j to the specific heat per unit volume, v_j is the velocity of the carrier, and λ_j is the mean free path. The dominant carrier mode in pure metals (resistivities up to 5 μΩ cm) is electron flow [Touloukian (1970)]. In semiconductors, virtually all of the heat is transferred by phonons at temperatures below 600°K [Maycock (1967)].

The mean free path of the carrier is of importance, because if it is too large, it will be necessary to make corrections in the heat conduction equation that accounts for the microscopic theory of heat flow. Conversely, if the mean free path is small compared to the size of the device structures, then the macroscopic or continuum theory of conduction is adequate.

For moderate temperatures, it is known that the phonon mean free path decreases with increasing temperature. For example, Gereth and Hubner (1964) determined that silicon has a phonon mean free path of about 20 μm at 200°K, which decreases to about 11 μm at 260°K. Extrapolation of their results indicates that the phonon mean free path is much less than 10 μm at room temperature. Tuckerman (1984) presents a phonon mean free path of silicon at room temperature that is much smaller than 1 μm. Since the smallest dimension of the microchannel heat sink structures is typically greater than 50 μm, it appears reasonable to use the continuum theory of conduction if the operating temperature is kept above say 200°K.*

The thermal conductivity of several pure materials is shown in Figure 3.1. In general, the thermal conductivity of the metals is much higher than that of semiconductors due to the effectiveness of free electron carriers in pure metals. It is difficult to predict the thermal

* Literature searches in several data bases proved unsuccessful in determining the phonon mean free path of indium phosphide (InP), which is the material of primary interest for this study. It is expected that the phonon mean free path of InP will be in the sub-micron range at room temperature [Walpole (1986)].

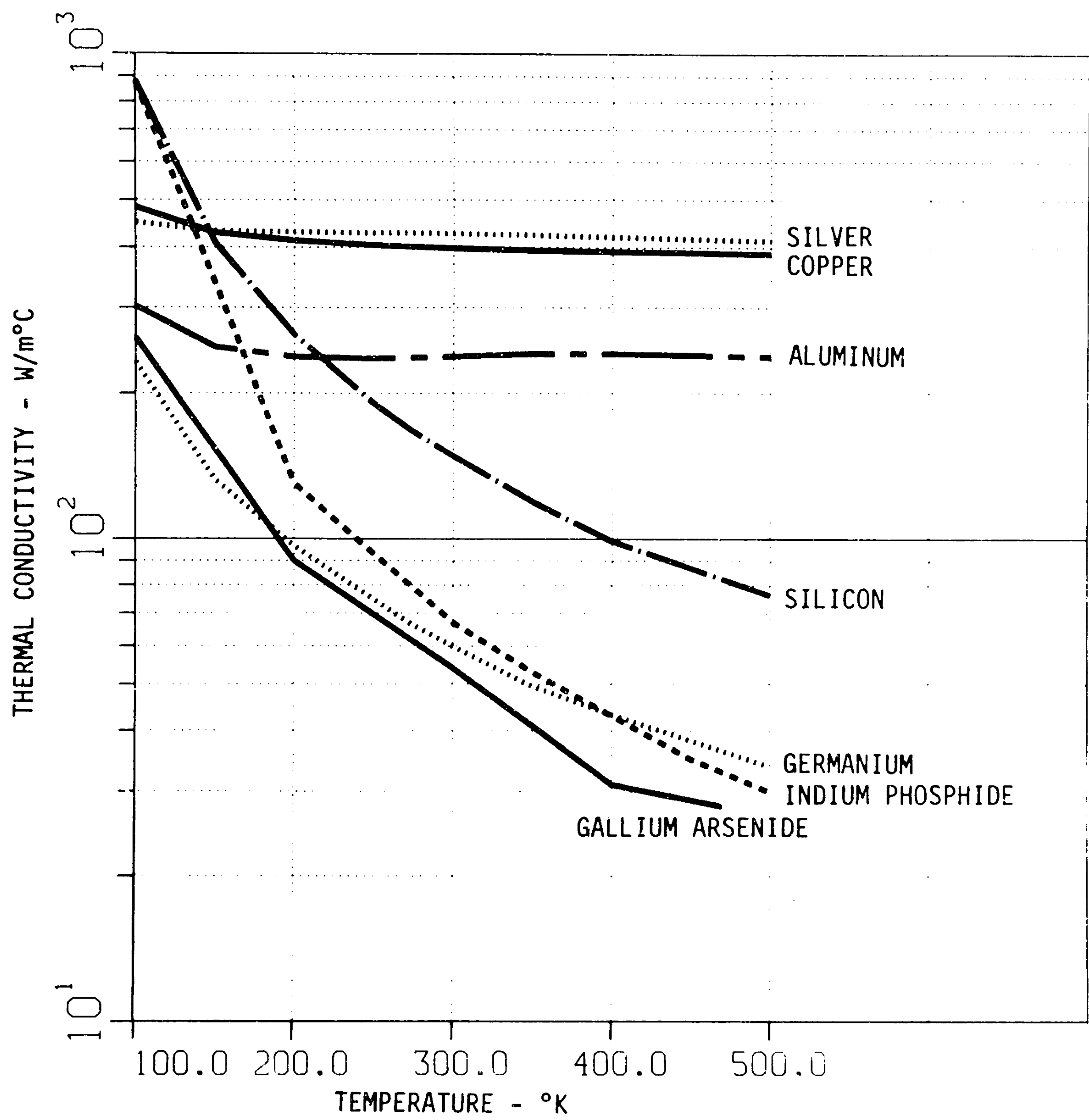

Figure 3.1. Thermal conductivity versus temperature of various materials. [Thermal conductivity values obtained from the sources listed in subroutines PROPS1-7 (see Appendix E).]

conductivity of a material due to variations in the number of dislocations, the doping level, and the amount of alloying. Maycock (1967) asserts that the thermal conductivity may be reduced by as much as 30 percent by high levels of doping.* The effect of alloying is even more severe, as Figure 3.2 clearly shows.

Clearly, small changes in the composition of a material can have a significant affect on the thermal conductivity. The validity of the thermal response predictions will be sensitive to the accuracy of the thermal conductivity values used (See Chapter 4).

3.2 Continuous and Discrete Heat Sources and Sinks

The purpose of this section is to present the equations that are used to compute the temperature gradients in several portions of the heat flow path, from the heat generating source(s) to the ultimate heat sink - the liquid coolant. Equations will be presented here for conduction through planar slabs, and for conduction through "constrictions" in the heat flow path.

Heat transfer by conduction through a continuous plane slab is shown in Figure 3.3 for the case of no internal heat generation, steady state, and uniform thermal conductivity. The heat flow is easily determined to be

$$q'' = -k_w \frac{dT}{dz} = \frac{k_w}{t} (T_1 - T_2) \qquad (3.2)$$

* Apparently, a good "rule of thumb" is to decease the conductivity obtained for pure semiconductors by 20 percent for highly doped samples [Maycock (1967)].

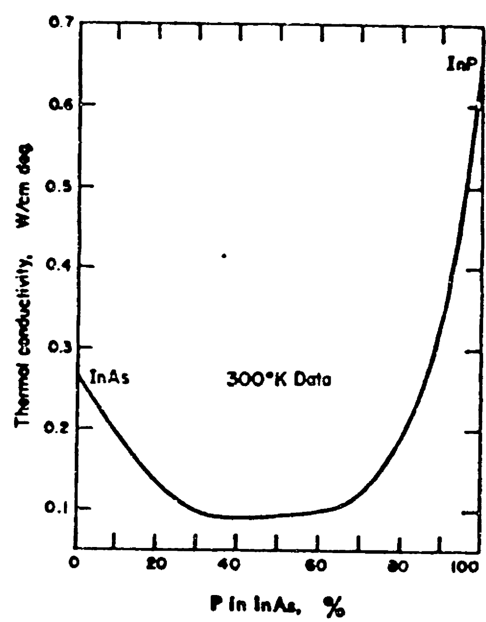

Figure 3.2. Thermal conductivity of In-As-P. [Taken from Maycock (1967).]

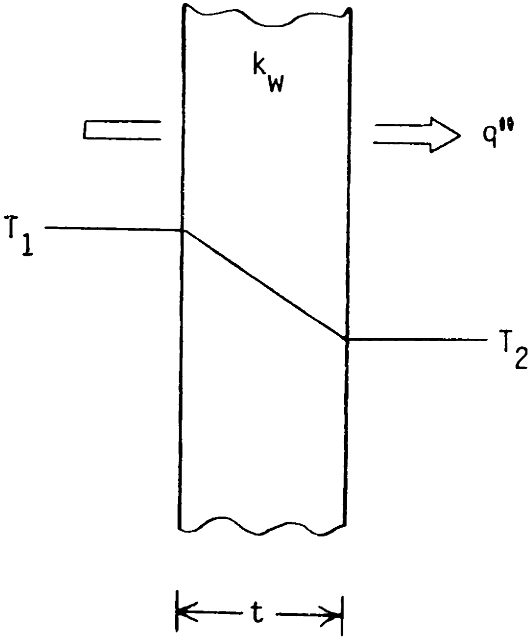

Figure 3.3. Heat transfer by conduction through a plane slab.

where q" is the heat flow rate per unit area, t is the slab thickness, T_1 is the hot surface temperature, and T_2 is the cool surface temperature.

Kraus and Bar-Cohen (1983) present the analysis done by Mikic' for determining the temperature at discrete heat sources and sinks on the face of the conducting medium. Figure 3.4 shows this "constriction effect" where the heat flow diverges (converges) in the region next to the heat source (sink). The temperature drop between the center of the heat source (sink) on one side of a planar slab, and a uniform heat sink (source) on the other side of the slab is given by

$$\Delta T_{tot} = \Delta T_o + \Delta T_c \tag{3.3}$$

where ΔT_{tot} is the overall temperature difference, ΔT_o is the temperature difference obtained assuming a uniform source on one side and a uniform sink on the other (Equation 3.2), and ΔT_c is the constriction effect.

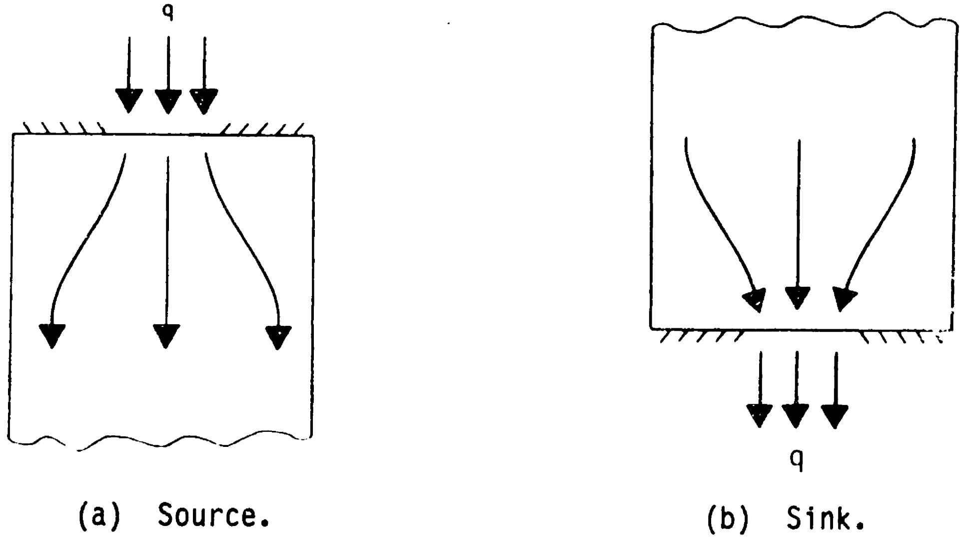

(a) Source. (b) Sink.

Figure 3.4. Heat flow "constriction effect".

Mikic' has determined the relationships for ΔT_c for a variety of cases. Three are of interest for this study. They are:

1. A circular heat source on an infinite conducting medium (Figure 3.5a)

$$\Delta T_c = \frac{q}{2\sqrt{\pi} a k_w} \tag{3.4}$$

2. A long strip heat source on a finite conducting medium (Figure 3.5b)

$$\Delta T_c = \frac{q}{\pi L k_w} \ln \left[\frac{1}{\sin(\pi a/2b)}\right] \tag{3.5}$$

where L >> a and L >> b, and finally

3. A finite length, strip heat source on a finite conducting medium (Figure 3.5c)

$$\Delta T_c = \Delta T_{c1} + \Delta T_{c2} + \Delta T_{c3} \tag{3.6}$$

where

$$\Delta T_{c1} = \frac{q}{2\pi^2 k_w} \cdot \frac{b}{ac} \sum_{m=1}^{\infty} \frac{\sin(m\pi a/b)}{m^2}$$

$$\Delta T_{c2} = \frac{q}{2\pi^2 k_w} \cdot \frac{c}{db} \sum_{m=1}^{\infty} \frac{\sin(m\pi d/b)}{m^2}$$

and $$\Delta T_{c3} = \frac{q}{2\pi^2 k_w} \cdot \frac{2}{ad} \sum_{m=1}^{\infty} \sum_{n=1}^{\infty} \frac{\sin(n\pi d/c)\ \sin(m\pi a/b)}{mn[(m\pi/b)^2 + (n\pi/c)^2]^{1/2}} .$$

The dimensions a, b, c, d, and L are defined as shown in Figure 3.5.

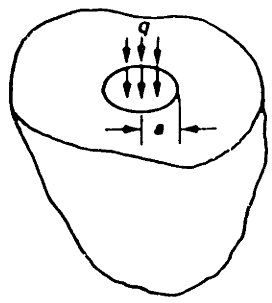

a) Circular heat source.

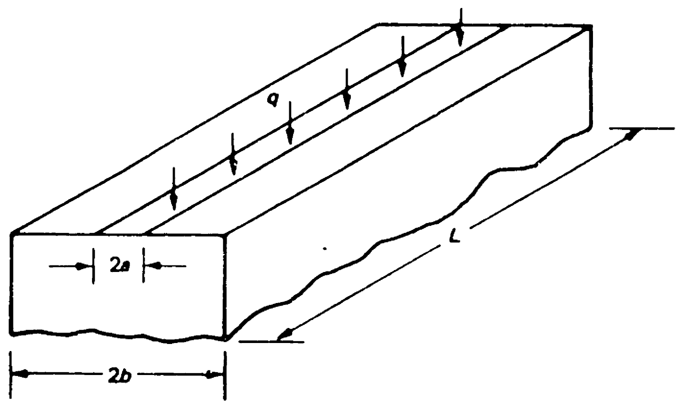

b) Long strip heat source.

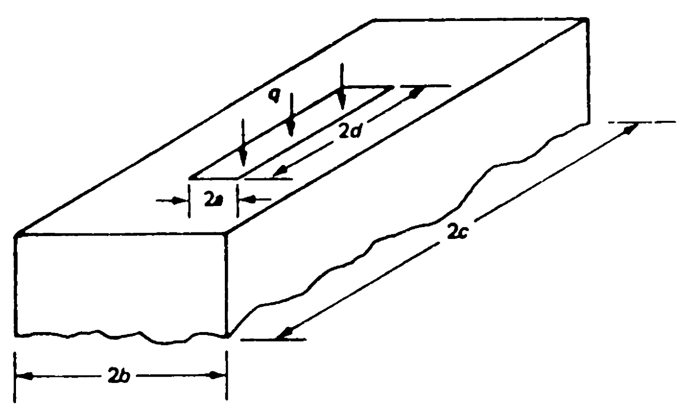

c) Short strip heat source.

Figure 3.5. Schematics of discrete heat sources.

3.3 Fin Heat Transfer

Inspection of the heat transfer equation $q = hA_{surf}\Delta T$ shows that in order to obtain a larger rate of heat transfer q, for the same (or smaller) ΔT, it is necessary to increase the hA_{surf} product. One way to increase the hA_{surf} product is to increase A_{surf} by using fins.

Several fin shapes are commonly used to augment heat transfer. In this study, only two shapes are good candidates. The channel fabrication methods of precision sawing and orientation dependent etching in indium phosphide result in the nearly rectangular and triangular channel configurations as shown in Figure 3.6. The triangular shape only increases the surface area by about 30 percent (if $w_w \approx 0$). The rectangular shape allows surface area increases of 400 percent for etching, and more than 1000 percent for precision sawing! Therefore, this study will limit itself to rectangular channels and rectangular fins.

Several assumptions are employed to limit and simplify the analysis of fin heat transfer. In this study, thirteen assumptions are used. Each assumption will be listed, and each one will be followed by a discussion of how realistic it is for this study. The solution of the fin heat transfer will be delayed until all thirteen assumptions have been discussed.

Assumption 1: The liquid coolant flow is steady and incompressible.

For all practical purposes, the liquid coolants used in this study are incompressible since the pressure drop across the heat sink is limited to a few atmospheres. Steady flow may be approximated if there is a suitably sized accumulator upstream of the heat sink.

a) Precision sawing.

$Br:CH_3OH$ (2:98) $H_3PO_4:HCl$ (3:1)

b) Orientation dependent etching [channels on 0.010 in. centers in the (01$\bar{1}$) direction].

Figure 3.6. Channel configurations obtained by precision sawing and orientation dependent etching.

Assumption 2: The power dissipated by the integrated circuit is constant spatially and temporally.

As a consequence of this and the previous assumption, the fin temperature profile does not vary with time. The primary interest of this study is to compute the worst-case thermal resistance under steady state conditions. Transient thermal response will occur when the chip is turned "on" ("off"), and when individual gates in the integrated circuit are turned "on" ("off"). For this study, the chip time constants are much less than one second. Therefore, the use of steady state analysis to model "reality" is a good approximation provided that the frequency of operation (cycling) is small enough (say << 1.0 cycles/second). The time constants for the individual integrated circuit gates are very small. This is due to their small feature size. It is reasonable to assume that the effect of individual gates becoming active (inactive) is small since the overall power dissipation does not change much.

Assumption 3: The fin thermal conductivity is isotropic (independent of crystal orientation) and constant over the entire length of the fin.

Anisotropicity of the fin thermal conductivity does not appear to be important for the heat sink materials used in this study, and therefore will be ignored in the analysis. The thermal conductivity is, though, a function of the fin temperature which does vary along the fin length. In this study, the thermal conductivity is evaluated at an "average" fin temperature to help compensate for this effect. If the heating rate is enormous, the variation in the thermal conductivity would be very large.

It would then be necessary to solve the fin conduction equation with temperature dependent thermal conductivity, or to divide the fin into several short sections with locally constant thermal conductivity. The latter method was used in the early stages of this study, but was abandoned due to the small increase in computational "accuracy" obtained with a large increase in computer costs. Appendix A presents a solution procedure for the sectioned-fin case that the reader can use to modify the computer program.

Assumption 4: The thickness of the fin is constant.

The accuracy of this assumption will of course depend on method(s) used to fabricate the microchannels. As shown in Figure 3.6, it is apparent that the fin thickness is <u>not</u> constant for sawn channels, which show "rounded" channel bases and some fin tapering. The rounded region is generally limited to less than five to ten percent of the overall fin length. Assuming that the fin thickness is constant is conservative because the thermal contraction resistance will be slightly smaller than that predicted using Equation 3.5 where the channel base is assumed to have sharp corners. In addition, the rounding at the base of the channel will tend to reduce the non-uniformity in the heat transfer coefficient in that region (see Assumption 13). The fin thickness non-uniformity is not a problem for channels fabricated using orientation dependent acid etching in indium phosphide (see Figure 3.6).

Assumption 5: The temperature gradient through the fin thickness is much smaller than the temperature gradient along the height of the fin.

If a fin is thick or short, the isotherms through the fin thickness will be curved. Conversely, a thin fin has isotherms that are relatively straight Rohsenow and Choi (1961) provide the following criterion which must be satisfied for thin fins

$$\frac{2k_w}{hw_w} = \frac{2k_w D_e}{Nu k_f w_w} > 6.0 \tag{3.7}$$

where D_e is the equivalent diameter of the flow channel. For this study, the criterion is easily satisfied. For example, laminar flow of water ($k_f \approx 0.6$ W/m°C) in a large aspect ratio channel (D_e of order 100 μm) in indium phosphide ($k_w \approx 70$ W/m°C) with Nu ≈ 8.0 and w_w of order 50 μm, the fin criterion is satisfied because 58 >> 6.0. For the same case, but turbulent flow (Nu ≈ 50), the criterion is satisfied because 9.3 > 6.0.

Assumption 6: There are no heat sources within the fin.

For this study, this assumption is valid since electrical current does not flow through the fins. Appendix B presents the solution of a fin with internal heat generation that the reader can use to modify the computer program to suit their specific application.

Assumption 7: The fin tip is adiabatic (insulated).

The heat flow paths at the fin tip are shown in Figure 3.7. In reality, some heat will be conducted from the fin tip, through the epoxy layer and the cover plate, and finally convected away by the fluid. To be conservative, this heat flow is ignored.

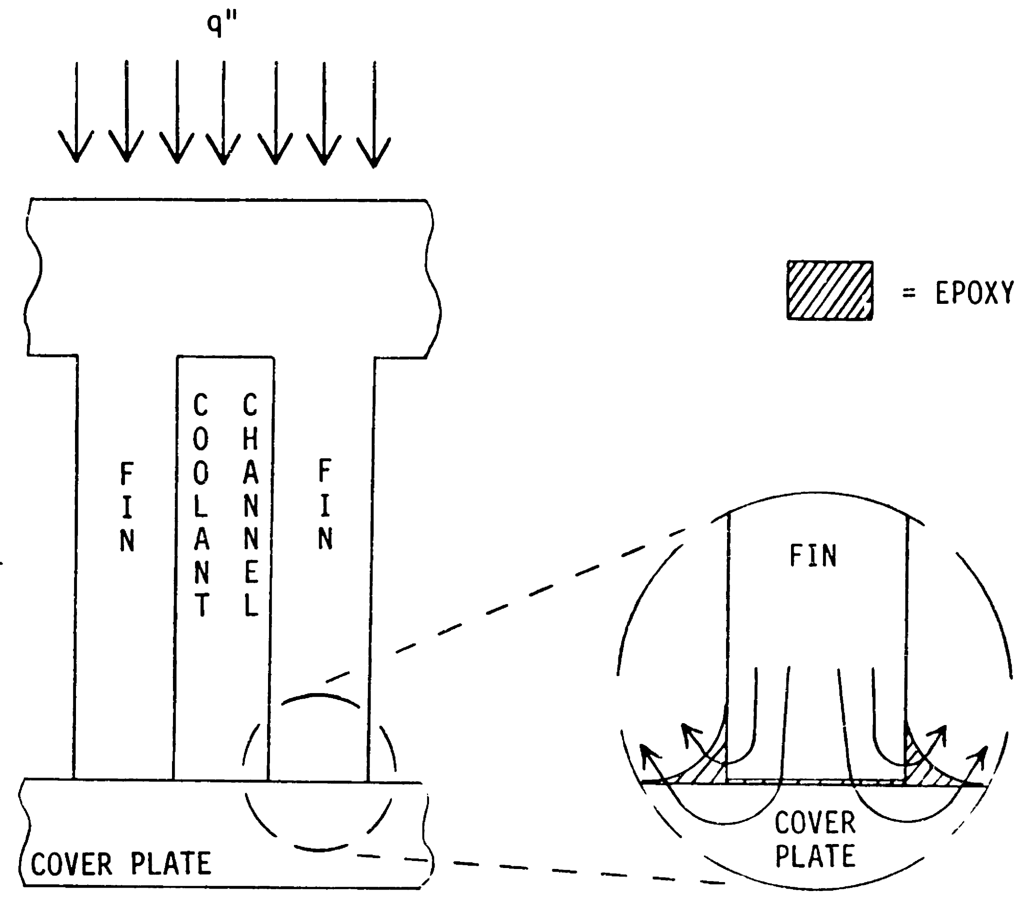

Figure 3.7. Heat flow paths in the region of the fin tip.

Assumption 8: The thin epoxy film on the sides of the fin tips has a negligible affect on the overall heat transfer.

Epoxy is used in this study to attach the cover plate to the heat sink (See Figure 3.7). A good seal is obtained because the epoxy "wets" the indium phosphide thereby forming the rounded appearance at the bottom of the channel. The epoxy film on the sides of the fins will reduce the heat transfer from the fin tip. Since a controlled amount of epoxy is used (typically $t_{epox} < 1.0$ µm, see Chapter 5), the thermal resistance of the epoxy film near the fin tip is ignored because it is nearly an order of magnitude smaller than the convective thermal resistance which is proportional to 1/h. The effect of this thin epoxy layer on the heat transfer is also ignored because some heat will be conducted through the fin tip (Assumption 7). This assumption (#8) would not be needed if other methods of cover plate attachment were used such that no foreign substance coats the fin sides (e.g., anodic bonding).

Assumption 9: Heat transfer due to radiation and superimposed natural convection is small and can be ignored.

The effect of superimposed natural convection was discussed in Section 2.5, where it was found to be negligible for the channel sizes commonly used in microchannel heat sinks.

The effect of radiation heat transfer is also small. For example, if the fin surface temperature is 100°C (definitely a worst case assumption for this study), and if the fins ($\epsilon = 1.0$) increased the surface area by a factor of ten, then the heat transferred by radiation can be no more than 1.1 W/cm^2 per unit chip circuit area. This is a small

portion of the overall heat dissipation which can be much larger than 100 W/cm^2 per unit chip circuit area.

Assumption 10: The fin base temperature is uniform.

The coolant temperature will increase with distance from the channel entrance. This will cause the fin base temperature to increase in the downstream direction. If the coolant flow rate is small, the temperature non-uniformity will be large. Conversely, if the flow rate is large, the bulk temperature rise of the coolant will be smaller, which will result in a more uniform fin base temperature. The effect of the coolant temperature gradient is to cause conduction of heat from the downstream end of the chip (hot end) to the upstream end of the chip (cold end). Axial heat conduction in the coolant has already been discussed in Section 2.3, where it was found to be small enough to ignore. Axial heat conduction in the fin material can be significant, but will be ignored in order to be conservative. It is conservative to ignore it because the thermal resistance (See Chapter 4) computed at the downstream end of the heat source will be larger than that computed if axial conduction is considered. Note that the effect of lateral heat spreading at the periphery of the heat source will be discussed in Section 3.4.

Assumption 11: The temperature of the primary surface (channel base) and the fin base are the same.

The temperature of the fin base will be lower than the temperature of the channel base because of the higher rate of heat transfer through the fin base compared to that from the channel base. Shah in Rohsenow, Hartnett, and Ganic (1985a) provides an overview of this effect where it

is found that the fin base temperature depression results in lower heat transfer from the channel base. It is also found that the total heat transfer rate from straight fins computed using a two-dimensional analysis is always higher than that computed using one-dimensional analysis. Therefore, ignoring the fin base temperature depression will result in a conservative prediction of the heat transfer rate.

Assumption 12: The temperature of the coolant surrounding the fin is uniform at a given axial distance from the channel entrance.

This assumption implies that the properties of the coolant are also constant, and that they should be evaluated at some average or bulk temperature of the coolant. It is known that the temperature of the coolant in the base region of the fin will be greater than the coolant temperature in the tip region. This results in a somewhat lower heat transfer rate at the base of the fin than would normally be expected. In reality, some thermal mixing of the coolant does occur, but this mixing is not complete. Coolant temperature non-uniformity should not be a problem for turbulent flow in moderate aspect ratio channels due to turbulent mixing. To simplify the analysis of the heat transfer coefficient, it is necessary to assume that there is complete thermal mixing of the coolant (discussed with the following assumption).

Assumption 13: The heat transfer coefficient is uniform over the surface of the fin at a given axial distance from the channel entrance.

The local heat transfer coefficient varies along the fin height and is defined at every axial distance (x) downstream from the channel entrance by

$$q'' = h(z)\left[T_w(z) - T_f(z)\right] \tag{3.8}$$

where q" is the rate of heat transfer per unit area, h(z) is the local heat transfer coefficient, $T_w(z)$ is the local fin temperature, and $T_f(z)$ is the local coolant temperature. It is very difficult to determine $T_f(z)$ without the aid of a two-dimension flow field analysis. Therefore, an alternate definition of the heat transfer coefficient is often used which is

$$q'' = h(z)\left[T_w(z) - T_b\right] \tag{3.9}$$

where T_b is the bulk temperature of the coolant at the distance of interest downstream from the channel entrance. It should be noted that the value of the local heat transfer coefficient h(z) determined by Equations 3.8 and 3.9 will be different. Equation 3.9 is used more often, because T_b is more easily determined than $T_f(z)$.

Several researchers have modeled fin heat transfer using Equations 3.8 and 3.9. The most notable ones that this author is aware of are: Han (1959), Sparrow, Baliga, and Patankar (1978), and Kadle and Sparrow (1986).

Han (1959) analyzed the flow in moderate-aspect-ratio rectangular channels that were heated as shown in Figure 3.8. Heat is conducted through the fins, thereby forming a non-uniform temperature profile around the channel. Han defines a corrected Nusselt number using

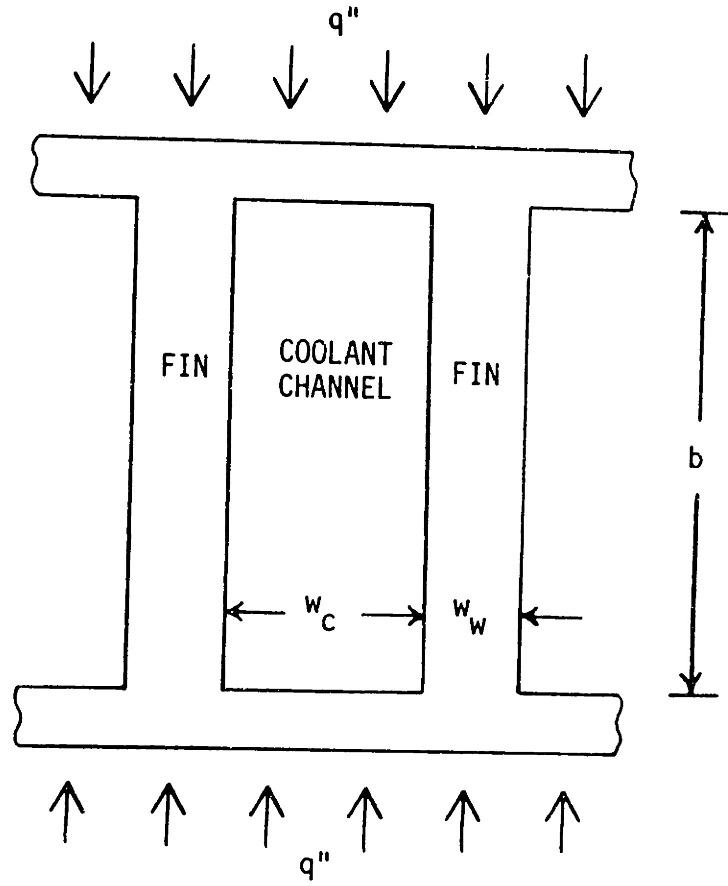

Figure 3.8. Flow channel configuration used by Han (1959).

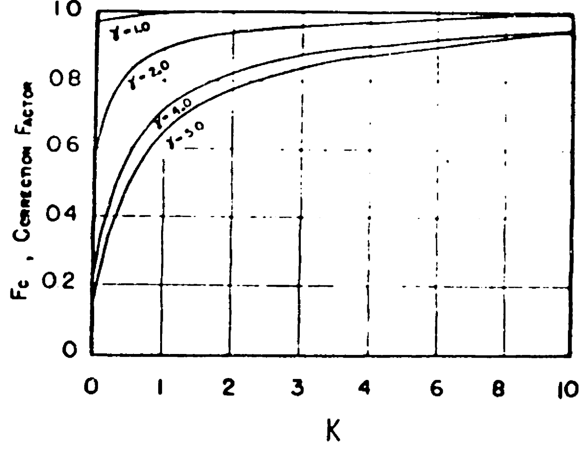

Figure 3.9. Correction factor for finite fin conductivity. [Taken from Han (1978).]

$$Nu = Nu(k_w = \infty)Fc(K,\alpha) \qquad (3.10)$$

where Fc is a dimensionless correction factor which is a function of the fin parameter $K = w_w k_w/2bk_f$, and the channel aspect ratio α. The Nusselt number for the case of infinite fin thermal conductivity, $Nu(k_w = \infty)$, has already been discussed in Chapter 2. Han's results for the correction factor are plotted in Figure 3.9. The curves clearly show that there is only a small reduction in the Nusselt number if the fin parameter K is large. In this study, K is large. For example, water ($k_f \approx 0.6$ W/m°C) flowing through indium phosphide ($k_w \approx 70$ W/m°C) with a channel height of order 200 μm and a fin thickness of order 50 μm results in $K \approx 14.5$. Therefore, the variation of the average Nusselt number should be small (at least for moderate aspect ratio channels).

A channel geometry very similar to the one used for this study was analyzed for laminar flow by Sparrow, Baliga, and Patankar (1978), and for turbulent flow by Kadle and Sparrow (1986). The channel configuration is shown in Figure 3.10.

The results indicate that the Nusselt number is relatively uniform in the central region of the fin, and then drops off very rapidly near the fin base and the fin tip. The Nusselt number at the fin base was nearly zero due to the two-dimensional heat transfer and the warmer coolant temperatures in that region. At the fin tip, the Nusselt number was about half the value of the central region. The Nusselt number along the base of the channel varied from a maximum at the center of the channel to nearly zero near the base of the fin. The maximum channel base Nusselt number was about half to three quarters of the value in the central

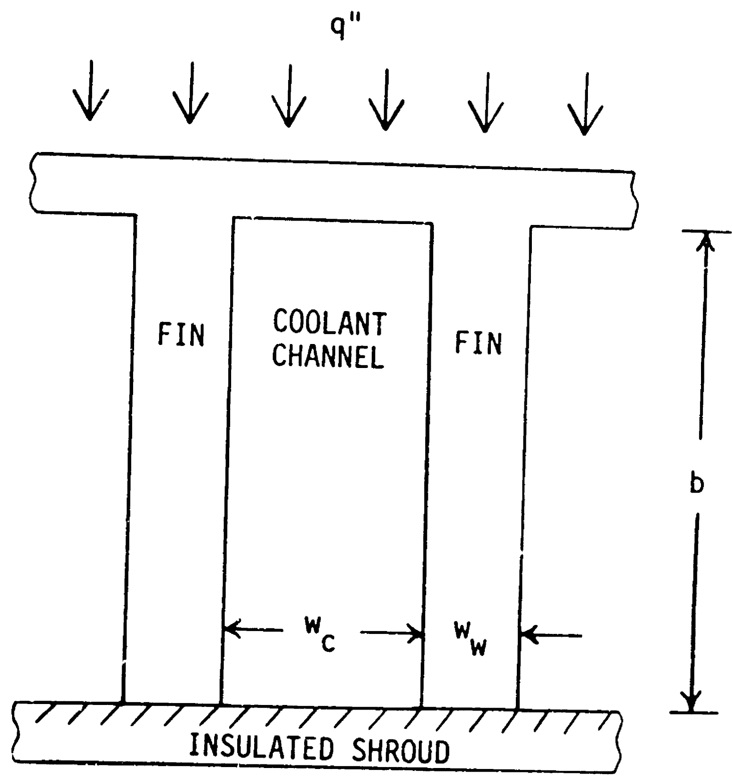

Figure 3.10. Flow channel configuration used by Sparrow, Baliga and Patankar (1978), and Kadle and Sparrow (1986).

region of the fin. Kadle and Sparrow (1986) compared their numerical values for the average Nusselt number with their experimental data. They found excellent agreement between the experimental data, their complicated numerical model, and the traditional fin analysis.

A simplified fin conduction model, which is based on the thirteen assumptions discussed above, should provide a reasonable estimate of the fin thermal response. Gardner (1945) discusses the results of several other researchers who arrive at a similar conclusion. Note that Shah in Rohsenow, Harnett, and Ganic (1985a) finds that the violation of Assumptions 11 through 13 will reduce the actual fin efficiency from calculated values if $\eta_f < 80$ percent.

The remainder of this section is devoted to solving the fin conduction equation. The differential equation modeling the one-dimensional heat conduction through the fin shown in Figure 3.11 is

$$\frac{d^2\theta}{dz^2} - m^2\theta = 0 \tag{3.11}$$

where $\theta = [T(z) - T_b]$ and $m^2 = 2h/k_w w_w$. The distance measured from the fin tip is z, the fin temperature at z is T(z), the coolant bulk temperature is T_b, the average heat transfer coefficient is h, the average fin thermal conductivity is k_w, and the fin thickness is w_w. The boundary conditions for Equation 3.11 are: $\theta = \theta_b = T(z = b) - T_b$ at $z = b$, and $d\theta/dz = 0$ at $z = 0$. The solution for the fin temperature profile is easily obtained as

$$\frac{\theta}{\theta_b} = \frac{\cosh (mz)}{\cosh (mb)} \quad . \tag{3.12}$$

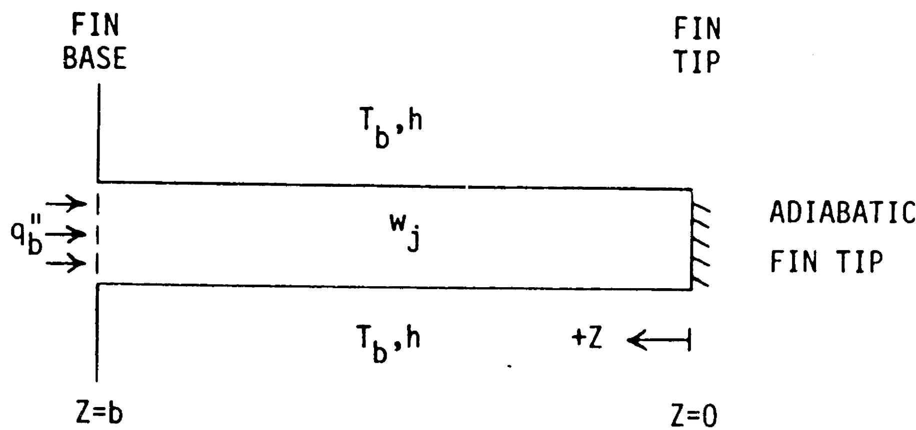

Figure 3.11. One-dimensional fin model.

Using $q''_b = k_w d\theta/dz$, the heat flow per unit area at the fin base is found to be

$$q''_b = k_w m\theta_b \tanh(mb) = \eta_f(2\delta)h\theta_b \tag{3.13}$$

where the aspect ratio of the fin is $\delta = b/w_w$, and the fin efficiency is $\eta_f = [\tanh\,(mb)]/mb$.

Kern and Kraus (1972) have computed the optimum lengths of w_w and b for the case of a fin with a fixed profile area $A_p = w_w b$ (See Appendix C). The optimum fin thickness is

$$w_w = 0.791\ (\frac{2h\ b^2}{k_w})^{1/3} \tag{3.14}$$

and the corresponding optimum fin length is

$$b = 1.262\ (\frac{k_w w_w b}{2h})^{1/3}\quad . \tag{3.15}$$

Equations 3.14 and 3.15 can be used to obtain an optimum aspect ratio $\delta = b/w_w$ (See Appendix C). The result is

$$\delta = -\frac{1}{2}\frac{w_c}{w_w} + \frac{1}{2}\ [(\ \frac{w_c}{w_w}\ )^2 + 8.056\ \frac{k_w\ \ w_c}{k_f Nu w_w}\ ]^{0.5} \tag{3.16}$$

where w_c is the channel width. Equation 3.16 is particularly useful in the analysis of large aspect ratio channels (See Section 4.3.2). It does not consider the heat transfer from base surface of the coolant channel.

3.4 Thermal Spreading At The Heat Source Perimeter

In the model of the heat transfer through the fins in the z-direction (through the thickness of the chip), it was assumed that the

fin base temperature was uniform (Assumption 10). This assumption implies that there is an abrupt drop in temperature at the periphery of the heat source where the heat flux suddenly changes to zero. This situation is not in agreement with reality since lateral heat conduction at the heater perimeter will provide for a gradual transition in temperature.

The fin shown in Figure 3.12 will be used to model thermal spreading at the heat source perimeter. The thirteen assumptions used in Section 3.3 will also be used here. In addition, if the coolant flow rate is large, then it can be assumed that the bulk temperature rise of the coolant is small. Therefore, the coolant temperature is assumed uniform everywhere. For simplicity, it is also assumed that the heat transfer coefficient is uniform over the entire length of the channel (ignores developing flow). Since the fluids used in this study have thermal conductivities that are much smaller than those of the chip materials, the effects of conduction within the liquid coolant will be ignored. Finally, it is also assumed that the thermal spreading effect can be evaluated by superimposing two, one-dimensional models - one in the streamwise (flow) direction, and the other in the transverse direction. This assumption is valid near the centers of the sides of a large rectangular heat source, but breaks down near the corners of the heat source where the heat flow is two-dimensional.

The differential equation modeling the thermal spreading for the heated region is

$$\frac{d^2\theta_1}{d\,x_1^2} - m^2\theta_1 + \frac{q''}{k_w H_{eff}} = 0 \tag{3.17}$$

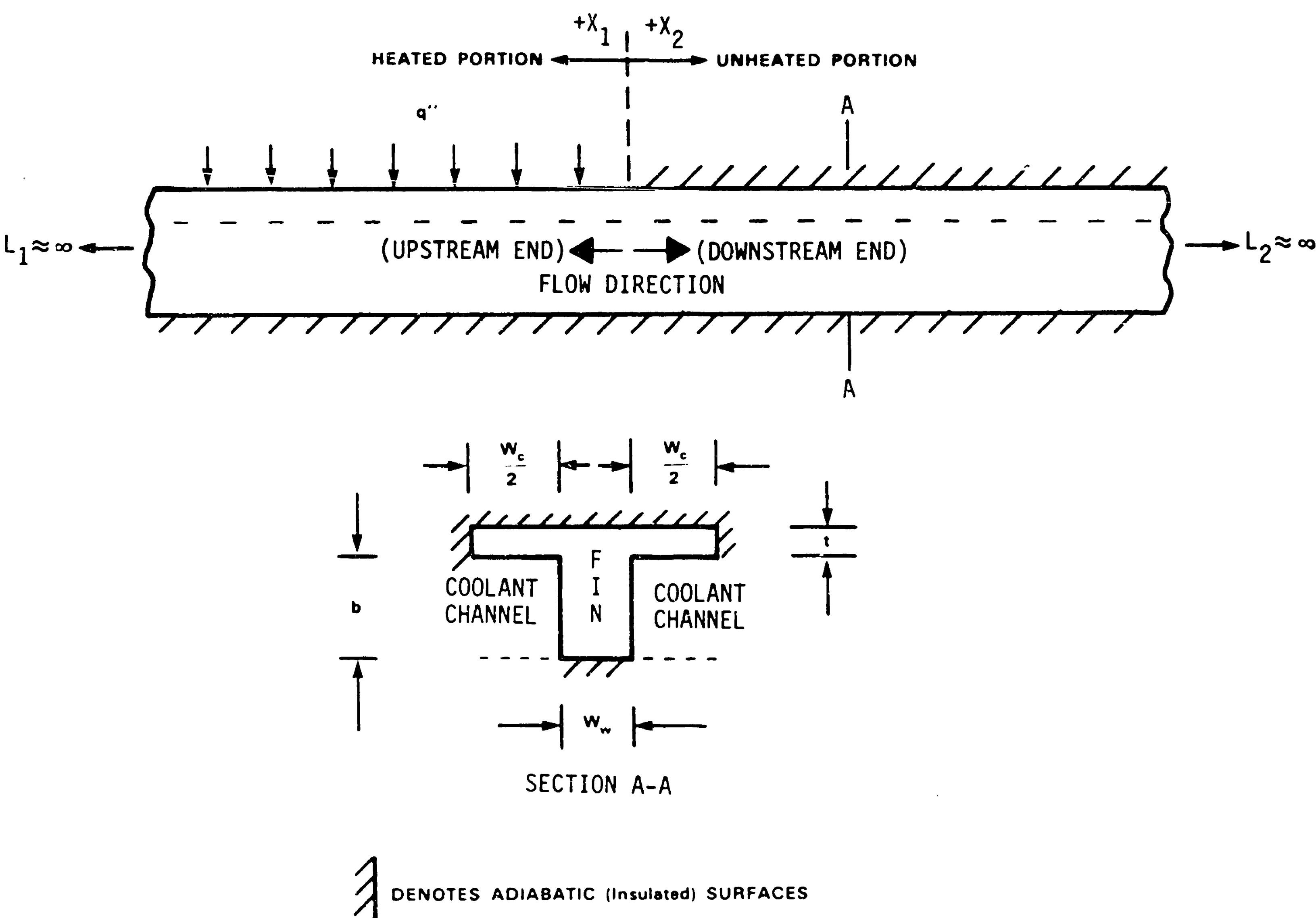

Figure 3.12. Fin model for thermal spreading at the heater perimeter.

and for the unheated region is

$$\frac{d^2\theta_2}{d\,x_2^2} - m^2\theta_2 + 0 = 0 \tag{3.18}$$

where $m^2 = hP/k_w H_{eff} W$, $\theta = T_w(x) - T_b$, q'' is the surface heat flux per flux per unit circuit area, k_w is the fin thermal conductivity, h is the heat transfer coefficient, P is the length of the convective heat transfer perimeter, W is the fin width over which P is determined, and H_{eff} is the effective fin thickness.

In the streamwise direction (x-direction), the effective fin thickness is assumed to be $H_{eff} \approx [w_c t + w_w(b+t)]/(w_w + w_c)$ and the convective heat transfer perimeter is $P \approx w_c + 2b$ (note that $W \approx w_w + w_c$), where t is the substrate thickness, w_c is the channel width, and w_w is the extended surface thickness (of the fins that define the coolant channels). For the transverse direction (y-direction), the effective fin thickness is the same or perhaps as small as $H_{eff} \approx t$. The convective heat transfer perimeter for the transverse direction is $P \approx x(2b + w_c)/(w_w + w_c)$, and $W = x$.

If the heater is large enough, the temperature gradients at the center of the heater are approximately zero. At the sides of the heat sinks the gradients are also zero. Consequently, the boundary conditions for Equations 3.17 and 3.18 are: at $x_1 = L_1$, $d\theta_1/dx_1 = 0$, at $x_2 = L_2$, $d\theta_2/dx_2 = 0$, and at $x_1 = x_2 = 0$, $\theta_1 = \theta_2$ and $-(d\theta_1/dx_1) = d\theta_2/dx_2$. If it is assumed that the thermal spreading decay length $L_d = 1/m$ is is small compared to $L_1 \approx \infty$ and $L_2 \approx \infty$, then the solutions to Equations 3.17 and 3.18 are

$$\theta_1 = \frac{q''W}{2hP} \left[2 - e^{-(x_1/L_d)}\right] \tag{3.19}$$

and

$$\theta_2 = \frac{q''W}{2hP} \left[e^{-(x_2/L_d)}\right] \tag{3.20}$$

where $L_d = (k_w H_{eff} W/hP)^{0.5} = (D_e K_w H_{eff} W/Nuk_f P)^{0.5}$, and the positive directions of x_1 and x_2 are as defined in Figure 3.12.

A typical plot of the dimensionless temperature profiles obtained from Equations 3.19 and 3.20 is shown in Figure 3.13 for a water-cooled indium phosphide heat sink. The results clearly show that thermal spreading can cause a significant temperature non-uniformity at the heater periphery.

Section 4.6 presents a novel method which can be used to minimize the effect of thermal spreading at the periphery of integrated circuits.

3.5 Chapter Summary

To conclude this chapter, some of the main points will be summarized.

The physics of the conduction process were reviewed, and it was found that the use of the continuum theory of conduction should be adequate to model the microchannel heat sinks used in this study.

Heat transfer through a continuous slab can be modeled using Equation 3.2. Conduction of heat from discrete heat sources can be modeled using Equations 3.3 through 3.6.

Thirteen assumptions were listed for the fin heat transfer analysis. The combined effect of these assumptions was to provide

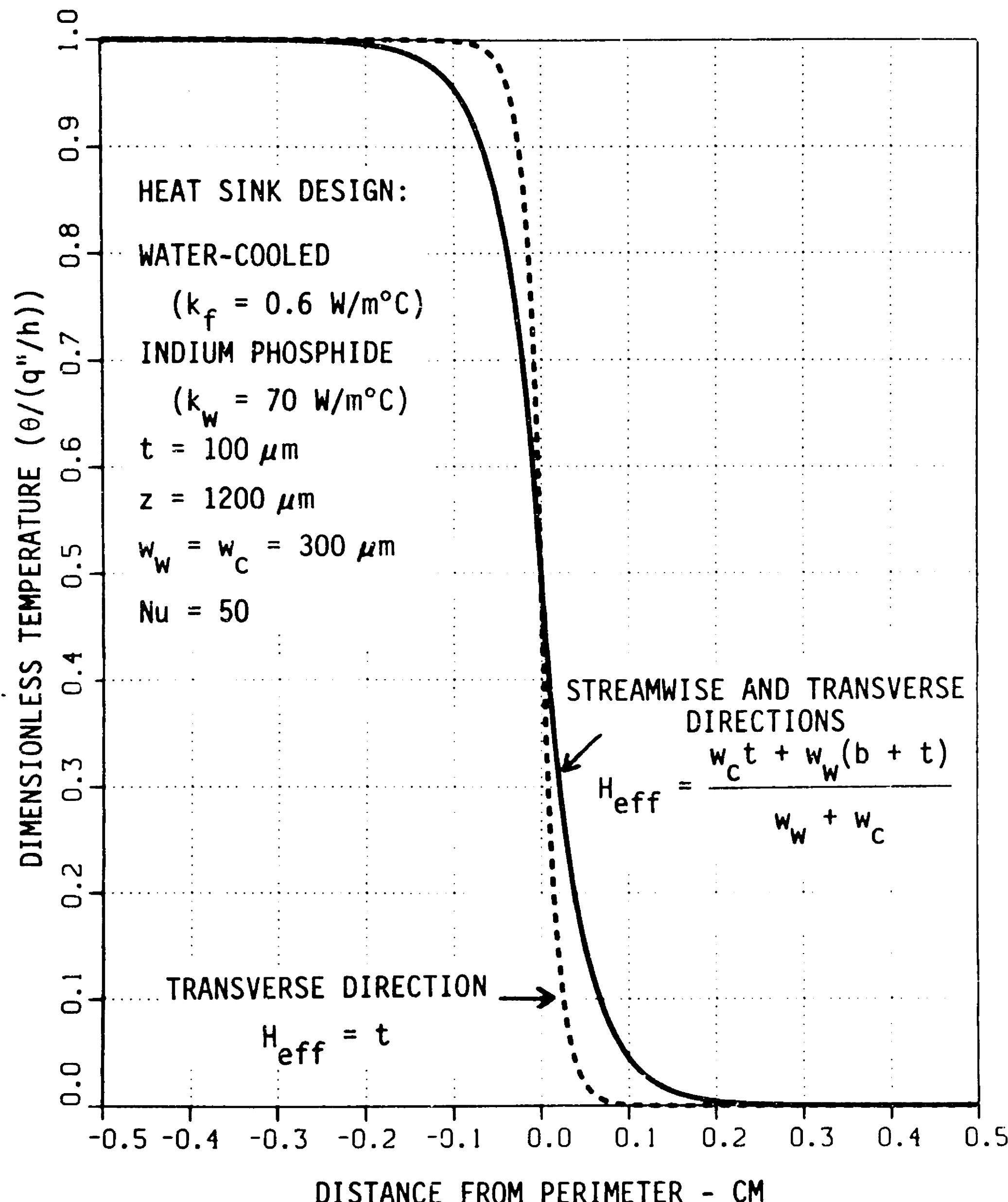

Figure 3.13. Example of chip thermal spreading.

conservative heat transfer estimates. The heat transfer rate through the fin base was modeled using Equation 3.13.

Thermal spreading at the periphery of a heat source was modeled using simplified one-dimensional models (Equations 3.19 and 3.20). It was found that thermal spreading can cause significant temperature non-uniformity.

4.0 MICROCHANNEL HEAT SINK DESIGN

The purpose of this chapter is to present the analytical models used to predict the thermal and hydraulic performance of forced-convection, liquid-cooled microchannel heat sinks. The concept of thermal resistance will be defined first, and the various components that make up the total thermal resistance will be defined. Thermal resistance models will be constructed for large, moderate, and small aspect ratio ducts. A simplified solution, used by the Stanford researchers, of the large aspect ratio duct model will be presented for the design constraint of specified coolant pressure drop. A more complicated solution procedure for the thermal resistance models is then presented for the design constraints of specified coolant pressure drop, specified coolant volumetric flow rate, and specified pumping power. The discussion then turns to an overview of a new computer program used in this study to predict the thermal performance. The programs capabilities will be reviewed, and sample numerical results will be presented and discussed. The use of "compensation heaters" and "interrupted-fins" to improve the thermal performance will then be discussed. The chapter concludes with a brief review of the main points that were covered in this chapter.

4.1 Components of Thermal Resistance

The thermal performance of microelectronics is often specified in terms of the thermal resistance of the device. The total thermal resistance R_{tot} is given by $R_{tot} = \Delta T/Q$, where ΔT is the peak temperature rise above an ambient reference temperature, and Q is the total heating

rate. In this study, a modified thermal resistance R''_{tot} is used. It is given by

$$R''_{tot} = R_{tot}A_{cross} = \frac{\Delta T}{Q} A_{cross} = \frac{\Delta T}{q''} \tag{4.1}$$

where A_{cross} is the surface area over which the heat input Q occurs, and q" is the heating rate per unit surface area which is assumed to be uniform over A_{cross}. Using the modified thermal resistance makes it possible to formulate the thermal analysis based on a single channel and an adjacent fin. This is allowed since neighboring channels and fins are symmetrical in thermal response (assumes that the heat source is large enough). Therefore, R''_{tot} will be based on $A_{cross} = L(w_W + w_C)$.

The total thermal resistance can be thought of as being made up of several components. The arrangement of these thermal resistances is similar to an electrical network of resistors in series and/or parallel. The network will be slightly different for each class of duct aspect ratio (large, moderate, and small). Six types of thermal resistance have been identified for this study. Each one will be discussed next.

The first thermal resistance is R_{spread}, which is the "constriction resistance" due to thermal spreading from each discrete heat source (e.g. integrated circuit feature or gate) on the surface of the chip. This so-called spreading thermal resistance has been said to be the limiting indicator of transistor speed improvement. This is because the speed of some types of transistors (e.g. bipolar devices) goes up as the supplied power goes up (which is mostly dissipated as heat). Therefore, the transistor speed can be increased only so much because the high heating rate will eventually drive the device temperature too high.

The thermal spreading resistance will be a function of the size and shape of the heat source. Equation 3.4 can be used to model thermal spreading from a circular heat source with $R_{spread} = \Delta T_C/q = 1/(2\ k_w a\sqrt{\pi})$, where a is the radius of the heat source. Equation 3.6 could be used to determine R_{spread} for rectangular shapes. If the heat source is square, Joy and Schlig (1970) recommend using

$$R_{spread} \approx \frac{1}{4\ k_w a} \tag{4.2}$$

where k_w is the thermal conductivity of the material evaluated at the device temperature, and a is the characteristic length.

Currently, thermal spreading accounts for on the order of 10°C of the total temperature rise of about 100°C in typical silicon chips. To get an idea of how significant the thermal spreading resistance might be in the future, consider the requirements for artificial intelligence predicted in Section 1.2. There, it was mentioned that 10^9 transistors per chip would be required, and that the heat dissipation per transistor would hopefully be of order 10^{-5} watts or less. The characteristic feature sizes should be at least 0.1 μm and perhaps as small as 0.025 μm. The temperature rise due to thermal spreading in silicon ($k_w \approx 100$ W/m°C @ 400°C) should therefore be in the neighborhood of 0.1 - 1.0°C. This is a highly idealized prediction of the future, but the trend is reasonably clear that the temperature rise due to thermal spreading should decrease as the level of circuit integration increases.

The peak temperature rise of the chip above ambient will probably not decrease quite as rapidly. Therefore, the effect of thermal spreading will not be included in the thermal resistance models.*

The second type of thermal resistance is R''_{solid}, which is due to the conduction of heat through the solid material between the heating surface (e.g. integrated circuit) and the fin base and channel base plane. From Equation 3.2, the modified thermal resistance is given by

$$R''_{solid} = \frac{t}{k_w} \tag{4.3}$$

where k_w is the wall thermal conductivity evaluated at the average substrate temperature, and t is the substrate thickness (see Figure 1.4). Note that if there is a thermal interface (discussed next), then R''_{solid} will be the sum of the contributions between the heating surface and the interface (material 1), and between the interface and the fin base and channel base plane (material 2).

The third type of thermal resistance is R''_{int}, which is due to the thermal interface (if any) between the microchannel heat sink and the heat source (e.g., an integrated circuit chip). If there is an interface, then the microchannel heat sink may be considered a "cold plate." Attachment of the heat source can be done using various types of bonding (solder, epoxy, etc.), thermal grease, gas layers, etc. A newly proposed

* The decision to ignore the gate thermal spreading resistance is also based on the fact that it varies with the transistor technology. The reader can easily include the thermal spreading resistance by modifying the computer program used in this study to predict the thermal performance. Note that the spreading modified thermal resistance should be added to the total thermal resistance (it is a "series" resistance).

interfacing method, called a "microcapillary thermal interface," is discussed in Appendix D. The thermal resistance models presented in Section 4.2 assume that the microchannel heat sink is manufactured directly into the substrate of the heat source, and therefore do not include R''_{int}.*

The fourth type of thermal resistance is R''_{cont}, which is due to the "constriction effect" at the base of the fin (if there is a fin). If fins are used, it is intended that they transfer more heat than if the fin base surface area were exposed directly to the fluid. This necessitates that the heat flow be "funneled" into the base of the fin. For this study, the fins act as a long-strip heat sink for which the constriction thermal resistance may be obtained from Equation 3.5. Substituting $a = w_w/2$, $b = (w_w + w_c)/2$, and $q = q''A_{cross} = q''\ (L(w_w + w_c))$ into Equation 3.5 gives

$$R''_{cont} = \frac{(w_w + w_c)}{\pi\ k_w} \ln \left[\frac{1}{\sin\ [\pi w_w/(2(w_w + w_c))]}\right] \tag{4.4}$$

where k_w is the material thermal conductivity which is evaluated at the average substrate temperature. Equation 4.4 is based on q'' and A_{cross}, and therefore applies for large aspect ratio channels. For moderate aspect ratio channels, some heat is convected from the channel base thereby making the constriction thermal resistance somewhat smaller. Compared to the overall thermal resistance, this reduction is small and therefore

* The reader can easily include the interface thermal resistance by modifying the computer program used in this study to predict the thermal performance. Note that the interface modified thermal resistance should be added to the total thermal resistance (it is a "series" resistance).

will be ignored for simplicity and conservatism. The contraction thermal resistance is zero for small aspect ratio channels because the fins are used for structural purposes and are assumed to transfer no heat. The fin thickness is assumed to be much smaller than the channel width, and therefore there is also no constriction thermal resistance for the heat flow into the channel base.

The fifth type of thermal resistance is R''_{conv}, which is due to the convection of heat from the channel base and/or the fin. If there is a fin, R''_{conv} also includes the thermal resistance of heat conduction in the fin. Note that the fin and channel base are connected in "parallel." Therefore Equations 2.10 and 3.13 can be used to obtain the convective thermal resistance which is given by

$$R''_{conv} = R_{conv}\ (L(w_c + w_c)) = \frac{(L(w_w + w_c))}{hA_{bc} + k_w m A_{bf} \tanh(mb)} \qquad (4.5)$$

where $m = (2h/k_w w_w)^{0.5}$, A_{bc} is the area of the channel base (Lw_c), and A_{bf} is the area of the fin base (Lw_w). Using the definition of the fin efficiency, $\eta_f = (\tanh(mb))/mb$, and doing some rearranging gives

$$R''_{conv} = \frac{(w_w + w_c)}{hw_c + 2hb\eta_f} \qquad (4.6)$$

which represents the convective thermal resistance between the fin base and channel base plane and the local coolant, for moderate aspect ratio

channels. Equation 4.6, of course, assumes that the temperatures of the fin base and the channel base are equal (assumption 11 - see Section 3.3). Note that for large aspect ratio ducts, $hw_c \approx 0$, and for small aspect ratio ducts $2hb\eta_f \approx 0$.

Remember that the overall thermal resistance is based on the difference between the peak chip surface temperature and the inlet coolant temperature. Thus an effective thermal resistance can be defined which is to be added to the local thermal resistance at a given distance from the channel entrance. Therefore, the sixth type of thermal resistance is R''_{bulk}, which is due to the bulk temperature rise of the coolant from the channel entrance caused by absorption of heat from the microchannel heat sink. The bulk thermal resistance is given by

$$R''_{bulk} = R_{bulk}(L(w_w + w_c)) = \frac{(L(w_w + w_c))}{\rho_f Cp_f V} = \frac{L(w_w + w_c)}{\rho_f Cp_f b w_c V_c} \tag{4.7}$$

where V is the volumetric flow rate of the coolant per channel, and V_c is the velocity of the coolant in the channel.

There is one phenomenon that cannot be put into the form of a thermal resistance since it is independent of the heating rate. This is the temperature rise of the coolant due to viscous heating. The coolant temperature rises due to the conversion of mechanical energy (fluid pressure) into thermal energy (fluid temperature rise). The temperature rise is given by Equation 2.22 as $\Delta T_{pump} = \Delta P/\rho_f Cp_f J$, where ΔP is the coolant pressure drop (between the inlet plenum and the channel exit - see Figure 2.9), and J is the mechanical equivalent of heat.

To summarize, the total modified thermal resistance is given by the sum of six thermal resistance terms as

$$R''_{tot} = R''_{spread} + R''_{solid} + R''_{int} + R''_{cont} + R''_{conv} + R''_{bulk} \quad . \tag{4.8}$$

R''_{spread} is ignored since it should become small as the level of circuit integration increases, and because it is highly dependent on the transistor technology. R''_{int} is in general not required for integrated circuits and is also ignored. Therefore, the thermal resistance models presented in the next section will consider the total thermal resistance as being given by

$$R''_{tot} = R''_{solid} + R''_{cont} + R''_{conv} + R''_{bulk} \quad . \tag{4.9}$$

Since viscous heating cannot be accounted for using a thermal resistance, the total temperature rise at the channel exit is given by

$$\Delta T_{tot} = R''_{tot}\, q'' + \Delta T_{pump} \tag{4.10}$$

where it is implied that R''_{tot} and ΔT_{pump} are independent of q". To be accurate, the properties must be evaluated at proper average temperatures.

At this point, it is wise to pause for a moment and consider if the thermal performance of microchannel heat sinks can be formulated in terms of Equation 4.10. To facilitate comparison between heat sink designs, it is necessary to have a common ambient reference temperature (the inlet coolant temperature in this study). But this is not enough. It is

obvious that different heating rates will result in different average properties of the liquid coolant and the heat sink material as well. Therefore, the total thermal resistance of the same heat sink with the same inlet coolant temperature will be different for different heating rates - especially if a comparison is attempted between very small and very large heating rates. Therefore, when comparing various heat sink designs, the heating rate must also be prescribed.

Figure 4.1 shows how the chip temperature varies in the streamwise direction. If thermal spreading at the heater perimeter is ignored, then the coolant temperature rise ΔT_{bulk} will increase linearly from the channel inlet to the exit. The temperature difference between the local coolant temperature and the chip surface temperature will also increase with distance from the channel entrance due to the reduction in the Nusselt number with distance from the channel entrance. All of these effects result in the peak surface temperature being located at the channel exit.

If thermal spreading at the heater perimeter is included (which is different from the gate thermal spreading resistance R''_{spread}), then the coolant temperature will look like the dotted curve, and the surface temperature will look like the dashed curve. The peak surface temperature does not occur at the heater perimeter when thermal spreading is considered. The thermal resistance models presented below do not account for thermal spreading at the heater perimeter. The effect of this thermal spreading is handled separately and will be discussed in Section 4.6.

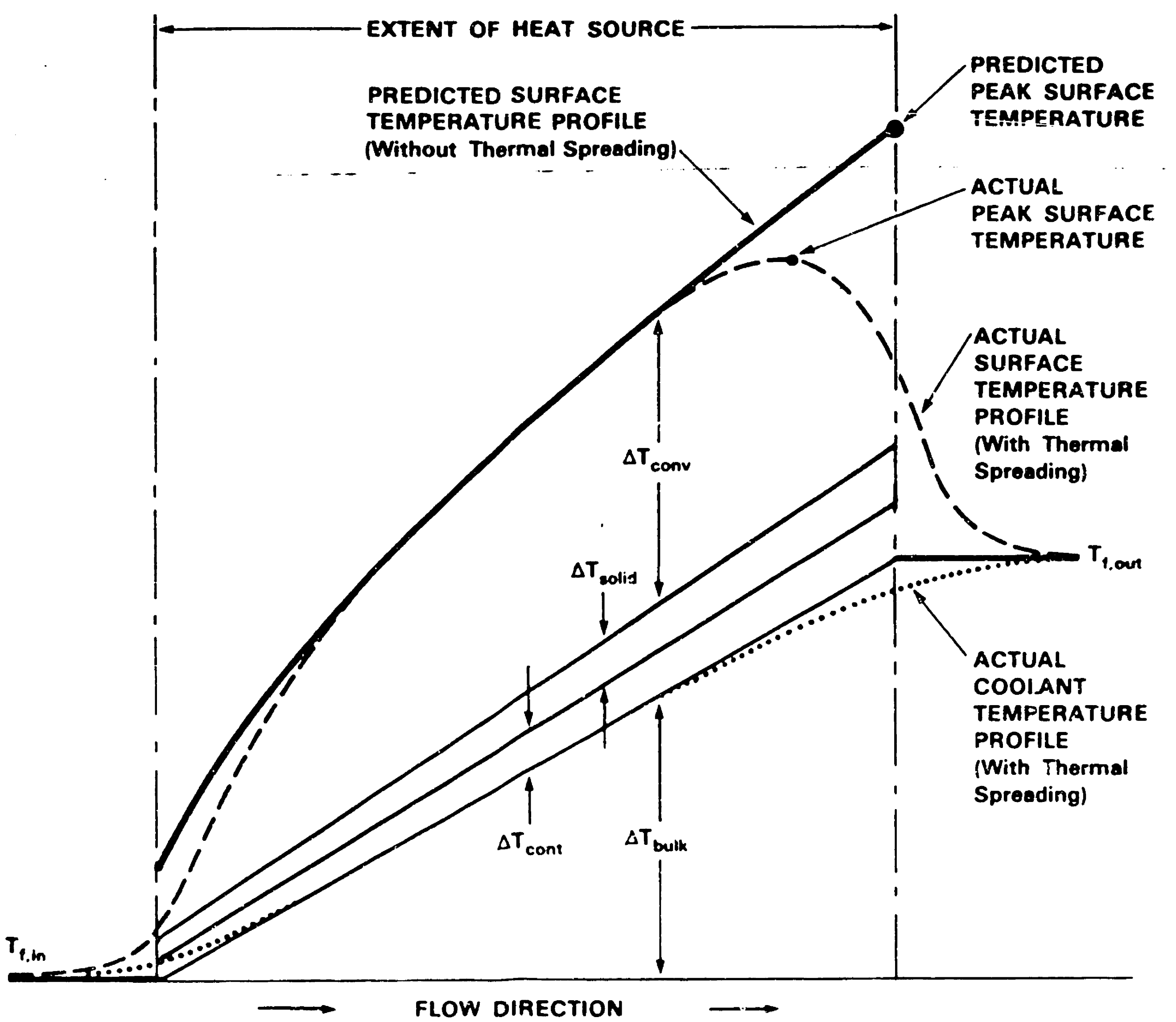

Figure 4.1. Temperature trends in the streamwise direction.

4.2 Thermal Resistance Models

In this study, three types of channel aspect ratios ($\alpha = b/w_c$) are analyzed. They are large ($\alpha > 10$), moderate ($0.1 < \alpha < 10$), and small ($\alpha < 1.0$). The thermal resistance model will be presented next for each type of channel aspect ratio. Following this there is a discussion of where the thermal resistance should be evaluated to obtain the worst case prediction of thermal performance. This section ends with a review of "knowns" and "unknowns" of the thermal resistance models.

Large aspect ratio channels have large fin heights. The surface area for convective heat transfer of the channel base is small compared to the surface area of the fins. Therefore the contribution of the channel base to the overall heat transfer is small and can be ignored even though the channel base surface temperature is on average higher than the fin temperature. Substituting Equations 4.3, 4.4, 4.6, and 4.7 into Equation 4.9, and ignoring the contribution of the channel base ($hw_c \approx 0$) in R''_{conv}, gives the following model for the total thermal resistance

$$R''_{tot,large} = \frac{t}{k_w} + \frac{(w_w + w_c)}{\pi k_w} \ln \left[\frac{1}{\sin(\pi w_w/(2(w_w + w_c)))}\right] + \frac{(w_w + w_c)}{2hb\eta_f} + \frac{L(w_w + w_c)}{\rho_f Cp_f b w_c V_c} \tag{4.11}$$

where $R''_{tot,large}$ is the total modified thermal resistance for large aspect ratio channels.

Moderate aspect ratio channels have shorter fin heights such that the heat transfer from the channel base is also significant. The total thermal resistance is obtained by direct substitution of Equations 4.3, 4.4, 4.6, and 4.7 into Equation 4.9, and is given by

$$R''_{tot,moderate} = \frac{t}{k_w} + \frac{(w_w + w_c)}{\pi k_w} \ln \left[\frac{1}{\sin(\pi w_w/(2(w_w + w_c)))}\right] + \frac{(w_w + w_c)}{hw_c + 2hb\eta_f} + \frac{L(w_w + w_c)}{\rho_f Cp_f b w_c V_c} \tag{4.12}$$

where $R''_{tot,moderate}$ is the total modified thermal resistance for moderate aspect ratio channels.

Small aspect ratio channels have fins which are primarily used for structural purposes. The fins are small in thickness compared to the channel width ($w_w << w_c$), and are very short in height ($b << w_c$). Therefore, the contribution of the fins to the overall heat transfer is small and can be ignored. Since $w_w << w_c$, it is assumed that $w_w \approx 0$, which results in $R''_{cont} \approx 0$. Substituting Equations 4.3, 4.6, and 4.7 into Equation 4.9 gives the following model for the total thermal resistance

$$R''_{tot,small} = \frac{t}{k_w} + \frac{1}{h} + \frac{L}{\rho_f Cp_f b V_c} \tag{4.13}$$

where $R''_{tot,small}$ is the total modified thermal resistance for small aspect ratio ducts.

The models for the total modified thermal resistance, Equations 4.11 - 4.13, need to be solved such that the worst case thermal performance is predicted. The models ignore axial heat conduction, and thermal

spreading at the periphery of the surface heat source. Therefore, the worst case thermal performance will be predicted to occur at the downstream edge ($x = L$) of the heat source where the Nusselt number is at its lowest value (see Figure 4.1). The assumptions which are made in the analysis of fin heat transfer (Section 3.3) have collectively been found to conservatively model the fin heat transfer. Therefore, it is expected that the thermal performance predicted by Equations 4.11 and 4.12 at $x = L$ will be conservative. Equations 4.11 and 4.13 are also conservative because the channel base heat transfer and the fin heat transfer have respectively been ignored.

A scan of the variables in Equations 4.11 - 4.13 shows that the thermal performance is a function of the type of coolant (ρ_f, Cp_f), the heat sink material (k_w), various geometrical parameters (t, w_w, w_c, b, L), and the convective parameters (h, V_c). In addition, the coolant and heat sink properties are a function of the inlet coolant temperature ($T_{f,in}$) and the heating rate (q''). The only "unknowns" on the right hand side are the convective parameters. The heat transfer coefficient is obtained from the Nusselt number at the channel exit using $h = Nuk_f/D_e$. Therefore, the unknowns are now Nu and V_c since D_e is a known geometrical parameter and k_f is known from the type of coolant. The Nusselt number was shown to be in general a function of the thermal entrance length $x^* = L/D_eRePr$ and the channel aspect ratio $\alpha = b/w_c$. Therefore, the unknowns are now Re and V_c since Pr is known from the type of coolant, and L, D_e, and α are all geometrical parameters. The Reynolds number is given by $Re = V_cD_e\rho_f/\mu_f$ where D_e

is a known geometrical parameter, and ρ_f and μ_f are known from the choice of coolant. Therefore, the only unknown is the coolant velocity V_c, which will be provided by any one of three design constraints placed on the liquid coolant flow.

Section 4.3 reviews the solution of the large aspect ratio channel model done by the Stanford researchers for the fixed-pressure-drop coolant flow constraint. Section 4.4 outlines a more comprehensive solution procedure for the thermal resistance models for three coolant flow constraints.

4.3 Simplified Solution of The Large Aspect Ratio Channel Model

The analysis in this section was presented in Tuckerman and Pease (1981a). The analysis presented here is done in terms of the modified thermal resistance, and the symbols for some of the analysis variables have been changed to correspond to the notation used in this thesis.

The important feature of Tuckerman and Pease (1981a) is that they were able to show that there is an "optimum" design for microchannel heat sinks operating in the fully-developed laminar flow regime. This is done by minimizing the sum of R''_{conv} and R''_{bulk} as a function of the channel width.

For large aspect ratio channels, there is a surface area multiplication factor $\delta = 2b/(w_w + w_c)$ due to the fins. Assuming fully developed laminar flow at the channel exit provides the friction factor as $f = 24/Re = 24\mu_f/(\rho_f V_c 2w_c)$. The Nusselt number is constant for a given channel aspect ratio and is obtained from Figure 2.12. The coolant pressure drop is a design constraint and is given by

$\Delta P = 4f(L/D_e)\ \rho_f V_c^2/2g_c$, where K_{90}, Kc, and Ke re assumed to be zero (see Equation 2.9). Upon substitution into Equations 4.6 and 4.7, the following thermal resistance model is obtained*

$$R'' = \frac{2w_c}{k_f Nu \delta \eta_f} + \frac{24\mu_f L^2}{\rho_f Cp_f \Delta P w_c^3 \delta} . \tag{4.14}$$

When δ is large, it can be shown that $w_w = w_c$ maximizes η_f (which is less than 1.0 and therefore minimizes R"). "For practical design," the surface area enhancement is given by $\delta = (k_w/k_f Nu)^{0.5}$ which results in $\eta_f \approx 0.76$. With these values for δ and η_f substituted into Equation 4.14, the "optimum" channel width is given by taking dR''/dw_c = 0 which gives

$$w_c \approx 2.29\ [\mu_f L^2 k_f Nu/\rho_f Cp_f \Delta P]^{0.25} \tag{4.15}$$

* Tuckerman (1984) divides R''_{bulk} by η_f to provide a conservative estimate of R". This is apparently done to account for the effect of non-uniform coolant temperature along the fin height. Section 3.3 of this thesis discussed the effect of non-uniform coolant temperature along the fin height and found that the traditional fin model quite accurately predicted the thermal performance (based on experimental data for moderate aspect ratio ducts). For very large aspect ratio channels, some correction might be required, but a correction should be done to R''_{conv} not R''_{bulk} (in the opinion of this author).

for which the "optimum" modified thermal resistance is given by

$$R'' = \frac{4}{3} R''_{conv} = 4R''_{bulk} = 8.01[\mu_f L^2/k_f \rho_f Cp_f k_w^2 Nu\Delta P]^{0.25} \quad . \tag{4.16}$$

To get an idea of the typical "optimum," consider forced convection of water ($k_f \approx 0.6$ W/m°C, $\mu_f \approx 9.8 \times 10^{-4}$ kg/ms, $\rho_f \approx 997.4$ kg/m^3) with a pressure drop of 30 psi (206843 Pa) in a silicon heat sink ($k_w \approx 148$ W/m°C). It can be shown that if the flow is laminar and fully developed that Nu ≈ 6, which gives $\delta \approx 6.4$, $w_w = w_c \approx 58$ µm, b ≈ 370 µm, $\dot{V} \approx 0.127$ cm^3/s per channel, Re ≈ 700, $x^* \approx 0.018$, and $R'' \approx 0.086$ °C/(W/cm^2).** Note that the total thermal resistance is $R_{tot} \approx 0.1$ °C/W for a 1 cm^2 heater, which is about two orders of magnitude lower than that of todays state-of-the-art, high-performance computer class (R_{tot} of 10°C/W or lower - see Section 1.2). This is why there is so much interest in microchannel heat sink technology.

The Stanford analysis is very simple and can provide a sense of which analysis variables are most important [see Tuckerman (1984)]. The selection of $\delta = (k_w/k_f Nu)^{0.5}$ may seem a little arbitrary. Since $w_w = w_c$, the "optimum" fin aspect ratio is equivalent to the channel aspect ratio. Therefore Equation 3.16 could be used to give δ as

$$\delta = -0.5 + 0.5[1 + 8.056\ k_w/k_f Nu]^{0.5} \tag{4.17}$$

** Note that the values listed here differ slightly from those presented in Tuckerman and Pease (1981a). This is probably due to the differences in the water and silicon properties.

which results in $\delta = 8.6$ for this example. This value of δ would be perhaps more "accurate" but would be more difficult to manufacture.

The Stanford analysis assumes that the flow is fully developed. Since $x^* = 0.018 < 0.2$, the flow is not fully developed - though it is close! Because of this, Nu will be larger which makes δ smaller and w_c larger. The effect of making δ smaller does tend to compensate by reducing the fully developed value of Nu. The Stanford researchers do recognize that the flow is not fully developed, but they apparently did not modify their model (Equation 4.14) to account explicitly for developing flow.

In this study, a computer program is used to do the tedious iterative solution of the thermal resistance models for both fully developed and developing flow. It will be shown that there often is no distinct "optimum" heat sink design. Instead, there is a continuum of designs which offer essentially the same level of thermal performance. The solution procedure used in this study to solve Equations 4.11 - 4.13 for three design constraints is discussed next.

4.4 Iterative Solution Procedure

The purpose of this section is to provide an overview of the solution of the thermal resistance models (Equations 4.11 - 4.13) for three design constraints on the coolant flow rate. The three design constraints will be introduced first. Then the procedure to obtain the coolant velocity V_c will be discussed for each constraint for smooth and repeated-rib-roughened channels. The procedure to obtain the Nusselt number Nu will be discussed for smooth and repeated-rib-roughened

channels. The discussion then turns to accounting for the effect of the heating rate q". The entire solution procedure will be presented in graphical form at the end of this section. Sample numerical results will be presented in Section 4.5.2 after the computer program used to obtain them is introduced in Section 4.5.1.

There are three types of design constraints which are used in the study to obtain the coolant velocity V_c. The first design constraint is fixed pressure drop ΔP, which may be required due to supply pressure limitations of the circulation pump or due to structural (stress) limitations of the heat sink design. The second design constraint is fixed volumetric flow rate per unit heater surface area V", which may be required since the circulation pump may be of the positive-displacement type. The third design constraint is fixed pumping power per unit heater surface area P" = ΔPV", which may be required to limit the power consumption of the cooling system. Notice that these three constraints really are not totally independent when a practical heat sink design is being sought. In general, all three constraints must be satisfied in that the pressure drop does not exceed ΔP, that the volumetric flow rate does not exceed V", and that the pumping power does not exceed P".

To determine the thermal performance of a heat sink, several analysis parameters must be known in advance. They are: the heat sink material, the liquid coolant, the inlet temperature of the liquid coolant $T_{f,in}$, the heating rate q", the channel width w_c, the fin thickness w_w (or the ratio w_w/w_c), the fin height b (or the channel aspect ratio $\alpha = b/w_c$), the channel length L, the ratio of the channel and

plenum cross-sectional areas A_c/A_p, the substrate thickness t, and one design constraint (ΔP, V", or P"). This adds up to ten variables plus the design constraint. If the channels are roughened with repeated ribs, there are four additional analysis parameters which must also be known in advance. These roughness parameters are: the ratio of the rib height to the channel hydraulic diameter e/D_e, the ratio of the distance between repeated-ribs to the rib height p/e, the rib shape angle ϕ, and the flow attack angle ψ. The computer program used in this study can only treat one design constraint at a time. Therefore, the solution procedures used to obtain the coolant velocity V_c for each design constraint are discussed separately.

Since the coolant velocity is not in general known in advance, the Reynolds number is not also known. To avoid problems with satisfying the Reynolds number criterion for laminar versus turbulent flow, the flow is first assumed to be laminar. The entire solution procedure is then completed assuming that the flow is laminar. The flow is then assumed to be turbulent and the entire solution procedure is repeated. If the laminar case Reynolds number turns out to be greater than Re_{crit}, the numerical results are discarded. Similarly, if the turbulent case Reynolds number turns out to be lower than Re_{crit}, the numerical results are discarded.

For the fixed pressure drop constraint, V_c can be obtained using Equation 2.9. If the ratio of the channel and plenum cross-sectional areas Ac/Ap is substituted into Equation 2.9 ($V_p = V_c Ac/Ap$), the

coolant velocity can be obtained after re-arrangement as

$$V_c^2 = \Delta P(\frac{2g_c}{\rho_f}) \left[(Ac/Ap)^2 (2K_{90}) + (Kc + Ke) + 4f_{app}L/D_e\right]^{-1} \qquad (4.18)$$

where $K_{90} = 1.2$, and Figures 2.10 or 2.11 are used to obtain Kc and Ke at a given Ac/Ap, and Re (for turbulent flow) or $4L^+ = 4L/D_eRe$ (for laminar flow). For laminar flow in smooth channels, the apparent friction factor f_{app} is obtained from Table 2.5 as a function of $\alpha = b/w_c$ and $L^+ = L/D_eRe$. For turbulent flow in smooth channels, the apparent friction factor is obtained from Equation 2.6 as a function of L/D_e and Re. For fully-developed turbulent flow in repeated-rib-roughened channels, the apparent friction factor is given by f_1 or f_2 which are obtained from Equations 2.16 - 2.18 as a function of De, the roughness parameters (e/D_e, p/e, ϕ and ψ), and Re. Therefore, Kc, Ke, and f_{app} are all functions of Re and other known analysis parameters. Since Re is a function of V_c and other known analysis parameters, it becomes clear that trial-and-error solution using successive guesses of V_c is required.

For the fixed volumetric flow rate constraint, the solution for the coolant velocity is easy. The volumetric flow rate per unit heater surface area V" must first by converted to a volumetric flow rate per channel. This is done by multiplying V" by the heater surface area directly over one channel and an adjacent fin ($L(w_w + w_c)$). The

velocity is directly obtained by dividing the result by the cross-sectional flow area of one channel (bw_c). Therefore, the coolant velocity is given by

$$V_c = \frac{V''(L(w_w + w_c))}{bw_c} \tag{4.19}$$

where V" is the design constraint, and the geometrical parameters (L, w_w, w_c, and b) are all known.

For the fixed pumping power constraint, the coolant velocity can be obtained using Equations 4.18 and 4.19 solved for ΔP and V" respectively. The resulting equations are then substituted into P" = ΔPV" and rearranged to give

$$V_c^3 = P''\left(\frac{2g_c}{\rho_f}\right) \left[(Ac/Ap)^2 (2K_{90}) + (Kc + Ke) + 4fapp\ L/D_e\right]^{-1} \frac{(L(w_w + w_c)}{bw_c} \tag{4.20}$$

where the solution procedure is the same as that discussed above with the fixed pressure drop constraint.

Now that the coolant velocity is known, the heat transfer coefficient can be obtained from the Nusselt number $Nu = hD_e/k_f$. For laminar flow in smooth channels, Nu is obtained from Table 2.11 as a function of α and $x^* = L/D_eRePr$. For turbulent flow in smooth channels, the heat transfer coefficient is obtained from Equation 2.15 as a function of Pr and Re. For fully-developed turbulent flow in repeated-rib-roughened channels, Nu is obtained from Equations 2.19 and 2.20 as a function of

D_e, the roughness parameters (e/D_e, p/e, ϕ, and ψ), the coolant parameters (ρ_f, μ_f, and Pr), and Re.

The total thermal resistance can now be obtained by substituting the values for the coolant velocity and the heat transfer coefficient into the thermal resistance models (Equations 4.11 - 4.13). This solution is "accurate" if the correct values of the heat sink material properties and the coolant properties are known. It was previously mentioned that the heating rate q" and the inlet coolant temperature $T_{f,in}$ both affect the properties of the heat sink and the coolant. To account for the effect of the heating rate, the following procedure is used. First the properties of the coolant and the heat sink material are evaluated at $T_{f,in}$ and assumed constant over the entire channel length. Then the coolant velocity and the heat transfer coefficient (at the channel exit) are obtained using the solution procedure discussed above. At this point, the individual thermal resistance components are computed and summed to give the total thermal resistance. Several temperatures* are then computed using the heating rate, the thermal resistances, and ΔT_{pump} (see Equation 4.10). The relative error between the "new" and "old" temperatures is computed, and the solution is obtained if all of the errors are sufficiently small. If one or more of the errors is too large, then average values for the temperatures are computed and used to evaluate the heat sink and coolant properties.

* These temperatures include: the coolant temperature at the channel outlet (at $x = L$), the average fin temperature (at $x = L/2$), the average fin temperature at the channel outlet (at $x = L$), the fin base temperature at the channel exit (at $x = L$), and the heated surface temperature at the channel exit (at $x = L$).

The entire solution procedure is then repeated using these new properties, and Equations 2.24 and 2.25 are used to account for variations of Nu and f_{app} due to non-uniform coolant properties. This process continues until all of the temperature errors are small enough. It is only after this final solution is obtained that the Reynolds number can be checked for being in the flow regime that was assumed in the beginning. If Re is not in the proper flow regime, the solution is discarded because it is not valid.

Figure 4.2 summarizes the iterative solution procedure used in this study. The solution procedure requires considerable numerical computation. Because of this, a new computer program has been written to do the numerical work. It is discussed in the next section.

4.5 Computer Solution of the Thermal Resistance Models

The purpose of this section is to introduce a computer program which can be used to compute the thermal and fluid performance of microchannel heat sinks. The capabilities of this computer program will be enumerated. Sample numerical results will be presented and discussed. The computer program quite accurately predicts the available experimental data for microchannel heat sinks (see Chapter 6).

4.5.1 The MICROHEX Computer Program

A new computer program called "MICROHEX" has been written by the author to compute the thermal and fluid performance of forced-convection, liquid-cooled, microchannel heat sinks. MICROHEX will handle small, moderate, and large aspect ratio channels with fully developed and developing flow in the laminar and turbulent regimes. The channel surfaces can

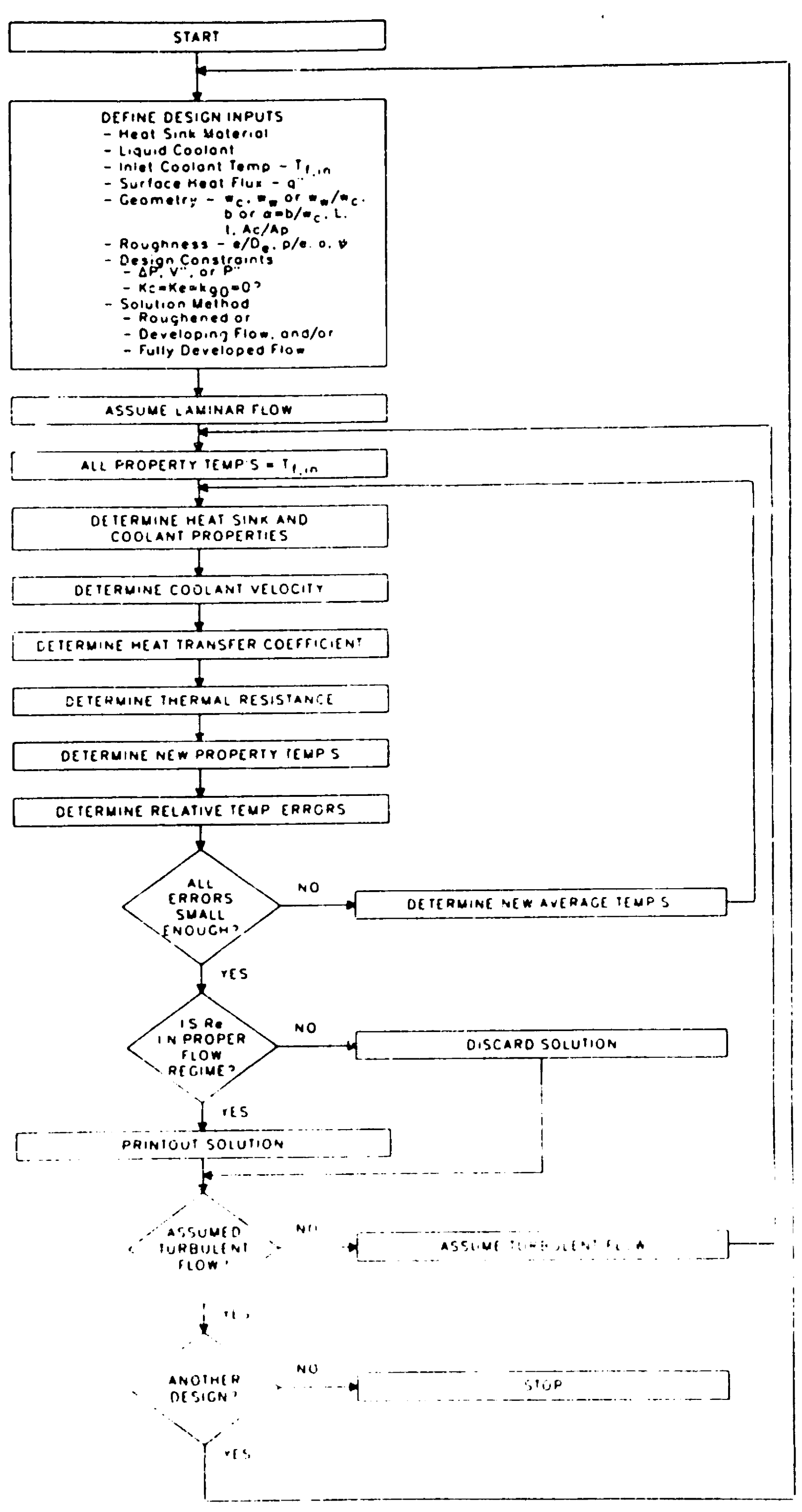

Figure 4.2. Flow chart of the iterative solution procedure.

be smooth or roughened with repeated-ribs. Variable property effects are included for the chip material and the liquid coolant (compressibility effects have not been included). The effect of viscous dissipation in the liquid coolant is included. Thermal spreading at the periphery of the heat source is also taken into account with simplified one-dimensional models.

Program MICROHEX and its 19 subroutines are written in Fortran IV. It has been successfully run on an IBM 3081, a MICROVAX II, and an IBM PC. A complete listing of the entire computer program is provided in Appendix E. Table 4.1 briefly discusses what each subroutine does, and Figure 4.3 presents the program flow chart which shows when each subroutine is called. The computational procedure used by MICROHEX to arrive at the thermal and fluid performance predictions is the same as the solution procedure outlined in Section 4.4. MICROHEX typically takes about 5 to 10 seconds of CPU time on an IBM 3081 computer to do the computations for each generic heat sink design (e.g. all of Figure 4.4). This CPU time also includes the time required to prepare plots of the thermal and fluid performance. The plotting is done using the DISSPLA graphics package. The reader/user may wish to use a different plotting package to suit their own in-house capabilities. It is for this reason that the plotting is done in two subroutines (PINPUT and PPLOTT), which can be easily "updated" with the user's own plotting routines.

The input for MICROHEX is provided via initializing up to 25 variables in the MICROHEX program data statements. These variables will now be introduced. (See Table 4.2 for a summary of the input variables.)

TABLE 4.1

OVERVIEW OF MICROHEX ROUTINES

Routine	Type		Purpose
ABRUPT	(fortran)	-	Computes the Kc, Ke, and K_{90} loss coefficients
MICROHEX	(exec)	-	Initializes the output data files (IBM 3081).
MICROHEX	(fortran)	-	Initializes the design variables.
PINPUT	(fortran)	-	Writes a modified "echo" of the 25 variables initialized in the MICROHEX (fortran) data statements, as the first plot page of the plotting output.
PPLOTT	(fortran)	-	Either plots the thermal resistance and the pumping power as a function of the channel width, or plots the thermal resistance as a function of the distance from the channel entrance, as the second plot page of the plotting output.
PRINTO	(fortran)	-	Initializes the column headings for the printout files.
PROP	(fortran)	-	Calls the appropriate subroutine (PROPF# and PROPS#) to initialize the property arrays for the liquid coolant and the heat sink material.
PROPF#	(fortran)	-	Contains the property data for liquid coolant #.
PROPS#	(fortran)	-	Contains the property data for heat sink material #.
RESIST	(fortran)	-	Computes the thermal and fluid performance.
RTOTAL	(fortran)	-	Finalizes the initialization of all computational input parameters, prints the thermal and fluid results, and stores valid data points for plotting.

TABLE 4.1

(Continued)

Routine	Type		Purpose
RTURF	(fortran)	-	Computes the repeated-rib roughened channel, fully developed flow friction factor.
RTURNU	(fortran)	-	Computes the repeated-rib roughened channel, fully developed flow Nusselt number.
SFFD	(fortran)	-	Computes the smooth-channel, laminar friction factor for fully developed flow everywhere.
SLAMF	(fortran)	-	Computes the smooth-channel, fully developed/developing laminar friction factor.
SLAMNU	(fortran)	-	Computes the smooth-channel, fully developed/developing laminar Nusselt number.
SNUFD	(fortran)	-	Computes the smooth-channel, laminar Nusselt number for fully developed flow everywhere.
STURF	(fortran)	-	Computes the smooth-channel fully developed/developing turbulent friction factor.
STURNU	(fortran)	-	Computes the smooth-channel, fully developed/developing turbulent Nusselt number.
TEMPS	(fortran)	-	Computes the coolant and heat sink temperatures.

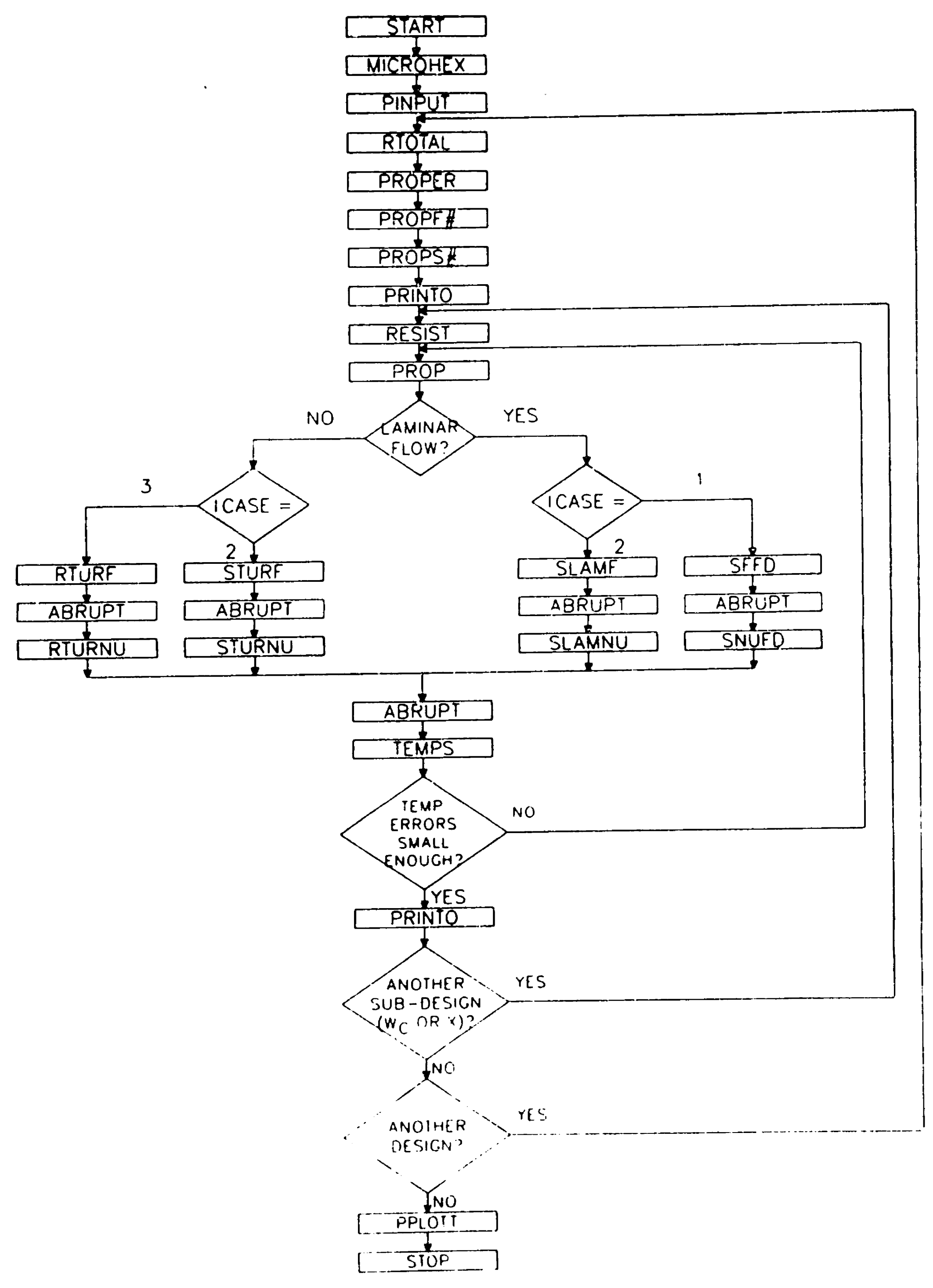

Figure 4.3. Flow chart of subroutine calls for Program MICROHEX.

Table 4.2

MICROHEX DATA STATEMENT VARIABLES

Variable	Units	Description
NCURVE	-	Number of generic heat sink designs.
IX	-	Vary channel width or channel position.
NSINK	-	Heat sink material identification number.
NFLUID	-	Liquid coolant identification number.
ICASE	-	Specifies flow regime and channel surface type.
Q	W/cm^2	Surface heating rate.
TFLUIN	°K	Inlet coolant temperature.
WCSTAR	microns	Smallest channel width.
WCEND	microns	Largest channel width.
WCINCR	microns	Channel width increment.
WWBYWC	-	Ratio of the fin thickness to the channel width.
IZ	-	Fixed fin height or channel aspect ratio.
B	microns	Fin height.
ASPECT	-	Channel aspect ratio.
L	m	Channel length.
T	microns	Solid material thickness between heated surface and the channel base and fin base plane.
IKLOSS	-	Specifies if inlet, exit, and 90 deg. bend pressure loss is to be computed.
ICONS	-	Determines the coolant velocity constraint.
DELP	psi	Coolant pressure drop.
VOLUME	$(cm^3/s)/cm^2$	Coolant volumetric flow rate per unit heater surface area.
POWER	W/cm^2	Coolant pumping power per unit heater surface area.
EBYDE	-	Ratio of the rib-height to the channel hydraulic diameter.
PBYE	-	Ratio of the rib separation to the rib height.
PHI	deg	Rib shape angle.
ZI	deg	Flow attack angle.

The variable NCURVE determines how many generic heat sink designs will be analyzed. From one to five designs are allowed, and each design will have its thermal and fluid performance plotted using a unique curve type.

The variable IX determines if either the channel width w_c or the channel length x is fixed (constant). If the channel length is constant (IX = 1), then the thermal and fluid performance will be plotted as a function of the channel width with all results provided at the channel exit (thermal spreading at the heater periphery is not included here since the channel exit is not the location of the peak, total thermal resistance if thermal spreading is considered). If the channel width is constant (IX = 2), then the thermal and fluid performance will be plotted as a function of the channel length (thermal spreading along the channel length at the heater periphery will be included).

The variable NSINK is used to specify the heat sink material. MICROHEX contains data for Gallium Arsenide, Germanium, Indium Phosphide, Silicon, Aluminum, Copper, and Silver. The user can easily include other materials simply by adding additional PROPS# subroutines.

The variable NFLUID is used to specify the liquid coolant. MICROHEX contains data for FC-77, Freon 12 (CCl_2F_2), and water. The user can easily include other liquid coolants simply by adding additional PROPF# subroutines.

The variable ICASE is used to specify the flow regime(s) and channel surface type. Three ICASE's are currently used. They are: 1) fully

developed laminar flow everywhere (smooth surfaces), 2) fully developed/developing, laminar/turbulent flow (smooth channels), and 3) fully developed turbulent flow everywhere (repeated-rib roughened surfaces).

The variable Q is used to specify the surface heat input q" in watts per square centimeter of heater surface area. The variable TFLUIN is used to specify the inlet temperature of the liquid coolant in degrees K.

The variable WCSTAR is used to specify the smallest channel width w_c in microns that will be analyzed. The variable WCEND is used to specify the largest channel width in microns that will be analyzed. The variable WCINCR is used to specify the increment in channel width between WCSTAR and WCEND for intermediate channel widths that will be analyzed. If IX = 1, then the thermal performance will be computed for channel widths w_c = WCSTAR, WCSTAR + 1WCINCR, WCSTAR + 2WCINCR, ... , WCEND. If IX = 2, then WCSTAR = WCEND, and WCINCR ≠ 0 is required since the channel width is constant.

The variable WWBYWC is used to specify the ratio of the fin width w_w to the channel width w_c.

The variable IZ is used to determine whether the channel height (fin height) b is constant, or if the channel aspect ratio $\alpha = b/w_c$ is constant. If IZ = 1, then the variable B is used to specify the channel height (fin height) b in microns. If IZ = 2, then the variable ASPECT is used to specify the constant channel aspect ratio.

The variable L is used to specify the channel length in meters. The variable T is used to specify the thickness in microns of the solid material between the surface of heat input and the channel base and fin base plane.

The variable IKLOSS is used to determine if the inlet and exit header pressure losses will be included or not. If IKLOSS = 0, then $Kc = Ke = K_{90} = 0$, and only the channel friction will be used to determine the overall pressure drop. If IKLOSS = 1, then Kc, Ke, and K_{90} will be computed and included in the overall pressure drop.

The variable ICONS is used to determine which flow constraint will be used to determine the velocity of the liquid in the microchannels. If ICONS = 1, then the variable DELP is used to specify the coolant pressure drop ΔP in psi. If ICONS = 2, then the variable VOLUME is used to specify the coolant flow rate V" in cubic centimeters per second per square centimeter of heater surface area. If ICONS = 3, then the variable POWER is used to specify the coolant pumping power P" in watts per square centimeter of heater surface area.

If the channel surfaces are roughened with repeated-ribs ($\alpha < 0.1$ or $\alpha > 10.$), then the following four variables must be initialized. The variable EBYDE is used to specify the ratio of the rib height e to the channel equivalent diameter D_e. The variable PBYE is used to specify the ratio of the spacing between repeated ribs p and the rib height e. The variable PHI is used to specify the rib shape angle ϕ in degrees. The variable ZI is used to specify the flow attack angle ψ in degrees.

4.5.2 Sample Numerical Results

This sub-section presents typical thermal and fluid performance predictions that are obtained using MICROHEX. A "reference" microchannel heat sink design will first be described. After this, there will be a

comparison of the thermal and fluid performance for the reference case with other design cases where one analysis parameter is temporarily varied while all others are held constant.

The reference case design is a water-cooled silicon heat sink. The modified "echo" (produced by subroutine PINPUT) of the input variables is provided as Table 4.3. From this table, it can be seen that all thermal and fluid performance calculations were done at the channel exit and therefore the effect of thermal spreading at the heater perimeter was not included. The calculations were done for fully developed/developing, laminar/turbulent flow in smooth channels. The inlet coolant temperature is $T_{f,in}$ = 300°K. For simplicity, the surface heat flux is assumed negligible, and therefore the properties of the heat sink material and the liquid coolant are constant all along the channel. The computations begin with a channel width of 5 µm and proceed in 5 µm increments up to w_c = 500 µm. The ratio of the fin thickness to the channel width is unity, and the channel aspect ratio is constant at 4.0. The channel length is 1.0 cm, and the substrate thickness t is 100 µm. The pressure drop through the 90° bends, the inlet contraction, and the exit expansion are assumed to be small compared to the friction pressure drop along the 1.0 cm long channel. The coolant velocity is determined for a 68.9 kPa (10 psi) pressure drop for all channel widths.

The thermal and fluid performance predictions are plotted in Figure 4.4 for the reference case. The upper graph is a plot of the total thermal resistance per unit area as a function of the channel width. The lower graph is a plot of the pumping power required per unit

TABLE 4.3

INPUT DATA FOR MICROHEX COMPUTATIONS

IX: CALCS. DONE AT CHANNEL EXIT - CHANNEL WIDTH VARIED

LINE TYPE:	SOLID	DOT	DASH	CHNDOT	CHNDSH
ICASE:	FD/D,LAM/TUR	NA	NA	NA	NA
MATERIAL:	SI	NA	NA	NA	NA
COOLANT:	WATER	NA	NA	NA	NA
TFLUIN:	300. DEG. K	NA	NA	NA	NA
Q:	0.000 W/CM*2	NA	NA	NA	NA
WCSTAR:	5.00 MICRONS	NA	NA	NA	NA
WCEND:	500. MICRONS	NA	NA	NA	NA
WCINCR:	5.00 MICRONS	NA	NA	NA	NA
WWBYWC:	1.000	NA	NA	NA	NA
B:	NA	NA	NA	NA	NA
ASPECT:	4.0000	NA	NA	NA	NA
L:	0.010 M	NA	NA	NA	NA
T:	100. MICRONS	NA	NA	NA	NA
IKLOSS:	KC-KE-K90-0.	NA	NA	NA	NA
DELP:	10.0 PSI	NA	NA	NA	NA
VOLUME:	NA	NA	NA	NA	NA
POWER:	NA	NA	NA	NA	NA
EBYDE:	NA	NA	NA	NA	NA
PBYE:	NA	NA	NA	NA	NA
PHI:	NA	NA	NA	NA	NA
ZI:	NA	NA	NA	NA	NA

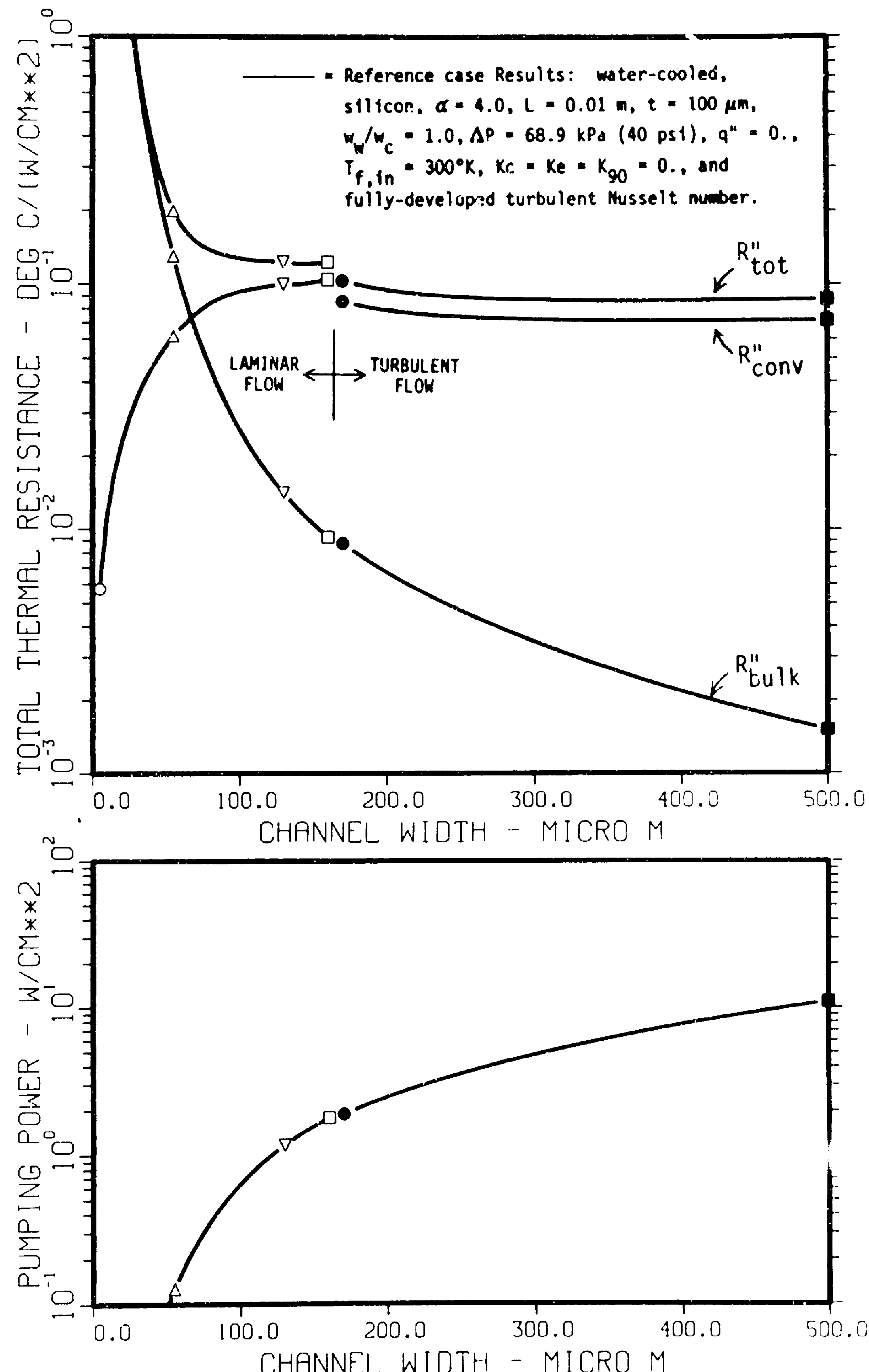

Figure 4.4. Thermal resistance and pumping power versus channel width for the reference case.

surface area as a function of the channel width. On both graphs, the laminar flow results begin with open circles (small w_c), and end with open squares (large w_c). Similarly, the turbulent flow results begin with closed circles (smallest turbulent w_c), and end with closed squares (largest w_c). The transition Reynolds number determines where the laminar flow curve ends, and where the turbulent flow curve begins (see Table 2.1). The upward pointing triangular symbols indicate the separation between fully-developed flow (to the left) and developing flow (to the right). The downward pointing triangular symbols* on the laminar flow curves indicate where the thermal entrance length $x^* = L/D_e RePr$ becomes less than 0.005 (to the right).

Three thermal resistance curves are shown for the reference case. They are the coolant bulk temperature rise thermal resistance (R''_{bulk}), the convective thermal resistance (R''_{conv}), and the total thermal resistance (R''_{tot}). The total thermal resistance also includes the solid substrate thermal resistance (R''_{solid}) and the contraction thermal resistance (R''_{cont}). The solid substrate thermal resistance was not plotted since it is constant for all channel widths ($q'' = 0.$). The contraction thermal resistance was not plotted since it is small and nearly constant.

* Downwards pointing triangles do not appear on the turbulent flow curves since $Re < 28{,}000$ for the range of channel widths shown. These symbols will appear on future turbulent flow curves as required to indicate when $Re \geq 28{,}000$.

Some interesting features of the curves should be noted. The magnitude of R''_{bulk} continuously gets smaller with channel width since more coolant can be forced through the larger channels at the same pressure drop. It is quite interesting to note that the turbulent flow R''_{bulk} appears to be an extension of the laminar flow results. This is a purely fortuitous result.

The laminar flow R''_{conv} continuously gets larger with increasing channel width. This is an intuitively correct result. For example, for fully-developed laminar flow, $Nu = hD_e/k_f = const.$ Since the channel hydraulic diameter increases with channel width, the heat transfer coefficient must decrease, thereby causing the thermal resistance to increase. For developing laminar flow, the Nusselt number increases as the flow at the channel exit becomes less fully developed, and therefore R''_{conv} increases less rapidly. The turbulent flow R''_{conv} is shown initially to decrease slowly with increasing channel width, and then to increase slowly. This is due to a steady increase in the flow Reynolds number which is required to meet the specified pressure drop. The Nusselt number gets bigger quite rapidly due to the increase in the Reynolds number. In fact, this effect is initially stronger than the reduction in h due to increases in D_e. One should also remember that the Nusselt number was determined assuming that the flow was fully developed, when in this case it really is not fully developed at the channel exit.

Perhaps the most interesting fact to note here is that the laminar flow R''_{tot} curve does not show any distinct optimum as predicted by the

Stanford researchers. Instead, the total thermal resistance tends to more-or-less level off with sufficiently large channel widths. In fact, it is found that the total thermal resistance for turbulent flow is lower! It is significantly lower - on the order of 20-30 percent. Remember also that the turbulent flow thermal and fluid performance predictions should be conservative (too large a friction factor, and too small a Nusselt number).

One does not get better thermal performance for nothing, though. As can be seen from the pumping power versus channel width plot, the required pumping power continuously increases with channel width. The pumping power is generally less than 10 w/cm^2, which is considered to be a very reasonable pumping cost in light of the thermal performance obtained.

Four separate output files are provided as output by MICROHEX. The numerical results contained in those output files for the reference case have been included as Appendix F of this thesis. At the top of each output column is the variable name and the units of the output results. The description of what each variable name represents is included in the comment header section of the RTOTAL subroutine (see Appendix E). Note that some variable names are different from the notation used in the text of this thesis. The MICROHEX numerical results have been checked and verified with a hand-held calculator for several channel widths.

The typical values of several analysis parameters for the reference case will now be reviewed. For simplicity, the following channel widths are selected: fully-developed laminar flow (w_c = 50 μm), developing

laminar flow (w_c = 100 μm), and developing turbulent flow (w_c = 300 μm). The liquid coolant and heat sink material properties are uniformly constant since the surface heat input is zero (q" = 0.). The properties are evaluated at TFLUIN = 300°K. The silicon thermal conductivity is k_w = 148 W/m°C. The water thermal conductivity is k_f = 0.613 W/m°C, the specific heat is Cp_f = 4177.6 J/kg°C, the Prandtl number is Pr = 6.033, the density is ρ_f = 995.5 kg/m^3, and the dynamic viscosity is μ_f = 0.00088 kg/ms. From Equation 2.22, the coolant temperature rise due to viscous dissipation is is ΔT_{pump} = 0.017°C. This is a very small temperature change, and therefore the properties are still essentially constant.

The heat sinks have a channel height b = 200 μm, 400 μm, and 1200 μm respectively for w_c = 50 μm, 100 μm, and 300 μm (α = 4.0). The corresponding fin widths are w_w = 50 μm, 100 μm, and 300 μm. The channel hydraulic diameters are D_e = 4A/P = 80 μm, 160 μm, and 480 μm for the same channel widths. From Equation 2.3, the laminar equivalent diameter is D_{le} = 416.3 μm for w_c = 300 μm (turbulent flow).

The average coolant velocity in the channels is V_c = 1.40 m/s, 4.67 m/s, and 11.59 m/s respectively for w_c = 50 μm, 100 μm, and 300 μm. From Equation 2.1, the corresponding Reynolds numbers are Re = 127, 845, and 6290. The laminar equivalent Reynolds number given by Equation 2.4 is Re^* = 5450 for w_c = 300 μm (turbulent flow). The hydrodynamic entrance length is given by $L^+ = L/D_eRe$ = 0.99, 0.074, and 0.0033 respectively. From Equation 2.13, the corresponding thermal entrance lengths are x^* = 0.164, 0.0123, and 0.0005.

The laminar flow friction factor can be obtained from Table 2.5 as $f_{app} = ((f_{app}Re)/Re) \approx 0.142$ and 0.0254 respectively for w_c = 50 μm and 100 μm. From Equation 2.6, the turbulent flow friction factor is $f_{app} \approx 0.0124$. From Equation 4.18, the aforementioned coolant velocities are obtained ($Kc = Ke = K_{90} = 0$). The coolant volumetric flow per unit heater surface area can be obtained from Equation 4.19 as $V'' \approx 1.4$ (cm^3/s)/cm^2, 9.35 (cm^3/s)/cm^2, and 69.53 (cm^3/s)/cm^2 respectively for w_c = 50 μm, 100 μm, and 300 μm. The corresponding coolant pumping power per unit heater surface area is $P'' = \Delta PV'' \approx 0.10$ W/cm^2, 0.64 W/cm^2, and 4.79 W/cm^2.

The laminar flow Nusselt number can be obtained from Equation 2.12 using Tables 2.8 and 2.11 to give Nu ≈ 5.86 and 7.17 respectively for w_c = 50 μm and 100 μm. The turbulent flow Nusselt number can be obtained from Equation 2.15 to give Nu ≈ 42.8 for w_c = 300 μm. The corresponding heat transfer coefficients are $h = Nuk_f/D_e \approx 44{,}900$ W/m^2°C, 27,470 W/m^2°C, and 54,600 W/m^2°C. From Equation 3.13, the corresponding fin efficiencies are 86.4 percent, 84.0 percent, and 50.7 percent. From Equation 3.7, the corresponding values of the fin criterion are $2k_w/hw_w \approx 132$, 108, and 18.1. The fin criteria are all greater than 6.0, and therefore fin analysis assumption #5 is not violated. Note though that the turbulent flow fin efficiency is less than the 80 percent limit specified in order for the fin model to be accurate. Therefore, the thermal performance will probably not be quite as good as predicted. Note though, that the turbulent Nusselt number was assumed to be fully developed when in actuality the flow is not fully developed. Therefore the thermal performance may be better.

The thermal resistance was computed for a moderate aspect ratio since $\alpha = 4.0$. From Equation 4.3, the solid material thermal resistance between the heater surface and the fin base and channel base plane is $R''_{solid} \approx 0.0068°C/(W/cm^2)$ for all three channel widths. From Equation 4.4, the contraction thermal resistance is $R''_{cont} \approx 0.0007$ $°C/(W/cm^2)$, $0.0015°C/(W/cm^2)$, and $0.0045°C/(W/cm^2)$. From Equation 4.6, the convective thermal resistance is $R''_{conv} \approx 0.0563°C/(W/cm^2)$, $0.0943°C/(W/cm^2)$, and $0.0724°C/(W/cm^2)$. From Equation 4.7, the coolant bulk temperature rise thermal resistance is $R''_{bulk} \approx 0.1718°C/(W/cm^2)$, $0.0257°C/(W/cm^2)$, and $0.0035°C/(W/cm^2)$. From Equation 4.9, the total thermal resistance is $R''_{tot} \approx 0.2356°C/(W/cm^2)$, $0.1282°C/(W/cm^2)$, and $0.0871°C/(W/cm^2)$.

The total thermal resistance of the three representative channel widths for the reference case is plotted in Figure 4.5 as a function of the distance from the upstream heater edge. The actual channel length is longer than the 1.0 cm long heat source. The effect of thermal spreading along the channel length has been included by using

$$R''_{tot} = [R''_{solid} + R''_{cont} + R''_{conv}][1.-e^{-(x/L_d)}][1.-e^{-((L-x)/L_d)}] + R''_{bulk} \qquad (4.21)$$

where L_d is defined in conjunction with Equation 3.19 (thermal spreading was not accounted for in Figure 4.4.) Note that thermal spreading in the transverse direction was not included here since it

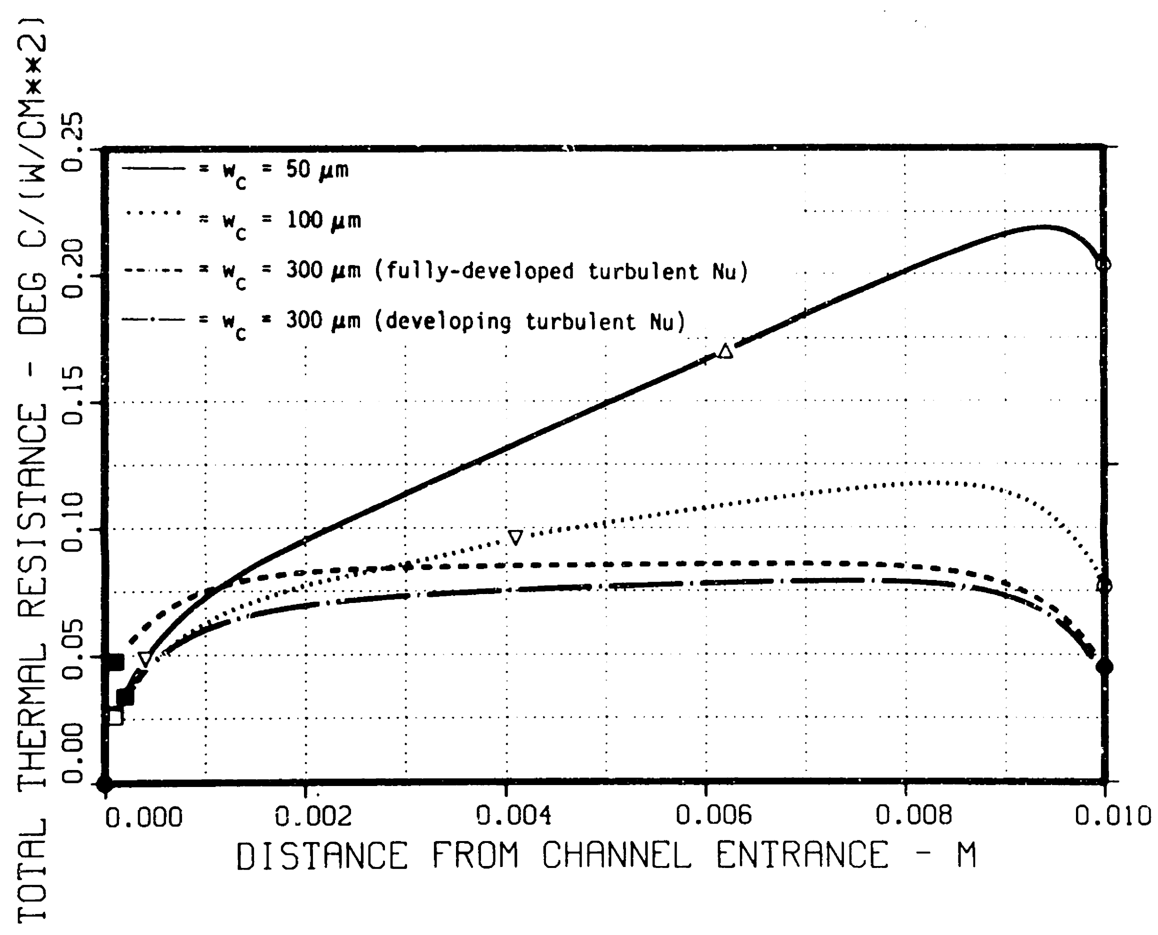

Figure 4.5. Thermal resistance as a function of distance from the upstream heater edge for several reference case channel widths.

is assumed that the heat source is very wide in the transverse direction. For the curves with the triangles, the results to the right of the upwards pointing triangle is fully developed, and the flow to the left of the downward pointing triangle is for $x^* < 0.005$.

Two curves are shown for turbulent flow. The dashed curve assumes that the Nusselt number is fully developed everywhere (which is the assumption used everywhere else in this treatise - except as noted). The solid-dot curve multiplies the turbulent Nusselt number by $[1+(D_e/L)^{2/3}]$ to approximate the effect of developing flow on the Nusselt number.* A comparison of the two curves shows that the flow at the channel exit is nearly fully developed for w_c = 300 μm. A comparison of the curves in Figure 4.5 shows that the effect of R''_{bulk} is very important for laminar flow. This leads to greater non-uniformity in R''_{tot} along the channel. The average R''_{tot} is consequently much smaller for turbulent flow. Section 4.6 will discuss how "compensation heaters" can be used to enhance the uniformity in R''_{tot}.

Having reviewed the results for the reference case, it is instructive to see what happens when some of the input variables are temporarily changed one at a time relative to the reference case values. A comparison between the early Stanford thermal and fluid performance prediction theory, and that theory which is used in this study, is shown in

---

* As discussed in Section 2.4, this conversion does not include the effect of Re and Pr on the developing turbulent Nusselt number, and therefore should be used with caution.

Figure 4.6. The solid curve is for the reference case where the calculations are done for fully-developed/developing, laminar/turbulent flow. The dotted curve is for the same reference case except that the flow is assumed to be fully developed and laminar for all channel widths. When the flow really is laminar and fully developed (to the left of the upward pointing triangles), the two computational methods yield virtually identical results, which indeed they should. The small difference between the two curves in this region is due to the inherent disagreement between using polynomial equations to model fully-developed laminar flow, (see subroutines SFFD and SNUFD in Appendix E), and using interpolation in the lookup tables used in this study (see Tables 2.5 and 2.11, and subroutines SLAMF and SLAMNU in Appendix E).

To the right of the upward pointing triangles, the flow is not fully developed. The R''_{tot} for the case where the flow is always assumed to be laminar and fully developed is higher than that for the reference case. The error increases with increasing channel width. In fact, there is a distinct minimum in the thermal resistance, which is an artifact of the assumption that the flow is always fully developed. Since the total thermal resistance rises quickly for smaller channel widths, this author considers the so-called "optimum" to instead be a "lower bound" to the range of channel widths that should be used.

Figure 4.6 also presents thermal and fluid performance results for a channel aspect ratio of $\alpha = 10.01$ (the solid-dot and dashed curves). The solid-dot curve gives the results where the flow is assumed to be fully

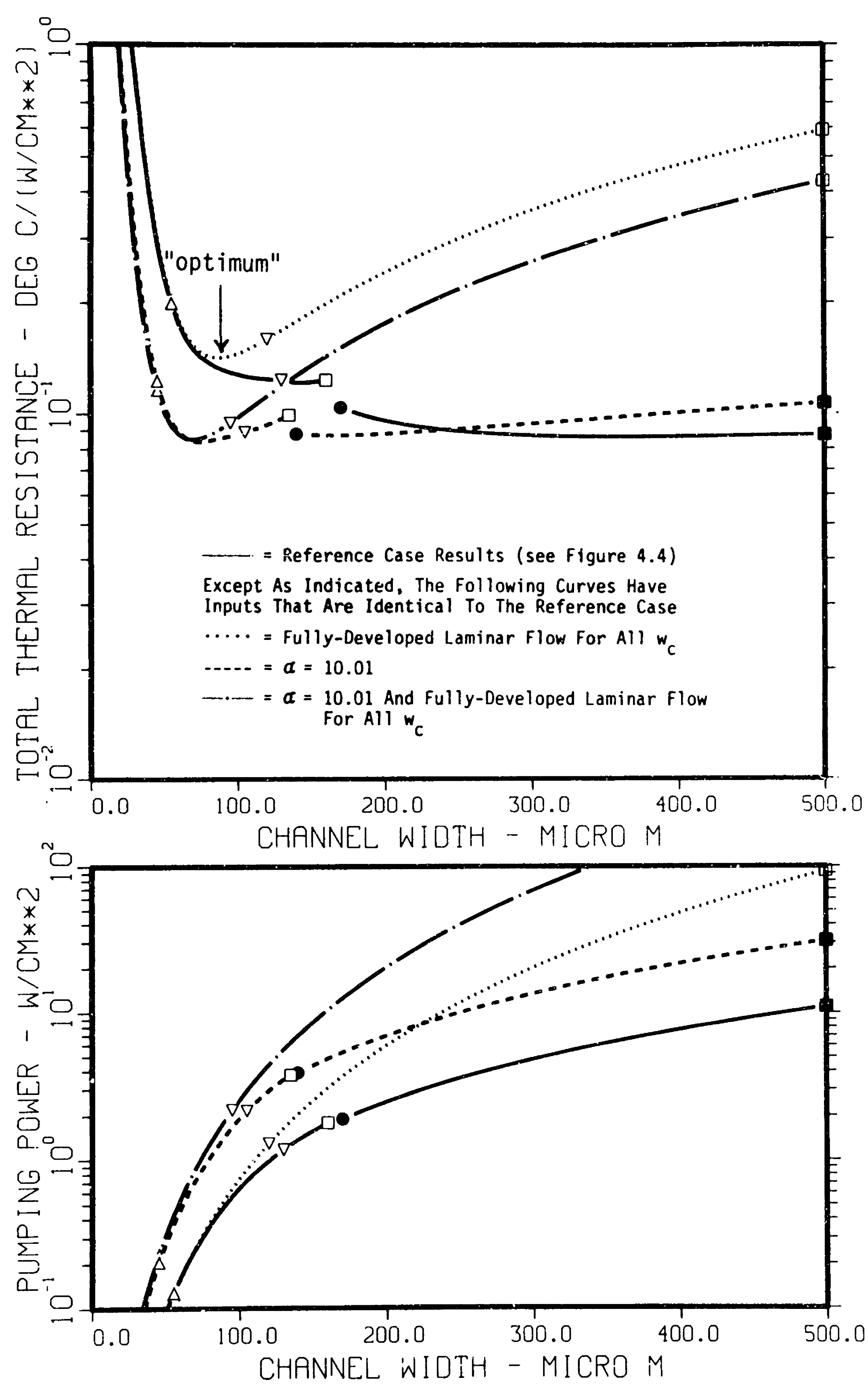

Figure 4.6. Thermal resistance and pumping power versus channel width for the reference case and fully-developed laminar flow at two channel aspect ratios.

developed and laminar for all channel widths. The dashed curve gives the results for fully developed/developing, laminar/turbulent flow. The reader should note that the computational differences between the two models are greater for $\alpha = 10.01$ than for $\alpha = 4.0$. This difference is due to the fact that $\alpha > 10.0$ is assumed to be equivalent to flow between infinite parallel plates for the model used in this study. The difference is notably small ($< \sim 10$ percent), which is the reason why $\alpha = 10.0$ is used to delineate between moderate and large aspect ratio channels. The reader should note that the thermal resistance in laminar flow is about 50 percent smaller for $\alpha = 10.01$ than for $\alpha = 4.0$. The turbulent flow thermal performance "crosses-over" at $w_c \approx 240$ μm. This effect is due to the fact that the fin efficiency for $\alpha = 10.01$ is much smaller than that for $\alpha = 4.0$ (even though the $\alpha = 10.01$ Nusselt number is larger). Note that the pumping power requirements for the $\alpha = 10.01$ case are always larger.

Figure 4.7 presents the thermal and fluid performance results for a comparison of the three coolant flow rate constraints. Note that the thermal performance for constant volumetric flow continuously increases with channel width. This is due to the decrease in coolant velocity related to the increase in the flow cross-sectional area (α = const). The pumping power therefore also continuously decreases with channel width. The thermal performance for the constant pumping power constraint behaves very similar to that of the reference case, except that the thermal performance for laminar flow shows an obvious optimum. The primary intent of this comparison, though, is to show that the three coolant flow rate constraints provide identical thermal and fluid

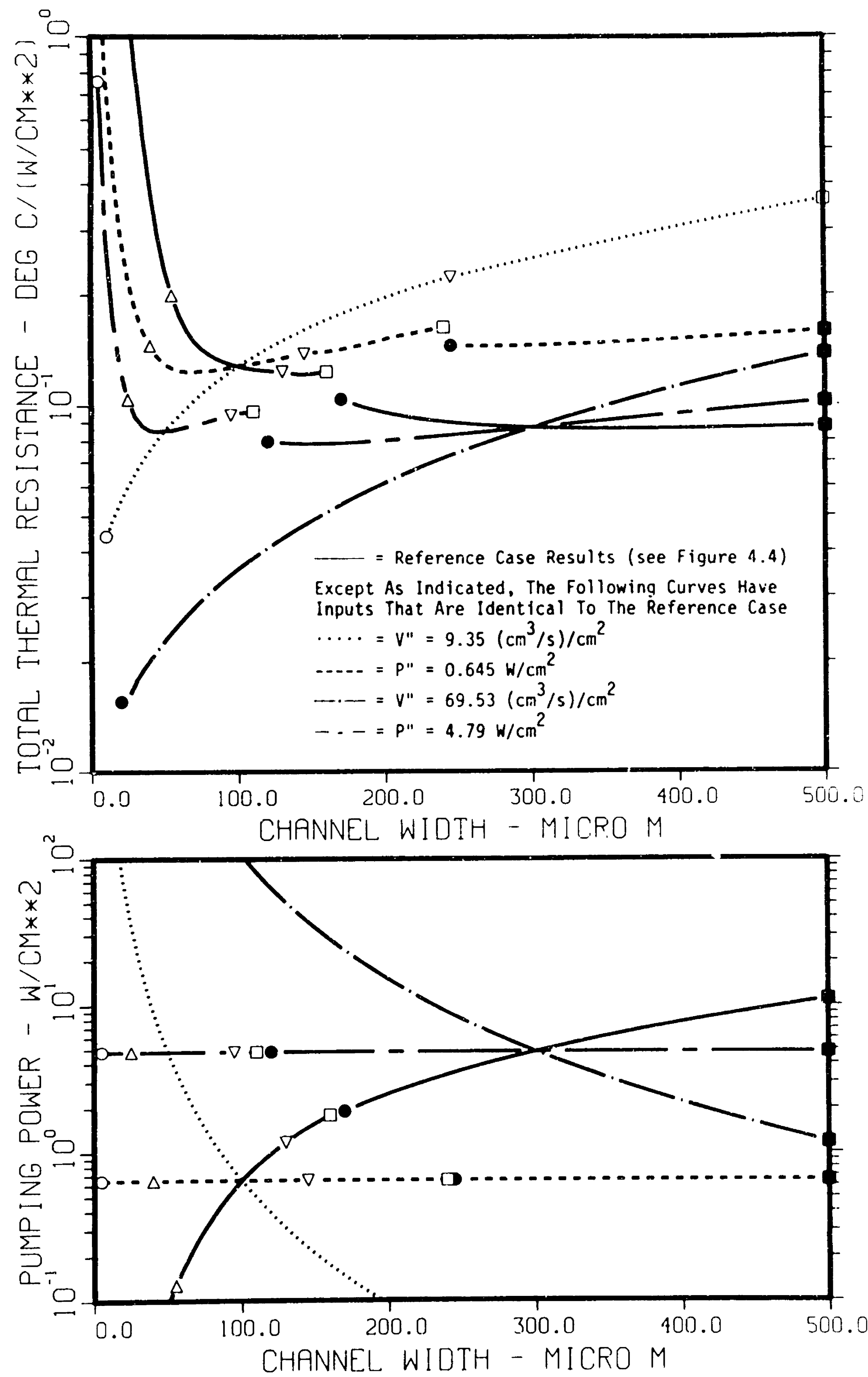

Figure 4.7. Thermal resistance and pumping power versus channel width for the reference case with several coolant velocity constraints.

performance in both the laminar and turbulent regimes when $P'' = \Delta PV''$. This is a sensitive test of the computational accuracy of the MICROHEX program.*

Figure 4.8 presents the thermal and fluid performance results for a comparison of various heat sink materials. As expected, the total thermal resistance decreases with higher heat sink thermal conductivity (the pumping power requirements of course do not change). The dotted and dashed curves terminate at somewhat smaller channel widths since the fin criterion is not satisfied for large channel widths.

Making the microchannel heat sink directly into the back of an IC chip does have potential problems, like reduced reliability and reduced manufacturing yield. Since copper and aluminum offer better thermal performance, the microchannel heat sink might be made in copper or aluminum and then interfaced with the chip. The heat sink therefore becomes a "cold plate", which can have good thermal performance if the interface thermal resistance (R''_{int}) is small enough. A relatively new interfacing method called a "microcapillary thermal interface" has been developed by Tuckerman and Pease (1983) and Tuckerman (1984). As discussed in Appendix D, the thermal resistance for this type of interface can be of the order $R''_{int} \approx 0.02°C/(W/cm^2)$! Therefore, a silicon IC chip could be attached to a microchannel heat sink made of copper, and the overall thermal resistance could be lower than if the

* Note that single precision calculations are used by MICROHEX. Numerical roundoff errors do appear on occasion for relatively large channel widths (say $w_c > 400$ µm). The errors can usually be eliminated with an appropriate selection of WCSTAR and WCINCR.

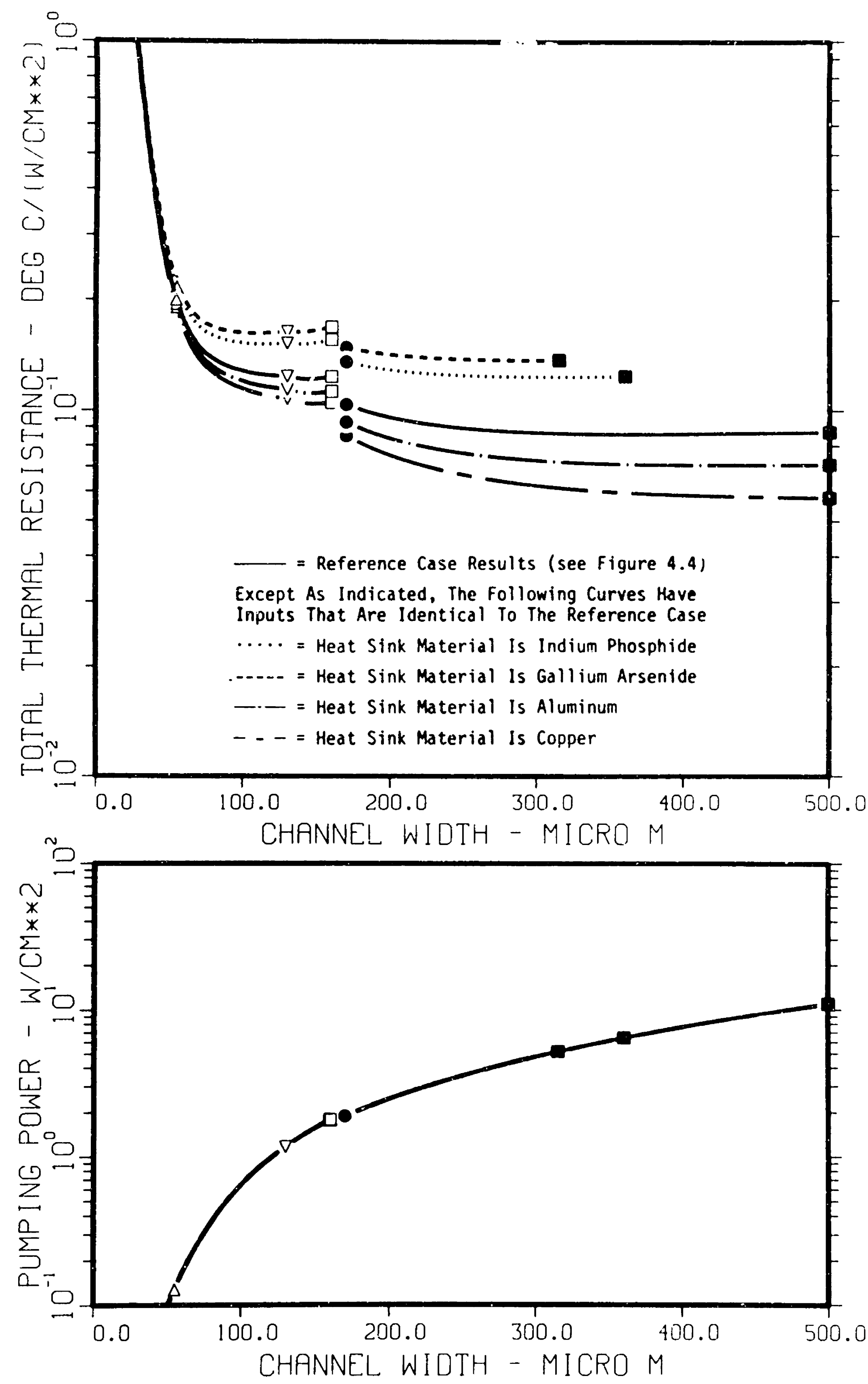

Figure 4.8. Thermal resistance and pumping power versus channel width for the reference case with several heat sink materials.

microchannel heat sink had been fabricated directly in the back of the IC chip!

Figure 4.9 presents the thermal and fluid performance results for a comparison of three liquid coolants. The solid curve is for the usual water-cooled reference case. The dashed curve is for freon (CCl_2F_2), and the dotted curve is for FC-77 (3M Company). As expected, using water as the coolant provides superior thermal performance. The pumping power requirements are essentially the same for all three coolants. Freon and FC-77 may be preferable to water because of possible contamination of the chip due to impurities in the water. (Freon and FC-77 are commonly used in pool boiling cooling of electronics where the coolant is in direct contact with the IC). The superior thermal performance of water is another good reason to make the heat sink as a cold plate and mate it with the chip with a low-thermal-resistance interface. As an aside, the reader should notice some "waviness" in the FC-77 thermal resistance for $x^* < 0.005$ (to the right of the downward pointing triangle). This effect is due to numerical errors in obtaining the Nusselt number via linear extrapolation for $x^* < 0.005$. This error, though, is barely perceptible.

Figure 4.10 presents the thermal and fluid performance for a comparison of various inlet coolant temperatures. The thermal resistance is reduced when the coolant temperature is increased. This effect is due to a reduction in the coolant dynamic viscosity and a larger coolant thermal conductivity. Note that R''_{tot} decreases even though the silicon thermal conductivity decreases.

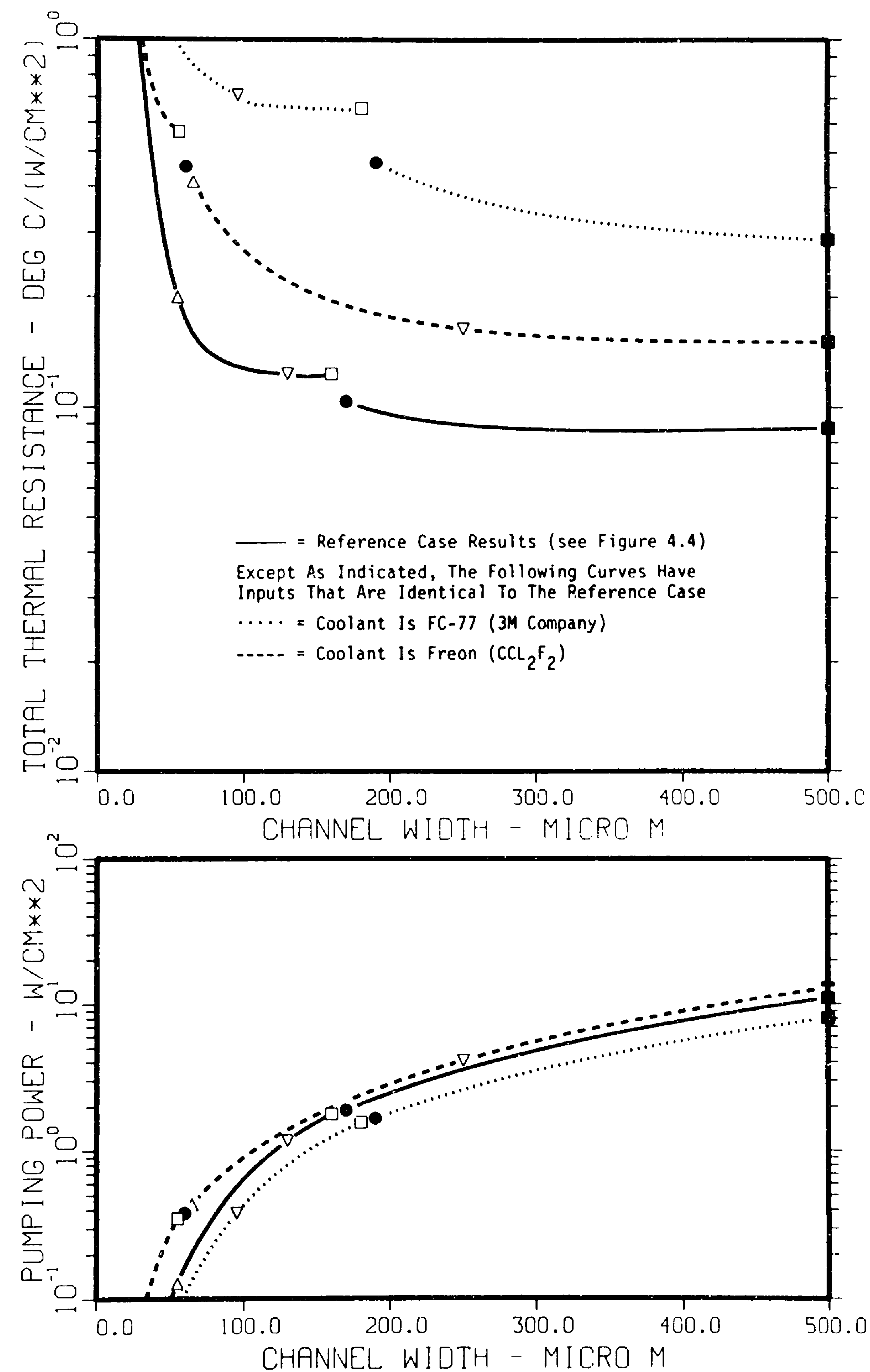

Figure 4.9. Thermal resistance and pumping power versus channel width for the reference case with several liquid coolants.

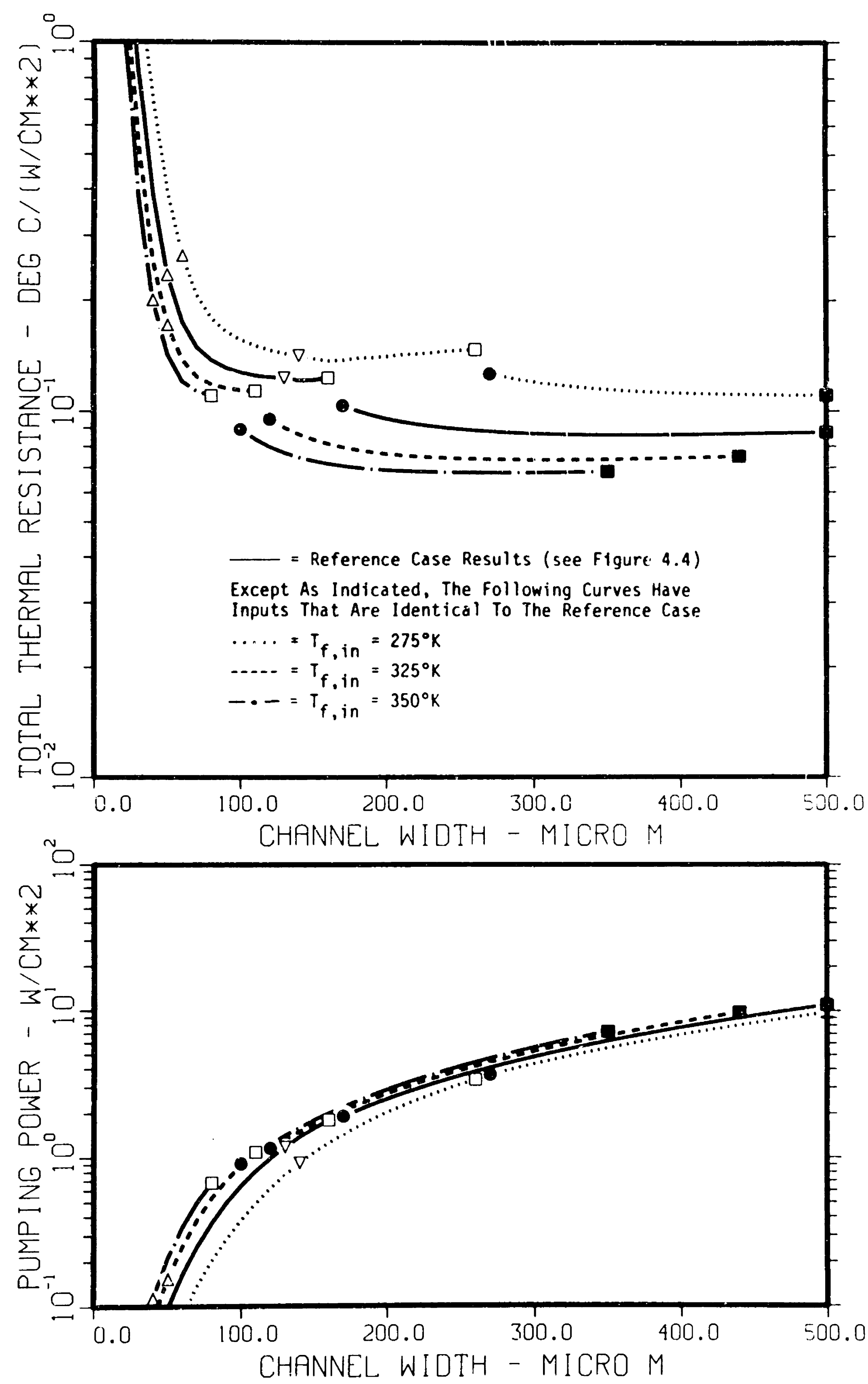

Figure 4.10. Thermal resistance and pumping power versus channel width for the reference case with several inlet coolant temperatures.

Increasing the inlet coolant temperature to get lower R''_{tot} can be misleading since the ultimate concern usually is the peak surface temperature of the chip. For small heating rates, increasing the coolant temperature will result in higher surface temperatures. For large heating rates, increasing the coolant temperature may prove to reduce the surface temperatures. The requirement to be met is that

$$(T_{surf})_{cold} > (T_{surf})_{hot} \tag{4.22}$$

which is equivalent to

$$(T_{f,in} + q''R''_{tot})_{cold} > (T_{f,in} + q''R''_{tot})_{hot} \tag{4.23}$$

or that

$$\Delta T_{f,in} + q''\Delta R''_{tot} < 0 \tag{4.24}$$

where the subscripts hot and cold represent respectively the hot and cold inlet coolant temperatures.* The reader should note, though, that there is a slight increase in the pumping power for the higher inlet coolant temperatures. This is due to the higher mass flow rate associated with the reduction in the coolant viscosity (at the same ΔP).

Figure 4.11 presents the thermal and fluid performance predictions for comparison on various heating rates. Several notable things happen

* Ignores the change in the viscous heating coolant temperature rise.

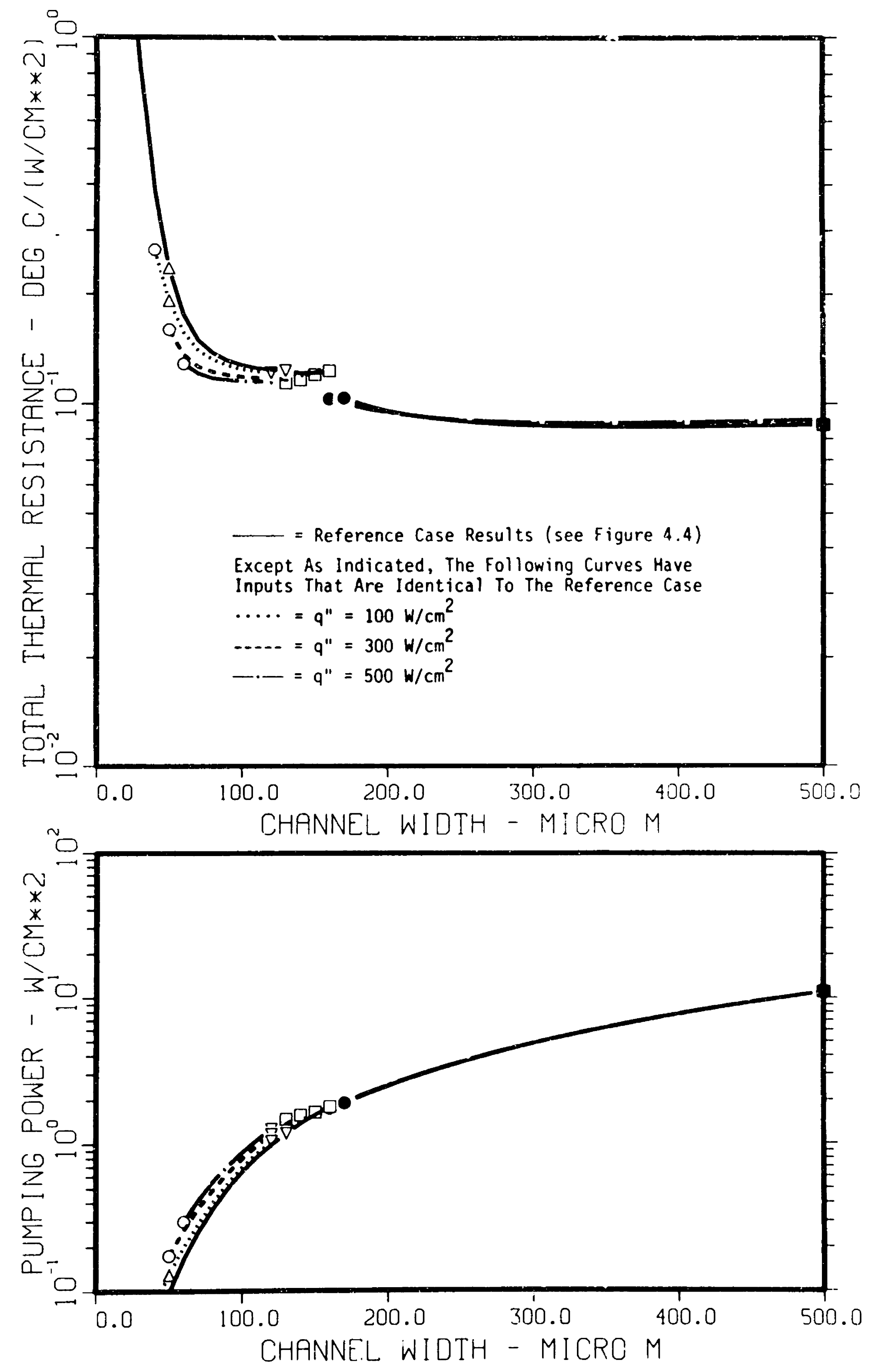

Figure 4.11. Thermal resistance and pumping power versus channel width for the reference case with several surface heating rates.

as the heat input per unit surface area is increased. For the small channel widths, the flow rate is so small that the liquid turns to a gas before reaching the channel exit - these solutions have been discarded. The total thermal resistance is reduced with increasing q" for the small channel widths where the coolant does not boil before reaching the channel exit. This effect is mostly due to the reduction in the coolant dynamic viscosity, which is the reason why the coolant pumping power increases with the surface heating rate.

For moderate channel widths, the total thermal resistance increases slightly due to the reduced substrate thermal conductivity and the higher average coolant viscosity. The turbulent flow results do not show a large change in the thermal resistance. The trend towards higher R''_{tot} at large channel widths is due to reduced substrate thermal conductivity and increased average coolant viscosity. It is interesting to note that as the heating rate increases, the transition Reynolds number criterion (see Table 2.1) is satisfied for larger channel widths in laminar flow, and for smaller channel widths for turbulent flow. This results in "dual" solutions in that both laminar and turbulent flow designs exist for the same channel widths. This is probably not a desirable design channel width because the flow might alternate being sometimes laminar and sometimes turbulent. This in turn could cause fairly large periodic swings in the chip temperatures, which could result in timing and reliability problems for IC chips.

Figure 4.12 presents the thermal and fluid performance predictions for a comparison of various channel lengths. As expected, the shorter channels have lower thermal resistance, but larger pumping power

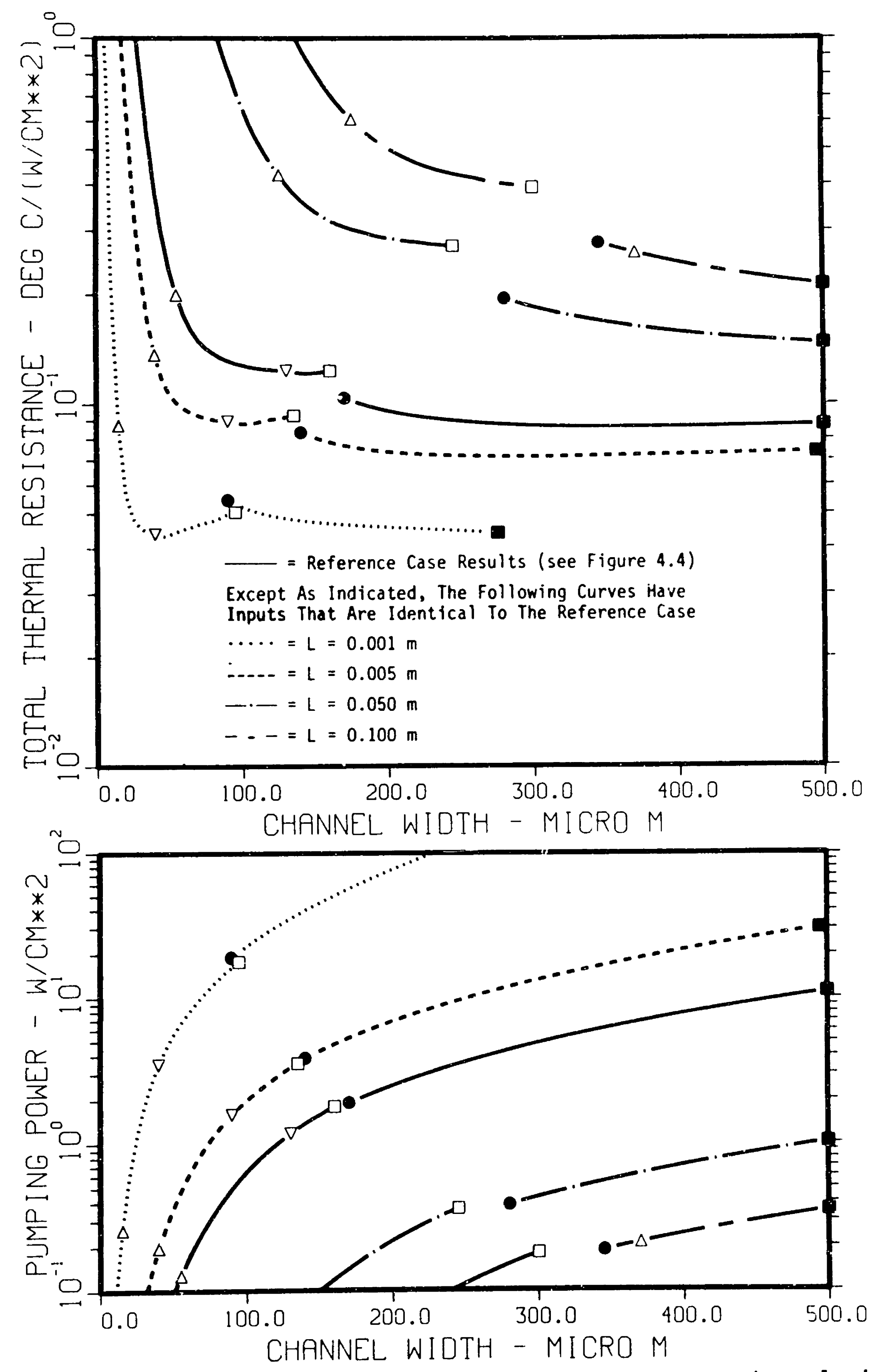

Figure 4.12. Thermal resistance and pumping power versus channel width for the reference case with several channel lengths.

requirements. It is interesting to note that the thermal performance for the very long channels is still very good. This implies that an entire circuit board could quite conceivably be used as a microchannel heat sink.

Figure 4.13 presents the thermal and fluid performance predictions for a comparison of various ratios of the fin thickness and the channel width. It is clear that there is an optimum w_w/w_c ratio, which appears to increase in magnitude as the channel width is increased. If this ratio is too small, then the fin thermal resistance will be high. Conversely, if this ratio is too large, then R''_{bulk} will be high. The trends are the same for laminar and turbulent flow. Note that the pumping power decreases proportional to increases in the w_w/w_c ratio because there are fewer channels per unit width of the chip. Note also that the $w_w/w_c = 1.5$ curve terminates for turbulent flow at large channel widths since the fin criterion is violated.

Figure 4.14 presents the thermal and fluid performance predictions for a comparison of the constant aspect ratio reference case design and several fixed fin height designs. The constant fin height designs show an obvious optimum in the thermal performance. As expected, the thermal and fluid performance of the fixed fin height designs is identical to the reference case when the channel aspect ratios are identical. The reader will notice a "zig-zag" in the thermal and fluid performance curves for the fixed channel height designs when the channel aspect ratio passes through $\alpha = 10.0$. This effect is due to the previously mentioned error in assuming that the friction factor and Nusselt number for flow between

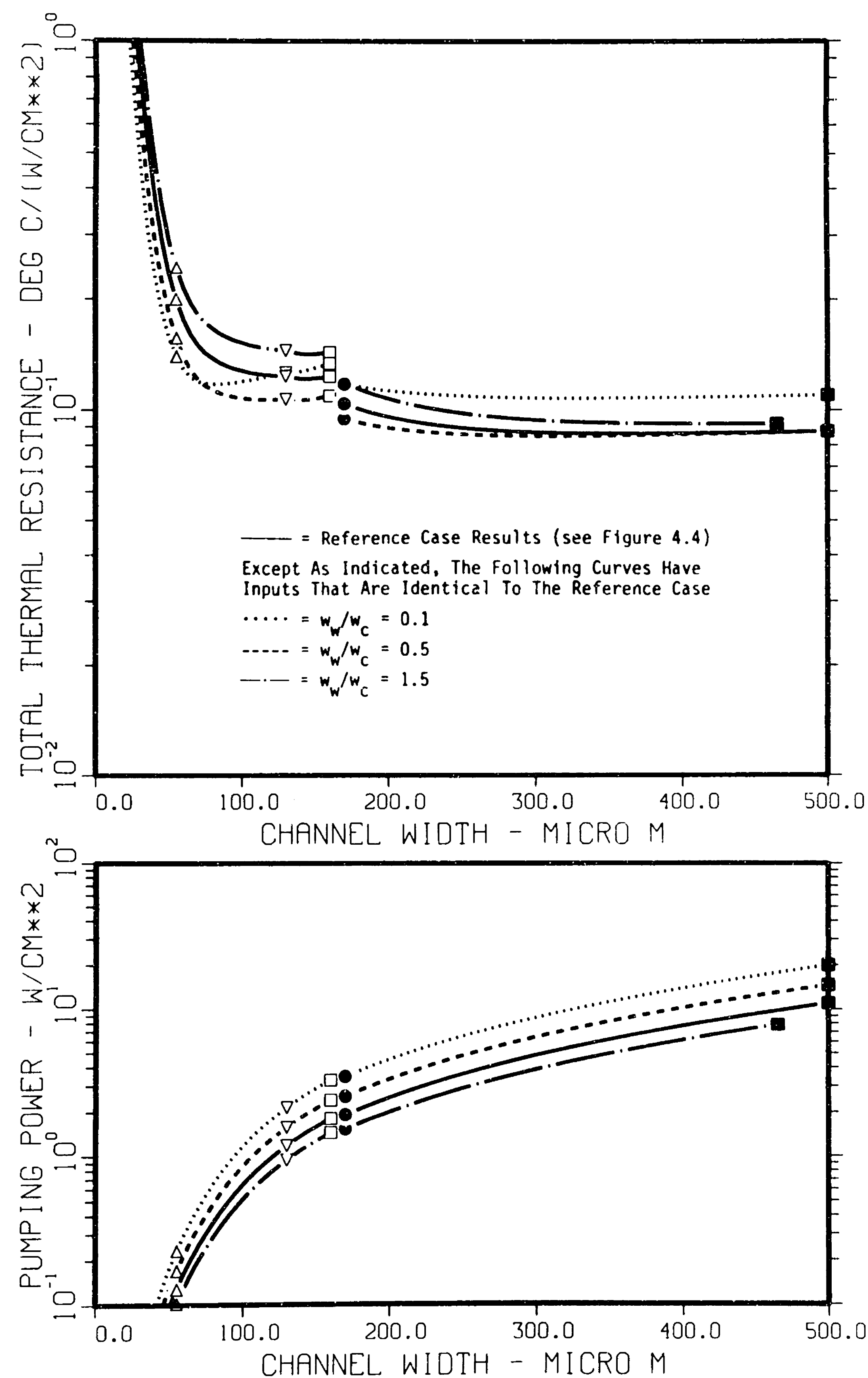

Figure 4.13. Thermal resistance and pumping power versus channel width for the reference case with several values of the fin thickness to channel width ratio.

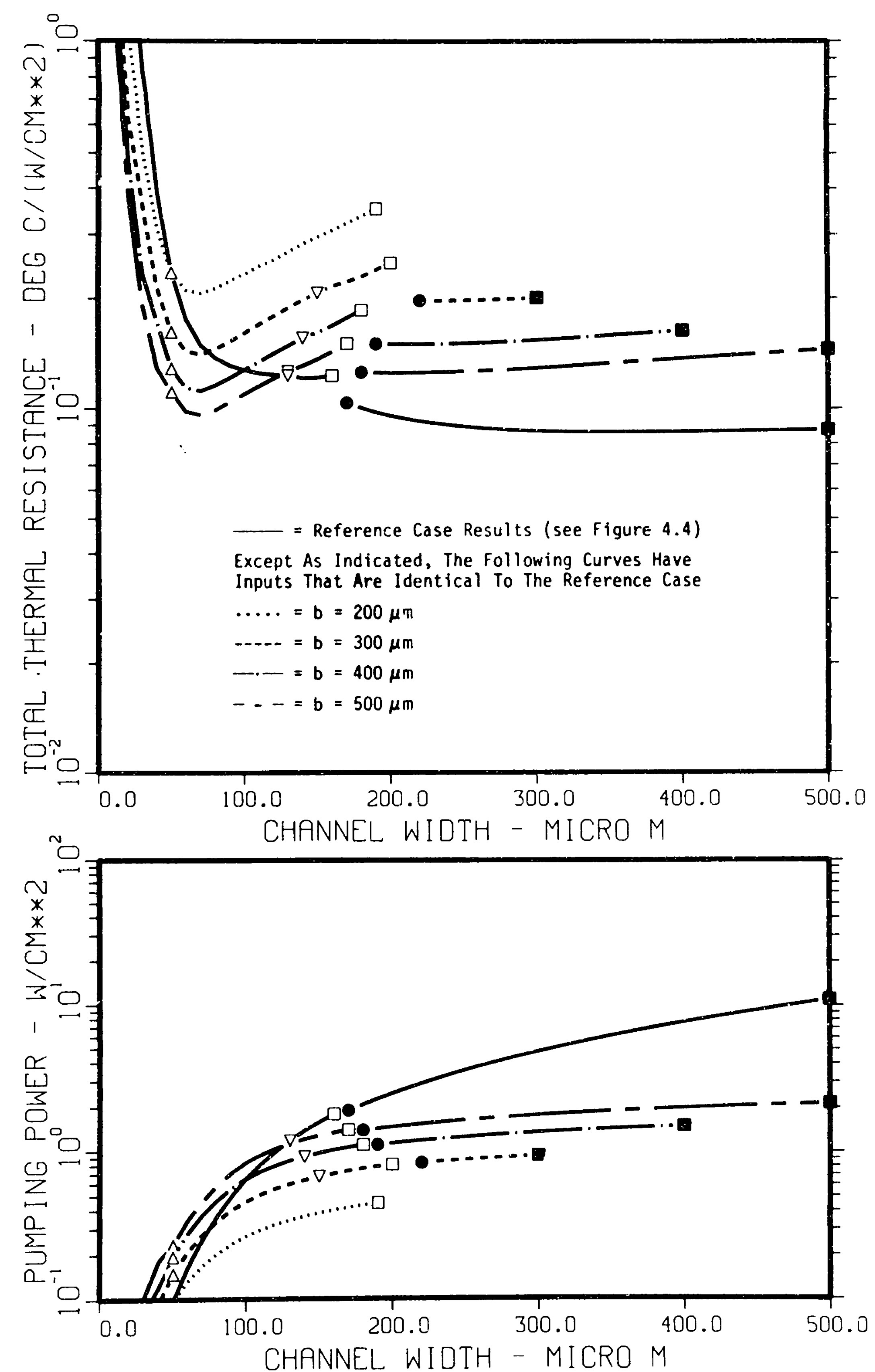

Figure 4.14. Thermal resistance and pumping power versus channel width for the reference case with several constant fin heights.

infinite parallel plates can be used to model $\alpha > 10.0$. Note that the thermal and fluid performance of the constant fin height designs was not computed for $\alpha < 1.0$.

Figure 4.15 presents the thermal and fluid performance predictions for a comparison of various thicknesses of the solid material between the heat source and the fin base and channel base plane. As expected, the R''_{tot} increases as the material thickness increases. Generally speaking, at least ~100 μm of solid material is required to withstand manufacturing handling as well as the coolant pressure.

Figure 4.16 presents the thermal and fluid performance predictions for a comparison of large, moderate, and small aspect ratio channels. The large and moderate aspect ratio channel results were previously discussed in conjunction with Figure 4.6 The main point to notice here is that the small aspect ratio channel design has poor thermal performance for the range of channel widths shown. The thermal performance for larger channel widths does continue to improve, but the coolant pressure induced stress may become too excessive to make small aspect ratio channel designs viable. Because of this, small aspect ratio channel designs probably will not be used much. The pumping power requirements for the small aspect ratio channel designs are small and fall below the bottom of the pumping power plot.

Figure 4.17 presents the thermal and fluid performance predictions for a comparison of inlet and exit pressure losses on the overall pressure drop. As expected, the predicted thermal resistance increases

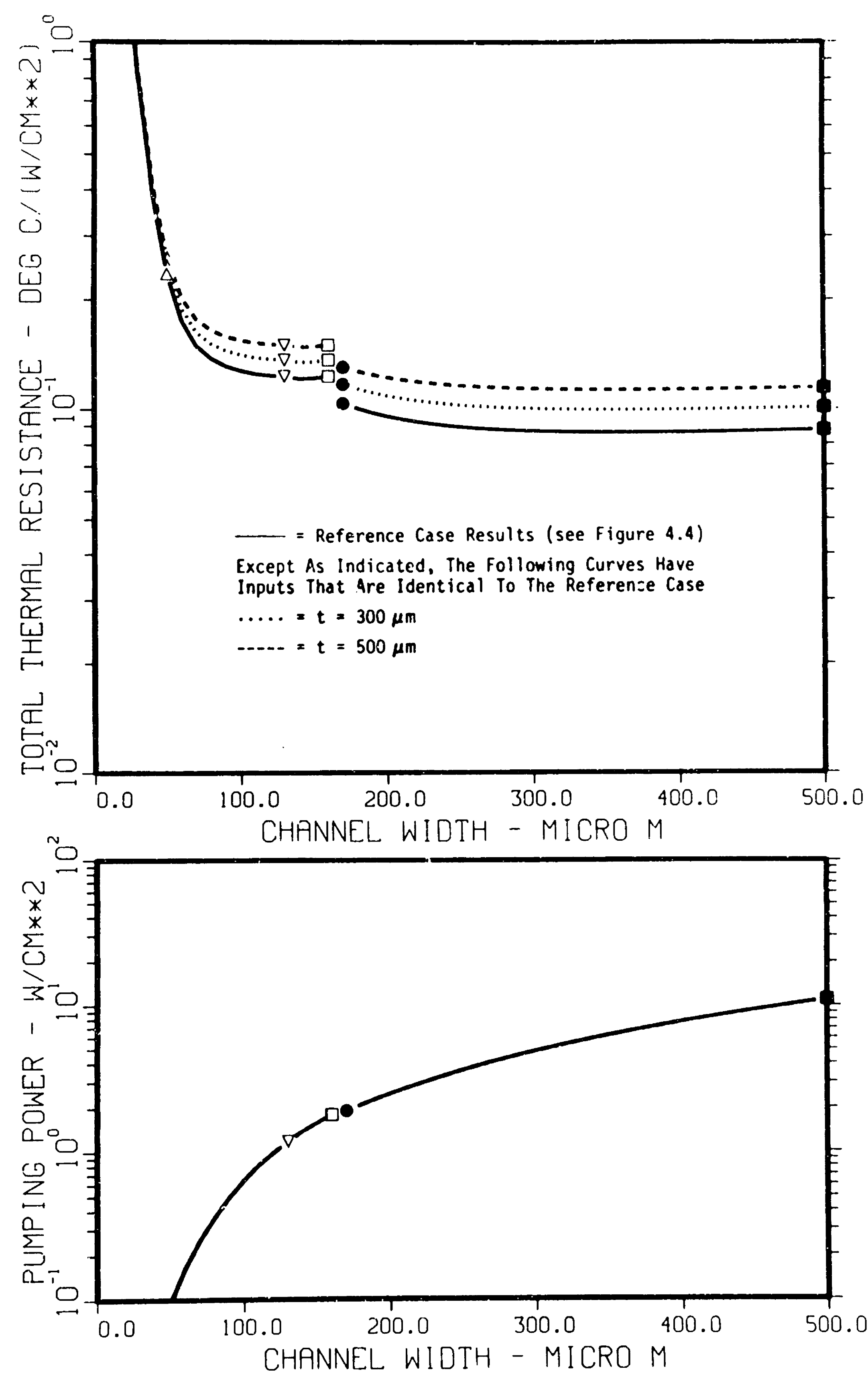

Figure 4.15. Thermal resistance and pumping power versus channel width for the reference case with several solid substrate thicknesses.

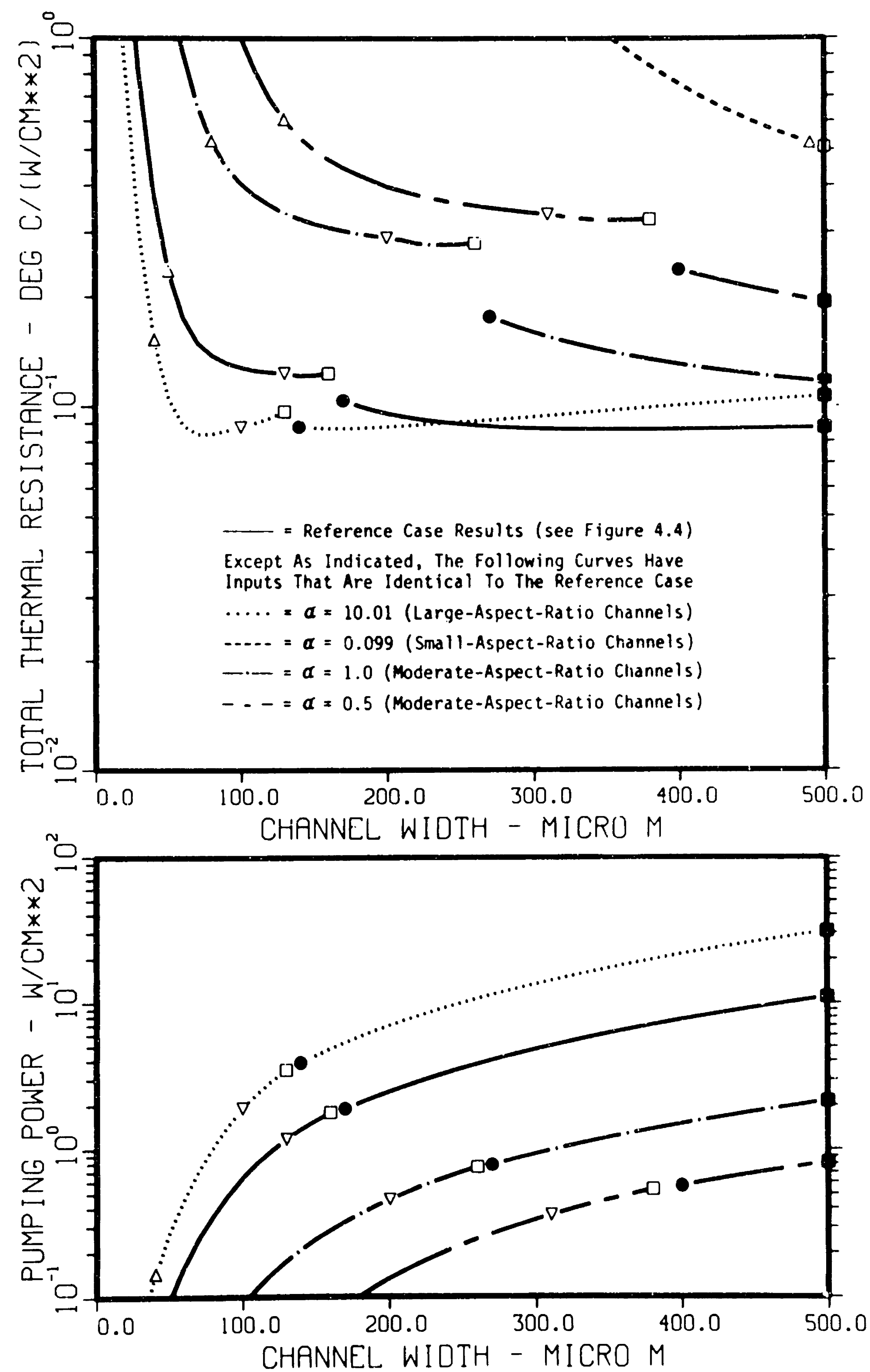

Figure 4.16. Thermal resistance and pumping power versus channel width for the reference case with several channel aspect ratios.

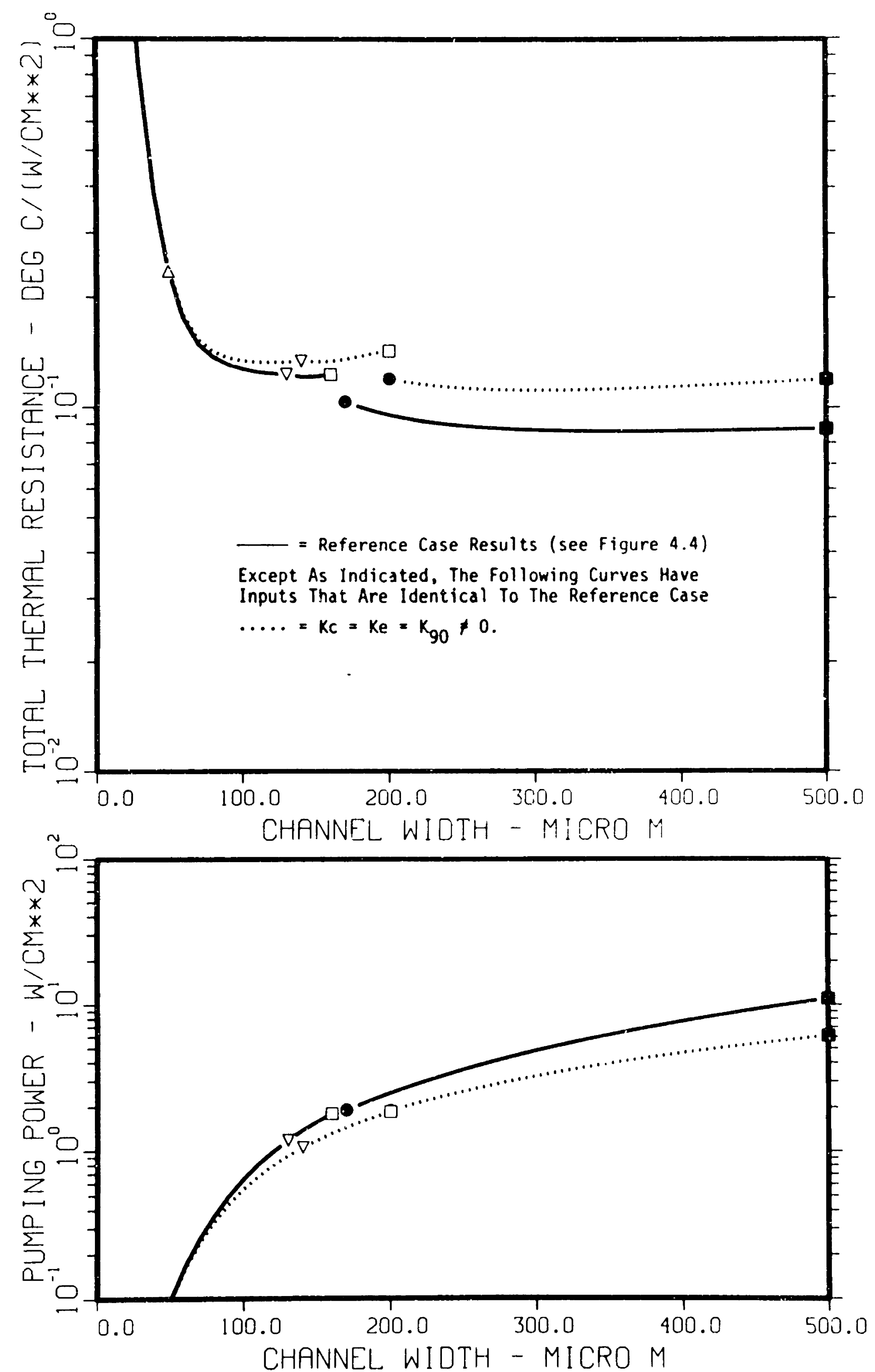

Figure 4.17. Thermal resistance and pumping power versus channel width for the reference case with and without entrance and exit losses.

when Kc, Ke, and K_{90} are included in the overall pressure drop. Note that their effect is larger for turbulent flow than for laminar flow. Note also that the turbulent thermal performance is still better than that for laminar flow.

Figure 4.18 presents the thermal and fluid performance predictions for a comparison of smooth, and repeated-rib-roughened channels. The coolant flow rate is 70 $(cm^3/s)/cm^2$ and $\alpha = 10.01$. The roughened channel designs have better thermal performance. The only question now is whether the roughened channels can be manufactured in the small dimensional sizes implicated for microchannel heat sinks.

The reader should note that some roughened designs are predicted by MICROHEX to require less pumping power than for comparable smooth surface designs. This is an erroneous prediction since an "apples and oranges" comparison is made with respect to the friction factors for large channel widths. The roughened designs assumed that the flow was fully developed, and entrance region effects on the apparent friction factor were not included. The smooth channel designs include the entrance effects. If the entrance effects are ignored for both surface characteristics (i.e. if the channels are very long), then the pumping power requirement for smooth channels is indeed smaller.

4.6 Use of Compensation Heaters

Thermal spreading at the edge of an IC heat source can cause significant variation in temperature across an IC. This non-uniformity in temperature can lead to reliability problems owing to thermal stress caused by differential thermal expansion across the IC. Timing problems

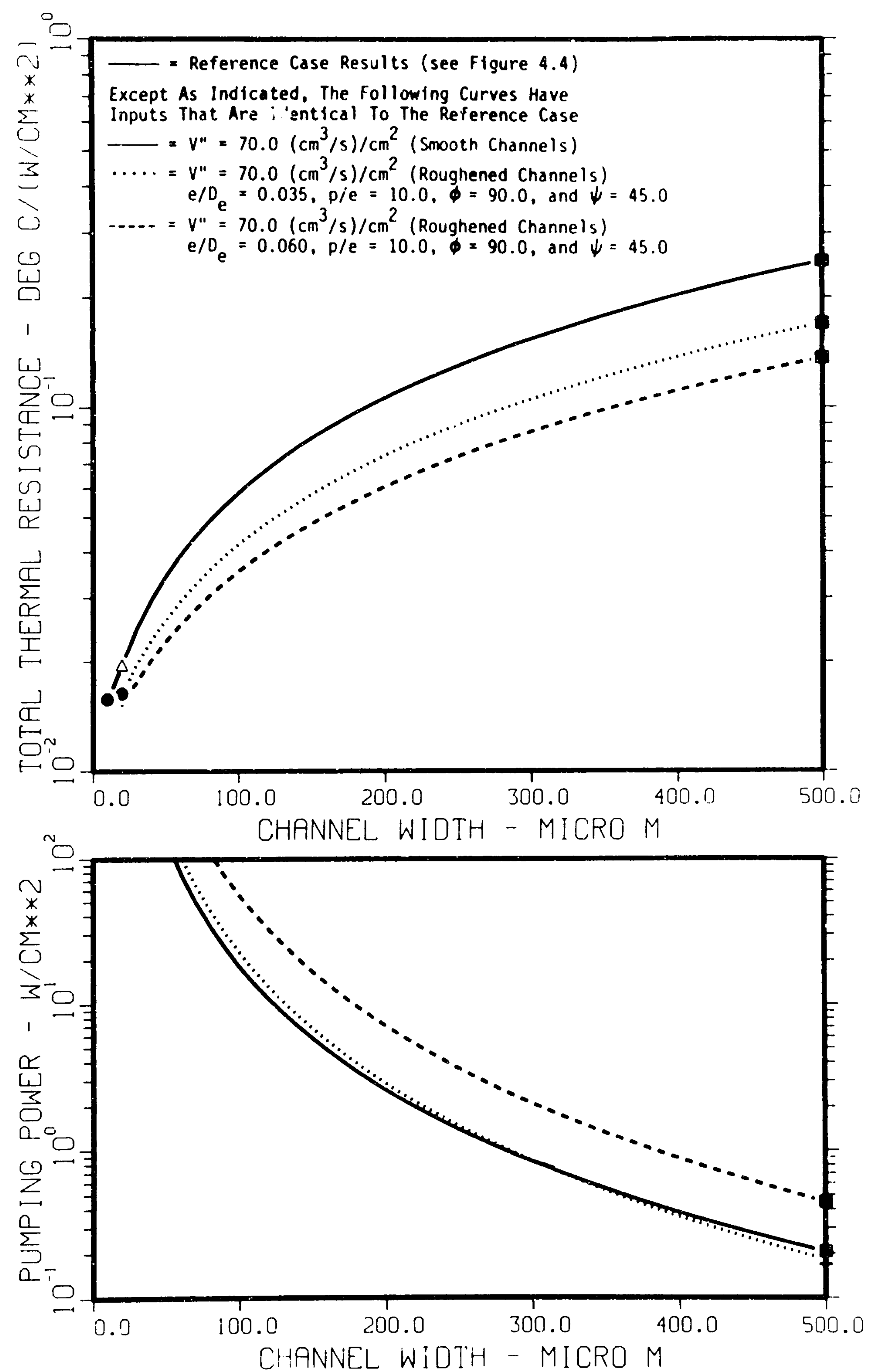

Figure 4.18. Thermal resistance and pumping power versus channel width for the reference case with smooth and repeated-rib-roughened surfaces.

may also arise because the path lengths between devices will change due to differential thermal expansion. If the IC temperature is more uniform, these problems can be virtually eliminated.

Several techniques can be used to make the IC temperature more uniform. The two most important techniques related to microchannel heat sinks are: 1) to keep the coolant bulk temperature rise as small as possible; and 2) to use "compensation heaters." The coolant bulk temperature rise can be reduced by increasing the coolant flow rate per unit surface area V". This can be achieved by increasing the coolant pressure drop for a specified channel width, and by increasing the channel width for a specified coolant pressure drop. The effect of thermal spreading at the heater perimeter can still be a serious problem even if the coolant flow is large.

As shown in Figure 4.19, if an IC is surrounded by a heater with the same heating rate q", then the zone of thermal spreading can be displaced outwards from the IC. The heater which surrounds the IC heat source is called a "compensation heater" because it compensates for thermal spreading at the IC heat source perimeter. This author is not aware of other applications in microelectronics where this method has been used at the chip level, and therefore the concept of a "compensation heater" is considered to be original.

The simplified one-dimensional thermal spreading models at the heater perimeter presented in Section 3.4 can be used to size the minimum width of compensation heaters. Consider, for example, the reference case discussed in Section 4.5.2 with a channel width w_c = 300 μm (turbulent

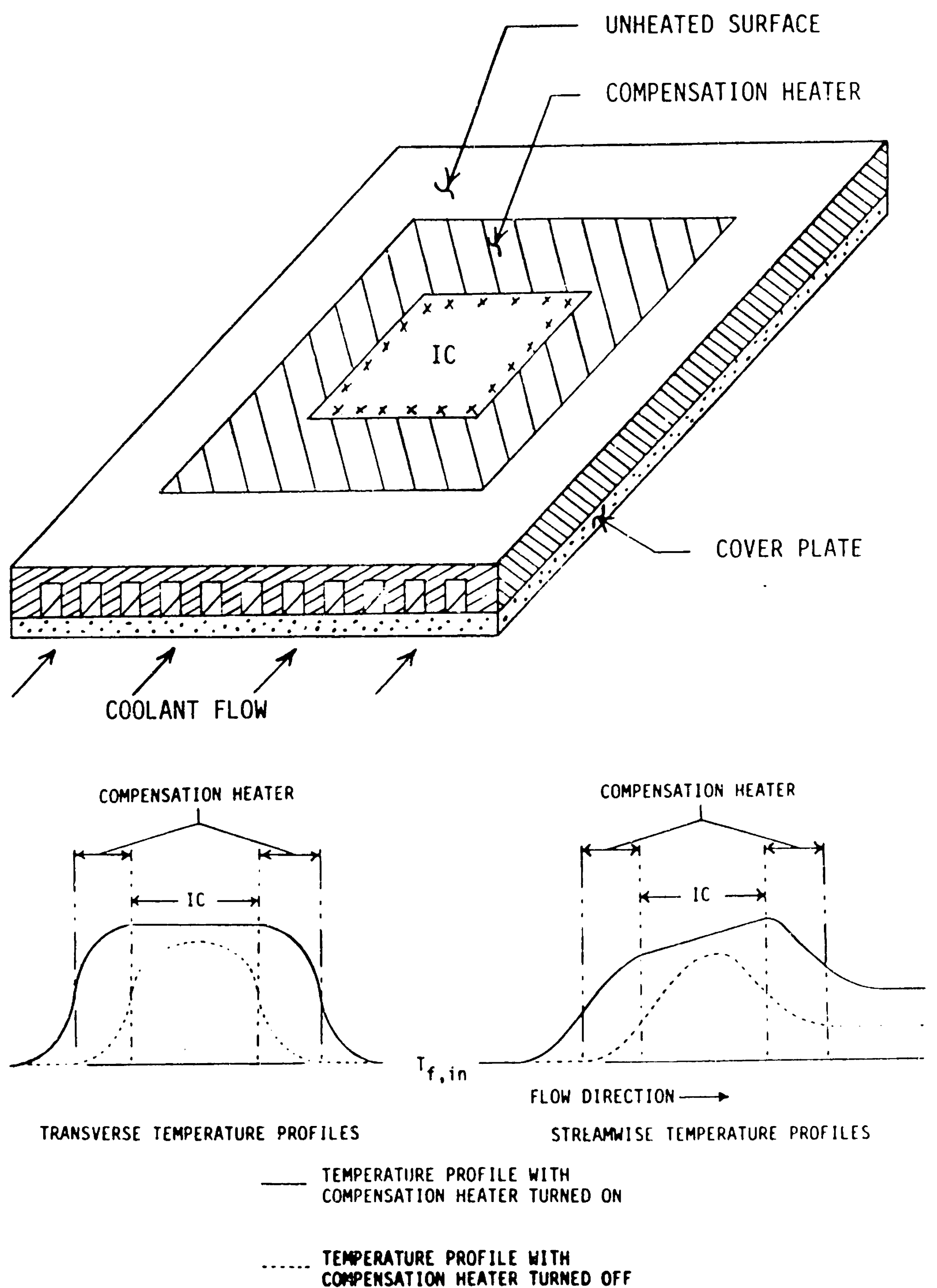

Figure 4.19. Compensation heater concept.

flow). The average Nusselt number along the channel length is about Nu ≈ 50, when the effect of developing flow is included. The thermal spreading diffusion length in the streamwise direction is therefore $L_d \approx 625$ μm, and in the transverse direction $L_d \approx 235$ μm (see Equations 3.19 and 3.20). The compensation heater can be sized such that there is no more than a one percent reduction in the total thermal resistance at the edge of an IC (corresponds to a heater width of $4.8L_d$). Therefore, the compensation heater width, in the streamwise direction is Zs ≈ 3000 μm, and in the transverse direction Zt ≈ 1125 μm.

Figure 4.20 represents the thermal performance prediction obtained by MICROHEX for a comparison of the IC with and without the "compensation heater" energized. The dotted and solid-dot curves are for the IC without the "compensation heater" energized, and the solid and dashed curves are for both the IC and the "compensation heater" energized. The solid and dotted curves are for the center of the IC in the streamwise direction. The dashed and solid-dot curves are for the edge of the IC in the streamwise direction. Note that the effect of the two-dimensional heat transfer near the corners of the IC and the "compensation heater" has been crudely modeled by superimposing the one-dimensional models for the two directions. This is a serious simplification of the actual heat transfer, but useful conclusions can still be drawn.

From Figure 4.20, it is apparent that the thermal resistance over the region of the IC heat source is much more uniform when the "compensation heater" is energized. The average total thermal resistance, though,

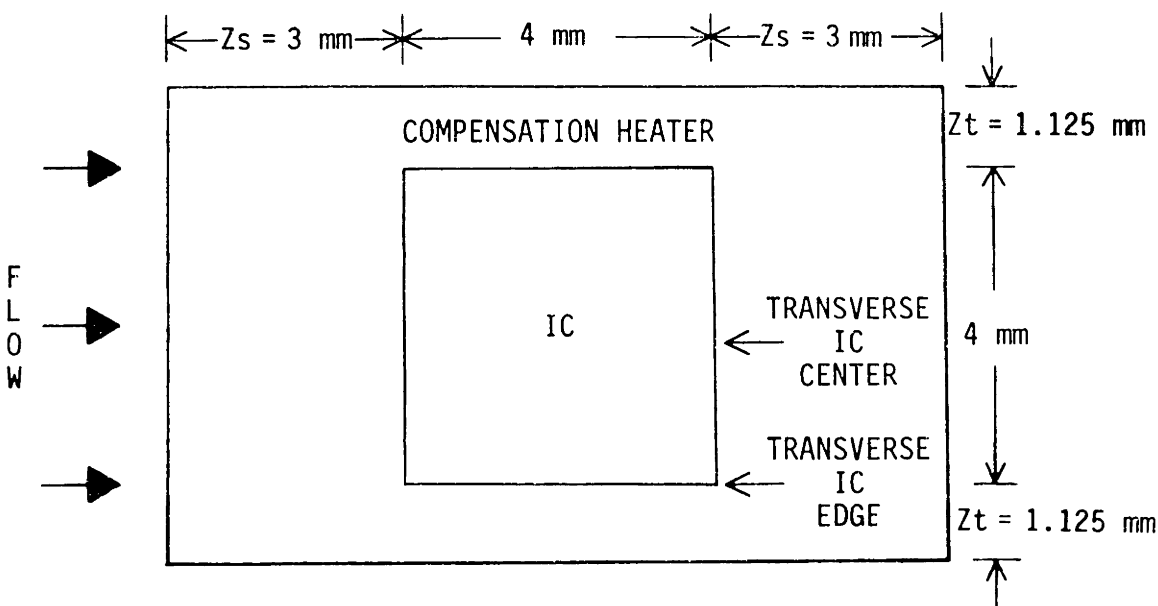

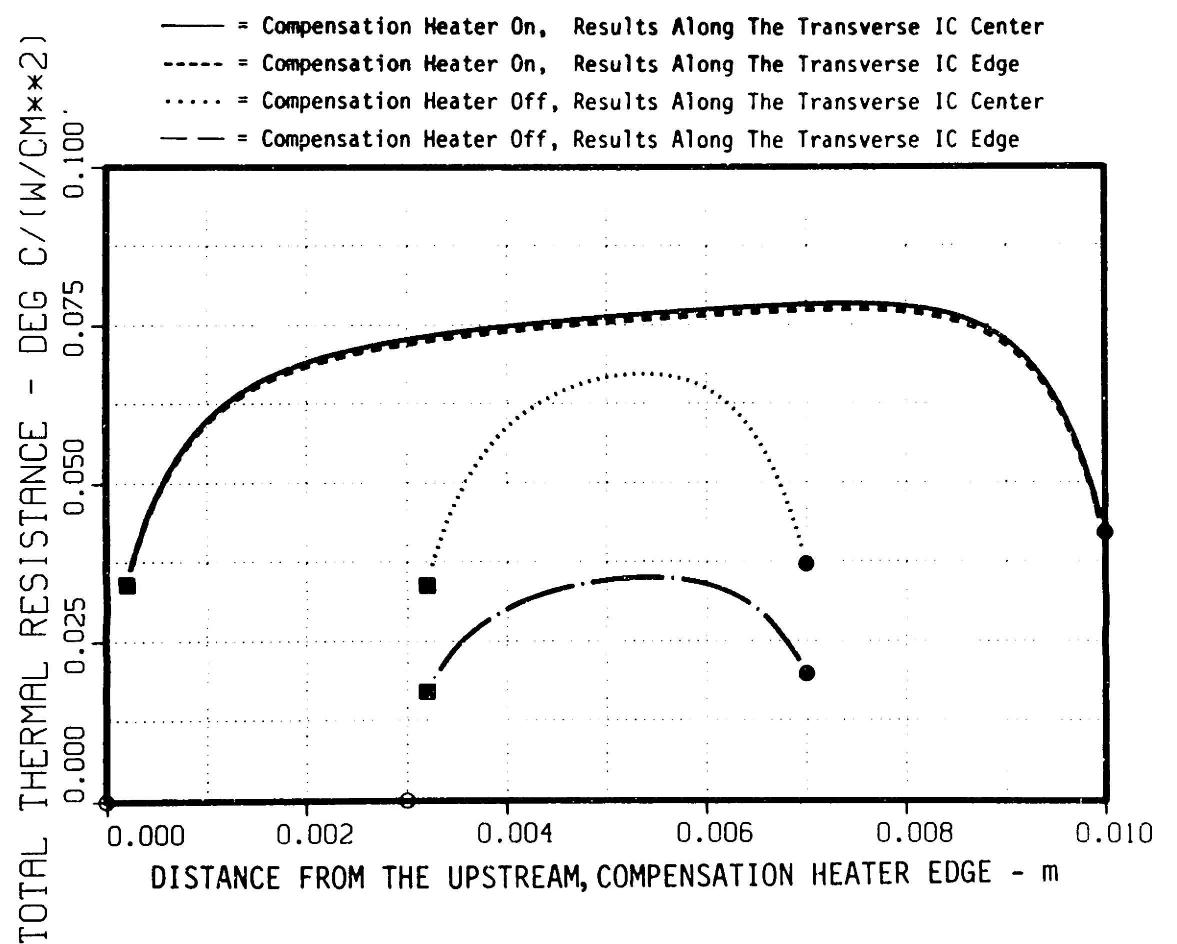

Figure 4.20. Thermal resistance as a function of distance from the upstream heater edge with and without a compensation heater energized for the reference case channel width of 300 μm.

is somewhat larger than when the "compensation heater" is off. The average thermal resistance is about $R''_{tot} \approx 0.0825°C/(W/cm^2)$ and $0.05°C/(W/cm^2)$ when the "compensation heater" is on and off, respectively. This means that the inlet coolant temperature would need to be only about 3.0 to 3.5°C lower when the compensation heater is on ($q'' = 100\ W/cm^2$) to maintain the same average surface temperature. In this example, the additional power required for the "compensation heater" is 2.75 times that of the IC heat source (the IC requires 16 W and the "compensation heater" requires 44 W).

This author will be the first to admit that the thermal spreading models need to be upgraded to include two-dimensional heat transfer at the corners, and to account for temperature gradients within the fins and the liquid coolant. Practical issues also need to be answered on a case by case basis as to whether the additional power requirements are too excessive. Questions about how to make the electrical connections to the IC, and what the thermal stresses are, need to be answered. Ultimately, chip-level reliability testing will need to be conducted in order to prove if "compensation heaters" can be used to improve chip reliability.

4.7 Use of Interrupted Fins

The total thermal performance of an interrupted-fin design should be at least as good as that for an equivalent continuous-fin design. A scan of the thermal resistance components discussed in Section 4.1 shows that for the same coolant velocity, the contraction thermal resistance and the convective thermal resistance will change if interrupted fins are used. The contraction thermal resistance can be obtained from Equation 3.6

(after a few substitutions and rearrangement), and will be slightly larger in magnitude for interrupted fins. Equation 4.6 can be used directly to obtain the convective thermal resistance at the channel exit, which will be slightly smaller in magnitude because the Nusselt number is larger for interrupted fins. Therefore, the worst case thermal resistance (at the channel exit) should be lower for interrupted-fin arrays.

The average thermal resistance (between the channel entrance and exit) may not necessarily be lower for interrupted-fin arrays. For this discussion, it is assumed that the differences in the contraction thermal resistance are small and can be ignored. It is also assumed that the heat transfer from the channel base can be ignored (large aspect ratio channels), that there is negligible heat transfer from the additional "channel base" area created by the gap between interrupted fins in the streamwise direction, and that there is negligible heat transfer from the leading and trailing ends of each interrupted fin. If the average thermal resistance of interrupted-fin arrays is to be competitive with continuous-fin arrays, it is required that $R''_{conv,interrupted} \leq R''_{conv,continuous}$.

Using this criterion and substituting $A_{cross} = n(L+S)(w_w+w_c)$, $A_{bf} = n(L+S)w_w$ for continuous-fin arrays, and $A_{bf} = nLw_w$ for interrupted-fin arrays (where n is the number of interrupted fins in the length L_{ex}) into Equation 4.5 and rearranging gives

$$\frac{(Nu_m \eta_f)_{interrupted}}{(Nu_m \eta_f)_{continuous}} \geq \frac{L+S}{L} \quad . \tag{4.25}$$

Since the fin efficiency decreases with increasing Nusselt number, the ratio of the interrupted-fin and continuous-fin mean Nusselt numbers must be larger than $(L+S)/L \approx 1.5$ (based on design criterion #1 in Section 2.8). In fact, the interrupted-fin mean Nusselt number must be about twice as large as that for continuous fins. It was shown in Section 4.5 that the best continuous-fin designs have flows which generally are not fully developed, and therefore already have relatively large mean Nusselt numbers. The mean Nusselt number for interrupted-fin arrays must therefore be very large. Such large increases in the mean Nusselt number can not be easily obtained by reducing the fin length while adhering to the design recommendations listed in Section 2.8. Instead, an increase in the coolant velocity appears to be necessary, which will also increase the pressure drop. It is for this reason that this author does not expect a significant improvement in the overall thermal-hydraulic performance when interrupted-fins are used. Instead, it appears that interrupted-fins will be used primarily because of their other advantages. That is because they allow transverse mixing (between channels) downstream from "hot-spots", and because they help prevent catastrophic failure due to channel clogging.

4.8 Chapter Summary

To conclude this chapter, several of the major results will be summarized.

Six thermal resistance components for microchannel heat sinks were identified and discussed. Overall thermal resistance models were formulated for large, moderate, and small aspect ratio channel designs (see Equations 4.11 to 4.13).

A simplified solution performed by Tuckerman and Pease at Stanford for large aspect ratio channels was presented. Their analysis predicts an "optimum" laminar flow channel width, which is supposed to exhibit the best possible thermal performance for the given design inputs. This "optimum" was shown to be an artifact of the assumption that the channel flow was laminar and fully developed.

A more complicated solution procedure was done for this work. A new computer program called MICROHEX was written to do the tedious numerical computations. The organization of the program was reviewed, and sample thermal and fluid performance predictions were presented. The numerical results indicate that turbulent flow can provide better thermal performance than comparable laminar flow designs. The pumping power requirements are somewhat higher, but are still within practical limits.

The so-called "optimum" channel design obtained by the Stanford researchers is considered to be instead a "lower bound" to the range of channel widths that should be used for microchannel heat sinks. No criterion was obtained for the upper bound to the range of channel widths, but this limit will probably be based in part on limitation of the pumping power requirements.

Microchannel heat sinks can be made as a "cold plate" of high thermal conductivity materials, such as aluminum and copper. IC chip heat

sources can then be interfaced to the heat sink with a low-thermal-resistance interface such as the "microcapillary thermal interface" developed by Tuckerman and Pease at Stanford. The overall thermal resistance can be lower than if the channels were fabricated directly in the back of the IC chip.

Thermal spreading at the IC heat source perimeter can cause significant non-uniformity in temperature across an IC heat source. A "compensation heater" about the circumference of the IC can be used to significantly improve the temperature uniformity across the IC. More uniform temperature implies enhanced reliability and fewer timing problems. Chip-level reliability testing is required to verify if "compensation heaters" indeed improve chip reliability.

Interrupted-fins probably will not be used to improve the thermal performance of microchannel heat sinks due to the large increase in the pumping power requirement. Interrupted-fins will instead be used because they allow transverse mixing of coolant (between channels) downstream from hot spots, and because they help prevent catastrophic failure due to channel clogging.

5.0 EXPERIMENTAL VERIFICATION OF MICROCHANNEL HEAT SINK PERFORMANCE

The purpose of this chapter is to review the experimental program that was used to characterize the performance of microchannel heat sinks fabricated in indium phosphide chips. The reasons why indium phosphide was chosen as the heat sink material will first be briefly discussed. The design and fabrication of the test ships and the manifold block will be reviewed. The testing apparatus and the data acquisition system will be discussed. Following this, there will be a discussion of the experimental errors and the overall experimental accuracy.

5.1 Purpose of the Experimental Investigation

This study was initiated to determine if microchannel heat sinking could be used to cool an array of electronic devices constructed in indium phosphide. These devices are anticipated to dissipate on the order of 100 - 300 W/cm^2 continuously over a large two-dimensional array of chips that may exceed tens of centimeters on each side.

The theoretical predictions indicated "on paper" that microchannel heat sinks could be designed to meet this high heating with reasonable surface temperatures. The question now was whether the channels could be fabricated in indium phosphide. Since indium phosphide is a fragile material that cleaves easily, it was also questioned if the indium phosphide chips would reliably withstand the coolant pressures without leaking. Finally, there is the question as to how accurately the theory predicts the experimental thermal and fluid performance data (see Chapter 6). Unfortunately, there was not enough time to experimentally test compensation heaters, interrupted fins, and microcapillary thermal interfaces.

5.2 Heat Sink Fabrication

This section reviews how microchannel heat sinks were made in indium phosphide chips. One method for constructing channels in aluminum is also presented.

5.2.1 Manufacturing the Microchannels in Indium Phosphide

The ability to fabricate the microchannels is the first prerequisite for allowing their application. All of the microchannels in any given chip must be nearly identical to each other since manufacturing tolerances more adversely affect the heat transfer than the flow friction (see Section 2.7). Two methods were used in this study to fabricate moderate aspect ratio channels in indium phosphide. These are precision sawing and orientation dependent etching.

5.2.1.1 Precision Sawing

Precision mechanical sawing of the microchannels can be done using conventional semiconductor dicing saws (such as the Tempress<R> 604 used in this study). Precision sawing is "relatively" insensitive to crystal orientation, and is therefore a viable fabrication method when the channels must be oriented in directions which are different from that preferred for orientation dependent etching. The cutting was done with a diamond-impregnated blade (e.g., Microautomation<R> #15.361), rotating typically at 25 krpm, with horizontal feed rates of 0.02-0.03 cm/s. A water jet was used to continuously bathe and cool the cutting blade. No coolant additives were used to enhance lubrication.

Precision sawing of microchannels in indium phosphide proved to be very time consuming due to the very slow horizontal feed rates that were

required to minimize breakage of the fins. Indium phosphide is a brittle material that cleaves very easily. The indium phosphide wafers used in this study were (100) slices which cleaves into rectangular shapes along the (011) and (01$\bar{1}$) directions. Channel cutting along those two directions resulted in frequent fin breakage when $w_w/w_c < 1.0$. Channel cutting at 45 degrees to these directions resulted in a significant reduction in breakage, but did not eliminate it. In addition to fin breakage, the fin tips showed occasional chipping that appeared to be unaffected by the sawing orientation.

In an attempt to get around the fin breakage problem, it was hypothesized that larger w_w/w_c ratios could be sawn, and then the channels could be widened by acid etching. It was also hypothesized that this etching could remove substrate damage created during the sawing process. Unfortunately, all of the acids tried in this study had etching rates and etching profiles that show a very strong dependence on the crystal orientation. Therefore, the saw-etch method did not work.

It has been concluded that precision sawing is not a good fabrication method for indium phosphide microchannel heat sinks. This is due to the slow cutting rates, and the excessive fin breakage and chipping. Precision sawing works well in other materials such as silicon [see Tuckerman (1984)]. It will be shown in Section 5.2.5 that microchannels can be fabricated very rapidly in aluminum substrates, which shows good promise for "cold plate" microchannel heat sinks.

5.2.1.2 Orientation Dependent Etching

Conventional wet chemical etching was used in this study to fabricate the microchannel heat sinks for thermal and fluid performance testing. The manufacturing process used to fabricate the test chip microchannels will be detailed in Section 5.2.4.

The rate of etching, and the channel shape, depends on the crystallographic orientation of the chip, and upon the etchant being used [see Buchmann and Houghton (1982) and Coldren, Furuya, and Miller (1983)]. In this study, microchannels with nearly rectangular cross-sections were fabricated in the (011) direction of indium phosphide using a 3:1 mixture by volume of H_3PO_4:HCl. The side of the indium phosphide chips that was to have the microchannels fabricated in it was first lapped and then polished in a 1% solution of bromine methanol. The polished surface was then pre-etched with full strength potassium ferricyanide for five minutes in order to allow good adhesion of the 3000 Å thick layer of PSG deposited on the surface ("wild" undercutting occurs when the mask does not adhere well). The PSG is then patterned and etched to form slots in the (011) direction where the indium phosphide surface is exposed. The width of the slots, and the width of the PSG between the slots, depends on the desired channel size and shape after etching. For 3:1 H_3PO_4:HCl, it was found that 1) the channel depth etching rate was on average about 0.62 μm/min, and 2) the undercutting etching rate was on average about 0.22 μm/min. This means that the largest possible channel aspect ratio that can be obtained for this etchant is 0.62/0.22=2.8. Buchmann and Houghton (1982) obtained etching rates of 0.6 μm/min in the channel

depth, and the undercutting rate was 0.05-0.20 μm/min depending on the agitation of the acid. This suggests that the channel aspect ratio could be in the range of 3-12 if less acid agitation is used.

Figure 5.1 shows three views of indium phosphide chips with microchannels fabricated using orientation dependent etching. As can be seen from the top view, this particular chip has channels which end before reaching the edge of the chip. This eliminates the need to seal the ends of the channels as would normally be required in "side-fed" channel designs (see Section 1.3). The channel end shape is shown in the streamwise view where the angle of the solid material was typically found to be 35-38 degrees. This angle helps deflect the coolant flow, and therefore has the additional benefit of reducing the coolant pressure drop.

Returning to the top view, it can be seen that there is a "wavy" appearance to the fin tips. This effect is due to drooping of the PSG mask caused by undercutting. The waviness results in local changes in the channel width that propagate to the fin base in triangular shapes which have angles that are also in the range of ± (35-38) degrees (see streamwise view in Figure 5.1). This waviness can be useful if the flow is turbulent since it can act as a turbulence promoter (a fortuitous result). The waviness could be eliminated if the PSG thickness is different. Unfortunately, there was insufficient time to determine the optimum PSG thickness.

Returning again to the top view in Figure 5.1, it can be seen that there is a "granular" texture to the channel bottoms. This effect is due to small triangular mounds (again 35-38 degree sides) which are formed

a) Top view (~ 210 μm wide channels on 375 μm centers);

b) Streamwise view (b ~ 160 μm);

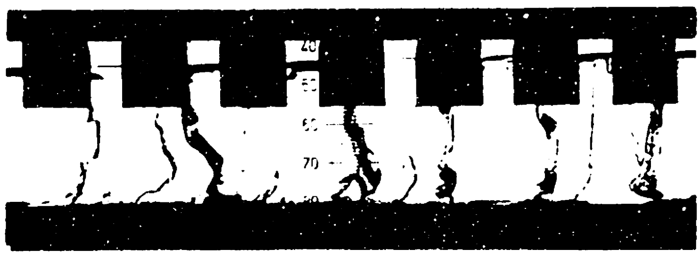

c) Transverse view (~ 160 μm wide channels on 250 μm centers, $\alpha \sim 1.0$).

Figure 5.1. Views of microchannels fabricated in indium phosphide using orientation dependent etching with H_3PO_4:HCl (3:1).

due to minute differences in etching in the $(01\bar{1})$ direction along the (011) channels. The size of these mounds appears to decrease as the etching time is increased. This is apparently due to more mounds being created with time. These mounds can also be useful in turbulent flow since they can act as turbulence promoters (a fortuitous result).

The transverse view in Figure 5.1 shows that the channel cross-sections can be quite uniform. Generally, the channel uniformity is within about five percent, but may be worse if the mask slots are not precisely aligned along the (011) direction.

5.2.2 Packaging and Headering

The three-sided channels in the indium phosphide chips must be packaged to provide coolant flow to and from the chip. The packaging design used in this study is shown in Figure 5.2. A glass "cover plate" with inlet and outlet manifold slots cut into it is epoxied to the chip. The cover plate was 0.043-in.-thick #7059 glass which was provided by Corning Glass of Corning, New York. This particular type of glass was selected since it has a coefficient of thermal expansion of $4.6\times10^{-6}{}^{\circ}C^{-1}$ (0-300°C), which is reasonably close to that of indium phosphide which is $6.17\times10^{-6}{}^{\circ}C^{-1}$ (16-63°C) and $4.32\times10^{-6}{}^{\circ}C^{-1}$ (63-107°C). The manifold slots in the glass were fabricated at 2750 rpm using a standard milling machine and a 0.040-in.-diameter Amplex<R> #S-40 diamond plated drill.

The epoxy used in this study to attach the indium phosphide chip to the cover plate is Trabond<R> F-113. This epoxy is commonly used in bonding glass, and was found to "wet" the indium phosphide surfaces quite nicely. The epoxy appears to have good stability at the chip operating

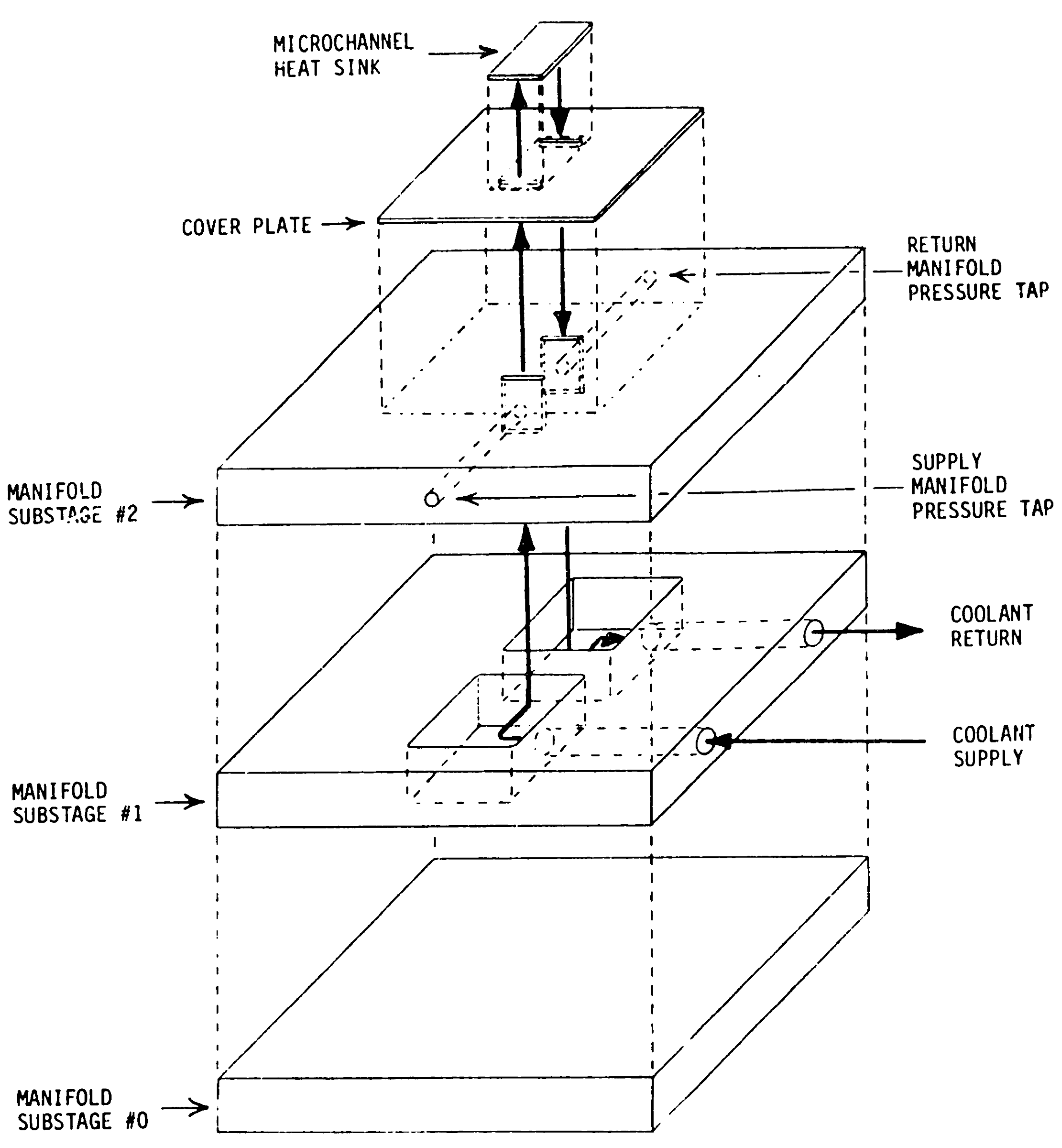

Figure 5.2. Test block assembly and coolant flow path. (See Figure 1.4 for a close-up view of a microchannel heatsink.)

temperatures for short time periods (no long term tests were conducted in this study).

The epoxy was applied to the glass cover plate and spun-down to a thin layer. The layer thickness was determined using

$$t_{epox} = \text{const}\left[\frac{3\nu}{4\ \omega^2 t}\right]^{0.5} \quad (5.1)$$

where t_{epox} is the epoxy thickness, ν is the kinematic viscosity, ω is the rpm, and t is the spin time in seconds. The constant accounts for deviations from Newtonian theory and is about 2.25 for the epoxy used here. Note that the epoxy thickness was selected assuming that the epoxy under the fins is displaced into the channels. This is due to the fact that since the epoxy wets the indium phosphide, a capillary suction force is generated which "sucks" the chip to the cover plate. To ensure a good seal about the periphery of the chip, a controlled amount of epoxy was also applied at the edges of the chip.

The cover plate was attached to the coolant manifold which was made out of Lexan<R>. Five-minute epoxy was used as the adhesive.

5.2.3 Resistor Heat Source Fabrication

In order to test the thermal performance of the microchannel heat sinks used in this study, it was necessary to fabricate large heat sources in the chips. The method used here was to fabricate the resistor(s) directly into the top surface of the chips. This was accomplished by implanting silicon ions into the surface of semi-insulating indium phosphide. The silicon ions were implanted such that the maximum implantation depth was about 0.5 µm. Therefore, the resistor(s) could be

electrically isolated from the rest of the chip by etching grooves into the chip that were deeper than the maximum implantation depth. Electrical contact to the chip was accomplished by piezoelectrically bonding 0.001-in.-diameter aluminum wires to gold contacts at opposite sides of the resistor(s). The manufacturing process used to fabricate the test chip resistors will be detailed in Section 5.2.4.

Figure 5.3 shows the resistor heat source design used in this study for experimentation (four-resistor-chips). The first design used four 0.25 cm square resistors, and the second used a single 1.0 cm square resistor. The four-resistor design was used specifically to investigate the thermal spreading phenomenon since the thermal spreading diffusion length (L_d) can be on the order of 0.1 cm. Each resistor can be turned on/off independently of the others.

Each resistor had an electrical resistance on the order of 15-20 Ω/□ at room temperature. This is comparably much smaller than the electrical resistivity of the semi-insulating indium phosphide (iron doped), which was typically greater than 100,000 Ω-cm. The uniformity of the heat dissipation over the surface of each individual resistor was not explicitly determined. Table 5.1 lists the room temperature electrical resistance of the chips used for experimentation. The variation of resistance among all chips is within ± 8.5 percent, and the maximum variation among the resistors on the four resistor chips is within ± 1.1 percent (resistance data for HEX1 and HEX5 not included). The effect of this nonuniformity on the experimental uncertainty is discussed in Section 5.3.3.

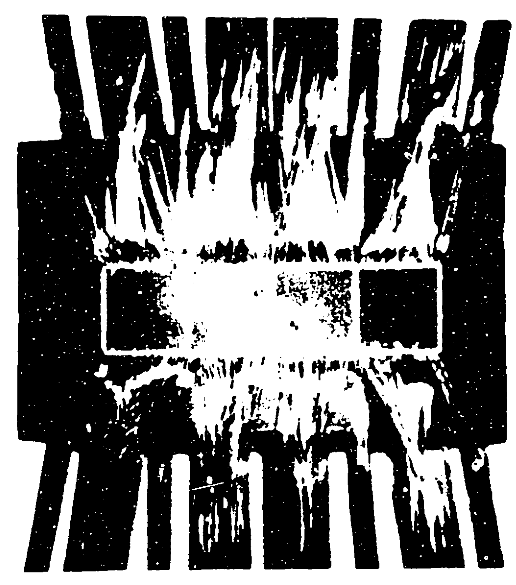

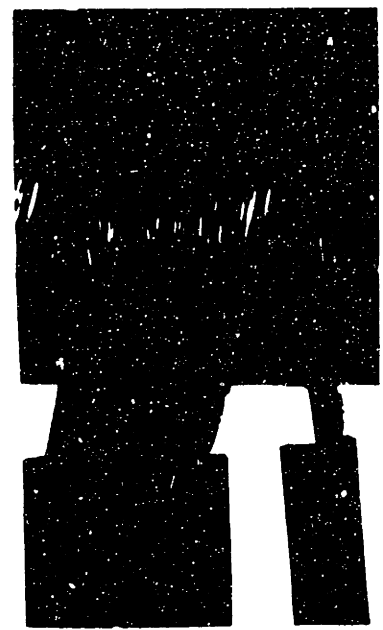

a) Photographs of a typical test chip.

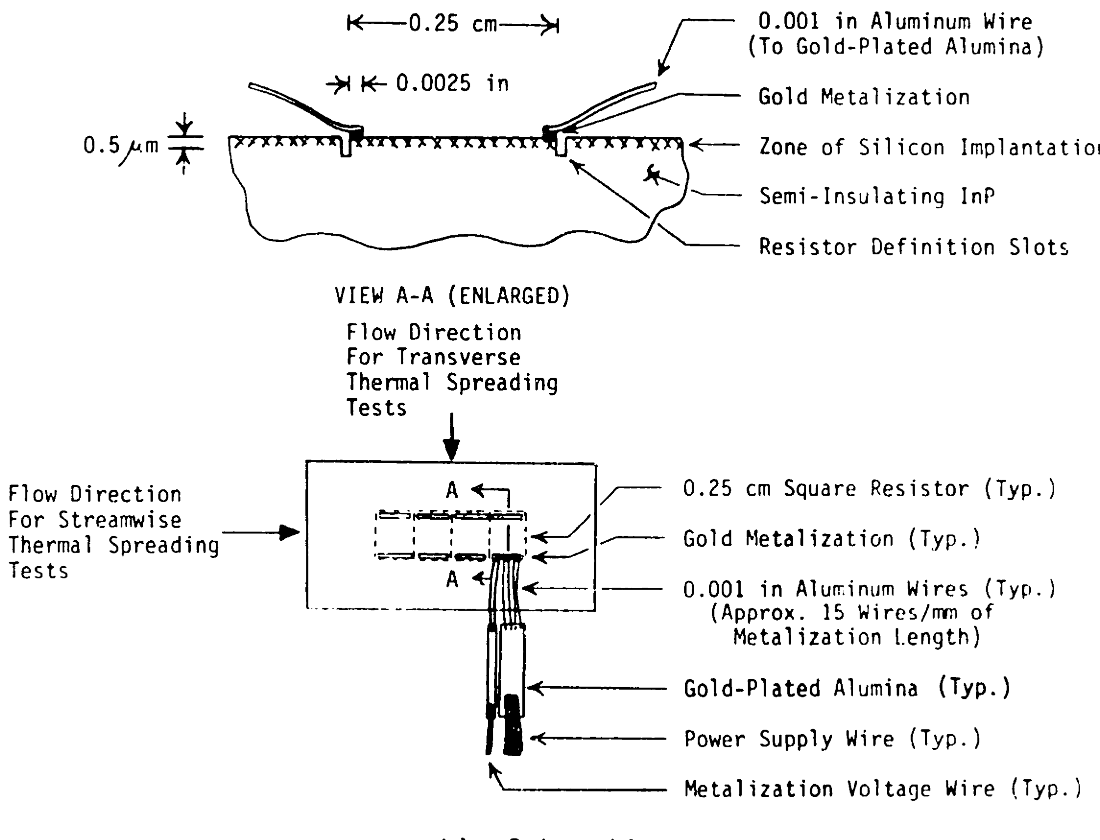

b) Schematics.

Figure 5.3. Test chip resistor electrical connection.

TABLE 5.1

RESISTANCE VALUES FOR TEST CHIPS

Chip #	Resistor Size	Resistor	Resistance (Ω)
HEX1*	0.25 cm x 0.25 cm	1	24.4**
HEX2*	0.25 cm x 0.25 cm	1	18.1
HEX3	0.25 cm x 0.25 cm	1	18.87
	" "	2	18.47
	" "	3	18.75
	" "	4	18.49
HEX4	0.25 cm x 0.25 cm	1	17.96
	" "	2	17.91
	" "	3	17.94
	" "	4	17.84
HEX5†,††	0.25 cm x 0.25 cm	1	27.1
	" "	2	19.5
	" "	3	20.4
	" "	4	660.0
HEX6†	0.25 cm x 0.25 cm	1	16.1
	" "	2	16.0
	" "	3	16.1
	" "	4	16.2
HEX7†,†††	1.0 cm x 1.0 cm	1	16.9

* This heat sink has a single resistor because it was obtained from a four-resistor chip that broke during fabrication.

** Total resistance between gold-plated alumina strips.

† Thermal and fluid performance testing has not been conducted on these chips at the publication date of this thesis. They will be tested at a later date.

†† This chip has some scratches on the resistor surfaces, which is the reason for the poor resistance characteristics.

††† The resistor metalizations pulled off from this chip at some locations.

5.2.4 Summary of Manufacturing Process Steps for Indium Phosphide Chips

The manufacturing process used to fabricate the microchannel heat sink test chips is listed in Table 5.2. It is hoped that sufficient detail has been provided such that interested parties may replicate this work.

TABLE 5.2

SUMMARY OF MANUFACTURING PROCESS FOR INDIUM PHOSPHIDE TEST CHIPS

Process Step	Process Description
1. Starting Wafers	Obtain 0.024-in.-thick slices (100) of iron-doped, semi-insulating (>100,000 Ω-cm) indium phosphide
2. Polish	Lap both sides of wafers
	Polish both sides of wafers in 1% bromine methanol
3. Implantation	Implant Si+ ions ($1.0 \times 10^{+15}$ dose per square cm) at 200°C, 7° tilt, 400 kEv (SiH_4 gas with He carrier)
	Mark the implanted side for identification
4. Obtain Test Chip	Cleave off test chip of desired size from wafer
	Mark the implanted side for identification
5. Implantation Damage Repair	Clean chip - Trico, Acetone, Methanol, DI water/soap spray, DI water, Methanol, and Isopropyl (T,A,M,W/S,W,M,I) and dry
	Soak in BHF for 2 minutes
	Wash with DI water and dry
	Deposit 3000 Å PSG
	Anneal at 750°C for 10 minutes
	Remove PSG by soaking in BHF for 1 minute
	Wash with DI water and dry

TABLE 5.2 (Continued)

Process Step	Process Description
5. (Continued)	Clean with AZ1112A:DI water (1:1) for 15 minutes
	Wash with DI water and dry
6. Crystal Orientation	Cleave off a small piece from the test chip
	Clean the small piece (T,A,M,W/S,W,M,I) and dry
	Soak in BHF for 2 minutes
	Wash with DI water and dry
	Immediately deposit 3000 Å PSG on the unimplanted side (channel side) of the small piece
	Melt several small drops of black wax on the PSG
	Etch the exposed PSG with BHF for 15 seconds
	Remove black wax with Trico
	Etch the chip in pure HCl for 20 seconds
	Obtain the crystal orientation by viewing under a microscope
7. Resistor Metalizations	Clean chip (T,A,M,W/S,W,M,I) and dry
	Soak in BHF for 1 minute
	Wash with DI water and dry
	Deposit 3000 Å PSG
	Apply HMDS, 1400-30 series photoresist at 5000 rpm for 30 seconds
	Bake at 80°C for 25 minutes
	Expose with metalizations contact mask for 7.0 seconds
	Develop photoresist with AZ606 developer: DI water (1:7) for 6.0 seconds or until fully developed
	Bake at 120°C for 10 minutes
	Etch the exposed PSG with BHF for 15 seconds
	Wash with DI water and dry

TABLE 5.2 (Continued)

Process Step	Process Description
7. (Continued)	Evaporate 300 Å Sn followed by 1000 Å Au in e-beam system at approximately $5x10^{-7}$ torr
	Lift-off photoresist and the Sn-Au over the photoresist with AZ1112A:DI water (1:1) for 10 minutes
	Wash with DI water and dry
	Alloy Sn-Au into InP at 390°C for 10 seconds
	Evaporate 1000 Å Au at approximately $1.0x10^{-6}$ torr or lower
	Apply HMDS, 1400-30 series photoresist at 5000 rpm for 30 seconds
	Bake at 80°C for 25 minutes
	Expose with metalizations contact mask for 7.0 seconds
	Expose with chrome mask the two opposite chip edges (silver paint contact locations) for 50 seconds
	Develop photoresist with AZ606 developer: DI water (1:7) for 8.0 seconds or until fully developed
	Bake at 120°C for 10 minutes
	Apply silver paint at the chip edges to make contact with the plating electrodes
	Cover the silver paint and any Au areas (other than the chip metalizations) with KTFR resist, and let dry for 20 minutes
	Plate in OROTEMP24 Au solution at 40°C, 60 µAmps and slow stirring for 5 minutes
	Remove silver paint and photoresist with Trico and Acetone
	Remove evaporated Au (unplated) by blasting with soap spray
	Wash with DI water and dry
8. Define Resistors	Apply HMDS, 1400-30 series photoresist at 5000 rpm for 30 seconds
	Bake at 80°C for 25 minutes

TABLE 5.2 (Continued)

Process Step	Process Description
8. (Continued)	Expose with resistor edge definition mask for 7.0 seconds
	Develop photoresist with AZ606 developer: DI water (1:7) for 6.0 seconds or until fully developed
	Bake at 120°C for 10 minutes
	Etch the exposed PSG with BHF for 15 seconds
	Wash with DI water and dry
	Etch the exposed InP with pure HCl for 10 seconds
	Wash with DI water and dry
	Remove photoresist with Acetone
	Wash with DI water and dry
	Do not remove remaining PSG (acts as electrical insulator)
9. Microchannel Fabrication	Flip chip over
	Clean chip (T,A,M,W/S,W,M,I) and dry
	Mount chip with bee's wax to a glass slide (be sure wax coats the entire resistor side of the chip)
	Soak in BHF for 3 minutes
	Wash with DI water and dry
	Demount chip from glass slide
	Mount chip with bee's wax to a polishing chuck (be sure wax coats entire resistor side of chip)
	Polish the surface with 1% bromine methanol
	Demount chip from polishing chuck
	Clean chip (T,A,M,W/S,W,M,I) and dry
	Pre-etch the surface with full strength potassium ferricyanide for 5 minutes (do not use solvents after this step to insure good adhesion of mask)
	Wash with DI water and dry

TABLE 5.2 (Continued)

Process Step	Process Description
9. (Continued)	Immediately deposit 3000 Å PSG
	Apply HMDS, 1400-30 series photoresist at 5000 rpm for 30 seconds
	Bake at 80°C for 25 minutes
	Position channel slots mask so that: 1) the slots are parallel to the (011) direction, 2) the slots pass underneath the resistor(s) on the other side of the chip, and 3) the slots do not extend beyond the edges of the chip
	Expose with the channel slots mask for 7.0 seconds
	To minimize risk of channel blockages due to exposure anomalies: 1) Translate the mask in the direction of the slots by about 0.05 cm, and 2) Re-expose with the channel slots mask for 7.0 seconds
	Develop photoresist with AZ606 developer: DI water (1:/) for 8.0 seconds or until fully developed.
	Bake at 120°C for 10 minutes
	Etch the exposed PSG with BHF for 15 seconds
	Remove photoresist with Acetone
	Wash with DI water and dry
	Mount chip with bee's wax to glass slide (be sure wax coats entire resistor side of chip and the edges of the chip)
	Etch the microchannels in H_3PO_4:HCl (3:1) at room temperature (normally 20°C) with stirring for the desired amount of time
	Wash with DI water and dry
	Remove PSG by soaking in BHF for 15 seconds
	Wash with DI water and dry
	Demount chip from glass slide
	Clean chip (T,A,M,W/S,W,M,I) and dry

TABLE 5.2 (Continued)

Process Step	Process Description
10. Cover Plate Fabrication	Saw 0.043-in.-thick 7059 glass to a 2-in. x 2-in. square piece
	Mill the coolant manifold headers through the glass with an Amplex S-40 drill at 2750 rpm (bathe the drill with water to keep it cool)
11. Bond Chip to Cover Plate	Clean glass cover plate (T,A,M,W/S,W,M,I) and dry
	Mix and degas Tracon F-113 epoxy
	Apply epoxy to glass slide and spin down to the desired thickness
	Position the chip on the glass slide
	Apply a controlled amount of epoxy about the periphery of the chip
	Let epoxy cure at room temperature for 24 hours
12. Bond Cover Plate to Lexan Manifold Block	Mix five-minute epoxy
	Apply a controlled amount of epoxy to the glass slide
	Position the cover plate on the Lexan manifold block
13. Electrical Wiring	Cut 0.2 cm x 1.0 cm gold-plated (0.001-in.-Au) alumina strips
	Attach one 14 awg wire to one end of each gold-plated alumina strip
	Mix five-minute epoxy
	Apply epoxy to the cover plate
	Position gold plated alumina strips on the cover plate
	Let epoxy cure at room temperature for 24 hours
	Piezoelectrically bond 0.001-in.-diameter aluminum wires between the resistor metalizations and their corresponding gold-plated alumina strips

5.2.5 Manufacturing the Microchannels in Aluminum

Using microchannel heat sinks in the form of a cold plate and mating the chip(s) with a low-thermal-resistance interface can result in a total thermal resistance which can be smaller than if the microchannels were fabricated directly in the chip(s) themselves (see Section 4.5.2). The use of a higher-thermal-conductivity material for the cold plate is in general required. Copper and aluminum are good candidates for the cold plate material since they have a thermal conductivity which is higher than most chip materials. This section briefly describes one method which was used to fabricate microchannels in aluminum. No attempt was made to fabricate microchannels in copper.

A numerically controlled milling machine (Cincinnatti Milacron<R> Model 5VC) was used to mill channels in 6061-T6 aluminum. An arbor was constructed with five 1.25-in.-diameter, 0.010-in.-thick, Poland<R> high-speed-steel, jewelers' blades (30 teeth/in.), which were separated by 0.0095-in.-thick shim stock. The arbor rotated at 6 krpm, and the blades were continuously bathed with water soluble cutting oil (60:1) to keep them cool. The horizontal feed rate was 0.5 in./minute and the cutting depth was 0.050 inch. The resulting production rate was 3.0 $in.^2$/hour, which could be increased if more blades were added to the arbor.

The fabricated channels had a nearly rectangular shape (the channel bottoms were slightly rounded). The uniformity in channel cross-sectional area was within about ± 10 percent. Most of this error is due to non-uniformity in the channel width (blade curf width). The curf width uniformity might be improved if the blades were trimmed as

installed in the arbor by a laser. More work is needed to improve the channel uniformity, but this fabrication method holds good promise for mass production of cold plate, microchannel heat sinks.

5.3 Experiments

This section provides an overview of the apparatus used to test the thermal and fluid performance of the test chips. The method of data acquisition and reduction will be reviewed, and estimates of the experimental errors will be presented. The experimental results will be presented in Chapter 6.

5.3.1 Test Apparatus

The test apparatus is shown schematically in Figure 5.4. The test loop was constructed almost entirely of 316 stainless steel in order to keep corrosion to a minimum. Some brass piping, valves, and fittings were used for the differential pressure transducers. An Oberdorfer(R) Chemical Gear Pump (Model #2146) was used for the circulator. A pressure relief valve was provided to keep the coolant pressure below 100 psi, which was the pressure rating of the circulator. This pump supply pressure limitation resulted in a maximum coolant pressure drop of about 70 psi across the test chips. Since the circulator was a positive displacement pump, a bypass loop was provided with a metering valve to adjust the bypass flow.

The flow that continued towards the test chip was first diverted through one of two flow metering sections. The flow rate was determined by monitoring the pressure drop across an ASME orifice plate. The pressure drop was measured using a Validyne(R) differential pressure

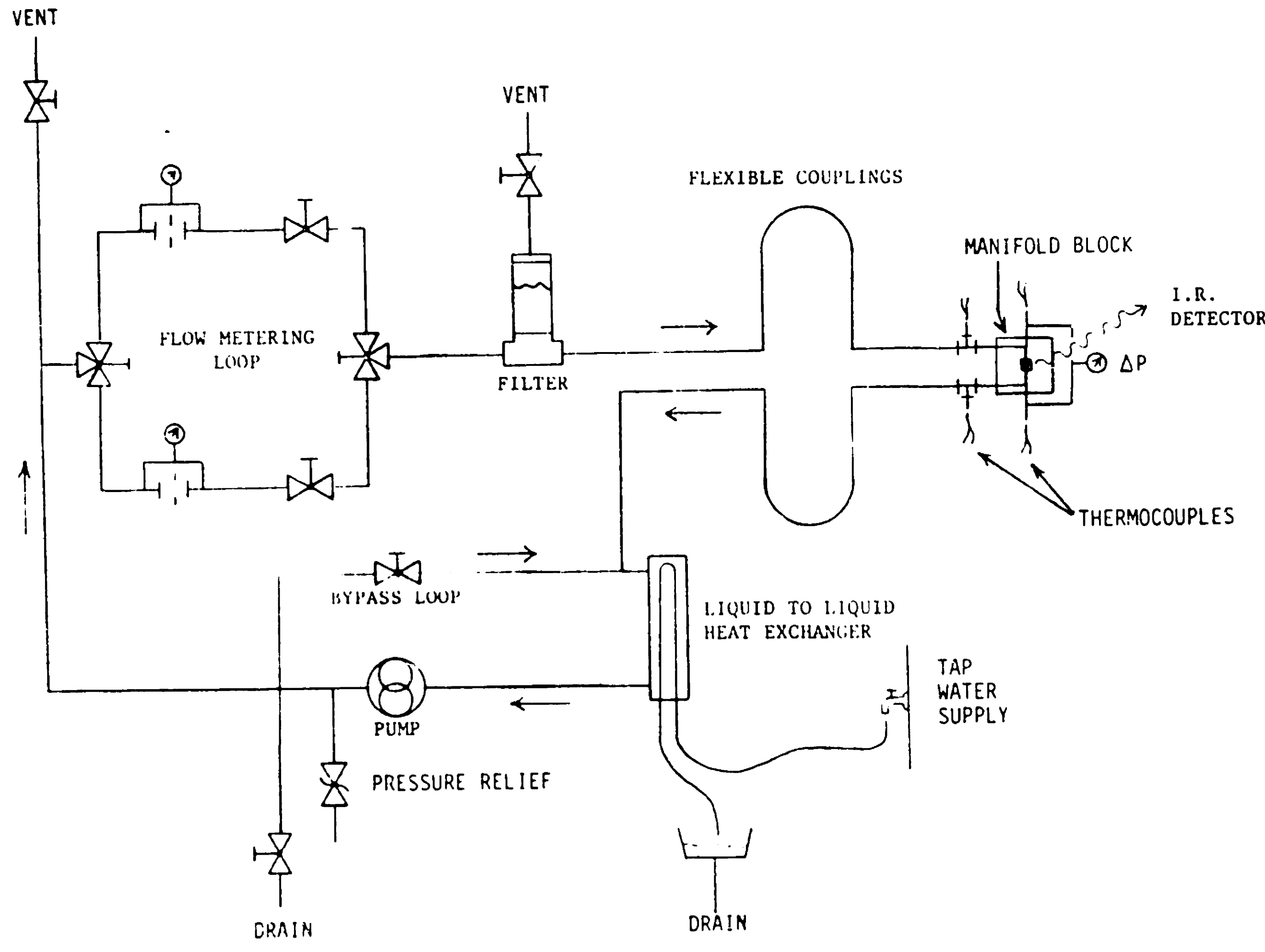

Figure 5.4. Test loop schematic.

transducer (Model #P305D). The flow rate to the chip was also adjusted with a flow metering valve.

The flow then passed through a Balston<R> 25 μm filter (Model #45-G). The flow then went through a flexible coupling to reach the manifold block containing the test chip. The manifold block was shown schematically in Figure 5.2. The coolant pressure drop across the chip was measured with another Validyne<R> differential pressure transducer. The temperature rise of the coolant across the chip was monitored by a series of type K thermocouples. Electrical power was provided to the test chip by a regulated DC power supply. The surface temperature of the chip was measured using a Barnes<R> infrared microscope (Model #RM-2A). The infrared microscope had an X-Y scanning capability (which is why the flexible couplings were provided). The microscope substage position was monitored using mechanical micrometers.

The test loop was designed to be operated as a closed-loop system, but was usually operated as an open-loop system in order to improve the accuracy of the coolant flow rate measurements. The coolant flow from the test chip was therefore either dumped into a vessel for flow rate measurement, or merged with the bypass flow. Finally, the flow passed through a Young Radiator<R>, shell and tube, liquid-to-liquid heat exchanger (Model #55F-303-HY-2P).

The test loop was designed to test a large array of microchannel heat sink test chips. Those tests will be conducted at a later date. For those tests, a pressure regulator and an expansion tank will be added to the test loop just downstream from the circulator.

The entire test apparatus was fabricated on a "tee cart" in order to allow ease of transport of the test loop to various locations for testing demonstrations. Figure 5.5 is a photograph of the test apparatus and its accompanying data acquisition system, which is on a separate utility cart. Figure 5.6 is a photograph of the manifold electronics substage with a test chip wired-up for testing.

5.3.2 Data Acquisition and Reduction

The data acquisition and reduction was performed using an IBM-PC/XT equipped with PCTHERM<R>, which is a machine language library of basic-callable subroutines that drive data acquisition boards. A BASIC computer program was written (not included in this thesis), which prompted the user for the chip micrometer positions, and performed the data acquisition when the user was ready. The acquired data was then processed and displayed on the computer monitor. A hard-copy printout was also provided for future reference. All of the sensor wires were routed through OMEGA<R> jack panels with rotary selector switches so that manual data acquisition could be readily performed as required.

The coolant flow rate was determined two ways. The primary method was to discharge the coolant flow from the test chip into a vessel. The discharge time was noted and the volume of coolant was weighed. The other method used to determine the coolant flow rate was to measure the differential pressure across an ASME flow orifice. The orifice was calibrated as installed in the apparatus. A 0-to-5 vdc signal from a Validyne<R> differential pressure transducer was used with the calibration curve to indicate the flow rate.

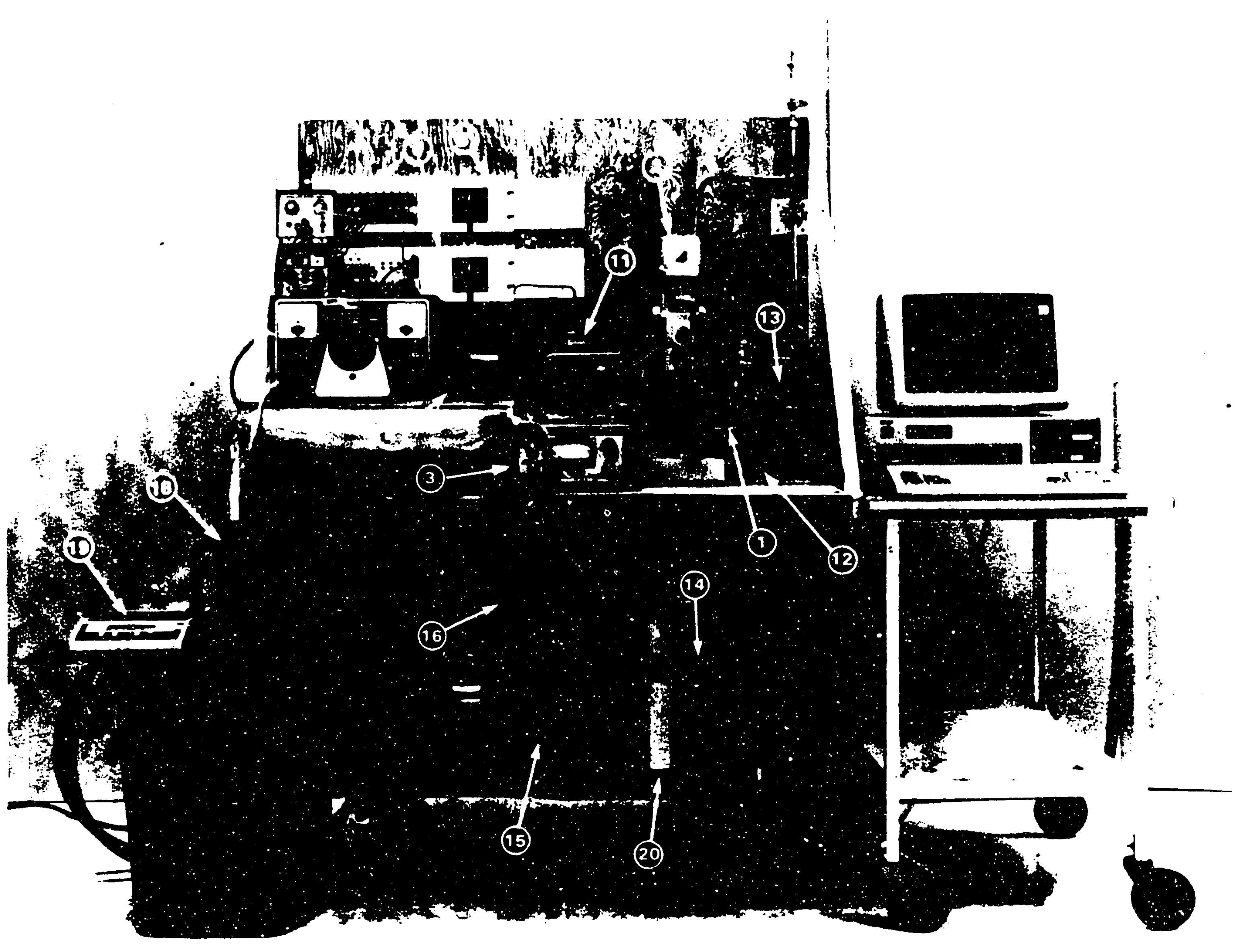

Figure 5.5. Microchannel heat sink test apparatus.

1 MANIFOLD ELECTRONICS SUBSTAGE
2 INFRARED MICROSCOPE
3 INFRARED MICROSCOPE CONTROL UNIT
4 CHIP RESISTOR(S) POWER ON/OFF SWITCH BOX
5 CHIP RESISTOR(S) POWER SUPPLY
6 DIFFERENTIAL PRESSURE TRANSDUCERS POWER SUPPLY
7 CURRENT-RESISTOR(S)-COOLING-FAN POWER SUPPLY
8 THERMOCOUPLE JACK PANEL
9 VOLTAGE JACK PANEL
10 IBM PC WITH DATA ACQUISITION SYSTEM
11 FLOW FILTER
12 ORIFICE FLOW METER (TYP)
13 VALVES FOR ORIFICE DIFFERENTIAL PRESSURE TRANSDUCER (TYP)
14 BYPASS LOOP FLOW CONTROL VALVE
15 GEAR PUMP CIRCULATOR
16 LIQUID/LIQUID HEAT EXCHANGER
17 COOLANT RESERVOIR (Open Loop Operation)
18 COOLANT FLOW RATE MEASUREMENT RESERVOIR
19 DIGITAL SCALE
20 ACOUSTIC INSULATION WALL (Show Partially Removed)

Figure 5.5. (Continued) - Labels.

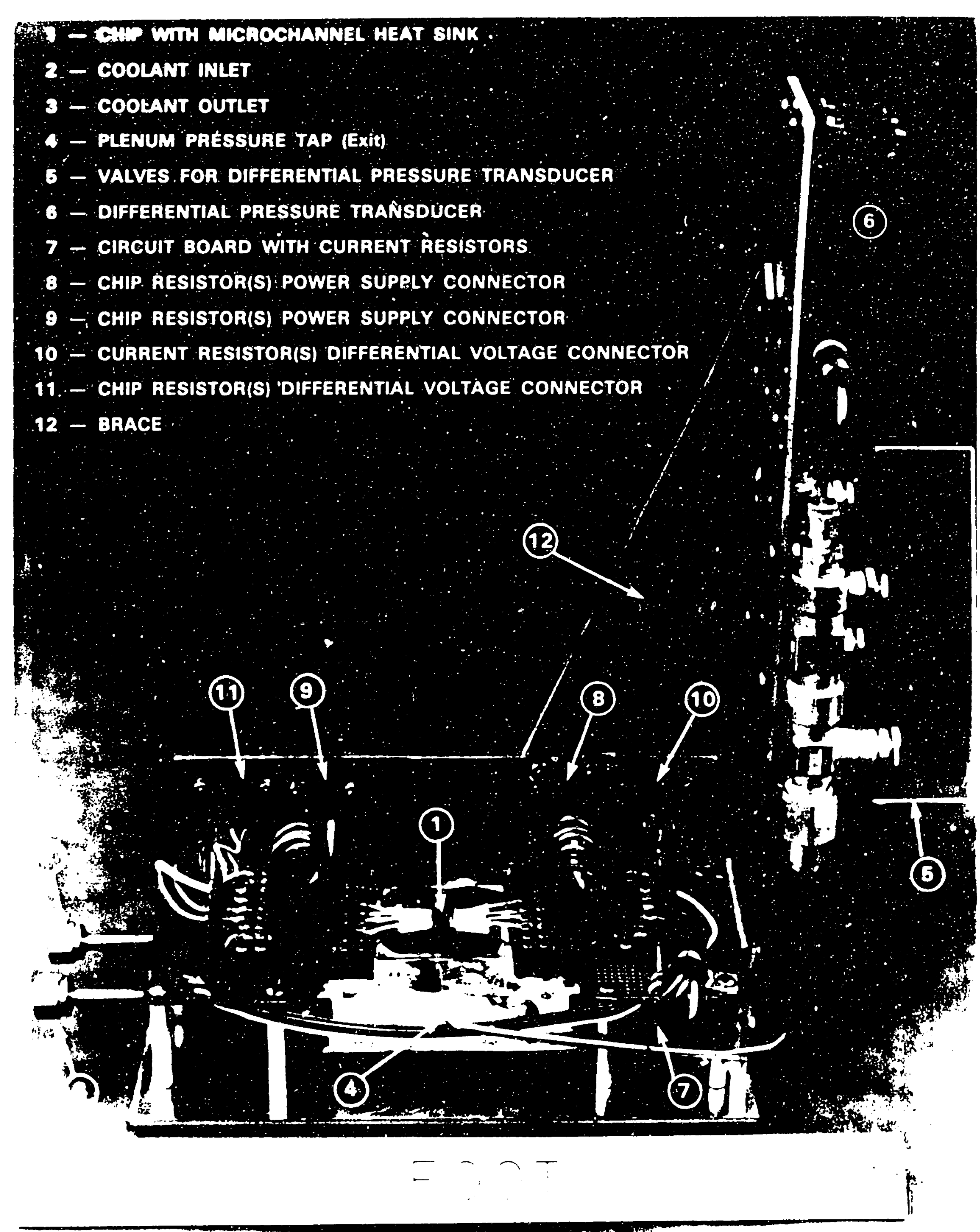

Figure 5.6. Manifold electronics substage.

The pressure drop across the chip was measured with another Validyne<R> differential pressure transducer. The pressure drop was measured between the inlet and outlet manifolds at the pressure taps indicated in Figure 5.2. Care was taken to bleed trapped gas from the pressure tap lines of each differential pressure transducer.

The power supplied to the test chip resistor(s) was determined by measuring the voltage drop across the test chip resistor metalizations, and by measuring the current-voltage-drop across precision resistors. The Dale<R> 0.01 Ω precision wirewound resistors (Model #LVR-3) were calibrated as installed in the manifold electronics substage, where the voltage drop was measured for various current flow rates and ambient temperatures. Note that a small fan is used to cool the precision resistors in order to minimize the effect of the resistance temperature coefficient

The surface temperature of the chip was measured using a Barnes<R> infrared microscope. The spot size for radiometric measurements was 0.0014 in. (35 µm). Since indium phosphide is fairly transparent in the near-infrared spectrum, the chip surface was painted with a "flat black" paint. The IR microscope was calibrated by flowing water of a known temperature through the test chips, and adjusting the microscope emissivity until the microscope control unit indicated the proper coolant temperature (typically, $\epsilon \approx 0.85$). The output voltage signal for data logging was 0-to-1 vdc at 10 kohms.

Several system temperatures are monitored using type K thermocouples. The offset for each thermocouple was obtained by calibrating

them at 0°C and 100°C. This offset was subtracted from all subsequent temperature measurements. Temperature measurements were taken for the ambient temperature, the precision resistor ambient temperature, the circulator coolant discharge temperature, and the heat exchanger shell side and tube side inlets and outlets. One thermocouple was used to monitor the temperature of the coolant in the inlet manifold, and another in the exit manifold. In addition, two thermocouples were installed and encapsulated in a Swagelok<R> fitting in the inlet and exit coolant supply lines (about 6 inches from the test chip). The three inlet and three exit coolant temperatures agreed well (within 0.2°C) upon insulating the stainless steel tubing between the manifold block and the thermocouple swagelok fittings.

The remaining testing parameters that need to be determined are the microchannel heat sink dimensions. The dimensions (t, b, L, w_W, w_C, and the number of channels) were evaluated either during chip fabrication and/or during a postmortem examination.

5.3.3 Experimental Errors

The experimental errors for the testing program include the inherent error in the measurement devices, errors in the instrumentation calibration, and systematic effects which change the magnitude of the quantity to be measured. The most common systematic errors are due to heat transfer related issues.

The most significant systematic error is the dissipated power in the chip that does not show up as coolant enthalpy rise. Convection heat transfer to the ambient air from the chip is very small owing to the

liquid coolant heat transfer coefficient being about three orders of magnitude larger. Convection heat transfer from the Lexan<R> manifold block and the stainless steel piping is also small. Radiation heat transfer from the chip is also small. The accuracy in determining the coolant temperature rise across the chip was found to be about ± 0.2°C; provided that steady-state thermal response had been achieved. All other thermocouple readings were accurate to within about ± 0.1°C.

The accuracy in determining the chip surface temperature depends on the accuracy of the infrared microscope, and on the uniformity of the chip surface emissivity. The indium phosphide chips were coated with a "flat black" paint which had a nominal emissivity of about 0.85. The paint emissivity was found to be very uniform across the chips. Therefore, the accuracy of the chip surface temperature measurements should be within the stated accuracy of the infrared microscope which was better than ± 0.5°C.

The error in determining the power dissipated by the test chip resistors is given by the accuracy of the voltage drop across the chip resistor(s) and the voltage drop across the precision resistors for current flow. The accuracy of both measurements is about ± 0.1 percent.

The uniformity of the power dissipation over each test chip resistor will be affected by the uniformity of the electrical resistance. It was shown in Section 5.2.3 that the resistor-to-resistor resistance uniformity was within ± 1.1 percent. This variance will result in an experimental thermal resistance which is too high by + 1.1 percent. The heat dissipation at the test chip resistors is assumed to occur uniformly

over the entire resistor area, which includes the resistor area directly underneath the gold metalizations. This assumption will result in an experimental thermal resistance which can be high by as much as 5.0 percent.

The total coolant flow rate measurements were accurate to within about ± 0.2 percent when the "bucket and stopwatch" method was used. The accuracy was within about ± 5.0 percent when the pressure drop across the flow orifices was used to determine the flow (in comparison to the flow rate determined by the "bucket and stopwatch" method).

The distribution of the coolant underneath the test chip heater resistors will be higher than the unheated portions of the chip due to the lower coolant viscosity at the heated regions. If it is assumed that the coolant flow rate per unit surface area under the unheated portions remains unchanged, then the flow rate under the resistors is approximately given by

$$f_{heated} = f_{hot} - f_{cold}\left[1 - \frac{W}{n(w_w + w_c)}\right] \quad (5.2)$$

where f_{heated} is the flow rate under the heaters, f_{hot} is the measured flow rate for the entire heat sink when the chip power is turned on, f_{cold} is the flow rate when the chip power is turned off, W is the transverse width of the heater, and n is the total number of coolant channels.

The accuracy in determining the channel geometry values is estimated to be: t ± 5 μm, b ± 5 μm, L ± 25 μm, w_w ± 2 μm, and w_c ± 2 μm. Note

that there is no error in the number of coolant channels. No problems were noted due to channel clogging and erosion during the testing. Some problems were caused by the epoxy used to bond the chip to the cover plate. The most serious problem was epoxy-plugged channels. This problem made it difficult to predict the thermal performance of the affected test chips (see Chapter 6). Note that the spun-down epoxy thickness (t_{epox}) multiplied by $(w_w+w_w)/w_c$, was subtracted from the channel height (b) in order to account for the reduction in channel cross-sectional area.

5.4 Chapter Summary

To conclude this chapter, some major results will be summarized.

This experimental program was initiated to see if microchannel heat sinks could be fabricated in indium phosphide chips. The orientation dependent etching method of fabrication was successfully used. Precision sawing was time consuming and resulted in occasional fin breakage. The manufacturing process used to fabricate the indium phosphide test chips is summarized by Table 5.2. A promising fabrication method for aluminum "cold plate" microchannel heat sinks was also introduced.

The apparatus used to test the thermal and fluid performance of the microchannel heat sink test chips was described. The experimental errors were discussed, and are used in the next chapter to establish overall uncertainty predictions in the thermal and fluid performance of the test chips.

6.0 COMPARISON OF ANALYTICAL AND EXPERIMENTAL RESULTS

The purpose of this chapter is to present thermal and fluid performance data, and to compare that data with the performance predicted by the MICROHEX computer program. The geometry of the microchannel heat sink test chips will be described first. Fluid performance results, and thermal performance results, will be presented and compared with theory. The chapter concludes with an overview of the modes of failure for the chips tested in this study.

6.1 Heat Sink Geometry

This author is currently aware of only two other research teams that have published information about microchannel heat sinks in the open literature. The original work was done by Tuckerman and Pease at Stanford University, Stanford, California, U.S.A. Their work concentrated on silicon microchannel heat sinks with moderate aspect ratio channels and small channel widths. The typical dimensions of their heat sinks were: $w_c \approx 50$ µm, $w_w \approx 40$ to 45 µm, $t \approx 100$ to 200 µm, $b \approx 300$ to 400 µm, $L \approx 1.4$ to 2.0 cm, $w_s \approx 1.5$ to 2.0 cm, and the surface heater was 1.0 cm square. The Stanford work is best summarized by Tuckerman (1984).*

Additional work on microchannel heat sinks was done by Kishimoto, Ohsaki, and Sasaki at Nippon Telegraph and Telephone Corporation (NTT),

* The reader should be aware that there are some critical typographical errors in Tuckerman (1984). This author was the first to discover several critical errors which have been confirmed by Dr. Tuckerman. An addendum sheet is being prepared by Dr. Tuckerman (currently of Lawrence Livermore National Laboratory, Livermore, CA, U.S.A.). Those interested in reading Tuckerman (1984) should make every effort to obtain the addendum.

Tokyo, Japan. Their work concentrated on alumina and silicon microchannel heat sinks with moderate aspect ratio channels, much larger channel widths, and very low coolant pressure drop ($\Delta P < 5$ psi). One of their designs had w_c = 800 μm, b = 400 μm, and L ≈ 10.0 cm. Another set of designs had a constant fin height of b = 900 μm, with several different channel widths [w_c = 70 μm, 140 μm, 340 μm,, and 20 mm (no fins)]. The NTT work is discussed in Sasaki and Kishimoto (1986), and Kishimoto and Ohsaki (1986).

This author is aware of some other microchannel heat sink work being done for the United States Department of Defense, and by many computer companies. This author is prevented from discussing their work because of restricted distribution and proprietary concerns.

The geometry of the indium phosphide test chips used in this study is presented in Table 6.1. The plenum geometry is also included in that table. All chip measurements were made by viewing the microchannel heat sink chips under a high-power microscope equipped with a calibrated reticle. All plenum measurements were done with a dial caliper.

The number of open and clogged channels was obtained by placing a drop of water in one plenum, and by observing the flow of the water to the other plenum (caused by microcapillary suction). (The "color" of the channels with water in them is different than those without water.) This method proved to be most useful just after epoxying the chip to the glass cover plate, since the chip could be detatched, cleaned, and re-epoxied without damage. Note that the epoxy used to attach the chip to the cover plate was first spun-down to about a 3-μm thick layer. The spun-down

TABLE 6.1

HEAT SINK GEOMETRY

Chip	w_w(µm)	w_c(µm)	w_w/w_c	b(µm)	$\alpha=b/w_c$	t(µm)	L(mm)	x_s(mm)††	w_s(mm)††
HEX 1	160 ± 2	90 ± 2	1.777	100 ± 5	1.111	310 ± 5	2.670 ± .025	1.016 ± .025	8.250 ± .025
HEX 2	65 ± 2	60 ± 2	1.083	80 ± 5	1.333	360 ± 5	2.670 ± .025	1.016 ± .025	6.250 ± .025
HEX 3	90 ± 2	160 ± 2	.5625	160 ± 5	1.000	260 ± 5	9.525 ± .025	1.016 ± .025	6.000 ± .025
HEX 4	155 ± 2	220 ± 2	.7045	165 ± 5	0.750	255 ± 5	9.703 ± .025	1.016 ± .025	5.842 ± .025
HEX 5†	205 ± 2	170 ± 2	1.206	170 ± 5	1.000	270 ± 5	4.801 ± .025	1.016 ± .025	12.750 ± .025
HEX 6†	235 ± 2	140 ± 2	1.679	162 ± 5	1.157	110 ± 5	4.750 ± .025	1.016 ± .025	12.776 ± .025
HEX 7†	210 ± 2	165 ± 2	1.273	170 ± 5	1.030	240 ± 5	12.065 ± .025	1.016 ± .025	11.862 ± .025

				Number of Channels			Overall Chip Size	
Chip	D_e(µm)	ε(µm)*	ϵ/D_e	Open	Clogged	Total	Length(cm)	Width(cm)
HEX 1	99.0	10 ± 3	0.101	5	28	33	0.9	0.7
HEX 2	68.6	8 ± 3	0.117	21	29	50	0.9	0.9
HEX 3	160.0	5 ± 2	0.031	24	0	24	1.3	0.8
HEX 4	185.3	10 ± 3	0.054	15	1	16	1.5	0.8
HEX 5†	172.5	5 ± 2	0.029	34	0	34	1.35	0.9
HEX 6†	153.0	8 ± 3	0.052	34	0	34	1.5	0.8
HEX 7†	167.5	8 ± 3	0.048	31	0	31	1.65	1.4

† Thermal and fluid performance testing has not been conducted on these chips at the publication date of this thesis. They will be tested at a later date.

†† Schematic of plenum geometry.

* Estimated characteristic height of surface roughness.

epoxy tended to build-up at the plenum slots in the cover plate. This phenomenon appears to be the reason for the serious channel clogging found in HEX1 and HEX2. To solve the problem, the epoxy layer was then reduced to < 1 μm by scraping the excess epoxy off the cover plate with a razor blade roughened with #600 grit sandpaper. This latter method proved very successful in controlling channel clogging, but care must also be taken to clean the excess epoxy from the inside of the manifold slots in the glass.

6.2 Fluid Performance

The pumping power required to operate a microchannel heat sink is directly proportional to the coolant flow rate and the associated pressure drop. The fluid performance of the microchannel heat sinks studied by the Stanford researchers was relatively straight forward to characterize [see Tuckerman (1984)]. Their tested designs were limited to laminar flow (Re < 1000), which was usually fully developed at the channel exit. They found that the friction factor-Reynolds number product agreed well between theory and data. They also found that the overall entrance and exit pressure loss coefficient $[(Ac/Ap)^2 2K_{90} + Kc + Ke] = K$ was somewhat higher than expected (K should be about two). Their end-fed designs (see Figure 1.4) had K ≈ 3, and the side-fed designs had K ≈ 4 to 5. The discrepancy is probably due to deviation from the ideal flow patterns assumed for the calculation of Kc, Ke, and K_{90}.

The Stanford researchers have published limited pressure drop versus flow rate data [see Tuckerman and Pease (1981a)]. A comparison between this data and the MICROHEX computer program was performed (see

Table 6.2). The comparison shows that the computer program underpredicts the pressure drop by as much as nearly 50 percent!. It is conjectured that the pressure drops listed in Tuckerman and Pease (1981a) were corrected and presented for a 1.0 cm channel length [instead of the 1.4 cm channel length listed in Tuckerman (1984)].* The agreement will be much improved if this is true. If it is not true, then it is unclear why there is such a large difference.

The fluid performance of the microchannel heat sinks studied by the NTT researchers was not documented explicitly in their papers. Their coolant pressure drop was typically less than 2000 Pa (2.85 psi). No pressure drop versus flow rate data were published, so no comparison can be made with the MICROHEX computer program.

The fluid performance of the microchannel heat sinks tested thus far in this study is shown in Figure 6.1, where the pressure drop is plotted versus Reynolds number. The uncertainty in the Reynolds number is shown for each data point, and is due primarily to the uncertainty in the channel hydraulic diameter. The uncertainty in the pressure drop is approximately equal to the size of the data points themselves.

The curves plotted in Figure 6.1 are the pressure drop predicted by the MICROHEX program. It can be seen that the agreement is quite good. The reader should note the relative decrease in the predicted pressure drop for HEX4 in the turbulent regime. The pressure drop data do show a slight change in the velocity-squared curvature for Re > 2500, which

* This author has had several conversations with Dr. Tuckerman, but the three heat sinks listed in Table 6.2 were not discussed.

TABLE 6.2

COMPARISON OF PRESSURE DROP PREDICTED BY THE MICROHEX COMPUTER PROGRAM AND EXPERIMENTAL DATA OBTAINED BY THE STANFORD RESEARCHERS

CHIP No.	80D6	80D19	81F9
Header Design	End-fed	End-fed	End-fed
Fabrication	Etched	Etched	Etched
L (mm)	14.0	14.0	14.0
w_s (mm)	20.0	20.0	20.0
x_s (mm)	3.0	3.0	3.0
w_c (μm)	56.0	55.0	50.0
w_w (μm)	44.0	45.0	50.0
b (μm)	320.0	287.0	302.0
t + b (μm)	533.0	430.0	458.0
f_{heated} $(cm^3/s)/cm^2$	4.7	6.5	8.6
Measured ΔP (psi)	15.0	17.0	31.0
Predicted ΔP (psi)	20.0	33.0	40.0

* Data taken from Tuckerman (1984), and Tuckerman and Pease (1981a).

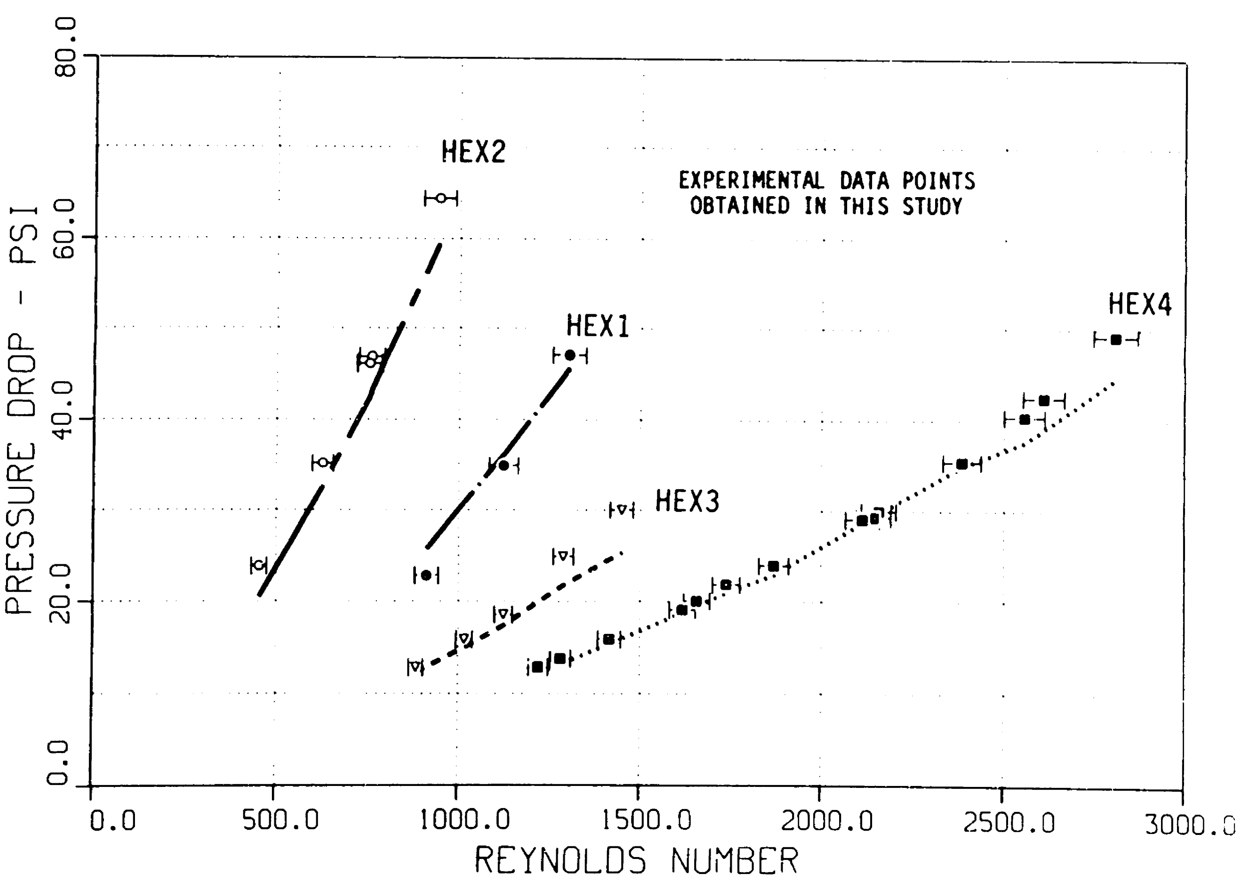

Figure 6.1. Comparison of experimental data and MICROHEX program predictions for pressure drop versus Reynolds number.

indicates that the transition from laminar to turbulent flow may have occurred. The discrepancy between the data and the theory may also be due to the increase in the friction factor due to the roughened channel surfaces, which occurs for turbulent flow.

The overall pressure loss coefficient has been computed using the MICROHEX program. The results show that $K \approx 1.7$ to 2.0 for laminar flow, and $K \approx 1.3$ for turbulent flow. The value of K was found to decrease slowly as the Reynolds number increased. The reduction in K for turbulent flow is due to the reduction in the tabulated values of Kc and Ke (w.r.t. laminar flow).

Figure 6.2 is a plot of the pressure drop versus the hydrodynamic entrance length L^+ based on the total channel length. The uncertainty in L^+ is primarily due to the inverse square of the uncertainty in the channel hydraulic diameter. The uncertainty in the pressure drop is again approximately equal to the size of the smaller data points (the squares). It should be noticed that the uncertainty is largest for small hydraulic diameters and small Reynolds numbers. The main point to note here is that the flow in the microchannels tested thus far in this study is not fully developed at the channel exit.

6.3 Thermal Performance

The ultimate reason for using microchannel heat sinks is that very high thermal performance can be achieved. This fact was proven by Tuckerman (1984), where one heat sink was tested to about 1300 W/cm^2 for a 1.0 cm square heater.

It has been found that the MICROHEX computer program quite accurately predicts the thermal performance data of the Stanford researchers.

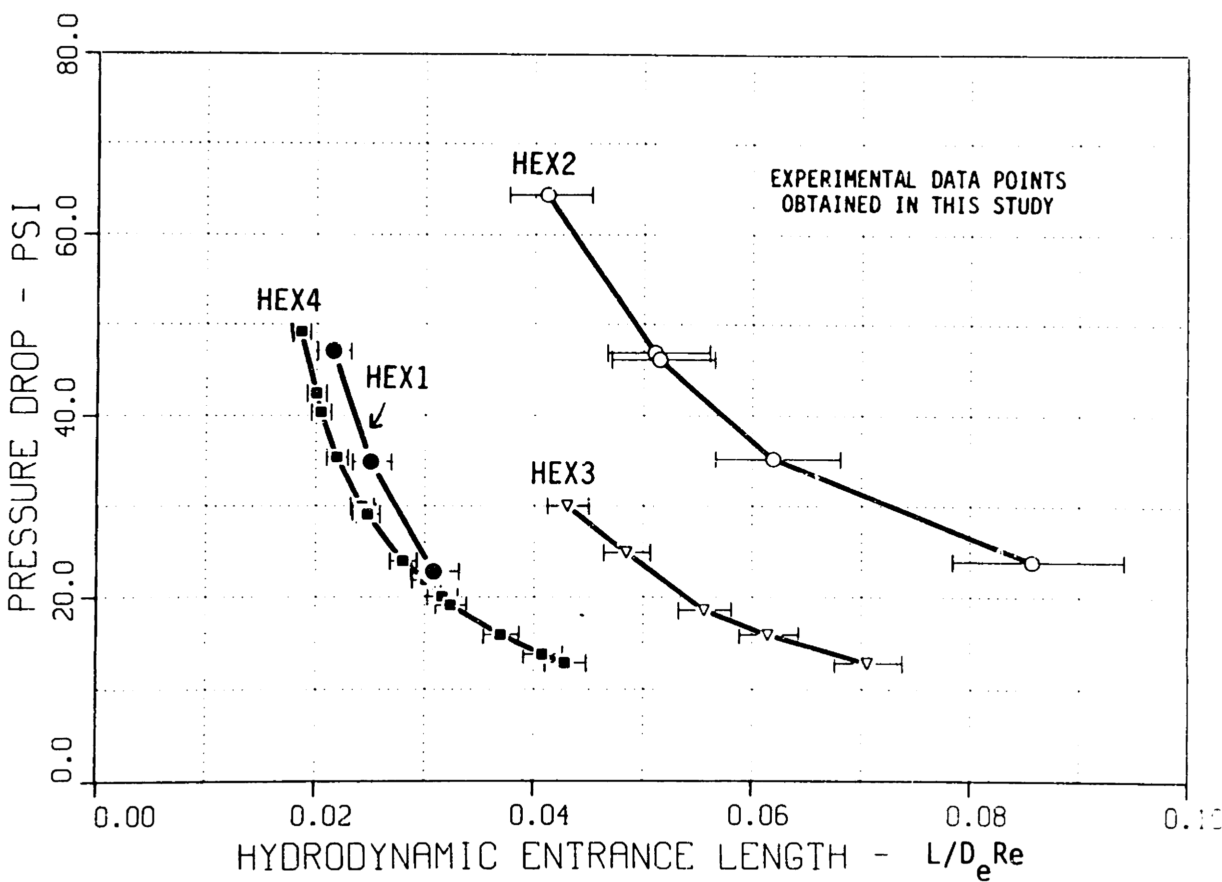

Figure 6.2. Comparison of experimental data and MICROHEX program predictions for pressure drop versus hydrodynamic entrance length.

In fact, the program is so accurate, that disagreement with the published data pointed towards documentation errors in Tuckerman (1984). The discrepancies were resolved when the documentation errors were discovered [Tuckerman (1986)].

The thermal resistance versus thermal entrance length data* presented in Tuckerman (1984) is compared with the MICROHEX program predictions in Figure 6.3. The channels for that heat sink were sawn, which means that an equivalent rectangular channel must be assumed for computational purposes. The numerical predictions in Figure 6.3 assume that w_c = 88.5 μm, w_w = 61.5 μm, b = 225 μm, t = 270 μm, L = 1.0 cm (heated), $T_{f,in.}$ = 288°K, and q" = 118 W/cm^2. It can be seen that the computer program quite accurately predicts the data. The predicted thermal resistance is lower in the regions where thermal spreading is important [unfortunately, no comparison is possible here in the thermal spreading region since no data in this region is provided by Tuckerman (1984)].

The thermal resistance data versus position from the upstream heater edge presented in Tuckerman (1984) is compared with the MICROHEX program predictions in Figure 6.4. Again, the channels were sawn, for which an equivalent smooth channel is assumed for computational purposes. The predictions in Figure 6.4 assume that w_c = 64 μm, w_w = 136 μm, b = 245 μm, T = 244 μm, L = 1.0 cm (heated), f_{heated} = 1.277 $(cm^3/s)/(cm^2)$, $T_{f,in}$ = 290°K, and q" = 34 W/cm^2. It can be

* Note that Tuckerman (1984) does not mention that R''_{cond} was subtracted from R''_{tot}, which results in the values shown in Figure 6.3 (confirmed by Dr. Tuckerman).

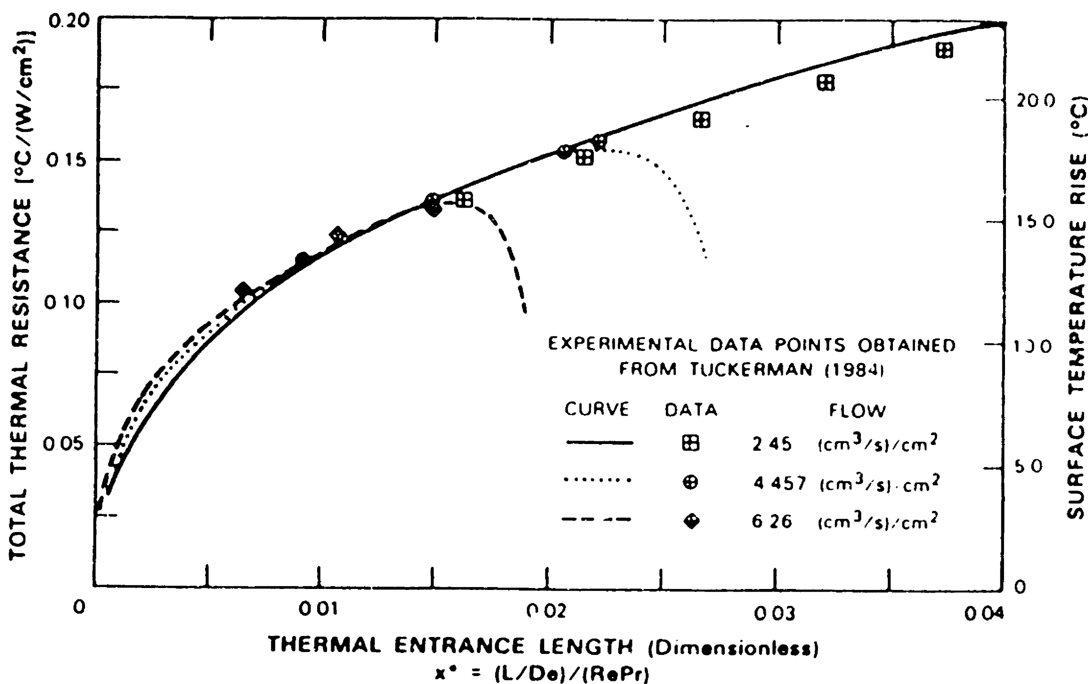

Figure 6.3. Comparison of experimental data and MICROHEX program predictions for thermal resistance versus thermodynamic entrance length.

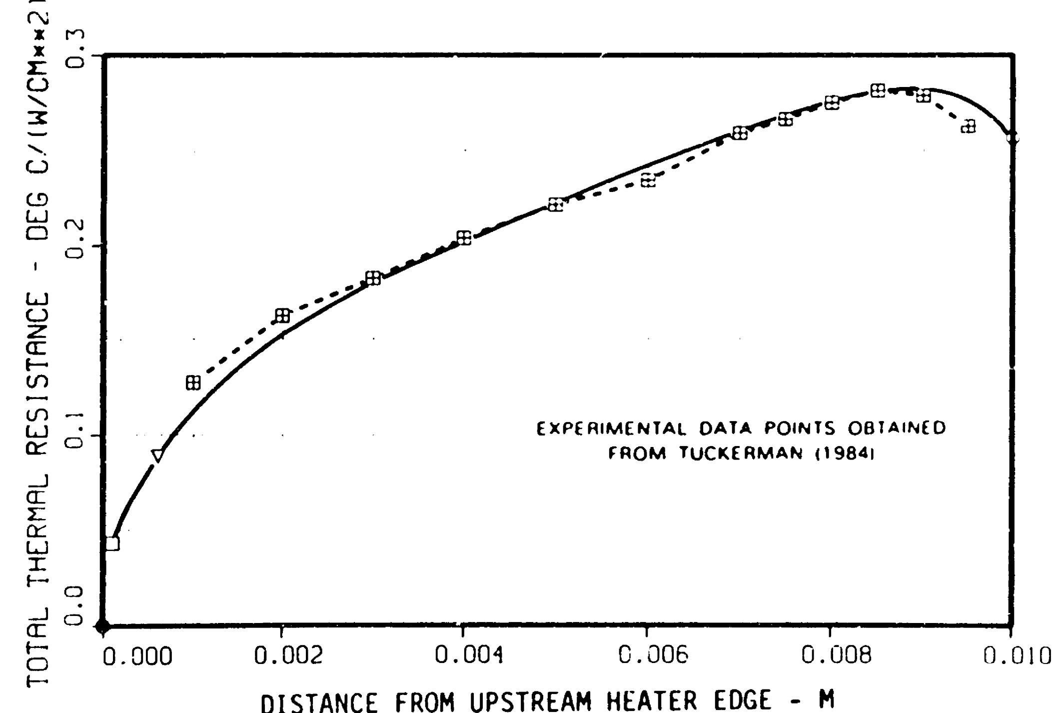

Figure 6.4. Comparison of experimental data and MICROHEX program predictions for thermal resistance versus distance from the upstream heater edge.

seen that the agreement is quite good. The thermal resistance at the entrance is low due to developing flow and thermal spreading at the heater perimeter. The thermal resistance is also low at the exit due to thermal spreading. Note that the predicted thermal resistance is slightly too high in the exit thermal spreading zone.

The NNT researchers do not present sufficient information in their articles to allow the direct comparison of MICROHEX program predictions and their experimental results. It is interesting to note, that they predict analytically, that there is an optimum channel width design when the pressure drop and channel height (b) are held constant. The existence of an optimum channel width is predicted by the MICROHEX computer program (see for example Figure 4.14), but this predicted optimum is at a somewhat smaller channel width.

The indium phosphide microchannel heat sinks tested in this study were found to have very good thermal performance. The maximum tested thermal performance for each heat sink is listed in Table 6.3. Note that HEX4 is still operational at the publication date, and that there is good potential for much better thermal performance if the pressure drop is increased (to provide more coolant flow). Note that HEX1 and HEX2 had numerous channels that were blocked with epoxy (see Table 6.1). No additional thermal performance information will be presented here for those two test chips due to the clogged channel problem.

The typical temperature profiles for a four-resistor chip are shown in Figure 6.5. The reader should note a few main points. First, the uncertainty in T_{surf} is within about ± 0.5°C at T_{surf} = 65°C, and

TABLE 6.3

EXPERIMENTAL THERMAL PERFORMANCE OF InP TEST CHIPS

Chip	$T_{f,in.}$(°C)	T_{surf}(°C)	Q (W)*	q" (W/cm^2)	R''_{tot}[°C/(W/cm^2)]
HEX1	23.0	110.0	13.95	223.0	0.390
HEX2	22.9	110.0	31.49	504.0	0.173
HEX3**	27.3	95.0	42.31	677.0	0.100
HEX4***	33.8	110.0	66.19	1059.0	0.072

* Total heating rate for a single 0.25 cm square resistor.
** This chip failed prematurely when the author over-pressured the chip while purging air from the differential pressure lines (no power was being dissipated by the chip resistors).
*** This chip is still operational at the publication date.

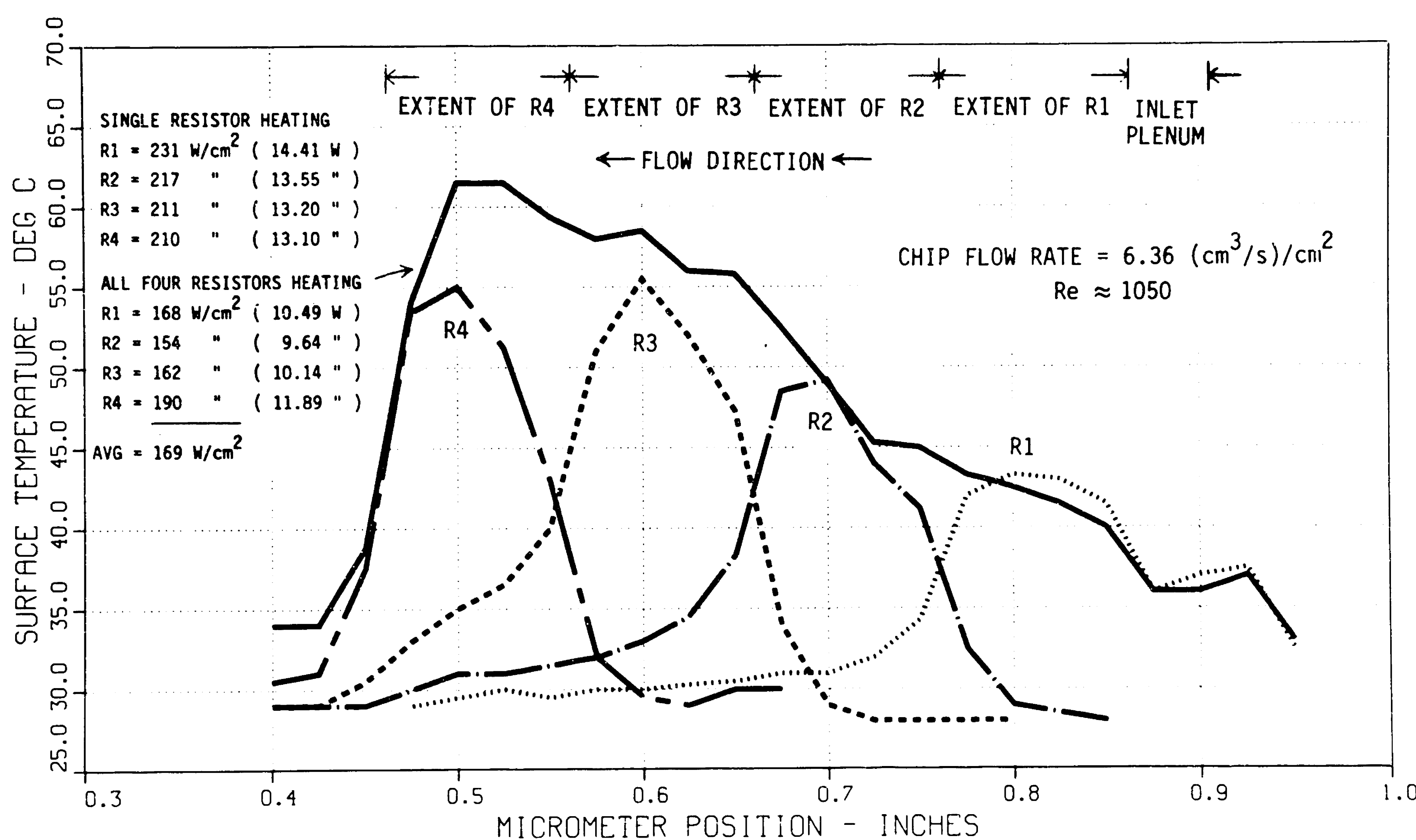

Figure 6.5. Surface temperature for HEX3 as a function of the microscope substage micrometer position.

within about ± 2.0°C at T_{surf} = 30°C. The increase in uncertainty for lower surface temperatures is due to the lower resolution in the analog meter output from the infrared microscope (for the 15°C to 65°C scale). (The uncertainty is within about ± 0.5°C at T_{surf} = 110°C, and within about ± 3.0°C at T_{surf} = 30°C for the 15°C to 165°C scale).

The second main point to note is that the power dissipated by each resistor was significantly different. This is because one power supply was used to supply power to all four resistors. This makes analysis of the results somewhat more difficult and, therefore, most of the results presented in the remainder of this chapter were obtained for a single resistor powered-up at a time.

The third main point to note is that the thermal spreading diffusion length in the streamwise direction is on the order of 1.5 to 2.0 mm. This is somewhat larger in magnitude than predicted by the thermal spreading theory presented in Section 3.4. This means that the MICROHEX computer program will predict surface temperatures that are too high. There are two reasons for this effect. First, the thermal spreading model ignored the temperature gradient in the streamwise direction caused by developing flow and coolant temperature rise. Second, the two-dimensional thermal spreading that occurs in reality is modeled by two one-dimensional models that are superimposed. It is expected that a thermal spreading model that accounts for these two effects will be more accurate.

The fourth main point to note from Figure 6.5 has to do with the location of the inlet coolant plenum. The chip surface temperature increases slightly over the top of the plenum, which indicates reduced

cooling efficiency in that region. This effect was not anticipated since the plenum flow "impacts" the chip similar to a jet on a flat plate, which gives locally enhanced heat transfer. The entrance flow may be separating, though, which would have an accompanying reduction in heat transfer (for laminar flow as in Figure 6.5).

The fifth main point to note from Figure 6.5 has to do with the thermal resistance of the two upstream resistors (R1 and R2). These two resistors exhibit lower thermal resistance than resistors R3 and R4! This is probably due to the local enhancement in the heat transfer caused by simultaneously developing flow in the upstream region of the channels.

Figure 6.6 plots some typical surface temperature profiles for HEX4. Note that the uniformity in thermal resistance among the four resistors is much improved. This can be seen by comparing the heating rates and the peak surface temperatures. Note that some entrance-region enhancement is again detectable for heater R1.

Figure 6.7 plots a comparison of the MICROHEX program predictions, and the experimental data for resistor R2 in Figure 6.6. It is clear that the computer program predicts higher thermal resistance. The error is about +20 percent when thermal spreading at the heater perimeter is accounted for, and about +50 percent when thermal spreading is ignored. The discrepancy is probably due entirely to the simplified one-dimensional modeling used to account for the effect of thermal spreading at the heater perimeter. The indium phosphide thermal conductivity was not measured, and may be slightly different from the tabulated thermal conductivity data. Note that there is a "bump" in the predicted thermal

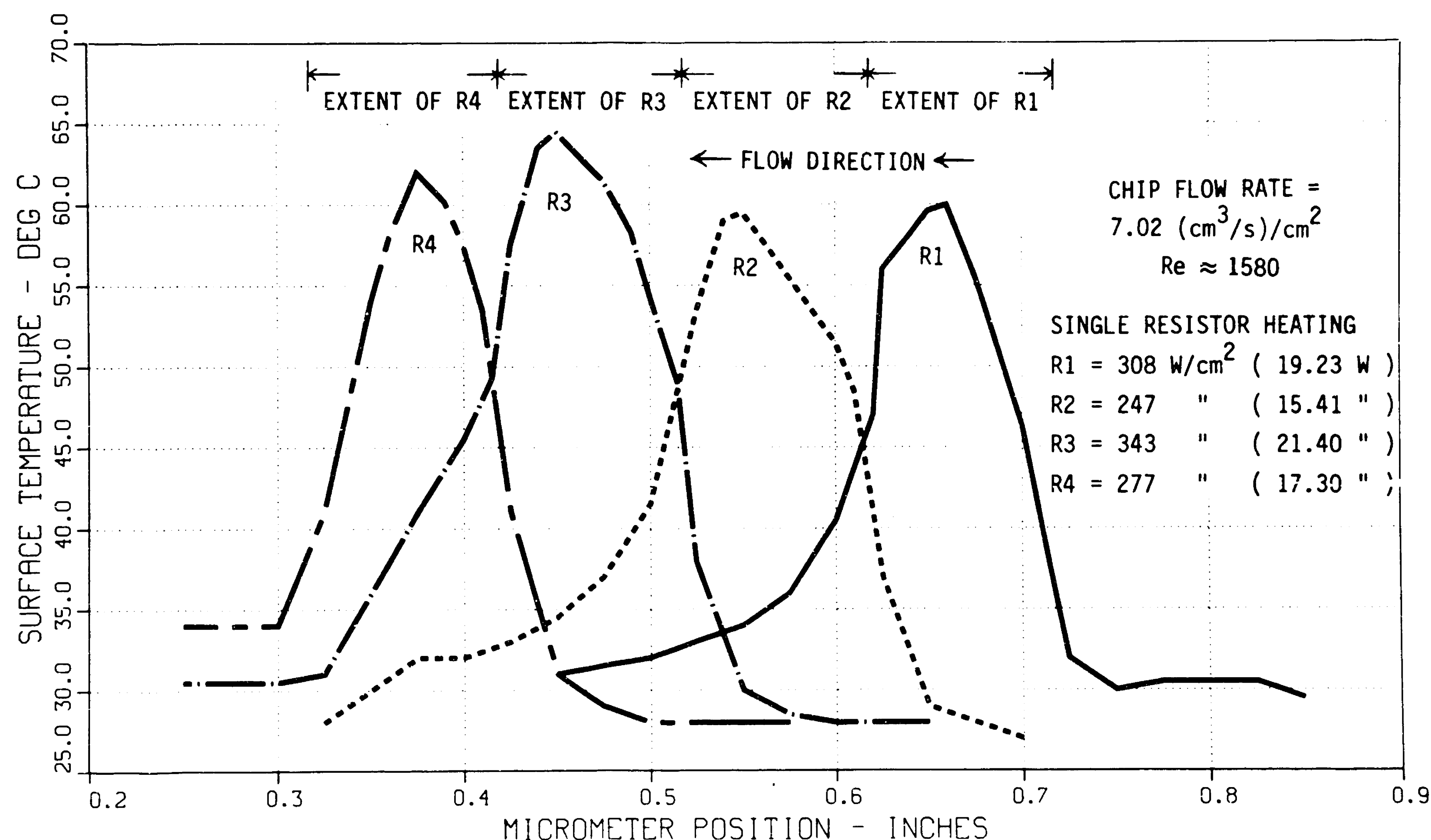

Figure 6.6. Surface temperature for HEX4 as a function of the microscope substage micrometer position.

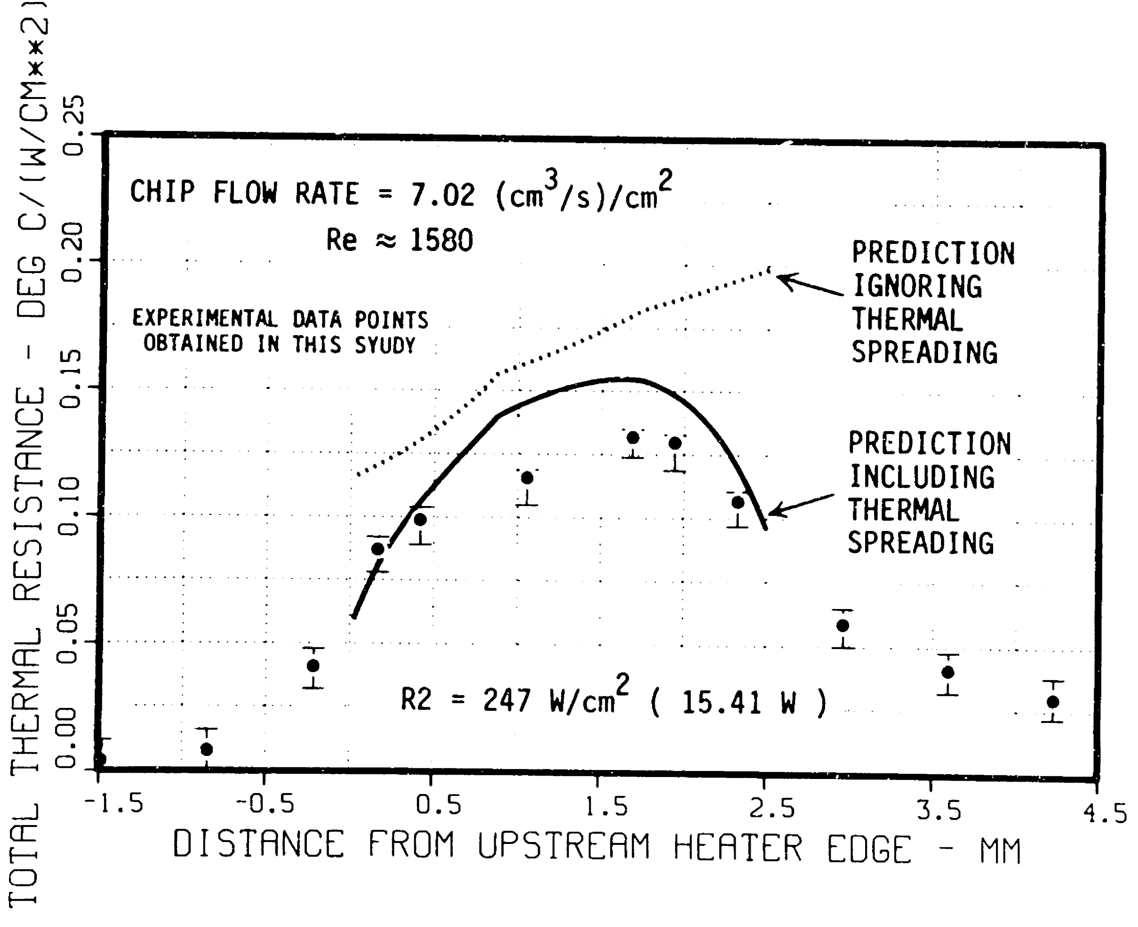

Figure 6.7. Comparison of experimental data and MICROHEX program predictions for thermal resistance versus distance from the upstream heater edge of HEX4 resistor R2.

performance at the 0.9 mm position. The bump is due to the error in obtaining the Nusselt number by using linear interpolation in Table 2.11.

Figure 6.8 is a plot of the peak surface temperature versus the dissipated power for HEX4 at two coolant flow rates. The uncertainty in the dissipated power is about equal to the width of the data points. The uncertainty in the peak surface temperature is about ±0.5°C at T_{surf} = 110°C and about ±2.1°C at T_{surf} = 60°C. The main point to notice here is that the surface temperature increases in a linear fashion with increasing power dissipation. The thermal resistance is lower for the higher coolant flow rate as is expected.

Figure 6.9 is a plot of the thermal resistance versus the dissipated power of HEX4, which is obtained from the data presented in Figure 6.8. The uncertainty in the dissipated power is again about equal to the width of the data points. The uncertainty in the thermal resistance is quite large, and is due to uncertainty in the surface temperature and the heat flux. The main point to notice here is that the thermal resistance does not appear to be a function of chip surface temperature. Indeed, the resistance seems to decrease with increasing surface temperature. This indicates that the decrease in the chip thermal conductivity is less important than the increase in the thermal conductivity of the water. The coolant flow rate did not change significantly as the dissipated power was increased, but the pressure drop did become slightly smaller. This is expected due to the reduction in the friction factor owing to a reduction in the dynamic viscosity with increasing coolant (and fin) temperature.

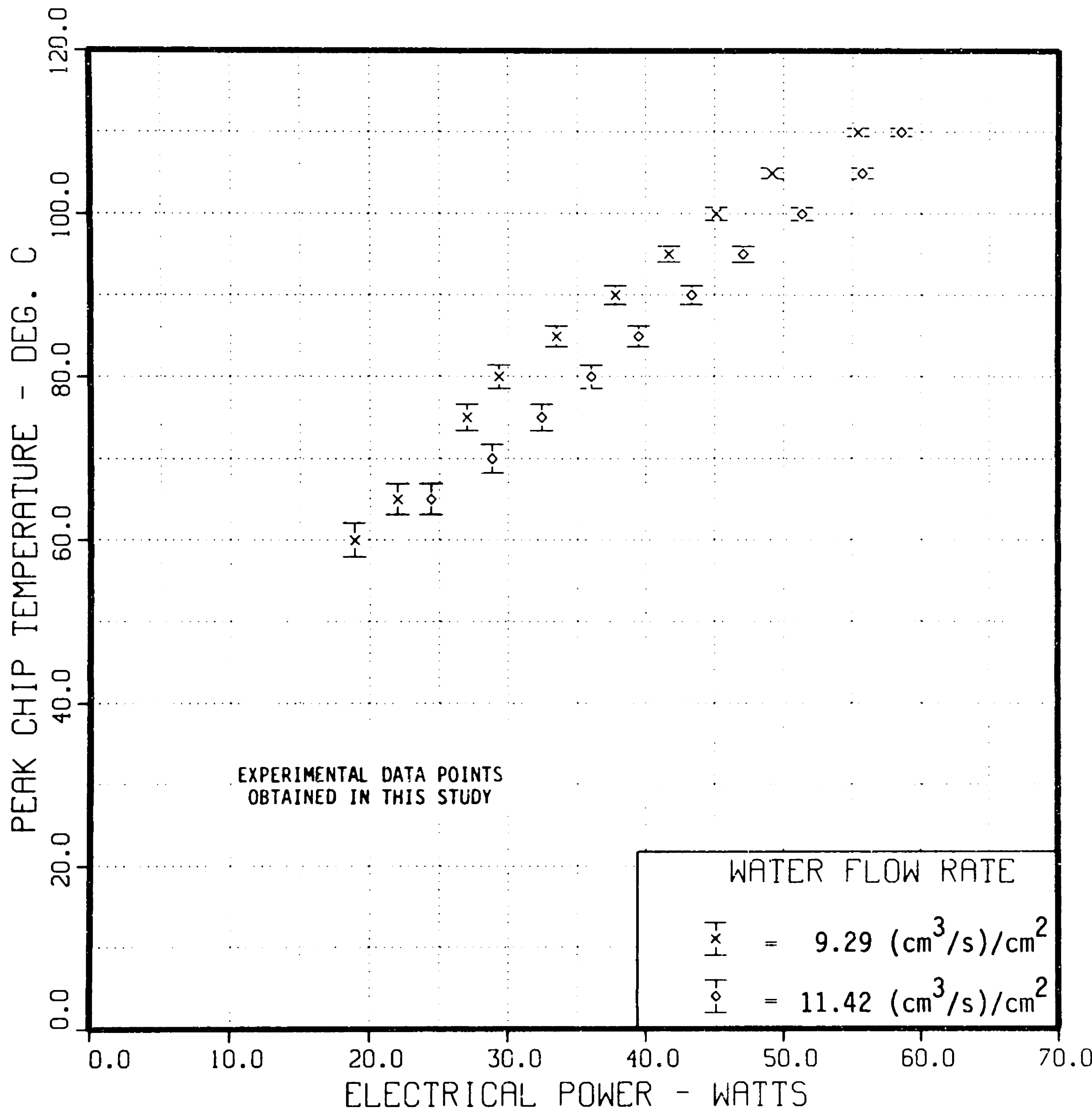

Figure 6.8. Peak surface temperatures versus dissipated power for HEX4 at two coolant flow rates.

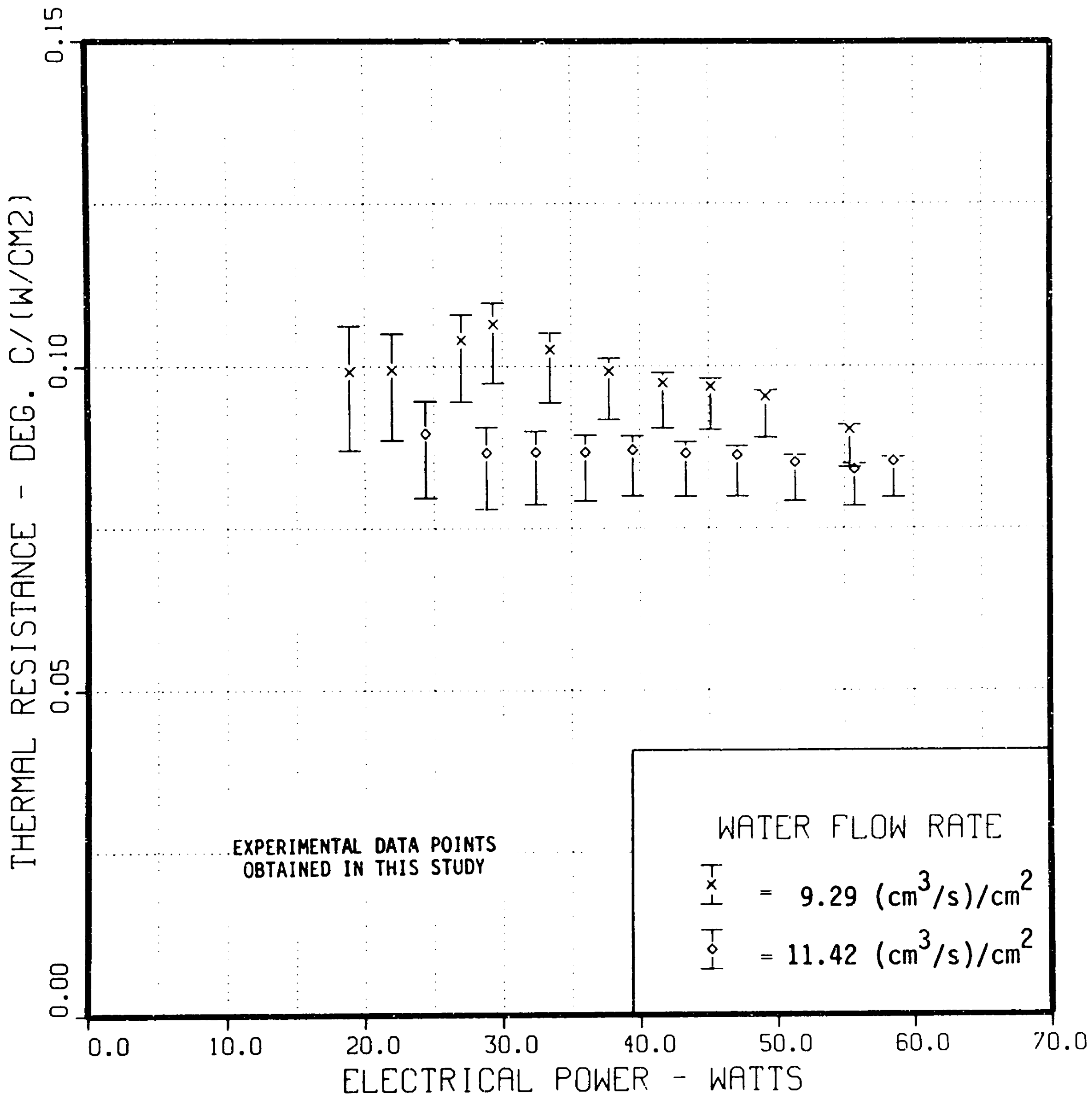

Figure 6.9. Thermal resistance versus dissipated power for HEX4 at two coolant flow rates.

The thermal performance of the indium phosphide test chips may be affected by the surface roughness created by the orientation dependent etching of the channels (see Figure 5.1). The effect would be to increase the turbulent friction factor and the Nusselt number compared to the same channel with smooth surfaces. (No effect should be noticeable in laminar flow.) The roughness may be significant if the characteristic height of the roughness ϵ is larger than the thickness of the turbulent-flow laminar sublayer. A criterion for the minimum roughness height can be obtained using the "universal velocity distribution" for turbulent flow in smooth tubes [see Rohsenow and Choi (1961)]. The minimum roughness height criterion obtained in this way is

$$\epsilon/D_e \geq 25.14 \; Re^{-0.875} \tag{6.1}$$

where the friction factor was obtained using the Blasius equation. Figure 6.10 is a plot of Equation 6.1, where the solid curve is for turbulent flow (the dashed curve is an extension of the results into the laminar Reynolds number range, and would apply if the flow was tripped into the turbulent regime). The estimated relative roughness for the indium phosphide microchannels was listed in Table 6.1. The minimum roughness height criterion appears to be satisfied by the test chips for low-Reynolds-number turbulent flow. Therefore, it is expected that the channel roughness may affect the thermal and fluid performance.

A crude estimate of the increase in the Nusselt number due to surface roughening can be made by assuming that the Nusselt number increases proportional to the relative increase in the friction factor.

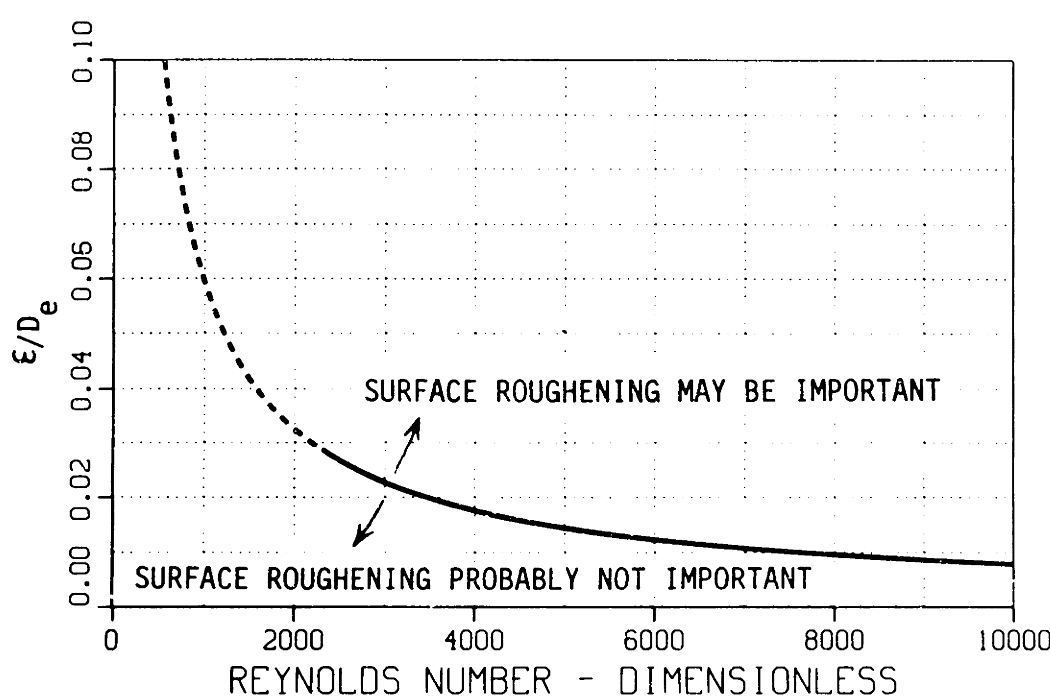

Figure 6.10. Roughness height criterion versus flow Reynolds number.

For HEX4, this means that the Nusselt number could be doubled due to surface roughening.* A comparison of the experimental data shown in Figure 6.9 and the MICROHEX predicted performance for HEX4 is shown in Figure 6.11. The uncertainty in the data is the same as discussed with Figure 6.9. The main point to notice here is that the computer program predicts significantly worse thermal performance. This discrepancy is probably due in part to the inadequate thermal spreading model as discussed above. Some of the discrepancy might be explained by enhanced heat transfer owing to surface roughness. It can be seen that tripling the Nusselt number provides results that, on average, agree pretty well with the data. The computer program, though, predicts increasing thermal resistance for higher power dissipation.

Overall, the MICROHEX computer program predicts the experimental data of several researchers quite well. Discrepancies appear to be largest when the heat sources are small (owing to the model used for thermal spreading at the heater perimeter), and when surface roughening may be affecting the turbulent flow performance.

6.4 Modes of Failure

Several heated and unheated (no resistors) microchannel heat sink chips were tested. All of the chips were made of indium phosphide, which is a material that cleaves very readily when stressed. All of the testing was done over relatively short time periods (<12 hours continuously). (One chip, HEX4, has been tested intermittently for approximately 24 hours, and is still operational at the date of this publication.)

* See White (1984).

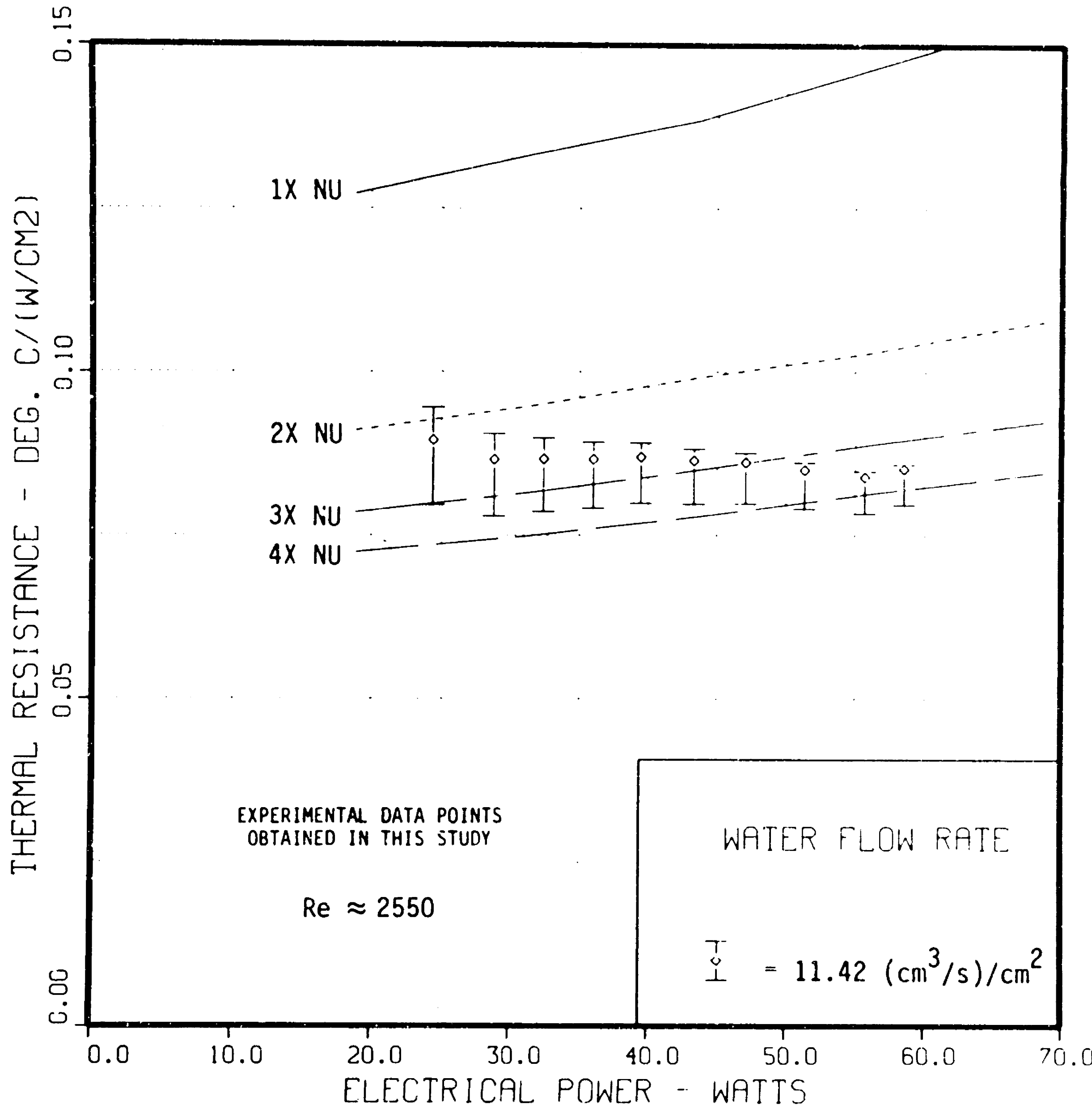

Figure 6.11. Comparison of experimental data and MICROHEX program predictions for thermal resistance versus dissipated power for HEX4.

It is interesting to note that the epoxy did not appear to fail in any test. The chips did not "pull up" from the epoxy and/or the glass cover plate, which indicates retention of bond strength. The chips did not leak about their outer periphery.

The author was not able to determine if the coefficient of thermal expansion of the epoxy had any impact on the chip failures. It is possible that the epoxy could have had an impact since its coefficient of thermal expansion is about 55 x $10^{-6}°C^{-1}$, which is about an order of magnitude larger than that of the glass cover plate and the indium phosphide.

All chips were deemed to have failed when pool(s) of the liquid coolant (here water) appeared on the chip surface. In all cases, the water came from microcracks in the directions of the (011) and $(01\bar{1})$ cleavage planes. The pool(s) of coolant usually first appeared looking like small "bead(s) of perspiration," which grew slowly in size. The rate of growth was slowed due to the high evaporation when power was being dissipated by the resistors. When the power was turned off, the pool(s) grew at a much faster rate. No "geyser(s)" of coolant have been created (so far).

The most common location of failure was over the top of the inlet coolant plenum, which is the location of the highest coolant pressure. This happens because the chip over the top of the plenum is not supported by the cover plate (here, x_s = 1.016 mm = 0.040 in.). Reducing the width of the inlet plenum would significantly improve the structural rigidity, but the plenum width probably should not be smaller than the fin height (b) in order to keep down the pressure losses.

Increasing the thickness of the solid material will provide additional stiffness, but will at the same time increase the thermal resistance.

6.5 Chapter Summary

This chapter has been devoted primarily to comparing the available experimental data on microchannel heat sinks with the analytical model of the thermal and fluid performance (the MICROHEX computer program). The comparisons were limited to moderate aspect ratio channel designs, since the author is not aware of any data for small and large aspect ratio channel designs.

The MICROHEX computer program was found to predict quite well the thermal performance data of the Stanford researchers, but predicted larger pressure drop than their data. The computer program predicts quite well the fluid performance data obtained in this study, but predicts larger thermal resistance than indicated by the data. The discrepancy in the thermal performance predictions should be due to the simplified, one-dimensional thermal spreading models used to account for thermal spreading at the heater perimeter. There may also be some effect for turbulent flow due to the surface roughness created when the channels are fabricated using orientation dependent acid etching.

The modes of failure for the indium phosphide test chips were discussed. Failure was indicated by pool(s) of coolant appearing on the chip surface. The leaking originated at microcracks in the (011) and $(01\bar{1})$ cleavage plane directions. The most common location for failure was directly above the inlet coolant plenum. The epoxy did not appear to fail for any of the test chips.

7.0 SUMMARY AND CONCLUSIONS

This chapter provides a brief review of the major conclusions of this research project. Several areas for additional design and development of microchannel heat sink technology are also provided.

7.1 Conclusions

The main conclusions and results of this work are:

1. It was found analytically that turbulent flow should provide equivalent or better thermal performance than similar laminar flow heat sink designs. Insufficient experimental data exists to verify or negate this claim. The pumping power requirements for the turbulent flow designs can be kept below 10 W/cm^2 and the thermal resistance can be lower than 0.1°C/(W/cm^2). The typical minimum channel widths for turbulent flow designs are in the range of 200 to 300 µm [for a 68.9 kPa (10 psi) pressure drop]. These large channels are much easier to manufacture than the much smaller laminar flow channel designs recommended by the Stanford researchers (Tuckerman and Pease). In fact, it becomes feasible to make the microchannel heat sink in high thermal conductivity materials such as copper and aluminum using conventional machine shop technology.
2. A generic computer program has been written that can compute the thermal and fluid performance of microchannel heat sinks. The entire computer program listing is provided as Appendix E of this document. This program, called MICROHEX, predicts quite well the available microchannel heat sink experimental

data. The computer program conservatively predicts the thermal performance of the heat sinks tested in this study. The discrepancy is thought to be due to the simplified model used to account for thermal spreading at the heater perimeter (a better model that accounts for two-dimensional thermal spreading should solve the problem). Surface roughening in turbulent flow can be important also.

3. It was found that a "compensation heater" can be used to improve the temperature uniformity across an IC heat source, which may lead to an improvement in IC reliability. This may also result in simplified IC design and fewer timing problems. This concept needs to be evaluated experimentally using chip-level reliability testing to verify its validity.

4. It was found that microchannel heat sinks can be fabricated directly into the back of indium phosphide chips. Both precision sawing and orientation dependent acid etching may be used to fabricate the channels, but the sawing method has problems with fin breakage and chipping. Water-cooled indium phosphide microchannel heat sinks have been tested at pressure drops up to about 414 kPa (60 psi), and thermal resistance as low as 0.072 °C/(W/cm^2) has been obtained. The maximum heat dissipation to date has been 1059 W/cm^2 for a 0.25 cm square 160 µm tall, and 1.0 cm long.

7.2 Future Work

There is a considerable amount of work that can be done to further develop microchannel heat sink design and use. Some areas which show good promise are:

1. developing a more accurate model of thermal spreading at the heater perimeter that accounts for two-dimensional effects (and incorporating the new model into the MICROHEX computer program),
2. developing cold-plate microchannel heat sink fabrication technology for mass production of metallic heat sinks,
3. developing alternate fabrication technology for microcapillary thermal interfaces (particularly on polished metallic cold plates),
4. developing ways to artificially roughen the microchannel surfaces to enhance heat transfer,
5. developing ways to incorporate microchannel heat sinks directly into printed circuit boards,
6. developing a sensible multiple header/plenum coolant distribution system for short channel length designs,
7. experimentally testing the possible enhancement in IC reliability using compensation heaters,
8. experimentally testing more microchannel heat sinks in the turbulent flow regime,
9. experimentally testing the thermal and fluid performance for coolants other than water,

10. experimentally testing the long-term reliability of microchannel heat sinks fabricated directly in IC chips (fouling, chip contamination, channel erosion due to flow, biological contamination (bugs), etc.),
11. developing finite-difference, and finite-element, models of the thermal and structural response,
12. researching the friction factor and Nusselt number characteristics of low-Reynolds-number turbulent flow, and
13. looking into the possible performance enhancement if "pulsating" coolant flow is used (instead of steady coolant flow).

The reader can probably see many other areas of research opportunity in this field.

This author will continue working on microchannel heat sink design, and would be very interested in corresponding with other researchers working in this field. The author is employed at:

M.I.T. Lincoln Laboratory
244 Wood Street
Lexington, Massachusetts 02173-0073
617-863-5500 Ext. 4512

BIBLIOGRAPHY

Aliev, S. A., Nashel'skii, A. Y., and Shalyt, S. S., 1965, "Thermal Conductivity and Thermoelectric Power of n-Type Indium Phosphide at Low Temperatures," Soviet Physics - Solid State, Vol. 7, pp. 1287-8.

Baker, D., 1972, Physical Design of Electronic Systems, Volume IV: Design Process. Prentice-Hall, Englewood Cliffs.

Bar-Cohen, A., 1985, "Thermal Management of Air and Liquid-Cooled Multi-Chip Modules," 23rd ASME/AICHE National Heat Transfer Conference, Denver, Colorado, August 4-7, 1985, pp. 1-36.

Bodoia, J. R., 1959, Presented in Shah, R. K. and London, A. L., 1978, Laminar Flow Forced Convection in Ducts, Supplement 1 in Advances in Heat Transfer. Eds. Irvine, T. F. and Hartnett, J. P., Academic, New York.

Boelter, L. M. K., Young, G., and Iversen, H. W., 1948, presented in Kays, W. M. and Crawford, M. E., 1980, Convective Heat and Mass Transfer. McGraw-Hill, New York.

Buchmann, P. and Houghton, A. J. N., 1982, "Optical Y-Junctions and S-Bends Formed By Preferentially Etched Single-Mode Rib Waveguides in InP," Electronics Letters, Vol. 18, pp. 850-2.

Carlson, R. O., Slack, G. A., and Silverman, S. J., 1965, "Thermal Conductivity of GaAs and $GaAs_{1-x}P_x$ Laser Semiconductors," Journal of Applied Physics, Vol. 36, pp. 505-7.

Coldren, L. A., Furuya, K., and Miller, B. I., 1983, "On the Formation of Planar-Etched Facets in GaInAsP/InP Double Heterostructures," Solid-State Science and Technology, Vol. 130, pp. 1918-26.

Cur, N. and Sparrow, E. M., 1978, "Experiments on Heat Transfer and Pressure Drop for a Pair of Colinear, Interrupted Plates Aligned With the Flow," International Journal of Heat and Mass Transfer, Vol. 21, pp. 1069-80.

Curr, R. M., Sharma, D., and Tatchell, D. G., 1972, presented in Shah, R. K. and London, A. L., 1978, Laminar Flow Forced Convection in Ducts, Supplement 1 in Advances in Heat Transfer. Eds. Irvine, T. F. and Hartnett, J. P., Academic, New York.

Deissler, R. G., 1955, "Turbulent Heat Transfer and Friction in the Entrance Regions of Smooth Passages," Transactions of the ASME, Vol. 77, pp. 1221-33.

Gardner, K. A., 1945, "Efficiency of Extended Surface," Transactions of the ASME, Vol. 67, pp. 621-31.

Gereth, R., and Hubner, K., 1964, "Phonon Mean Free Path in Silicon Between 77 and 250°K," Physical Review, Vol. 134, pp. A235-40.

Gnielinski, V., 1976, "New Equations for Heat and Mass Transfer in Turbulent Pipe and Channel Flow," International Chemical Engineering, Vol. 16, pp. 359-68.

Han, J. C., Glicksman, L. R., and Rohsenow, W. M., 1978, "An Investigation of Heat Transfer and Friction for Rib-Roughened Surfaces," International Journal of Heat and Mass Transfer, Vol. 21, pp. 1143-56.

Han, L. S., 1959, "Laminar Heat Transfer In Rectangular Channels," Journal of Heat Transfer, Vol. 81, pp. 121-28.

Hanneman, R. J., 1980, "Computer Systems Of The Eighties: The Impact Of Physical Design," Advances in Computer Technology, A.S.M.E., Vol. 1, pp. 348-54.

Hartnett, J. P., 1955, "Experimental Determination of the Thermal-Entrance Length for the Flow of Water and of Oil in Circular Pipes," Transactions of the ASME, Vol. 77, pp. 1211-20.

Hartnett, J. P., Koh, J. C. Y., and McComas, S. T., 1962, "A Comparison of Predicted and Measured Friction Factors for Turbulent Flow Through Rectangular Ducts," Journal of Heat Transfer, Vol. 84, pp. 82-8.

Holman, J. P., 1976, Heat Transfer. McGraw-Hill, New York.

Howard, R. E., 1986, "Nanostructures: A New Dimension In Electronics Research," VLSI Seminar, Massachusetts Institute of Technology (speech presented on 1 April 1986).

Johnson, C. O. and Loehrke, R. I., 1984, "An Experimental Investigation of Wake Edge Tones," AIAA Journal, Vol. 22, pp. 1249-53.

Jones, Jr., O. C., 1976, "An Improvement in the Calculation of Turbulent Friction in Rectangular Ducts," Journal of Fluids Engineering, Vol. 98, pp. 173-81.

Joy, R. C. and Schlig, E. S., 1970, "Thermal Properties of Very Fast Transistors," IEEE Transactions on Electron Devices, Vol. ED-17, pp. 586-94.

Kadle, D. S. and Sparrow, E. M., 1986, "Numerical and Experimental Study of Turbulent Heat Transfer and Fluid Flow in Longitudinal Fin Arrays," Journal of Heat Transfer, Vol. 108, pp. 16-23.

Kays, W. M. and Crawford, M. E., 1980, Convective Heat and Mass Transfer. McGraw-Hill, New York.

Kays, W. M. and London, A. L., 1984, Compact Heat Exchangers. McGraw-Hill, New York.

Kern, D. Q. and Kraus, A. D., 1972, Extended Surface Heat Transfer. McGraw-Hill, New York.

Kishimoto, T. and Ohsaki, T., 1986, "VLSI Packaging Using Liquid-Cooled Channels," 36th Electronics Components Conference Proceedings, pp. 595-601.

Kraus, A. D., and Bar-Cohen, A., 1983, Thermal Analysis and Control of Electronic Equipment. McGraw-Hill, New York.

Kudman, I. and Steigmeier, E. F., 1964, "Thermal Conductivity and Seebeck Coefficient of InP," Physical Review, Vol. 133, pp. A1665-7.

Lane, J. C., 1980, presented in Zelenka, R. L. and Loehrke, R. I., 1983, "Heat Transfer From Interrupted Plates," Journal of Heat Transfer, Vol. 105, pp. 172-7.

Lane, J. C. and Loehrke, R. I., 1980, "Leading Edge Separation From a Blunt Plate at Low Reynolds Number," Journal of Fluids Engineering, Vol. 102, pp. 494-6.

Liang, C. Y., 1975, presented in Loehrke, R. I., Roadman, R. E., and Read, G. W., 1976, "Low Reynolds Number Flow in Plate Wakes," ASME Paper No. 76-WA/HT-30.

Liu, J., 1974, presented in Shah, R. K. and London, A. L., 1978, Laminar Flow Forced Convection in Ducts, Supplement 1 in Advances in Heat Transfer. Eds. Irvine, T. F. and Hartnett, J. P., Academic, New York.

Loehrke, R. I., Roadman, R. E., and Read, G. W., 1976, "Low Reynolds Number Flow in Plate Wakes," ASME Paper No. 76-WA/HT-30.

Lundberg, R. E., Reynolds, W. C., and Kays, W. M., 1963, presented in Kays, W. M. and Crawford, M. E., 1980, Convective Heat and Mass Transfer. McGraw-Hill, New York.

Malina, J. A. and Sparrow, E. M., 1964, "Variable-Property, Constant-Property, and Entrance-Region Heat Transfer Results for Turbulent Flow of Water and Oil in a Circular Tube," Chemical Engineering Science, Vol. 19, pp. 953-62.

Maycock, P. D., 1967, "Thermal Conductivity of Silicon, Germanium, III-V Compounds and III-V Alloys," Solid-State Electronics, Vol. 10, pp. 161-8.

Metais, B. and Eckert, E. R. G., 1964, presented in Rohsenow, W. M., Hartnett, J. P., and Ganic', E. N., 1985b, Handbook of Heat Transfer Fundamentals. McGraw-Hill, New York.

Military Handbook 217D, 1983, Reliability Prediction of Electronic Equipment. Rome Air Development Center, Griffiss Air Force Base, New York.

Morkoc, H. and Solomon, P. M., 1984, "The HEMT: a superfast transistor," IEEE Spectrum, Vol. 21, pp. 28-35.

Neuberger, M., 1971, Handbook of Electronic Materials. IFI/Plenum, New York.

Oktay, S., Hannemann, R., and Bar-Cohen, A., 1986, "High Heat from A Small Package," Mechanical Engineering, Vol. 108, pp. 36-42.

Patankar, S. V. and Prakash, C., 1981, "An Analysis of the Effect of Plate Thickness on Laminar Flow and Heat Transfer in Interrupted-Plate Passages," International Journal of Heat and Mass Transfer, Vol. 24, pp. 1801-10.

Product Manual, 1984, Fluorinert Electronic Liquids. 3M-Company, St. Paul, Minnesota.

Rohsenow, W. M. and Choi, H. Y., 1961, Heat, Mass, and Momentum Transfer. Prentice-Hall, Englewood Cliffs.

Rohsenow, W. M., Hartnett, J. P., and Ganic', E. N., 1985a, Handbook of Heat Transfer Applications. McGraw-Hill, New York.

Rohsenow, W. M., Hartnett, J. P., and Ganic', E. N., 1985b, Handbook of Heat Transfer Fundamentals. McGraw-Hill, New York.

Roadman, R. E. and Loehrke, R. I., 1983, "Low Reynolds Number Flow Between Interrupted Flat Plates," Journal of Heat Transfer, Vol. 105, pp. 166-71.

Sasaki, S. and Kishimoto, T., 1986, "Optimal Structure for Microgrooved Cooling Fin for High-Power LSI Devices," Electronics Letters, Vol. 22, pp. 1332-34.

Schmidt, F. W., 1971, presented in Shah, R. K. and London, A. L., 1978, Laminar Flow Forced Convection in Ducts, Supplement 1 in Advances in Heat Transfer. Eds. Irvine, T. F. and Hartnett, J. P., Academic, New York.

Shah, R. K., 1979, "Discussion," Journal of Heat Transfer, Vol. 101, pp. 188-9.

Shah, R. K. and Johnson, R. S., 1981, "Correlations For Fully Developed Flow Through Circular and Noncircular Channels," 6th National Heat and Mass Transfer Conference Proceedings, Madras, India, December 29-31, 1981, pp. D75-96.

Shah, R. K. and London, A. L., 1978, Laminar FLow Forced Convection in Ducts, Supplement 1 in Advances in Heat Transfer. Eds. Irvine, T. F. and Hartnett, J. P., Academic, New York.

Shah, R. K. and London, A. L., 1980, "Effects of Nonuniform Passages On Compact Heat Exchanger Performance," Journal of Engineering for Power, Vol. 102, pp. 653-9.

Shah, R. K. and Osborn, H. H., 1967, presented in Loehrke, R. I., Roadman, R. E., and Read, G. W., 1976, "Low Reynolds Number Flow in Plate Wakes," ASME Paper No. 76-WA/HT-30.

Sheriff, N. and Gumley, P., 1966, "Heat-Transfer and Friction Properties of Surfaces With Discrete Roughness," International Journal of Heat and Mass Transfer, Vol. 9, pp. 1297-320.

Sparrow, E. M., Baliga, B. R., and Patankar, S. V., 1977, "Heat Transfer and Fluid Flow Analysis of Interrupted-Wall Channels, With Application to Heat Exchangers," Journal of Heat Transfer, Vol. 99, pp. 4-11.

Sparrow, E. M., Baliga, B. R., and Patankar, S. V., 1978, "Forced Convection Heat Transfer from a Shrouded Fin Array With and Without Tip Clearance," Journal of Heat Transfer, Vol. 100, pp. 572-9.

Sparrow, E. M., Hallman, T. M., and Siegel, R., 1957, "Turbulent Heat Transfer in the Thermal Entrance Region of a Pipe With Uniform Heat Flux," Applied Science Research, Vol. 7, pp. 37-52.

Sparrow, E. M. and Liu, C. H., 1979, "Heat-Transfer, Pressure-Drop and Performance Relationships for In-Line, Staggered, and Continuous Plate Heat Exchangers," International Journal of Heat and Mass Transfer, Vol. 22, pp. 1613-25.

Touloukian, Y. S., 1970, Thermophysical Properties of Matter. IFI/Plenum, New York.

Trimberger, S., 1983, "Reaching for the Million-Transistor Chip," IEEE Spectrum, Vol. 20, pp. 100-5.

Tuckerman, D. B., 1984, "Heat-Transfer Microstructures for Integrated Circuits," Ph.D. Thesis, Stanford University, Stanford, CA.

Tuckerman, D. B., 1986, private communication, Cambridge, Massachusetts.

Tuckerman, D. B. and Pease, R. F. W., 1981a, "High-Performance Heat Sinking for VLSI," IEEE Electron Device Letters, Vol. EDL-2, pp. 126-9.

Tuckerman, D. B. and Pease, R. F. W., 1981b, "Ultrahigh Thermal Conductance Microstructures for Cooling Integrated Circuits," 32nd Electronics Components Conference Proceedings, pp. 145-9.

Tuckerman, D. B. and Pease, R. F. W., 1982, "Optimized Convective Cooling Using Micromachined Structures," Electrochemical Society Extended Abstract #125, Vol. 82, pp. 197-8.

Tuckerman, D. B. and Pease, R. F. W., 1983, "Microcapillary Thermal Interface Technology for VLSI Packaging," Symposium on VLSI Technology, Digest of Technical Papers, pp. 60-1.

Tye, R. P., 1969, Thermal Conductivity. Academic Press, New York.

Walpole, J. N., 1986, private communication, Lexington, Massachusetts.

Webb, R. L., Eckert, E. R. G., and Goldstein, R. J., 1971, "Heat Transfer and Friction in Tubes With Repeated-Rib Roughness," International Journal of Heat and Mass Transfer, Vol. 14, pp. 601-17.

White, F. M., 1984, Heat Transfer. Addison-Wesley, Reading, MA.

Wibulswas, P., 1966, presented in Shah, R. K. and London, A. L., 1978, Laminar Flow Forced Convection in Ducts, Supplement 1 in Advances in Heat Transfer. Eds. Irvine, T. F. and Hartnett, J. P., Academic, New York.

Wieting, A. R., 1975, "Empirical Correlations for Heat Transfer and Flow Friction Characteristics of Rectangular Offset-Fin, Plate-Fin Heat Exchangers," Journal of Heat Transfer, Vol. 97, pp. 488-90.

Zelenka, R. L. and Loehrke, R. I., 1983, "Heat Transfer from Interrupted Plates," Journal of Heat Transfer, Vol. 105, pp. 172-7.

APPENDIX A: Fins With Non-Uniform Thermal Conductivity, Heat Transfer Coefficient, and Coolant Temperature

The analysis presented here is based on the thirteen assumptions listed in Section 3.3. They are assumed to be "locally" valid in that the thermal conductivity and/or the heat transfer coefficient and/or the coolant temperature are not uniform over the entire fin height. Instead they are considered constant over smaller sections of the fin height. The original fin is therefore made up of several smaller fins connected in series as shown in Figure A.1.

The differential equation modeling each fin section is

$$\frac{d^2\theta_j}{dz_j^2} - m_j^2\theta_j = 0 \tag{A.1}$$

and $\theta_j = T_{wj}(z) - T_{bj}$, $m_j^2 = 2h_j/k_{wj}w_w$, where T_{bj} is the bulk coolant temperature of the jth fin, $T_{wj}(z)$ is the temperature profile of the jth fin, h_j is the heat transfer coefficient of the jth fin, k_{wj} is the thermal conductivity of the jth fin, and w_w is the fin width. The boundary conditions are: $\theta_j = \theta_{base,j}$ at $z_j = 0$, and $-k_{wj}Ad\theta_j/dz_j = Q_j = q''_jA$ at $z_j = 0$ where A is the fin base area, q''_j is the heat flux at the fin base, and Q_j is the heating rate at the fin base. The solution of Equation A.1 is readily obtained as

$$\theta_j = \theta_{base,j}\cosh(m_jz_j) - \frac{Q_j}{Ak_{wj}m_j}\sinh(m_jz_j) \quad . \tag{A.2}$$

The heating rate from the fin tip is evaluated using Equation A.2 and the boundary condition $Q_{j+1} = -k_{wj} A d\theta_j/dz_j$ at $z_j = b_j$. The result is

$$Q_{j+1} = Q_j \cos(m_j b_j) - k_{wj} A m_j \theta_{base,j} \sinh(m_j b_j) \qquad (A.3)$$

where Q_{j+1} is the positive heat loss from the tip of fin j to the base of fin j+1. The heat transferred to the coolant is $Q_{fj} = Q_j - Q_{j+1}$.

The solution of Equations A.2 and A.3 for j = 1, 2, 3,..., n is very tedious. In general, the solution is easiest if all T_{bj} and h_j are known in advance, and if each k_{wj} is assumed constant over the length b_j and and evaluated at $\theta_{base,j}$. The solution is readily obtained by trial and error guessing of $\theta_{base,1}$ such that $Q_{n+1} = 0$.

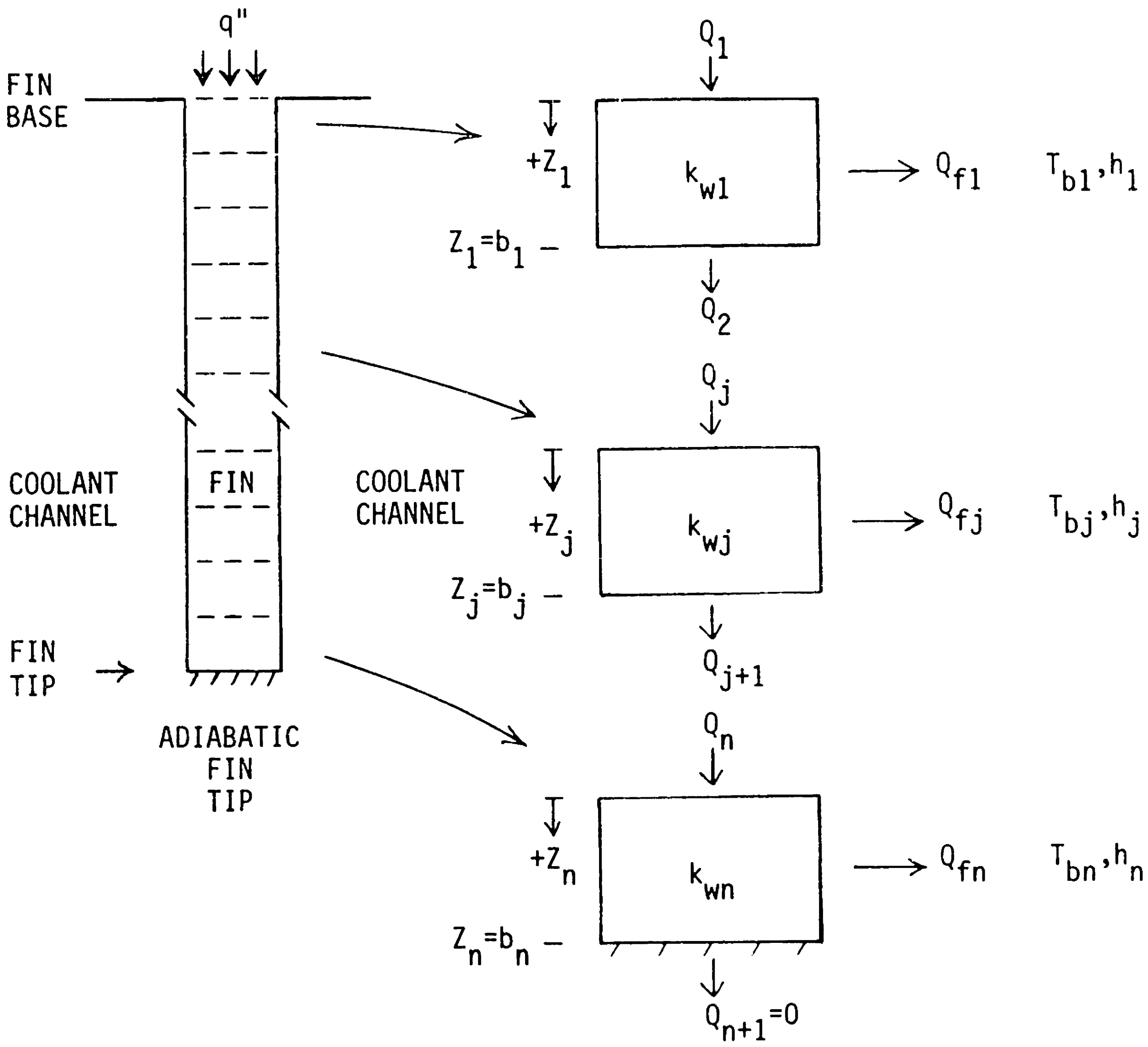

Figure A.1. Sub-divided fin model.

APPENDIX B: Fin With Internal Heat Generation

A fin with resistive heating is shown in Figure B.1. The electric current flows between the fin base and the fin tip, and it is assumed that no current "leaks" into the liquid coolant. It is assumed that the assumptions listed in Section 3.3 apply here also (except of course assumption 6).

The governing differential equation is

$$\frac{d^2\theta}{dz^2} - m^2\theta + \frac{w_j}{k_w} = 0 \qquad \text{(B.1)}$$

where $\theta = T_w(z) - T_b$, $m^2 = 2h/k_w w_w$, T_b is the coolant bulk temperature, h is the heat transfer coefficient, k_w is the fin thermal conductivity, w_w is the fin thickness, and w_j is the internal heat generation per unit volume. The boundary conditions are: $d\theta/dz = 0$ at $z = 0$, and $\theta = \theta_{base}$ at $z = b$. The solution of Equation B.1 is readily obtained as

$$\theta = \theta_{base}\frac{\cosh(mz)}{\cosh(mb)} + \frac{w_j w_w}{2h}\left[1 - \frac{\cosh(mz)}{\cosh(mb)}\right] . \qquad \text{(B.2)}$$

The heat flow rate through the fin base is found using $q'' = k_w d\theta/dz$, which is evaluated at $z = b$ to give

$$q'' = k_w m\theta_{base}\tanh(mb) - \frac{w_j w_w k_w m}{2h}\tanh(mb) . \qquad \text{(B.3)}$$

The definition of a fin efficiency is not appropriate here.

To determine the rate of internal heat generation per unit volume, it is necessary to know the electrical resistivity ρ and the electrical

current distribution. If it is assumed that the resistivity is independent of temperature, and that the current flow is uniform, it is easy to show that the internal heat generation per unit volume is given by

$$w_j = \frac{I^2 R}{V} = \frac{I^2 (\rho \frac{z}{w_w x})}{w_w z x} = \frac{I^2 \rho}{w_w^2 x^2} \qquad \text{(B.4)}$$

where I is the current flowing through the fin base length x, and ρ is the electrical resistivity (Ω - m).

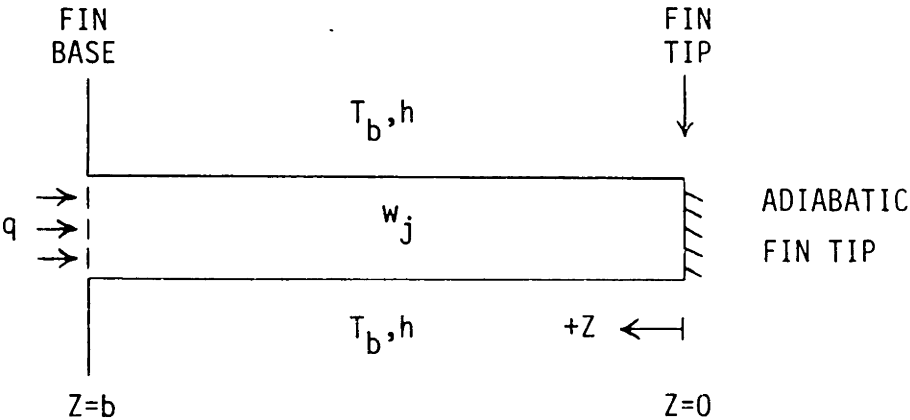

Figure B.1. Fin with internal heat generation.

APPENDIX C: Optimum Fin Aspect Ratio

The analysis presented here is based on the thirteen assumptions listed in Section 3.3. In that section, the heat flow per unit fin base area was obtained (Equation 3.13), which leads to the heat flow rate per unit fin length given by

$$q' = q'' w_w = k_w w_w m \theta_{base} \tanh(\beta) \qquad \text{(C.1)}$$

where $m = (2h/k_\omega w_w)^{0.5}$, q' is the heating rate at the fin base per unit fin base length, q'' is the fin base heating rate per unit fin base area, w_w is the fin thickness, k_w is the fin thermal conductivity, θ_{base} is the fin-base-to-liquid-coolant temperature excess, h is the heat transfer coefficient, and β is the optimizing parameter given by

$$\beta = mb = b\left(\frac{2h}{k_w w_w}\right)^{0.5} = A_p\left(\frac{2h}{k_w}\right)^{0.5} w_w^{-1.5} \qquad \text{(C.2)}$$

where b is the fin length, and A_p is the fin profile area (bw_w). Substituting Equation C.2 into Equation C.1 and re-grouping terms gives

$$q' = k_w \theta_{base}\left(\frac{2h}{k_w}\right)^{0.5} w_w^{0.5} \tanh\left[A_p\left(\frac{2h}{k_w}\right)^{0.5} w_w^{-1.5} \right] . \qquad \text{(C.3)}$$

Taking the derivative of Equation C.3 with respect to w_w and evaluating where the derivative vanishes gives $\beta \approx 1.4192$. Substituting this value into Equation C.2 gives the "optimum" fin thickness as

$$w_w \approx 0.791 \left(\frac{2hA_p^2}{k_w}\right)^{0.33} \qquad \text{(C.4)}$$

and using $b = A_p/w_w$ gives the "optimum" fin length as

$$b \approx 1.262 \left(\frac{k_w A_p}{2h}\right)^{0.33} . \tag{C.5}$$

Equations C.4 and C.5 apply for fins with a fixed profile area. No sensible optimum was found for b and w_w when the derivatives with respect to b and w_w were taken after $A_p = bw_w$ was substituted into Equation C.3.

The optimum fin aspect ratio is obtained by dividing Equation C.5 by Equation C.4 which gives

$$\delta = (b/w_w) \approx 1.595 \left(\frac{k_w^2}{4h^2 A_p}\right)^{0.33} . \tag{C.6}$$

The profile area may be written as

$$A_p = bw_w = (b/w_w)w_w^2 = \delta\, w_w^2 \tag{C.7}$$

and the heat transfer coefficient can be obtained from the Nusselt number by

$$h = \frac{Nuk_f}{D_e} \tag{C.8}$$

where Nu is the Nusselt number, k_f is the fluid thermal conductivity, D_e is the equivalent diameter given by

$$D_e = \frac{4A}{p} = \frac{4bw_c}{2b + 2w_c} \tag{C.9}$$

where w_c is the channel width, and the heating from the bottom of the channel has been ignored. Substituting Equations C.7, C.8, and C.9 into Equation C.6 gives

$$\delta \approx 1.419 \left[\frac{k_w}{k_f} \frac{1}{N_u} \frac{(w_c/w_w)\delta}{(\delta + (w_c/w_w))} \right]^{0.5} . \qquad (C.10)$$

Equation C.10 can be put into quadratic form of which the quadratic expansion solution is

$$\delta \approx -0.5 \frac{w_c}{w_w} \mp 0.5 \left[\left(\frac{w_c}{w_w}\right)^2 + 8.056 \frac{k_w}{k_f} \frac{1}{N_u} \frac{w_c}{w_w} \right]^{0.5} . \qquad (C.11)$$

Clearly the "+" solution is the only one that makes sense.

To get an idea of the typical "optimum" α, consider the case when water ($k_f \approx 0.6$ W/m°C) is used to cool a indium phosphide ($k_w \approx 70$ W/m°C) heat sink when $w_w/w_c \approx 1.0$ and Nu $\approx$ 8.0. Equation C.11 indicates that $\delta \approx 4.9$ will give the most heat transfer from the fin for a given profile area. Note that the analysis does <u>not</u> consider heat transfer from the base of the channel.

APPENDIX D: Microcapillary Thermal Interface

This appendix provides a brief discussion of a relatively new type of thermal interface that can be used in conjunction with microchannel heat sinks. The information presented here on the so-called "microcapillary thermal interface" has been abstracted from Tuckerman and Pease (1983), and Tuckerman (1984). It has been included in this thesis in an attempt to provide the reader with a more complete understanding of how microchannel heat sinks could be manufactured separately from the device they are intended to cool and then joined via a low-thermal-resistance interface.

The fabrication and use of microchannel heat sinks raises a number of questions about the manufacturing yield and the device reliability. For example, the integrated circuit might be damaged during heat sink fabrication. There may also be problems associated with the diffusion of contaminates from the liquid coolant into the integrated circuit chip. There may also be a systems design problem of delivering coolant to each chip in a multichip array.

To avoid these problems, the chip and the heat sink could be manufactured separately and then packaged together with an interface between them. For microelectronics, it would be preferable to have the heat sink manufactured directly within the printed circuit board.

Several methods can be used to provide a low-thermal-resistance interface. Various types of bonding (epoxy, solder, etc.) can be used to provide a "solid" interface, but such interfaces have problems with

mechanical stress limitations, high thermal resistance (due to gas voids), and are generally non-reusable (meaning a chip can't be easily removed and reused). Gas layer interfaces (eg. helium) can be used, but they have problems since they require very small separations between the two surfaces, the surfaces should be optically flat (and dust free), and a hermetic seal is required for the package. Liquid layer interfaces (e.g., thermal grease) often require that the two surfaces be held under large compressive loads to keep the surface separation small.

An alternative liquid interface, called a microcapillary thermal interface, has been recently developed by the Stanford researchers. Shown in Figure D.1, this interface has re-entrant cavities which use the liquid's surface tension to create a very strong attractive (suction) force between the two surfaces. This attractive force guarantees a small interfacial gap that has a very small thermal resistance. The re-entrant cavities are long channels that act as partially filled reservoirs and allow trapped air to escape (virtually eliminates gas voids in the interface). Transverse "tunnels" are provided between the re-entrant-cavity channels that allow the interfacial liquid to equilibriate between the channels. In order to guarantee a void-free interface, the width of the re-entrant cavity channels (at the nominal meniscus level) is selected such that it is slightly larger than the maximum gap between the surfaces (at the relevant contact pressure).

The re-entrant cavity channels used by the Stanford researchers were manufactured in basically a two-step process. First, channels were etched into the top surface of a silicon wafer containing a microchannel

heat sink. The channels were typically 5 μm wide, 30 μm deep, and on 10 μm centers. The channels were then electrolessly plated with nickel to form the re-entrant shape where the gap width at the channel top was typically 1 μm. Nickel was chosen because its thickness (typically less than 2 μm) provided a semi-ductile stress-absorbing interface that was resistant to peeling. Dow Corning 704 silicone oil was used as an interfacial liquid. It was applied to the smooth integrated-circuit surface, and spun-down to a thickness of typically 3 μm. Due to the inherent attractive (suction) force developed by the interface, the interfacial gap was typically less than 0.7 μm. Such small gaps were obtained even when the integrated circuit chips were intentionally prepared with concave bows of 15 μm between the edge and the center of chip!

The thermal performance of the microcapillary thermal interface was truly amazing. Typically, $R''_{int} < 0.1°C/(W/cm^2)$, and values as low as $R''_{int} \approx 0.02°C/(W/cm^2)$ have been obtained. This interface is reusable in the sense that the integrated circuit chip can be detached from the heat sink and reattached without damage and has about the same thermal resistance. It was also found that R''_{int} decreases with large amounts of thermal cycling. This is probably due to the smoothing of the interface surfaces caused by sliding owing to thermal expansion and contraction.

Clearly the interface thermal resistance is pretty low, and therefore won't significantly degrade the overall thermal performance. In fact, using such an interface could improve the thermal performance when the heat source substrate has a low thermal conductivity. In this case,

the microcapillary thermal interface could be used which would allow the microchannel heat sink to be made separately in a high thermal conductivity material. The resulting total thermal resistance could therefore be much lower.

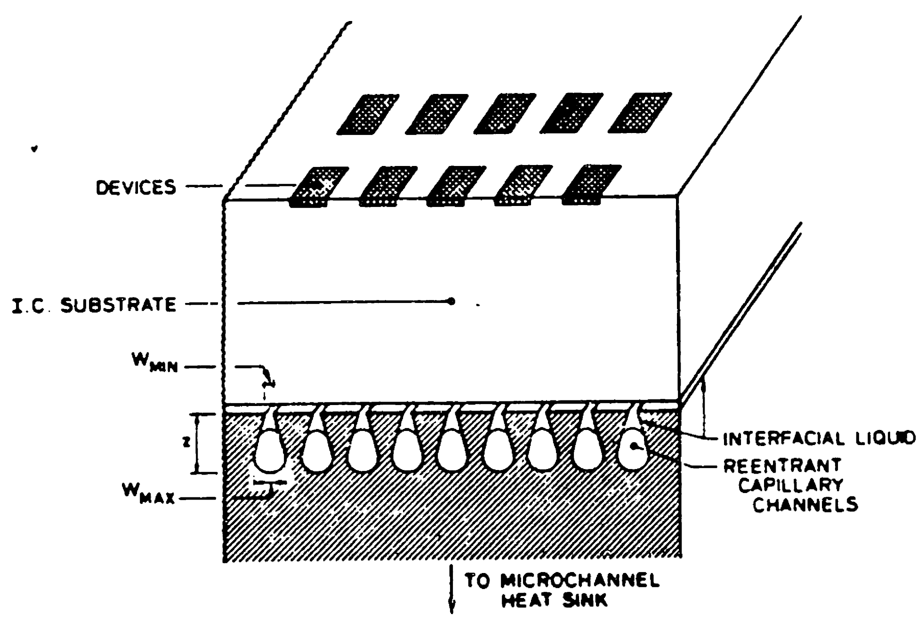

Figure D.1. Microcapillary thermal interface concept. [Taken from Tuckerman (1984).]

APPENDIX E: MICROHEX Computer Program Listing

This appendix contains the entire listing of the computer program used to compute the thermal and fluid performance of forced-convection, liquid-cooled, microchannel heat sinks. The computer program is written in FORTRAN IV, and has been successfully run on an IBM 3081, a Microvax II, and an IBM PC/XT.

The computer code listed herein is the version that was used on an IBM 3081. The MICROHEX EXEC file is needed only for the IBM 3081 to setup the output files. Output file setup for the Microvax II and the IBM PC/XT is accomplished by un-commenting the appropriate lines in the MICROHEX FORTRAN program as indicated.

Plotting of the thermal and fluid performance results is done using the DISSPLA<R> graphics package. Other plotting packages can of course be used provided that subroutines PINPUT and PPLOTT are revised as required.

Program MICROHEX computes the thermal and fluid performance for up to five heat sink designs, which have been initialized with the data statements in the MICROHEX FORTRAN program. A description of the heat sink design parameters that must be initialized is provided in the comment header block of the MICROHEX FORTRAN program, and in Section 4.5.1 as well.

When MICROHEX is run, the user will be prompted for a plotting output device name. This is the only "interactive" response that is required.

The author has very carefully checked the accuracy of the numerical computations. All of the computations are done using "single precision." Numerical roundoff errors do on occasion occur such that incorrect performance is predicted. Erroneous results are readily noticeable (usually) when looking at the plot of the thermal and fluid performance. These errors can usually be eliminated by selecting different values for WCSTAR and WCINCR. Ultimately, the best solution would be to convert the entire program to at least "double precision," but that conversion has not been done to date.

The author is not aware of any programming errors. The author also will admit that some programming changes could result in a reduction in the CPU time required to do the numerical computations. The author would be very grateful if the reader would bring to his attention any potential programming errors and/or computational enhancements.

```
      . REAL DUMMY,COMMAND,LINE
C-----------------------------------------------------------------------
C NOTES TO THE USER FROM THE AUTHOR OF THIS PROGRAM......
C
C THIS COMPUTER PROGRAM HAS BEEN DOCUMENTED BY DEFINING THE ANALYSIS
C VARIABLES IN THE TOP OF EACH SUBROUTINE, AND BY DEFINING THE PRIMARY
C ANALYSIS EQUATIONS THAT ARE BEING USED.  MOST OF THE DOCUMENTATION
C HERE WAS DONE BY THE AUTHOR IN ORDER TO AVOID HIS OWN CONFUSION WHILE
C WRITING AND DEBUGGING THE CODE.  HOPEFULLY YOU WILL FIND IT RELATIVELY
C EASY TO UNDERSTAND THE CODE, BUT BEFORE YOU DO SO, IT PROBABLY WOULD
C BE BEST IF YOU READ THE THESIS TEXT FIRST.  THE AUTHOR IS NOT AWARE OF
C ANY BUGS IN THIS PROGRAM AT THE TIME OF PUBLICATION.  THERE ARE SOME
C TIMES WHEN NUMERICAL ROUNDOFF ERRORS DO SHOW UP, BUT THESE USUALLY
C DISAPPEAR WHEN THE INPUT PARAMETER 'WCSTAR' IS ADJUSTED (USE OF
C INCREMENTS OF TEN APPEAR TC BE MOST ACCURATE (10,20,30,...)).  THE
C AUTHOR WOULD APPRECIATE IT IF ANY COMPUTATIONAL ENHANCEMENTS OR BUGS
C ARE BROUGHT TO HIS ATTENTION, SO THAT OTHER INTERESTED PARTIES MAY BE
C INFORMED.  GOOD LUCK, AND HAPPY PROGRAMMING!
C                                                  SINCERELY,
C                                                  RICHARD J. PHILLIPS
C                                                  16 JAN 87
C
C-----------------------------------------------------------------------
C MICROHEX:  WRITTEN BY RICHARD J. PHILLIPS.  MICROHEX CONTAINS THE
C            INPUT DATA ARRAYS THAT ARE USED TO COMPUTE THE THERMAL-
C            HYDRAULIC PERFORMANCE OF MICROCHANNEL HEAT SINKS.
C-----------------------------------------------------------------------
C DISCRIPTION OF INPUT VARIABLES
C
C NUMBER OF CURVES AND TYPE OF OUTPUT
C
C             NCURVE : NUMBER OF GENERIC DESIGNS TO BE ANALYZED
C             IX     : CONTROL FOR IF CHANNEL WIDTH OR AXIAL POSITION
C                      IS TO BE VARIED.  NOTE THAT THE CALCULATIONS MUST
C                      BE DONE FOR WC=WCSTAR=WCEND.
C                      1 - WC VARIED, OR 2 - X VARIED
C
C HEAT SINK MATERIAL
C                                             TEMP. RANGE OF DATA
C             NSINK  : 1 = GALLIUM ARSENIDE  20. K - 470. K
C                      2 = GERMANIUM         10. K - 500. K
C                      3 = INDIUM PHOSPHIDE  20. K - 500. K
C                      4 = SILICON           10. K - 500. K
C                      5 = ALUMINUM          10. K - 500. K
C                      6 = COPPER            10. K - 500. K
C                      7 = SILVER            10. K - 500. K
C
C TYPE OF LIQUID COOLANT AND INLET TEMPERATURE
C                                             TEMP. RANGE OF DATA
C             NFLUID : 1 = FC-77            273. K - 353. K
C                      2 = FREON            223. K - 323. K
C                      3 = WATER            273. K - 377. K
C             TFLUIN : INLET COOLANT TEMP.  (DEG KELVIN)
C
C HEATING RATE
C
C             Q      : SURFACE HEATING RATE (W/CM**2)
C
C ANALYSIS METHOD
C
```

```
C              ICASE  : 1 = FULLY DEVELOPED LAMINAR FLOW IN SMOOTH
C                           CHANNELS
C                       2 = FULLY DEVELOPED/DEVELOPING LAMINAR AND
C                           TURBULENT FLOW IN SMOOTH CHANNELS
C                       3 = FULLY DEVELOPED TURBULENT FLOW IN REPEATED-
C                           RIB ROUGHENED CHANNELS
C
C GEOMETRICAL PARAMETERS
C
C              WCSTAR : INITIAL CHANNEL WIDTH (MICRONS)
C              WCEND  : FINAL CHANNEL WIDTH (MICRONS)
C              WCINCR : INCREMENT IN CHANNEL WIDTH (MICRONS)
C              WWBYWC : RATIO OF FIN THICKNESS TO CHANNEL WIDTH (-)
C              IZ     : CONTROL FOR WHICH CRITERION USED FOR FIN LENGTH
C                       1 - B, OR 2 - ASPEC
C              B      : FIN HEIGHT (MICRONS)
C              ASPECT : CHANNEL ASPECT RATIO (-)
C              L      : CHANNEL LENGTH (M)
C              T      : SUBSTRATE HEIGHT (MICRONS)
C
C COOLANT VELOCITY CONSTRAINTS
C
C              IKLOSS : CONTROL FOR INCLUDING K90, KC, AND KE
C                       0 - NO  1 - YES
C              ICONS  : CONTROL FOR WHICH FLOW CONSTRAINT SHOULD BE USED
C                       1 - DELP, 2 - VOLUME, OR 3 - POWER
C              DELP   : CONSTANT PRESSURE DROP CONSTRAINT (PSI)
C              VOLUME : CONSTANT VOLUMETRIC FLOW CONSTRAINT((CC/S)/CM*2)
C              POWER  : CONSTANT PUMPING POWER CONSTAINT (W/CM**2)
C
C ROUGHNESS PARAMETERS
C
C              EBYDE  : RATIO OF REPEATED RIB HEIGHT TO CHANNEL
C                       HYDRAULIC DIAMETER (-)
C              PBYE   : RATIO OF RIB SEPARATION TO RIB HEIGHT (-)
C              PHI    : FLOW ATTACK ANGLE (DEGREES)
C              ZI     : RIB SHAPE ANGLE (DEGREES)
C-----------------------------------------------------------------------
C INITIALIZE ARRAYS
      REAL L
      INTEGER WCSTAR,WCEND,WCINCR
      DIMENSION NSINK(5),NFLUID(5),TFLUIN(5),Q(5),ICASE(5),IZ(5),
     &          WCSTAR(5),WCEND(5),WCINCR(5),WWBYWC(5),B(5),ASPECT(5),
     &          L(5),T(5),IKLOSS(5),DELP(5),VOLUME(5),POWER(5),
     &          ICONS(5),EBYDE(5),PBYE(5),PHI(5),ZI(5),
     &          X1(5,2,100),Y1A(5,2,100),Y2(5,2,100),Y3(5,2,100),
     &          IINUM(5,2),Y1B(5,2,100),Y1C(5,2,100),
     &          XX(5,2,100),XSTARX(5,2,100)
C ************ INPUT DATA FOR UP TO FIVE CURVES ************
      DATA NCURVE/1/
      DATA IX    /1/
      DATA ICASE /      2,      0,      0,      0,      0/
      DATA NSINK /      4,      0,      0,      0,      0/
      DATA NFLUID/      3,      0,      0,      0,      0/
      DATA TFLUIN/  300.0,     0.,     0.,     0.,     0./
      DATA Q     /     0.,     0.,     0.,     0.,     0./
      DATA WCSTAR/      5,      0,      0,      0,      0/
      DATA WCEND /    500,      0,      0,      0,      0/
      DATA WCINCR/      5,      0,      0,      0,      0/
      DATA WWBYWC/    1.0,     0.,     0.,     0.,     0./
```

```
      DATA IZ     /       2,       0,       0,       0,       0/
      DATA B      /  0.E-6,  0.E-6,  0.E-6,  0.E-6,  0.E-6/
      DATA ASPECT/      4.,      0.,      0.,      0.,      0./
      DATA L      / .01000,      0.,      0.,      0.,      0./
      DATA T      /100.E-6,  0.E-6,  0.E-6,  0.E-6,  0.E-6/
      DATA IKLOSS/       0,       0,       0,       0,       0/
      DATA ICONS /       1,       0,       0,       0,       0/
      DATA DELP  /    10.0,      0.,      0.,      0.,      0./
      DATA VOLUME/      0.,      0.,      0.,      0.,      0./
      DATA POWER /      0.,      0.,      0.,      0.,      0./
      DATA EBYDE /      0.,      0.,      0.,      0.,      0./
      DATA PBYE  /      0.,      0.,      0.,      0.,      0./
      DATA PHI   /      0.,      0.,      0.,      0.,      0./
      DATA ZI    /      0.,      0.,      0.,      0.,      0./
C INITIALIZE OUTPUT DATA FILES FOR MICROVAX
      OPEN (UNIT=11, FILE='MICROHEX.OUTPUT1',
     &       ORGANIZATION='SEQUENTIAL', STATUS='NEW')
      OPEN (UNIT=13, FILE='MICROHEX.OUTPUT2',
     &       ORGANIZATION='SEQUENTIAL', STATUS='NEW')
      OPEN (UNIT=15, FILE='MICRCHEX.OUTPUT3',
     &       ORGANIZATION='SEQUENTIAL', STATUS='NEW')
      OPEN (UNIT=17, FILE='MICROHEX.OUTPUT4',
     &       ORGANIZATION='SEQUENTIAL', STATUS='NEW')
C DETERMINE EXECUTION TIME (HUMAN CLOCK) FOR MICROVAX
      T1=SECNDS(0.0)
CC PROMPT FOR PLOT OUTPUT DEVICE
C      WRITE(6,10)
C10    FORMAT(
C     &' +-----------------------------------+',/,
C     &' + SEND PLOT OUTPUT TO ......        +',/,
C     &' +     0 = DO NOT PLOT RESULTS       +',/,
C     &' +     1 = COMPRS                    +',/,
C     &' +     2 = TEKTRONIX 4015            +',/,
C     &' +     3 = TEKTRONIX 4114            +',/,
C     &' +     4 = BENSON                    +',/,
C     &' +     5 = COMP80                    +',/,
C     &' + MAKE NEGATIVE FOR NO DATA ECHO    +',/,
C     &' + ENTER SELECTION NUMBER AND <CR>   +',/,
C     &' +-----------------------------------+')
C      IECHO=1
C      READ(6,*)IPLOT
C      IF(IPLOT.LT.0)IECHO=0
C      IF(IPLOT.LT.0)IPLOT=-1*IPLOT
C      IF(IPLOT.EQ.1)CALL COMPRS
C      IF(IPLOT.EQ.2)CALL TEKALL(4015,480,0,1,0)
C      IF(IPLOT.EQ.3)CALL TEKALL(4114,480,0,1,0)
C      IF(IPLOT.EQ.4)CALL BENSN2(0)
C      IF(IPLOT.EQ.5)CALL COMP80(69,16,0,0,1)
C      IF((IPLOT.NE.0).AND.(IECHO.NE.0))
C     &CALL PINPUT(NCURVE,ICASE,NSINK,NFLUID,TFLUIN,Q,WCSTAR,WCEND,
C     &              WCINCR,WWBYWC,IZ,IX,B,ASPECT,L,T,IKLOSS,
C     &              ICONS,DELP,VOLUME,POWER,EBYDE,PBYE,PHI,ZI)
C LOOP FOR UP TO FIVE CURVES
      DO 100 I=1,NCURVE,1
C        CONVERT W/CM*2 TO W/M*2
         Q(I)=Q(I)*(1.E+4)
C        CONVERT (CC/S)/CM**2 TO (M**3/S)/CM**2
         VOLUME(I)=VOLUME(I)*(1.E-6)
C        CONVERT PSI TO PA
         DELP(I)=DELP(I)*6894.8
```

```
         CALL RTOTAL(
     1         I,NSINK(I),NFLUID(I),TFLUIN(I),Q(I),ICASE(I),
     1         WCSTAR(I),WCEND(I),WCINCR(I),WWBYWC(I),B(I),IZ(I),IX,
     1         ASPECT(I),L(I),T(I),IKLOSS(I),ICONS(I),DELP(I),VOLUME(I),
     1         POWER(I),EBYDE(I),PBYE(I),PHI(I),ZI(I),X1,Y1A,Y1B,Y1C,Y2,
     1         Y3,IINUM,XX,XSTARX)
100   CONTINUE
C PLOT OUT RESULTS
C       IF(IPLOT.NE.0)
C      1CALL PPLOTT(X1,Y1A,Y1B,Y1C,Y2,Y3,IINUM,NCURVE,ICASE,IX,XX,XSTARX)
C PRINT OUT EXECUTION TIME (HUMAN TIME) FOR MICROVAX
      DELTA=SECNDS(T1)
      WRITE(5,1000)DELTA
1000  FORMAT(/,' ELAPSED TIME = ',F8.2,' SECONDS',/)
      STOP
      END
C END OF FILE FOR PROGRAM MICROHEX
C-----------------------------------------------------------------------
C ABRUPT:  WRITTEN BY RICHARD J. PHILLIPS.  ABRUPT
C          COMPUTES THE ENTRANCE AND EXIT PRESSURE LOSS COEFFICIENTS.
C          THE POLYNOMIAL EQUATIONS FOR KC AND KE WERE OBTAINED FROM
C          FIGURES 2.10 AND 2.11 USING HP-41C PROGRAMS (SUM)POLYC
C          AND (SUM)LIN.  THE CIRCULAR-TUBE, TURBULENT FLOW EQUATIONS
C          WERE OBTAINED FOR RE=5000, AND THE PARALLEL-PLATE, TURBULENT
C          -FLOW EQUATIONS WERE OBTAINED FOR RE=10000.  NOTE THAT THE
C          POLYNOMIAL EQUATIONS ARE FOR LPLUS=X/DE*RE BECAUSE THE FACTOR
C          OF FOUR HAS BEEN USED TO OBTAIN THE LPLUS = .05, .025, AND
C          .0125 VALUES.
C-----------------------------------------------------------------------
C ANALYSIS VARIABLES
C A,AA,AAA . DUMMY CALCULATION VARIABLES                        (-)
C ACBYAP ... RATIO OF FREE-FLOW TO FRONTAL CROSS-SECTIONAL
C              AREAS                                            (-)
C ASPECT ... CHANNEL ASPECT RATIO                               (-)
C IFLOW  ... FLOW REGIME INDICATOR                              (-)
C IKLOSS ... CONTROL FOR INCLUDING K90, KC, AND KE              (-)
C KC     ... ENTRANCE PRESSURE LOSS COEFFICIENT                 (-)
C KCXXX  ... ENTRANCE PRESSURE LOSS COEFFICIENT AT
C              LPLUS=.XXX                                       (-)
C KE     ... EXIT PRESSURE LOSS COEFFICIENT                     (-)
C KEXXX  ... EXIT PRESSURE LOSS COEFFICIENT AT LPLUS=.XXX       (-)
C K90    ... NINETY DEGREE BEND PRESSURE LOSS COEFFICIENT       (-)
C LPLUS  ... HYDRODYNAMIC ENTRY LENGTH                          (-)
C-----------------------------------------------------------------------
      SUBROUTINE ABRUPT(ACBYAP,ASPECT,IFLOW,IKLOSS,KC,KE,K90,LPLUS)
      REAL KC,KC05,KC025,KC0125,KE,KE05,KE025,KE0125,K90,LPLUS
C CHECK IF K90, KC, AND KE ARE TO BE ZERO
      IF(IKLOSS.NE.0)GO TO 10
         K90=0.
         KC=0.
         KE=0.
         RETURN
10    CONTINUE
C LOSS COEFFICIENTS ARE TO BE COMPUTED
      K90=1.2
      A=ACBYAP
      AA=A*ACBYAP
      AAA=AA*ACBYAP
C DETERMINE IF CIRCULAR TUBE OR PARALLEL PLATE COEFFICIENTS ARE USED
      IF((ASPECT.LE.0.1).OR.(ASPECT.GE.10.))GO TO 1000
```

```
C
C****************
C CIRCULAR TUBES
C****************
C  DETERMINE FLOW REGIME
      IF(IFLOW.EQ.2)GO TO 500
C  LAMINAR FLOW
      IF((LPLUS.LT.0.05).AND.(LPLUS.GE.0.025))GO TO 100
      IF((LPLUS.LT.0.025).AND.(LPLUS.GE.0.0125))GO TO 200
      IF(LPLUS.LT.0.0125)GO TO 300
C  LPLUS>=0.05
      KC=1.0600-0.4000*A
      KE=0.9998-2.6248*A+0.8958*AA+0.0694*AAA
      RETURN
100   CONTINUE
C  0.05<LPLUS>=0.025
      KC05=1.0600-0.4000*A
      KC025=1.0000-0.4000*A
      KE05=0.9998-2.6248*A+0.8958*AA+0.0694*AAA
      KE025=0.9973-2.6089*A+1.0903*AA-0.0810*AAA
      FACTOR=(0.05-LPLUS)/0.025
      KC=(KC025-KC05)*FACTOR+KC05
      KE=(KE025-KE05)*FACTOR+KE05
      RETURN
200   CONTINUE
C  0.025<LPLUS>=0.0125
      KC025=1.0000-0.4000*A
      KC0125=0.8800-0.4000*A
      KE025=0.9973-2.6089*A+1.0903*AA-0.0810*AAA
      KE0125=1.0006-2.4414*A+0.8790*AA+0.0926*AAA
      FACTOR=(0.025-LPLUS)/0.0125
      KC=(KC0125-KC025)*FACTOR+KC025
      KE=(KE0125-KE025)*FACTOR+KE025
      RETURN
300   CONTINUE
C  LPLUS<0.0125
      KC=0.8800-0.4000*A
      KE=1.0006-2.4414*A+0.8790*AA+0.0926*AAA
      RETURN
500   CONTINUE
C  TURBULENT FLOW
      KC=0.5200-0.4000*A
      KE=1.0000-2.1000*A+1.0000*AA+0.0000*AAA
      K90=(1.70-KC-KE)/(2.*ACBYAP*ACBYAP)
      RETURN
C
1000  CONTINUE
C****************
C INFINITE PARALLEL PLATES
C****************
C  DETERMINE FLOW REGIME
      IF(IFLOW.EQ.2)GO TO 1500
C  LAMINAR FLOW
      KC=0.7990+0.0392*A-0.4439*AA+0.0058*AAA
      KE=1.0009-2.4356*A+1.1171*AA-0.0810*AAA
      RETURN
1500  CONTINUE
C  TURBULENT FLOW
      KC=0.4604+0.0362*A-0.4841*AA+0.0579*AAA
      KE=0.9993-2.0226*A+0.9152*AA+0.0521*AAA
```

```
      RETURN
      END
C END OF FILE FOR SUBROUTINE ABRUPT
C-------------------------------------------------------------------
C SFFD:    WRITTEN BY RICHARD J. PHILLIPS.  SFFD COMPUTES THE SMOOTH-
C          CHANNEL COOLANT VELOCITY AND OTHER ANALYSIS VARIABLES
C          ASSUMING FULLY DEVELOPED FLOW FOR ALL CHANNEL WIDTHS.
C-------------------------------------------------------------------
C ANALYSIS VARIABLES
C A      ... INTERMEDIATE DUMMY VARIABLE FOR FIXED PRESSURE
C                DROP CONSTRAINT                            (M*2/S*2)
C ACBYAP ... RATIO OF FREE-FLOW TO FRONTAL CROSS-SECTIONAL
C                AREAS                                      (-)
C ASPECT ... CHANNEL ASPECT RATIO                           (-)
C B,C    ... INTERMEDIATE DUMMY VARIABLES FOR FIXED PRESSURE
C                DROP CONSTRAINT                            (-)
C DE     ... HYDRAULIC DIAMETER                             (M)
C DELP   ... PRESSURE DROP                                  (N/M*2)
C DUMPHI ... FRICTION FACTOR CORRECTION FOR CHANNEL SHAPE   (-)
C E      ... INTERMEDIATE DUMMY VARIABLE FOR FIXED PRESSURE
C                DROP CONSTRAINT                            (S/M)
C FACT   ... VARIABLE PROPERTIES COMPENSATION FACTOR        (-)
C FAPP   ... APPARANT FRICTION FACTOR                       (-)
C ICONS  ... COOLANT FLOW CONSTRAINT                        (-)
C IFLOW  ... FLOW REGIME INDICATOR                          (-)
C IKLOSS ... CONTROL FOR INCLUDING K90, KC AND KE           (-)
C KC     ... ENTRANCE PRESSURE LOSS COEFFICIENT             (-)
C KE     ... EXIT PRESSURE LOSS COEFFICIENT                 (-)
C K90    ... NINETY DEGREE BEND PRESSURE LOSS COEFFICIENT   (-)
C L      ... CHANNEL LENGTH                                 (M)
C LPLUS  ... HYDRODYNAMIC ENTRY LENGTH                      (-)
C MUFILA ... AVERAGE COOLANT DYNAMIC VISCOSITY AT THE
C                AVERAGE FIN TEMPERATURE BETWEEN THE
C                CHANNEL ENTRANCE AND EXIT                  (KG/M S)
C MUFLLA ... AVERAGE COOLANT DYNAMIC VISCOSITY AT THE
C                AVERAGE COOLANT TEMPERATURE BETWEEN THE
C                CHANNEL ENTRANCE AND EXIT                  (KG/M S)
C MUFLUL ... COOLANT DYNAMIC VISCOSITY AT CHANNEL EXIT       (KG/M S)
C MUFLUX ... COOLANT DYNAMIC VISCOSITY AT POSITION X        (KG/M S)
C NCHAN  ... NUMBER OF CHANNELS PER CENTIMETER CHIP WIDTH   (-)
C NPARAL ... NUMBER OF CHANNELS IN SERIES PER CENTIMETER    (-)
C PPOWER ... PUMPING POWER PER UNIT CIRCUIT SURFACE AREA    (W/CM*2)
C PRFLUL ... COOLANT PRANDTL NUMBER AT CHANNEL EXIT         (-)
C PRFLUX ... COOLANT PRANDTL NUMBER AT POSITION X           (-)
C REL    ... REYNOLDS NUMBER AT CHANNEL EXIT                (-)
C REX    ... REYNOLDS NUMBER AT POSITION X                  (-)
C RHOFLL ... COOLANT DENSITY AT CHANNEL EXIT                (KG/M*3)
C RHOFLX ... COOLANT DENSITY AT POSITION X                  (KG/M*3)
C V1CL   ... COOLANT FLOW VELOCITY AT CHANNEL EXIT          (M/S)
C V1CX   ... COOLANT FLOW VELOCITY AT POSITION X            (M/S)
C VOLUME ... COOLANT FLOW RATE PER UNIT
C                CIRCUIT SURFACE AREA                     ((M*3/S)/CM*2)
C WC     ... CHANNEL WIDTH                                  (M)
C WW     ... FIN WIDTH                                      (M)
C X      ... POSITION FROM CHANNEL ENTRANCE                 (M)
C XSTARL ... THERMAL ENTRY LENGTH AT CHANNEL EXIT           (-)
C XSTARX ... THERMAL ENTRY LENGTH AT POSITION X             (-)
C Z      ... FIN HEIGHT                                     (M)
C-------------------------------------------------------------------
      SUBROUTINE SFFD(IFLOW,WW,WC,Z,L,X,DE,ASPECT,ACBYAP,
```

```
     *                 RHOFLL,RHOFLX,MUFLUL,MUFLUX,MUFLLA,MUFILA,
     *                 PRFLUL,PRFLUX,IKLOSS,ICONS,DELP,VOLUME,PPOWER,
     *                 REL,REX,V1CL,V1CX,LPLUS,FAPP,XSTARL,XSTARX)
      REAL KC,KE,K90,L,LPLUS,MUFLLA,MUFILA,MUFLUL,MUFLUX,NCHAN,NPARAL
C DETERMINE SOLUTION METHOD - NO SOLUTION IS GIVEN FOR FIXED PUMPING
C    POWER
      IF(ICONS.EQ.2)GO TO 200
      IF(ICONS.EQ.3)RETURN
C
C                          ******************************
C                          *    PRESSURE DROP FIXED     *
C                          ******************************
C
C NONUNIFORM PROPERTIES - EQN. 2.24
      FACT=(MUFILA/MUFLLA)**0.58
C CORRECTION FOR DUCT SHAPE - EQN. 2.3
      DUMPHI=(2./3.)+(11./24.)*(WC/Z)*(2.-(WC/Z))
      CALL ABRUPT(ACBYAP,ASPECT,IFLOW,IKLOSS,KC,KE,K90,9999.)
C COMPUTE REYNOLDS NUMBER - EQN. 4.18
      A=DELP*2.*1./RHOFLL
      B=((ACBYAP*ACBYAP*2.*K90)+(KC+KE))
      C=(4.*L/DE)*(16./DUMPHI)*FACT
      E=RHOFLL*DE/MUFLUL
      IF(IKLOSS.NE.0)
     *REL=((-1.*C)+((C*C)+(4.*A*B*E*E)))/(2.*B)
      IF(IKLOSS.EQ.0)
     *REL=A*E*E/C
C COMPUTE MISC. STUFF
      V1CL=REL/E
      V1CX=V1CL*RHOFLL/RHOFLX
      REX=RHOFLX*V1CX*DE/MUFLUX
      XSTARL=L/(DE*REL*PRFLUL)
      XSTARX=X/(DE*REX*PRFLUX)
      LPLUS=L/(DE*REL)
C COMPUTE FULLY DEVELOPED FRICTION FACTOR
      FAPP=(16./(DUMPHI*REL))*FACT
C COMPUTE FLOW STUFF
      NCHAN=0.01/(WW+WC)
      NPARAL=0.01/L
      VOLUME=(V1CL*WC*Z)*(NCHAN*NPARAL)
      PPOWER=DELP*VOLUME
      RETURN
C
C                          ********************************
C                          * VOLUMETRIC FLOW RATE FIXED *
C                          ********************************
C
200   CONTINUE
C NONUNIFORM PROPERTIES - EQN. 2.24
      FACT=(MUFILA/MUFLLA)**0.58
C CORRECTION FOR DUCT SHAPE - EQN. 2.3
      DUMPHI=(2./3.)+(11./24.)*(WC/Z)*(2.-(WC/Z))
      CALL ABRUPT(ACBYAP,ASPECT,IFLOW,IKLOSS,KC,KE,K90,9999.)
C COMPUTE COOLANT VELOCITY - EQN. 4.19
      V1CL=VOLUME*10000.*L*(WW+WC)/(WC*Z)
C COMPUTE MISC. STUFF
      REL=RHOFLL*V1CL*DE/MUFLUL
      V1CX=V1CL*RHOFLL/RHOFLX
      REX=RHOFLX*V1CX*DE/MUFLUX
      XSTARL=L/(DE*REL*PRFLUL)
```

```
      XSTARX=X/(DE*REX*PRFLUX)
      LPLUS=L/(DE*REL)
C COMPUTE FULLY DEVELOPED FRICTION FACTOR
      FAPP=(16./(DUMPHI*REL))*FACT
C COMPUTE PRESSURE DROP - EQN. 2.9
      DELP=(RHOFLL*V1CL*V1CL/2.)*
     $     ((ACBYAP*ACBYAP*2.*K90)+(KC+KE)+(4.*FAPP*FACT*L/DE))
      PPOWER=DELP*VOLUME
      RETURN
      END
C END OF FILE FOR SUBROUTINE SFFD
C-----------------------------------------------------------------------
C  SLAMF:  WRITTEN BY RICHARD J. PHILLIPS.  SLAMF COMPUTES THE
C          SMOOTH-CHANNEL COOLANT VELOCITY AND SOME OTHER ANALYSIS
C          VARIABLES FOR FULLY DEVELOPED/DEVELOPING LAMINAR FLOW.
C-----------------------------------------------------------------------
C ANALYSIS VARIABLES
C A      ... INTERMEDIATE DUMMY VARIABLE FOR FIXED PRESSURE
C                DROP CONSTRAINT                            (M*2/S*2)
C ACBYAP ... RATIO OF FREE-FLOW TO FRONTAL CROSS-SECTIONAL
C              AREAS                                        (-)
C ASPEC  ... ARRAY OF CHANNEL ASPECT RATIOS FOR FAPRE       (-)
C ASPECT ... CHANNEL ASPECT RATIO(FIN LENGTH/CHANNEL WIDTH)(-)
C B1,B2  ... Y - INTERCEPTS FOR LPLUS LOCATION              (-)
C B,C    ... INTERMEDIATE DUMMY VARIABLES FOR FIXED PRESSURE
C                DROP CONSTRAINT                            (-)
C DE     ... CHANNEL HYDRAULIC DIAMETER                     (M)
C DELP   ... PRESSURE DROP                                  (N/M*2)
C DUMF   ... ARRAY OF INTERMEDIATE FAPPRE VALUES            (-)
C E      ... INTERMEDIATE DUMMY VARIABLE FOR FIXED PRESSURE
C                DROP CONSTRAINT                            (S/M)
C ELARGE ... ERROR OF EQUATION 4.18 USING VLARGE            (-)
C EMED   ... ERROR OF EQUATION 4.18 USING VMED              (-)
C ERROR  ... RELATIVE ERROR BETWEEN VLARGE AND VSMALL       (-)
C ESMALL ... ERROR OF EQUATION 4.18 USING VSMALL            (-)
C FACT   ... VARIABLE PROPERTIES COMPENSATION FACTOR        (-)
C FACTOR ... INTERPOLATION DUMMY VARIABLE                   (-)
C FAPP   ... APPARANT FRICTION FACTOR                       (-)
C FAPRE  ... APPARANT FRICTION FACTOR AND RE PRODUCT DATA   (-)
C FAPPRE ... FLOW APPARANT FRICTION FACTOR AND RE PRODUCT   (-)
C ICONS  ... COOLANT FLOW CONSTRAINT                        (-)
C IFLOW  ... FLOW REGIME INDICATOR                          (-)
C IKLOSS ... CONTROL FOR INCLUDING K90, KC, AND KE          (-)
C KC     ... ENTRANCE PRESSURE LOSS COEFFICIENT             (-)
C KE     ... EXIT PRESSURE LOSS COEFFICIENT                 (-)
C K90    ... NINETY DEGREE BEND PRESSURE LOSS COEFFICIENT   (-)
C L      ... CHANNEL LENGTH                                 (M)
C LLPLUS ... ARRAY OF MOMENTUM ENTRY LENGTH DATA FOR FAPRE (-)
C LOOP   ... DUMMY COUNTER                                  (-)
C LPLUS  ... MOMENTUM ENTRY LENGTH                          (-)
C MUFILA ... AVERAGE COOLANT DYNAMIC VISCOSITY AT THE
C              AVERAGE FIN TEMPERATURE BETWEEN THE
C              CHANNEL ENTRANCE AND EXIT                    (KG/M S)
C MUFLLA ... AVERAGE COOLANT DYNAMIC VISCOSITY AT THE
C              AVERAGE COOLANT TEMPERATURE BETWEEN THE
C              CHANNEL ENTRANCE AND EXIT                    (KG/M S)
C MUFLUL ... COOLANT DYNAMIC VISCOSITY AT CHANNEL EXIT      (KG/M S)
C MUFLUX ... COOLANT DYNAMIC VISCOSITY AT POSITION X        (KG/M S)
C NCHAN  ... NUMBER OF CHANNELS PER CENTIMETER CHIP WIDTH   (-)
C NPARAL ... NUMBER OF CHANNELS IN SERIES PER CENTIMETER
```

```
C                CHIP LENGTH                                          (-)
C PPOWER ... PUMPING POWER PER UNIT CIRCUIT SURFACE AREA   (W/CM*2)
C PRFLUL ... COOLANT PRANDTL NUMBER AT CHANNEL EXIT         (-)
C PRFLUX ... COOLANT PRANDTL NUMBER AT POSITION X           (-)
C REL    ... REYNOLDS NUMBER AT CHANNEL EXIT                (-)
C REX    ... REYNOLDS NUMBER AT POSITION X                  (-)
C RE1,RE2... ARRAYS OF INTERMEDIATE REYNOLDS NUMBERS
C            FOR LOCATION OF THE APPROPRIATE LPLUS          (-)
C RHOFLL ... COOLANT DENSITY AT CHANNEL EXIT                (KG/M*3)
C RHOFLX ... COOLANT DENSITY AT POSITION X                  (KG/M*3)
C SLOPE1,2.. SLOPES FOR LPLUS LOCATION                      (-)
C V1CL   ... COOLANT FLOW VELOCITY AT CHANNEL EXIT          (M/S)
C V1CX   ... COOLANT FLOW VELOCITY AT POSITION X            (M/S)
C VLARGE ... HIGH ESTIMATE OF COOLANT VELOCITY              (M/S)
C VMED   ... NEW ESTIMATE OF COOLANT VELOCITY               (M/S)
C VOLUME ... COOLANT FLOW RATE PER UNIT SURFACE AREA        (M*3/CM*2)
C VSMALL ... LOW ESTIMATE OF COOLANT VELOCITY               (M/S)
C WC     ... CHANNEL WIDTH                                  (M)
C WW     ... FIN THICKNESS                                  (M)
C X      ... POSITION FROM CHANNEL ENTRANCE                 (M)
C XSTARL ... THERMAL ENTRY LENGTH AT CHANNEL EXIT           (-)
C XSTARX ... THERMAL ENTRY LENGTH AT POSITION X             (-)
C Z      ... FIN HEIGHT                                     (M)
C----------------------------------------------------------------------
      SUBROUTINE SLAMF(IFLOW,WW,WC,Z,L,X,DE,ASPECT,ACBYAP,
     &           RHOFLL,RHOFLX,MUFLUL,MUFLUX,MUFLLA,MUFILA,
     &           PRFLUL,PRFLUX,IKLOSS,ICONS,DELP,VOLUME,PPOWER,
     &           REL,REX,V1CL,V1CX,LPLUS,FAPP,XSTARL,XSTARX)
      DIMENSION FAPRE(5,19),DUMF(19),LLPLUS(19),ASPEC(5),RE1(19),RE2(19)
      REAL L,K90,KC,KE,LLPLUS,LPLUS,MUFLUL,MUFLUX,MUFLLA,MUFILA,
     &     NCHAN,NPARAL
C DATA FOR FAPRE, LLPLUS, AND ASPEC WERE OBTAINED FROM TABLE 2.5.
      DATA FAPRE/
     &         287.,142.,142.,142.,287.,
     &         112.,111.,111.,111.,112.,
     &         67.5,66.0,66.0,66.1,67.5,
     &         53.0,51.8,51.8,52.5,53.0,
     &         46.2,44.6,44.6,45.3,46.2,
     &         42.1,39.9,40.0,40.6,42.1,
     &         40.4,38.0,38.2,38.9,40.4,
     &         35.6,32.1,32.5,33.3,35.6,
     &         32.4,28.6,29.1,30.2,32.4,
     &         29.7,24.6,25.3,26.7,29.7,
     &         28.2,22.4,23.2,24.9,28.2,
     &         27.4,21.0,21.8,23.7,27.4,
     &         27.1,20.0,20.8,22.9,26.8,
     &         26.9,19.3,20.1,22.4,26.4,
     &         26.7,18.7,19.6,22.0,26.1,
     &         26.5,18.2,19.1,21.7,25.8,
     &         26.2,17.8,18.8,21.4,25.6,
     &         24.7,15.8,17.0,20.1,24.7,
     &         24.0,14.2,15.5,19.1,24.0/
      DATA LLPLUS/0.0000001,.001,.003,.005,.007,.009,.01,.015,
     &         .02,.03,.04,.05,.06,.07,.08,.09,.10,0.20,1./
      DATA ASPEC/0.1,1.,2.,5.,10./
C INTERPOLATION BETWEEN COLUMNS OF FAPPRE AT PROPER CHANNEL ASPECT RATIO
C
      IF(ASPECT.GT.ASPEC(1))GO TO 10
C  SMALL ASPECT RATIO CHANNELS
      DO 5 II=1,19
```

```
         DUMF(II)=FAPRE(1,II)
5     CONTINUE
      GO TO 50
10    CONTINUE
      IF(ASPECT.LT.ASPEC(5))GO TO 20
C  LARGE ASPECT RATIO CHANNELS
      DO 15 II=1,19
         DUMF(II)=FAPRE(5,II)
15    CONTINUE
      GO TO 50
C MODERATE ASPECT RATIO CHANNELS
20    CONTINUE
      DO 30 I=1,4
         IF((ASPECT.GE.ASPEC(I)).AND.(ASPECT.LT.ASPEC(I+1)))GO TO 40
30    CONTINUE
40    CONTINUE
      FACTOR=(ASPECT-ASPEC(I))/(ASPEC(I+1)-ASPEC(I))
      DO 45 II=1,19
         DUMF(II)=FACTOR*(FAPRE(I+1,II)-FAPRE(I,II))+FAPRE(I,II)
45    CONTINUE
50    CONTINUE
C
C DETERMINE COOLANT FLOW RATE CONSTRAINT
C  1) DELP FIXED
         IF(ICONS.EQ.1)GO TO 1000
C  2) VOLUME FIXED
         IF(ICONS.EQ.2)GO TO 2000
C  3) POWER FIXED
         IF(ICONS.EQ.3)GO TO 3000
1000  CONTINUE
C
C                          ******************************
C                          *    PRESSURE DROP FIXED     *
C                          ******************************
C
C   THE APPROPRIATE LPLUS WILL BE LOCATED WHERE RE1 AND RE2 ARE THE
C   SAME.  IN GENERAL, IF LPLUS IS TOO SMALL, RE1 WILL BE LARGER THAN
C   RE2.  WHEN THE NEXT VALUE OF LPLUS RESULTS IN A RE1 THAT IS LESS
C   THAN RE2, THE CORRECT VALUE OF LPLUS HAS BEEN BRACKETED.
C
C
C NONUNIFORM PROPERTIES - EQN. 2.24
      FACT=(MUFILA/MUFLLA)**0.58
      DO 200 I=1,19,1
C        DETERMINE ENTRANCE AND EXIT PRESSURE LOSS COEFFICIENTS
         CALL ABRUPT(ACBYAP,ASPECT,IFLOW,IKLOSS,KC,KE,K90,LLPLUS(I))
C        RE1(I) IS DETERMINED DIRECTLY FROM LLPLUS(I)
         RE1(I)=(L/DE)/LLPLUS(I)
C        RE2(I) IS OBTAINED FROM EQUATION 4.18 AT LLPLUS(I). NOTE THAT
C        V**2=A/(B+C/(EV))
C COMPUTE REYNOLDS NUMBER - EQN. 4.18
         A=DELP*2.*1./RHOFLL
         B=(ACBYAP*ACBYAP*2.*K90)+(KC+KE)
         C=(4.*L/DE)*(DUMF(I)*FACT)
         E=RHOFLL*DE/MUFLUL
         IF(IKLOSS.NE.0)
     &   RE2(I)=((-1.*C)+SQRT((C*C)+(4.*A*B*E*E)))/(2.*B)
         IF(IKLOSS.EQ.0)
     &   RE2(I)=A*E*E/C
         IF(RE2(I).GT.RE1(I))GO TO 300
```

```
200   CONTINUE
C
C     IF THE PROGRAM GETS TO THIS POINT, RE1 AND RE2 DO NOT CROSS.  THIS
C     CAN ONLY HAPPEN IF THE FLOW IS FULLY DEVELOPED.
C
C     IF(I.EQ.19)WRITE(11,202)
202   FORMAT(' CHECK THAT FLOW IS FULLY DEVELOPED AT EXIT')
      REL=RE2(19)
      LPLUS=L/(DE*REL)
      FAPPRE=DUMF(19)
      GO TO 350
300   CONTINUE
C
C   RE1 AND RE2 HAVE CROSSED.  GENERATE LINEAR CURVES TO FIND THE
C   INTERSECTION.  THIS IS DONE WITH 1/LPLUS SO THAT LINEAR
C   INTERPOLATION GIVES MORE ACCURATE RESULTS AT LARGE LPLUS VALUES.
C   THE RESULTS AT SMALL LPLUS'S DON'T APPEAR TO BE AFFECTED BY THE
C   INTERPOLATION METHOD.
C
      SLOPE1=(RE1(I)-RE1(I-1))/(1./LLPLUS(I)-1./LLPLUS(I-1))
      SLOPE2=(RE2(I)-RE2(I-1))/(1./LLPLUS(I)-1./LLPLUS(I-1))
      B1=RE1(I)-SLOPE1/LLPLUS(I)
      B2=RE2(I)-SLOPE2/LLPLUS(I)
      LPLUS=(B2-B1)/(SLOPE1-SLOPE2)
      LPLUS=1./LPLUS
C INTERPOLATE AT APPROXIMATE INTERSECTION POINT
      FAPPRE=((LPLUS-LLPLUS(I-1))/(LLPLUS(I)-LLPLUS(I-1)))
     *       *(DUMF(I)-DUMF(I-1))+DUMF(I-1)
      REL=(L/DE)/LPLUS
C
350   CONTINUE
C COMPUTE MISC. STUFF
      FAPP=FAPPRE/REL
      V1CL=(REL*MUFLUL)/(RHOFLL*DE)
      V1CX=V1CL*RHOFLL/RHOFLX
      REX=RHOFLX*V1CX*DE/MUFLUX
      XSTARL=L/(DE*REL*PRFLUL)
      XSTARX=X/(DE*REX*PRFLUX)
C COMPUTE FLOW STUFF
      NCHAN=0.01/(WW+WC)
      NPARAL=0.01/L
      VOLUME=(V1CL*WC*Z)*(NCHAN*NPARAL)
      PPOWER=VOLUME*DELP
      RETURN
C
2000  CONTINUE
C
C                          ********************************
C                          * VOLUMETRIC FLOW RATE FIXED *
C                          ********************************
C
C COMPUTE COOLANT VELOCITY - EQN. 4.19
      V1CL=VOLUME*10000.*(L*(WW+WC))/(WC*Z)
C COMPUTE MISC. STUFF
      REL=V1CL*RHOFLL*DE/MUFLUL
      LPLUS=(L/DE)/REL
C
C     INTERPOLATE FAPPRE AND THE DESIRED LPLUS
C
      DO 2200 I=1,18
```

```
         IF((LPLUS.GE.LLPLUS(I)).AND.(LPLUS.LT.LLPLUS(I+1)))GO TO 2300
2200  CONTINUE
      IF(LPLUS.LT.LLPLUS(1))FAPPRE=DUMF(1)
      IF(LPLUS.GE.LLPLUS(19))FAPPRE=DUMF(19)
      GO TO 2400
2300  CONTINUE
      FAPPRE=((LPLUS-LLPLUS(I))/(LLPLUS(I+1)-LLPLUS(I)))
     &        *(DUMF(I+1)-DUMF(I))+DUMF(I)
2400  CONTINUE
C
C     COMPUTE OTHER NUMBERS
C
      FAPP=FAPPRE/REL
      V1CX=V1CL*RHOFLL/RHOFLX
      REX=RHOFLX*V1CX*DE/MUFLUX
      XSTARL=L/(DE*REL*PRFLUL)
      XSTARX=X/(DE*REX*PRFLUX)
C DETERMINE ENTRANCE AND EXIT PRESSURE LOSS COEFFICIENTS
      CALL ABRUPT(ACBYAP,ASPECT,IFLOW,IKLOSS,KC,KE,K90,LPLUS)
C NONUNIFORM PROPERTIES - EQN. 2.24
      FACT=(MUFILA/MUFLLA)**0.58
C COMPUTE PRESSURE DROP - EQN. 2.9
      DELP=(RHOFLL*V1CL*V1CL/2.)*
     &((ACBYAP*ACBYAP*2.*K90)+(KC+KE)+(4.*FAPP*FACT*L/DE))
C COMPUTE PUMPING POWER
      PPOWER=VOLUME*DELP
      RETURN
C
3000  CONTINUE
C
C                          ******************************
C                          *    PUMPING POWER FIXED     *
C                          ******************************
C
C   THE APPROPRIATE LPLUS WILL BE LOCATED WHERE RE1 AND RE2 ARE THE
C   SAME.  IN GENERAL, IF LPLUS IS TOO SMALL, RE1 WILL BE LARGER THAN
C   RE2.  WHEN THE NEXT VALUE OF LPLUS RESULTS IN A RE1 THAT IS LESS
C   THAN RE2, THE CORRECT VALUE OF LPLUS HAS BEEN BRACKETED.
C
C NONUNIFORM PROPERTIES - EQN. 2.24
      FACT=(MUFILA/MUFLLA)**0.58
      DO 3200 I=1,19,1
C         DETERMINE ENTRANCE AND EXIT PRESSURE LOSS COEFFICIENTS
          CALL ABRUPT(ACBYAP,ASPECT,IFLOW,IKLOSS,KC,KE,K90,LLPLUS(I))
C         RE1(I) IS DETERMINED DIRECTLY FROM LLPLUS(I)
          RE1(I)=(L/DE)/LLPLUS(I)
C         RE2(I) IS OBTAINED FROM EQUATION 4.20 AT LLPLUS(I).
C         NOTE THAT V**3=A/(B+C/(EV))
C COMPUTE REYNOLDS NUMBER - EQN. 4.20
          A=(PPOWER*10000.*2.*1./RHOFLL)*(L*(WW+WC)/(WC*Z))
          B=(ACBYAP*ACBYAP*2.*K90)+(KC+KE)
          C=(4.*L/DE)*(DUMF(I)*FACT)
          E=RHOFLL*DE/MUFLUL
          IF(IKLOSS.EQ.0)
     &    RE2(I)=SQRT(A*E*E*E/C)
          IF(IKLOSS.EQ.0)GO TO 3190
C
C         TRIAL AND ERROR SOLUTION FOR V1C AT LLPLUS(I).  NOTE THAT
C         EQUATION 4.20 GIVES V**3=A/(B+C/(EV)),
C         AND ERROR=B*V**3+(C/E)*V**2-A.
```

```
C
C         VLARGE: ASSUMES K90=KC=KE=0.
          VLARGE=SQRT(A*E/C)
          ELARGE=(VLARGE*VLARGE*VLARGE*B)+(VLARGE*VLARGE*C/E)-A
C         INITIAL GUESS OF VSMALL IS VERY SMALL
          VSMALL=0.00001
          ESMALL=(VSMALL*VSMALL*VSMALL*B)+(VSMALL*VSMALL*C/E)-A
C
C         NOTE THAT VSMALL GIVES RHS<0, AND VLARGE GIVES RHS>0, AND
C         THEREFORE THE SOLUTION IS SOMEWHERE BETWEEN.
C
          LOOP=0
3110      CONTINUE
          LOOP=LOOP+1
          IF(LOOP.EQ.20)STOP
          VMED=(VLARGE+VSMALL)/2.
          EMED=(VMED*VMED*VMED*B)+(VMED*VMED*C/E)-A
          IF(EMED.GT.0.)GO TO 3150
C         UPDATE VSMALL
          VSMALL=VMED
          ERROR=ABS((VLARGE-VSMALL)/VMED)
          IF(ERROR.LT.0.0001)GO TO 3155
          ESMALL=EMED
          GO TO 3110
C         UPDATE VLARGE
3150      CONTINUE
          VLARGE=VMED
          ERROR=ABS((VLARGE-VSMALL)/VMED)
          IF(ERROR.LT.0.0001)GO TO 3155
          ELARGE=EMED
          GO TO 3110
3155   CONTINUE
C
C         THE COOLANT VELOCITY IS APPROXIMATELY KNOWN FOR THIS LLPLUS(I)
C
          RE2(I)=RHOFLL*DE*((VLARGE+VSMALL)/2.)/MUFLUL
3190   CONTINUE
          IF(RE2(I).GT.RE1(I))GO TO 3220
3200   CONTINUE
C
C      IF THE PROGRAM GETS TO THIS POINT, RE1 AND RE2 DO NOT CROSS.  THIS
C      CAN ONLY HAPPEN IF THE FLOW IS FULLY DEVELOPED.
C
C      IF(I.EQ.19)WRITE(11,3202)
3202   FORMAT(' CHECK THAT FLOW IS FULLY DEVELOPED AT EXIT')
       REL=RE2(19)
       LPLUS=L/(DE*REL)
       FAPPRE=DUMF(19)
       GO TO 3350
3220   CONTINUE
C
C    RE1 AND RE2 HAVE CROSSED.  GENERATE LINEAR CURVES TO FIND THE
C    INTERSECTION.  THIS IS DONE WITH 1/LPLUS SO THAT LINEAR
C    INTERPOLATION GIVES MORE ACCURATE RESULTS AT LARGE LPLUS VALUES.
C    THE RESULTS AT SMALL LPLUS'S DON'T APPEAT TO BE AFFECTED BY THE
C    INTERPOLATION METHOD.
C
       SLOPE1=(RE1(I)-RE1(I-1))/(1./LLPLUS(I)-1./LLPLUS(I-1))
       SLOPE2=(RE2(I)-RE2(I-1))/(1./LLPLUS(I)-1./LLPLUS(I-1))
       B1=RE1(I)-SLOPE1/LLPLUS(I)
```

```
      B2=RE2(I)-SLOPE2/LLPLUS(I)
      LPLUS=(B2-B1)/(SLOPE1-SLOPE2)
      LPLUS=1./LPLUS
C     INTERPOLATE AT APPROXIMATE INTERSECTION POINT
      FAPPRE=((LPLUS-LLPLUS(I-1))/(LLPLUS(I)-LLPLUS(I-1)))
     1       *(DUMF(I)-DUMF(I-1))+DUMF(I-1)
      REL=(L/DE)/LPLUS
C
C     COMPUTE OTHER NUMBERS
C
3350  CONTINUE
C COMPUTE MISC. STUFF
      CALL ABRUPT(ACBYAP,ASPECT,IFLOW,IKLOSS,KC,KE,K90,LPLUS)
      FAPP=FAPPRE/REL
      V1CL=(REL*MUFLUL)/(RHOFLL*DE)
      V1CX=V1CL*RHOFLL/RHOFLX
      REX=RHOFLX*V1CX*DE/MUFLUX
      XSTARL=L/(DE*REL*PRFLUL)
      XSTARX=X/(DE*REX*PRFLUX)
C COMPUTE COOLANT FLOW STUFF
      DELP=(RHOFLL*V1CL*V1CL/2.)*((ACBYAP*ACBYAP*2.*K90)+(KC+KE)
     1                              +(4.*FAPP*FACT*L/DE))
      NCHAN=0.01/(WW+WC)
      NPARAL=0.01/L
      VOLUME=(V1CL*WC*Z)*(NCHAN*NPARAL)
      RETURN
      END
C END OF FILE FOR SUBROUTINE SLAMF
C-----------------------------------------------------------------------
C  STURF:  WRITTEN BY RICHARD J. PHILLIPS.  STURF COMPUTES THE
C          SMOOTH-CHANNEL COOLANT VELOCITY AND SOME OTHER ANALYSIS
C          VARIABLES FOR FULLY DEVELOPED/DEVELOPING TURBULENT FLOW.
C-----------------------------------------------------------------------
C ANALYSIS VARIABLES
C A1,A2,A3.. DUMMY ANALYSIS VARIABLES FOR EQUATION 4.18      (-)
C A,B    ... DUMMY ANALYSIS PARAMETERS FOR EQUATION 2.6      (-)
C ACBYAP ... RATIO OF CHANNEL AND PLENUM CROSS-SECTIONAL
C                AREAS                                       (-)
C ASPECT ... CHANNEL ASPECT RATIO                            (-)
C DE     ... CHANNEL HYDRAULIC DIAMETER                      (M)
C DELP   ... ASSUMED CHANNEL PRESSURE LOSS                   (N/M*2)
C DLE    ... LAMINAR EQUIVALENT DIAMETER (ONLY FOR RESTAR)   (-)
C ELARGE ... ERROR OF EQUATION 4.18 USING VLARGE             (-)
C EMED   ... ERROR OF EQUATION 4.18 USING VMED               (-)
C ERROR  ... RELATIVE ERROR BETWEEN VLARGE AND VSMALL        (-)
C ESMALL ... ERROR OF EQUATION 4.18 USING VSMALL             (-)
C FACT   ... VARIABLE PROPERTIES COMPENSATION FACTOR         (-)
C FAPP   ... APPARANT FRICTION FACTOR                        (-)
C ICONS  ... CONTROL FOR WHICH FLOW CONSTRAINT IS USED       (-)
C IFLOW  ... ACTIVE LOOP INDICATOR FOR FLOW REGIME           (-)
C IKLOSS ... CONTROL FOR INCLUDING K90, KC, AND KE           (-)
C KC     ... ENTRANCE PRESSURE LOSS COEFFICIENT              (-)
C KE     ... EXIT PRESSURE LOSS COEFFICIENT                  (-)
C K90    ... NINETY DEGREE BEND PRESSURE LOSS COEFFICIENT    (-)
C L      ... CHANNEL LENGTH                                  (M)
C LOOP   ... DUMMY COUNTER                                   (-)
C LPLUS  ... MOMENTUM ENTRY LENGTH                           (-)
C MUFILA ... AVERAGE COOLANT DYNAMIC VISCOSITY AT THE
C              AVERAGE FIN TEMPERATURE BETWEEN THE
C              CHANNEL ENTRANCE AND EXIT                     (KG/M S)
```

```
C MUFLLA ... AVERAGE COOLANT DYNAMIC VISCOSITY AT THE
C               AVERAGE COOLANT TEMPERATURE BETWEEN THE
C               CHANNEL ENTRANCE AND EXIT                    (KG/M S)
C MUFLUL ... COOLANT DYNAMIC VISCOSITY AT CHANNEL EXIT       (KG/M S)
C MUFLUX ... COOLANT DYNAMIC VISCOSITY AT POSITION X         (KG/M S)
C NCHAN  ... NUMBER OF CHANNELS PER CENTIMETER CHIP WIDTH    (-)
C NPARAL ... NUMBER OF CHANNELS IN SERIES PER CENTIMETER
C                 CHIP LENGTH                                (-)
C PPOWER ... COOLANT PUMPING POWER PER UNIT SURFACE AREA     (W/CM*2)
C PRFLUL ... COOLANT PRANDTL NUMBER AT CHANNEL EXIT          (-)
C PRFLUX ... COOLANT PRANDTL NUMBER AT POSITION X            (-)
C REL    ... REYNOLDS NUMBER AT CHANNEL EXIT                 (-)
C REX    ... REYNOLDS NUMBER AT POSITION X                   (-)
C RESTAL ... MODIFIED REYNOLDS NUMBER AT CHANNEL EXIT        (-)
C RESTAX ... MODIFIED REYNOLDS NUMBER AT POSITION X          (-)
C RHOFLL ... COOLANT DENSITY AT CHANNEL EXIT                 (KG/M*3)
C RHOFLX ... COOLANT DENSITY AT POSITION X                   (KG/M*3)
C V1CL   ... COOLANT FLOW VELOCITY AT CHANNEL EXIT           (M/S)
C V1CX   ... COOLANT FLOW VELOCITY AT POSITION X             (M/S)
C VLARGE ... HIGH ESTIMATE OF COOLANT VELOCITY               (M/S)
C VMED   ... NEW ESTIMATE OF COOLANT VELOCITY                (M/S)
C VOLUME ... COOLANT FLOW RATE PER UNIT SURFACE AREA         (M*3/CM*2)
C VSMALL ... LOW ESTIMATE OF COOLANT VELOCITY                (M/S)
C WC     ... CHANNEL WIDTH                                   (M)
C WW     ... FIN THICKNESS                                   (M)
C X      ... POSITION FROM CHANNEL ENTRANCE                  (M)
C XSTARL ... THERMAL ENTRY LENGTH AT CHANNEL EXIT            (-)
C XSTARX ... THERMAL ENTRY LENGTH AT POSITION X              (-)
C Z      ... FIN LENGTH                                      (M)
C-----------------------------------------------------------------------
      SUBROUTINE STURF(IFLOW,WW,WC,Z,L,X,DE,DLE,ASPECT,ACBYAP,
     1                 RHOFLL,RHOFLX,MUFLUL,MUFLUX,MUFLLA,MUFILA,
     1                 PRFLUL,PRFLUX,IKLOSS,ICONS,DELP,VOLUME,PPOWER,
     1                 REL,REX,RESTAL,RESTAX,V1CL,V1CX,LPLUS,FAPP,
     1                 XSTARL,XSTARX)
      REAL L,K90,KC,KE,LPLUS,MUFLUL,MUFLUX,MUFLLA,MUFILA,NCHAN,NPARAL
C
C DETERMINE COOLANT FLOW RATE CONSTRAINT
C  1) DELP FIXED
        IF(ICONS.EQ.1)GO TO 1000
C  2) VOLUME FIXED
        IF(ICONS.EQ.2)GO TO 2000
C  3) PUMPING POWER FIXED
        IF(ICONS.EQ.3)GO TO 3000
1000  CONTINUE
C
C                         ******************************
C                         *    PRESSURE DROP FIXED     *
C                         ******************************
C
C DETERMINE ENTRANCE AND EXIT PRESSURE LOSS COEFFICIENTS
      CALL ABRUPT(ACBYAP,ASPECT,IFLOW,IKLOSS,KC,KE,K90,LPLUS)
C NONUNIFORM PROPERTIES - EQN. 2.24
      FACT=(MUFILA/MUFLLA)**0.25
C FRICTION FACTOR - EQN. 2.6 - REMEMBER THAT B IS NEGATIVE
      A=0.09290+(1.01612/(L/DE))
      B=0.26800+(0.31930/(L/DE))
C     CONSTANTS FOR PRESSURE DROP EQUATION 4.18
C     NOTE THAT V**2=(A1)/(A2+A3*V**(-B))
      A1=DELP*2.*1./RHOFLL
```

```
      A2=(ACBYAP*ACBYAP*2.*K90)+(KC+KE)
      A3=(4.*L/DE)*A/((RHOFLL*DLE/MUFLUL)**B)
      IF(IKLOSS.EQ.0)V1CL=(A1/A3)**(1./(2.-B))
      IF(IKLOSS.EQ.0)GO TO 300
C
C     TRIAL AND ERROR ESTIMATION OF V1CL
C     EQUATION 4.18 GIVES V**2=(A1)/(A2+A3*V**(-B))
C     WHICH CAN BE REARRANGED TO (V**2)*A2+(V**(2-B))*A3-A1=0.
C
C     VLARGE: ASSUMES K90=KC=KE=0.
      VLARGE=(A1/A3)**(1./(2.-B))
      ELARGE=(VLARGE*VLARGE*A2)+((VLARGE**(2.-B))*A3)-A1
C     INITIAL GUESS OF VSMALL IS VERY SMALL
      VSMALL=0.00001
      ESMALL=(VSMALL*VSMALL*A2)+((VSMALL**(2.-B))*A3)-A1
C
C     NOTE THAT VSMALL GIVES RHS<0, AND VLARGE GIVES RHS>0, THEREFORE
C     THE SOLUTION IS SOMEWHERE BETWEEN.
C
      LOOP=0
100   CONTINUE
      LOOP=LOOP+1
      IF(LOOP.EQ.20)STOP
      VMED=(VLARGE+VSMALL)/2.
      EMED=(VMED*VMED*A2)+((VMED**(2.-B))*A3)-A1
      IF(EMED.GT.0.)GO TO 200
C     UPDATE VSMALL
      VSMALL=VMED
      ERROR=ABS((VLARGE-VSMALL)/VMED)
      IF(ERROR.LT.0.00001)GO TO 300
      ESMALL=EMED
      GO TO 100
200   CONTINUE
C     UPDATE VLARGE
      VLARGE=VMED
      ERROR=ABS((VLARGE-VSMALL)/VMED)
      IF(ERROR.LT.0.00001)GO TO 300
      ELARGE=EMED
      GO TO 100
300   CONTINUE
      IF(IKLOSS.NE.0)V1CL=(VLARGE+VSMALL)/2.
C
C     THE COOLANT VELOCITY IS APPROXIMATELY KNOWN
C
C COMPUTE MISC. STUFF
      REL=RHOFLL*V1CL*DE/MUFLUL
      RESTAL=RHOFLL*V1CL*DLE/MUFLUL
C     REMEMBER THAT B IS NEGATIVE
      FAPP=A/(RESTAL**B)
      LPLUS=(L/DE)/REL
      V1CX=V1CL*RHOFLL/RHOFLX
      REX=RHOFLX*V1CX*DE/MUFLUX
      RESTAX=RHOFLX*V1CX*DLE/MUFLUX
      XSTARL=L/(DE*REL*PRFLUL)
      XSTARX=X/(DE*REX*PRFLUX)
C COMPUTE FLOW STUFF
      NCHAN=0.01/(WW+WC)
      NPARAL=0.01/L
      VOLUME=(V1CL*WC*Z)*(NCHAN*NPARAL)
      PPOWER=VOLUME*DELP
```

```
      RETURN
C
2000  CONTINUE
C
C                          ******************************
C                          * VOLUMETRIC FLOW RATE FIXED *
C                          ******************************
C
C NONUNIFORM PROPERTIES - EQN. 2.24
      FACT=(MUFILA/MUFLLA)**0.25
C COMPUTE COOLANT VELOCITY - EQN. 4.19
      V1CL=VOLUME*10000.*(L*(WW+WC))/(WC*Z)
C COMPUTE MISC. STUFF
      REL=V1CL*RHOFLL*DE/MUFLUL
      RESTAL=V1CL*RHOFLL*DLE/MUFLUL
      LPLUS=(L/DE)/REL
      V1CX=V1CL*RHOFLL/RHOFLX
      REX=RHOFLX*V1CX*DE/MUFLUX
      RESTAX=RHOFLX*V1CX*DLE/MUFLUX
      XSTARL=L/(DE*REL*PRFLUL)
      XSTARX=X/(DE*REX*PRFLUX)
C DETERMINE ENTRANCE AND EXIT PRESSURE LOSS COEFFICIENTS
      CALL ABRUPT(ACBYAP,ASPECT,IFLOW,IKLOSS,KC,KE,K90,LPLUS)
C DETERMINE APPARENT FRICTION FACTOR - EQN. 2.6
      A=0.09290+(1.01612/(L/DE))
      B=0.26800+(0.31930/(L/DE))
C     REMEMBER THAT B IS NEGATIVE
      FAPP=A/(RESTAL**B)
C DETERMINE PRESSURE DROP - EQN. 2.9
      DELP=(RHOFLL*V1CL*V1CL/2.)*
     *(((ACBYAP**2.)*2.*K90)+(KC+KE)+(4.*FAPP*FACT*L/DE))
      PPOWER=VOLUME*DELP
      RETURN
3000  CONTINUE
C
C                          ******************************
C                          *    PUMPING POWER FIXED     *
C                          ******************************
C
C DETERMINE ENTRANCE AND EXIT PRESSURE LOSS COEFFICIENTS
      CALL ABRUPT(ACBYAP,ASPECT,IFLOW,IKLOSS,KC,KE,K90,LPLUS)
C NONUNIFORM PROPERTIES - EQN. 2.24
      FACT=(MUFILA/MUFLLA)**0.25
C COMPUTE FRICTION FACTOR - EQN. 2.6 -  REMEMBER THAT B IS NEGATIVE
      A=0.09290+(1.01612/(L/DE))
      B=0.26800+(0.31930/(L/DE))
C CONSTANTS FOR PRESSURE DROP EQUATION 4.20
C     NOTE THAT V**3=(A1)/(A2+A3*V**(-B))
      A1=(PPOWER*2.*1./RHOFLL)*(10000.*L*(WW+WC)/(WC*Z))
      A2=(ACBYAP*ACBYAP*2.*K90)+(KC+KE)
      A3=(4.*L/DE)*A/((RHOFLL*DLE/MUFLUL)**B)
      IF(IKLOSS.EQ.0)V1CL=(A1/A3)**(1./(3.-B))
      IF(IKLOSS.EQ.0)GO TO 3300
C
C     TRIAL AND ERROR ESTIMATION OF V1C
C     EQUATION 4.20 GIVES V**3=(A1)/(A2+A3*V**(-B))
C     WHICH CAN BE REARRANGED TO (V**3)*A2+(V**(3-B))*A3-A1=0
C
C     VLARGE: ASSUMES K90=KC=KE=0.
      VLARGE=(A1/A3)**(1./(3.-B))
```

```
      ELARGE=(VLARGE*VLARGE*VLARGE*A2)+((VLARGE**(3.-B))*A3)-A1
C     INITIAL GUESS OF VSMALL IS VERY SMALL
      VSMALL=0.00001
      ESMALL=(VSMALL*VSMALL*VSMALL*A2)+((VSMALL**(3.-B))*A3)-A1
C
C     NOTE THAT VSMALL GIVES RHS<0, AND VLARGE GIVES RHS>0, THEREFORE
C     THE SOLUTION IS SOMEWHERE BETWEEN.
C
      LOOP=0
3100  CONTINUE
      LOOP=LOOP+1
      IF(LOOP.EQ.20)STOP
      VMED=(VLARGE+VSMALL)/2.
      EMED=(VMED*VMED*VMED*A2)+((VMED**(3.-B))*A3)-A1
      IF(EMED.GT.0.)GO TO 3200
C     UPDATE VSMALL
      VSMALL=VMED
      ERROR=ABS((VLARGE-VSMALL)/VMED)
      IF(ERROR.LT.0.00001)GO TO 3300
      ESMALL=EMED
      GO TO 3100
3200  CONTINUE
C     UPDATE VLARGE
      VLARGE=VMED
      ERROR=ABS((VLARGE-VSMALL)/VMED)
      IF(ERROR.LT.0.00001)GO TO 3300
      ELARGE=EMED
      GO TO 3100
3300  CONTINUE
      IF(IKLOSS.NE.0)V1CL=(VLARGE+VSMALL)/2.
C
C     THE COOLANT VELOCITY IS APPROXIMATELY KNOWN
C
C COMPUTE MISC. STUFF
      REL=RHOFLL*V1CL*DE/MUFLUL
      RESTAL=RHOFLL*V1CL*DLE/MUFLUL
      V1CX=V1CL*RHOFLL/RHOFLX
      REX=RHOFLX*V1CX*DE/MUFLUX
      RESTAX=RHOFLX*V1CX*DLE/MUFLUX
      XSTARL=L/(DE*REL*PRFLUL)
      XSTARX=X/(DE*REX*PRFLUX)
      LPLUS=(L/DE)/REL
C COMPUTE FRICTION FACTOR - EQN. 2.6 - REMEMBER THAT B IS NEGATIVE
      FAPP=A/(RESTAL**B)
      CALL ABRUPT(ACBYAP,ASPECT,IFLOW,IKLOSS,KC,KE,K90,LPLUS)
C COMPUTE PRESSURE DROP - EQN. 2.9
      DELP=(RHOFLL*V1CL*V1CL/2.)*((ACBYAP*ACBYAP*2.*K90)+(KC+KE)
     &                            +(4.*FAPP*FACT*L/DE))
C COMPUTE VOLUMETRIC FLOW RATE
      NCHAN=0.01/(WW+WC)
      NPARAL=0.01/L
      VOLUME=(V1CL*WC*Z)*(NCHAN*NPARAL)
      RETURN
      END
C END OF FILE FOR SUBROUTINE STURF
C-----------------------------------------------------------------------
C  RTURF:  WRITTEN BY RICHARD J. PHILLIPS.  RTURF COMPUTES THE REPEATED-
C          RIB ROUGHENED CHANNEL COOLANT VELOCITY AND SOME OTHER
C          VARIABLES FOR TURBULENT FLOW.
C-----------------------------------------------------------------------
```

```
C ANALYSIS VARIABLES
C A1,A2,
C   A3,A4... DUMMY VARIABLES FOR TERMS OF EQUATION 2.16    (-)
C ACBYAP ... RATIO OF CHANNEL AND PLENUM CROSS-SECTIONAL
C                AREAS                                      (-)
C ASPECT ... CHANNEL ASPECT RATIO                           (-)
C DE     ... CHANNEL HYDRAULIC DIAMETER                     (M)
C DELP   ... ASSUMED CHANNEL PRESSURE LOSS                  (N/M*2)
C EBYDE  ... RATIO OF RIB HEIGHT TO EQUIVALENT DIAMETER     (-)
C EPLUS  ... ROUGHNESS REYNOLDS NUMBER                      (-)
C EPLUS1 ... PREVIOUS ROUGHNESS REYNOLDS NUMBER             (-)
C ERROR  ... RELATIVE ERROR IN ROUGHNESS REYNOLDS NUMBER    (-)
C FO     ... SMOOTH CHANNEL FRICTION FACTOR                 (-)
C F1     ... ONE SIDE ROUGHENED FRICTION FACTOR             (-)
C F2     ... BOTH SIDES ROUGHENED FRICTION FACTOR           (-)
C FACT   ... VARIABLE PROPERTIES COMPENSATION FACTOR        (-)
C FAPP   ... APPARANT FRICTION FACTOR                       (-)
C ICONS  ... CONTROL FOR WHICH FLOW CONSTRAINT IS USED      (-)
C IFLOW  ... ACTIVE LOOP INDICATOR FOR FLOW REGIME          (-)
C IKLOSS ... CONTROL FOR INCLUDING K90, KC, AND KE          (-)
C IRETUR ... CONTROL VARIABLE FOR OUT OF RANGE DATA         (-)
C KC     ... ENTRANCE PRESSURE LOSS COEFFICIENT             (-)
C KE     ... EXIT PRESSURE LOSS COEFFICIENT                 (-)
C K90    ... NINETY DEGREE BEND PRESSURE LOSS COEFFICIENT   (-)
C L      ... CHANNEL LENGTH                                 (M)
C LOOP   ... DUMMY COUNTER                                  (-)
C LPLUS  ... MOMENTUM ENTRY LENGTH                          (-)
C MUFILA ... AVERAGE COOLANT DYNAMIC VISCOSITY AT THE
C              AVERAGE FIN TEMPERATURE BETWEEN THE
C              CHANNEL ENTRANCE AND EXIT                    (KG/M S)
C MUFLLA ... AVERAGE COOLANT DYNAMIC VISCOSITY AT THE
C              AVERAGE COOLANT TEMPERATURE BETWEEN THE
C              CHANNEL ENTRANCE AND EXIT                    (KG/M S)
C MUFLUL ... COOLANT DYNAMIC VISCOSITY AT CHANNEL EXIT      (KG/M S)
C MUFLUX ... COOLANT DYNAMIC VISCOSITY AT POSITION X        (KG/M S)
C PBYE   ... RATIO OF RIB SEPARATION TO RIB HEIGHT          (-)
C PHI    ... REPEATED-RIB FLOW ATTACK ANGLE                 (DEGREES)
C PPOWER ... COOLANT PUMPING POWER PER UNIT SURFACE AREA    (W/CM*2)
C PRFLUL ... COOLANT PRANDTL NUMBER AT CHANNEL EXIT         (-)
C PRFLUX ... COOLANT PRANDTL NUMBER AT POSITION X           (-)
C REPLUS ... ROUGHNESS FUNCTION                             (-)
C REL    ... REYNOLDS NUMBER AT CHANNEL EXIT                (-)
C REX    ... REYNOLDS NUMBER AT POSITION X                  (-)
C RHOFLL ... COOLANT DENSITY AT CHANNEL EXIT                (KG/M*3)
C RHOFLX ... COOLANT DENSITY AT POSITION X                  (KG/M*3)
C RESTAL ... MODIFIED REYNOLDS NUMBER AT CHANNEL EXIT       (-)
C RESTAX ... MODIFIED REYNOLDS NUMBER AT POSITION X         (-)
C V1CL   ... COOLANT FLOW VELOCITY AT CHANNEL EXIT          (M/S)
C V1CX   ... COOLANT FLOW VELOCITY AT POSITION X            (M/S)
C VOLUME ... COOLANT FLOW RATE PER UNIT SURFACE AREA        (M*3/CM*2)
C WC     ... CHANNEL WIDTH                                  (M)
C WW     ... FIN THICKNESS                                  (M)
C X      ... POSITION FROM CHANNEL ENTRANCE                 (M)
C XSTARL ... THERMAL ENTRY LENGTH AT CHANNEL EXIT           (-)
C XSTARX ... THERMAL ENTRY LENGTH AT POSITION X             (-)
C Z      ... FIN LENGTH                                     (M)
C ZI     ... REPEATED-RIB SHAPE ANGLE                       (DEGREES)
C-----------------------------------------------------------------------
      SUBROUTINE RTURF(IFLOW,WW,WC,Z,L,X,DE,DLE,ASPECT,ACBYAP,
     1                 RHOFLL,RHOFLX,MUFLUL,MUFLUX,MUFLLA,MUFILA,
```

```
     *                    PRFLUL,PRFLUX,IKLOSS,ICONS,DELP,VOLUME,PPOWER,
     *                    REL,REX,V1CL,V1CX,RESTAL,RESTAX,LPLUS,F1,F2,FAPP,
     *                    XSTARL,XSTARX,IRETUR,EBYDE,PBYE,ZI,PHI)
      REAL L,K90,KC,KE,LPLUS,MUFLUL,MUFLUX,MUFLLA,MUFILA
C
C CHECK IF CORRECT ASPECT RATIO
C
      IF((ASPECT.GT.0.1).AND.(ASPECT.LT.10.))RETURN
C
C DETERMINE COOLANT FLOW RATE CONSTRAINT
C  1) DELP FIXED
         IF(ICONS.EQ.1)RETURN
C  2) VOLUME FIXED
         IF(ICONS.EQ.2)GO TO 10
C  3) PUMPING POWER FIXED
         IF(ICONS.EQ.3)RETURN
C
10    CONTINUE
C
C                         ******************************
C                         * VOLUMETRIC FLOW RATE FIXED *
C                         ******************************
C
C COMPUTE COOLANT VELOCITY - EQN. 4.19
      V1CL=VOLUME*10000.*(L*(WW+WC))/(Z*WC)
      REL=V1CL*RHOFLL*DE/MUFLUL
      LPLUS=(L/DE)/REL
C CHECK IF THE VARIABLES ARE WITHIN THE VALID RANGE
      IRETUR=0
      IF((REL.LT.3000.).OR.(REL.GT.30000))IRETUR=1
      IF((EBYDE.LT.0.032).OR.(EBYDE.GT.0.102))IRETUR=1
      IF(IRETUR.EQ.1)RETURN
C
C     BOTH SIDES ROUGHENED FRICTION FACTOR OBTAINED USING EQUATION 2.16
C
C FOLLOW STUFF FROM EQN. 2.16
      A1=(PHI/90.)**0.35
      IF(PBYE.LT.10.)A2=1./((10./PBYE)**0.13)
      IF(PBYE.GE.10.)A2=(10./PBYE)**(0.53*((ZI/90.)**0.71))
      A3=(ZI/45.)**0.57
C ASSUME EPLUS >= 35
      A4=4.9
      REPLUS=A4/(A1*A2*A3)
      F2=2./((REPLUS-(2.5*ALOG(2.*EBYDE))-3.75)**2.)
      EPLUS=EBYDE*REL*SQRT(F2/2.)
C CHECK ASSUMPTION ON EPLUS
      IF(EPLUS.GE.35.)GO TO 500
C
C     ASSUMPTION ON EPLUS WAS WRONG - USE TRIAL AND ERROR TO OBTAIN
C     THE CORRECT VALUE OF EPLUS.
C
      LOOP=0
100   CONTINUE
      LOOP=LOOP+1
      IF(LOOP.GT.20)STOP
      EPLUS1=EPLUS
      A4=4.9/((EPLUS1/35.)**0.4)
      REPLUS=A4/(A1*A2*A3)
      F2=2./((REPLUS-(2.5*ALOG(2.*EBYDE))-3.75)**2.)
      EPLUS=EBYDE*REL*SQRT(F2/2.)
```

```
C     CHECK ERROR
      ERROR=ABS((EPLUS-EPLUS1)/EPLUS1)
      IF(ERROR.GT.0.0001)GO TO 100
500   CONTINUE
C
C     APPARENT FRICTION FACTOR IS APPROXIMATELY KNOWN
C
      FAPP=F2
C DETERMINE ENTRANCE AND EXIT PRESSURE LOSS COEFFICIENTS
      CALL ABRUPT(ACBYAP,ASPECT,IFLOW,IKLOSS,KC,KE,K90,LPLUS)
C NONUNIFORM PROPERTIES - EQN. 2.24
      FACT=(MUFILA/MUFLLA)**0.25
      IF(ASPECT.GE.10.)GO TO 1000
C SMALL ASPECT RATIO DUCT PRESSURE DROP - ONLY ONE SIDE IS ROUGHENED
C USE INSTEAD, EQUATIONS 2.17 AND 2.18.
      F0=0.079/(REL**0.25)
      F1=F0+(F2-F0)/2.
      FAPP=F1
1000  CONTINUE
C COMPUTE PRESSURE DROP - EQN. 2.9
      DELP=(RHOFLL*V1CL*V1CL/2.)*
     &((ACBYAP*ACBYAP*2.*K90)+(KC+KE)+(4.*FAPP*FACT*L/DE))
      PPOWER=VOLUME*DELP
C COMPUTE MISC. STUFF
      V1CX=V1CL*RHOFLL/RHOFLX
      REX=RHOFLX*V1CX*DE/MUFLUX
      RESTAL=RHOFLL*V1CL*DLE/MUFLUL
      RESTAX=RHOFLX*V1CX*DLE/MUFLUX
      XSTARL=L/(DE*REL*PRFLUL)
      XSTARX=X/(DE*REX*PRFLUX)
      RETURN
      END
C END OF FILE FOR SUBROUTINE RTURF
C-----------------------------------------------------------------------
C SNUFD:   WRITTEN BY RICHARD J. PHILLIPS.  SFFD COMPUTES THE SMOOTH-
C          CHANNEL NUSSELT NUMBER ASSUMING FULLY DEVELOPED FLOW ALWAYS.
C-----------------------------------------------------------------------
C ANALYSIS VARIABLES
C ASPECT ... CHANNEL ASPECT RATIO(FIN LENGTH/CHANNEL WIDTH)(-)
C FACT   ... VARIABLE PROPERTIES COMPENSATION FACTOR        (-)
C IRETUR ... CONTROL VARIABLE FOR OUT OF RANGE PROP. DATA   (-)
C MUFILA ... AVERAGE COOLANT DYNAMIC VISCOSITY AT THE
C              AVERAGE FIN TEMPERATURE BETWEEN THE
C              CHANNEL ENTRANCE AND EXIT                    (KG/M S)
C MUFIXA ... AVERAGE COOLANT DYNAMIC VISCOSITY AT THE
C              AVERAGE FIN TEMPERATURE BETWEEN THE
C              CHANNEL ENTRANCE AND POSITION X              (KG/M S)
C MUFLLA ... AVERAGE COOLANT DYNAMIC VISCOSITY AT THE
C              AVERAGE COOLANT TEMPERATURE BETWEEN THE
C              CHANNEL ENTRANCE AND EXIT                    (KG/M S)
C MUFLXA ... AVERAGE COOLANT DYNAMIC VISCOSITY AT THE
C              AVERAGE COOLANT TEMPERATURE BETWEEN THE
C              CHANNEL ENTRANCE AND POSITION X              (KG/M S)
C NUL    ... NUSSELT NUMBER AT CHANNEL EXIT                 (-)
C NUX    ... NUSSELT NUMBER AT CHANNEL POSITION X           (-)
C NUTL   ... NUSSELT NUMBER AT CHANNEL EXIT INCUDING
C              EFFECT OF NONUNIFORM COOLANT TEMPERATURE     (-)
C NUTX   ... NUSSELT NUMBER AT CHANNEL POSITION X INCUDING
C              EFFECT OF NONUNIFORM COOLANT TEMPERATURE     (-)
C-----------------------------------------------------------------------
```

```
      SUBROUTINE SNUFD(ASPECT,NUL,NUX,NUTL,NUTX,
     &                 MUFILA,MUFIXA,MUFLLA,MUFLXA,IRETUR)
      REAL NUL,NUX,NUTL,NUTX,MUFILA,MUFIXA,MUFLLA,MUFLXA
      IRETUR=0
C INTERPOLATION EQUATIONS FOR FULLY-DEVELOPED FLOW DETERMINED USING
C HP41C PROGRAM (SUM)POLYC, AND TABLE 2.8
      IF(ASPECT.GE.10.)NUL=
     & 8.229-(10.9893/ASPECT)+(14.7321/(ASPECT**2.))-(9.75/(ASPECT**3.))
      IF((ASPECT.GE.1.).AND.(ASPECT.LT.10.))NUL=
     & 8.227-(14.6284/ASPECT)+(21.5484/(ASPECT**2.))-(14.4/(ASPECT**3.))
      IF((ASPECT.GE.0.1).AND.(ASPECT.LT.1.0))IRETUR=1
      IF(ASPECT.LT.0.1)NUL=
     & 1.6607+(1.2740/ASPECT)-(0.1954/(ASPECT**2.))+(0.01/(ASPECT**3.))
      IF(IRETUR.EQ.1)RETURN
C ACCOUNT FOR VARIABLE PROPERTIES - EQN. 2.25
      NUX=NUL
      FACT=(MUFLLA/MUFILA)**0.14
      NUTL=NUL*FACT
      FACT=(MUFLXA/MUFIXA)**0.14
      NUTX=NUX*FACT
      RETURN
      END
C END OF FILE FOR SUBROUTINE SNUFD
C-----------------------------------------------------------------------
C SLAMNU:  WRITTEN BY RICHARD J. PHILLIPS.  SLAMNU COMPUTES THE SMOOTH
C          CHANNEL FULLY DEVELOPED/DEVELOPING LAMINAR NUSSELT NUMBER.
C-----------------------------------------------------------------------
C ANALYSIS PARAMETERS
C ASPEC  ... CHANNEL ASPECT RATIO DATA FOR NNUX                 (-)
C ASPECT ... CHANNEL ASPECT RATIO                               (-)
C DUMNUX ... ARRAY OF DEVELOPING-FLOW, LAMINAR NUSSELT
C              NUMBERS AT ASPECT.                               (-)
C F3TO4  ... RATIO OF FULLY-DEVELOPED 3-SIDE AND 4-SIDE
C              HEATED CHANNELS.                                 (-)
C FACT   ... PROPERTY RATIO METHOD INTERPOLATION FACTOR         (-)
C FACTOR ... INTERPOLATION VARIABLE                             (-)
C MUFILA ... AVERAGE COOLANT DYNAMIC VISCOSITY AT THE
C              AVERAGE FIN TEMPERATURE BETWEEN THE
C              CHANNEL ENTRANCE AND EXIT                        (KG/M S)
C MUFIXA ... AVERAGE COOLANT DYNAMIC VISCOSITY AT THE
C              AVERAGE FIN TEMPERATURE BETWEEN THE
C              CHANNEL ENTRANCE AND POSITION X                  (KG/M S)
C MUFLLA ... AVERAGE COOLANT DYNAMIC VISCOSITY AT THE
C              AVERAGE COOLANT TEMPERATURE BETWEEN THE
C              CHANNEL ENTRANCE AND EXIT                        (KG/M S)
C MUFLXA ... AVERAGE COOLANT DYNAMIC VISCOSITY AT THE
C              AVERAGE COOLANT TEMPERATURE BETWEEN THE
C              CHANNEL ENTRANCE AND POSITION X                  (KG/M S)
C NNU3   ... FULLY-DEVELOPED, LAMINAR NUSSELT NUMBER DATA
C               FOR 3-SIDED CHANNELS.                           (-)
C NNU4   ... FULLY-DEVELOPED, LAMINAR NUSSELT NUMBER DATA
C               FOR 4-SIDED CHANNELS.                           (-)
C NNUX   ... DEVELOPING-FLOW, LAMINAR NUSSELT NUMBER DATA
C              FOR CHANNELS WITH ALL FOUR SIDES HEATED.         (-)
C NU3    ... 3-SIDE HEATED MODERATE ASPECT RATIO DUCT NU        (-)
C NU4    ... 4-SIDE HEATED MODERATE ASPECT RATIO DUCT NU        (-)
C NUL    ... NUSSELT NUMBER AT CHANNEL EXIT                     (-)
C NUX    ... NUSSELT NUMBER AT CHANNEL POSITION X               (-)
C NUTL   ... NUSSELT NUMBER AT CHANNEL EXIT INCUDING
C              EFFECT OF NONUNIFORM COOLANT TEMPERATURE         (-)
```

```
C NUTX   ... NUSSELT NUMBER AT CHANNEL POSITION X INCUDING
C              EFFECT OF NONUNIFORM COOLANT TEMPERATURE    (-)
C WWCBYZ ... CHANNEL ASPECT RATIO DATA FOR NNU3 AND NNU4.  (-)
C XSTARL ... THERMAL ENTRY LENGTH AT CHANNEL EXIT          (-)
C XSTARX ... THERMAL ENTRY LENGTH AT POSITION X            (-)
C XTHERM ... THERMAL ENTRANCE LENGTH DATA FOR NNUX         (-)
C----------------------------------------------------------------------
      SUBROUTINE SLAMNU(ASPECT,MUFLLA,MUFILA,XSTARL,NUL,NUTL,
     &                          MUFLXA,MUFIXA,XSTARX,NUX,NUTX)
      DIMENSION ASPEC(6),NNUX(6,19),XTHERM(19),NNU3(11),NNU4(11),
     &          WWCBYZ(11),DUMNUX(19)
      REAL MUFLLA,MUFLXA,MUFILA,MUFIXA,NUL,NUX,NUTL,NUTX,
     &     NNUX,NU3,NNU3,NU4,NNU4
C DATA FOR NNUX, ASPEC, AND XTHERM OBTAINED FROM TABLE 2.11, AND APPLY
C     FOR FOUR-SIDED CHANNELS WITH ALL FOUR WALLS HEATING DEVELOPING
C     FLOW.
C DATA POINTS BETWEEN 0.005 AND 0. WERE EXPONENTIALLY EXTRAPOLATED TO
C     PROVIDE LESS 'WAVINESS' IN THE RESULTS
      DATA NNUX/
     &          31.6,25.2,23.7,27.0,26.7,31.4,
     &          18.8,15.0,14.7,16.4,16.6,19.3,
     &          15.0,12.0,12.0,13.2,13.6,15.7,
     &          13.2,10.5,10.6,11.7,12.0,13.9,
     &          12.0, 9.6, 9.8,10.7,11.1,12.7,
     &          11.2, 8.9, 9.2, 9.9,10.4,11.9,
     &           9.0,7.10,7.46,8.02,8.44,10.0,
     &           8.8,6.86,7.23,7.76,8.18, 9.8,
     &           8.5,6.60,6.96,7.50,7.92, 9.5,
     &           8.2,6.32,6.68,7.22,7.63, 9.3,
     &           7.9,6.02,6.37,6.92,7.32, 9.1,
     &          7.49,5.69,6.05,6.57,7.00,8.80,
     &           7.2,5.33,5.70,6.21,6.63, 8.6,
     &           6.7,4.91,5.28,5.82,6.26, 8.5,
     &           6.2,4.45,4.84,5.39,5.87, 8.4,
     &           5.9,4.18,4.61,5.17,5.77, 8.3,
     &          5.55,3.91,4.38,5.00,5.62,8.25,
     &           5.4,3.71,4.22,4.85,5.45,8.24,
     &          5.38,3.60,4.11,4.77,5.35,8.23/
      DATA ASPEC/0.1,1.,2.,3.,4.,10./
      DATA XTHERM/0.,.0005,.0010,.0015,.0020,.0025,
     &           .005,.00556,.00625,.00714,.00833,.01,.0125,
     &          .0167,.025,.033,.05,.1,1./
C DATA FOR NNU4, AND WWCBYZ WERE OBTAINED FROM TABLE 2.8, AND ARE
C     FOR FOUR-SIDED CHANNELS WITH ALL FOUR WALLS HEATING FULLY
C     DEVELOPED FLOW.
      DATA NNU4/3.599,3.612,3.655,3.740,3.884,4.111,4.457,4.969,
     &          5.704,6.700,8.235/
      DATA WWCBYZ/1.,1.11,1.25,1.43,1.67,2.,2.5,3.33,5.,10.,9999./
C DATA FOR NNU3, AND WWCBYZ WERE OBTAINED FROM TABLE 2.8, AND ARE
C     FOR FOUR-SIDED CHANNELS WITH THREE WALLS HEATING FULLY
C     DEVELOPED FLOW.
      DATA NNU3/3.556,3.701,3.846,3.991,4.248,4.505,4.885,5.393,
     &          6.072,6.939,8.235/
C
C DETERMINE IF MODERATE ASPECT RATIO DUCT
C
      IF((ASPECT.LE.ASPEC(1)).OR.(ASPECT.GE.ASPEC(6)))GO TO 210
C
C CALCULATE RATIO OF 4-SIDED AND 3-SIDED FULLY DEVELOPED VALUES FOR
C EQUATION 2.12.  NOTE THAT NO CORRECTION IS NEEDED FOR LARGE AND
```

```
C SMALL ASPECT RATIO CHANNELS.
      DO 100 I=1,10
         IF((ASPECT.GE.WWCBYZ(I)).AND.(ASPECT.LT.WWCBYZ(I+1)))GO TO 200
100   CONTINUE
200   CONTINUE
      FACTOR=(ASPECT-WWCBYZ(I))/(WWCBYZ(I+1)-WWCBYZ(I))
      NU3=FACTOR*(NNU3(I+1)-NNU3(I))+NNU3(I)
      NU4=FACTOR*(NNU4(I+1)-NNU4(I))+NNU4(I)
      F3TO4=NU3/NU4
210   CONTINUE
C
C INTERPOLATION BETWEEN COLUMNS OF NNUX AT PROPER CHANNEL ASPECT RATIO
C
C  SMALL ASPECT RATIO CHANNELS
      IF(ASPECT.GE.ASPEC(1))GO TO 250
      DO 225 II=1,19
         DUMNUX(II)=NNUX(1,II)
225   CONTINUE
      GO TO 475
250   CONTINUE
      IF(ASPECT.LE.ASPEC(6))GO TO 280
C  LARGE ASPECT RATIO CHANNELS
      DO 275 II=1,19
         DUMNUX(II)=NNUX(6,II)
275   CONTINUE
      GO TO 475
280   CONTINUE
C MODERATE ASPECT RATIO CHANNELS
      DO 300 I=1,5
         IF((ASPECT.GE.ASPEC(I)).AND.(ASPECT.LT.ASPEC(I+1)))GO TO 400
300   CONTINUE
400   CONTINUE
      FACTOR=(ASPECT-ASPEC(I))/(ASPEC(I+1)-ASPEC(I))
      DO 450 II=1,19
         DUMNUX(II)=FACTOR*(NNUX(I+1,II)-NNUX(I,II))+NNUX(I,II)
450   CONTINUE
475   CONTINUE
C
C INTERPOLATION BETWEEN ROWS AT THE CORRECT THERMAL ENTRANCE LENGTH AT
C THE CHANNEL EXIT
C
      DO 500 J=1,18
         IF((XSTARL.GE.XTHERM(J)).AND.(XSTARL.LT.XTHERM(J+1)))GO TO 600
500   CONTINUE
      IF(XSTARL.GE.XTHERM(19))J=19
600   CONTINUE
      IF(J.NE.19)FACTOR=(XSTARL-XTHERM(J))/(XTHERM(J+1)-XTHERM(J))
      IF(J.NE.19)NUL=FACTOR*(DUMNUX(J+1)-DUMNUX(J))+DUMNUX(J)
      IF(J.EQ.19)NUL=DUMNUX(19)
C COMPUTE DEVELOPING-FLOW, LAMINAR NUSSELT NUMBER USING EQUATION 2.12.
      IF((ASPECT.GT.ASPEC(1)).AND.(ASPECT.LT.ASPEC(6)))NUL=NUL*F3TO4
C ACCOUNT FOR NONUNIFORM PROPERTIES - EQN. 2.25
      FACT=(MUFLLA/MUFILA)**0.14
      NUTL=NUL*FACT
C
C INTERPOLATION BETWEEN ROWS AT THE CORRECT THERMAL ENTRANCE LENGTH AT
C POSITION X
C
      DO 700 J=1,18
         IF((XSTARX.GE.XTHERM(J)).AND.(XSTARX.LT.XTHERM(J+1)))GO TO 800
```

```
700   CONTINUE
      IF(XSTARX.GE.XTHERM(19))J=19
800   CONTINUE
      IF(J.NE.19)FACTOR=(XSTARX-XTHERM(J))/(XTHERM(J+1)-XTHERM(J))
      IF(J.NE.19)NUX=FACTOR*(DUMNUX(J+1)-DUMNUX(J))+DUMNUX(J)
      IF(J.EQ.19)NUX=DUMNUX(19)
C COMPUTE DEVELOPING-FLOW, LAMINAR NUSSELT NUMBER USING EQUATION 2.12.
      IF((ASPECT.GT.ASPEC(1)).AND.(ASPECT.LT.ASPEC(6)))NUX=NUX*F3TO4
C ACCOUNT FOR NONUNIFORM PROPERTIES - EQN. 2.25
      FACT=(MUFLXA/MUFIXA)**0.14
      NUTX=NUX*FACT
      RETURN
      END
C END OF FILE FOR SUBROUTINE SLAMNU
C-----------------------------------------------------------------------
C STURNU:  WRITTEN BY RICHARD J. PHILLIPS.  STURNU COMPUTES
C          THE TURBULENT NUSSELT NUMBER FOR FLOW IN A TUBE.
C-----------------------------------------------------------------------
C ANALYSIS VARIABLES
C DE     ... HYDRAULIC DIAMETER                                 (M)
C FACT   ... PROPERTY RATIO METHOD INTERPOLATION FACTOR         (-)
C L      ... CHANNEL LENGTH                                     (M)
C MUFILA ... AVERAGE COOLANT DYNAMIC VISCOSITY AT THE
C              AVERAGE FIN TEMPERATURE BETWEEN THE
C              CHANNEL ENTRANCE AND EXIT                        (KG/M S)
C MUFIXA ... AVERAGE COOLANT DYNAMIC VISCOSITY AT THE
C              AVERAGE FIN TEMPERATURE BETWEEN THE
C              CHANNEL ENTRANCE AND POSITION X                  (KG/M S)
C MUFLLA ... AVERAGE COOLANT DYNAMIC VISCOSITY AT THE
C              AVERAGE COOLANT TEMPERATURE BETWEEN THE
C              CHANNEL ENTRANCE AND EXIT                        (KG/M S)
C MUFLXA ... AVERAGE COOLANT DYNAMIC VISCOSITY AT THE
C              AVERAGE COOLANT TEMPERATURE BETWEEN THE
C              CHANNEL ENTRANCE AND POSITION X                  (KG/M S)
C NUL    ... NUSSELT NUMBER AT CHANNEL EXIT                     (-)
C NUX    ... NUSSELT NUMBER AT CHANNEL POSITION X               (-)
C NUTL   ... NUSSELT NUMBER AT CHANNEL EXIT INCUDING
C              EFFECT OF NONUNIFORM COOLANT TEMPERATURE         (-)
C NUTX   ... NUSSELT NUMBER AT CHANNEL POSITION X INCUDING
C              EFFECT OF NONUNIFORM COOLANT TEMPERATURE         (-)
C PRFLUL ... COOLANT PRANDTL NUMBER AT CHANNEL EXIT             (-)
C PRFLUX ... COOLANT PRANDTL NUMBER AT POSITION X               (-)
C REL    ... REYNOLDS NUMBER AT CHANNEL EXIT                    (-)
C REX    ... REYNOLDS NUMBER AT POSITION X                      (-)
C X      ... POSITION FROM CHANNEL ENTRANCE                     (M)
C-----------------------------------------------------------------------
      SUBROUTINE STURNU(MUFLLA,MUFILA,PRFLUL,REL,NUL,NUTL,
     *                  MUFLXA,MUFIXA,PRFLUX,REX,NUX,NUTX,DE,L,X)
      REAL MUFLLA,MUFLXA,MUFILA,MUFIXA,NUL,NUX,NUTL,NUTX,L
C DITTUS - BOELTER EQUATION
C     NUL=0.023*((REL)**0.8)*(PRFLUL**0.4)
C SIMPLIFIED GNIELINSKI CORRELATION FOR 1.5<PR<500. - EQN. 2.15
      IF(REL.LE.650.)NUL=1.0
      IF(REL.GT.650.)NUL=0.012*((REL**0.87)-280.)*(PRFLUL**0.4)
C NEXT LINE ACCOUNTS FOR DEVELOPING TURBULENT NUSSELT NUMBER
C     NUL=NUL*(1.+(DE/L)**(2./3.))
C ACCOUNT FOR NONUNIFORM PROPERTIES - EQN. 2.25
      FACT=(MUFLLA/MUFILA)**0.11
      NUTL=NUL*FACT
C DITTUS - BOELTER EQUATION
```

```
C     NUX=0.023*((REX)**0.8)*(PRFLUX**0.4)
C SIMPLIFIED GNIELINSKI CORRELATION FOR 1.5<PR<500. - EQN. 2.15
      IF(REX.LE.650.)NUX=1.0
      IF(REX.GT.650.)NUX=0.012*((REX**0.87)-280.)*(PRFLUX**0.4)
C NEXT LINE ACCOUNTS FOR DEVELOPING TURBULENT NUSSELT NUMBER
C     NUX=NUX*(1.+(DE/X)**(2./3.))
C ACCOUNT FOR NONUNIFORM PROPERTIES - EQN. 2.25
      FACT=(MUFLXA/MUFIXA)**0.11
      NUTX=NUX*FACT
      RETURN
      END
C END OF FILE FOR SUBROUTINE STURNU
C-----------------------------------------------------------------------
C RTURNU: WRITTEN BY RICHARD J. PHILLIPS.  RTURNU COMPUTES THE NUSSELT
C         NUMBER FOR REPEATED-RIB ROUGHENED CHANNELS.
C-----------------------------------------------------------------------
C ANALYSIS PARAMETERS
C A1,A2,A3.. DUMMY VARIABLES FOR TERMS OF EQUATION 2.19     (-)
C ASPECT ... CHANNEL ASPECT RATIO                           (-)
C EBYDE  ... RATIO OF RIB HEIGHT TO EQUIVALENT DIAMETER     (-)
C EPLUS  ... ROUGHNESS REYNOLDS NUMBER                      (-)
C F2     ... BOTH SIDES ROUGHENED FRICTION FACTOR           (-)
C FACT   ... PROPERTY RATIO METHOD INTERPOLATION FACTOR     (-)
C HEPLUS ... HEAT TRANSFER FUNCTION                         (-)
C MUFILA ... AVERAGE COOLANT DYNAMIC VISCOSITY AT THE
C              AVERAGE FIN TEMPERATURE BETWEEN THE
C              CHANNEL ENTRANCE AND EXIT                    (KG/M S)
C MUFLLA ... AVERAGE COOLANT DYNAMIC VISCOSITY AT THE
C              AVERAGE COOLANT TEMPERATURE BETWEEN THE
C              CHANNEL ENTRANCE AND EXIT                    (KG/M S)
C NUL    ... NUSSELT NUMBER AT CHANNEL EXIT                 (-)
C NUX    ... NUSSELT NUMBER AT CHANNEL POSITION X           (-)
C NUTL   ... NUSSELT NUMBER AT CHANNEL EXIT INCUDING
C              EFFECT OF NONUNIFORM COOLANT TEMPERATURE     (-)
C NUTX   ... NUSSELT NUMBER AT CHANNEL POSITION X INCUDING
C              EFFECT OF NONUNIFORM COOLANT TEMPERATURE     (-)
C PRFLUL ... COOLANT PRANDTL NUMBER AT CHANNEL EXIT         (-)
C REL    ... REYNOLDS NUMBER AT CHANNEL EXIT                (-)
C REPLUS ... ROUGHNESS FUNCTION                             (-)
C STANTO ... AVERAGE STANTON NUMBER                         (-)
C ZI     ... REPEATED-RIB SHAPE ANGLE                       (DEGREES)
C-----------------------------------------------------------------------
      SUBROUTINE RTURNU(ASPECT,EBYDE,ZI,MUFLLA,MUFILA,PRFLUL,REL,F2,
     &                  NUL,NUTL,NUX,NUTX)
      REAL MUFLLA,MUFILA,NUL,NUX,NUTL,NUTX
C
C CHECK IF CORRECT ASPECT RATIO
C
      IF((ASPECT.GT.0.1).AND.(ASPECT.LT.10.))RETURN
C COMPUTE STANTON NUMBER - EQN. 2.19
      EPLUS=EBYDE*REL*SQRT(F2/2.)
      REPLUS=(SQRT(2./F2))+(2.5*ALOG(2.*EBYDE))+3.75
      IF(ZI.LT.45.)A1=(ZI/45.)**0.5
      IF(ZI.GE.45.)A1=1./((ZI/45.)**0.45)
      IF(EPLUS.LT.35.)A2=10.
      IF(EPLUS.GE.35.)A2=10.*((EPLUS/35.)**0.28)
      A3=(0.72/PRFLUL)**0.57
      HEPLUS=A2/(A1*A3)
      STANTO=(F2/2.)/(((HEPLUS-REPLUS)*SQRT(F2/2.))+1.)
C COMPUTE NUSSELT NUMBER - EQN. 2.20
```

```
      NUL=STANTO*REL*PRFLUL
      NUX=NUL
C ACCOUNT FOR NONUNIFORM PROPERTIES - EQN 2.25
      FACT=(MUFLLA/MUFILA)**0.11
      NUTL=NUL*FACT
      NUTX=NUTL
      RETURN
      END
C END OF FILE FOR SUBROUTINE RTURNU
C-----------------------------------------------------------------------
C PROPER: WRITTEN BY RICHARD J. PHILLIPS.  PROPER
C         CALLS THE APPRIATE SUBROUTINES TO INITIALIZE THE COOLANT
C         AND SUBSTRATE MATERIAL PROPERTY DATA ARRAYS.
C-----------------------------------------------------------------------
C ANALYSIS VARIABLES
C CPFF   ... COOLANT SPECIFIC HEAT DATA                      (J/KG DEG K)
C FLUID  ... ALPHANUMERIC FOR COOLANT TYPE                   (-)
C KFF    ... COOLANT THERMAL CONDUCTIVITY DATA               (W/M DEG K)
C KWW    ... SUBSTRATE THERMAL CONDUCTIVITY DATA             (W/M DEG K)
C MUFF   ... COOLANT DYNAMIC VISCOSITY DATA                  (KG/M S)
C NFLUID ... COOLANT IDENTIFIER NUMBER                       (-)
C               1)  FC-77
C               2)  FREON
C               3)  WATER
C NPROPF ... NUMBER OF COOLANT DATA ENTRIES                  (-)
C NPROPW ... NUMBER OF SUBSTRATE MATERIAL DATA ENTRIES       (-)
C NSINK  ... SUBSTRATE MATERIAL INDENTIFIER NUMBER           (-)
C               1)  GALLIUM ARSENIDE
C               2)  GERMANIUM
C               3)  INDIUM PHOSPHIDE
C               4)  SILICON
C               5)  ALUMINUM
C               6)  COPPER
C               7)  SILVER
C PRFF   ... COOLANT PRANDTL NUMBER DATA                     (-)
C RHOFF  ... COOLANT DENSITY DATA                            (KG/M*3)
C SINK   ... ALPHANUMERIC FOR SUBSTRATE TYPE                 (-)
C TPROPF ... TEMPERATURES FOR FLUID PROPERTY DATA            (DEG K)
C TPROPW ... TEMPERATURES FOR SUBSTRATE PROPERTY DATA        (DEG K)
C-----------------------------------------------------------------------
      SUBROUTINE PROPER(NFLUID,NSINK,FLUID,SINK,
     &                  NPROPF,TPROPF,CPFF,KFF,MUFF,PRFF,RHOFF,
     &                  NPROPW,TPROPW,KWW)
      DIMENSION TPROPF(20),CPFF(20),KFF(20),MUFF(20),PRFF(20),RHOFF(20)
      DIMENSION TPROPW(20),KWW(20)
      CHARACTER*4 FLUID(3),SINK(4)
      REAL KFF,KWW,MUFF
C CALL PROPER SUBROUTINES FOR COOLANT AND SUBSTRATE PROPERTIES
C     COOLANT
      IF(NFLUID.EQ.1)CALL PROPF1(NPROPF,TPROPF,CPFF,KFF,MUFF,PRFF,RHOFF,
     &FLUID)
      IF(NFLUID.EQ.2)CALL PROPF2(NPROPF,TPROPF,CPFF,KFF,MUFF,PRFF,RHOFF,
     &FLUID)
      IF(NFLUID.EQ.3)CALL PROPF3(NPROPF,TPROPF,CPFF,KFF,MUFF,PRFF,RHOFF,
     &FLUID)
C     SUBSTRATE
      IF(NSINK.EQ.1)CALL PROPS1(NPROPW,TPROPW,KWW,SINK)
      IF(NSINK.EQ.2)CALL PROPS2(NPROPW,TPROPW,KWW,SINK)
      IF(NSINK.EQ.3)CALL PROPS3(NPROPW,TPROPW,KWW,SINK)
      IF(NSINK.EQ.4)CALL PROPS4(NPROPW,TPROPW,KWW,SINK)
```

```
      IF(NSINK.EQ.5)CALL PROPS5(NPROPW,TPROPW,KWW,SINK)
      IF(NSINK.EQ.6)CALL PROPS6(NPROPW,TPROPW,KWW,SINK)
      IF(NSINK.EQ.7)CALL PROPS7(NPROPW,TPROPW,KWW,SINK)
      RETURN
      END
C END OF FILE FOR SUBROUTINE PROPER
C-----------------------------------------------------------------------
C PROPF1:  WRITTEN BY RICHARD J. PHILLIPS.  PROPF1 CONTAINS
C          THE COOLANT PROPERTY DATA FOR FC-77 AS TAKEN FROM
C          3M PRODUCT MANUAL (1984).
C-----------------------------------------------------------------------
C ANALYSIS VARIABLES
C CPF     ... COOLANT SPECIFIC HEAT DATA                     (J/KG DEG K)
C FLUID   ... ALPHANUMERIC FOR COOLANT TYPE                  (-)
C KF      ... COOLANT THERMAL CONDUCTIVITY DATA              (W/M DEG K)
C MUF     ... COOLANT DYNAMIC VISCOSITY DATA                 (KG/M S)
C NPROPF  ... NUMBER OF COOLANT DATA ENTRIES                 (-)
C PRF     ... COOLANT PRANDTL NUMBER DATA                    (-)
C RHOF    ... COOLANT DENSITY DATA                           (KG/M*3)
C TPROPF  ... TEMPERATURES FOR FLUID PROPERTY DATA           (DEG K)
C-----------------------------------------------------------------------
      SUBROUTINE PROPF1(NPROPF,TPROPF,CPFF,KFF,MUFF,PRFF,RHOFF,FLUID)
      DIMENSION TPROPF(20),CPFF(20),KFF(20),MUFF(20),PRFF(20),RHOFF(20)
      DIMENSION TPROP(9),CPF(9),KF(9),MUF(9),PRF(9),RHOF(9)
      CHARACTER*4 FLUID(3),FLU(3)
      REAL KF,KFF,MUF,MUFF
      DATA FLU  /'FC-7','7   ','    '/
      DATA TPROP/ 273., 283., 293., 303., 313., 323., 333., 343., 353./
      DATA CPF  /1010.,1025.,1040.,1055.,1070.,1085.,1100.,1115.,1130./
      DATA KF   /.0651,.0643,.0635,.0627,.0619,.0611,.0603,.0595,.0588/
      DATA MUF  /.00230,.00188,.00155,.00129,.00109,.00093,.00080,
     &           .00071,.00062/
      DATA PRF  / 35.6, 30.0, 25.4, 21.7, 18.8, 16.5, 14.6, 13.3, 11.9/
      DATA RHOF /1836.,1812.,1786.,1762.,1737.,1713.,1687.,1663.,1638./
      NPROPF=9
C TRANSFER VALUES
      DO 10 I=1,3
         FLUID(I)=FLU(I)
10    CONTINUE
      DO 100 I=1,NPROPF
         TPROPF(I)=TPROP(I)
         CPFF(I)=CPF(I)
         KFF(I)=KF(I)
         MUFF(I)=MUF(I)
         PRFF(I)=PRF(I)
         RHOFF(I)=RHOF(I)
100   CONTINUE
      RETURN
      END
C END OF FILE FOR SUBROUTINE PROPF1
C-----------------------------------------------------------------------
C PROPF2:  WRITTEN BY RICHARD J. PHILLIPS.  PROPF2 CONTAINS
C          THE COOLANT PROPERTY DATA FOR FREON (CCL2F2) AS TAKEN FROM
C          HOLMAN (1976).
C-----------------------------------------------------------------------
C ANALYSIS VARIABLES
C CPF     ... COOLANT SPECIFIC HEAT DATA                     (J/KG DEG K)
C FLUID   ... ALPHANUMERIC FOR COOLANT TYPE                  (-)
C KF      ... COOLANT THERMAL CONDUCTIVITY DATA              (W/M DEG K)
C MUF     ... COOLANT DYNAMIC VISCOSITY DATA                 (KG/M S)
```

```
C NPROPF ... NUMBER OF COOLANT DATA ENTRIES                   (-)
C PRF    ... COOLANT PRANDTL NUMBER DATA                      (-)
C RHOF   ... COOLANT DENSITY DATA                             (KG/M*3)
C TPROPF ... TEMPERATURES FOR FLUID PROPERTY DATA             (DEG K)
C-----------------------------------------------------------------------
      SUBROUTINE PROPF2(NPROPF,TPROPF,CPFF,KFF,MUFF,PRFF,RHOFF,FLUID)
      DIMENSION TPROPF(20),CPFF(20),KFF(20),MUFF(20),PRFF(20),RHOFF(20)
      DIMENSION TPROP(6),CPF(6),KF(6),MUF(6),PRF(6),RHOF(6)
      CHARACTER*4 FLUID(3),FLU(3)
      REAL KF,KFF,MUF,MUFF
      DATA FLU  /'FREO','N   ','    '/
      DATA TPROP/   223.,    243.,    263.,    283.,    303.,    323./
      DATA CPF  /   875.,    896.,    920.,    950.,    984.,   1022./
      DATA KF   /   .067,    .069,    .073,    .073,    .071,    .067/
      DATA MUF  /.000480,.000377,.000316,.000277,.000251,.000231/
      DATA PRF  /    6.2,     4.8,     4.0,     3.6,     3.5,     3.5/
      DATA RHOF /  1547.,   1490.,   1429.,   1364.,   1295.,   1216./
      NPROPF=6
C TRANSFER VALUES
      DO 10 I=1,3
         FLUID(I)=FLU(I)
10    CONTINUE
      DO 100 I=1,NPROPF
         TPROPF(I)=TPROP(I)
         CPFF(I)=CPF(I)
         KFF(I)=KF(I)
         MUFF(I)=MUF(I)
         PRFF(I)=PRF(I)
         RHOFF(I)=RHOF(I)
100   CONTINUE
      RETURN
      END
C END OF FILE FOR SUBROUTINE PROPF2
C-----------------------------------------------------------------------
C PROPF3:  WRITTEN BY RICHARD J. PHILLIPS.  PROPF3 CONTAINS
C          THE COOLANT PROPERTY DATA FOR WATER AS TAKEN FROM
C          HOLMAN (1976).
C-----------------------------------------------------------------------
C ANALYSIS VARIABLES
C CPF    ... COOLANT SPECIFIC HEAT DATA                       (J/KG DEG K)
C FLUID  ... ALPHANUMERIC FOR COOLANT TYPE                    (-)
C KF     ... COOLANT THERMAL CONDUCTIVITY DATA                (W/M DEG K)
C MUF    ... COOLANT DYNAMIC VISCOSITY DATA                   (KG/M S)
C NPROPF ... NUMBER OF COOLANT DATA ENTRIES                   (-)
C PRF    ... COOLANT PRANDTL NUMBER DATA                      (-)
C RHOF   ... COOLANT DENSITY DATA                             (KG/M*3)
C TPROPF ... TEMPERATURES FOR FLUID PROPERTY DATA             (DEG K)
C-----------------------------------------------------------------------
      SUBROUTINE PROPF3(NPROPF,TPROPF,CPFF,KFF,MUFF,PRFF,RHOFF,FLUID)
      DIMENSION TPROPF(20),CPFF(20),KFF(20),MUFF(20),PRFF(20),RHOFF(20)
      DIMENSION TPROP(7),CPF(7),KF(7),MUF(7),PRF(7),RHOF(7)
      CHARACTER*4 FLUID(3),FLU(3)
      REAL KF,KFF,MUF,MUFF
      DATA FLU  /'WATE','R   ','    '/
      DATA TPROP/  273.,  283.,  294.,   316.,   333.,   355.,   377./
      DATA CPF  / 4225., 4195., 4179.,  4174.,  4179.,  4195.,  4216./
      DATA KF   /  .566,  .585,  .604,   .637,   .654,   .673,   .684/
      DATA MUF  /.00179,.00131,.00098,.000616,.000471,.000347,.000267/
      DATA PRF  / 13.25,  9.40,  6.78,   4.04,   3.01,   2.16,   1.66/
      DATA RHOF / 999.8, 999.2, 997.4,  990.6,  983.3,  970.2,  955.1/
```

```
      NPROPF=7
C TRANSFER VALUES
      DO 10 I=1,3
         FLUID(I)=FLU(I)
10    CONTINUE
      DO 100 I=1,NPROPF
         TPROPF(I)=TPROP(I)
         CPFF(I)=CPF(I)
         KFF(I)=KF(I)
         MUFF(I)=MUF(I)
         PRFF(I)=PRF(I)
         RHOFF(I)=RHOF(I)
100   CONTINUE
      RETURN
      END
C END OF FILE FOR SUBROUTINE PROPF3
C-----------------------------------------------------------------------
C PROPS1:  WRITTEN BY RICHARD J. PHILLIPS.  PROPS1 CONTAINS
C          THE SUBSTRATE PROPERTY DATA FOR GALLIUM ARSENIDE AS TAKEN
C          FROM TYE (1969), NEUBERGER (1971), AND CARLSON ET AL. (1965).
C-----------------------------------------------------------------------
C ANALYSIS VARIABLES
C KW     ... COOLANT THERMAL CONDUCTIVITY DATA               (W/M DEG K)
C NPROPW ... NUMBER OF SUBSTRATE MATERIAL DATA ENTRIES       (-)
C MAT    ... ALPHANUMERIC FOR SUBSTRATE TYPE                 (-)
C TPROPW ... TEMPERATURES FOR FLUID PROPERTY DATA            (DEG K)
C-----------------------------------------------------------------------
      SUBROUTINE PROPS1(NPROPW,TPROPW,KWW,SINK)
      DIMENSION TPROPW(20),KWW(20)
      DIMENSION TPROP(8),KW(8)
      CHARACTER*4 SINK(4),MAT(4)
      REAL KW,KWW
      DATA MAT  /'GALL','IUM ','ARSE','NIDE'/
      DATA TPROP/  20.,  50.,  80., 100., 200., 300., 400., 470./
      DATA KW   /4500., 600., 400., 260.,  90.,  54.,  31.,  28./
      NPROPW=8
C TRANSFER VALUES
      DO 10 I=1,4
         SINK(I)=MAT(I)
10    CONTINUE
      DO 100 I=1,NPROPW
         TPROPW(I)=TPROP(I)
         KWW(I)=KW(I)
100   CONTINUE
      RETURN
      END
C END OF FILE FOR SUBROUTINE PROPS1
C-----------------------------------------------------------------------
C PROPS2:  WRITTEN BY RICHARD J. PHILLIPS.  PROPS2 CONTAINS
C          THE SUBSTRATE PROPERTY DATA FOR GERMANIUM AS TAKEN FROM
C          TOULOUKIAN (1970).
C-----------------------------------------------------------------------
C ANALYSIS VARIABLES
C KW     ... COOLANT THERMAL CONDUCTIVITY DATA               (W/M DEG K)
C NPROPW ... NUMBER OF SUBSTRATE MATERIAL DATA ENTRIES       (-)
C MAT    ... ALPHANUMERIC FOR SUBSTRATE TYPE                 (-)
C TPROPW ... TEMPERATURES FOR FLUID PROPERTY DATA            (DEG K)
C-----------------------------------------------------------------------
      SUBROUTINE PROPS2(NPROPW,TPROPW,KWW,SINK)
      DIMENSION TPROPW(20),KWW(20)
```

```
      DIMENSION TPROP(18),KW(18)
      CHARACTER*4 SINK(4),MAT(4)
      REAL KW,KWW
      DATA MAT  /'GERM','ANIU','M   ','    '/
      DATA TPROP/  10.,  20.,  30.,  40.,
     &              50.,  60.,  70.,  80.,  90., 100., 150., 200., 250.,
     &            273.2, 300., 350., 400., 500./
      DATA KW   /1770.,1490.,1080., 798.,
     &             615., 487., 393., 325., 270., 232., 132., 96.8, 74.9,
     &             66.7, 59.9, 49.5, 43.2, 33.8/
      NPROPW=18
C TRANSFER VALUES
      DO 10 I=1,4
         SINK(I)=MAT(I)
10    CONTINUE
      DO 100 I=1,NPROPW
         TPROPW(I)=TPROP(I)
         KWW(I)=KW(I)
100   CONTINUE
      RETURN
      END
C END OF FILE FOR SUBROUTINE PROPS2
C-----------------------------------------------------------------------
C PROPS3:  WRITTEN BY RICHARD J. PHILLIPS.  PROPS3 CONTAINS
C          THE SUBSTRATE PROPERTY DATA FOR INDIUM PHOSPHIDE TAKEN FROM
C          KUDMAN AND STEIGMEIER (1964), ALIEV ET AL. (1965), AND
C          NEUBERGER (1971).
C-----------------------------------------------------------------------
C ANALYSIS VARIABLES
C KW      ... COOLANT THERMAL CONDUCTIVITY DATA              (W/M DEG K)
C NPROPW ... NUMBER OF SUBSTRATE MATERIAL DATA ENTRIES       (-)
C MAT     ... ALPHANUMERIC FOR SUBSTRATE TYPE                (-)
C TPROPW ... TEMPERATURES FOR FLUID PROPERTY DATA            (DEG K)
C-----------------------------------------------------------------------
      SUBROUTINE PROPS3(NPROPW,TPROPW,KWW,SINK)
      DIMENSION TPROPW(20),KWW(20)
      DIMENSION TPROP(11),KW(11)
      CHARACTER*4 SINK(4),MAT(4)
      REAL KW,KWW
      DATA MAT  /'INDI','UM P','HOSP','HIDE'/
      DATA TPROP/  20.,  30.,  50.,  80., 100., 200., 300.,  350.,
     &             400., 450., 500./
      DATA KW   /3000.,2000.,1000., 500., 880., 130.,  67.,   53.,
     &              43.,  35.,  30./
      NPROPW=11
C TRANSFER VALUES
      DO 10 I=1,4
         SINK(I)=MAT(I)
10    CONTINUE
      DO 100 I=1,NPROPW
         TPROPW(I)=TPROP(I)
         KWW(I)=KW(I)
100   CONTINUE
      RETURN
      END
C END OF FILE FOR SUBROUTINE PROPS3
C-----------------------------------------------------------------------
C PROPS4:  WRITTEN BY RICHARD J. PHILLIPS.  PROPS4 CONTAINS
C          THE SUBSTRATE PROPERTY DATA FOR SILICON AS TAKEN FROM
C          TOULOUKIAN (1970).
```

```
C-----------------------------------------------------------------------
C ANALYSIS VARIABLES
C KW      ... COOLANT THERMAL CONDUCTIVITY DATA               (W/M DEG K)
C NPROPW ... NUMBER OF SUBSTRATE MATERIAL DATA ENTRIES        (-)
C MAT     ... ALPHANUMERIC FOR SUBSTRATE TYPE                 (-)
C TPROPW ... TEMPERATURES FOR FLUID PROPERTY DATA             (DEG K)
C-----------------------------------------------------------------------
      SUBROUTINE PROPS4(NPROPW,TPROPW,KWW,SINK)
      DIMENSION TPROPW(20),KWW(20)
      DIMENSION TPROP(18),KW(18)
      CHARACTER*4 SINK(4),MAT(4)
      REAL KW,KWW
      DATA MAT  /'SILI','CON ','    ','    '/
      DATA TPROP/  10.,  20.,  30.,  40.,
     &             50.,  60.,  70.,  80.,  90., 100., 150., 200., 250.,
     &           273.2, 300., 350., 400., 500./
      DATA KW   /2110.,4940.,4810.,3530.,
     &           2680.,2110.,1680.,1340.,1080., 884., 409., 264., 191.,
     &            168., 148., 119., 98.9, 76.2/
      NPROPW=18
C TRANSFER VALUES
      DO 10 I=1,4
         SINK(I)=MAT(I)
10    CONTINUE
      DO 100 I=1,NPROPW
         TPROPW(I)=TPROP(I)
         KWW(I)=KW(I)
100   CONTINUE
      RETURN
      END
C END OF FILE FOR SUBROUTINE PROPS4
C-----------------------------------------------------------------------
C PROPS5:  WRITTEN BY RICHARD J. PHILLIPS.  PROPS4 CONTAINS
C          THE SUBSTRATE PROPERTY DATA FOR ALUMINUM AS TAKEN FROM
C          TOULOUKIAN (1970).
C-----------------------------------------------------------------------
C ANALYSIS VARIABLES
C KW      ... COOLANT THERMAL CONDUCTIVITY DATA               (W/M DEG K)
C NPROPW ... NUMBER OF SUBSTRATE MATERIAL DATA ENTRIES        (-)
C MAT     ... ALPHANUMERIC FOR SUBSTRATE TYPE                 (-)
C TPROPW ... TEMPERATURES FOR FLUID PROPERTY DATA             (DEG K)
C-----------------------------------------------------------------------
      SUBROUTINE PROPS5(NPROPW,TPROPW,KWW,SINK)
      DIMENSION TPROPW(20),KWW(20)
      DIMENSION TPROP(18),KW(18)
      CHARACTER*4 SINK(4),MAT(4)
      REAL KW,KWW
      DATA MAT  /'ALUM','INUM','    ','    '/
      DATA TPROP/   10.,   20.,  30.,  40.,
     &              50.,   60.,  70.,  80.,  90., 100., 150., 200.,
     &             250., 273.2, 300., 350., 400., 500./
      DATA KW   /23500.,11700.,5180.,2380.,
     &            1230.,  754., 532., 414., 344., 302., 248., 237.,
     &             235.,  236., 237., 240., 240., 237./
      NPROPW=18
C TRANSFER VALUES
      DO 10 I=1,4
         SINK(I)=MAT(I)
10    CONTINUE
      DO 100 I=1,NPROPW
```

```
         TPROPW(I)=TPROP(I)
         KWW(I)=KW(I)
100   CONTINUE
      RETURN
      END
C END OF FILE FOR SUBROUTINE PROPS5
C----------------------------------------------------------------------
C PROPS6: WRITTEN BY RICHARD J. PHILLIPS.  PROPS5 CONTAINS
C         THE SUBSTRATE PROPERTY DATA FOR COPPER AS TAKEN FROM
C         TOULOUKIAN (1970).
C----------------------------------------------------------------------
C ANALYSIS VARIABLES
C KW     ... COOLANT THERMAL CONDUCTIVITY DATA               (W/M DEG K)
C NPROPW ... NUMBER OF SUBSTRATE MATERIAL DATA ENTRIES       (-)
C MAT    ... ALPHANUMERIC FOR SUBSTRATE TYPE                 (-)
C TPROPW ... TEMPERATURES FOR FLUID PROPERTY DATA            (DEG K)
C----------------------------------------------------------------------
      SUBROUTINE PROPS6(NPROPW,TPROPW,KWW,SINK)
      DIMENSION TPROPW(20),KWW(20)
      DIMENSION TPROP(18),KW(18)
      CHARACTER*4 SINK(4),MAT(4)
      REAL KW,KWW
      DATA MAT  /'COPP','ER  ','    ','    '/
      DATA TPROP/   10.,   20.,  30.,  40.,
     &              50.,   60.,  70.,  80.,  90., 100., 150., 200.,
     &             250., 273.2, 300., 350., 400., 500./
      DATA KW   /19600.,10500.,4300.,2050.,
     &            1220.,  850., 670., 570., 514., 483., 428., 413.,
     &             404.,  401., 398., 394., 392., 388./
      NPROPW=18
C TRANSFER VALUES
      DO 10 I=1,4
         SINK(I)=MAT(I)
10    CONTINUE
      DO 100 I=1,NPROPW
         TPROPW(I)=TPROP(I)
         KWW(I)=KW(I)
100   CONTINUE
      RETURN
      END
C END OF FILE FOR SUBROUTINE PROPS6
C----------------------------------------------------------------------
C PROPS7: WRITTEN BY RICHARD J. PHILLIPS.  PROPS6 CONTAINS
C         THE SUBSTRATE PROPERTY DATA FOR SILVER AS TAKEN FROM
C         TOULOUKIAN (1970).
C----------------------------------------------------------------------
C ANALYSIS VARIABLES
C KW     ... COOLANT THERMAL CONDUCTIVITY DATA               (W/M DEG K)
C NPROPW ... NUMBER OF SUBSTRATE MATERIAL DATA ENTRIES       (-)
C MAT    ... ALPHANUMERIC FOR SUBSTRATE TYPE                 (-)
C TPROPW ... TEMPERATURES FOR FLUID PROPERTY DATA            (DEG K)
C----------------------------------------------------------------------
      SUBROUTINE PROPS7(NPROPW,TPROPW,KWW,SINK)
      DIMENSION TPROPW(20),KWW(20)
      DIMENSION TPROP(18),KW(18)
      CHARACTER*4 SINK(4),MAT(4)
      REAL KW,KWW
      DATA MAT  /'SILV','ER  ','    ','    '/
      DATA TPROP/   10.,  20.,  30.,  40.,
     &              50.,  60.,  70.,  80.,  90., 100., 150., 200., 250.,
```

```
      &           273.2, 300., 350., 400., 500./
       DATA KW   /16800.,5100.,1930.,1050.,
      &             700., 550., 497., 471., 460., 450., 432., 430., 428.,
      &             428., 427., 424., 420., 413./
       NPROPW=18
C TRANSFER VALUES
       DO 10 I=1,4
          SINK(I)=MAT(I)
10     CONTINUE
       DO 100 I=1,NPROPW
          TPROPW(I)=TPROP(I)
          KWW(I)=KW(I)
100    CONTINUE
       RETURN
       END
C END OF FILE FOR SUBROUTINE PROPS7
C-----------------------------------------------------------------------
C PRINTO:  WRITTEN BY RICHARD J. PHILLIPS. PRINTO INITIALIZES
C          AND TERMINATES THE PRINTOUTS OF ANALYSIS RESULTS.
C-----------------------------------------------------------------------
C FLUID  ... ALPHANUMERIC FOR COOLANT TYPE                    (-)
C TFLUIN ... ASSUMED COOLANT   .ET TEMPERATURE                (DEG K)
C Q      ... SURFACE HEATING RATE                             (W/CM*2)
C SINK   ... ALPHANUMERIC FOR SUBSTRATE TYPE                  (-)
C IDUM   ... DUMMY VARIABLE FOR PRINTOUT CONTROL              (-)
C-----------------------------------------------------------------------
       SUBROUTINE PRINTO(FLUID,TFLUIN,SINK,Q,IDUM)
       CHARACTER*4 FLUID(3),SINK(4)
C******** FILE 11
C GEOMETRY, FLOW CONSTRAINTS, AND THERMAL RESISTANCE
C LABEL PRINTOUT
       IF(IDUM.EQ.0)WRITE(11,500)SINK,FLUID,TFLUIN,Q
500    FORMAT(' SUBSTRATE = ',4A4,
      &'      LIQUID COOLANT = ',3A4,'      TFLUIN = ',F5.1,' DEG K      ',
      &' Q = ',F6.0,' W/CM**2')
C TOP OF PRINTOUT
       IF(IDUM.EQ.0)WRITE(11,800)
800    FORMAT(
      &' -----+-----+----+------+-----+-----+------+-----+----+---+---+'
      &,
      &'----+------+-----++------+------+------+------+------+------+'
      &,/,
      &'  WC    WW    X     Z      T   ASPEC ACBYAP EBYDE PBYE PHI ZI  '
      &,
      &'DELP   V'    P'     RCOND     RC    RCONV  RBULK   RTOT  DTPUMP '
      &,/,
      &' -----+-----+----+------+-----+-----+------+-----+----+---+---+'
      &,
      &'----+------+-----++------+------+------+------+------+------+')
       IF(IDUM.EQ.0)WRITE(11,801)
801    FORMAT(
      &'                                                                '
      &,
      &'LBF    CC/S    W    DEG. C DEG. C DEG. C DEG. C DEG. C         '
      &,/,
      &'   M      M     M     M      M    ---     --     ---    -- DEG DEG '
      &,
      &'----  ----- -----  ------ ------ ------ ------ ------ DEG. C '
      &,/,
      &'                                                                '
```

```
     &,
     &'IN*2  CM*2  CM*2   W/CM*2 W/CM*2 W/CM*2 W/CM*2 W/CM*2          '
     &,/,
     &' -----+-----+----+------+-----+-----+------+-----+----+---+---+'
     &,
     &'----+------+-----++------+------+------+------+------+------+')
      IF(IDUM.EQ.0)WRITE(11,802)
802   FORMAT(
     &' *E-6  *E-6        *E-6  *E-6                                   '
     &,
     &'                                                               '
     &,/,
     &' -----+-----+----+------+-----+-----+------+-----+----+---+---+'
     &,
     &'----+------+-----++------+------+------+------+------+------+')
C BOTTOM OF PRINTOUT
      IF(IDUM.EQ.1)WRITE(11,803)
803   FORMAT(
     &' -----+-----+----+------+-----+-----+------+-----+----+---+---+'
     &,
     &'----+------+-----++------+------+------+------+------+------+')
C******** FILE 13
C FLOW AND HEAT TRANSFER VARIABLES
C LABEL PRINTOUT
      IF(IDUM.EQ.0)WRITE(13,500)SINK,FLUID,TFLUIN,Q
C TOP OF PRINTOUT
      IF(IDUM.EQ.0)WRITE(13,901)
901   FORMAT(
     &' -----+-----+-----+------+------+------+------+'
     &,
     &'------+------+------+----+----+----+------+------+'
     &,/,
     &'  DE    DLE   VC     RE   RESTAR XSTAR  LPLUS  '
     &,
     &'  NU    NUT    FAPP  K90    KC    KE  FINCRI  EFF    '
     &,/,
     &' -----+-----+-----+------+------+------+------+'
     &,
     &'------+------+------+----+----+----+------+------+')
      IF(IDUM.EQ.0)WRITE(13,902)
902   FORMAT(
     &'   M     M    M/S    --     --     --     --   '
     &,
     &'  --    ---     --   ---    --    --     --    ---    '
     &,/,
     &' -----+-----+-----+------+------+------+------+'
     &,
     &'------+------+------+----+----+----+------+------+')
C BOTTOM OF PRINTOUT
      IF(IDUM.EQ.1)WRITE(13,903)
903   FORMAT(
     &' -----+-----+-----+------+------+------+------+'
     &,
     &'------+------+------+----+----+----+------+------+')
C******** FILE 15
C TEMPERATURES
C LABEL PRINTOUT
      IF(IDUM.EQ.0)WRITE(15,500)SINK,FLUID,TFLUIN,Q
C TOP OF PRINTOUT
      IF(IDUM.EQ.0)WRITE(15,10001)
```

```
10001 FORMAT(
     &' ------+------+------+------+------+------+------+------+------+'
     &,
     &'------+------+------+------+------+------+------+'
     &,/,
     &' TFINL  TFLUL   TTBL  TFLLAV TFILAV TFINX  TFLUX   TTBX  TFLXAV '
     &,
     &'TFIXAV  TTX    TTB   TTIPX  TFLUO  DTPUML DTPUMX '
     &)
      IF(IDUM.EQ.0)WRITE(15,10002)
10002 FORMAT(
     &' ------+------+------+------+------+------+------+------+------+'
     &,
     &'------+------+------+------+------+------+------+'
     &,/,
     &' DEG. C DEG. C DEG. C DEG. C DEG. C DEG. C DEG. C DEG. C DEG. C '
     &,
     &'DEG. C DEG. C DEG. C DEG. C DEG. C DEG. C DEG. C '
     &,/,
     &' ------+------+------+------+------+------+------+------+------+'
     &,
     &'------+------+------+------+------+------+------+'
     &)
C BOTTOM OF PRINTOUT
      IF(IDUM.EQ.1)WRITE(15,10003)
10003 FORMAT(
     &' ------+------+------+------+------+------+------+------+------+'
     &,
     &'------+------+------+------+------+------+------+'
     &)
C******** FILE 17
C PROPERTIES
C LABEL PRINTOUT
      IF(IDUM.EQ.0)WRITE(17,500)SINK,FLUID,TFLUIN,Q
C TOP OF PRINTOUT
      IF(IDUM.EQ.0)WRITE(17,20001)
20001 FORMAT(
     &' ------+------+------+------+------+------+------+------+------+'
     &,
     &'------+------+------+------+------+------+------+------+------+'
     &,/,
     &' CPFLUL CPFLUX KFLUL  KFLUX  PRFLUL PRFLUX RHOFLL RJOFLX MUFLUL '
     &,
     &'MUFLUX MUFLLA MUFLXA MUFILA MUFIXA KFINL  KFINX   KTBL   KTBX  '
     &)
      IF(IDUM.EQ.0)WRITE(17,20002)
20002 FORMAT(
     &' ------+------+------+------+------+------+------+------+------+'
     &,
     &'------+------+------+------+------+------+------+------+------+'
     &,/,
     &' J/KG C J/KG C W/M C  W/M C    --     --   KG/M*3 KG/M*3 KG/M S '
     &,
     &'KG/M S KG/M S KG/M S KG/M S KG/M S W/M C  W/M C  W/M C  W/M C  '
     &,/,
     &' ------+------+------+------+------+------+------+------+------+'
     &,
     &'------+------+------+------+------+------+------+------+------+'
     &)
C BOTTOM OF PRINTOUT
```

```
      IF(IDUK.EQ.1)WRITE(17,20003)
20003 FORMAT(
     &' ------+------+------+------+------+------+------+------+------+'
     &,
     &'------+------+------+------+------+------+------+------+------+'
     &)
      RETURN
      END
C END OF FILE FOR SUBROUTINE PRINTO
C-----------------------------------------------------------------------
C PPLOTT:  WRITTEN BY RICHARD J. PHILLIPS.  PPLOTT PLOTS THE THERMAL-
C          HYDRAULIC RESULTS USING THE DISSPLA PLOTTING PACKAGE.  NOTE
C          THAT A 'C' HAS BEEN ADDED BEFORE COLUMN 1 TO COMMENT OUT
C          THE ENTIRE SUBROUTINE.
C-----------------------------------------------------------------------
C ANALYSIS VARIABLES
C ICASE  ... ANALYSIS METHOD CONTROL PARAMETER              (-)
C IINUM  ... ARRAY OF THE NUMBER OF CURVE DATA POINTS       (-)
C IX     ... CONTROL FOR IF X OR WC IS VARIED               (-)
C NCURVE ... NUMBER OF CURVE SETS TO BE PLOTTED             (-)
C X1     ... CHANNEL WIDTH ARRAY DATA POINTS                (M)
C XX     ... ARRAY OF CHANNEL POSITION X VALUES             (M)
C XSTARX ... ARRAY OF THERMAL ENTRANCE LENGTHS              (-)
C Y1A    ... TOTAL THERMAL RESISTANCE ARRAY DATA POINTS (DEG C/(W/CM*2))
C Y1B    ... CONVECTIVE THERMAL RESISTANCE ARRAY DATA
C              POINTS                                   (DEG C/(W/CM*2))
C Y1C    ... COOLANT BULK TEMPERATURE RISE THERMAL
C              RESISTANCE ARRAY DATA POINTS             (DEG C/(W/CM*2))
C Y2     ... COOLANT PUMPING POWER PER UNIT SURFACE AREA
C              ARRAY DATA POINTS                            (W/CM*2)
C Y3     ... ARRAY FOR LOCATION OF MARKER SYMBOLS           (-)
C-----------------------------------------------------------------------
C     SUBROUTINE PPLOTT(X1,Y1A,Y1B,Y1C,Y2,Y3,IINUM,NCURVE,ICASE,
C    &                  IX,XX,XSTARX)
C     DIMENSION X1(5,2,100),Y1A(5,2,100),Y2(5,2,100),Y3(5,2,100),
C    &IINUM(5,2),ICASE(5),X(100),Y(100),Y1B(5,2,100),Y1C(5,2,100),
C    &XX(5,2,100),XSTARX(5,2,100)
CC DETERMINE IF X OR WC WAS VARIED
C     IF(IX.EQ.2)GO TO 50000
CC THE CHANNEL WIDTH WAS VARIED
CC DEFINE THERMAL RESISTANCE PLOT
C     CALL HWSCAL('SCREEN')
C     CALL HWROT('AUTO')
C     CALL NOBRDR
C     CALL NOCHEK
C     CALL SETDEV(20,20)
C     CALL GRACE(0.)
C     CALL PAGE(8.5,11.)
C     CALL PHYSOR(2.0,4.6)
C     CALL AREA2D(5.,5.)
C     CALL FRAME
C     CALL YNAME('TOTAL THERMAL RESISTANCE - DEG C/(W/CM**2)',42)
C     CALL XNAME('CHANNEL WIDTH - MICRO M',23)
C     CALL YLOG(0.,100.,0.010,2.5)
CC    CALL YLOG(0.,100.,0.001,1.6667)
C     CALL BLSYM
C     CALL THKCRV(0.02)
CC LOOP FOR UP TO FIVE SETS OF CURVES
C     DO 1000 I=1,NCURVE,1
C        IF(I.EQ.2)CALL DOT
```

```
C          IF(I.EQ.3)CALL DASH
C          IF(I.EQ.4)CALL CHNDOT
C          IF(I.EQ.5)CALL CHNDSH
C          IF(ICASE(I).EQ.1)JMIN=1
C          IF(ICASE(I).EQ.1)JMAX=1
C          IF(ICASE(I).EQ.2)JMIN=1
C          IF(ICASE(I).EQ.2)JMAX=2
C          IF(ICASE(I).EQ.3)JMIN=2
C          IF(ICASE(I).EQ.3)JMAX=2
CC LOOP FOR FLOW REGIME
C       DO 500 J=JMIN,JMAX,1
C          INUM=IINUM(I,J)
CC LOOP FOR INUM DATA POINTS FOR EACH CURVE SET
CC    TOTAL THERMAL RESISTANCE
C       DO 175 K=1,INUM,1
C          X(K)=X1(I,J,K)
C          Y(K)=Y1A(I,J,K)
C          IF(K.EQ.1)GO TO 50
C          IF(K.EQ.INUM)GO TO 50
C          IF(Y3(I,J,K).EQ.(Y3(I,J,K+1)))GO TO 175
C50         CONTINUE
C          IF(Y3(I,J,K).EQ.1)CALL MARKER(2)
C          IF(Y3(I,J,K).EQ.2)CALL MARKER(6)
C          IF((J.EQ.1).AND.(K.EQ.1))CALL MARKER(16)
C          IF((J.EQ.2).AND.(K.EQ.1))CALL MARKER(15)
C          IF((J.EQ.1).AND.(K.EQ.INUM))CALL MARKER(17)
C          IF((J.EQ.2).AND.(K.EQ.INUM))CALL MARKER(18)
C          IF((J.NE.1).OR.(Y3(I,J,K).NE.1))GO TO 175
C          IF(K.EQ.1)GO TO 175
C          CALL CURVE(X(K),Y(K),1,-1)
C175    CONTINUE
C       CALL CURVE(X,Y,INUM,0)
CC    CONVECTIVE THERMAL RESISTANCE
C       DO 200 K=1,INUM,1
C          X(K)=X1(I,J,K)
C          Y(K)=Y1B(I,J,K)
C          IF(K.EQ.1)GO TO 150
C          IF(K.EQ.INUM)GO TO 150
C          IF(Y3(I,J,K).EQ.(Y3(I,J,K+1)))GO TO 200
C150        CONTINUE
C          IF(Y3(I,J,K).EQ.1)CALL MARKER(2)
C          IF(Y3(I,J,K).EQ.2)CALL MARKER(6)
C          IF((J.EQ.1).AND.(K.EQ.1))CALL MARKER(16)
C          IF((J.EQ.2).AND.(K.EQ.1))CALL MARKER(15)
C          IF((J.EQ.1).AND.(K.EQ.INUM))CALL MARKER(17)
C          IF((J.EQ.2).AND.(K.EQ.INUM))CALL MARKER(18)
C          IF((J.NE.1).OR.(Y3(I,J,K).NE.1))GO TO 200
C          IF(K.EQ.1)GO TO 200
C          CALL CURVE(X(K),Y(K),1,-1)
C200    CONTINUE
C       CALL CURVE(X,Y,INUM,0)
CC    COOLANT BULK TEMPERATURE RISE THERMAL RESISTANCE
C       DO 300 K=1,INUM,1
C          X(K)=X1(I,J,K)
C          Y(K)=Y1C(I,J,K)
C          IF(K.EQ.1)GO TO 250
C          IF(K.EQ.INUM)GO TO 250
C          IF(Y3(I,J,K).EQ.(Y3(I,J,K+1)))GO TO 300
C250        CONTINUE
C          IF(Y3(I,J,K).EQ.1)CALL MARKER(2)
```

```
C          IF(Y3(I,J,K).EQ.2)CALL MARKER(6)
C          IF((J.EQ.1).AND.(K.EQ.1))CALL MARKER(16)
C          IF((J.EQ.2).AND.(K.EQ.1))CALL MARKER(15)
C          IF((J.EQ.1).AND.(K.EQ.INUM))CALL MARKER(17)
C          IF((J.EQ.2).AND.(K.EQ.INUM))CALL MARKER(18)
C          IF((J.NE.1).OR.(Y3(I,J,K).NE.1))GO TO 300
C          IF(K.EQ.1)GO TO 300
C          CALL CURVE(X(K),Y(K),1,-1)
C300    CONTINUE
C       CALL CURVE(X,Y,INUM,0)
C500    CONTINUE
C1000   CONTINUE
C       IF(NCURVE.EQ.2)CALL RESET('DOT')
C       IF(NCURVE.EQ.3)CALL RESET('DASH')
C       IF(NCURVE.EQ.4)CALL RESET('CHNDOT')
C       IF(NCURVE.EQ.5)CALL RESET('CHNDSH')
CC      LABEL SURFACE TEMPERATURE RISE - YOU PROVIDE THE HEATING RATE
CC      CALL YLGAXS(0.1,2.0,6.,'PEAK SURFACE TEMPERATURE RISE - DEG C$',
CC     1-100,7.,0.)
C       CALL YNONUM
C       CALL YLGAXS(1.0,2.5,5.,' $',-100,5.,0.)
CC      CALL YLGAXS(1.0,1.6667,5.,' $',-100,5.,0.)
C       CALL RESET('YNONUM')
C       CALL ENDGR(0)
CC DEFINE PUMPING POWER PLOT
C       CALL PAGE(8.5,11.)
C       CALL PHYSOR(2.0,1.0)
C       CALL AREA2D(5.,3.)
C       CALL FRAME
C       CALL YNAME('PUMPING POWER - W/CM**2',23)
C       CALL XNAME('CHANNEL WIDTH - MICRO M',23)
C       CALL YLOG(0.,100.,0.10,1.0)
C       CALL YNONUM
C       CALL YLGAXS(0.10,1.0,3.,' ',-1,5.,0.)
C       CALL RESET('YNONUM')
C       CALL BLSYM
C       CALL THKCRV(0.02)
CC LOOP FOR UP TO FIVE CURVES
C       DO 2000 I=1,NCURVE,1
C          IF(I.EQ.2)CALL DOT
C          IF(I.EQ.3)CALL DASH
C          IF(I.EQ.4)CALL CHNDOT
C          IF(I.EQ.5)CALL CHNDSH
C          IF(ICASE(I).EQ.1)JMIN=1
C          IF(ICASE(I).EQ.1)JMAX=1
C          IF(ICASE(I).EQ.2)JMIN=1
C          IF(ICASE(I).EQ.2)JMAX=2
C          IF(ICASE(I).EQ.3)JMIN=2
C          IF(ICASE(I).EQ.3)JMAX=2
CC LOOP FOR FLOW REGIME
C       DO 1500 J=JMIN,JMAX,1
C          INUM=IINUM(I,J)
CC LOOP FOR INUM DATA POINTS
C       DO 1100 K=1,INUM,1
C          X(K)=X1(I,J,K)
C          Y(K)=Y2(I,J,K)
C          IF(K.EQ.1)GO TO 1050
C          IF(K.EQ.INUM)GO TO 1050
C          IF(Y3(I,J,K).EQ.(Y3(I,J,K+1)))GO TO 1100
C1050      CONTINUE
```

```
C          IF(Y3(I,J,K).EQ.1)CALL MARKER(2)
C          IF(Y3(I,J,K).EQ.2)CALL MARKER(6)
C          IF((J.EQ.1).AND.(K.EQ.1))CALL MARKER(16)
C          IF((J.EQ.2).AND.(K.EQ.1))CALL MARKER(15)
C          IF((J.EQ.1).AND.(K.EQ.INUM))CALL MARKER(17)
C          IF((J.EQ.2).AND.(K.EQ.INUM))CALL MARKER(18)
C          IF((J.NE.1).OR.(Y3(I,J,K).NE.1))GO TO 1100
C          IF(K.EQ.1)GO TO 1100
C          CALL CURVE(X(K),Y(K),1,-1)
C1100   CONTINUE
C       CALL CURVE(X,Y,INUM,0)
C1500   CONTINUE
C2000   CONTINUE
C       CALL ENDPL(0)
C       CALL DONEPL
C       RETURN
C50000 CONTINUE
CC THE POSITION FROM THE CHANNEL ENTRANCE WAS VARIED
CC DEFINE THERMAL RESISTANCE PLOT
C       CALL HWSCAL('SCREEN')
C       CALL HWROT('AUTO')
C       CALL NOBRDR
C       CALL NOCHEK
C       CALL SETDEV(20,20)
C       CALL GRACE(0.)
C       CALL PAGE(8.5,11.)
C       CALL PHYSOR(2.,2.)
C       CALL AREA2D(5.5,3.5)
C       CALL FRAME
C       CALL HEADIN('MICROCHANNEL THERMAL RESISTANCE',31,1.,1)
CC      NOTE THAT PLOTS VERSUS THERMAL ENTRANCE LENGTH USE XSTARX, AND
CC        PLOTS VERSUS DISTANCE FROM UPSTREAM HEATER EDGE USE XX ARRAYS
C       CALL YNAME('TOTAL THERMAL RESISTANCE - DEG C/(W/CM**2)',42)
CC      CALL XNAME('THERMAL ENTRANCE LENGTH - DIMENSIONLESS',39)
CC      CALL GRAF(0.,.01,.04,0.,.05,.2)
C       CALL XNAME('DISTANCE FROM CHANNEL ENTRANCE - M',34)
C       CALL GRAF(0.0,0.002,0.01,0.,.05,.30)
C       CALL BLSYM
C       CALL THKCRV(0.02)
CC LOOP FOR UP TO FIVE SETS OF CURVES
C       DO 51000 I=1,NCURVE,1
C          IF(I.EQ.2)CALL DOT
C          IF(I.EQ.3)CALL DASH
C          IF(I.EQ.4)CALL CHNDOT
C          IF(I.EQ.5)CALL CHNDSH
C          IF(ICASE(I).EQ.1)JMIN=1
C          IF(ICASE(I).EQ.1)JMAX=1
C          IF(ICASE(I).EQ.2)JMIN=1
C          IF(ICASE(I).EQ.2)JMAX=2
C          IF(ICASE(I).EQ.3)JMIN=2
C          IF(ICASE(I).EQ.3)JMAX=2
CC LOOP FOR FLOW REGIME
C       DO 50500 J=JMIN,JMAX,1
C          INUM=IINUM(I,J)
CC LOOP FOR INUM DATA POINTS FOR EACH CURVE SET
CC    TOTAL THERMAL RESISTANCE
C       DO 50100 K=1,INUM,1
CC         X(K)=XSTARX(I,J,K)
C          X(K)=XX(I,J,K)
C          Y(K)=Y1A(I,J,K)
```

```
C          IF(K.EQ.1)GO TO 50050
C          IF(K.EQ.INUM)GO TO 50050
C          IF(Y3(I,J,K).EQ.(Y3(I,J,K+1)))GO TO 50100
C50050     CONTINUE
C          IF(Y3(I,J,K).EQ.1)CALL MARKER(2)
C          IF(Y3(I,J,K).EQ.2)CALL MARKER(6)
C          IF((J.EQ.1).AND.(K.EQ.1))CALL MARKER(16)
C          IF((J.EQ.2).AND.(K.EQ.1))CALL MARKER(15)
C          IF((J.EQ.1).AND.(K.EQ.INUM))CALL MARKER(17)
C          IF((J.EQ.2).AND.(K.EQ.INUM))CALL MARKER(18)
C          IF((J.NE.1).OR.(Y3(I,J,K).NE.1))GO TO 50100
C          IF(K.EQ.1)GO TO 50100
C          CALL CURVE(X(K),Y(K),1,-1)
C50100 CONTINUE
C       CALL CURVE(X,Y,INUM,0)
CC    CONVECTIVE THERMAL RESISTANCE
C       DO 50200 K=1,INUM,1
CC         X(K)=XSTARX(I,J,K)
C          X(K)=XX(I,J,K)
C          Y(K)=Y1B(I,J,K)
C          IF(K.EQ.1)GO TO 50150
C          IF(K.EQ.INUM)GO TO 50150
C          IF(Y3(I,J,K).EQ.(Y3(I,J,K+1)))GO TO 50200
C50150     CONTINUE
C          IF(Y3(I,J,K).EQ.1)CALL MARKER(2)
C          IF(Y3(I,J,K).EQ.2)CALL MARKER(6)
C          IF((J.EQ.1).AND.(K.EQ.1))CALL MARKER(16)
C          IF((J.EQ.2).AND.(K.EQ.1))CALL MARKER(15)
C          IF((J.EQ.1).AND.(K.EQ.INUM))CALL MARKER(17)
C          IF((J.EQ.2).AND.(K.EQ.INUM))CALL MARKER(18)
C          CALL CURVE(X(K),Y(K),1,-1)
C50200 CONTINUE
C       CALL CURVE(X,Y,INUM,0)
CC    COOLANT BULK TEMPERATURE RISE THERMAL RESISTANCE
C       DO 50300 K=1,INUM,1
CC         X(K)=XSTARX(I,J,K)
C          X(K)=XX(I,J,K)
C          Y(K)=Y1C(I,J,K)
C          IF(K.EQ.1)GO TO 50250
C          IF(K.EQ.INUM)GO TO 50250
C          IF(Y3(I,J,K).EQ.(Y3(I,J,K+1)))GO TO 50300
C50250     CONTINUE
C          IF(Y3(I,J,K).EQ.1)CALL MARKER(2)
C          IF(Y3(I,J,K).EQ.2)CALL MARKER(6)
C          IF((J.EQ.1).AND.(K.EQ.1))CALL MARKER(16)
C          IF((J.EQ.2).AND.(K.EQ.1))CALL MARKER(15)
C          IF((J.EQ.1).AND.(K.EQ.INUM))CALL MARKER(17)
C          IF((J.EQ.2).AND.(K.EQ.INUM))CALL MARKER(18)
C          CALL CURVE(X(K),Y(K),1,-1)
C50300 CONTINUE
C       CALL CURVE(X,Y,INUM,0)
C50500 CONTINUE
C51000 CONTINUE
C       IF(NCURVE.EQ.2)CALL RESET('DOT')
C       IF(NCURVE.EQ.3)CALL RESET('DASH')
C       IF(NCURVE.EQ.4)CALL RESET('CHNDOT')
C       IF(NCURVE.EQ.5)CALL RESET('CHNDSH')
C       CALL RESET('THKCRV')
C       CALL DOT
C       CALL GRID(2,2)
```

```
C       CALL RESET('DOT')
CC      NOTE THAT YOU MUST PROVIDE THE HEATING RATE TO LABEL TEMP. RISE
CC      CALL YGRAXS(0.,5.,10.0,3.5,'SURFACE TEMPERATURE RISE - DEG C$',
CC     $-100,5.5,0.)
C       CALL YNONUM
CC      CALL YGRAXS(0.,5.,10.0,3.5,' $',-100,5.5,0.)
C       CALL RESET('YNONUM')
C       CALL ENDPL(0)
C       CALL DONEPL
C       RETURN
C       END
CC END OF FILE FOR SUBROUTINE PPLOTT
C-----------------------------------------------------------------------
C PINPUT:  WRITTEN BY RICHARD J. PHILLIPS.  PINPUT PLOTS THE INPUT
C          ARRAY DATA.   NOTE THAT A 'C' HAS BEEN ADDED BEFORE COLUMN 1
C          TO COMMENT OUT THE ENTIRE SUBROUTINE.
C-----------------------------------------------------------------------
C ASPECT ... CHANNEL ASPECT RATIO                              (-)
C B      ... FIN HEIGHT                                        (M)
C DELP   ... PRESSURE DROP                                     (PSI)
C EBYDE  ... RATIO OF RIB HEIGHT TO HYDRAULIC DIAMETER         (-)
C ICASE  ... CASE SELECTION CONTROL VARIABLE                   (-)
C ICONS  ... COOLANT FLOW CONSTRAINT                           (-)
C IKLOSS ... CONTROL FOR INCLUDING K90, KC AND KE              (-)
C IX     ... CONTROL VARIABLE FOR IF X OR WC IS VARIED         (-)
C IZ     ... CONTROL VARIABLE FOR FIN HEIGHT CONSTRAINT        (-)
C L      ... CHANNEL LENGTH                                    (M)
C NCURVE ... CONTROL VARIBLE FOR STORAGE OF PLOTTING DATA      (-)
C NFLUID ... COOLANT IDENTIFIER NUMBER                         (-)
C NSINK  ... SUBSTRATE MATERIAL INDENTIFIER NUMBER             (-)
C PBYE   ... RATIO OF RIB SEPARATION TO RIB HEIGHT             (-)
C PHI    ... REPEATED-RIB FLOW ATTACK ANGLE                    (DEGREES)
C POWER  ... PUMPING POWER PER UNIT CIRCUIT SURFACE AREA       (W/CM*2)
C Q      ... INPUT HEAT FLUX FROM THE SURFACE                  (W/CM*2)
C T      ... SUBSTRATE THICKNESS                               (M)
C TFLUIN ... COOLANT INLET TEMPERATURE                         (DEG K)
C VOLUME ... COOLANT FLOW RATE PER UNIT
C                CIRCUIT SURFACE AREA                       ((CM*3/S)/CM*2)
C WCEND  ... MAXIMUM CHANNEL WIDTH CONTROL VARIABLE            (M)
C WCINCR ... CHANNEL WIDTH INCREMENT CONTROL VARIABLE          (M)
C WCSTAR ... MINIMUM CHANNEL WIDTH CONTROL VARIABLE            (M)
C WWBYWC ... RATIO OF FIN WIDTH TO THE CHANNEL WIDTH           (-)
C XI     ... DUMMY VARIABLE                                    (-)
C ZI     ... REPEATED-RIB SHAPE ANGLE                          (DEGREES)
C-----------------------------------------------------------------------
C       SUBROUTINE PINPUT(NCURVE,ICASE,NSINK,NFLUID,TFLUIN,Q,WCSTAR,WCEND,
C      $                  WCINCR,WWBYWC,IZ,IX,B,ASPECT,L,T,IKLOSS,
C      $                  ICONS,DELP,VOLUME,POWER,EBYDE,PBYE,PHI,ZI)
C       DIMENSION NSINK(5),NFLUID(5),TFLUIN(5),Q(5),WCSTAR(5),WCEND(5),
C      $WCINCR(5),WWBYWC(5),IZ(5),B(5),ASPECT(5),L(5),T(5),IKLOSS(5),
C      $ICONS(5),DELP(5),VOLUME(5),POWER(5),EBYDE(5),PBYE(5),PHI(5),ZI(5),
C      $ICASE(5),XI(5)
C       DATA XI/1.2,2.4,3.6,4.8,6./
CC SET UP PLOTTER
C       CALL HWSCAL('SCREEN')
C       CALL HWROT('AUTO')
C       CALL NOBRDR
C       CALL NOCHEK
C       CALL SETDEV(20,20)
C       CALL GRACE(0.)
```

```
CC PLOT OUT THE ARRAY INFORMATION
C      CALL PAGE(8.5,11.)
C      CALL PHYSOR(1.,0.)
C      CALL AREA2D(7.,9.)
C      CALL MESSAG('INPUT DATA FOR MICROHEX COMPUTATIONS$',100,1.6,8.6)
C      CALL HEIGHT(0.1)
C      CALL MESSAG('       IX:  ',11,0.,8.3)
C      IF(IX.EQ.1)CALL MESSAG(
C     &'CALCS. DONE AT CHANNEL EXIT - CHANNEL WIDTH VARIED$',100,XI(1),8.
C     &3)
C      IF(IX.EQ.2)CALL MESSAG(
C     &'CALCS. ALONG CHANNEL - CHANNEL WIDTH IS CONSTANT$',100,XI(1),8.3)
C      CALL MESSAG('LINE TYPE:$',100,-0.1,8.0)
C      CALL MESSAG('       SOLID',12,XI(1),8.0)
C      CALL MESSAG('         DOT',12,XI(2),8.0)
C      CALL MESSAG('        DASH',12,XI(3),8.0)
C      CALL MESSAG('      CHNDOT',12,XI(4),8.0)
C      CALL MESSAG('      CHNDSH',12,XI(5),8.0)
C      CALL MESSAG('   ICASE:  ',11,0.,7.7)
C      DO 99 I=1,5,1
C         IF(I.GT.NCURVE)GO TO 98
C         IF(ICASE(I).EQ.1)CALL MESSAG('      FD LAM',12,XI(I),7.7)
C         IF(ICASE(I).EQ.2)CALL MESSAG('FD/D,LAM/TUR',12,XI(I),7.7)
C         IF(ICASE(I).EQ.3)CALL MESSAG('FD,TUR,ROUGH',12,XI(I),7.7)
C         GO TO 99
C98    CONTINUE
C         CALL MESSAG('          NA',12,XI(I),7.7)
C99    CONTINUE
C      CALL MESSAG('MATERIAL:  ',11,0.,7.4)
C      DO 101 I=1,5,1
C         IF(I.GT.NCURVE)GO TO 100
C         IF(NSINK(I).EQ.1)CALL MESSAG('        GAAS',12,XI(I),7.4)
C         IF(NSINK(I).EQ.2)CALL MESSAG('          GE',12,XI(I),7.4)
C         IF(NSINK(I).EQ.3)CALL MESSAG('         INP',12,XI(I),7.4)
C         IF(NSINK(I).EQ.4)CALL MESSAG('          SI',12,XI(I),7.4)
C         IF(NSINK(I).EQ.5)CALL MESSAG('          AL',12,XI(I),7.4)
C         IF(NSINK(I).EQ.6)CALL MESSAG('          CU',12,XI(I),7.4)
C         IF(NSINK(I).EQ.7)CALL MESSAG('          AG',12,XI(I),7.4)
C         GO TO 101
C100   CONTINUE
C         CALL MESSAG('          NA',12,XI(I),7.4)
C101   CONTINUE
C      CALL MESSAG(' COOLANT:  ',11,0.,7.1)
C      DO 103 I=1,5,1
C         IF(I.GT.NCURVE)GO TO 102
C         IF(NFLUID(I).EQ.1)CALL MESSAG('       FC-77',12,XI(I),7.1)
C         IF(NFLUID(I).EQ.2)CALL MESSAG('       FREON',12,XI(I),7.1)
C         IF(NFLUID(I).EQ.3)CALL MESSAG('       WATER',12,XI(I),7.1)
C         GO TO 103
C102   CONTINUE
C         CALL MESSAG('          NA',12,XI(I),7.1)
C103   CONTINUE
C      CALL MESSAG('  TFLUIN:  ',11,0.,6.8)
C      DO 105 I=1,5,1
C         IF(I.GT.NCURVE)GO TO 104
C         CALL REALNO(TFLUIN(I),103,XI(I),6.8)
C         CALL MESSAG(' DEG. K',7,'ABUT','ABUT')
C         GO TO 105
C104   CONTINUE
C         CALL MESSAG('          NA',12,XI(I),6.8)
```

```
C105    CONTINUE
C       CALL MESSAG('       Q:  ',11,0.,6.5)
C       DO 107 I=1,5,1
C          IF(I.GT.NCURVE)GO TO 106
C          CALL REALNO(Q(I),104,XI(I),6.5)
C          CALL MESSAG('W/CM*2',6,'ABUT','ABUT')
C          GO TO 107
C106    CONTINUE
C          CALL MESSAG('          NA',12,XI(I),6.5)
C107    CONTINUE
C       CALL MESSAG('  WCSTAR:  ',11,0.,6.2)
C       DO 109 I=1,5,1
C          IF(I.GT.NCURVE)GO TO 108
C          CALL REALNO(WCSTAR(I),103,XI(I),6.2)
C          CALL MESSAG('MICRONS',7,'ABUT','ABUT')
C          GO TO 109
C108    CONTINUE
C          CALL MESSAG('          NA',12,XI(I),6.2)
C109    CONTINUE
C       CALL MESSAG('   WCEND:  ',11,0.,5.9)
C       DO 111 I=1,5,1
C          IF(I.GT.NCURVE)GO TO 110
C          CALL REALNO(WCEND(I),103,XI(I),5.9)
C          CALL MESSAG('MICRONS',7,'ABUT','ABUT')
C          GO TO 111
C110    CONTINUE
C          CALL MESSAG('          NA',12,XI(I),5.9)
C111    CONTINUE
C       CALL MESSAG('  WCINCR:  ',11,0.,5.6)
C       DO 113 I=1,5,1
C          IF(I.GT.NCURVE)GO TO 112
C          CALL REALNO(WCINCR(I),103,XI(I),5.6)
C          CALL MESSAG('MICRONS',7,'ABUT','ABUT')
C          GO TO 113
C112    CONTINUE
C          CALL MESSAG('          NA',12,XI(I),5.6)
C113    CONTINUE
C       CALL MESSAG('  WWBYWC:  ',11,0.,5.3)
C       DO 115 I=1,5,1
C          IF(I.GT.NCURVE)GO TO 114
C          CALL MESSAG('    ',6,XI(I),5.3)
C          CALL REALNO(WWBYWC(I),104,'ABUT','ABUT')
C          GO TO 115
C114    CONTINUE
C          CALL MESSAG('          NA',12,XI(I),5.3)
C115    CONTINUE
C       CALL MESSAG('       B:  ',11,0.,5.0)
C       DO 117 I=1,5,1
C          IF(I.GT.NCURVE)GO TO 116
C          BB=B(I)*1.E+6
C          IF(IZ(I).EQ.1)CALL REALNO(BB,103,XI(I),5.0)
C          IF(IZ(I).EQ.1)CALL MESSAG('MICRONS',7,'ABUT','ABUT')
C          IF(IZ(I).NE.1)CALL MESSAG('          NA',12,XI(I),5.0)
C          GO TO 117
C116    CONTINUE
C          CALL MESSAG('          NA',12,XI(I),5.0)
C117    CONTINUE
C       CALL MESSAG('  ASPECT:  ',11,0.,4.7)
C       DO 119 I=1,5,1
C          IF(I.GT.NCURVE)GO TO 118
```

```
C          CALL MESSAG('      ',5,XI(I),4.7)
C          IF(IZ(I).EQ.2)CALL REALNO(ASPECT(I),105,'ABUT','ABUT')
C          IF(IZ(I).NE.2)CALL MESSAG('           NA',12,XI(I),4.7)
C          GO TO 119
C118    CONTINUE
C          CALL MESSAG('           NA',12,XI(I),4.7)
C119    CONTINUE
C       CALL MESSAG('        L:  ',11,0.,4.4)
C       DO 121 I=1,5,1
C          IF(I.GT.NCURVE)GO TO 120
C          CALL MESSAG('    ',4,XI(I),4.4)
C          CALL REALNO(L(I),104,'ABUT','ABUT')
C          CALL MESSAG(' M',2,'ABUT','ABUT')
C          GO TO 121
C120    CONTINUE
C          CALL MESSAG('           NA',12,XI(I),4.4)
C121    CONTINUE
C       CALL MESSAG('        T:  ',11,0.,4.1)
C       DO 123 I=1,5,1
C          IF(I.GT.NCURVE)GO TO 122
C          TT=T(I)/1.E-6
C          CALL REALNO(TT,103,XI(I),4.1)
C          CALL MESSAG('MICRONS',7,'ABUT','ABUT')
C          GO TO 123
C122    CONTINUE
C          CALL MESSAG('           NA',12,XI(I),4.1)
C123    CONTINUE
C       CALL MESSAG('  IKLOSS:  ',11,0.,3.8)
C       DO 125 I=1,5,1
C          IF(I.GT.NCURVE)GO TO 124
C          IF(IKLOSS(I).EQ.0)CALL MESSAG('KC=KE=K90=0.',12,XI(I),3.8)
C          IF(IKLOSS(I).NE.0)CALL MESSAG(' KC=KE=K90=?',12,XI(I),3.8)
C          GO TO 125
C124    CONTINUE
C          CALL MESSAG('           NA',12,XI(I),3.8)
C125    CONTINUE
C       CALL MESSAG('    DELP:  ',11,0.,3.5)
C       DO 127 I=1,5,1
C          IF(I.GT.NCURVE)GO TO 126
C          IF(ICONS(I).NE.1)CALL MESSAG('           NA',12,XI(I),3.5)
C          IF(ICONS(I).EQ.1)CALL MESSAG('   ',3,XI(I),3.5)
C          IF(ICONS(I).EQ.1)CALL REALNO(DELP(I),103,'ABUT','ABUT')
C          IF(ICONS(I).EQ.1)CALL MESSAG(' PSI',4,'ABUT','ABUT')
C          GO TO 127
C126    CONTINUE
C          CALL MESSAG('           NA',12,XI(I),3.5)
C127    CONTINUE
C       CALL MESSAG('  VOLUME:  ',11,0.,3.2)
C       DO 129 I=1,5,1
C          IF(I.GT.NCURVE)GO TO 128
C          IF(ICONS(I).NE.2)CALL MESSAG('           NA',12,XI(I),3.2)
C          IF(ICONS(I).EQ.2)CALL REALNO(VOLUME(I),106,XI(I),3.2)
C          IF(ICONS(I).EQ.2)CALL MESSAG('CC/S',4,'ABUT','ABUT')
C          GO TO 129
C128    CONTINUE
C          CALL MESSAG('           NA',12,XI(I),3.2)
C129    CONTINUE
C       CALL MESSAG('   POWER:  ',11,0.,2.9)
C       DO 131 I=1,5,1
C          IF(I.GT.NCURVE)GO TO 130
```

```
C          IF(ICONS(I).NE.3)CALL MESSAG('          NA',12,XI(I),2.9)
C          IF(ICONS(I).EQ.3)CALL REALNO(POWER(I),105,XI(I),2.9)
C          IF(ICONS(I).EQ.3)CALL MESSAG('W/CM2',5,'ABUT','ABUT')
C          GO TO 131
C130    CONTINUE
C          CALL MESSAG('          NA',12,XI(I),2.9)
C131    CONTINUE
C       CALL MESSAG('   EBYDE:  ',11,0.,2.6)
C       DO 133 I=1,5,1
C          IF(I.GT.NCURVE)GO TO 132
C          IF(ICASE(I).NE.3)CALL MESSAG('          NA',12,XI(I),2.6)
C          IF(ICASE(I).EQ.3)CALL MESSAG('    ',4,XI(I),2.6)
C          IF(ICASE(I).EQ.3)CALL REALNO(EBYDE(I),106,'ABUT','ABUT')
C          GO TO 133
C132    CONTINUE
C          CALL MESSAG('          NA',12,XI(I),2.6)
C133    CONTINUE
C       CALL MESSAG('    PBYE:  ',11,0.,2.3)
C       DO 135 I=1,5,1
C          IF(I.GT.NCURVE)GO TO 134
C          IF(ICASE(I).NE.3)CALL MESSAG('          NA',12,XI(I),2.3)
C          IF(ICASE(I).EQ.3)CALL MESSAG('    ',4,XI(I),2.3)
C          IF(ICASE(I).EQ.3)CALL REALNO(PBYE(I),106,'ABUT','ABUT')
C          GO TO 135
C134    CONTINUE
C          CALL MESSAG('          NA',12,XI(I),2.3)
C135    CONTINUE
C       CALL MESSAG('     PHI:  ',11,0.,2.)
C       DO 137 I=1,5,1
C          IF(I.GT.NCURVE)GO TO 136
C          IF(ICASE(I).NE.3)CALL MESSAG('          NA',12,XI(I),2.)
C          IF(ICASE(I).EQ.3)CALL MESSAG('    ',4,XI(I),2.)
C          IF(ICASE(I).EQ.3)CALL REALNO(PHI(I),106,'ABUT','ABUT')
C          GO TO 137
C136    CONTINUE
C          CALL MESSAG('          NA',12,XI(I),2.)
C137    CONTINUE
C       CALL MESSAG('      ZI:  ',11,0.,1.7)
C       DO 139 I=1,5,1
C          IF(I.GT.NCURVE)GO TO 138
C          IF(ICASE(I).NE.3)CALL MESSAG('          NA',12,XI(I),1.7)
C          IF(ICASE(I).EQ.3)CALL MESSAG('    ',4,XI(I),1.7)
C          IF(ICASE(I).EQ.3)CALL REALNO(ZI(I),106,'ABUT','ABUT')
C          GO TO 139
C138    CONTINUE
C          CALL MESSAG('          NA',12,XI(I),1.7)
C139    CONTINUE
C       CALL RESET('HEIGHT')
C       CALL ENDPL(0)
C       RETURN
C       END
CC END OF FILE FOR SUBROUTINE PINPUT
C----------------------------------------------------------------------
C RTOTAL:    WRITTEN BY RICHARD J. PHILLIPS.  RTOTAL FINALIZES THE
C            INITIALIZATION OF THE COMPUTATIONAL INPUTS, CALLS
C            SUBROUTINE RESIST (WHICH COMPUTES THE THERMAL RESISTANCE),
C            WRITES OUT THE COMPUTATIONAL RESULTS, AND STORES THE
C            VALID RESULTS INTO ARRAYS WHICH CAN BE PLOTTED.
C----------------------------------------------------------------------
C NAME       DESCRIPTION                                        UNITS
```

```
C ACBYAP ... RATIO OF FREE-FLOW TO FRONTAL CROSS-SECTIONAL
C              AREAS                                        (-)
C ASPECT ... CHANNEL ASPECT RATIO                           (-)
C ASPINV ... INVERSE OF THE CHANNEL ASPECT RATIO            (-)
C B      ... FIN HEIGHT                                     (M)
C CPFF   ... COOLANT SPECIFIC HEAT DATA                     (J/KG DEG K)
C CPFLUL ... COOLANT SPECIFIC HEAT AT CHANNEL EXIT          (J/KG DEG K)
C CPFLUX ... COOLANT SPECIFIC HEAT AT POSITION X            (J/KG DEG K)
C DE     ... HYDRAULIC DIAMETER                             (M)
C DEO    ... HYDRAULIC DIAMETER                             (MICRONS)
C DELP   ... PRESSURE DROP                                  (N/M*2)
C DELPO  ... PRESSURE DROP                                  (PSI)
C DLE    ... LAMINAR EQUIVALENT DIAMETER                    (M)
C DLEO   ... LAMINAR EQUIVALENT DIAMETER                    (MICRONS)
C DTPUML ... VISCOUS HEATING TEMPERATURE RISE AT CHANNEL
C              EXIT                                         (DEG K)
C DTPUMX ... VISCOUS HEATING TEMPERATURE RISE AT POSITION X(DEG K)
C EBYDE  ... RATIO OF RIB HEIGHT TO HYDRAULIC DIAMETER      (-)
C EFFX   ... FIN EFFICIENCY AT CHANNEL POSITION X           (-)
C FAPP   ... APPARANT FRICTION FACTOR                       (-)
C FINCRI ... FIN CRITERION                                  (-)
C FLUID  ... ALPHANUMERIC FOR COOLANT TYPE                  (-)
C ICASE  ... CASE SELECTION CONTROL VARIABLE                (-)
C ICONS  ... COOLANT FLOW CONSTRAINT                        (-)
C IFLOW  ... FLOW REGIME INDICATOR                          (-)
C IINUM  ... ARRAY OF INUM VALUES FOR PLOTTING CONTROL      (-)
C IKLOSS ... CONTROL FOR INCLUDING K90, KC AND KE           (-)
C IMIN,IMAX. DUMMY LOOP BEGIN/END VARIABLES                 (-)
C INUM   ... NUMBER OF DATA POINTS IN PLOTTING ARRAY DATA   (-)
C IPOINT ... PLOTTING CONTROL VARIABLE FOR XSTAR            (-)
C IRETUR ... CONTROL VARIABLE FOR OUT OF RANGE PROP. DATA   (-)
C IWC    ... LOOP INDICATOR FOR CHANNEL WIDTH               (-)
C IX     ... CONTROL VARIABLE FOR IF X OR WC IS VARIED      (-)
C IXX    ... LOOP INDICATOR FOR CHANNEL POSITION X          (-)
C IZ     ... CONTROL VARIABLE FOR FIN HEIGHT CONSTRAINT     (-)
C KC     ... ENTRANCE PRESSURE LOSS COEFFICIENT             (-)
C KE     ... EXIT PRESSURE LOSS COEFFICIENT                 (-)
C K90    ... NINETY DEGREE BEND PRESSURE LOSS COEFFICIENT   (-)
C KFF    ... COOLANT THERMAL CONDUCTIVITY DATA              (W/M DEG K)
C KFINL  ... AVERAGE FIN THERMAL CONDUCTIVITY AT
C              CHANNEL EXIT                                 (W/M DEG K)
C KFINX  ... AVERAGE FIN THERMAL CONDUCTIVITY AT
C              POSITION X                                   (W/M DEG K)
C KFLUL  ... COOLANT THERMAL CONDUCTIVITY AT
C              CHANNEL EXIT                                 (W/M DEG K)
C KFLUX  ... COOLANT THERMAL CONDUCTIVITY AT
C              POSITION X                                   (W/M DEG K)
C KTBL   ... AVERAGE SUBSTRATE THERMAL CONDUCTIVITY
C              AT CHANNEL EXIT                              (W/M DEG K)
C KTBX   ... AVERAGE SUBSTRATE THERMAL CONDUCTIVITY
C              AT POSITION X                                (W/M DEG K)
C KWW    ... SUBSTRATE THERMAL CONDUCTIVITY DATA            (W/M DEG K)
C L      ... CHANNEL LENGTH                                 (M)
C LAST   ... PREVIOUS RESULTS FOR PRINTOUT TO SCREEN  (M, (DEG K/(W/CM2)))
C LPLUS  ... HYDRODYNAMIC ENTRY LENGTH                      (-)
C MUFF   ... COOLANT DYNAMIC VISCOSITY DATA                 (KG/M S)
C MUFILA ... AVERAGE COOLANT DYNAMIC VISCOSITY AT THE
C              AVERAGE FIN TEMPERATURE BETWEEN THE
C              CHANNEL ENTRANCE AND EXIT                    (KG/M S)
C MUFIXA ... AVERAGE COOLANT DYNAMIC VISCOSITY AT THE
```

```
C               AVERAGE FIN TEMPERATURE BETWEEN THE
C               CHANNEL ENTRANCE AND POSITION X             (KG/M S)
C MUFLLA ... AVERAGE COOLANT DYNAMIC VISCOSITY AT THE
C               AVERAGE COOLANT TEMPERATURE BETWEEN THE
C               CHANNEL ENTRANCE AND EXIT                   (KG/M S)
C MUFLUL ... COOLANT DYNAMIC VISCOSITY AT CHANNEL EXIT       (KG/M S)
C MUFLUX ... COOLANT DYNAMIC VISCOSITY AT POSITION X         (KG/M S)
C MUFLXA ... AVERAGE COOLANT DYNAMIC VISCOSITY AT THE
C               AVERAGE COOLANT TEMPERATURE BETWEEN THE
C               CHANNEL ENTRANCE AND POSITION X             (KG/M S)
C NCURVE ... CONTROL VARIBLE FOR STORAGE OF PLOTTING DATA   (-)
C NUX    ... NUSSELT NUMBER AT CHANNEL POSITION X           (-)
C NUTX   ... NUSSELT NUMBER AT CHANNEL POSITION X INCUDING
C               EFFECT OF NONUNIFORM COOLANT TEMPERATURE    (-)
C NFLUID ... COOLANT IDENTIFIER NUMBER                      (-)
C NPROPF ... NUMBER OF COOLANT DATA ENTRIES                 (-)
C NPROPW ... NUMBER OF SUBSTRATE DATA ENTRIES               (-)
C NSINK  ... SUBSTRATE MATERIAL INDENTIFIER NUMBER          (-)
C PBYE   ... RATIO OF RIB SEPARATION TO RIB HEIGHT          (-)
C PHI    ... REPEATED-RIB FLOW ATTACK ANGLE                 (DEGREES)
C POWERO ... PUMPING POWER PER UNIT CIRCUIT SURFACE AREA    (W/CM*2)
C PPOWER ... PUMPING POWER PER UNIT CIRCUIT SURFACE AREA    (W/CM*2)
C PRFF   ... COOLANT PRANDTL NUMBER DATA                    (-)
C PRFLUL ... COOLANT PRANDTL NUMBER AT CHANNEL EXIT         (-)
C PRFLUX ... COOLANT PRANDTL NUMBER AT POSITION X           (-)
C Q      ... INPUT HEAT FLUX FROM THE SURFACE               (W/M*2)
C QO     ... INPUT HEAT FLUX FROM THE SURFACE               (W/CM*2)
C RBFO   ... SAME AS RBFX                                 (DEG K/(2/CM*2)
C RBFX   ... FIN AND CHANNEL BASE TO COOLANT THERMAL
C               RESISTANCE AT POSITION X                  (DEG K/(W/M*2))
C RCO    ... SAME AS RCX                                 (DEG K/(W/CM*2))
C RCX    ... CONTRACTION THERMAL RESISTANCE AT POSITION X(DEG K/(W/M*2))
C REX    ... REYNOLDS NUMBER AT POSITION X                  (-)
C RESTAX ... MODIFIED REYNOLDS NUMBER AT POSITION X         (-)
C RFFO   ... SAME AS RFFX                                 (DEG K/(2/CM*2)
C RFFX   ... COOLANT BULK TEMPERATURE RISE THERMAL
C               RESISTANCE AT POSITION X                  (DEG K/(W/M*2))
C RHOFF  ... COOLANT DENSITY DATA                           (KG/M*3)
C RHOFLL ... COOLANT DENSITY AT CHANNEL EXIT                (KG/M*3)
C RHOFLX ... COOLANT DENSITY AT POSITION X                  (KG/M*3)
C RTBO   ... SAME AS RTBX                                (DEG K/(2/CM*2))
C RTBX   ... CIRCUIT SIDE OF THE SUBSTRATE TO THE FIN
C               AND CHANNEL BASE THERMAL RESISTANCE
C               AT POSITION X                             (DEG K/(W/M*2))
C RTOTO  ... TOTAL THERMAL RESISTANCE AT POSITION X      (DEG K/(W/CM*2))
C RTOTX  ... TOTAL THERMAL RESISTANCE AT POSITION X       (DEG K/(W/M*2))
C SINK   ... ALPHANUMERIC FOR SUBSTRATE TYPE                (-)
C T      ... SUBSTRATE THICKNESS                            (M)
C TO     ... SUBSTRATE THICKNESS                            (MICRONS)
C TBX    ... FIN BASE TEMPERATURE AT POSITION X             (DEG K)
C TFINL  ... AVERAGE FIN TEMPERATURE AT CHANNEL EXIT        (DEG K)
C TFINX  ... AVERAGE FIN TEMPERATURE AT POSITION X          (DEG K)
C TFILAV ... AVERAGE FIN TEMPERATURE MIDWAY BETWEEN
C               THE CHANNEL ENTRANCE AND CHANNEL EXIT       (DEG K)
C TFIXAV ... AVERAGE FIN TEMPERATURE MIDWAY BETWEEN
C               THE CHANNEL ENTRANCE AND POSITION X         (DEG K)
C TFLLAV ... AVERAGE COOLANT TEMPERATURE MIDWAY BETWEEN
C               THE CHANNEL ENTRANCE AND CHANNEL EXIT       (DEG K)
C TFLUIN ... COOLANT INLET TEMPERATURE                      (DEG K)
C TFLUL  ... COOLANT MIXED MEAN TEMPERATURE AT
```

```
C              CHANNEL EXIT                                      (DEG K)
C TFLUO   ... OUTLET COOLANT TEMPERATURE                         (DEG K)
C TFLUX   ... COOLANT MIXED MEAN TEMPERATURE AT
C              POSITION X                                        (DEG K)
C TFLXAV  ... AVERAGE COOLANT TEMPERATURE MIDWAY BETWEEN
C              THE CHANNEL ENTRANCE AND POSITION X               (DEG K)
C TMAX    ... MAXIMUM SURFACE TEMPERATURE                        (DEG K)
C TOTK    ... TOTAL PRESSURE LOSS COEFFICIENT                    (-)
C TPROPF  ... TEMPERATURES FOR FLUID PROPERTY DATA               (DEG K)
C TPROPW  ... TEMPERATURES FOR SUBSTRATE PROPERTY DATA           (DEG K)
C TRANS   ... TRANSITION REYNOLDS NUMBER                         (-)
C TTBL    ... AVERAGE SUBSTRATE TEMPERATURE AT
C              CHANNEL EXIT                                      (DEG K)
C TTBX    ... AVERAGE SUBSTRATE TEMPERATURE AT
C              POSITION X                                        (DEG K)
C TTIPX   ... FIN TIP TEMPERATURE AT POSITION X                  (DEG K)
C TTX     ... TOP SURFACE        (CIRCUIT SIDE) TEMPERATURE
C              AT POSITION X                                     (DEG K)
C VOLUME  ... COOLANT FLOW RATE PER UNIT
C              CIRCUIT SURFACE AREA                          ((M*3/S)/CM*2)
C VOLUMO  ... COOLANT FLOW RATE PER UNIT
C              CIRCUIT SURFACE AREA                          ((CM*3/S)/CM*2)
C V1CX    ... COOLANT FLOW VELOCITY AT POSITION X                (M/S)
C WC      ... CHANNEL WIDTH                                      (M)
C WCO     ... CHANNEL WIDTH                                      (MICRONS)
C WCEND   ... MAXIMUM CHANNEL WIDTH CONTROL VARIABLE             (-)
C WCINCR  ... CHANNEL WIDTH INCREMENT CONTROL VARIABLE           (-)
C WCSTAR  ... MINIMUM CHANNEL WIDTH CONTROL VARIABLE             (-)
C WW      ... FIN WIDTH                                          (M)
C WWBYWC  ... RATIO OF FIN WIDTH TO THE CHANNEL WIDTH            (-)
C WWO     ... FIN WIDTH                                          (MICRONS)
C X       ... POSITION FROM CHANNEL ENTRANCE                     (M)
C X1      ... CHANNEL WIDTH PLOTTING DATA                        (MICRONS)
C XX      ... POSITION FROM CHANNEL ENTRANCE PLOTTING DATA       (M)
C XSTAR   ... THERMAL ENTRY LENGTH                               (-)
C XSTARX  ... THERMAL ENTRY LENGTH PLOTTING DATA                 (-)
C Y1A     ... RTOTO PLOTTING DATA                            (DEG K/(W/CM*2))
C Y1B     ... RBFO PLOTTING DATA                             (DEG K/(W/CM*2))
C Y1C     ... RFFO PLOTTING DATA                             (DEG K/(W/CM*2))
C Y2      ... POWERO PLOTTING DATA                               (W/CM*2)
C Y3      ... IPLOINT PLOTTING DATA                              (-)
C Z       ... FIN HEIGHT                                         (M)
C ZO      ... FIN HEIGHT                                         (MICRONS)
C ZI      ... REPEATED-RIB SHAPE ANGLE                           (DEGREES)
C------------------------------------------------------------------------------
      SUBROUTINE RTOTAL(NCURVE,NSINK,NFLUID,TFLUIN,Q,ICASE,
     &                  WCSTAR,WCEND,WCINCR,WWBYWC,B,IZ,IX,
     &                  ASPECT,L,T,IKLOSS,ICONS,DELP,VOLUME,PPOWER,
     &                  EBYDE,PBYE,PHI,ZI,X1,Y1A,Y1B,Y1C,Y2,Y3,IINUM,
     &                  XX,XSTARX)
C INITIALIZE ARRAYS
      DIMENSION WC(400),RTOTX(400),
     &          TPROPF(20),CPFF(20),KFF(20),MUFF(20),PRFF(20),RHOFF(20),
     &          TPROPW(20),KWW(20),
     &          TTX(2),TBX(2),TTIPX(2),TFLUO(2),
     &          X1(5,2,100),Y1A(5,2,100),Y2(5,2,100),Y3(5,2,100),
     &          IINUM(5,2),Y1B(5,2,100),Y1C(5,2,100),XX(5,2,100),
     &          XSTARX(5,2,100),LAST(6)
      CHARACTER*4 FLUID(3),SINK(4)
      INTEGER WCSTAR,WCEND,WCINCR
```

```
      REAL KC,KE,K90,L,LPLUS,NUX,NUTX,KFF,KWW,MUFF,
     &     KFINL,KFINX,KFLUL,KFLUX,KTBL,KTBX,MUFILA,MUFIXA,MUFLLA,
     &     MUFLXA,MUFLUL,MUFLUX,LAST
C OBTAIN PROPERTY DATA ARRAYS FOR THE COOLANT AND THE SUBSTRATE
      CALL PROPER(NFLUID,NSINK,FLUID,SINK,
     &           NPROPF,TPROPF,CPFF,KFF,MUFF,PRFF,RHOFF,
     &           NPROPW,TPROPW,KWW)
C PRINTOUT INITIALIZATION FOR EACH NCURVE
      Q0=Q/10000.
      IIMAX=0
      CALL PRINTO(FLUID,TFLUIN,SINK,Q0,0)
C
C FLOW REGIME LOOP FOR THE THREE CASES
C
      IF(ICASE.EQ.2)GO TO 510
      IF(ICASE.EQ.3)GO TO 520
C     ICASE=1 - FULLY DEVELOPED LAMINAR FLOW IN SMOOTH
C               CHANNELS
      IMIN=1
      IMAX=1
      GO TO 530
510   CONTINUE
C     ICASE=2 - FULLY DEVELOPED AND DEVELOPING, LAMINAR AND
C               TURBULENT FLOW IN SMOOTH CHANNELS
      IMIN=1
      IMAX=2
      GO TO 530
520   CONTINUE
C     ICASE=3 - FULLY DEVELOPED TURBULENT FLOW IN REPEATED-RIB
C               ROUGHENED CHANNELS
      IMIN=2
      IMAX=2
530   CONTINUE
      DO 70000 IFLOW=IMIN,IMAX,1
C LABEL OUTPUT FILES
         DO 580 II=11,17,2
            IF(ICASE.EQ.1)WRITE(II,600)
            IF((IFLOW.EQ.1).AND.(ICASE.EQ.2))WRITE(II,601)
            IF((IFLOW.EQ.2).AND.(ICASE.EQ.2))WRITE(II,602)
            IF(ICASE.EQ.3)WRITE(II,603)
580      CONTINUE
600      FORMAT(' FULLY DEVELOPED LAMINAR FLOW IN SMOOTH CHANNELS')
601      FORMAT(' FULLY DEVELOPED/DEVELOPING LAMINAR FLOW IN SMOOTH ',
     &          'CHANNELS')
602      FORMAT(' FULLY DEVELOPED/DEVELOPING TURBULENT FLOW IN SMOOTH ',
     &          'CHANNELS')
603      FORMAT(' FULLY DEVELOPED TURBULENT FLOW IN REPEATED-',
     &          'RIB ROUGHENED CHANNELS')
C
C POSITION FROM CHANNEL ENTRANCE IMPLIED DO LOOP
C
      INUM=0
      IRETUR=1
      IXX=0
C
50    IXX=IXX+1
      IF(IXX.GT.100)GO TO 2000
C COMPUTE CHANNEL POSITION
         IF(IX.EQ.1)IXX=100
         X=L*0.01*FLOAT(101-IXX)
```

```
         IF(IX.EQ.1)X=L
C
C CHANNEL WIDTH LOOP
C
      DO 1000 IWC=WCSTAR,WCEND,WCINCR
         WC(IWC)=FLOAT(IWC)*01.E-06
         WW=WWBYWC*WC(IWC)
C       COMPUTE ASPECT RATIO AND Z
         IF(IZ.EQ.1)ASPECT=B/WC(IWC)
         IF(IZ.EQ.1)Z=B
         IF(IZ.EQ.2)Z=WC(IWC)*ASPECT
         ASPINV=1./ASPECT
C       THE NEXT LINE ASSUMES THAT THE PLENUM WIDTH IS 0.040 INCH
         ACBYAP=(WC(IWC)*Z)/((WW+WC(IWC))*0.040*0.0254)
C       COMPUTE HYDRAULIC DIAMETER
         IF(ASPECT.LE.0.1)DE=2.*Z
         IF((ASPECT.GT.0.1).AND.(ASPECT.LT.10.))
     &                   DE=4.*WC(IWC)*Z/(2.*(WC(IWC)+Z))
         IF(ASPECT.GE.10.)DE=2.*WC(IWC)
C        IF(ICASE.EQ.1)DE=2.*WC(IWC)
C       IF DE IS TOO SMALL DON'T DO COMPUTATIONS BECAUSE OF ERRORS
         IF(DE.LT.5.E-6)GO TO 55
C       COMPUTE LAMINAR EQUIVALENT DIAMETER - EQN. 2.3
         IF(IFLOW.NE.2)DLE=0.
         IF((IFLOW.EQ.2).AND.(ASPECT.GE.1.))
     &   DLE=DE*((2./3.)+(11./24.)*(ASPINV)*(2.-(ASPINV)))
         IF((IFLOW.EQ.2).AND.(ASPECT.LT.1.))
     &   DLE=DE*((2./3.)+(11./24.)*(ASPECT)*(2.-(ASPECT)))
C COMPUTE THERMAL RESISTANCE
        CALL RESIST(NCURVE,ICASE,IFLOW,IX,
     &  Q,WC(IWC),WW,X,L,T,ASPECT,ASPINV,Z,DE,DLE,ACBYAP,
     &  IKLOSS,ICONS,DELP,VOLUME,PPOWER,
     &  EBYDE,PBYE,PHI,ZI,
     &  TFLUIN,NPROPF,TPROPF,CPFF,KFF,MUFF,PRFF,RHOFF,
     &  NPROPW,TPROPW,KWW,
     &  IRETUR,TTX,TBX,TTIPX,TFLUO,DTPUML,DTPUMX,
     &  TFINL,TFLUL,TTBL,TFINX,TFLUX,TTBX,TFLLAV,TFLXAV,TFILAV,TFIXAV,
     &  CPFLUL,KFLUL,MUFLUL,PRFLUL,RHOFLL,MUFLLA,MUFILA,KFINL,KTBL,
     &  CPFLUX,KFLUX,MUFLUX,PRFLUX,RHOFLX,MUFLXA,MUFIXA,KFINX,KTBX,
     &  NUX,NUTX,V1CX,K90,KC,KE,FAPP,FINCRI,EFFX,
     &  TRANS,REX,RESTAX,XSTAR,LPLUS,
     &  RTBX,RCX,RBFX,RFFX,RTOTX(IWC))
C COME TO THIS LOCATION IF DE IS TOO SMALL
55    CONTINUE
C IF RE>3000 FOR LAMINAR FLOW, STOP LAMINAR FLOW CALCS.
C       IF((ICASE.NE.1).AND.((IFLOW.EQ.1).AND.(REX.GT.3000.)))GO TO 1009
C CHECK IF CHIP SURFACE TEMPERATURE (K) IS TOO LARGE TO BE OF INTEREST
        TMAX=Q*RTOTX(IWC)+(TFLUIN+DTPUML)
C       IF(TMAX.GT.400.)GO TO 900
C MODIFY UNITS FOR PRINTOUT
        WCO=WC(IWC)*1.E+6
        WWO=WW*1.E+6
        DEO=DE*1.E+6
        DLEO=DLE*1.E+6
        ZO=Z*1.E+6
        TO=T*1.E+6
        DELPO=DELP/6894.8
        VOLUMO=VOLUME*1.E+6
        POWERO=PPOWER
        RTBO=RTBX*1.E+4
```

```
          RCO=RCX*1.E+4
          RBFO=RBFX*1.E+4
          RFFO=RFFX*1.E+4
          RTOTO=RTOTX(IWC)*1.E+4
C CHECK IF RESULTS ARE TO BE PRINTED OUT (IF RE IS IN PROPER RANGE)
      IF((IFLOW.EQ.1).AND.(REX.GT.TRANS))GO TO 1008
      IF((IFLOW.EQ.2).AND.(REX.LT.TRANS))GO TO 1008
C WRITE SOME GOODIES TO THE SCREEN
C       TOTK=(ACBYAP**2.)*2.*K90+KC+KE
C       WRITE(6,999)NCURVE,REX,DELPO,TOTK
C999    FORMAT(' NCURVE = ',I1,'  REX = ',F6.0,'  DELP = ',F5.1,
C       &' PSI   TOTK = ',F4.1)
C PRINTOUT RESULTS
      WRITE(11,1001,ERR=1002)
     &              WCO,WWO,X,ZO,TO,ASPECT,ACBYAP,EBYDE,PBYE,PHI,ZI,
     &              DELPO,VOLUMO,POWERO,RTBO,RCO,RBFO,RFFO,RTOTO,DTPUML
1001  FORMAT(2(1X,F5.1),1X,F4.3,1X,F6.1,1X,F5.1,1X,F5.2,1X,F5.2,1X,
     &       1X,F5.3,1X,F4.1,2(1X,F3.0),1X,F4.0,1X,F6.2,1X,F5.2,1X,
     &       5(1X,F6.4),1X,F6.3)
1002  CONTINUE
      WRITE(13,1003,ERR=1004)
     &              DEO,DLEO,V1CX,REX,RESTAX,XSTAR,LPLUS,NUX,NUTX,FAPP,
     &              K90,KC,KE,FINCRI,EFFX
1003  FORMAT(2(1X,F5.1),1X,F5.2,2(1X,F6.0),2(1X,F6.4),2(1X,F6.2),
     &       1X,F6.5,3(1X,F4.2),1X,F6.2,1X,F6.5)
1004  CONTINUE
      WRITE(15,1005,ERR=1006)
     &              TFINL,TFLUL,TTBL,TFLLAV,TFILAV,TFINX,TFLUX,TTBX,
     &              TFLXAV,TFIXAV,TTX(2),TBX(2),TTIPX(2),TFLUO(2),
     &              DTPUML,DTPUMX
1005  FORMAT(14(1X,F6.1),2(1X,F6.3))
1006  CONTINUE
      WRITE(17,1007,ERR=1008)
     &              CPFLUL,CPFLUX,KFLUL,KFLUX,PRFLUL,PRFLUX,
     &              RHOFLL,RHOFLX,MUFLUL,MUFLUX,MUFLLA,MUFLXA,MUFILA,
     &              MUFIXA,KFINL,KFINX,KTBL,KTBX
1007  FORMAT(2(1X,F6.1),2(1X,F6.4),2(1X,F6.3),2(1X,F6.1),
     &       6(1X,F6.5),4(1X,F6.2))
1008  CONTINUE
C CHECK IF VALID DATA FOR PLOTTING
      IF(IRETUR.EQ.1)GO TO 900
      IF(RTOTO.LT.1.E-10)GO TO 900
C IDENTIFY POINT TYPES FOR PPLOTT
      IF((IFLOW.EQ.1).AND.(XSTAR.GT.0.1))IPOINT=1
      IF((IFLOW.EQ.2).AND.(XSTAR.GT.0.01))IPOINT=1
      IF((IFLOW.EQ.1).AND.(XSTAR.LE.0.1))IPOINT=2
      IF((IFLOW.EQ.2).AND.(XSTAR.LE.0.01))IPOINT=2
      IF((IFLOW.EQ.1).AND.(XSTAR.LT.0.005))IPOINT=3
      IF((IFLOW.EQ.2).AND.(REX.GT.28000.))IPOINT=3
C FILL PLOTTING ARRAYS
      INUM=INUM+1
      XX(NCURVE,IFLOW,INUM)=X
      XSTARX(NCURVE,IFLOW,INUM)=XSTAR
      X1(NCURVE,IFLOW,INUM)=WCO
      Y1A(NCURVE,IFLOW,INUM)=RTOTO
      Y1B(NCURVE,IFLOW,INUM)=RBFO
      Y1C(NCURVE,IFLOW,INUM)=RFFO
      Y2(NCURVE,IFLOW,INUM)=POWERO
      Y3(NCURVE,IFLOW,INUM)=IPOINT
900   CONTINUE
```

```
      IF(IXX.EQ.1)GO TO 905
C WRITE MAXIMUM THERMAL RESISTANCE VALUES TO THE SCREEN
      IF(((IX.EQ.2).AND.(RTOTO.LT.LAST(6))).AND.(IIMAX.EQ.0))
     &WRITE(5,902)(LAST(ILAST),ILAST=1,6),REX
902   FORMAT(/,' ...X... ..RTBX.. ...RCX.. ..RBFX.. ..RFFX.. ..RTOTX..
     & ..REX..',/,1X,F7.6,2X,F6.4,3X,F6.4,3X,F6.4,3X,F6.4,3X,F7.4,2X,
     &F6.1)
      IF(((IX.EQ.2).AND.(RTOTO.LT.LAST(6))).AND.(IIMAX.EQ.0))
     &IIMAX=1
905   CONTINUE
C FILL PREVIOUS VALUE ARRAY FOR PRINTOUT WHEN MAXIMUM REACHED
      LAST(1)=X
      LAST(2)=RTBO
      LAST(3)=RCO
      LAST(4)=RBFO
      LAST(5)=RFFO
      LAST(6)=RTOTO
C ZERO COMPUTED VALUES SO THAT IF EXECUTION RETURNS TO THIS RTOTAL
C SUBROUTINE, IT CAN BE MORE READILY DETERMINED WHICH CRITERION WAS
C NOT SATISFIED.
      RTBX=0.
      RCX=0.
      RBFX=0.
      RFFX=0.
      RTOTX(IWC)=0.
      DTPUMX=0.
      NUX=0.
      NUTX=0.
      FINCRI=0.
      EFFX=0.
      V1CX=0.
      REX=0.
      RESTAX=0.
      LPLUS=0.
      XSTAR=0.
      FAPP=0.
1000  CONTINUE
1009  CONTINUE
C     CHANNEL WIDTH LOOP TERMINATED
      IF(IX.EQ.1)GO TO 2001
      GO TO 50
2000  CONTINUE
2001  CONTINUE
C     POSITION FROM CHANNEL ENTRANCE LOOP TERMINATED
      IINUM(NCURVE,IFLOW)=INUM
70000 CONTINUE
C     FLOW REGIME LOOP TERMINATED
C PRINTOUT TERMINATION FOR EACH NCURVE
      CALL PRINTO(FLUID,TFLUIN,SINK,Q,1)
      RETURN
      END
C END OF FILE FOR SUBROUTINE RTOTAL
C-----------------------------------------------------------------------
C TEMPS:  WRITTEN BY RICHARD J. PHILLIPS.  TEMPS COMPUTES THE
C         NEW COOLANT AND SUBSTRATE TEMPERATURES AT VARIOUS LOCATIONS
C         SO THAT THE AVERAGE PROPERTIES MAY BE COMPUTED.
C-----------------------------------------------------------------------
C NAME       DESCRIPTION                                       UNITS
C DTPUML ... VISCOUS HEATING COOLANT TEMPERATURE RISE
C               UP TO CHANNEL EXIT                             (DEG K)
```

```
C DTPUMX ... VISCOUS HEATING COOLANT TEMPERATURE RISE
C               UP TO POSITION X                              (DEG K)
C EFFL    ... FIN EFFICIENCY AT CHANNEL EXIT                  (-)
C EFFX    ... FIN EFFICIENCY AT POSITION X                    (-)
C ERROR1-4.. RELATIVE ERROR                                   (-)
C ICLOSE ... ITERATION CONTROL VARIABLE                       (-)
C MZL,MZX... FIN EFFICIENCY VARIABLE                          (-)
C Q       ... INPUT HEAT FLUX FROM THE SURFACE                (W/CM*2)
C RBFL    ... FIN AND CHANNEL BASE TO COOLANT THERMAL
C               RESISTANCE AT CHANNEL EXIT               (DEG K/(W/M*2))
C RBFX    ... FIN AND CHANNEL BASE TO COOLANT THERMAL
C               RESISTANCE AT POSITION X                 (DEG K/(W/M*2))
C RFFL    ... COOLANT BULK TEMPERATURE RISE THERMAL
C               RESISTANCE AT CHANNEL EXIT               (DEG K/(W/M*2))
C RFFX    ... COOLANT BULK TEMPERATURE RISE THERMAL
C               RESISTANCE AT POSITION X                 (DEG K/(W/M*2))
C RTBL    ... CIRCUIT SIDE OF THE SUBSTRATE TO THE FIN
C               AND CHANNEL BASE THERMAL RESISTANCE
C               AT CHANNEL EXIT                          (DEG K/(W/M*2))
C RTBX    ... CIRCUIT SIDE OF THE SUBSTRATE TO THE FIN
C               AND CHANNEL BASE THERMAL RESISTANCE
C               AT POSITION X                            (DEG K/(W/M*2))
C RTOTL   ... TOTAL THERMAL RESISTANCE AT CHANNEL EXIT(DEG K/(W/M*2))
C RTOTX   ... TOTAL THERMAL RESISTANCE AT POSITION X  (DEG K/(W/M*2))
C TBL     ... FIN BASE TEMPERATURE AT CHANNEL EXIT            (DEG K)
C TBX     ... FIN BASE TEMPERATURE AT POSITION X              (DEG K)
C TFILAV ... AVERAGE FIN TEMPERATURE MIDWAY BETWEEN
C               THE CHANNEL ENTRANCE AND CHANNEL EXIT         (DEG K)
C TFINL   ... AVERAGE FIN TEMPERATURE AT CHANNEL EXIT         (DEG K)
C TFINX   ... AVERAGE FIN TEMPERATURE AT POSITION X           (DEG K)
C TFIXAV ... AVERAGE FIN TEMPERATURE MIDWAY BETWEEN
C               THE CHANNEL ENTRANCE AND POSITION X           (DEG K)
C TFLLAV ... AVERAGE COOLANT TEMPERATURE MIDWAY BETWEEN
C               THE CHANNEL ENTRANCE AND CHANNEL EXIT         (DEG K)
C TFLUIN ... COOLANT INLET TEMPERATURE                        (DEG K)
C TFLUL   ... COOLANT MIXED MEAN TEMPERATURE AT
C               CHANNEL EXIT                                  (DEG K)
C TFLUO   ... OUTLET COOLANT TEMPERATURE                      (DEG K)
C TFLUX   ... COOLANT MIXED MEAN TEMPERATURE AT
C               POSITION X                                    (DEG K)
C TFLXAV ... AVERAGE COOLANT TEMPERATURE MIDWAY BETWEEN
C               THE CHANNEL ENTRANCE AND POSITION X           (DEG K)
C TTBL    ... AVERAGE SUBSTRATE TEMPERATURE AT
C               CHANNEL EXIT                                  (DEG K)
C TTBX    ... AVERAGE SUBSTRATE TEMPERATURE AT
C               POSITION X                                    (DEG K)
C TTL     ... TOP SURFACE    (CIRCUIT SIDE) TEMPERATURE
C               AT CHANNEL EXIT                               (DEG K)
C TTX     ... TOP SURFACE       (CIRCUIT SIDE) TEMPERATURE
C               AT POSITION X                                 (DEG K)
C TTIPL   ... FIN TIP TEMPERATURE AT CHANNEL EXIT             (DEG K)
C TTIPX   ... FIN TIP TEMPERATURE AT POSITION X               (DEG K)
C------------------------------------------------------------------------
      SUBROUTINE TEMPS(TTX,TBX,TTIPX,TFLUIN,TFLUO,
     &                 TFLUL,TFLUX,TFINL,TFINX,TTBL,TTBX,
     &                 TFLLAV,TFLXAV,TFILAV,TFIXAV,
     &                 RTBL,RBFL,RFFL,RTOTL,RTBX,RBFX,RFFX,RTOTX,
     &                 Q,DTPUML,DTPUMX,MZL,EFFL,MZX,EFFX,ICLOSE)
C INITIALIZE VARIABLE ARRAYS
      DIMENSION TTX(2),TBX(2),TTIPX(2),TFLUO(2)
```

```
      REAL MZL,MZX
C COMPUTE NEW TEMPERATURES
C   COOLANT AT CHANNEL EXIT
      TFLUL=RFFL*Q+(TFLUIN+DTPUML)
      TFLUO(2)=TFLUL
      TFLLAV=(TFLUL+TFLUIN)/2.
C   COOLANT AT POSITION X
      TFLUX=RFFX*Q+(TFLUIN+DTPUMX)
      TFLXAV=(TFLUX+TFLUIN)/2.
C   FIN AT CHANNEL EXIT
      TBL=(RFFL+RBFL)*Q+(TFLUIN+DTPUML)
      IF(MZL.EQ.0.)RETURN
      TTIPL=((TBL-TFLUL)/COSH(MZL))+TFLUL
      TFINL=((TBL-TFLUL)*EFFL)+TFLUL
      TFILAV=(TFINL+TFLUIN)/2.
C   FIN AT POSITION X
      TBX(2)=(RFFX+RBFX)*Q+(TFLUIN+DTPUMX)
      IF(MZX.EQ.0.)RETURN
      TTIPX(2)=((TBX(2)-TFLUX)/COSH(MZX))+TFLUX
      TFINX=((TBX(2)-TFLUX)*EFFX)+TFLUX
      TFIXAV=(TFINX+TFLUIN)/2.
C   CAP SUBSTRATE AT CHANNEL EXIT
      TTL=RTOTL*Q+(TFLUIN+DTPUML)
      TTBL=(TTL+TBL)/2.
C   CAP SUBSTRATE AT POSITION X
      TTX(2)=RTOTX*Q+(TFLUIN+DTPUMX)
      TTBX=(TTX(2)+TBX(2))/2.
C  CHECK TEMPERATURE ERRORS
      ERROR1=ABS((TFLUO(1)-TFLUO(2))/TFLUO(1))
      ERROR2=ABS((TBX(1)-TBX(2))/TBX(1))
      ERROR3=ABS((TTIPX(1)-TTIPX(2))/TTIPX(1))
      ERROR4=ABS((TTX(1)-TTX(2))/TTX(1))
C     WRITE(6,*)TFLUO,TBX,TTIPX,TTX
C     WRITE(6,*)ERROR1,ERROR2,ERROR3,ERROR4
      IF(ERROR1.GT.0.0001)GO TO 500
      IF(ERROR2.GT.0.0001)GO TO 500
      IF(ERROR3.GT.0.0001)GO TO 500
      IF(ERROR4.GT.0.0001)GO TO 500
C     CLOSE ENOUGH
      ICLOSE=0
      RETURN
500   CONTINUE
C  RESET TEMPERATURES AND TRY AGAIN
      ICLOSE=1
      TFLUO(1)=(TFLUO(2)+TFLUO(1))/2.
      TBX(1)=(TBX(2)+TBX(1))/2.
      TTIPX(1)=(TTIPX(2)+TTIPX(1))/2.
      TTX(1)=(TTX(2)+TTX(1))/2.
      RETURN
      END
C END OF FILE FOR SUBROUTINE TEMPS
C-----------------------------------------------------------------------
C PROP:  WRITTEN BY RICHARD J. PHILLIPS.  PROP COMPUTES THE
C        LIQUID COOLANT AND SUBSTRATE MATERIAL PROPERTIES.
C-----------------------------------------------------------------------
C NAME       DESCRIPTION                                        UNITS
C CPFF   ... COOLANT SPECIFIC HEAT DATA                         (J/KG DEG K)
C CPFLUL ... COOLANT SPECIFIC HEAT AT CHANNEL EXIT              (J/KG DEG K)
C CPFLUX ... COOLANT SPECIFIC HEAT AT POSITION X                (J/KG DEG K)
C FACTOR ... INTERPOLATION PARAMETER                            (-)
```

```
C IRETUR ... CONTROL VARIABLE FOR OUT OF RANGE DATA           (-)
C KFF    ... COOLANT THERMAL CONDUCTIVITY DATA                (W/M DEG K)
C KFINL  ... AVERAGE FIN THERMAL CONDUCTIVITY AT
C              CHANNEL EXIT                                   (W/M DEG K)
C KFINX  ... AVERAGE FIN THERMAL CONDUCTIVITY AT
C              POSITION X                                     (W/M DEG K)
C KFLUL  ... COOLANT THERMAL CONDUCTIVITY AT
C              CHANNEL EXIT                                   (W/M DEG K)
C KFLUX  ... COOLANT THERMAL CONDUCTIVITY AT
C              POSITION X                                     (W/M DEG K)
C KTBL   ... AVERAGE SUBSTRATE THERMAL CONDUCTIVITY
C              AT CHANNEL EXIT                                (W/M DEG K)
C KTBX   ... AVERAGE SUBSTRATE THERMAL CONDUCTIVITY
C              AT POSITION X                                  (W/M DEG K)
C KWW    ... SUBSTRATE THERMAL CONDUCTIVITY DATA              (W/M DEG K)
C MUFF   ... COOLANT DYNAMIC VISCOSITY DATA                   (KG/M S)
C MUFILA ... AVERAGE COOLANT DYNAMIC VISCOSITY AT THE
C              AVERAGE FIN TEMPERATURE BETWEEN THE
C              CHANNEL ENTRANCE AND EXIT                      (KG/M S)
C MUFIXA ... AVERAGE COOLANT DYNAMIC VISCOSITY AT THE
C              AVERAGE FIN TEMPERATURE BETWEEN THE
C              CHANNEL ENTRANCE AND POSITION X                (KG/M S)
C MUFLLA ... AVERAGE COOLANT DYNAMIC VISCOSITY AT THE
C              AVERAGE COOLANT TEMPERATURE BETWEEN THE
C              CHANNEL ENTRANCE AND EXIT                      (KG/M S)
C MUFLXA ... AVERAGE COOLANT DYNAMIC VISCOSITY AT THE
C              AVERAGE COOLANT TEMPERATURE BETWEEN THE
C              CHANNEL ENTRANCE AND POSITION X                (KG/M S)
C MUFLUL ... COOLANT DYNAMIC VISCOSITY AT CHANNEL EXIT        (KG/M S)
C MUFLUX ... COOLANT DYNAMIC VISCOSITY AT POSITION X          (KG/M S)
C NPROP  ... DUMMY VARIABLE                                   (-)
C NPROPF ... NUMBER OF COOLANT DATA ENTRIES                   (-)
C NPROPW ... NUMBER OF SUBSTRATE MATERIAL DATA ENTRIES        (-)
C PRFF   ... COOLANT PRANDTL NUMBER DATA                      (-)
C PRFLUL ... COOLANT PRANDTL NUMBER AT CHANNEL EXIT           (-)
C PRFLUX ... COOLANT PRANDTL NUMBER AT POSITION X             (-)
C RHOFF  ... COOLANT DENSITY DATA                             (KG/M*3)
C RHOFLL ... COOLANT DENSITY AT CHANNEL EXIT                  (KG/M*3)
C RHOFLX ... COOLANT DENSITY AT POSITION X                    (KG/M*3)
C TFILAV ... AVERAGE FIN TEMPERATURE MIDWAY BETWEEN
C              THE CHANNEL ENTRANCE AND CHANNEL EXIT          (DEG K)
C TFIXAV ... AVERAGE FIN TEMPERATURE MIDWAY BETWEEN
C              THE CHANNEL ENTRANCE AND POSITION X            (DEG K)
C TFLLAV ... AVERAGE COOLANT TEMPERATURE MIDWAY BETWEEN
C              THE CHANNEL ENTRANCE AND CHANNEL EXIT          (DEG K)
C TFLXAV ... AVERAGE COOLANT TEMPERATURE MIDWAY BETWEEN
C              THE CHANNEL ENTRANCE AND POSITION X            (DEG K)
C TFINX  ... AVERAGE FIN TEMPERATURE AT POSITION X            (DEG K)
C TFINL  ... AVERAGE FIN TEMPERATURE AT CHANNEL EXIT          (DEG K)
C TFLUL  ... COOLANT MIXED MEAN TEMPERATURE AT
C              CHANNEL EXIT                                   (DEG K)
C TFLUX  ... COOLANT MIXED MEAN TEMPERATURE AT
C              POSITION X                                     (DEG K)
C TPROPF ... TEMPERATURES FOR FLUID PROPERTY DATA             (DEG K)
C TPROPW ... TEMPERATURES FOR SUBSTRATE PROPERTY DATA         (DEG K)
C TTBL   ... AVERAGE SUBSTRATE TEMPERATURE AT
C              CHANNEL EXIT                                   (DEG K)
C TTBX   ... AVERAGE SUBSTRATE TEMPERATURE AT
C              POSITION X                                     (DEG K)
C-----------------------------------------------------------------------
```

```
      SUBROUTINE PROP(NPROPF,TPROPF,CPFF,KFF,MUFF,PRFF,RHOFF,
     &                NPROPW,TPROPW,KWW,
     &                TFLUX,CPFLUX,KFLUX,MUFLUX,PRFLUX,RHOFLX,
     &                TFINX,KFINX,TTBX,KTBX,
     &                TFLUL,CPFLUL,KFLUL,MUFLUL,PRFLUL,RHOFLL,
     &                TFINL,KFINL,TTBL,KTBL,
     &                TFLLAV,MUFLLA,TFLXAV,MUFLXA,
     &                TFILAV,MUFILA,TFIXAV,MUFIXA,IRETUR)
C INITIALIZE VARIABLE ARRAYS
      DIMENSION TPROPF(20),CPFF(20),KFF(20),MUFF(20),PRFF(20),RHOFF(20),
     &          TPROPW(20),KWW(20)
      REAL MUFF,KFF,KWW,KFLUX,MUFLUX,KFINX,KTBX,KFLUL,MUFLUL,KFINL,KTBL,
     &     MUFLLA,MUFLXA,MUFILA,MUFIXA
C OUT OF TEMPERATURE RANGE CONTROL
C      0 = WITHIN RANGE
C      1 = OUT OF RANGE
      IRETUR=0
C**********
C CONSTANT PROPERTY VALUES OBTAINED AT CHANNEL POSITION X
C**********
C COOLANT
      NPROP=NPROPF-1
      DO 100 I=1,NPROP
         IF((TFLUX.GE.TPROPF(I)).AND.(TFLUX.LT.TPROPF(I+1)))GO TO 150
100   CONTINUE
      WRITE(11,101)
101   FORMAT(' TFLUX IS OUT OF RANGE OF PROPERTY DATA ')
      IRETUR=1
      RETURN
150   CONTINUE
      FACTOR=(TFLUX-TPROPF(I))/(TPROPF(I+1)-TPROPF(I))
      CPFLUX=FACTOR*(CPFF(I+1)-CPFF(I))+CPFF(I)
      KFLUX=FACTOR*(KFF(I+1)-KFF(I))+KFF(I)
      MUFLUX=FACTOR*(MUFF(I+1)-MUFF(I))+MUFF(I)
      PRFLUX=FACTOR*(PRFF(I+1)-PRFF(I))+PRFF(I)
      RHOFLX=FACTOR*(RHOFF(I+1)-RHOFF(I))+RHOFF(I)
C FIN
      NPROP=NPROPW-1
      DO 200 I=1,NPROP,1
         IF((TFINX.GE.TPROPW(I)).AND.(TFINX.LT.TPROPW(I+1)))GO TO 250
200   CONTINUE
      WRITE(11,201)
201   FORMAT(' TFINX IS OUT OF RANGE FOR PROPERTY DATA ')
      IRETUR=1
      RETURN
250   CONTINUE
      FACTOR=(TFINX-TPROPW(I))/(TPROPW(I+1)-TPROPW(I))
      KFINX=FACTOR*(KWW(I+1)-KWW(I))+KWW(I)
C CAP (SOLID SUBSTRATE MATERIAL)
      NPROP=NPROPW-1
      DO 300 I=1,NPROP,1
         IF((TTBX.GE.TPROPW(I)).AND.(TTBX.LT.TPROPW(I+1)))GO TO 350
300   CONTINUE
      WRITE(11,301)
301   FORMAT(' TTBX IS OUT OF RANGE FOR PROPERTY DATA')
      IRETUR=1
      RETURN
350   CONTINUE
      FACTOR=(TTBX-TPROPW(I))/(TPROPW(I+1)-TPROPW(I))
      KTBX=FACTOR*(KWW(I+1)-KWW(I))+KWW(I)
```

```
C**********
C CONSTANT PROPERTY VALUES OBTAINED AT THE CHANNEL EXIT
C**********
C COOLANT
      NPROP=NPROPF-1
      DO 400 I=1,NPROP
         IF((TFLUL.GE.TPROPF(I)).AND.(TFLUL.LT.TPROPF(I+1)))GO TO 450
400   CONTINUE
      WRITE(11,401)
401   FORMAT(' TFLUL IS OUT OF RANGE OF PROPERTY DATA ')
      IRETUR=1
      RETURN
450   CONTINUE
      FACTOR=(TFLUL-TPROPF(I))/(TPROPF(I+1)-TPROPF(I))
      CPFLUL=FACTOR*(CPFF(I+1)-CPFF(I))+CPFF(I)
      KFLUL=FACTOR*(KFF(I+1)-KFF(I))+KFF(I)
      MUFLUL=FACTOR*(MUFF(I+1)-MUFF(I))+MUFF(I)
      PRFLUL=FACTOR*(PRFF(I+1)-PRFF(I))+PRFF(I)
      RHOFLL=FACTOR*(RHOFF(I+1)-RHOFF(I))+RHOFF(I)
C FIN
      NPROP=NPROPW-1
      DO 500 I=1,NPROP,1
         IF((TFINL.GE.TPROPW(I)).AND.(TFINL.LT.TPROPW(I+1)))GO TO 550
500   CONTINUE
      WRITE(11,501)
501   FORMAT(' TFINL IS OUT OF RANGE FOR PROPERTY DATA ')
      IRETUR=1
      RETURN
550   CONTINUE
      FACTOR=(TFINL-TPROPW(I))/(TPROPW(I+1)-TPROPW(I))
      KFINL=FACTOR*(KWW(I+1)-KWW(I))+KWW(I)
C CAP (SOLID SUBSTRATE MATERIAL)
      NPROP=NPROPW-1
      DO 600 I=1,NPROP,1
         IF((TTBL.GE.TPROPW(I)).AND.(TTBL.LT.TPROPW(I+1)))GO TO 650
600   CONTINUE
      WRITE(11,601)
601   FORMAT(' TTBL IS OUT OF RANGE FOR PROPERTY DATA')
      IRETUR=1
      RETURN
650   CONTINUE
      FACTOR=(TTBL-TPROPW(I))/(TPROPW(I+1)-TPROPW(I))
      KTBL=FACTOR*(KWW(I+1)-KWW(I))+KWW(I)
C**********
C VISCOSITY VALUE OBTAINED AT THE MIXED-MEAN COOLANT
C TEMPERATURE (BETWEEN THE CHANNEL ENTRANCE AND EXIT)
C**********
      NPROP=NPROPF-1
      DO 700 I=1,NPROP
         IF((TFLLAV.GE.TPROPF(I)).AND.(TFLLAV.LT.TPROPF(I+1)))
     &   GO TO 750
700   CONTINUE
      WRITE(11,701)
701   FORMAT(' TFLLAV IS OUT OF RANGE OF PROPERTY DATA ')
      IRETUR=1
      RETURN
750   CONTINUE
      FACTOR=(TFLLAV-TPROPF(I))/(TPROPF(I+1)-TPROPF(I))
      MUFLLA=FACTOR*(MUFF(I+1)-MUFF(I))+MUFF(I)
C**********
```

```
C VISCOSITY VALUE OBTAINED AT THE MIXED-MEAN COOLANT
C TEMPERATURE (BETWEEN THE CHANNEL ENTRANCE AND CHANNEL POSITION X)
C**********
      NPROP=NPROPF-1
      DO 800 I=1,NPROP
         IF((TFLXAV.GE.TPROPF(I)).AND.(TFLXAV.LT.TPROPF(I+1)))
     &   GO TO 850
800   CONTINUE
      WRITE(11,801)
801   FORMAT(' TFLXAV IS OUT OF RANGE OF PROPERTY DATA ')
      IRETUR=1
      RETURN
850   CONTINUE
      FACTOR=(TFLXAV-TPROPF(I))/(TPROPF(I+1)-TPROPF(I))
      MUFLXA=FACTOR*(MUFF(I+1)-MUFF(I))+MUFF(I)
C**********
C VISCOSITY VALUE OBTAINED AT THE AVERAGE FIN
C TEMPERATURE (BETWEEN THE CHANNEL ENTRANCE AND EXIT)
C**********
      NPROP=NPROPF-1
      DO 900 I=1,NPROP
         IF((TFILAV.GE.TPROPF(I)).AND.(TFILAV.LT.TPROPF(I+1)))
     &   GO TO 950
900   CONTINUE
      WRITE(11,901)
901   FORMAT(' TFILAV IS OUT OF RANGE OF PROPERTY DATA ')
      IRETUR=1
      RETURN
950   CONTINUE
      FACTOR=(TFILAV-TPROPF(I))/(TPROPF(I+1)-TPROPF(I))
      MUFILA=FACTOR*(MUFF(I+1)-MUFF(I))+MUFF(I)
C**********
C VISCOSITY VALUE OBTAINED AT THE AVERAGE FIN
C TEMPERATURE (BETWEEN THE CHANNEL ENTRANCE AND CHANNEL POSITION X)
C**********
      NPROP=NPROPF-1
      DO 1000 I=1,NPROP
         IF((TFIXAV.GE.TPROPF(I)).AND.(TFIXAV.LT.TPROPF(I+1)))
     &   GO TO 1050
1000  CONTINUE
      WRITE(11,1001)
1001  FORMAT(' TFIXAV IS OUT OF RANGE OF PROPERTY DATA ')
      IRETUR=1
      RETURN
1050  CONTINUE
      FACTOR=(TFIXAV-TPROPF(I))/(TPROPF(I+1)-TPROPF(I))
      MUFIXA=FACTOR*(MUFF(I+1)-MUFF(I))+MUFF(I)
      RETURN
      END
C END OF FILE FOR SUBROUTINE PROP
C----------------------------------------------------------------------
C RESIST:  WRITTEN BY RICHARD J. PHILLIPS.  RESIST COMPUTES THE THERMAL-
C          HYDRAULIC PERFORMANCE.
C----------------------------------------------------------------------
C NAME       DESCRIPTION                                        UNITS
C ACBYAP ... RATIO OF FREE-FLOW TO FRONTAL CROSS-SECTIONAL
C               AREAS                                            (-)
C ASPEC  ... CHANNEL ASPECT RATIO FOR SMOOTH-CHANNEL
C               F AND NU CALCULATIONS                            (-)
C ASPECT ... CHANNEL ASPECT RATIO(FIN LENGTH/CHANNEL WIDTH)(-)
```

```
C ASPINV ... INVERSE OF THE CHANNEL ASPECT RATIO              (-)
C CPFF   ... COOLANT SPECIFIC HEAT DATA                       (J/KG DEG K)
C CPFLUL ... COOLANT SPECIFIC HEAT AT CHANNEL EXIT            (J/KG DEG K)
C CPFLUX ... COOLANT SPECIFIC HEAT AT POSITION X              (J/KG DEG K)
C DE     ... HYDRAULIC DIAMETER                               (M)
C DELP   ... PRESSURE DROP                                    (N/M*2)
C DLE    ... LAMINAR EQUIVALENT DIAMETER                      (M)
C DTPUML ... VISCOUS HEATING TEMPERATURE RISE AT CHANNEL
C              EXIT                                           (DEG K)
C DTPUMX ... VISCOUS HEATING TEMPERATURE RISE AT POSITION X(DEG K)
C DUMPHI ... FRICTION FACTOR CORRECTION FOR CHANNEL SHAPE     (-)
C EBYDE  ... RATIO OF RIB HEIGHT TO HYDRAULIC DIAMETER        (-)
C EFFL   ... FIN EFFICIENCY AT CHANNEL EXIT                   (-)
C EFFX   ... FIN EFFICIENCY AT CHANNEL POSITION X             (-)
C F1,F2  ... ONE-SIDE AND TWO-SIDE REPEATED-RIB ROUGHENED
C              FRICTION FACTORS                               (-)
C FACT   ... VARIABLE PROPERTIES COMPENSATION FACTOR          (-)
C FACTX  ... THERMAL SPREADING FACTOR IN X-DIRECTION          (-)
C FACTY  ... THERMAL SPREADING FACTOR IN Y-DIRECTION          (-)
C FAPP   ... APPARANT FRICTION FACTOR                         (-)
C FINCRI ... FIN CRITERION                                    (-)
C HL     ... HEAT TRANSFER COEFFICIENT AT CHANNEL EXIT        (W/M DEG K)
C HX     ... HEAT TRANSFER COEFFICIENT AT POSITION X          (W/M DEG K)
C ICASE  ... CASE SELECTION CONTROL VARIABLE                  (-)
C ICONS  ... COOLANT FLOW CONSTRAINT                          (-)
C ICLOSE ... ITERATION CONTROL VARIABLE                       (-)
C IFLOW  ... FLOW REGIME INDICATOR                            (-)
C IKLOSS ... CONTROL FOR INCLUDING K90, KC AND KE             (-)
C IRETUR ... CONTROL VARIABLE FOR OUT OF RANGE PROP. DATA     (-)
C IX     ... CONTROL VARIABLE FOR IF X OR WC IS VARIED        (-)
C KC     ... ENTRANCE PRESSURE LOSS COEFFICIENT               (-)
C KE     ... EXIT PRESSURE LOSS COEFFICIENT                   (-)
C K90    ... NINETY DEGREE BEND PRESSURE LOSS COEFFICIENT     (-)
C KFF    ... COOLANT THERMAL CONDUCTIVITY DATA                (W/M DEG K)
C KFINL  ... AVERAGE FIN THERMAL CONDUCTIVITY AT
C              CHANNEL EXIT                                   (W/M DEG K)
C KFINX  ... AVERAGE FIN THERMAL CONDUCTIVITY AT
C              POSITION X                                     (W/M DEG K)
C KFLUL  ... COOLANT THERMAL CONDUCTIVITY AT
C              CHANNEL EXIT                                   (W/M DEG K)
C KFLUX  ... COOLANT THERMAL CONDUCTIVITY AT
C              POSITION X                                     (W/M DEG K)
C KTBL   ... AVERAGE SUBSTRATE THERMAL CONDUCTIVITY
C              AT CHANNEL EXIT                                (W/M DEG K)
C KTBX   ... AVERAGE SUBSTRATE THERMAL CONDUCTIVITY
C              AT POSITION X                                  (W/M DEG K)
C KWW    ... SUBSTRATE THERMAL CONDUCTIVITY DATA              (W/M DEG K)
C L      ... CHANNEL LENGTH                                   (M)
C LPLUS  ... HYDRODYNAMIC ENTRY LENGTH                        (-)
C ML     ... FIN ANALYSIS PARAMETER AT CHANNEL EXIT           (1/M)
C MX     ... FIN ANALYSIS PARAMETER AT POSITION X             (1/M)
C MUFF   ... COOLANT DYNAMIC VISCOSITY DATA                   (KG/M S)
C MUFILA ... AVERAGE COOLANT DYNAMIC VISCOSITY AT THE
C              AVERAGE FIN TEMPERATURE BETWEEN THE
C              CHANNEL ENTRANCE AND EXIT                      (KG/M S)
C MUFIXA ... AVERAGE COOLANT DYNAMIC VISCOSITY AT THE
C              AVERAGE FIN TEMPERATURE BETWEEN THE
C              CHANNEL ENTRANCE AND POSITION X                (KG/M S)
C MUFLLA ... AVERAGE COOLANT DYNAMIC VISCOSITY AT THE
C              AVERAGE COOLANT TEMPERATURE BETWEEN THE
```

```
C                 CHANNEL ENTRANCE AND EXIT                        (KG/M S)
C MUFLUL ... COOLANT DYNAMIC VISCOSITY AT CHANNEL EXIT             (KG/M S)
C MUFLUX ... COOLANT DYNAMIC VISCOSITY AT POSITION X               (KG/M S)
C MUFLXA ... AVERAGE COOLANT DYNAMIC VISCOSITY AT THE
C                 AVERAGE COOLANT TEMPERATURE BETWEEN THE
C                 CHANNEL ENTRANCE AND POSITION X                  (KG/M S)
C MZL    ... FIN EFFICIENCY VARIABLE AT CHANNEL EXIT               (-)
C MZX    ... FIN EFFICIENCY VARIABLE AT POSITION X                 (-)
C NCHAN  ... NUMBER OF CHANNELS PER CENTIMETER CHIP WIDTH          (-)
C NFLUID ... COOLANT IDENTIFIER NUMBER                             (-)
C NPARAL ... NUMBER OF CHANNELS IN SERIES PER CENTIMETER
C                 CHIP WIDTH                                       (-)
C NPROPF ... NUMBER OF COOLANT DATA ENTRIES                        (-)
C NPROPW ... NUMBER OF SUBSTRATE DATA ENTRIES                      (-)
C NSINK  ... SUBSTRATE MATERIAL INDENTIFIER NUMBER                 (-)
C NUL    ... NUSSELT NUMBER AT CHANNEL EXIT                        (-)
C NUX    ... NUSSELT NUMBER AT CHANNEL POSITION X                  (-)
C NUTL   ... NUSSELT NUMBER AT CHANNEL EXIT INCUDING
C                 EFFECT OF NONUNIFORM COOLANT TEMPERATURE         (-)
C NUTX   ... NUSSELT NUMBER AT CHANNEL POSITION X INCUDING
C                 EFFECT OF NONUNIFORM COOLANT TEMPERATURE         (-)
C PBYE   ... RATIO OF RIB SEPARATION TO RIB HEIGHT                 (-)
C PHI    ... REPEATED-RIB FLOW ATTACK ANGLE                        (DEGREES)
C PPOWER ... PUMPING POWER PER UNIT CIRCUIT SURFACE AREA           (W/CM*2)
C PRFF   ... COOLANT PRANDTL NUMBER DATA                           (-)
C PRFLUL ... COOLANT PRANDTL NUMBER AT CHANNEL EXIT                (-)
C PRFLUX ... COOLANT PRANDTL NUMBER AT POSITION X                  (-)
C Q      ... INPUT HEAT FLUX FROM THE SURFACE                      (W/CM*2)
C RBFL   ... FIN AND CHANNEL BASE TO COOLANT THERMAL
C                 RESISTANCE AT CHANNEL EXIT                     (DEG K/(W/M*2))
C RBFX   ... FIN AND CHANNEL BASE TO COOLANT THERMAL
C                 RESISTANCE AT POSITION X                       (DEG K/(W/M*2))
C RCL    ... CONTRACTION THERMAL RESISTANCE AT
C                 CHANNEL EXIT                                   (DEG K/(W/M*2))
C RCX    ... CONTRACTION THERMAL RESISTANCE AT POSITION X(DEG K/(W/M*2))
C REL    ... REYNOLDS NUMBER AT CHANNEL EXIT                       (-)
C REX    ... REYNOLDS NUMBER AT POSITION X                         (-)
C RESTAL ... MODIFIED REYNOLDS NUMBER AT CHANNEL EXIT              (-)
C RESTAX ... MODIFIED REYNOLDS NUMBER AT POSITION X                (-)
C RFFL   ... COOLANT BULK TEMPERATURE RISE THERMAL
C                 RESISTANCE AT CHANNEL EXIT                     (DEG K/(W/M*2))
C RFFX   ... COOLANT BULK TEMPERATURE RISE THERMAL
C                 RESISTANCE AT POSITION X                       (DEG K/(W/M*2))
C RHOFF  ... COOLANT DENSITY DATA                                  (KG/M*3)
C RHOFLL ... COOLANT DENSITY AT CHANNEL EXIT                       (KG/M*3)
C RHOFLX ... COOLANT DENSITY AT POSITION X                         (KG/M*3)
C RTBL   ... CIRCUIT SIDE OF THE SUBSTRATE TO THE FIN
C                 AND CHANNEL BASE THERMAL RESISTANCE
C                 AT CHANNEL EXIT                                (DEG K/(W/M*2))
C RTBX   ... CIRCUIT SIDE OF THE SUBSTRATE TO THE FIN
C                 AND CHANNEL BASE THERMAL RESISTANCE
C                 AT POSITION X                                  (DEG K/(W/M*2))
C RTOTL  ... TOTAL THERMAL RESISTANCE AT CHANNEL EXIT            (DEG K/(W/M*2))
C RTOTX  ... TOTAL THERMAL RESISTANCE AT POSITION X              (DEG K/(W/M*2))
C T      ... SUBSTRATE THICKNESS                                   (M)
C TBL    ... FIN BASE TEMPERATURE AT CHANNEL EXIT                  (DEG K)
C TBX    ... FIN BASE TEMPERATURE AT POSITION X                    (DEG K)
C TFINL  ... AVERAGE FIN TEMPERATURE AT CHANNEL EXIT               (DEG K)
C TFINX  ... AVERAGE FIN TEMPERATURE AT POSITION X                 (DEG K)
C TFILAV ... AVERAGE FIN TEMPERATURE MIDWAY BETWEEN
```

```
C                   THE CHANNEL ENTRANCE AND CHANNEL EXIT       (DEG K)
C TFIXAV ... AVERAGE FIN TEMPERATURE MIDWAY BETWEEN
C                   THE CHANNEL ENTRANCE AND POSITION X         (DEG K)
C TFLLAV ... AVERAGE COOLANT TEMPERATURE MIDWAY BETWEEN
C                   THE CHANNEL ENTRANCE AND CHANNEL EXIT       (DEG K)
C TFLUIN ... COOLANT INLET TEMPERATURE                          (DEG K)
C TFLUL  ... COOLANT MIXED MEAN TEMPERATURE AT
C                   CHANNEL EXIT                                (DEG K)
C TFLUO  ... OUTLET COOLANT TEMPERATURE                         (DEG K)
C TFLUX  ... COOLANT MIXED MEAN TEMPERATURE AT
C                   POSITION X                                  (DEG K)
C TFLXAV ... AVERAGE COOLANT TEMPERATURE MIDWAY BETWEEN
C                   THE CHANNEL ENTRANCE AND POSITION X         (DEG K)
C TPROPF ... TEMPERATURES FOR FLUID PROPERTY DATA               (DEG K)
C TPROPW ... TEMPERATURES FOR SUBSTRATE PROPERTY DATA           (DEG K)
C TRANS  ... TRANSITION REYNOLDS NUMBER                         (-)
C TTBL   ... AVERAGE SUBSTRATE TEMPERATURE AT
C                   CHANNEL EXIT                                (DEG K)
C TTBX   ... AVERAGE SUBSTRATE TEMPERATURE AT
C                   POSITION X                                  (DEG K)
C TTIPX  ... FIN TIP TEMPERATURE AT POSITION X                  (DEG K)
C TTL    ... TOP SURFACE (CIRCUIT SIDE) TEMPERATURE
C                   AT CHANNEL EXIT                             (DEG K)
C TTX    ... TOP SURFACE (CIRCUIT SIDE) TEMPERATURE
C                   AT POSITION X                               (DEG K)
C VOLUME ... COOLANT FLOW RATE PER CHANNEL                 ((M*3/S)/CM*2)
C V1CL   ... COOLANT FLOW VELOCITY AT CHANNEL EXIT              (M/S)
C V1CX   ... COOLANT FLOW VELOCITY AT POSITION X                (M/S)
C W      ... WIDTH OF HEATER TRANSVERSE TO FLOW DIRECTION       (M)
C WC     ... CHANNEL WIDTH                                      (M)
C WW     ... FIN WIDTH                                          (M)
C WWBYWC ... RATIO OF FIN WIDTH TO THE CHANNEL WIDTH            (-)
C X      ... POSITION FROM CHANNEL ENTRANCE                     (M)
C XSTARL ... THERMAL ENTRY LENGTH AT CHANNEL EXIT               (-)
C XSTARX ... THERMAL ENTRY LENGTH AT POSITION X                 (-)
C Y      ... DISTANCE FROM ONE TRANSVERSE SIDE OF HEATER        (M)
C Z      ... FIN HEIGHT                                         (M)
C ZI     ... REPEATED-RIB SHAPE ANGLE                           (DEGREES)
C-----------------------------------------------------------------------
      SUBROUTINE RESIST(NCURVE,ICASE,IFLOW,IX,
     & Q,WC,WW,X,L,T,ASPECT,ASPINV,Z,DE,DLE,ACBYAP,
     & IKLOSS,ICONS,DELP,VOLUME,PPOWER,
     & EBYDE,PBYE,PHI,ZI,
     & TFLUIN,NPROPF,TPROPF,CPFF,KFF,MUFF,PRFF,RHOFF,
     & NPROPW,TPROPW,KWW,
     & IRETUR,TTX,TBX,TTIPX,TFLUO,DTPUML,DTPUMX,
     & TFINL,TFLUL,TTBL,TFINX,TFLUX,TTBX,TFLLAV,TFLXAV,TFILAV,TFIXAV,
     & CPFLUL,KFLUL,MUFLUL,PRFLUL,RHOFLL,MUFLLA,MUFILA,KFINL,KTBL,
     & CPFLUX,KFLUX,MUFLUX,PRFLUX,RHOFLX,MUFLXA,MUFIXA,KFINX,KTBX,
     & NUX,NUTX,V1CX,K90,KC,KE,FAPP,FINCRI,EFFX,
     & TRANS,REX,RESTAX,XSTARX,LPLUS,
     & RTBX,RCX,RBFX,RFFX,RTOTX)
C INITIALIZE VARIABLE ARRAYS
      DIMENSION TTX(2),TBX(2),TTIPX(2),TFLUO(2),
     &          TPROPF(20),CPFF(20),KFF(20),MUFF(20),PRFF(20),RHOFF(20),
     &          TPROPW(20),KWW(20)
      REAL L,K90,KC,KE,KWW,KFF,MUFF,NUL,NUX,NUTL,NUTX,ML,MX,MZL,MZX,
     &     LPLUS,NCHAN,NPARAL,
     &     KFINL,KFLUL,KTBL,KFINX,KFLUX,KTBX,
     &     MUFLUL,MUFLUX,MUFLLA,MUFLXA,MUFILA,MUFIXA
```

```
C INITIALIZE TEMPERATURES TO EQUAL INLET COOLANT TEMP. - FIRST ITERATION
      DO 15 I=1,2,1
         TTX(I)=TFLUIN
         TBX(I)=TFLUIN
         TTIPX(I)=TFLUIN
         TFLUO(I)=TFLUIN
15    CONTINUE
      TFLUX=TFLUIN
      TFINX=TFLUIN
      TTBX=TFLUIN
      TFLUL=TFLUIN
      TFINL=TFLUIN
      TTBL=TFLUIN
      TFLLAV=TFLUIN
      TFILAV=TFLUIN
      TFLXAV=TFLUIN
      TFIXAV=TFLUIN
      IITER=0
100   CONTINUE
      IITER=IITER+1
C DETERMINE COOLANT AND SUBSTRATE PROPERTIES
      CALL PROP(NPROPF,TPROPF,CPFF,KFF,MUFF,PRFF,RHOFF,
     &          NPROPW,TPROPW,KWW,
     &          TFLUX,CPFLUX,KFLUX,MUFLUX,PRFLUX,RHOFLX,
     &          TFINX,KFINX,TTBX,KTBX,
     &          TFLUL,CPFLUL,KFLUL,MUFLUL,PRFLUL,RHOFLL,
     &          TFINL,KFINL,TTBL,KTBL,
     &          TFLLAV,MUFLLA,TFLXAV,MUFLXA,
     &          TFILAV,MUFILA,TFIXAV,MUFIXA,IRETUR)
      IF(IRETUR.EQ.1)RETURN
C
C COMPUTE FRICTION FACTOR AND COOLANT VELOCITY
C
C     IF THE CHANNEL ASPECT RATIO IS LESS THAN 1.0, FAKE OUT THE
C     SMOOTH SURFACE F AND NU CALCULATION ROUTINES BY USING ASPINV
C     AS THE CHANNEL ASPECT RATIO.
C
      IF(ASPECT.GE.1.0)ASPEC=ASPECT
      IF(ASPECT.LT.1.0)ASPEC=ASPINV
C
      IF(ICASE.EQ.1)
     &CALL  SFFD(IFLOW,WW,WC,Z,L,X,DE,ASPEC,ACBYAP,
     &           RHOFLL,RHOFLX,MUFLUL,MUFLUX,MUFLLA,MUFILA,
     &           PRFLUL,PRFLUX,IKLOSS,ICONS,DELP,VOLUME,PPOWER,
     &           REL,REX,V1CL,V1CX,LPLUS,FAPP,XSTARL,XSTARX)
      IF((ICASE.EQ.2).AND.(IFLOW.EQ.1))
     &CALL SLAMF(IFLOW,WW,WC,Z,L,X,DE,ASPEC,ACBYAP,
     &           RHOFLL,RHOFLX,MUFLUL,MUFLUX,MUFLLA,MUFILA,
     &           PRFLUL,PRFLUX,IKLOSS,ICONS,DELP,VOLUME,PPOWER,
     &           REL,REX,V1CL,V1CX,LPLUS,FAPP,XSTARL,XSTARX)
      IF((ICASE.EQ.2).AND.(IFLOW.EQ.2))
     &CALL STURF(IFLOW,WW,WC,Z,L,X,DE,DLE,ASPEC,ACBYAP,
     &           RHOFLL,RHOFLX,MUFLUL,MUFLUX,MUFLLA,MUFILA,
     &           PRFLUL,PRFLUX,IKLOSS,ICONS,DELP,VOLUME,PPOWER,
     &           REL,REX,RESTAL,RESTAX,V1CL,V1CX,LPLUS,FAPP,
     &           XSTARL,XSTARX)
      IF(ICASE.EQ.3)
     &CALL RTURF(IFLOW,WW,WC,Z,L,X,DE,DLE,ASPECT,ACBYAP,
     &           RHOFLL,RHOFLX,MUFLUL,MUFLUX,MUFLLA,MUFILA,
     &           PRFLUL,PRFLUX,IKLOSS,ICONS,DELP,VOLUME,PPOWER,
```

```
     &           REL,REX,V1CL,V1CX,RESTAL,RESTAX,LPLUS,F1,F2,FAPP,
     &           XSTARL,XSTARX,IRETUR,EBYDE,PBYE,ZI,PHI)
      IF(IRETUR.EQ.1)RETURN
C
C COMPUTE TRANSITION REYNOLDS NUMBER - SEE TABLE 2.1
C
      IF(ASPECT.LE.0.2)TRANS=2500.
      IF((ASPECT.GT.0.2).AND.(ASPECT.LT.1.0))
     &                 TRANS=((ASPECT-0.2)/(1.0-0.2))*(2200.-2500.)+2500.
      IF((ASPECT.GT.1.0).AND.(ASPECT.LT.5.0))
     &                 TRANS=((ASPECT-1.0)/(5.0-1.0))*(2500.-2200.)+2200.
      IF(ASPECT.GE.5.0)TRANS=2500.
C
C COMPUTE NUSSELT NUMBER
C
      IF(ICASE.EQ.1)
     &CALL SNUFD(ASPEC,NUL,NUX,NUTL,NUTX,
     &           MUFILA,MUFIXA,MUFLLA,MUFLXA,IRETUR)
      IF((ICASE.EQ.2).AND.(IFLOW.EQ.1))
     &CALL SLAMNU(ASPEC,MUFLLA,MUFILA,XSTARL,NUL,NUTL,
     &                     MUFLXA,MUFIXA,XSTARX,NUX,NUTX)
      IF((ICASE.EQ.2).AND.(IFLOW.EQ.2))
     &CALL STURNU(MUFLLA,MUFILA,PRFLUL,REL,NUL,NUTL,
     &             MUFLXA,MUFIXA,PRFLUX,REX,NUX,NUTX,DE,L,X)
      IF(ICASE.EQ.3)
     &CALL RTURNU(ASPECT,EBYDE,ZI,MUFLLA,MUFILA,PRFLUL,REL,F2,
     &            NUL,NUTL,NUX,NUTX)
C
C COMPUTE HEAT TRANSFER COEFFICIENT
      HL=NUTL*KFLUL/DE
      HX=NUTX*KFLUX/DE
      IF(ASPECT.LT.0.1)GO TO 1010
C COMPUTE FIN CRITERION - EQN. 3.7
      FINCRI=2.*KFINX/(HX*WW)
      IF(FINCRI.LE.6.0)RETURN
C COMPUTE FIN EFFICIENCY - SEE EQN. 3.13
      ML=SQRT((HL*2.)/(KFINL*WW))
      MX=SQRT((HX*2.)/(KFINX*WW))
      MZL=ML*Z
      MZX=MX*Z
      EFFL=(TANH(MZL))/(MZL)
      EFFX=(TANH(MZX))/(MZX)
1010  CONTINUE
C COMPUTE THERMAL RESISTANCES
C     IF(ICASE.EQ.1)GO TO 1100
      IF(ASPECT.GE.10.)GO TO 1100
      IF((ASPECT.GE.0.1).AND.(ASPECT.LT.10.))GO TO 1200
      IF(ASPECT.LE.0.1)GO TO 1300
1100  CONTINUE
C     LARGE ASPECT RATIO CHANNELS EQN. 4.11
      RTBL=T/KTBL
      RCL=(WW+WC)/(3.14159*KTBL)*
     &   ALOG(1./SIN(3.14159*(WW/2.)/(WW+WC)))
      RBFL=(WW+WC)/(2.*HL*Z*EFFL)
      RFFL=(L*(WW+WC))/(RHOFLL*CPFLUL*Z*WC*V1CL)
      RTOTL=RTBL+RCL+RBFL+RFFL
C
      RTBX=T/KTBX
      RCX=(WW+WC)/(3.14159*KTBX)*
     &   ALOG(1./SIN(3.14159*(WW/2.)/(WW+WC)))
```

```
      RBFX=(WW+WC)/(2.*HX*Z*EFFX)
      RFFX=(X*(WW+WC))/(RHOFLX*CPFLUX*WC*Z*V1CX)
      RTOTX=RTBX+RCX+RBFX+RFFX
      GO TO 1400
1200  CONTINUE
C     MODERATE ASPECT RATIO CHANNELS - EQN. 4.12
      RTBL=T/KTBL
      RCL=(WW+WC)/(3.14159*KTBL)*
     &   ALOG(1./SIN(3.14159*(WW/2.)/(WW+WC)))
      RBFL=(WW+WC)/((HL*WC)+(2.*HL*Z*EFFL))
      RFFL=(L*(WW+WC))/(RHOFLL*CPFLUL*WC*Z*V1CL)
      RTOTL=RTBL+RCL+RBFL+RFFL
C
      RTBX=T/KTBX
      RCX=(WW+WC)/(3.14159*KTBX)*
     &   ALOG(1./SIN(3.14159*(WW/2.)/(WW+WC)))
      RBFX=(WW+WC)/((HX*WC)+(2.*HX*Z*EFFX))
      RFFX=(X*(WW+WC))/(RHOFLX*CPFLUX*WC*Z*V1CX)
C DIVIDE BY TUCKERMANS CONVERSION FOR NON-UNIFORM HEAT TRANSFER COEFF.
C     RFFX=RFFX/EFFX
      RTOTX=RTBX+RCX+RBFX+RFFX
      GO TO 1400
1300  CONTINUE
C     SMALL ASPECT RATIO CHANNELS - EQN. 4.13
      RTBL=T/KTBL
      RCL=0.
      RBFL=1./HL
      RFFL=L/(RHOFLL*CPFLUL*Z*V1CL)
      RTOTL=RTBL+RCL+RBFL+RFFL
C
      RTBX=T/KTBX
      RCX=0.
      RBFX=1./HX
      RFFX=X/(RHOFLX*CPFLUX*Z*V1CX)
      RTOTX=RTBX+RCX+RBFX+RFFX
1400  CONTINUE
C
C SEE IF THERMAL SPREADING IS TO BE INCLUDED
      IF(IX.EQ.1)GO TO 1450
C
C NOTE THAT THERMAL SPREADING CALCS. ARE VALID FOR CONSTANT PROPERTIES.
C AND CONSTANT H, BUT THEY ARE DONE AT EACH INDIVIDUAL CHANNEL LOCATION
C BASED ON THE LOCAL VALUES AND NOT THE AVERAGE VALUES.  THE USER MAY
C FIND IT PREFERABLE TO RUN THE PROGRAM ONCE, COMPUTE AN AVERAGE
C NUSSELT NUMBER ALONG THE CHANNEL (USE DATA FROM FILE MICROHEX.OUTPUT2)
C AND TO USE THIS AVERAGE VALUE FOR ALL THERMAL SPREADING CALCULATIONS.
C NOTE THAT ONLY 0.5 TIMES THE BRACKETED TERMS OF EQN.S 3.19 AND 3.20
C ARE USED TO COMPUTE THE DIMENSIONLESS TEMPERATURE CHANGE.  SINCE
C THE THERMAL SPREADING DIFFUSION LENGTH GETS SMALLER WITH INCREASING
C NUSSELT NUMBER, THE 'APPARENT' THERMAL RESISTANCE GOES UP!  THIS IS
C BECAUSE THE OTHER TERMS IN EQN.S 3.19 AND 3.20 WERE NOT USED.
C
C NOTE ALSO THAT THE PROPERTIES AND TEMPERATURES AT THE CHANNEL EXIT
C LISTED IN MICROHEX.OUTPUT4 DO NOT ACCOUNT FOR THERMAL SPREADING,
C  BUT THE LOCAL VALUES DO
      FACTX=1.
      FACTY=1.
C THERMAL SPREADING FOR CALCULATIONS TRANSVERSE TO THE CHANNEL LENGTH
C     HEFF=T+(WW*Z/(WW+WC))
      HEFF=T
```

```
      DLT=SQRT((DE*KTBX*HEFF*(WW+WC))/(NUX*KFLUX*(WC+Z+Z)))
C    - FINITE WIDTH OF COOLING PERIPHERY (NOT DISCUSSED IN TEXT OF THESIS)
C     WCOMP=1.0000
C     WRES=0.0025
C     YRES=0.00125
C     TML1=TANH(WRES/DLT)
C     TML2=TANH(WCOMP/DLT)
C     C4=(1./TML2)*(1./(1.+(TML1/TML2)))
C     FACTY=(1.+C4*(SINH(YRES/DLT)-(TML1*COSH(YRES/DLT))))
C    &      *(1.+C4*(SINH(YRES/DLT)-(TML1*COSH(YRES/DLT))))
C    - INFINITE WIDTH OF THE COOLING PERIPHERY
C
C     THE NEXT TWO VARIABLES SHOULD HAVE BEEN INCLUDED IN THE MICROHEX
C     DATA STATEMENTS, W IS THE TRANSVERSE HEATER WIDTH, AND Y IS THE
C     TRANSVERSE DISTANCE FROM THE HEATER EDGE FOR THE CALCULATION.
      W=0.010
      Y=0.005
      FACTY=(1.-(0.5/EXP(Y/DLT)))*(1.-(0.5/EXP((W-Y)/DLT)))
C THERMAL SPREADING FOR CALCULATIONS ALONG THE CHANNEL LENGTH
      HEFF=T+(WW*Z/(WW+WC))
      DLS=SQRT((DE*KTBX*HEFF*(WW+WC))/(NUX*KFLUX*(WC+Z+Z)))
C    - FINITE WIDTH OF COOLING PERIPHERY (NOT DISCUSSED IN THESIS)
C     WCOMP=1.0000
C     WRES=L
C     XRES=X
C     TML1=TANH(WRES/DLS)
C     TML2=TANH(WCOMP/DLS)
C     C4=(1./TML2)*(1./(1.+(TML1/TML2)))
C     FACTX=(1.+C4*(SINH(XRES/DLS)-(TML1*COSH(XRES/DLS))))
C    &      *(1.+C4*(SINH((L-XRES)/DLS)-(TML1*COSH((L-XRES)/DLS))))
C    - INFINITE WIDTH OF THE COOLING PERIPHERY
      FACTX=(1.-(0.5/EXP(X/DLS)))*(1.-(0.5/EXP((L-X)/DLS)))
C CHANGE THE THERMAL RESISTANCE VALUES TO ACCOUNT FOR THERMAL SPREADING
      RTBX=FACTX*FACTY*RTBX
      RCX=FACTX*FACTY*RCX
      RBFX=FACTX*FACTY*RBFX
      RFFX=RFFX
      RTOTX=RTBX+RBFX+RCX+RFFX
1450  CONTINUE
C
C VISCOUS HEATING COOLANT TEMPERATURE RISE
C     DETERMINE ENTRANCE AND EXIT PRESSURE LOSS COEFFICIENTS
      IF(ICASE.EQ.1)
     &CALL ABRUPT(ACBYAP,ASPECT,IFLOW,IKLOSS,KC,KE,K90,9999.)
      IF(ICASE.NE.1)
     &CALL ABRUPT(ACBYAP,ASPECT,IFLOW,IKLOSS,KC,KE,K90,LPLUS)
      IF(IFLOW.EQ.1)FACT=(MUFILA/MUFLLA)**0.58
      IF(IFLOW.EQ.2)FACT=(MUFILA/MUFLLA)**0.25
      DELPL=(RHOFLL*V1CL*V1CL/2.)*((ACBYAP*ACBYAP*1.*K90)+
     &                             (KC+KE)+(4.*FAPP*FACT*L/DE))
C COMPUTE TEMPERATURE RISE - EQN. 2.22
      DTPUML=DELPL/(RHOFLL*CPFLUL)
      IF(IFLOW.EQ.1)FACT=(MUFIXA/MUFLXA)**0.58
      IF(IFLOW.EQ.2)FACT=(MUFIXA/MUFLXA)**0.25
      DELPX=(RHOFLX*V1CX*V1CX/2.)*((ACBYAP*ACBYAP*1.*K90)+
     &                             (KC+KE)+(4.*FAPP*FACT*X/DE))
C COMPUTE TEMPERATURE RISE - EQN. 2.22
      DTPUMX=DELPX/(RHOFLX*CPFLUX)
C COMPUTE NEW TEMPERATURES
      CALL TEMPS(TTX,TBX,TTIPX,TFLUIN,TFLUO,
```

```
     &           TFLUL,TFLUX,TFINL,TFINX,TTBL,TTBX,
     &           TFLLAV,TFLXAV,TFILAV,TFIXAV,
     &           RTBL,RBFL,RFFL,RTOTL,RTBX,RBFX,RFFX,RTOTX,
     &           Q,DTPUML,DTPUMX,MZL,EFFL,MZX,EFFX,ICLOSE)
C CHECK IF ANOTHER ITERATION IS NEEDED
      IF(ICLOSE.EQ.1)GO TO 100
C CHECK IF REYNOLDS NUMBER IS OUT OF RANGE
      IF(ICASE.EQ.1)IRETUR=0
      IF((IFLOW.EQ.1).AND.(REX.GT.TRANS))IRETUR=1
      IF((IFLOW.EQ.2).AND.(REX.LE.TRANS))IRETUR=1
      IF((IFLOW.EQ.3).AND.((REX.LT.3000.).OR.(REX.GT.10000.)))IRETUR=1
C CHECK IF THERMAL ENTRY LENGTH IS OUT OF RANGE
C     IF((REX.LT.TRANS).AND.(XSTARX.LT.0.0025))IRETUR=1
C     IF((REX.GT.TRANS).AND.(XSTARX.LT.0.001))IRETUR=1
C CHECK IF FIN CRITERION IS NOT SATISFIED
      IF((ASPECT.GT.0.1).AND.(FINCRI.LE.6.0))IRETUR=1
      RETURN
      END
C END OF FILE FOR SUBROUTINE RESIST
C-----------------------------------------------------------------------
```

FILE: MHEX EXEC

```
FILEDEF 11 DISK MICROHEX OUTPUT1 (RECFM FB LRECL 132 BLOCK 1320
FILEDEF 13 DISK MICROHEX OUTPUT2 (RECFM FB LRECL 132 BLOCK 1320
FILEDEF 15 DISK MICROHEX OUTPUT3 (RECFM FB LRECL 132 BLOCK 1320
FILEDEF 17 DISK MICROHEX OUTPUT4 (RECFM FB LRECL 132 BLOCK 1320
FILEDEF 20 DISK DISSPLA MESSAG D(RECFM FB LRECL 132 BLOCK 1320
EXEC DISSPLA MICROHEX
* THE LINE ABOVE CAN BE REPLACED WITH 'RUN MICROHEX' IF THE
* DISSPLA GRAPHICS PACKAGE IS NOT USED (FILDEF 20 ... WILL NOT BE
* NEEDED IF DISSPLA IS NOT USED).
```

APPENDIX F: MICROHEX Numerical Results for the Reference Case

This appendix contains the listing of the files MICROHEX OUTPUT1-4, that were computed for the reference case heat sink design. MICROHEX OUTPUT1 is provided as Table F.1, and MICROHEX OUTPUT2 is provided as Table F.2. Portions of MICROHEX OUTPUT3 and MICROHEX OUTPUT4 are respectively provided as Tables F.3 and F.4. The entire listings of these latter two files were not provided since the values for all channel widths are the same due to the assumed heating rate ($q'' = 0$ W/cm^2). See the comment header block at the beginning of subroutine RTOTAL for a description of the variable names.

The reader will note that some of the values listed for the analysis variables here, are slightly different from those presented in Section 4.5.2. The small differences are due to using the rounded values for the coolant and heat sink properties (listed in Section 4.5.2) for the "hand calculator" results listed there.

The author regrets that more sample output file listings could not be provided due to space limitations.

TABLE F.1

MICROHEX OUTPUT1 FILE FOR THE REFERENCE CASE

SUBSTRATE = SILICON LIQUID COOLANT = WATER TFLUIN = 300.0 DEG K Q = 0. W/CM**2

WC	WW	X	Z	T	ASPEC	ACHYAP	ERYDE	PRYE	PHI	ZI	DELP	V'	P'	RCOND	RC	RCONV	RBULK	RTOT	DTPUMP
M	M	M	M	M	---	--	---	--	DEG	DEG	LBF / IN*2	CC/S / CM*2	W / CM*2	DEG. C / W/CM*2	DEG. C / W/CM*2	DEG. C / W/CM*2	DEG. C / W/CM*2	DEG. C / W/CM*2	DEG. C
*E-6	*E-6		*E-6	*E-6															
FULLY DEVELOPED/DEVELOPING LAMINAR FLOW IN SMOOTH CHANNELS																			
5.0	5.0	.010	20.0	100.0	4.00	0.01	0.000	0.0	0.	0.	10.	0.00	0.00	0.0068	0.0001	0.0057	******	******	0.017
10.0	10.0	.010	40.0	100.0	4.00	0.02	0.000	0.0	0.	0.	10.	0.01	0.00	0.0068	0.0001	0.0114	******	******	0.017
15.0	15.0	.010	60.0	100.0	4.00	0.03	0.000	0.0	0.	0.	10.	0.04	0.00	0.0068	0.0002	0.0171	6.3631	6.3872	0.017
20.0	20.0	.010	80.0	100.0	4.00	0.04	0.000	0.0	0.	0.	10.	0.09	0.01	0.0068	0.0003	0.0229	2.6844	2.7143	0.017
25.0	25.0	.010	100.0	100.0	4.00	0.05	0.000	0.0	0.	0.	10.	0.17	0.01	0.0068	0.0004	0.0286	1.3744	1.4101	0.017
30.0	30.0	.010	120.0	100.0	4.00	0.06	0.000	0.0	0.	0.	10.	0.30	0.02	0.0068	0.0004	0.0343	0.7954	0.8369	0.017
35.0	35.0	.010	140.0	100.0	4.00	0.07	0.000	0.0	0.	0.	10.	0.48	0.03	0.0068	0.0005	0.0398	0.5009	0.5479	0.017
40.0	40.0	.010	160.0	100.0	4.00	0.08	0.000	0.0	0.	0.	10.	0.72	0.05	0.0068	0.0006	0.0452	0.3356	0.3881	0.017
45.0	45.0	.010	180.0	100.0	4.00	0.09	0.000	0.0	0.	0.	10.	1.02	0.07	0.0068	0.0007	0.0507	0.2357	0.2938	0.017
50.0	50.0	.010	200.0	100.0	4.00	0.10	0.000	0.0	0.	0.	10.	1.40	0.10	0.0068	0.0007	0.0563	0.1718	0.2356	0.017
55.0	55.0	.010	220.0	100.0	4.00	0.11	0.000	0.0	0.	0.	10.	1.85	0.13	0.0068	0.0008	0.0619	0.1300	0.1995	0.017
60.0	60.0	.010	240.0	100.0	4.00	0.12	0.000	0.0	0.	0.	10.	2.38	0.16	0.0068	0.0009	0.0667	0.1011	0.1755	0.017
65.0	65.0	.010	260.0	100.0	4.00	0.13	0.000	0.0	0.	0.	10.	2.99	0.21	0.0068	0.0010	0.0715	0.0804	0.1596	0.017
70.0	70.0	.010	280.0	100.0	4.00	0.14	0.000	0.0	0.	0.	10.	3.68	0.25	0.0068	0.0010	0.0760	0.0653	0.1492	0.017
75.0	75.0	.010	300.0	100.0	4.00	0.15	0.000	0.0	0.	0.	10.	4.45	0.31	0.0068	0.0011	0.0803	0.0541	0.1423	0.017
80.0	80.0	.010	320.0	100.0	4.00	0.16	0.000	0.0	0.	0.	10.	5.29	0.37	0.0068	0.0012	0.0846	0.0454	0.1379	0.017
85.0	85.0	.010	340.0	100.0	4.00	0.17	0.000	0.0	0.	0.	10.	6.21	0.43	0.0068	0.0013	0.0875	0.0387	0.1342	0.017
90.0	90.0	.010	360.0	100.0	4.00	0.18	0.000	0.0	0.	0.	10.	7.19	0.50	0.0068	0.0013	0.0902	0.0335	0.1318	0.017
95.0	95.0	.010	380.0	100.0	4.00	0.19	0.000	0.0	0.	0.	10.	8.23	0.57	0.0068	0.0014	0.0923	0.0292	0.1297	0.017
100.0	100.0	.010	400.0	100.0	4.00	0.20	0.000	0.0	0.	0.	10.	9.35	0.64	0.0068	0.0015	0.0943	0.0257	0.1282	0.017
105.0	105.0	.010	420.0	100.0	4.00	0.21	0.000	0.0	0.	0.	10.	10.53	0.73	0.0068	0.0016	0.0955	0.0228	0.1267	0.017
110.0	110.0	.010	440.0	100.0	4.00	0.22	0.000	0.0	0.	0.	10.	11.74	0.81	0.0068	0.0016	0.0968	0.0205	0.1257	0.017
115.0	115.0	.010	460.0	100.0	4.00	0.23	0.000	0.0	0.	0.	10.	12.99	0.90	0.0068	0.0017	0.0980	0.0185	0.1250	0.017
120.0	120.0	.010	480.0	100.0	4.00	0.24	0.000	0.0	0.	0.	10.	14.27	0.98	0.0068	0.0018	0.0991	0.0169	0.1245	0.017
125.0	125.0	.010	500.0	100.0	4.00	0.25	0.000	0.0	0.	0.	10.	15.63	1.08	0.0068	0.0019	0.1001	0.0154	0.1241	0.017
130.0	130.0	.010	520.0	100.0	4.00	0.26	0.000	0.0	0.	0.	10.	17.00	1.17	0.0068	0.0019	0.1011	0.0141	0.1239	0.017
135.0	135.0	.010	540.0	100.0	4.00	0.27	0.000	0.0	0.	0.	10.	18.43	1.27	0.0068	0.0020	0.1009	0.0130	0.1228	0.017
140.0	140.0	.010	560.0	100.0	4.00	0.28	0.000	0.0	0.	0.	10.	19.90	1.37	0.0068	0.0021	0.1010	0.0121	0.1219	0.017
145.0	145.0	.010	580.0	100.0	4.00	0.29	0.000	0.0	0.	0.	10.	21.36	1.47	0.0068	0.0022	0.1016	0.0113	0.1218	0.017
150.0	150.0	.010	600.0	100.0	4.00	0.30	0.000	0.0	0.	0.	10.	22.78	1.57	0.0068	0.0022	0.1027	0.0106	0.1222	0.017
155.0	155.0	.010	620.0	100.0	4.00	0.31	0.000	0.0	0.	0.	10.	24.35	1.68	0.0068	0.0023	0.1039	0.0099	0.1229	0.017
160.0	160.0	.010	640.0	100.0	4.00	0.31	0.000	0.0	0.	0.	10.	25.92	1.79	0.0068	0.0024	0.1054	0.0093	0.1239	0.017

TABLE F.1 (Continued)

FULLY DEVELOPED/DEVELOPING TURBULENT FLOW IN SMOOTH CHANNELS

170.0	170.0	.010	680.0	100.0	4.00	0.33	0.000	0.0	0.	0.	10.	27.48	1.89	0.0068	0.0025	0.0861	0.0087	0.1041	0.017
175.0	175.0	.010	700.0	100.0	4.00	0.34	0.000	0.0	0.	0.	10.	28.83	1.99	0.0068	0.0026	0.0846	0.0083	0.1023	0.017
180.0	180.0	.010	720.0	100.0	4.00	0.35	0.000	0.0	0.	0.	10.	30.19	2.08	0.0068	0.0027	0.0833	0.0080	0.1007	0.017
185.0	185.0	.010	740.0	100.0	4.00	0.36	0.000	0.0	0.	0.	10.	31.56	2.18	0.0068	0.0028	0.0821	0.0076	0.0993	0.017
190.0	190.0	.010	760.0	100.0	4.00	0.37	0.000	0.0	0.	0.	10.	33.00	2.28	0.0068	0.0028	0.0811	0.0073	0.0980	0.017
195.0	195.0	.010	780.0	100.0	4.00	0.38	0.000	0.0	0.	0.	10.	34.43	2.37	0.0068	0.0029	0.0802	0.0070	0.0968	0.017
200.0	200.0	.010	800.0	100.0	4.00	0.39	0.000	0.0	0.	0.	10.	35.89	2.47	0.0068	0.0030	0.0793	0.0067	0.0958	0.017
205.0	205.0	.010	820.0	100.0	4.00	0.40	0.000	0.0	0.	0.	10.	37.38	2.58	0.0068	0.0031	0.0786	0.0064	0.0948	0.017
210.0	210.0	.010	840.0	100.0	4.00	0.41	0.000	0.0	0.	0.	10.	38.88	2.68	0.0068	0.0031	0.0779	0.0062	0.0940	0.017
215.0	215.0	.010	860.0	100.0	4.00	0.42	0.000	0.0	0.	0.	10.	40.41	2.79	0.0068	0.0032	0.0773	0.0060	0.0932	0.017
220.0	220.0	.010	880.0	100.0	4.00	0.43	0.000	0.0	0.	0.	10.	41.95	2.89	0.0068	0.0033	0.0767	0.0057	0.0925	0.017
225.0	225.0	.010	900.0	100.0	4.00	0.44	0.000	0.0	0.	0.	10.	43.52	3.00	0.0068	0.0034	0.0762	0.0055	0.0919	0.017
230.0	230.0	.010	920.0	100.0	4.00	0.45	0.000	0.0	0.	0.	10.	45.11	3.11	0.0068	0.0034	0.0758	0.0053	0.0913	0.017
235.0	235.0	.010	940.0	100.0	4.00	0.46	0.000	0.0	0.	0.	10.	46.73	3.22	0.0068	0.0035	0.0754	0.0051	0.0908	0.017
240.0	240.0	.010	960.0	100.0	4.00	0.47	0.000	0.0	0.	0.	10.	48.36	3.33	0.0068	0.0036	0.0750	0.0050	0.0903	0.017
245.0	245.0	.010	980.0	100.0	4.00	0.48	0.000	0.0	0.	0.	10.	50.01	3.45	0.0068	0.0037	0.0747	0.0048	0.0899	0.017
250.0	250.0	.010	1000.0	100.0	4.00	0.49	0.000	0.0	0.	0.	10.	51.69	3.56	0.0068	0.0037	0.0743	0.0047	0.0895	0.017
255.0	255.0	.010	1020.0	100.0	4.00	0.50	0.000	0.0	0.	0.	10.	53.38	3.68	0.0068	0.0038	0.0741	0.0045	0.0891	0.017
260.0	260.0	.010	1040.0	100.0	4.00	0.51	0.000	0.0	0.	0.	10.	55.10	3.80	0.0068	0.0039	0.0738	0.0044	0.0888	0.017
265.0	265.0	.010	1060.0	100.0	4.00	0.52	0.000	0.0	0.	0.	10.	56.83	3.92	0.0068	0.0040	0.0736	0.0042	0.0885	0.017
270.0	270.0	.010	1080.0	100.0	4.00	0.53	0.000	0.0	0.	0.	10.	58.59	4.04	0.0068	0.0040	0.0733	0.0041	0.0882	0.017
275.0	275.0	.010	1100.0	100.0	4.00	0.54	0.000	0.0	0.	0.	10.	60.36	4.16	0.0068	0.0041	0.0731	0.0040	0.0880	0.017
280.0	280.0	.010	1120.0	100.0	4.00	0.55	0.000	0.0	0.	0.	10.	62.16	4.29	0.0068	0.0042	0.0730	0.0039	0.0878	0.017
285.0	285.0	.010	1140.0	100.0	4.00	0.56	0.000	0.0	0.	0.	10.	63.97	4.41	0.0068	0.0042	0.0728	0.0038	0.0876	0.017
290.0	290.0	.010	1160.0	100.0	4.00	0.57	0.000	0.0	0.	0.	10.	65.81	4.54	0.0068	0.0043	0.0727	0.0037	0.0874	0.017
295.0	295.0	.010	1180.0	100.0	4.00	0.58	0.000	0.0	0.	0.	10.	67.66	4.66	0.0068	0.0044	0.0725	0.0036	0.0872	0.017
300.0	300.0	.010	1200.0	100.0	4.00	0.59	0.000	0.0	0.	0.	10.	69.53	4.79	0.0068	0.0045	0.0724	0.0035	0.0871	0.017
305.0	305.0	.010	1220.0	100.0	4.00	0.60	0.000	0.0	0.	0.	10.	71.42	4.92	0.0068	0.0045	0.0723	0.0034	0.0870	0.017
310.0	310.0	.010	1240.0	100.0	4.00	0.61	0.000	0.0	0.	0.	10.	73.33	5.06	0.0068	0.0046	0.0722	0.0033	0.0868	0.017
315.0	315.0	.010	1260.0	100.0	4.00	0.62	0.000	0.0	0.	0.	10.	75.26	5.19	0.0068	0.0047	0.0721	0.0032	0.0867	0.017
320.0	320.0	.010	1280.0	100.0	4.00	0.63	0.000	0.0	0.	0.	10.	77.21	5.32	0.0068	0.0048	0.0720	0.0031	0.0866	0.017
325.0	325.0	.010	1300.0	100.0	4.00	0.64	0.000	0.0	0.	0.	10.	79.18	5.46	0.0068	0.0048	0.0719	0.0030	0.0866	0.017
330.0	330.0	.010	1320.0	100.0	4.00	0.65	0.000	0.0	0.	0.	10.	81.16	5.60	0.0068	0.0049	0.0719	0.0030	0.0865	0.017
335.0	335.0	.010	1340.0	100.0	4.00	0.66	0.000	0.0	0.	0.	10.	83.17	5.73	0.0068	0.0050	0.0718	0.0029	0.0864	0.017
340.0	340.0	.010	1360.0	100.0	4.00	0.67	0.000	0.0	0.	0.	10.	85.19	5.87	0.0068	0.0051	0.0717	0.0028	0.0864	0.017
345.0	345.0	.010	1380.0	100.0	4.00	0.68	0.000	0.0	0.	0.	10.	87.23	6.01	0.0068	0.0051	0.0717	0.0028	0.0864	0.017
350.0	350.0	.010	1400.0	100.0	4.00	0.69	0.000	0.0	0.	0.	10.	89.29	6.16	0.0068	0.0052	0.0717	0.0027	0.0863	0.017
355.0	355.0	.010	1420.0	100.0	4.00	0.70	0.000	0.0	0.	0.	10.	91.36	6.30	0.0068	0.0053	0.0716	0.0026	0.0863	0.017
360.0	360.0	.010	1440.0	100.0	4.00	0.71	0.000	0.0	0.	0.	10.	93.46	6.44	0.0068	0.0054	0.0716	0.0026	0.0863	0.017
365.0	365.0	.010	1460.0	100.0	4.00	0.72	0.000	0.0	0.	0.	10.	95.57	6.59	0.0068	0.0054	0.0716	0.0025	0.0863	0.017
370.0	370.0	.010	1480.0	100.0	4.00	0.73	0.000	0.0	0.	0.	10.	97.70	6.74	0.0068	0.0055	0.0715	0.0025	0.0863	0.017
375.0	375.0	.010	1500.0	100.0	4.00	0.74	0.000	0.0	0.	0.	10.	99.85	6.88	0.0068	0.0056	0.0715	0.0024	0.0863	0.017

TABLE F.1 (Continued)

380.0	380.0	.010	1520.0	100.0	4.00	0.75	0.000	0.0	0.	0.	10.	102.01	7.03	0.0068	0.0057	0.0715	0.0024	0.0863	0.017
385.0	385.0	.010	1540.0	100.0	4.00	0.76	0.000	0.0	0.	0.	10.	104.20	7.18	0.0068	0.0057	0.0715	0.0023	0.0863	0.017
390.0	390.0	.010	1560.0	100.0	4.00	0.77	0.000	0.0	0.	0.	10.	106.40	7.34	0.0068	0.0058	0.0715	0.0023	0.0863	0.017
395.0	395.0	.010	1580.0	100.0	4.00	0.78	0.000	0.0	0.	0.	10.	108.62	7.49	0.0068	0.0059	0.0715	0.0022	0.0863	0.017
400.0	400.0	.010	1600.0	100.0	4.00	0.79	0.000	0.0	0.	0.	10.	110.86	7.64	0.0068	0.0060	0.0715	0.0022	0.0863	0.017
405.0	405.0	.010	1620.0	100.0	4.00	0.80	0.000	0.0	0.	0.	10.	113.11	7.80	0.0068	0.0060	0.0714	0.0021	0.0864	0.017
410.0	410.0	.010	1640.0	100.0	4.00	0.81	0.000	0.0	0.	0.	10.	115.38	7.96	0.0068	0.0061	0.0714	0.0021	0.0864	0.017
415.0	415.0	.010	1660.0	100.0	4.00	0.82	0.000	0.0	0.	0.	10.	117.67	8.11	0.0068	0.0062	0.0714	0.0020	0.0864	0.017
420.0	420.0	.010	1680.0	100.0	4.00	0.83	0.000	0.0	0.	0.	10.	119.98	8.27	0.0068	0.0063	0.0714	0.0020	0.0865	0.017
425.0	425.0	.010	1700.0	100.0	4.00	0.84	0.000	0.0	0.	0.	10.	122.30	8.43	0.0068	0.0063	0.0714	0.0020	0.0865	0.017
430.0	430.0	.010	1720.0	100.0	4.00	0.85	0.000	0.0	0.	0.	10.	124.64	8.59	0.0068	0.0064	0.0715	0.0019	0.0865	0.017
435.0	435.0	.010	1740.0	100.0	4.00	0.86	0.000	0.0	0.	0.	10.	127.00	8.76	0.0068	0.0065	0.0715	0.0019	0.0866	0.017
440.0	440.0	.010	1760.0	100.0	4.00	0.87	0.000	0.0	0.	0.	10.	129.38	8.92	0.0068	0.0066	0.0715	0.0019	0.0866	0.017
445.0	445.0	.010	1780.0	100.0	4.00	0.88	0.000	0.0	0.	0.	10.	131.77	9.09	0.0068	0.0066	0.0715	0.0018	0.0867	0.017
450.0	450.0	.010	1800.0	100.0	4.00	0.89	0.000	0.0	0.	0.	10.	134.18	9.25	0.0068	0.0067	0.0715	0.0018	0.0867	0.017
455.0	455.0	.010	1820.0	100.0	4.00	0.90	0.000	0.0	0.	0.	10.	136.61	9.42	0.0068	0.0068	0.0715	0.0018	0.0868	0.017
460.0	460.0	.010	1840.0	100.0	4.00	0.91	0.000	0.0	0.	0.	10.	139.05	9.59	0.0068	0.0069	0.0715	0.0017	0.0868	0.017
465.0	465.0	.010	1860.0	100.0	4.00	0.92	0.000	0.0	0.	0.	10.	141.51	9.76	0.0068	0.0069	0.0715	0.0017	0.0869	0.017
470.0	470.0	.010	1880.0	100.0	4.00	0.93	0.000	0.0	0.	0.	10.	143.99	9.93	0.0068	0.0070	0.0715	0.0017	0.0870	0.017
475.0	475.0	.010	1900.0	100.0	4.00	0.94	0.000	0.0	0.	0.	10.	146.49	10.10	0.0068	0.0071	0.0715	0.0016	0.0870	0.017
480.0	480.0	.010	1920.0	100.0	4.00	0.94	0.000	0.0	0.	0.	10.	149.00	10.27	0.0068	0.0072	0.0716	0.0016	0.0871	0.017
485.0	485.0	.010	1940.0	100.0	4.00	0.95	0.000	0.0	0.	0.	10.	151.53	10.45	0.0068	0.0072	0.0716	0.0016	0.0871	0.017
490.0	490.0	.010	1960.0	100.0	4.00	0.96	0.000	0.0	0.	0.	10.	154.07	10.62	0.0068	0.0073	0.0716	0.0016	0.0872	0.017
495.0	495.0	.010	1980.0	100.0	4.00	0.97	0.000	0.0	0.	0.	10.	156.64	10.80	0.0068	0.0074	0.0716	0.0015	0.0873	0.017
500.0	500.0	.010	2000.0	100.0	4.00	0.98	0.000	0.0	0.	0.	10.	159.22	10.98	0.0068	0.0075	0.0716	0.0015	0.0873	0.017

TABLE F.2

MICROHEX OUTPUT2 FILE FOR THE REFERENCE CASE

SUBSTRATE = SILICON LIQUID COOLANT = WATER TFLUIN = 300.0 DEG K Q = 0. W/CM**2

DE	DLE	VC	RE	RESTAR	XSTAR	LPLUS	NU	NUT	FAPP	K90	KC	KE	FINCRI	EFF
M	M	M/S	--	--	--	--	--	---	--	---	--	--	--	---
FULLY DEVELOPED/DEVELOPING LAMINAR FLOW IN SMOOTH CHANNELS														
8.0	0.0	0.01	0.	0.	******	******	5.76	5.76	******	0.00	0.00	0.00	134.18	.86643
16.0	0.0	0.06	1.	0.	******	******	5.76	5.76	******	0.00	0.00	0.00	134.18	.86643
24.0	0.0	0.13	3.	0.	******	******	5.76	5.76	******	0.00	0.00	0.00	134.18	.86643
32.0	0.0	0.22	8.	0.	6.3954	******	5.76	5.76	******	0.00	0.00	0.00	134.18	.86643
40.0	0.0	0.35	16.	0.	2.6196	******	5.76	5.76	******	0.00	0.00	0.00	134.18	.86643
48.0	0.0	0.50	27.	0.	1.2633	7.6211	5.76	5.76	.65481	0.00	0.00	0.00	134.18	.86643
56.0	0.0	0.69	43.	0.	0.6819	4.1137	5.80	5.80	.41236	0.00	0.00	0.00	133.29	.86569
64.0	0.0	0.90	65.	0.	0.3997	2.4114	5.83	5.83	.27625	0.00	0.00	0.00	132.57	.86503
72.0	0.0	1.13	92.	0.	0.2495	1.5054	5.85	5.85	.19402	0.00	0.00	0.00	132.12	.86469
80.0	0.0	1.40	127.	0.	0.1638	0.9879	5.86	5.86	.14160	0.00	0.00	0.00	131.88	.86449
88.0	0.0	1.68	167.	0.	0.1126	0.6795	5.86	5.86	.10983	0.00	0.00	0.00	131.75	.86437
96.0	0.0	1.98	215.	0.	0.0803	0.4842	5.94	5.94	.08670	0.00	0.00	0.00	130.11	.86294
104.0	0.0	2.30	270.	0.	0.0590	0.3557	6.02	6.02	.06969	0.00	0.00	0.00	128.42	.86144
112.0	0.0	2.63	333.	0.	0.0445	0.2683	6.10	6.10	.05699	0.00	0.00	0.00	126.63	.85981
120.0	0.0	2.96	402.	0.	0.0344	0.2072	6.20	6.20	.04739	0.00	0.00	0.00	124.67	.85797
128.0	0.0	3.31	479.	0.	0.0270	0.1632	6.29	6.29	.04095	0.00	0.00	0.00	122.82	.85621
136.0	0.0	3.65	562.	0.	0.0217	0.1309	6.48	6.48	.03573	0.00	0.00	0.00	119.14	.85254
144.0	0.0	3.99	650.	0.	0.0177	0.1069	6.69	6.69	.03144	0.00	0.00	0.00	115.55	.84879
152.0	0.0	4.33	744.	0.	0.0147	0.0884	6.93	6.93	.02608	0.00	0.00	0.00	111.47	.84428
160.0	0.0	4.67	845.	0.	0.0123	0.0740	7.17	7.17	.02540	0.00	0.00	0.00	107.69	.83987
168.0	0.0	5.01	952.	0.	0.0104	0.0625	7.48	7.48	.02317	0.00	0.00	0.00	103.34	.83446
176.0	0.0	5.34	1062.	0.	0.0089	0.0535	7.77	7.77	.02144	0.00	0.00	0.00	99.47	.82933
184.0	0.0	5.65	1175.	0.	0.0077	0.0463	8.06	8.06	.02004	0.00	0.00	0.00	95.81	.82417
192.0	0.0	5.94	1290.	0.	0.0067	0.0404	8.37	8.37	.01882	0.00	0.00	0.00	92.31	.81895
200.0	0.0	6.25	1413.	0.	0.0059	0.0354	8.68	8.68	.01784	0.00	0.00	0.00	89.00	.81371
208.0	0.0	6.54	1537.	0.	0.0052	0.0313	8.99	8.99	.01691	0.00	0.00	0.00	85.92	.80856
216.0	0.0	6.83	1667.	0.	0.0046	0.0278	9.42	9.42	.01622	0.00	0.00	0.00	82.03	.80163
224.0	0.0	7.11	1800.	0.	0.0041	0.0248	9.83	9.83	.01561	0.00	0.00	0.00	78.57	.79501
232.0	0.0	7.36	1931.	0.	0.0037	0.0223	10.18	10.18	.01502	0.00	0.00	0.00	75.89	.78958
240.0	0.0	7.59	2060.	0.	0.0034	0.0202	10.47	10.47	.01444	0.00	0.00	0.00	73.77	.78509
248.0	0.0	7.85	2202.	0.	0.0030	0.0183	10.74	10.74	.01404	0.00	0.00	0.00	71.93	.78103
256.0	0.0	8.10	2344.	0.	0.0028	0.0167	10.97	10.97	.01364	0.00	0.00	0.00	70.42	.77757

TABLE F.2 (Continued)

FULLY DEVELOPED/DEVELOPING TURBULENT FLOW IN SMOOTH CHANNELS

272.0	235.9	8.08	2485.	2155.	0.0025	0.0148	15.25	15.25	.01441	0.00	0.00	0.00	50.65	.71967
280.0	242.8	8.24	2607.	2261.	0.0023	0.0137	16.19	16.19	.01429	0.00	0.00	0.00	47.71	.70838
288.0	249.8	8.39	2730.	2368.	0.0021	0.0127	17.14	17.14	.01418	0.00	0.00	0.00	45.07	.69742
296.0	256.7	8.54	2856.	2477.	0.0020	0.0118	18.10	18.10	.01407	0.00	0.00	0.00	42.68	.68676
304.0	263.6	8.68	2984.	2588.	0.0018	0.0110	19.07	19.07	.01396	0.00	0.00	0.00	40.50	.67640
312.0	270.6	8.83	3114.	2700.	0.0017	0.0103	20.06	20.06	.01386	0.00	0.00	0.00	38.52	.66633
320.0	277.5	8.97	3246.	2815.	0.0016	0.0096	21.05	21.05	.01376	0.00	0.00	0.00	36.71	.65654
328.0	284.4	9.12	3380.	2931.	0.0015	0.0090	22.05	22.05	.01367	0.00	0.00	0.00	35.04	.64702
336.0	291.4	9.26	3516.	3049.	0.0014	0.0085	23.06	23.06	.01358	0.00	0.00	0.00	33.51	.63776
344.0	298.3	9.40	3654.	3169.	0.0013	0.0080	24.08	24.08	.01349	0.00	0.00	0.00	32.09	.62875
352.0	305.3	9.54	3794.	3290.	0.0012	0.0075	25.11	25.11	.01341	0.00	0.00	0.00	30.77	.61999
360.0	312.2	9.67	3936.	3413.	0.0012	0.0071	26.15	26.15	.01333	0.00	0.00	0.00	29.55	.61147
368.0	319.1	9.81	4080.	3538.	0.0011	0.0067	27.20	27.20	.01325	0.00	0.00	0.00	28.41	.60317
376.0	326.1	9.94	4225.	3664.	0.0010	0.0063	28.25	28.25	.01317	0.00	0.00	0.00	27.35	.59510
384.0	333.0	10.07	4373.	3792.	0.0010	0.0060	29.32	29.32	.01310	0.00	0.00	0.00	26.35	.58724
392.0	339.9	10.21	4523.	3922.	0.0009	0.0056	30.39	30.39	.01303	0.00	0.00	0.00	25.42	.57958
400.0	346.9	10.34	4674.	4053.	0.0009	0.0053	31.48	31.48	.01296	0.00	0.00	0.00	24.54	.57213
408.0	353.8	10.47	4827.	4186.	0.0008	0.0051	32.57	32.57	.01290	0.00	0.00	0.00	23.72	.56487
416.0	360.8	10.60	4982.	4321.	0.0008	0.0048	33.67	33.67	.01283	0.00	0.00	0.00	22.95	.55779
424.0	367.7	10.72	5139.	4457.	0.0008	0.0046	34.78	34.78	.01277	0.00	0.00	0.00	22.21	.55090
432.0	374.6	10.85	5298.	4594.	0.0007	0.0044	35.90	35.90	.01271	0.00	0.00	0.00	21.52	.54417
440.0	381.6	10.98	5459.	4734.	0.0007	0.0042	37.02	37.02	.01265	0.00	0.00	0.00	20.87	.53762
448.0	388.5	11.10	5621.	4874.	0.0007	0.0040	38.16	38.16	.01259	0.00	0.00	0.00	20.25	.53123
456.0	395.4	11.22	5785.	5017.	0.0006	0.0038	39.30	39.30	.01254	0.00	0.00	0.00	19.66	.52500
464.0	402.4	11.35	5951.	5160.	0.0006	0.0036	40.45	40.45	.01248	0.00	0.00	0.00	19.10	.51892
472.0	409.3	11.47	6118.	5306.	0.0006	0.0035	41.61	41.61	.01243	0.00	0.00	0.00	18.57	.51298
480.0	416.3	11.59	6288.	5453.	0.0005	0.0033	42.77	42.77	.01238	0.00	0.00	0.00	18.06	.50719
488.0	423.2	11.71	6459.	5601.	0.0005	0.0032	43.95	43.95	.01233	0.00	0.00	0.00	17.58	.50153
496.0	430.1	11.83	6631.	5751.	0.0005	0.0030	45.13	45.13	.01228	0.00	0.00	0.00	17.12	.49601
504.0	437.1	11.95	6806.	5902.	0.0005	0.0029	46.32	46.32	.01223	0.00	0.00	0.00	16.68	.49062
512.0	444.0	12.06	6982.	6055.	0.0005	0.0028	47.51	47.51	.01218	0.00	0.00	0.00	16.26	.48535
520.0	450.9	12.18	7160.	6209.	0.0004	0.0027	48.72	48.72	.01214	0.00	0.00	0.00	15.86	.48020
528.0	457.9	12.30	7339.	6365.	0.0004	0.0026	49.93	49.93	.01209	0.00	0.00	0.00	15.47	.47517
536.0	464.8	12.41	7521.	6522.	0.0004	0.0025	51.14	51.14	.01205	0.00	0.00	0.00	15.11	.47025
544.0	471.8	12.53	7703.	6680.	0.0004	0.0024	52.37	52.37	.01200	0.00	0.00	0.00	14.75	.46544
552.0	478.7	12.64	7888.	6840.	0.0004	0.0023	53.60	53.60	.01196	0.00	0.00	0.00	14.41	.46073
560.0	485.6	12.76	8074.	7002.	0.0004	0.0022	54.84	54.84	.01192	0.00	0.00	0.00	14.09	.45613
568.0	492.6	12.87	8262.	7165.	0.0004	0.0021	56.09	56.09	.01188	0.00	0.00	0.00	13.77	.45163
576.0	499.5	12.98	8451.	7329.	0.0003	0.0021	57.35	57.35	.01184	0.00	0.00	0.00	13.47	.44723
584.0	506.4	13.09	8642.	7495.	0.0003	0.0020	58.61	58.61	.01180	0.00	0.00	0.00	13.18	.44291
592.0	513.4	13.20	8835.	7662.	0.0003	0.0019	59.88	59.88	.01176	0.00	0.00	0.00	12.90	.43869
600.0	520.3	13.31	9029.	7830.	0.0003	0.0018	61.15	61.15	.01172	0.00	0.00	0.00	12.63	.43456

TABLE F.2 (Continued)

608.0	527.3	13.42	9225.	8000.	0.0003	0.0018	62.43	62.43	.01169	0.00	0.00	0.00	12.37	.43051
616.0	534.2	13.53	9423.	8171.	0.0003	0.0017	63.72	63.72	.01165	0.00	0.00	0.00	12.12	.42654
624.0	541.1	13.64	9622.	8344.	0.0003	0.0017	65.02	65.02	.01161	0.00	0.00	0.00	11.88	.42266
632.0	548.1	13.75	9822.	8518.	0.0003	0.0016	66.32	66.32	.01158	0.00	0.00	0.00	11.65	.41885
640.0	555.0	13.86	10025.	8693.	0.0003	0.0016	67.63	67.63	.01154	0.00	0.00	0.00	11.42	.41512
648.0	561.9	13.96	10229.	8870.	0.0003	0.0015	68.95	68.95	.01151	0.00	0.00	0.00	11.21	.41146
656.0	568.9	14.07	10434.	9048.	0.0002	0.0015	70.27	70.27	.01147	0.00	0.00	0.00	10.99	.40787
664.0	575.8	14.18	10641.	9228.	0.0002	0.0014	71.60	71.60	.01144	0.00	0.00	0.00	10.79	.40435
672.0	582.8	14.28	10850.	9409.	0.0002	0.0014	72.94	72.94	.01141	0.00	0.00	0.00	10.59	.40090
680.0	589.7	14.39	11060.	9591.	0.0002	0.0013	74.28	74.28	.01137	0.00	0.00	0.00	10.40	.39752
688.0	596.6	14.49	11271.	9774.	0.0002	0.0013	75.63	75.63	.01134	0.00	0.00	0.00	10.21	.39419
696.0	603.6	14.60	11485.	9959.	0.0002	0.0013	76.99	76.99	.01131	0.00	0.00	0.00	10.03	.39093
704.0	610.5	14.70	11699.	10146.	0.0002	0.0012	78.35	78.35	.01128	0.00	0.00	0.00	9.86	.38773
712.0	617.4	14.81	11916.	10333.	0.0002	0.0012	79.72	79.72	.01125	0.00	0.00	0.00	9.69	.38459
720.0	624.4	14.91	12134.	10522.	0.0002	0.0011	81.10	81.10	.01122	0.00	0.00	0.00	9.53	.38151
728.0	631.3	15.01	12353.	10713.	0.0002	0.0011	82.48	82.48	.01119	0.00	0.00	0.00	9.37	.37848
736.0	638.3	15.11	12574.	10904.	0.0002	0.0011	83.87	83.87	.01116	0.00	0.00	0.00	9.21	.37550
744.0	645.2	15.22	12797.	11097.	0.0002	0.0011	85.27	85.27	.01113	0.00	0.00	0.00	9.06	.37258
752.0	652.1	15.32	13021.	11292.	0.0002	0.0010	86.67	86.67	.01110	0.00	0.00	0.00	8.91	.36971
760.0	659.1	15.42	13247.	11487.	0.0002	0.0010	88.08	88.08	.01107	0.00	0.00	0.00	8.77	.36688
768.0	666.0	15.52	13474.	11684.	0.0002	0.0010	89.50	89.50	.01104	0.00	0.00	0.00	8.63	.36411
776.0	672.9	15.62	13702.	11883.	0.0002	0.0009	90.92	90.92	.01101	0.00	0.00	0.00	8.50	.36138
784.0	679.9	15.72	13933.	12082.	0.0002	0.0009	92.35	92.35	.01098	0.00	0.00	0.00	8.37	.35870
792.0	686.8	15.82	14165.	12283.	0.0001	0.0009	93.78	93.78	.01096	0.00	0.00	0.00	8.24	.35607
800.0	693.8	15.92	14398.	12486.	0.0001	0.0009	95.22	95.22	.01093	0.00	0.00	0.00	8.11	.35347

TABLE F.3

MICROHEX OUTPUT3 FILE FOR THE REFERENCE CASE *,**

SUBSTRATE = SILICON   LIQUID COOLANT = WATER   TFLUIN = 300.0 DEG K   Q = 0. W/CM**2

TFINL	TFLUL	TTBL	TFLLAV	TFILAV	TFINX	TFLUX	TTBX	TFLXAV	TFIXAV	TTX	TTB	TTIPX	TFLUO	DTPUML	DTPUMX
DEG. C	DEG. C	DEG. C	DEG. C	DEG. C	DEG. C	DEG. C	DEG. C	DEG. C	DEG. C	DEG. C	DEG. C	DEG. C	DEG. C	DEG. C	DEG. C
FULLY DEVELOPED/DEVELOPING LAMINAR FLOW IN SMOOTH CHANNELS															
300.0	300.0	300.0	300.0	300.0	300.0	300.0	300.0	300.0	300.0	300.0	300.0	300.0	300.0	0.017	0.017
* INTERMEDIATE LAMINAR FLOW VALUES ARE NOT SHOWN SINCE THEY ARE THE SAME FOR ALL w_c															
300.0	300.0	300.0	300.0	300.0	300.0	300.0	300.0	300.0	300.0	300.0	300.0	300.0	300.0	0.017	0.017
FULLY DEVELOPED/DEVELOPING TURBULENT FLOW IN SMOOTH CHANNELS															
300.0	300.0	300.0	300.0	300.0	300.0	300.0	300.0	300.0	300.0	300.0	300.0	300.0	300.0	0.017	0.017
** INTERMEDIATE TURBULENT FLOW VALUES ARE NOT SHOWN SINCE THEY ARE THE SAME FOR ALL w_c															
300.0	300.0	300.0	300.0	300.0	300.0	300.0	300.0	300.0	300.0	300.0	300.0	300.0	300.0	0.017	0.017

TABLE F.4

MICROHEX OUTPUT4 FILE FOR THE REFERENCE CASE *,**

SUBSTRATE = SILICON   LIQUID COOLANT = WATER   TFLUIN = 300.0 DEG K   Q = 0. W/CM**2

CPFLUL	CPFLUX	KFLUL	KFLUX	PRFLUL	PRFLUX	RHOFLL	RJOFLX	MUFLUL	MUFLUX	MUFLLA	MUFLXA	MUFILA	MUFIXA	KFINL	KFINX	KTBL	KTBX
J/KG C	J/KG C	W/M C	W/M C	--	--	KG/M*3	KG/M*3	KG/M S	KG/M S	KG/M S	KG/M S	KG/M S	KG/M S	W/M C	W/M C	W/M C	W/M C
FULLY DEVELOPED/DEVELOPING LAMINAR FLOW IN SMOOTH CHANNELS																	
4177.6	4177.6	0.6130	0.6130	6.033	6.033	995.5	995.5	.00088	.00088	.00088	.00088	.00088	.00088	148.00	148.00	148.00	148.00
* INTERMEDIATE LAMINAR FLOW VALUES ARE NOT SHOWN SINCE THEY ARE THE SAME FOR ALL w_c																	
4177.6	4177.6	0.6130	0.6130	6.033	6.033	995.5	995.5	.00088	.00088	.00088	.00088	.00088	.00088	148.00	148.00	148.00	148.00
FULLY DEVELOPED/DEVELOPING TURBULENT FLOW IN SMOOTH CHANNELS																	
4177.6	4177.6	0.6130	0.6130	6.033	6.033	995.5	995.5	.00088	.00088	.00088	.00088	.00088	.00088	148.00	148.00	148.00	148.00
** INTERMEDIATE TURBULENT FLOW VALUES ARE NOT SHOWN SINCE THEY ARE THE SAME FOR ALL w_c																	
4177.6	4177.6	0.6130	0.6130	6.033	6.033	995.5	995.5	.00088	.00088	.00088	.00088	.00088	.00088	148.00	148.00	148.00	148.00